OUTLOOK
Taste

nature

THE INTERNATIONAL WEEKLY JOURNAL OF SCIENCE

MILKING THE GREEN SAHARA

Chemical residues in pottery date earliest use of dairy products in Africa to fifth millennium BC

PAGE 390

CLINICAL RESEARCH

ILL-INFORMED CONSENT

Protecting subjects in the era of big data

PAGE 312

DIGITAL PHOTOGRAPHY

VERY CANDID CAMERA

Gigapixel revolution to change photographers' art

PAGE 386

GENOMICS

BREAST CANCER DIVERSITY

Whole-genome analysis yields multiple drug targets

PAGE 328

➲ NATURE.COM/NATURE
21 June 2012 £10
Vol. 486, No. 7403

MERCK MILLIPORE

Break free from routine sample prep. Go from boring to bold.

The Samplicity™ Filtration System takes sample prep in a flexible, new direction. This vacuum-powered system filters one sample or eight, of virtually any viscosity or composition, into HPLC vials in seconds—with minimal manual effort.

With the Samplicity filtration system and Millex Samplicity™ filters, Merck Millipore has transformed multi-sample filtration forever.

Samplicity makes it simple.

Discover how at www.millipore.com/GoBold

Merck Millipore is a division of MERCK

Merck Millipore, the M mark, Samplicity and Millex Samplicity are trademarks of Merck KGaA, Darmstadt, Germany.
© 2012 EMD Millipore Corporation, Billerica MA USA. All rights reserved.

MEETINGS OF NOBEL LAUREATES
LINDAU®

Lindau Nobel Community

the interactive home of the Lindau Meetings

Be part of our community

Scan this tag to access the site on your smartphone

The 2012 Nobel Laureate Meeting
28 Nobel Laureates, 588 young researchers, 69 countries.

The 62nd Lindau Meeting of Nobel Laureates, taking place from 1st to 6th July 2012, is dedicated to physics. We invite you to visit the Lindau Nobel Community site to access multilingual blogs, follow tweets about the event and view pictures from Instagram. You can also watch footage by *Nature Video* from past and present meetings and more.

lindau.nature.com

nature publishing group npg

Antibodies and Related Reagents for Signal Transduction Research

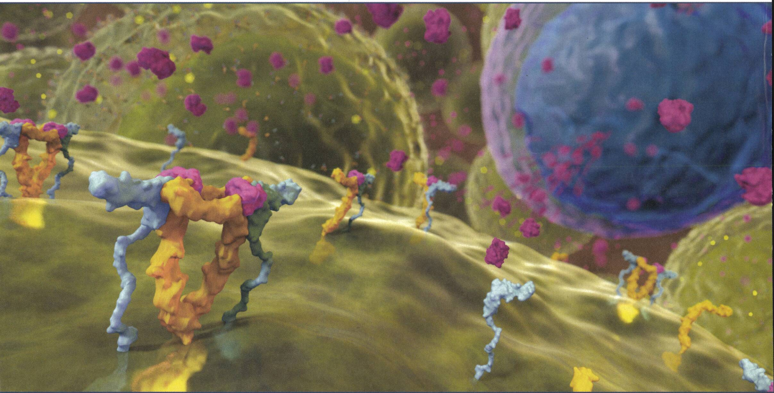

The Highest Quality
Cytokines & Growth Factors

...from Cell Signaling Technology

The world's highest quality antibody provider has now extended its expertise to cytokine production.

- Produced and bioassayed in house with the highest purity and bioactivity.
- Comparison of multiple lots, stringent product specifications, and rigorous quality control ensures maximum lot-to-lot consistency.
- Endotoxin levels are routinely tested and are less than 0.01 ng/µg cytokine.
- Many products are produced in mammalian cells to maximize natural conformation and glycosylation.
- Multi-milligram quantities available.

Human Interleukin-17A (hIL-17A) #8928

Purity

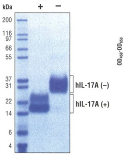

6 µg reduced (+) and non-reduced (-) recombinant hIL-17A.

Bioactivity

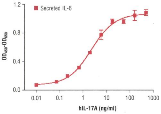

The production of IL-6 by human foreskin fibroblasts cultured with increasing concentrations of hIL-17A for 48 hours was assessed.

Downstream Signaling

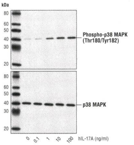

Human foreskin fibroblasts treated with hIL-17A for 15 minutes were examined using phospho- and total p38 MAPK antibodies.

for quality products you can trust...

www.cellsignal.com

Cell Signaling
TECHNOLOGY®

For Research Use Only. Not For Use In Diagnostic Procedures.

Orders (toll-free) 1-877-616-2355 | **Inquiries** info@cellsignal.com | **Environmental Commitment** eco.cellsignal.com

© 2012 Cell Signaling Technology, Inc. Cell Signaling Technology® is a trademark of Cell Signaling Technology, Inc.

CONTENTS

21 June 2012 / Vol 486 / Issue No 7403

THIS WEEK

EDITORIALS

293 INFORMED CONSENT
Time to open up
Scientists must be more up-front about how they will use the data they gather

293 STEM CELLS
Renewed vigour
Politicians need to be continually reminded of the merits of stem-cell work

294 LABORATORY PRACTICE
Serious questions
Nature asks researchers to participate in a survey on lab-safety procedures

WORLD VIEW

295 **Do not censor science in the name of biosecurity**
Tim Trevan
Why biosecurity professionals don't see mutant-flu papers as a threat

RESEARCH HIGHLIGHTS

296 SELECTIONS FROM THE SCIENTIFIC LITERATURE
Genomics used to track a pathogen / Desalination with graphene / Bats' role in rabies spread / Ice loss drives Arctic warming / Retinal repair

SEVEN DAYS

298 THE NEWS IN BRIEF
Chinese astronauts board home-made space station / Australia releases plans for world's largest marine-reserve network / Nobel chemist William Knowles dies / Monsanto one step closer to losing Brazilian revenue

CAREERS

429 LIFE SCIENCES
All jazzed up
The resurgent New Orleans area is attracting a good line in start-ups

431 COLUMN
Piled too high
Mariano A Loza-Coll
The scientific life — it's just like it is in the movies

NATUREJOBS ADVERTISING FEATURE
Spotlight on Genetics

NEWS IN FOCUS

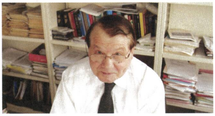

301 AIDS
Nobel laureates call for removal of African HIV centre's scientific director

302 PUBLISHING
Britain considers making all papers open-access from the start

304 COMMUNITY
Ranks of US biomedical researchers swell, but minorities still face challenges

305 ACADEMIC CONDUCT
Plagiarism allegations levelled at Romanian prime minister

306 ENVIRONMENT
Peru's attempts to crack down on mining impacts cause friction

308 ARCHAEOLOGY
Austerity measures are wreaking havoc on Greece's cultural heritage

FEATURES

312 INFORMED CONSENT
Broken contract
How consent forms don't always meet the needs of study participants

WILDLIFE BIOLOGY
Danger in the wind
Researchers seek ways to keep birds and bats away from wind turbines PAGE 310

COMMENT

315 INSTITUTES
Aspen physics turns 50
Michael S Turner
Why theoreticians head to the mountains every summer

BOOKS & ARTS

318 NOBEL PRIZE
A dark edge to the glory
Hidde Ploegh

319 BOOKS IN BRIEF

ANIMAL BEHAVIOUR
Death force
The life-enhancing power of decay impresses Clive Wynne PAGE 320

321 MATHEMATICS
A life computed
James Poskett

CORRESPONDENCE

323 Geoengineering controls / Burning spent nuclear fuel / How to prime the antibiotics pipeline / The HIV threat in China / El Niño and the dolphins

OBITUARY

324 **Akira Tonomura (1942–2012)**
Archie Howie

FUTURES

484 **21st-century girl**
Adrian Tchaikovsky

Free up your time

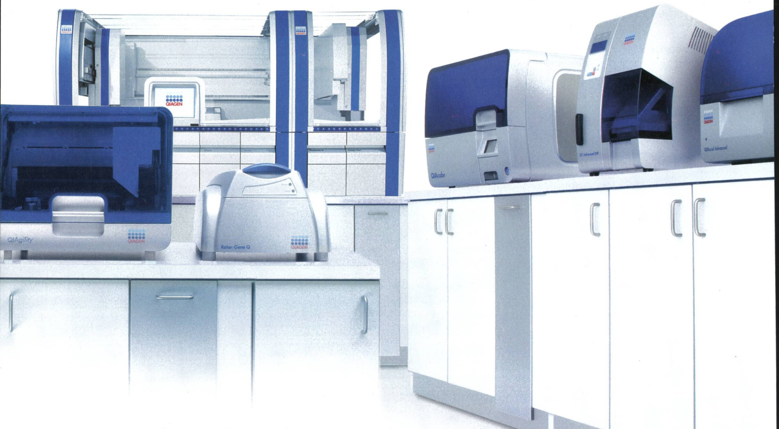

Automated sample and assay technologies by QIAGEN

Automated solutions from sample to result:

- The widest choice of sample processing protocols
- Low-, medium-, and high-throughput automation
- Leading solutions for molecular testing
- Plug-and-play automated sample preparation
- Quantitative, real-time PCR detection
- Automated analysis of DNA fragments and RNA
- High-resolution sequence-based DNA detection and quantification

Making improvements in life possible — www.qiagen.com

QIAGEN®

AUTOPortf0612N1WW

Sample & Assay Technologies

CONTENTS

21 June 2012 / Vol 486 / Issue No 7403

RESEARCH

NEW ONLINE

325 Papers published this week at nature.com

NEWS & VIEWS

326 DRUG DISCOVERY **Computer model predicts side effects**
Assessing the risks of drug candidates
Kyle Kolaja **SEE ARTICLE P.361**

327 MATERIALS CHEMISTRY **Carbon origami**
A reaction for making buckybowls from polynuclear aromatics
Jay S Siegel

328 GENOMICS **The breast cancer landscape**
Whole-genome analysis reveals tumour diversity and drug targets
Joe Gray & Brian Druker
SEE ARTICLES P.346 & P.353, LETTERS P.395, P.400 & P.405

330 NUCLEAR PHYSICS **Symmetrical tin**
Nature of the heaviest symmetrical doubly magic nucleus
Daniel Bazin **SEE ARTICLE P.341**

331 PLANETARY SCIENCE **Early start for rocky planets**
Chemical composition of stars hosting small exoplanet candidates
Debra Fischer **SEE LETTER P.375**

332 VIROLOGY **Bird flu in mammals**
Influenza with a mutated H5 haemagglutinin can transmit between mammals
Hui-Ling Yen & Joseph Sriyal Malik Peiris
SEE LETTER P.420

PERSPECTIVE

335 VIROLOGY **Engineering H5N1 avian influenza viruses to study human adaptation**
D M Morens, K Subbarao & J K Taubenberger

ARTICLES

341 PHYSICS **Superallowed Gamow–Teller decay of the doubly magic nucleus ^{100}Sn**
C B Hinke et al. **SEE N&V P. 330**

346 CANCER GENOMICS **The genomic and transcriptomic architecture of 2,000 breast tumours reveals novel subgroups**
C Curtis et al. **SEE N&V P. 328**

353 CANCER GENOMICS **Whole-genome analysis informs breast cancer response to aromatase inhibition**
M J Ellis et al. **SEE N&V P. 328**

361 CHEMICAL BIOLOGY **Large-scale prediction and testing of drug activity on side-effect targets**
E Lounkine et al. **SEE N&V P. 326**

368 STRUCTURAL BIOLOGY **Structure of yeast Argonaute with guide RNA**
K Nakanishi, D E Weinberg, D P Bartel & D J Patel

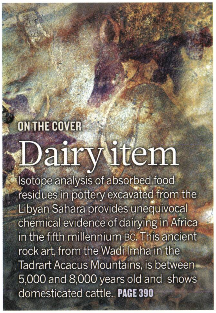

ON THE COVER

Dairy item

Isotope analysis of absorbed food residues in pottery excavated from the Libyan Sahara provides unequivocal chemical evidence of dairying in Africa in the fifth millennium BC. This ancient rock art, from the Wadi Imha in the Tadrart Acacus Mountains, is between 5,000 and 8,000 years old and shows domesticated cattle. **PAGE 390**

ROBERTO CECCACCI, SAPIENZA UNIV.

LETTERS

375 ASTRONOMY **An abundance of small exoplanets around stars with a wide range of metallicities**
L A Buchhave et al. **SEE N&V P. 331**

378 PLANETARY SCIENCE **Constraints on the volatile distribution within Shackleton crater at the lunar south pole**
M T Zuber et al.

382 PHYSICS **Electronic nematicity above the structural and superconducting transition in $BaFe_2(As_{1-x}P_x)_2$**
S Kasahara et al.

386 TECHNOLOGY **Multiscale gigapixel photography**
D J Brady et al.

390 EVOLUTION **First dairying in green Saharan Africa in the fifth millennium BC**
J Dunne et al.

395 CANCER GENOMICS **The clonal and mutational evolution spectrum of primary triple-negative breast cancers**
S P Shah et al. **SEE N&V P. 328**

400 CANCER GENOMICS **The landscape of cancer genes and mutational processes in breast cancer**
P J Stephens et al. **SEE N&V P. 328**

405 CANCER GENOMICS **Sequence analysis of mutations and translocations across breast cancer subtypes**
S Banerji et al. **SEE N&V P. 328**

410 NEUROSCIENCE **Astrocyte glypicans 4 and 6 promote formation of excitatory synapses via GluA1 AMPA receptors**
N J Allen et al.

415 DEVELOPMENTAL BIOLOGY **PGC7 binds histone H3K9me2 to protect against conversion of 5mC to 5hmC in early embryos**
T Nakamura et al.

420 VIROLOGY **Experimental adaptation of an influenza H5 HA confers respiratory droplet transmission to a reassortant H5 HA/H1N1 virus in ferrets**
M Imai et al. **SEE N&V P. 332**

PLANETARY SCIENCE

Lunar leak

The Moon's Shackleton crater may not contain water ice after all. **PAGE 378**

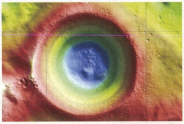

nature REVIEWS CANCER nature REVIEWS IMMUNOLOGY April 2012

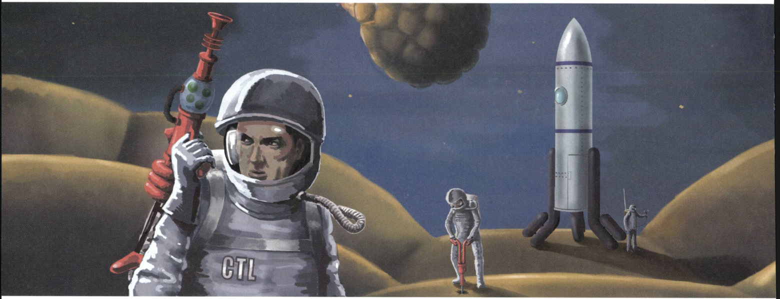

Focus on Tumour immunology & immunotherapy

Understanding how the immune system is able to protect us from cancer is an important goal for immunologists and cancer biologists alike. The progress that researchers have made in this field can be seen from the rapid expansion of new therapies that are based on boosting the immune response to tumours. This joint Focus issue from *Nature Reviews Cancer* and *Nature Reviews Immunology* features specially commissioned articles that discuss the promise of immunotherapy to treat cancer. The Focus also covers the recent insights that have been made into how key immune cells function in the tumour microenvironment — a better appreciation of this will hopefully improve the application and development of future tumour immunotherapies.

The Focus features ten articles by leading researchers, including:
The blockade of immune checkpoints in cancer immunotherapy
Drew Pardoll

Combining immunotherapy and targeted therapies in cancer treatment
Matthew Vanneman & Glenn Dranoff

Targeting natural killer cells and natural killer T cells in cancer
Eric Vivier, Sophie Ugolini, Didier Blaise, Christian Chabannon & Laurent Brossay

Access the Focus online for FREE until the end of September 2012.
www.nature.com/reviews/focus/tumourimmunology

Produced with support from Boehringer Ingelheim

nature publishing group npg

OUTLOOK

Supplement to 21 June 2012 / Vol 486 / Issue No. 7403

TASTE

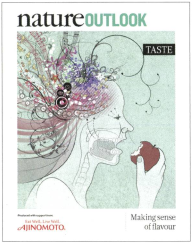
nature OUTLOOK

TASTE

Produced with support from:
Eat Well, Live Well.
AJINOMOTO.

Making sense
of flavour

Turn to page 324

S1 **EDITORIAL**
Taste
Herb Brody

S2 **GUSTATORY SYSTEM**
The finer points of taste
Discovery of the receptors that mediate taste is helping define the mechanisms of sensory perception

S4 **SENSORY SCIENCE**
Partners in flavour
The experience of flavour draws on more senses than taste

S6 **PERSPECTIVE**
Complexities of flavour
Barry Smith sorts the intrinsic qualities of food from the subjective experience

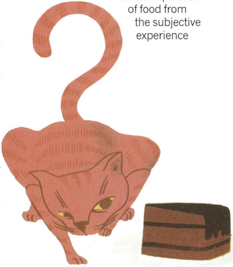

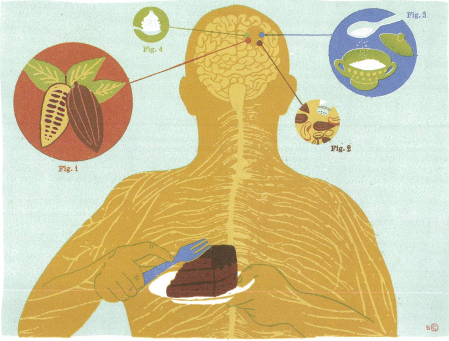

How can a flavour trigger evocative memories or instant repulsion (see page S7)?

S7 **NEUROSCIENCE**
Hardwired for taste
Just what could taste receptors be doing throughout the human body?

S10 **COOKING**
Delicious science
Chef scientists are serving up some stimulating dishes

S12 **OBESITY**
Insensitive issue
Does receptiveness to fatty foods influence a person's appetite and eating habits?

S14 **FOOD SCIENCE**
Taste bud hackers
Ingenious tricks that aim to make people prefer healthier foods

S16 **EVOLUTIONARY BIOLOGY**
The lost appetites
What tastes sweet to one species of vertebrate is bland to another

S18 **TECHNOLOGY**
The taste of things to come
Electronic tongues and other new taste-based devices could prove useful to the food industry

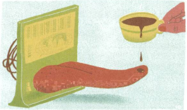

MORE ONLINE

NATURE.COM

- Researchers decode the flavour experience of a variety of world cuisines to see if there's any pattern to taste: go.nature.com/bw66nx

COLLECTION

- Visit our online edition to request a free print copy, which includes some of the latest research papers on taste: go.nature.com/igicko

nature

21 June 2012 / Vol 486 / Issue No. 7403

EDITORIAL

LONDON, MUNICH, WASHINGTON DC, NEW YORK, BOSTON, PARIS, SAN FRANCISCO, TOKYO nature@nature.com

EDITOR-IN-CHIEF: Philip Campbell
EXECUTIVE EDITOR: Nick Campbell
PUBLISHING EXECUTIVE EDITOR: Maxine Clarke **EXECUTIVE EDITOR:** Véronique Kiermer
CHIEF MAGAZINE EDITOR: Tim Appenzeller
THIS WEEK/NEWS/FEATURES: Alison Abbott, David Adam, Ananyo Bhattacharya, Geoff Brumfiel, Declan Butler, Ewen Callaway, Erika Check Hayden, Daniel Cressey, David Cyranoski, Natasha Gilbert, Eric Hand, Heidi Ledford, Corie Lok, Brendan Maher, Emma Marris, Richard Monastersky, Brian Owens, Helen Pearson, Mark Peplow, Eugenie Samuel Reich, Ivan Semeniuk, Quirin Schiermeier, Jeff Tollefson, Richard Van Noorden, Meredith Wadman, M Mitchell Waldrop **COMMENT:** Sara Abdulla, Joanne Baker, Rosalind Cotter, Barbara Kiser, Alison McCook, Lucy Odling-Smee, Sarah Tomlin **NATURE PODCAST/VIDEO:** Adam Rutherford, Thea Cunningham, Geoff Marsh, Kerri Smith, Charlotte Stoddart **NEWS AND VIEWS:** Sadaf Shadan, Ana Lopes, Andrew Mitchinson, Cesar Sanchez, Marian Turner **RESEARCH:** Ritu Dhand, Karl Ziemelis, Francesca Cesari, I-han Chou, Tanguy Chouard, Rosamund Daw, Alex Eccleston, Angela Eggleston, Joshua Finkelstein, Henry Gee, Patrick Goymer, Noah Gray, Marie-Thérèse Heemels, Magdalena Helmer, Karen Howell, Claudia Lupp, Barbara Marte, Andrew Mitchinson, Juliane Mössinger, Deepa Nath, Wayne Peng, Leslie Sage, Magdalena Skipper, Clare Thomas, Maria Trajkovska, John VanDecar, Liesbeth Venema, Ursula Weiss, Michael White **INSIGHTS/REVIEWS/PERSPECTIVES:** Ursula Weiss **CAREERS:** Gene Russo, Karen Kaplan **TECHNOLOGY FEATURES:** Monya Baker **FUTURES:** Henry Gee **SUPPLEMENTS:** Herb Brody, Michelle Grayson, Tony Scully **SUBEDITORS:** Colin Sullivan, Sarah Archibald, Nicola Bailey, Anne Blewett, Nicolas Fanget, Isobel Flanagan, Paul Fletcher, Afsaneh Gray, Sasha Lewis, Dinah Loon, Louisa Lyon, Anna Novitzky, Yukie Ozawa, Katherine Perry, David Price, Jenny Rooke, David Winters, Anna York **PRODUCTION:** Jenny Henderson, Leonora Dawson-Bowling, Dan Foley, Stewart Fraser, Susan Gray, Simon Gribbin, Hazel Mayhew, James McQuat, Emilia Orviss, Yvonne Strong, Robert Sullivan, Roberta Tarran, Charles Wenz **ART AND DESIGN:** Kelly Buckheit Krause, Wesley Fernandes, Madeline Hutchinson, Barbara Izdebska, Paul Jackman, Jasiek Krzysztofiak, Annthea Lewis, Chris Ryan, Nik Spencer, Claire Welsh, Mark Wood **JAPAN EDITION:** Eiji Matsuda, Mika Ishida, Mitsuyo Utsugi, Sayaka Ayame **PRESS OFFICE:** Ruth Francis, Neda Afsarmanesh, Lisa Boucher, Rachel Twinn, Rebecca Walton **ADMINISTRATION:** Paul Sng, Liz Bankes, Roseann Campbell, Peter Cary, Ffion Cleverley, Dana Coles, Faye Fornasier, Ashlee Gagui, Amy Invernizzi, Diane Kempinski, Caroline McLean, Rina Nozawa, Anastasia Panoutsou, Kenneth Simpson

PUBLISHING

LONDON feedback@nature.com

MANAGING DIRECTOR & PUBLISHER: Steven Inchcoombe
ASSOCIATE PUBLISHER: Arash Hejazi
PUBLISHING PROJECT MANAGER: Christian Manco

TOKYO feedback@natureasia.com

REGIONAL MANAGING DIRECTOR — ASIA-PACIFIC: David Swinbanks
DIRECTOR — ASIA-PACIFIC: Antoine E Bocquet
OPERATIONS DIRECTOR — ASIA-PACIFIC: Hiroshi Minemura

DISPLAY ADVERTISING, SPONSORSHIP & NATUREJOBS

GLOBAL HEAD: Andrew Douglas a.douglas@nature.com

DISPLAY ADVERTISING AND SPONSORSHIP

GLOBAL HEAD: Gerard Preston g.preston@nature.com
ASSISTANT SPONSORSHIP MANAGER: Reya Silao Tel: +44 (0)20 7843 4977 (r.silao@nature.com)

EUROPE/REST OF WORLD display@nature.com Tel: +44 (0)20 7843 4960

GERMANY/SWITZERLAND/AUSTRIA: Sabine Hugi-Fürst Tel: +41 52761 3386
UK/IRELAND/SCANDINAVIA/SPAIN/PORTUGAL: Evelina Rubio Hakansson Tel: +44 (0)20 7843 4079
FRANCE/BELGIUM/THE NETHERLANDS/LUXEMBOURG/ITALY/OTHER EUROPE: Nicola Wright Tel: +44 (0)20 7843 4959

NORTH AMERICA display@natureny.com

NEW ENGLAND/ EASTERN CANADA: Sheila Reardon Tel: +1 617 494 4900
NEW YORK/MID-ATLANTIC/SOUTHEAST: Jim Breault Tel: +1 212 726 9334
MIDWEST: Mike Rossi Tel: +1 212 726 9255
WEST COAST/ WESTERN CANADA: George Lui Tel: +1 415 781 3804
WEST COAST NORTH: Kayla McCutchan Tel: +1 415 403 9038

ASIA-PACIFIC display@natureasia.com

ASIA-PACIFIC HEAD: Kate Yoneyama
JAPAN: Ken Mikami Tel: +81 3 3267 8765
GREATER CHINA/SINGAPORE: Gloria To Tel: +852 2811 7191
INDIA: Vikas Chawla Tel: +91 124 288 1057

SPONSORSHIP

BUSINESS DEVELOPMENT MANAGER: David Bagshaw Tel: +1 212 726 9215
BUSINESS DEVELOPMENT MANAGER: Patrick Murphy Tel: +1 617 475 9216

NATUREJOBS

naturejobs@nature.com

EUROPEAN HEAD OFFICE, LONDON: Tel: +44 (0)20 7843 4961
EUROPEAN SALES MANAGER: Nils Moeller (n.moeller@nature.com) **BUSINESS DEVELOPMENT MANAGER, MIDDLE EAST:** Jon Giuliani (j.giuliani@nature.com) **ADVERTISING PRODUCTION MANAGER:** Stephen Russell **NATUREJOBS ONLINE PRODUCTION:** Dennis Chu
US HEAD OFFICE, NEW YORK: naturejobs@natureny.com **US SALES MANAGER:** Ken Finnegan
JAPAN HEAD OFFICE, TOKYO: Tel: +81 3 3267 8765 **ASIA-PACIFIC HEAD:** Kate Yoneyama
ASIA-PACIFIC SALES & BUSINESS DEVELOPMENT MANAGER: Yuki Fujiwara **BUSINESS DEVELOPMENT MANAGER, GREATER CHINA, SINGAPORE:** Gloria To Tel: +852 2811 7191
INDIA: Vikas Chawla Tel: +91 1242881057 (v.chawla@nature.com)

MARKETING & SUBSCRIPTIONS

USA/CANADA/LATIN AMERICA subscriptions@us.nature.com

Tel: (USA/Canada)+1 866 363 7860; (outside USA/Canada) +1 212 726 9223
MARKETING: Sara Girard **FULFILMENT:** Karen Dawson

JAPAN/CHINA/KOREA subscriptions@natureasia.com

Tel: +81 3 3267 8751 **MARKETING:** Sachiyo Ikeda **FULFILMENT:** Masayo Tanaka

EUROPE/REST OF WORLD subscriptions@nature.com

Tel: +44 (0)1256 329242
MARKETING: Elena Woodstock, Marcus Parker, Hannah Phipps **FULFILMENT:** Jean Burrows

INDIA npgindia@nature.com

Tel: +91 124 2881053/54
HEAD OF BUSINESS DEVELOPMENT, INDIA: Debashish Brahmachari **MARKETING:** Harpal Singh Gill

ANNUAL SUBSCRIPTIONS (UK/Europe, including post and packing)

FULL RATE: £1,400
PERSONAL RATES: UK £135; Europe €209; Rest of World £210
STUDENT RATES: UK £79; Europe €122; Rest of World £125
Individual rates apply to payments by personal cheque or credit card. Back issues: £20.00.

ANNUAL SUBSCRIPTIONS (USA, including post and packing)

INSTITUTIONAL/CORPORATE RATE: $2,730 ; **PERSONAL RATE:** $199; **STUDENT RATE:** $99; **POSTDOC RATE:** $119
Printed in USA. Individual rates available only to subscribers paying by personal check or credit card. Orders for student/postdoc subscriptions must be accompanied by a copy of student ID. Rates apply to USA, Canada, Mexico/Central & South America. Add 7% GST tax in Canada (Canadian GST number 140911595). **BACK ISSUES:** US$20.00.

ANNUAL SUBSCRIPTIONS (Asia, including post and packing)

JAPAN: **年間購読料金：** *Nature のみ* 437,800 円 +21,890 円(消費税)=459,690 円(合計)
Nature + Nature Digest 466,550 円 +23,328 円(消費税)=489,878 (合計)
お問い合わせ：日本出版貿易株式会社 国内営業 1 部
〒101-0064 東京都千代田区猿楽町1-2-1 Tel: 03-3292-3767 Fax: 03-3292-8766
個人/学生購読について
NPG ネイチャー アジア・パシフィック フルフィルメント & カスタマーサービス
〒162-0843 東京都新宿区市谷田町2-37 千代田ビル Tel: 03-3267-8759 Fax: 03-3267-8752
CHINA: www.natureasia.com/ch/subscribe; **KOREA:** www.natureasia.com/korea/subscribe

NATURE ONLINE

WWW.NATURE.COM/NATURE

CHIEF TECHNOLOGY OFFICER: Howard Ratner **ASSOCIATE DIRECTOR, NATURE.COM:** Daniel Pollock
PLATFORM DEVELOPMENT: Jeremy Macdonald **WEB PRODUCTION:** Alexander Thurrell, Deborah Anthony **WEB DESIGN:** Juan-Carlos Sobrino, Luke Stavenhagen **PLATFORM INTERFACES:** Amanda Ward

SITE LICENCES, FULFILMENT & CUSTOMER SERVICES

SITE LICENCES: npg.nature.com/libraries feedback@nature.com
CHIEF OPERATIONS OFFICER: John Carroll **ASSOCIATE DIRECTOR OF OPERATIONS:** Dominic Pettit
CUSTOMER SERVICE: Liz Davidson **ORDER PROCESSING OPERATIONS:** Steve Poulter

NATURE PUBLISHING GROUP OFFICES

LONDON: The Macmillan Building, 4 Crinan Street, London N1 9XW Tel: +44 (0)20 7833 4000 Fax: +44 (0)20 7843 4596/7
BASINGSTOKE: Nature Publishing Group, Subscriptions, Brunel Road, Basingstoke, Hants RG21 6XS, UK Tel: +44 (0)1256 329242
WASHINGTON DC: 968 National Press Building, 529 14th St NW, Washington DC 20045-1938 Tel: +1 202 737 2355
NEW YORK: 75 Varick St, 9th Floor, New York, NY 10013-1917 Tel: +1 212 726 9200
BOSTON: 25 First Street, Suite 104, Cambridge, MA 02141 Tel: +1 617 475 9275
SAN FRANCISCO: 225 Bush Street, Suite 1453, San Francisco, CA 94104 Tel: +1 415 403 9027
MUNICH: Nymphenburger Strasse 14, D-80335 München Tel: +49 89 549057-13
PARIS: Moulin de Malicorne, Sainte Maure de Touraine, Paris 37800 Tel: +33 2 47 35 72 15
TOKYO: Chiyoda Building, 2-37 Ichigayatamachi, Shinjuku-ku, Tokyo 162-0843 Tel: +81 3 3267 8751
INDIA: Nature Publishing Group, 3A, 4th Floor, DLF Corporate Park, Gurgaon 122002 Tel: +91 124 2881053/54

Nature® (ISSN 0028-0836) is published by Nature Publishing Group, a division of Macmillan Publishers Ltd (The Macmillan Building, 4 Crinan Street, London N19XW). Registered as a newspaper at the British Post Office. North and South American orders to subscriptions@natureny.com (Tel: +1 866 363 7860). Other orders to subscriptions@nature.com (Tel. +44 (0)1256 329242; Fax +44 (0)1256 812358). Authorization to photocopy material for internal or personal use, or internal or personal use of specific clients, is granted by *Nature* to libraries and others registered with the Copyright Clearance Center (CCC) Transactional Reporting Service, provided the relevant copyright fee is paid direct to CCC, 222 Rosewood Drive, Danvers MA 01923, USA. Identification code for *Nature*: 0028-0836/03. CPC PUB AGREEMENT #40032744. In the US, *Nature* (ISSN 0028-0836) is published weekly on Thursday, except the last week in December by Nature Publishing Group, 75 Varick St, 9th Fl, New York NY 10013-1917, USA. US Periodicals postage paid at New York NY, and additional mailing post offices. US POSTMASTER: send address changes to *Nature*, Subscription Dept, 75 Varick St, 9th Fl, New York NY 10013-1917, USA. Published in Japan by NPG Nature Asia-Pacific, Chiyoda Building, 2-37 Ichigayatamachi, Shinjuku-ku, Tokyo 162-0843, Japan. © 2012 Macmillan Publishers Limited. All rights reserved.

THIS WEEK

EDITORIALS

SAFETY FIRST Take our pioneering survey on laboratory practice **p.294**

WORLD VIEW The way to fight bioterror is to publish **p.295**

UNDEAD Keep vampire bats alive to help fight rabies spread **p.296**

Time to open up

If scientists want the public to continue to volunteer for research projects, they must learn to be a lot more forthcoming about the ways in which the information they garner will be used.

Few biomedical researchers who work with human volunteers are entirely happy with the rules that govern and preserve research ethics. Scientists working on an experiment or a clinical trial can find that the complex web of regulations that they must follow is a confusing burden. These rules, they feel, simply add time, cost and complication to their studies.

Institutions are wary of falling foul of regulations that even highly trained staff are hard-pressed to interpret. And research participants — the volunteers without whom research such as clinical trials would not be possible — often don't understand all the implications contained in the voluminous documents that they must sign before they take part in the research. Although these forms are ostensibly designed to protect participants, they are more often directed at protecting institutions from liability.

The notion of informed consent has become especially problematic in this modern age of 'big data'. The need to seek and obtain permission from volunteers can be traced back to research-ethics principles introduced in response to revelations about the way Nazi doctors tortured people during the Second World War. Decades ago, researchers could not glean much information from a piece of stored tissue. But now, it is no longer possible to explain to a research subject all the possible ways in which their offered data might be used in the future, and it is becoming less feasible to guarantee their privacy under (correct) rules that mandate the deposition of research data in public databanks. Some large data-collection projects have therefore adopted very broad informed-consent provisions, in which research participants simply agree that their data may be used for a wide and unspecified variety of purposes. But as potential volunteers become savvier to the value and vulnerability of their personal data, they may become less receptive to this approach. Indeed, as our feature on page 312 shows, this may already be happening.

Technology and some creative thinking should be able to provide a solution to this problem. In an era when people can control who sees what types of personal information on their Facebook page, programmers should be able to design similar tools to give research volunteers a degree of influence over who uses their data and for which types of research. Experiments along these lines are now being tried by the company Private Access, based in Irvine, California.

Scholars of ethics and law are also trying to think of new models for informed consent that could accommodate the needs of both researchers and research participants. For instance, a group based at Duke University in Durham, North Carolina, and the University of North Carolina at Chapel Hill has proposed remodelling consent provisions based on laws that protect trade secrets. In its favour, this model would provide the option of giving donors something in return for handing over their samples to a large data collection, such as a biobank. It would ask the donors what they want in return for the information embedded in the samples, such as financial compensation (which many already receive) or a say in the types of research their information is used for.

Other researchers have proposed reforms that head in the opposite direction — for instance, by relaxing the rules on consent for research involving 'de-identified' specimens, which are stripped of information that could link them back to their source.

This approach may seem attractive because it would seem to lessen cost and burden on the researchers, and could make the most of currently under-exploited medical records and data samples. Extreme caution is needed, however. It would take only one high-profile case of an unwanted data disclosure to undermine support for research — and not just for the field in question. Researchers need only look to the backlash against newborn screening in the United States and tissue research in the United Kingdom to realize how failing to obtain consent can set back their cause.

> ***"Scholars of ethics and law are trying to think of new models for informed consent."***

As this journal has argued previously, a more appropriate solution to the conundrum of informed consent is to introduce greater openness to the process.

Scientists could agree to give results containing medically relevant findings back to participants in genetic studies, such as information about their health. Although some have argued that this approach, as well as patient-controlled approaches, will add time, cost and complication to studies, no one really knows if this is the case. Such concerns must not be allowed to derail the idea.

Most large studies are funded by taxpayers or patient-advocacy groups. Researchers are therefore obliged to listen when patients and members of the public argue that they want to have more information — not less — to ensure that they agree to offer their continued participation in research. It might not make everybody happy, but it should keep everybody involved. ■

Renewed vigour

Stem-cell researchers must engage with politicians to keep their work alive in Europe.

Research involving human embryonic stem (ES) cells is once more under scrutiny in Europe. In a situation that will stir memories of the acrimonious debates of 2006, legislators must again assess whether this kind of work should still be funded under the forthcoming €80-billion (US$100-billion) Horizon 2020 research programme.

Now, as then, opinion is split. Some countries and some members of the European Parliament are in favour of the research, recognizing the long-term potential to treat debilitating disease. Others maintain that it is immoral to exploit a technique that uses human embryos — even spare embryos from *in vitro* fertilization clinics that would otherwise be destroyed, and from which nearly all experimental human ES cell lines are derived. The 2006 debate was resolved with both the European Parliament and Council agreeing to fund such research, provided that it didn't involve the creation of new human ES cells, and provided that it was not carried out in those countries — such as Germany — whose national law banned it.

Stem-cell researchers around the world breathed a sigh of relief, knowing how a decision in Europe could also influence funding decisions elsewhere. The outcome of the present debate offers similar influence. But there are already signs that some members of the European Parliament will once again try to outlaw funding of research involving human ES cells.

Rather than wait for these views to gain unchecked momentum, a group including UK research-funding bodies the Wellcome Trust, the Medical Research Council, the British Heart Foundation and Parkinson's UK last week issued a joint statement in support of the research, explaining the benefits of the work and the rationale to include it in Horizon 2020.

It is a wise move that should help to anchor the coming debate to reality. Biology is complicated, which makes it easy for politicians to mislead the public and colleagues — intentionally or unintentionally — in emotive areas. The general public, and politicians, have every right to question whether the ends justify the means used by medical researchers. But they also have the right to reliable information.

The statement outlines the remarkable progress that stem-cell researchers have made since 2006, which has led in the past 12 months to the first approvals for clinical trials of potential therapies involving human ES cells — for a type of blindness called macular degeneration and for spinal-cord injury. In addition, scientists have discovered how to force adult cells back to an embryonic-like state. The resulting induced pluripotent stem (iPS) cells can then be grown into particular cell types and used to understand mechanisms of disease at the cellular level. In the long term, they may also be useful for therapy.

The most insidious claim of those who oppose human ES cell research holds that iPS cells, which can be derived from a particular patient's own cells and are ethically unburdened, eliminate the need for human ES cells in research and therapy. That concept sounds appealing, but it is simply not true. Scientists understand little of the differences between the two sorts of stem cells and it will take years of comparative work to do so.

"The general public, and politicians, have every right to question whether the ends justify the means used by medical researchers."

One particular event that makes biomedical researchers worry is a decision taken last year by the European Court of Justice. In October it ruled that patenting of inventions involving human ES cells was illegal because it was immoral — and as a consequence, human ES cell research must also be immoral (see *Nature* **480,** 310–312; 2011). *Nature* condemned this ruling as being beyond the court's juridical and technical competencies (see *Nature* **480,** 291–292; 2011). But members of the European Parliament who oppose human ES cell research stealthily inserted a reference to it during an unrelated resolution on broad patenting of essential biological processes in animal and plant breeding, which was adopted on 10 May.

Horizon 2020 has to be approved by the European Parliament and Council by mid-2013 so that first calls for proposals can be launched at the start of 2014. The UK research funding agencies' statement is a good start to a continuous campaign of education and transparency that stem-cell researchers from all interested European countries must maintain for the next year. Just as cell-culture medium needs to be renewed to keep its cargo alive, a political message has to be constantly renewed if it is to stay alive in political minds. ■

Serious questions

Nature Publishing Group's reader survey on lab-safety practices needs your input.

Scientific laboratories are dangerous places. Noxious chemicals, naked flames and nasty microbes abound. The white laboratory coat, a long-standing symbol of science to many outsiders,offers some protection against these implicit threats. White coats are ubiquitous in fictional labs in films and on television, but how many lab scientists actually wear one? And, perhaps more importantly, how many should do, but don't? Are you wearing one right now? Are your colleagues? Does it matter? Would you tell anybody if it did? And, if not a lab coat, what about those protective goggles? They get so hot in summer, don't they? Is it really that big a deal if you leave them on the hook just this once?

It is easy for scientists, especially those who have been around for a while and so tend to be in charge, to take a cavalier attitude to safety, purely because science is so much safer now than it was when they began. And although it is true that laboratories and lab culture have improved since the reckless days of the 1950s and 1960s, accidents still happen. Sometimes, these accidents are fatal. Laboratories do still kill people.

In an Editorial on the subject last April (*Nature* **472,** 259; 2011), prompted by the death of physics and astronomy undergraduate student Michele Dufault in a workshop at Yale University in New Haven, Connecticut, this publication warned against complacency when it comes to lab safety. A common complaint among environmental health and safety officers in universities and elsewhere, we noted, is that "there is no good source of consistent data on laboratory accidents, which could be studied to determine effective safety interventions". That the working environment for scientists is safer now than in times past is less important than whether it is as safe now as it could, or should, be — and there is at present no way to say for sure that it is.

"It is easy for scientists to take a cavalier attitude to safety."

Nature Publishing Group (NPG) has now joined with the University of California, Los Angeles, and the software firm BioRAFT to try to fill in some of the blanks. (BioRAFT, based in Cambridge, Massachusetts, has investment from Digital Science, owned by NPG's parent company, Macmillan.) Together, the three have launched an online survey of international laboratory safety and working culture. Some readers will already have received invitations to participate, but everyone else is welcome, too: the survey can be found at go.nature.com/7ldjli. It should take about 15 minutes to complete and is anonymous — although there is an option to leave an e-mail address for follow-up questions. The organizers hope that tens of thousands of working scientists will respond to questions about the environments they work in and the attitudes that they and their colleagues have to health and safety regulations. The survey also addresses research practice, including how many people regularly work alone in a lab, and how often; training provision; and whether scientists feel able to raise concerns about safety. Please take the survey. Someone, some day, will benefit. ■

➲ NATURE.COM
To comment online, click on Editorials at:
go.nature.com/xhunqv

nature
nature

A key thread in your scientific career

Since 1869 we've made it our mission to share the greatest developments in science and advance the discussion among the global scientific community. Whether in print, online or mobile, *Nature* is always at the forefront of science and is your forum to read, watch, listen and engage with key research, news and opinion.

How will you access the next landmark discovery?

➲ NATURE.COM/NATURE

nature publishing group npg

CUSTOM MONOCLONAL ANTIBODIES
Rat mAb ∘ Mouse mAb ∘ Ascites

CUSTOM PROTEIN EXPRESSION
HEK293 ∘ Baculovirus ∘ *E. coli*

Superior Quality • Unriveled Expertise
www.promab.com
1.866.339.0871 | info@promab.com

ProMab
Biotechnologies, Inc.

naturejobs

Scientists stay informed of the latest:

- Hot jobs
- Career news
- Announcements

Sign-up to our **FREE** jobseeker newsletter:
www.naturejobs.com/newsletter

nature MIDDLE EAST
Emerging science in the Arab world

twitter facebook google+

RESEARCH, NEWS, JOBS, BLOGS, EVENTS

Ensure you're part of the scientific and medical community gaining access to **the latest research in the region**.

Nature Middle East is your free comprehensive portal keeping you at the centre of science in the Arabic speaking Middle East.

nature.com/nmiddleeast

Download the free app for your phone at http://gettag.mobi

Sponsored by

nature publishing group npg

sense about science

nature

The John Maddox Prize for standing up for science

The John Maddox Prize will reward an individual who has promoted sound science and evidence on a matter of public interest. Its emphasis is on those who have faced difficulty or hostility in doing so. Nominations of people at an early stage in their careers are particularly welcomed.

The prize is open to nominations for any kind of public activity, including all forms of writing, speaking and public engagement, in any of the following areas:

- Addressing misleading information about scientific or medical issues in any forum.
- Bringing sound evidence to bear in a public or policy debate.
- Helping people to make sense of a complex scientific issue.

Sir John Maddox, whose name this prize commemorates, was a passionate and tireless champion and defender of science, engaging with difficult debates and inspiring others to do the same. As a writer and editor, he changed attitudes and perceptions, and strove for better understanding and appreciation of science throughout his long working life.

The prize is a joint initiative of Nature, where Sir John was editor for 22 years, and Sense About Science, where he served as a trustee until his death in 2009. It is supported by a contribution from the Kohn Foundation.

The prize: £2000. An announcement of the winner will be published in *Nature*.

Candidates for the John Maddox Prize must be nominated. The nominator should normally be an individual who is familiar with the work of the candidate but self-nomination will be considered in exceptional circumstances. This is a global prize: people from and in any country can be nominated. Award criteria and an online nomination form can be found at: www.senseaboutscience.org. The deadline for nominations is midnight on 20th August 2012 BST. Announcement of the winner will be in November 2012.

Do not censor science in the name of biosecurity

Security officials should not be concerned about the publication of mutant-flu research, says bio-weapons expert **Tim Trevan**.

The recent controversy over research into mutated versions of the H5N1 flu virus has focused on biosecurity concerns. It is easy to get the impression that this debate has created a clear split between a scientific community that wants the research to proceed and the results to be published and a biosecurity community that doesn't.

As a member of this biosecurity community for more than 30 years — I was special adviser to the chairman of the United Nations weapons inspectors in Iraq and covered chemical and biological disarmament with the UK Foreign Office in both London and Geneva, Switzerland — I believe this to be a false dichotomy. The research should be published in full, as it will be this week.

In fact, I will go further and say that the whole concept of dual-use biological research that is 'of concern' is flawed. It is a dangerous distraction, an inappropriate hangover from nuclear-threat analysis. Almost all biological knowledge can be either misused or applied for good.

Those concerned about publishing full details of the mutant-flu work say that they fear the research will be misused to develop more-effective biological weapons. But who would want to use a live, highly transmissible, virulent organism as a weapon, and to what purpose? And would censorship stop them?

Although such a weapon would strike terror and harm economies, its impacts would be uncontrollable, indiscriminate and unpredictable. And compared with conventional weapons, it would be slow to take effect and relatively easy to combat, through prompt vaccination and treatment.

That severely restricts the number of potential users. An uncontrollable weapon is unsuited to targeted attacks and its use would heap opprobrium on the user. And if insurgents or terrorists unleashed a catastrophic and indiscriminate attack on civilians, it would devastate sympathy for their cause.

The only groups who might logically consider using such a weapon are those for whom humans are the problem, such as environmental extremists and animal-rights activists, or apocalyptic sects, such as the Japanese terrorist cult Aum Shinrikyo, which released sarin gas in the Tokyo underground in 1995. Then there are those who do not care about casualties, such as a state or a regime that believes it faces imminent existential threat, or suicide fighters.

Censorship of the H5N1 papers would not have kept the genie in the bottle. Suppressing such papers or limiting access to their findings might even encourage proliferation by drawing attention to the risks and by provoking those researchers denied access to the results to seek to replicate them.

Can we prevent proliferation by controlling research? Certainly, researchers, institutional review boards and funders must consider the implications of proposed research from the outset and implement a full biosafety and biosecurity plan. Major efforts have been made in this area. But to deny funding to projects with clear scientific or public-health value, even if they have some biosecurity risks, will drive research to undesirable sources of funding and prevent valuable research from being done.

➲ NATURE.COM
For more on mutant flu, see:
go.nature.com/mhmibi

If the knowledge and the science cannot be contained, then what about access to the materials and equipment required to turn research results into weapons? The direction in which technology and scientific services are heading does not bode well for controlling proliferation in this way. Companies already make genes for mail order. Free gene-design software exists. DNA printers will probably be on lab bench tops within the decade. But it cannot be morally or politically defensible to prevent wide distribution of tools that are indispensable to public health and basic research.

Warfare and terrorism are not the only biological risks that confront humanity. There is an entire spectrum of risks, from natural and accidental to deliberate. We are mostly helpless to prevent the periodic creation of new deadly diseases. We know that we face regular flu pandemics and that some will be particularly deadly.

CONTINUED RESEARCH INTO **MUTANT FLU** WILL ULTIMATELY DETER THE USE OF BIOLOGICAL **WEAPONS.**

An analysis of the effect of carrying out and publishing such research must compare two factors. The first — the cost — is the risk that publication will lead to deliberate release, multiplied by the impact of the release, multiplied by the frequency of release. The second — the benefit — is the possible reduction in the 250,000–500, 000 annual deaths worldwide due to seasonal flu and the more than 12 million lives lost annually to other infectious diseases, among other public-health benefits.

Precise calculation is not possible, but the evidence strongly suggests that the increase in risk is quite small. The known benefits of addressing public-health challenges from nature will almost always far outweigh the potential and unknowable increased risk of misuse.

The bigger argument in favour of continued research into viral transmissibility and pathogenicity (the focus of the mutant-flu work) is that it will ultimately deter the use of biological weapons.

The best strategy to stop biological attacks is to make biological weapons unattractive by making preparedness and responses so effective that the consequences are no worse than those of a train wreck. Increased understanding of transmissibility and pathogenicity will enable countries to identify threats earlier, develop better vaccines, produce them more quickly and develop broad-spectrum defences to diseases. This will protect against both nature and warfare. ■

Tim Trevan *is executive director of the International Council for the Life Sciences in McLean, Virginia.*
e-mail: trevan@iclscharter.org

RESEARCH HIGHLIGHTS

Selections from the scientific literature

INFECTIOUS DISEASE

Sequencing tracks outbreak

Whole-genome sequencing has enabled researchers to confirm which patients in a hospital were affected by a particular outbreak of an antibiotic-resistant pathogen — at a cost and on a timescale that are clinically relevant.

Sharon Peacock at the University of Cambridge, UK, and her team sequenced isolates of methicillin-resistant *Staphylococcus aureus* (MRSA) from 14 hospitalized patients, half of whom had become carriers of a specific strain of MRSA during an outbreak in the neonatal intensive care unit. In about 1.5 days and at a cost of some US$150 per isolate, the authors generated sequences that showed a clear genetic distinction between outbreak and non-outbreak isolates.

The researchers predict that, as whole-genome sequencing costs and turnaround times fall, this will become a standard tool for controlling the spread of dangerous pathogens.

N. Engl. J. Med. 366, **2267–2275 (2012)**

G. ZIESLER/GETTY

ECOLOGY

Bat culls do not stop spread of rabies

Culling adult vampire bats might not be an effective means of reducing outbreaks of rabies in humans and livestock.

Daniel Streicker at the University of Georgia in Athens and his colleagues tested common vampire bats (*Desmodus rotundus*; pictured) sampled from 20 colonies across Peru between 2007 and 2010 for exposure to the rabies virus. Exposure prevalence ranged from 3% to 28% and was highest in immature bats. Culling during the test period did not reduce the probability of exposure to rabies.

Adult bats might be developing immunity to rabies after repeated exposure to the virus, the authors suggest, so culling could increase virus transmission in part because it targets immune adults and leaves behind young bats that are more likely to carry and to transmit the disease.

Proc. R. Soc. B **http://dx.doi.org/10.1098/rspb.2012.0538 (2012)**

ANIMAL BEHAVIOUR

Castration boosts spider stamina

The male orb-web nephilid spider often castrates himself during sex, reducing his body weight by up to 9%. This could increase his endurance when defending his mate from competitors.

L. QI QI

Daiqin Li at the National University of Singapore and his colleagues partly or fully castrated male spiders (*Nephilengys malabarensis*; **fully castrated pictured right**) and then assessed their stamina by repeatedly poking them with a paintbrush to goad them into moving.

Spiders that retained their genitals, or palps, quickly became exhausted, whereas the much lighter eunuchs showed 80% greater locomotor endurance. Spiders with one remaining palp kept going for 32% longer than intact males (**left**).

Biol. Lett. **http://dx.doi.org/10.1098/rsbl.2012.0285 (2012)**

IMMUNOLOGY

Good microbes fight bad

Microbes living in the guts and airways of mammals help their hosts to fend off pathogens.

John Wherry and David Artis at the University of Pennsylvania in Philadelphia and their team treated mice with antibiotics to kill off their gut microbes and then infected them with an influenza virus. The mice lost more weight and were more likely to die than those that did not receive antibiotics. The antibiotic-fed mice also mounted a reduced immune response to the virus.

The authors suggest that the bacteria living in mammals prime the immune system to respond to pathogens, and say that harnessing this ability could aid in the treatment of viral infections in humans.

Immunity **http://dx.doi.org/10.1016/j.immuni.2012.04.011 (2012)**

MATERIALS

Graphene can desalinate water

Salt could be separated from water using an ultrathin porous membrane made up of a single sheet of carbon atoms, a computational study suggests.

David Cohen-Tanugi

and Jeffrey Grossman at the Massachusetts Institute of Technology in Cambridge simulated the molecular interactions between graphene, salt and water, and looked at the effects of different pore sizes on salt filtration. The researchers found that graphene with a pore size of 0.7–0.9 nanometres should stop the passage of salt while letting water through. Attaching hydroxyl groups to the edges of the graphene pores would boost water flow-rate but impair salt rejection — because the chemical groups can swap with water molecules surrounding the salt ions. By contrast, attaching hydrogen atoms to the pores would improve filtration.

Graphene promises to be many times more permeable to water than conventional membranes used in desalination, the authors say.

Nano Lett. **http://dx.doi.org/10.1021/nl3012853 (2012)**

MICROBIOLOGY

Bacterial border defence

Insects combat pathogenic bacteria by producing a polymer called melanin and depositing it onto the microbe's surface. But one bacterial species has a weapon of its own — a cell-surface molecule that inhibits insects' melanin-producing enzymes.

Jon Clardy at Harvard Medical School in Boston, Massachusetts, and his team pinpointed the molecule, rhabduscin, on the surface of the bacterium *Xenorhabdus nematophila*. Nanomolar levels of the chemical blocked the activity of a melanin-producing enzyme from waxmoth larvae. *X. nematophila* that lack a rhabduscin-producing enzyme were less effective at killing the larvae than were normal bacteria.

Genes that encode enzymes involved in rhabduscin production are also found in the pathogen that causes cholera, *Vibrio cholerae*. A similar defence mechanism might exist in this bacterium, the authors speculate.

Proc. Natl Acad. Sci. USA **http://dx.doi.org/10.1073/pnas.1201160109 (2012)**

APPLIED PHYSICS

Terahertz-wave detector

Devices that emit and detect radiation in the terahertz part of the spectrum — between the infrared and microwave regions — have potential applications in imaging, including in medical diagnostics. Researchers have developed a compact and efficient terahertz detector that works at room temperature.

Miriam Vitiello of the National Enterprise for nanoScience and nanoTechnology in Pisa, Italy, and her team built their detector out of indium arsenide nanowires 1.5 micrometres long and 30 nanometres in diameter. Radiation from a 1.5-terahertz emitter was funnelled to the detector from a bow-tie-shaped antenna.

The researchers suggest that the detector could be tuned to respond to even higher frequencies, and could be built into multi-pixel arrays, which are ideal for detectors.

Appl. Phys. Lett. **100, 241101 (2012)**

COMMUNITY CHOICE

The most viewed papers in science

CLIMATE CHANGE

Melting ice behind Arctic warming

✪ HIGHLY READ
on www.agu.org
4 June–11 June

Sea-ice loss seems to be the main culprit behind the rapid surface warming in the Arctic, but it contributes next to nothing to the heating of the area's lower atmosphere.

The climate is warming faster in the Arctic than elsewhere. Using simulations generated by two atmospheric circulation models, James Screen at the University of Melbourne in Australia and his team disentangled and quantified local and remote contributions to this 'Arctic amplification'.

Sea-ice retreat and related changes in local sea surface temperature are the main drivers of surface-level warming, the simulations suggest. By contrast, most lower atmosphere warming seems to result from increased atmospheric heat transport from lower latitudes. Apart from in July and August, greenhouse gases and aerosols make little direct contribution to Arctic warming, the authors note.

Geophys. Res. Lett. **http://dx.doi.org/10.1029/2012GL051598 (2012)**

STEM CELLS

Human eye parts in a dish

Retinal cells made from human embryonic stem cells could one day be used to help restore sight in people with certain forms of blindness.

Yoshiki Sasai at the RIKEN Center for Developmental Biology in Kobe, Japan, and his colleagues used the stem cells to generate retinal epithelial cells, which are precursors for the retina. After a few weeks, a single layer of these cells spontaneously formed a curved structure called an optic cup. After several more weeks, the cup developed into a multilayered structure with multiple retinal cell types, including light-sensitive photoreceptors.

The researchers also devised a method for cryopreserving the retinal tissue. They foresee that stored material could ultimately be triggered to develop into specific cell types that can be grafted onto a patient's retina.

Cell Stem Cell **10, 771–785 (2012)**

For a longer story on this research, see go.nature.com/ibgaqa

ARCHAEOLOGY

One mummy but three people

A mummy found at a site off the coast of Scotland consists of remains from at least three individuals.

Human skeletons dating from 1400–1100 BC were previously unearthed at the Cladh Hallan settlement. A male skeleton was identified as a composite of multiple individuals on the basis of isotope data, but the status of a female mummy (**pictured**) was less certain. Terry Brown at the University of Manchester, UK, and his colleagues extracted DNA from bones of the jaw, right arm and right leg of the female remains. After excluding possible contamination, the researchers found that all three body parts came from different individuals. DNA analysis of the skull was inconclusive.

The team suggests that the remains at Cladh Hallan were deliberately merged, perhaps to symbolically combine different ancestries into one lineage.

J. Archaeol. Sci. **http://dx.doi.org/10.1016/j.jas.2012.04.030 (2012)**

M. PARKER PEARSON

➲ NATURE.COM
For the latest research published by *Nature* visit:
www.nature.com/latestresearch

SEVEN DAYS *The news in brief*

CHINAFOTOPRESS/GETTY

China celebrates space-station success

In a milestone for China's space programme, three astronauts boarded the country's orbiting Tiangong 1 space module on 18 June. Their flight on the *Shenzhou 9* craft was the country's fourth manned space launch, but is the first of a series of missions in efforts to build a manned space station, the Tiangong ('Heavenly Palace'), by 2020 (see *Nature* **473**, 14–15; 2011). The mission carried China's first female astronaut, Liu Yang. See go.nature.com/f5qkka for more.

POLICY

Marine reserves

Australia's government has unveiled its final plans to create what will be the world's largest network of marine reserves, covering 3.1 million square kilometres of ocean along the nation's coasts. Researchers were worried by draft proposals last year (see *Nature* **480,** 14–15; 2011), but the plans released on 14 June addressed their concerns by including small but significant extensions to the reserve boundaries, to increase protection to regions such as the Coral Sea. The government expects the reserves to become law at the end of this year, after a public consultation. See go.nature.com/vnq8fw for more.

US research thrift

Research universities in the United States need to become more efficient and more productive, a 14 June report from the US National Academies urges. The report, requested by Congress in 2009, recommends ten fixes to maintain quality, including improving cost-effectiveness by sharing expensive research equipment and facilities, and encouraging greater collaboration. Federal funding has flattened or declined, and state funding has dropped by 25% on average and up to 50% in some cases, the report notes. See go.nature.com/6ppdtj for more.

Fisheries reform

Europe's attempts to overhaul its much-criticized fisheries policy took a step forward at a meeting in Luxembourg on 12 June. Ministers on the council of the European Union agreed to a partial ban on the practice of throwing away unwanted by-catch, and pledged to return fish stocks to levels that produce the maximum sustainable yield by 2020. But critics said that these agreements were insufficient, effectively allowing Europe's fisheries to continue on their current unsustainable path. Any reforms still need to be negotiated with the European Parliament. See go.nature.com/tn8oea for more.

Ocean acidity

The International Atomic Energy Agency (IAEA), based in Vienna, is to create a centre to facilitate and communicate research into ocean acidification, it announced on 18 June. The centre, to be launched this summer at the IAEA's Environmental Laboratories in Monaco, is part of the agency's remit to support peaceful uses of nuclear technology. Tracing of the radioisotope calcium-45, for example, allows sensitive measurements of calcium carbonate uptake in the skeletons of marine organisms, affected by acidifying oceans.

German excellence

Thirty-nine universities have each won a share of €2.4 billion (US$3 billion) in the second round of Germany's Excellence Initiative — a competition among the country's institutions to win elite status and funding for specialized research clusters and graduate schools for 2012–17. The decisions, announced on 15 June, spread cash across 99 separate projects.

Biomedical careers

The US National Institutes of Health on 14 June received two key reports on how to improve prospects for young biomedical scientists. One suggests raising minimum salaries for postdocs, among other recommendations, while the other addresses the plight of under-represented minorities in biomedical science. See page 304 for more.

Open access

A report commissioned by the UK government has laid out how the country should accelerate a shift to open-access publishing. The 19 June report, chaired by sociologist Janet Finch at the University of Manchester, UK, recommended that researchers should prepare to pay up front for the cost of publishing their research, a route known as gold open access. See page 302 for more.

Unethical research

A US court has dismissed a lawsuit by Guatemalan citizens against US officials over American researchers who intentionally infected Guatemalans with sexually transmitted diseases in the 1940s (see *Nature* **482**, 148–152; 2012). A presidential bioethics commission has already issued a series of reports condemning the experiments, but on 13 June a judge ruled that the government was immune to prosecution in the case. Lawyers said they would appeal. See go.nature.com/1ffh6l for more.

PEOPLE

Mikovits theft case

Chronic-fatigue-syndrome researcher Judy Mikovits is no longer facing criminal charges for stealing lab notebooks, computers and other material from her former employer, the Whittemore Peterson Institute for Neuro-Immune Disease in Reno, Nevada. A Nevada district attorney dropped the charges last week, although Mikovits (known for her now-retracted work linking chronic fatigue syndrome to a virus) still faces a civil suit from the institute. See go.nature.com/ukgegy for more.

Nobel chemist dies

Organic chemist William Knowles (**pictured**), who shared the 2001 Nobel Prize in Chemistry, died on 13 June aged 95. Knowles worked for four decades at the agricultural giant Monsanto in St Louis. He won the Nobel with Ryoji Noyori and Barry Sharpless for his work on chemical syntheses that selectively create one of two mirror-image forms (enantiomers) of a molecule.

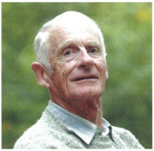

W. GREENBLATT/SYGMA/CORBIS

BUSINESS

GM soya levy

The biotechnology giant Monsanto is one step closer to losing billions of dollars in revenues from its genetically modified (GM) Roundup Ready soya beans in Brazil. Monsanto, headquartered in St Louis, Missouri, levies a charge on Brazilian farmers who grow soya beans that turn out to be GM. Farmers say it is impossible to avoid growing GM soya because of contamination, and in April they won a challenge in the state of Rio Grande do Sul, where a judge ruled that the company's levy was illegal. The ruling is currently suspended, pending consideration by a higher court. But on 12 June, the Brazilian Supreme Court of Justice said it should apply nationwide. See go.nature.com/mowmyh for more.

Fossil smuggling

A nearly complete tyrannosaurid fossil that sold for US$1 million was illegally smuggled out of Mongolia, according to a civil complaint seeking the fossil's return, which was filed on 18 June by the US Department of Justice. Despite a restraining order obtained by the Mongolian government from a Texas court to prevent the sale or transfer of the fossil, Heritage Auctions based in Dallas, Texas, auctioned off the *Tarbosaurus bataar* fossil in New York last month.

RESEARCH

Diesel cancer links

Diesel exhaust is carcinogenic to humans, the International Agency for Research on Cancer (IARC) declared on 12 June after a meeting in Lyons, France. Diesel emissions were previously classed as 'probably' carcinogenic; the latest conclusion followed the publication in March of a long-delayed US government study showing how exposure to diesel exhaust increases the risk of lung cancer in miners. The IARC's pronouncement is purely scientific; it will be up to national regulatory agencies to decide how to proceed. See go.nature.com/dddpaz for more.

COMING UP

24 JUNE–6 JULY
In St Petersburg, Russia, the United Nations Educational, Scientific and Cultural Organization's World Heritage Committee meets to discuss the state of conservation sites including Australia's Great Barrier Reef.
whc36-russia2012.ru

26–28 JUNE
In Washington, Seattle, marine scientists plan out an international network to monitor the acidification of the oceans.
go.nature.com/lopgt6

Space X-rays

NASA's NuSTAR telescope, which will examine high-energy X-rays produced at the thresholds of black holes (see *Nature* **483**, 255; 2012), was launched into low-Earth orbit on 13 June. The low-cost mission is one of only a few available to X-ray astronomers. See go.nature.com/dcye8k for more.

TREND WATCH

The United States, which two years ago yielded the title of host to the world's top supercomputer — bested first by China and then by Japan — has roared back into the lead in this month's list of the world's top 500 supercomputers, with the Sequoia machine at Lawrence Livermore National Laboratory in California. It also claimed third place with a supercomputer at Argonne National Laboratory in Illinois. Italy made its top-ten debut with a system at the CINECA computing centre near Bologna.

WORLD'S FASTEST COMPUTERS

The United States reclaims the top spot for first time in two years with a supercomputer at Lawrence Livermore National Laboratory in California.

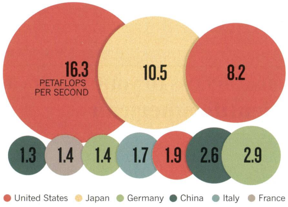

SOURCE: WWW.TOP500.ORG

CORRECTIONS

The story 'Nobel laureate dies' (*Nature* **486,** 11; 2012) should have said that Andrew Huxley did his award-winning work at the Laboratory of the Marine Biological Association in Plymouth, not the Plymouth Marine Laboratory. And 'Piezonuclear row' (*Nature* **486,** 162; 2012) gave the wrong name for INRiM: it is the National Institute for Metrological Research.

➲ NATURE.COM
For daily news updates see:
www.nature.com/news

SCIENTIFIC
AMERICAN™

Gain complete online access to the latest in science, technology and medicine **at your institution**

Recommend site license access to your library today!
www.nature.com/scientificamerican

™ Scientific American, Inc.

nature publishing group npg

NEWS IN FOCUS

POLITICS In Romania, plagiarism charges strike at the top **p.305**

ENVIRONMENT Gold rush tears at Peru's green heart **p.306**

ARCHAEOLOGY Greece's turmoil endangers its classical heritage **p.308**

ETHICS Genomics puts question marks over informed consent **p.312**

U. ANDERSEN/GETTY

Luc Montagnier has controversial scientific views that may harm Cameroon's AIDS institute, allege critics.

AIDS

Nobel fight over African HIV centre

Laureates question choice of interim scientific director.

BY DECLAN BUTLER

A fledgling AIDS research centre in Cameroon, already struggling to find a scientific leader, is now facing insurrection from an unlikely quarter: a group of 35 Nobel prizewinners.

The laureates are calling for the centre's interim scientific director, fellow prizewinner Luc Montagnier, to be removed from the part-time post. Observers say that unless the leadership crisis is resolved quickly and decisively, it could harm the prospects of the Chantal Biya International Reference Centre (CIRCB) in Yaoundé.

The centre has a comprehensive AIDS research and health-care programme, in particular testing and treating newborn babies to reduce maternal transmission of HIV. It is the only research institution in central Africa with the technology and expertise to monitor people with HIV thoroughly, and one of the few African sources of hard data about the spread of the disease. It has an annual budget of about US$1 million, an array of international collaborations and around 20 local staff members, most of whom trained abroad.

Nature has learned that the Nobel laureates wrote on 9 June to Paul Biya, president of Cameroon, asking him to reconsider Montagnier's appointment. Montagnier, head of the World Foundation for AIDS Research and Prevention in Paris, shared the 2008 Nobel Prize in Physiology or Medicine for discovering HIV.

The laureates argue that his embrace of theories that are far from the scientific mainstream, as well as what they claim are anti-vaccination views, risk hurting the CIRCB's research, health-care programme and reputation. Montagnier has suggested, for example, that water can retain a 'memory' of pathogens that are no longer present[1]; that the DNA sequences of pathogens emit electromagnetic waves that could be used to diagnose disease[2,3]; and that stimulating the immune system with antioxidants and nutritional supplements may help people to fight off AIDS[4].

HIGH-PROFILE OPPOSITION

The letter was coordinated by Richard Roberts, a Nobel-prizewinning molecular biologist and chief scientific officer of New England Biolabs in Ipswich, Massachusetts, who also wrote personally to Biya on 4 June, to resign from the CIRCB's scientific board. Roberts says he is concerned that Montagnier plans to pursue his unorthodox research at the centre. Several other board members have also resigned.

Robert Gallo, head of the Institute of Human Virology at the University of Maryland, Baltimore, who had battled with Montagnier over which of them had discovered HIV, has also entered the fray. On 4 June, Gallo wrote to Biya expressing concerns similar to those of the Nobel laureates and informing Biya that his institute, a founding sponsor of the CIRCB, was immediately severing its links with the centre.

Montagnier deplores what he describes as "ad hominem attacks" and "plain lies", and says that there is an "ignominious campaign" against him and his group. He says that history is full of pioneers whose ideas were at first given a chilly reception by a conservative research community. "I believe this is happening again to me, and it is very sad that it involves Nobel Prize laureates attacking a fellow laureate," he says.

The last straw for Montagnier's critics seems to have been his appearance in May alongside vaccine sceptics at a conference in Chicago, Illinois, organized by US patient-advocacy groups AutismOne and Generation Rescue. Montagnier's talk, on his hypothesis that bacterial infections may be one of many causes of autism spectrum disorder, states: "There is in

▶

▶ the blood of most autistic children — but not in healthy children — DNA sequences that emit, in certain conditions, electromagnetic waves."

Montagnier defends his research, pointing out that some clinicians have observed improvements in symptoms of autism after long-term treatment with antibiotics. He says that he has never argued that vaccination could cause autism. "Many parents have observed a temporal association, which does not mean causation, between a vaccination and the appearance of autism symptoms," he says. "Presumably vaccination, especially against multiple antigens, could be a trigger of a pre-existing pathological situation in some children."

LEADERSHIP CRISIS

The CIRCB, founded in 2006, is named after President Biya's wife, who has championed efforts to fight AIDS in Africa. Montagnier's AIDS foundation was a founding partner; Montagnier is also president of the now-defunct scientific advisory board, and vice-president of the management board.

The current crisis compounds problems caused by the centre's lack of stable full-time leadership. In March, its management committee appointed Montagnier to replace former interim scientific director Vittorio Colizzi, an AIDS researcher on secondment from the Tor Vergata University in Rome, who had held the post since 2009. Colizzi was standing in until a full-time scientific director could be hired, but a recruitment process last year failed to settle on an agreed candidate. Some candidates had also expressed misgivings about the job, because at the time the scientific director and administrative director had to share power, a situation that caused tensions, says Colizzi. To address this issue, a presidential decree issued on 31 May merged the positions to create the post of permanent director, with full control of the centre. The move should make it much easier to attract a leading scientist to the post, says Jacques Theze, an immunologist at the Pasteur Institute in Paris, a former member of the CIRCB's scientific board.

The decree also required that many of the centre's posts and committees be disbanded or renewed, creating an uncertain transitional period. On the day that Roberts resigned, for example, the scientific board was officially dissolved, and no clear timetable has been set to reestablish it. Colizzi is concerned that this deprives the centre of its main mechanism for enforcing rigorous peer-review and ethical oversight of research proposals. Montagnier says that he intends to continue all research previously approved by the board, and that he will ask the next board to review the programme. He also plans to embark on new research, including a "key project" using his electromagnetic-wave theory to detect reservoirs of HIV in the body that persist after antiretroviral treatment. Any new projects, including his own, will need to be approved by the centre's science board and ethics committee, he says.

Jean Stéphane Biatcha, head of the centre's management board and a presidential adviser, recognizes the "very serious disagreement" but says that the president and the Ministry of Health will quickly enact the 31 May decree, and so will renew the scientific advisory board and begin the search for a permanent director.

Theze says that he would have preferred Montagnier's detractors to have taken a more diplomatic approach, and warns that the high-level criticism, and the resulting controversy, risks tarnishing the credibility and reputation of the centre, which he says is unfair, because the CIRCB has enormous potential. He worries that the episode might also discourage scientists from applying for the position of director. ■

1. Montagnier, L., Aïssa, J., Ferris, S., Montagnier, J.-L. & Lavallée, C. *Interdisciplin. Sci.* **1,** 81–90 (2009).
2. Montagnier, L., *et al.* Preprint at http://arxiv.org/abs/1012.5166 (2010).
3. Montagnier, L. *et al. Interdisciplin. Sci.* **1,** 245–253 (2009).
4. Butler, D. *Nature* **468,** 743 (2010).

PUBLISHING

Britain aims for broad open access

But critics claim plan seeks to protect publishers' interests.

BY RICHARD VAN NOORDEN

For years, countries have been edging towards open access for research, with some funding agencies requiring that researchers make their papers publicly available within a set period after publication. A report commissioned by the UK government recommends a more radical step: making all papers open access from the start, with authors paying publishers up-front to make their work free to read.

The shift towards this 'gold' form of open access will create short-term financial burdens for research funders, the report acknowledges, but the economic and cultural benefits far outweigh the risks. Not everyone is convinced, however: research-intensive universities say they are concerned that the report plays down potentially cheaper ways to move to open access, in favour of sustaining publishers' profits.

"Momentum for open access is already under way, and it's important for the United Kingdom to embrace that change, to accelerate it, and to manage it," says Janet Finch, a sociologist at the University of Manchester, UK, who chaired the panel behind the report, which was released on 19 June. It is expected to set the national agenda for open access, and influence other countries to follow Britain's lead.

"The ultimate goal is to have a system where the full costs of research publication are met in advance," says Martin Hall, another member of the panel and vice-chancellor of the University of Salford in Manchester. Globally, the number of gold articles is growing by about 30% each year, aided by the rise of journals such as *PLoS ONE*. But they still make up a minority of the world's output — comprising about 12% of research articles indexed in Elsevier's Scopus database in 2011, according to preliminary estimates by Mikael Laakso and Bo-Christer Björk at the Hanken School of Economics in Helsinki (see 'Rise of gold'). UK researchers tend to publish in higher-impact selective journals, so only 5% of their articles are gold open access, according to data collected by Yassine Gargouri, a informatician at the University of Quebec in Montreal, Canada (see 'Open access in the UK').

As that proportion rises, the report notes, authors' open-access costs will grow — but university libraries will still have to subscribe to most of the journals that currently line their shelves. Subscription costs will fall substantially only when most research articles are freely available. During the transition period, gold and subscription models will exist side by side, potentially increasing the overall costs of access. The report also recommends subsidising subscription licences for health and business users to give them better access. Overall, the panel estimates that these transitional costs will amount to roughly £50 million–60 million (US$78 million–94 million) per year, on top of the country's existing annual spending of about £175 million to publish and access research. If the costs were to be met by research funders, they would total about 1% of Britain's annual science budget.

➲ NATURE.COM
For *Nature*'s policy on open access, see:
go.nature.com/pnxzup

The report does not recommend a figure for

OPEN ACCESS IN THE UK

Of the 85,215 research papers published by UK academics in 2010 (as indexed by Web of Science), around 5% were gold open access, whereby authors pay for open publication. Another 35% were green open access — published behind a pay wall and then put in a free repository. However, the proportion varied between disciplines.

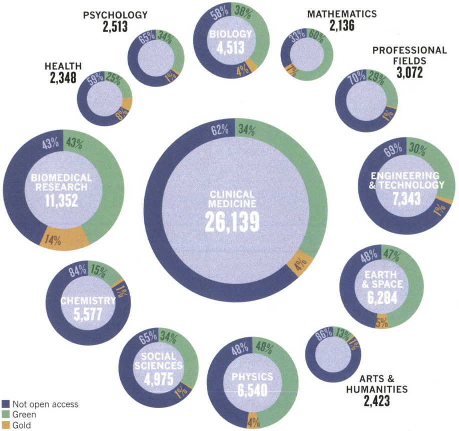

SOURCE: THOMSON REUTERS/Y. GARGOURI

the cost of a gold article, but notes that the UK Wellcome Trust, a major biomedical research funder, last year paid an average of £1,422 per paper on behalf of the scientists it supports. Costs could be greater in more selective journals — *Nature*'s editor-in-chief Philip Campbell says that the journal would have to charge more than £6,500 for gold open-access articles.

Universities and funders will have to work out how to transform their payment systems under a gold regime, with each institution likely to set up a central publishing fund supported by a percentage of every research grant. Whatever the solution, academics will be much more aware of the costs of publishing. This could, in turn, modify their behaviour, with researchers submitting papers to the journals they can afford to publish in, or trying to publish fewer, broader articles.

GOING GREEN

An alternative open-access model is already thriving around the world, and particularly in the United Kingdom. Under green open access, research funders can require that peer-reviewed papers be made openly accessible in online repositories, without the author paying a fee. This usually happens some months after publication, a time period that allows publishers to sell access to the paper for long enough to turn a profit. Researchers can also post pre-publication versions of their papers in institutional repositories.

Paul Ayris, director of library services at University College London, says that scaling up green publishing would be a cheaper short-term route to expanding open access, together with a nationwide scheme to pay for researchers' access to subscription journals en masse. "The gold route does nothing about publisher profits, which many commentators feel are already too high," he says. Open-access advocate Stevan Harnad, a cognitive scientist at the University of Montreal, is even more critical of the report's overt support for gold access. "Some publishers seem to be successfully persuading some politicians that what is at issue is protecting their current revenue streams and modus operandi from the threat of green open access," he says.

But the Finch group says that it was expressly asked to find sustainable ways to grow open access, which it says only a gold route can provide. "It's not in the interests of UK scholarship to make recommendations which undermine the sustainability of the publishing industry," says Philip Sykes, another Finch group member and a librarian at the University of Liverpool. Universities can use their collective lobbying power to drive down both subscription and gold costs, he adds. Gold open access will eventually result in lower incomes for publishers anyway, Finch members note, by making the research-publishing market more transparent and competitive.

RISE OF GOLD

The world's gold open-access articles are rising as a share of the total.

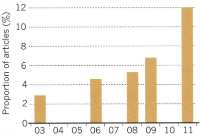

SOURCE: SCOPUS/ISI/M. LAAKSO/B.-C. BJÖRK

That's particularly worrying for learned societies, because they rely on subscription publishing for much of their income. The London-based Institute of Physics, for example, earns some £10 million each year — more than 60% of its total income — from publishing, which it spends on activities such as science education and outreach, says its president Peter Knight. "The mood of the community is to get costs down — but if scientific publishing only just covered its costs, an awful lot of our programmes would be in jeopardy," he says.

What matters now is how the agencies that support UK scientists require them to make their research freely available. Existing open-access mandates have been spottily enforced. The Wellcome Trust has only 55% compliance, although it will soon make grant funding conditional on open-access publishing. A similar condition from the US National Institutes of Health currently has 75% compliance.

In March, Research Councils UK (the umbrella body for the United Kingdom's seven government-funded grant agencies) released a draft policy that suggested it, too, would toughen up on open access. The Higher Education Funding Council for England, another major research funder, could go the same way. But the devil will be in the detail, says Hall. "If research funders go soft on open access, the Finch report will be of only academic interest."

Most uncertain of all is how rapidly the United Kingdom's efforts might drive other countries towards open access. British scientists produce 6% of the research papers published worldwide each year, and the country could find itself paying to make its research free for others' benefit. But there is growing momentum internationally. The European Commission hopes to push for an open-access mandate in its 2014–20 research-funding programme Horizon 2020, and the newly formed Global Research Council — a forum for funding-agency heads worldwide (see *Nature* **485,** 427; 2012) — has open access on its agenda for its second meeting next year in Berlin. As the report concludes, "measures to promote open access need to be ... international in scope if they are to achieve their full potential". ■

COMMUNITY

A workforce out of balance

Too many biomedical PhDs and too few minorities are a demographic dilemma for the NIH.

BY MEREDITH WADMAN

The US biomedical workforce has a glut of young researchers but a dearth of some minority groups, members of which are struggling to establish themselves in the field. The double-barrelled problem is laid out in detail in a pair of reports presented to the US National Institutes of Health (NIH) in Bethesda, Maryland, on 14 June.

NIH leaders have long worried about a steep increase in the number of biomedical PhDs, a consequence of the doubling of the NIH budget from 1998 to 2003. Now that boom is making it increasingly difficult for young scientists to launch academic careers (see 'Swelling ranks').

"This is dysfunctional and it's not sustainable in the long term," says Shirley Tilghman, president of Princeton University in New Jersey and a co-chair of the working group that authored a report on structural problems in the workforce. It calls for several measures to address the oversupply of PhDs, including a six-year cap on the number of years that a graduate student can be supported by NIH funds and an increase in the proportion of students on career-oriented training grants rather than on research grants.

A second report, focusing on diversity, was spurred by a study published in *Science* last year, which found that after factors such as education and publication record are controlled for, black applicants are 10% less likely than white applicants to win NIH research funding (D. K. Ginther *et al. Science* **333,** 1015–1019; 2011).

The diversity report confirms that minority applicants have significantly reduced success rates for grant applications (see 'Uneven playing field'). Confronted with data such as these, "there are a number of scientists of colour who feel, at the end of the day, 'What's the point?'" says Reed Tuckson, vice-president and chief of medical affairs at the health-insurance firm UnitedHealth Group in Minnetonka, Minnesota, and one of three co-chairs of the diversity working group. That sentiment "really, really bothers me", he adds. "We have got to turn [that] around."

The report recommends, among other things, that the NIH launch a "bold", well-funded competitive grant process to build infrastructure at institutions with a record of producing minority scientists, and that it launch an experiment to make applicants' identities and institutions anonymous in the review process.

Francis Collins, director of the NIH, has promised to respond to the recommendations by December. ■

SWELLING RANKS

The number of US biomedical PhDs has ballooned in the past decade, driven by NIH funding of research assistantships. These typically offer less career development compared with traineeships and fellowships.

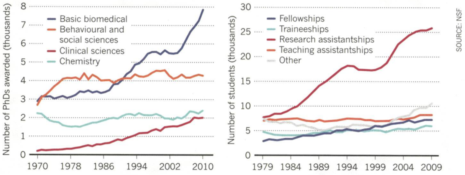

SOURCE: NSF

Researchers become faculty members and win a first NIH grant significantly later in life now than in 1980.

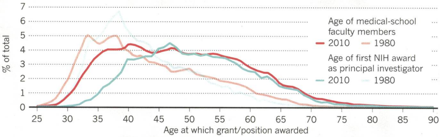

SOURCE: NIH; ASSOC. AM. MED. COLL.

A growing number of US biomedical scientists are foreign workers. Early salaries are lower than in other fields.

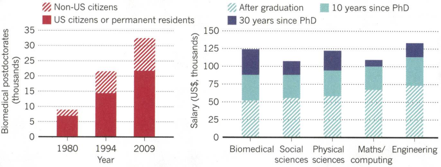

SOURCE: NSF

UNEVEN PLAYING FIELD

Relative to the US population, black and Hispanic people are under-represented in biomedical fields. Minority applicants have lower success rates than white applicants at winning new NIH grants (right).

2010 US Census*

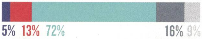

2010 NIH principal investigators*

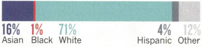

*Adds to more than 100% because some respondents declared two races.

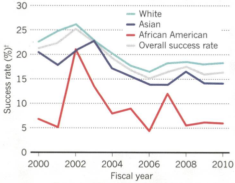

†Success rates of NIH new grant applications in basic sciences category.

SOURCE: 2010 US CENSUS BUREAU REPORT; NIH

ACADEMIC CONDUCT

Romanian prime minister accused of plagiarism

Allegations prompt questions about government's ability to tackle misconduct in academia.

BY QUIRIN SCHIERMEIER

Romania's new government, still reeling from a misconduct scandal that forced its research minister to resign last month, has been hit by fresh allegations of plagiarism that strike at the very top.

Prime Minister Victor Ponta has been accused of copying large sections of his 2003 PhD thesis in law from previous publications, without proper reference. If the charges are substantiated, they could spark public pressure for Ponta to resign, say political insiders. The allegations are also raising fresh doubts about the government's ability to tackle corruption in the higher-education system.

Nature has seen documents compiled by an anonymous whistle-blower indicating that more than half of Ponta's 432-page, Romanian-language thesis[1] on the functioning of the International Criminal Court consists of duplicated text. Moreover, the thesis was republished with very minor amendments as a Romanian-language book in 2004 (ref. 2), and also forms the basis of a 2010 book on liability in international humanitarian law[3]. A former PhD student of Ponta's, Daniela Coman, is named as co-author of the books.

Substantial sections of text in all three publications seem to be identical, or almost so, to material in monographs written in Romanian by law scholars Dumitru Diaconu[4] and Vasile Creţu[5]. They also feature direct Romanian translations of parts of an English-language publication by law scholar Ion Diaconu[6].

"The evidence of plagiarism is overwhelming," says Marius Andruh, a chemist at the University of Bucharest and president of the Romanian council for the recognition of university diplomas. If the allegations are borne out, "a serious discussion is needed in Romania and abroad to prevent this in the future," says Andruh.

"I understand that in law studies it can be necessary to copy extensive legal articles and definitions," says Paul Dragos Aligica, a Romanian political scientist at George Mason University in Arlington, Virginia. But Ponta's alleged plagiarism "goes way beyond that. It's astonishing", he adds. Ponta did not respond to *Nature*'s request for comment on the allegations, and Coman could not be contacted.

Ponta, leader of the Romanian Social Democratic Party, took office as prime minister only last month, replacing Emil Boc, who stepped down in February following protests against austerity measures that he had introduced. Ponta obtained his PhD from the University of Bucharest while acting as Secretary of State in the government of an earlier prime minister, Adrian Năstase — who was also his PhD supervisor.

> ***"There is very clear evidence in these excerpts that the matter should be investigated further."***

"There is very clear evidence in these excerpts that the matter should be investigated further," says Vlad Perju, a Romanian political scientist and director of the Clough Center for the Study of Constitutional Democracy at Boston College in Chestnut Hill, Massachusetts.

The episode follows the resignation last month of the education and research minister, computer scientist Ioan Mang, following accusations of plagiarism in at least eight papers[7]. An investigation of that case by the Romanian Research Ethics Council is ongoing.

The latest allegations add to complaints about declining academic standards in Romania. The previous government had introduced measures to make the country's struggling science and education system more competitive and transparent, but the plans met ferocious opposition from large parts of the academic establishment, and have been substantially relaxed by the current government.

"It's more than unlikely that this government is fit to create institutional structures in science that Romania urgently needs," says Aligica. "How can it be, when some of its leaders don't seem to even remotely understand, or care about, the standards of good science?"

Members of Romania's post-communist elite — including many politicians — have been eager to acquire academic credentials. In the view of some critics, a number of private and public universities in the country are consequently degenerating into 'degree mills' that care little about the quality or novelty of the knowledge that they produce, and which are a breeding ground for academic plagiarism.

"One could almost feel pity for all these guys who have power and money, and who are now craving intellectual recognition," says Aligica. "Unfortunately these incidents just add to the disrepute of Romanian academic standards and create extra pressure that real Romanian scholars and scientists will now have to fight against." ■

1. Ponta, V. *Curtea Penală Internaţională*. PhD thesis, Univ. Bucharest (2003).
2. Ponta, V. & Coman, D. *Curtea Penală Internaţionala* (Lumina Lex, 2004).
3. Coman, D. & Ponta, V. *Răspunderea în Dreptul Internaţional Umanitar* (Universul Juridic, 2010).
4. Diaconu, D. *Curtea Penală Internaţionlă, Istorie şi Realitate* (Editura All Beck, 1999).
5. Creţu, V. *Drept Internaţional Penal* (Editura Tempus, 1996).
6. Diaconu, I. *The International Criminal Court: A New Stage* (Nicolae Titulescu Romanian Inst. International Studies, 2002).
7. Abbott, A. *Nature* **485,** 289 (2012).

MORE ONLINE

TOP STORY

Biologists grow human-eye precursor from stem cells **go.nature.com/ibgaqa**

MORE NEWS

- Budget cuts threaten Japanese scientists' pay **go.nature.com/ahwioz**
- Risk assessment of US agro-biosafety lab found wanting **go.nature.com/ozze9w**
- Boron finally gets a triple bond **go.nature.com/3motmh**

NEWS SPECIAL

Rio+20 Earth summit kicks off in Brazil, with low expectations of progress **go.nature.com/d69weu**

D. WATERS/GETTY

JULENE HARRISON (PHOTO S. ACOSTA/SHUTTERSTOCK)

E. FELIX/AP PHOTO

Many unregulated gold mines in Madre de Dios, Peru, leave a trail of environmental devastation in their wake.

ENVIRONMENT

Peru battles the golden curse of Madre de Dios

Attempts to reduce the environmental and health impacts of mining cause unrest.

BY ELIE GARDNER IN LIMA

"You go out to these communities that are so incredibly poor, and there is money buried in the dirt," says Jason Scullion. "It is not surprising that they want to go out there and dig it up."

Scullion, a graduate student in environmental and forest sciences at the University of Washington, Seattle, arrived in the Peruvian region of Madre de Dios last September, just after the price of gold hit a record high of US$68 per gram. Madre de Dios is at ground zero of Peru's gold rush: an estimated 30,000 artisanal and small-scale miners work in this lush Amazonian area, one of the most biologically diverse places on Earth. Scientists and conservationists are alarmed by the damage that mining is causing to the land and its people.

In the 1930s, settlers armed with shovels, picks and pans came to search the riverbanks for deposits of gold washed down from the Andes mountains. Now, mechanical diggers and dump trucks are much more common. Peru is the sixth-largest producer of gold in the world, and the metal was its main export in the first quarter of this year. Yet about 20% of Peru's bullion is mined illegally, using techniques that destroy forests and pollute local rivers — as well as depriving the government of an estimated US$305 million in taxes each year. The informal operations rarely assess their effects on the environment, or develop plans for what to do with the mines once they are exhausted, and they leave behind mountains of sand and rock, dead trees and deep pits filled with murky water.

Now the government is tightening the screws on illegal mining, and scientists monitoring its impacts are on the front lines of a battle between miners, environmental campaigners and the authorities.

In February, the Peruvian government banned mining in Madre de Dios outside a designated 500,000-hectare corridor (see map) and ordered that all miners must formally register — a year-long process that requires the mine operators to produce a work plan, an environmental-impact assessment and a clean-up strategy, among other requirements. By setting aside a specific area for mining, the government hopes to regulate the industry more effectively and to protect parks and the territories of indigenous people. But miners who have worked outside this newly designated corridor for decades with the government's tacit approval fear for their livelihoods, and the Madre de Dios

➲ **NATURE.COM**
For *Nature*'s special on the changing Amazon, see:
go.nature.com/pvnkj5

Mining Federation in regional capital Puerto Maldonado has campaigned strongly against the legislation. In March, three people died as police clashed with federation-organized protests involving about 15,000 people. The government began raiding mining camps outside the corridor in late March, but in many of those areas miners have since returned to work.

Only around 4,000 miners in the region have met the government's deadline of 13 June to register their mining activities, suggesting that many more intend to disregard the order. Miners who have not registered, or who break environmental laws, will face up to 10 years in prison. But locals say that corruption and lack of government resources in Madre de Dios will make enforcing the law difficult.

SPOILT WILDERNESS

At stake are broad swathes of fertile rainforest, including that in the Tambopata National Reserve and Manu National Park, which is the largest national park in Peru and has been designated a World Heritage Site by the United Nations Educational, Scientific and Cultural Organization. "This is the epitome of a healthy ecosystem," says Enrique Ortiz, vice-president of the Amazon Conservation Association, based in Washington DC. "It's the capital of biodiversity." But mining is already beginning to encroach on these areas, and was threatening to become more widespread. A study published last year (J. J. Swenson *et al. PLoS ONE* **6**, e18875; 2011) showed that mining is deforesting Madre de Dios faster than any other activity. Using satellite imagery, the study's authors found that deforestation in two prominent mining zones increased sixfold between 2003 and 2009, destroying 6,600 hectares of wetlands and primary tropical forest. And they predicted that the trend will only get worse.

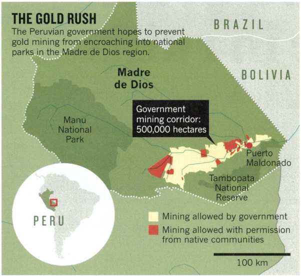
THE GOLD RUSH
The Peruvian government hopes to prevent gold mining from encroaching into national parks in the Madre de Dios region.

BRAZIL
BOLIVIA
Madre de Dios
Manu National Park
Government mining corridor: 500,000 hectares
Puerto Maldonado
Tambopata National Reserve
PERU
🟨 Mining allowed by government
🟥 Mining allowed with permission from native communities
100 km

Scullion came to Madre de Dios to find out whether that prediction is coming true. Funded by a 10-month grant from the US government's Fulbright Program, he is mapping 2 million hectares of the region, including many of the mining hotspots. Most previous mapping studies have assigned land to only two categories — forested and deforested — lumping agriculture, towns and mining areas together, and making it difficult to track the impact of the gold rush. Scullion's study will use ten categories, including mining, agriculture and five different classes of forestry.

Scullion says that there is a misconception among locals that researchers are against mining. Not so, he says — he just wants it to be done in a more sustainable way, staying out of parks and reserves, and ensuring that miners reforest areas after operations have finished. Scullion hopes that his maps will identify the most vulnerable areas in Madre de Dios, as well as the most biologically diverse, and says that they could provide the high-quality information that the government needs to decide whether land should be used for logging, mining or conservation. The data could also help to guide where — and how much — mining takes place in the designated corridor.

Mining is also taking its toll on local people. An estimated 45–50 tonnes of mercury are used each year in Madre de Dios to extract the prized gold, and a large proportion of that ends up in rivers or is released into the atmosphere.

Miners combine mercury with sediments that contain gold — typically using their feet to mix them in a bucket or drum — to form a solid amalgam of the two metals. That amalgam is then heated, often in frying pans over open flames in non-ventilated spaces, to boil off the mercury and leave gold behind.

In March, Katy Ashe, a graduate student in environmental engineering at Stanford University in California, published the first study (K. Ashe *PLoS ONE* **7**, e33305; 2012) to show the scale of the health threat from mercury in Madre de Dios. She found that in mining zones, the proportion of people burdened with unhealthy levels of the metal — 6 micrograms or more per gram of dry hair tested — was more than twice that in Puerto Maldonado. Mercury poisoning can cause vomiting and diarrhoea and, in more extreme cases, brain or kidney damage. Because the metal accumulates in rivers, elevated mercury levels were much more common in those who ate a lot of fish: 18% of people who ate 12 or more fish meals each month had unhealthy mercury levels, in contrast to just 6% and 7% of low and moderate fish consumers, respectively.

That finding tallies with as-yet unpublished research by Luis Fernandez, a tropical ecologist at the Carnegie Institution for Science in Stanford, with whom Ashe is about to begin working. In 2009, Fernandez discovered that the most-consumed fish species in Madre de Dios, such as the mota (*Calophysus macropterus*) and doncella (*Pseudoplatystoma fasciatum*), had the highest levels of mercury. Fernandez is now leading a project to conduct a more extensive survey of the levels of mercury in fish and humans.

Despite the overwhelming evidence of harm, Peruvians are still divided over the findings. Some march through Puerto Maldonado's main plaza shouting through megaphones that mercury is killing everyone, whereas others are willing to drink the toxic liquid metal to prove it is safe.

> ***"Mining is deforesting Madre de Dios faster than any other activity."***

Variations of the mercury-amalgamation technique have been used in gold mining for centuries, and it is difficult to dislodge such deep-rooted practices among artisanal miners. The global gold-mining industry, including leading mines in Peru, has mostly switched to an extraction process that uses cyanide, and recovers about twice as much gold as does mercury amalgamation. But cyanide requires more careful handling than mercury and few artisanal or small-scale miners have the necessary knowledge and skills. The more modern process of thiosulphate leaching might offer a non-toxic alternative, but it is most effective with very fine particles of gold — and Madre de Dios tends to yield larger, coarser grains.

To reduce miners' exposure to mercury, non-governmental organizations have distributed retorts that can capture the toxic vapour. Two years ago, Peruvian engineer Carlos Villachica unveiled the ECO-100V, a US$4,500 machine that uses water and jets of air to separate gold from sediments. And local development organizations such as Caritas Peru, based in Callao, and the Association for Integral Research and Development in Lima have developed other mercury-free technologies for extracting gold.

But Cesar Ascorra, director of Caritas Peru's office in Madre de Dios, says that miners will not switch methods unless the alternative works just as quickly, recovers at least as much gold, and is no more expensive than mercury amalgamation. For now, he adds, miners are more worried about the government's demands for them to formalize their work, and until the price of mercury goes up, or its use is banned, there is little incentive for them to change their practices.

Ortiz says that this underscores the value of research in the region — and the importance of disseminating the results through public-awareness campaigns. Studies such as Fernandez's are not done "for the sake of knowledge", says Ortiz. "This has a direction." ■

Y. KARAHALIS/REUTERS

Unlike the Acropolis, many classical sites are under threat from looting.

ARCHAEOLOGY

Cuts leave Greek heritage in ruins

Austerity measures damaging archaeological research.

BY LEIGH PHILLIPS

The economic and political turmoil in Greece is not just jeopardizing the country's economic future, it is also having a devastating effect on the country's rich cultural past, according to archaeologists in Athens.

Last month, the Association of Greek Archaeologists warned that the economic policies dictated by the European Union and the International Monetary Fund would cause "the destruction of both our country and our cultural heritage". The austerity measures intended to cut government debt have forced the state archaeological service to slash staff numbers by more than 10%, with a further 35–50% reduction possible. Research and excavations are being abandoned. Museums that can no longer afford to pay for security are being plagued by armed robbers. And organized criminals are exploiting the chaos in an explosion of illegal digs and the trafficking of illicitly procured antiquities.

Despina Koutsoumba, president of the archaeologists' association, says that the government no longer funds new research projects — other than those involving foreign partners to whom they are contractually obliged.

"Last year, a very important excavation underneath metro rail lines uncovered long walls connecting Athens to the port of Piraeus, built in the age of Pericles," she says. "The walls to the port were vital and played a major role in the Peloponnesian War as they linked Athens to the sea, and their strength was in their fleet." But the excavation was stopped uncompleted, she says, and there will be no opportunity to return to it once the rail lines are finished.

Koutsoumba says that the ministry also wanted to halt work at a site in Thessaloniki, after major buildings from the time of Roman emperor Gaius Galerius around AD 305–11 were discovered on land where a shopping centre was to be built. The archaeologists' association won a small victory when it persuaded the ministry to continue the work, she says, "but it is a continuous struggle". Net salaries for young archaeologists in the service have been cut by 35%, to €670 (US$842) a month, and many have taken part-time jobs to supplement their income. Meanwhile, senior employees with the highest salaries and most experience are being forced into early retirement. Those who remain are reduced to bureaucratic 'box-ticking' — visiting construction sites to assess whether excavation is needed. They no longer have time for research or analysis, says Koutsoumba.

➲ NATURE.COM
To read more on archaeology and ancient relics, see:
go.nature.com/QygA1o

"Excavation is of course part of our job, but we also need time and funds to do research, to publish our findings. We are not giving anything to the scientific community and letting people know about our new discoveries — we are just digging up pretty objects," she says.

While legitimate archaeology is being hampered, looting is on the rise. The country is pockmarked with holes dug by the poor and desperate hoping for 'buried treasure', and organized criminals perform more professional excavations. "There is no doubt that there has been an increase in the past 3–4 years in both organized and amateur illegal digs and this is definitely related to the cuts," says Christos Tsirogiannis, a forensic archaeologist and researcher at the University of Cambridge, UK, who specializes in investigating the criminal networks behind trafficking in antiquities. He escorts the Greek police art squad on raids to identify looted antiquities.

"There is always a rise in this form of crime in regions rich with antiquities during times of crisis — in recent years in Egypt, Iraq and Afghanistan," says Tsirogiannis.

He says that auction houses and museums are not doing enough to avoid dealing in artefacts of "unprovenanced origin". "I wouldn't be surprised if in the coming years there is a large increase in the number of unprovenanced Greek antiquities sold openly," he says.

Christie's, the London auction house, has strict internal policies to ensure they only offer objects for sale legally, says Matthew Patton, head of communications.

The European Commission denies that spending cuts are to blame. "Greece has received very large sums that go towards cultural heritage. Many cultural institutions have been saved in Greece because of the work of the European Union," says Dennis Abbott, spokesman for Androulla Vassiliou, European Commissioner for culture and education. "But there are limits to what we can do. The main responsibility lies with the states," he says. ■

CORRECTION
The News story 'Journal offers flat fee for "all you can publish"' (*Nature* **486,** 166; 2012) stated that all co-authors on a paper must be members of *PeerJ*. In fact, only 12 co-authors need to be paying members. It also wrongly noted that *mBio* does not assess for impact or importance: it does.

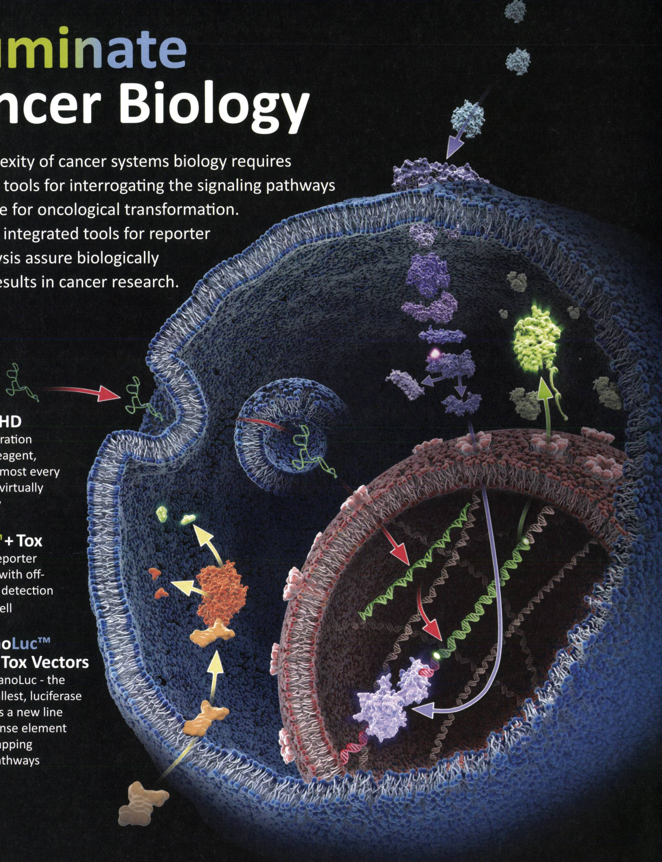

Illuminate
Cancer Biology

The complexity of cancer systems biology requires innovative tools for interrogating the signaling pathways responsible for oncological transformation. Promega's integrated tools for reporter gene analysis assure biologically relevant results in cancer research.

FuGENE® HD
The next generation transfection reagent, effective on almost every cell type with virtually no cell toxicity

ONE-Glo™ + Tox
Multiplexed reporter gene analysis with off-target toxicity detection in the same well

New! NanoLuc™ and pGL4 Tox Vectors
Introducing NanoLuc - the brightest, smallest, luciferase available - plus a new line of pGL4 response element vectors for mapping oncological pathways

Promega

To get a FREE sample of any one of these reagents, visit:
www.promega.com/futurebiology

AN ILL WIND

WITH TURBINES THREATENING SOME BIRD AND BAT POPULATIONS, RESEARCHERS ARE SEEKING WAYS TO KEEP THE SKIES SAFE FOR WILDLIFE.

BY MEERA SUBRAMANIAN

Marc Bechard turned a worried eye skywards as he walked among the limestone hills at the southern tip of Spain. It was October 2008, and thousands of griffon vultures — along with other vulnerable raptors — were winging towards the Strait of Gibraltar and beyond to Africa. But first they had to navigate some treacherous airspace. The landscape on either side of the strait bristles with wind turbines up to 170 metres high, armed with blades that slice the air at 270 kilometres per hour.

Bechard, a biologist at Boise State University in Idaho, and colleagues from the Doñana Biological Station in Seville, Spain, had been hired to help the birds make it safely past 13 wind farms in Cádiz province. Each time the researchers spotted a raptor heading towards a turbine, they called the wind farm's control tower. Within minutes the blades slowed to a stop, and one more migrating bird soared past unharmed. Then the turbine swung back into action.

When the biologists weren't looking up at the sky, they were scouring the ground for carcasses of griffon vultures (*Gyps fulvus*), Spanish imperial eagles (*Aquila adalberti*) and other species. The Spanish Ornithological Society in Madrid estimates that Spain's 18,000 wind turbines may be killing 6 million to 18 million birds and bats annually. “A blade will cut a griffon vulture in half,” says Bechard. “I've seen them just decapitated.”

Wind turbines kill far fewer birds in general each year than do many other causes linked to humans, including domestic cats and collisions with glass windows. But wind power has a disproportionate effect on certain species that are already struggling for survival, such as the precarious US population of golden eagles (*Aquila chrysaetos canadensis*).

“The troubling issue with wind development is that we're seeing a turbines,” says Albert Manville, a biologist with th US Fish and Wildlife Service in Arlington, Virginia

The deaths caused by turbines have the potentia to harm not only wildlife, but also the wind-energy industry, which i the fastest-growing source of power worldwide, according to the Worl Bank. With critics vilifying wind turbines as ‘bird blenders’, wind companies, governments and researchers are teaming up to mitigate the problem before it reaches a crisis point. Cádiz province, for example, require all wind-energy projects to consider environmental issues, and helps t fund research on reducing any damage.

The early signs are that with targeted efforts, wind power and wildlif can cautiously coexist. Bechard and his colleagues, for example, lowere mortality at the Cádiz wind farms by 50%, with only a 0.07% loss i energy production[1]. Others are finding that minor changes in the desig or operation of wind farms can bring major reductions in animal deaths

Bechard and others believe research is crucial to making wind energ viable: “In the long run it'll save a lot of money and a lot of headaches.”

THE GATHERING STORM

Wind power is poised to take off as the world seeks new sources o renewable energy. The industry is growing most quickly in China which plans a 60% increase in wind power in the next three years. Th US Department of Energy is aiming for a sixfold jump by 2030, an the European Union is working towards supplying 20% of its energ demand using renewable sources by 2020, much of that from wind.

But the rapid expansion of wind power can harm wildlife in multipl ways. Beyond direct collisions with turbines, wind farms threaten specie

Raptors favour sites ideal for turbines, like these in Cadiz, Spain.

as a result of air-pressure changes when they fly through the wake of a spinning blade.

The industry maintains that the effects on wildlife are minor. Although there are only a few, limited estimates of bird fatalities at a national level, the available data for the United States suggest that wind farms account for a tiny fraction of avian deaths (see 'Bird killers').

But the concern is that turbines threaten species that are already struggling, such as bats, which in North America have been hit hard by white-nose fungus. Another vulnerable group is raptors, which are slow to reproduce and favour the wind corridors that energy companies covet. "There are species of birds that are getting killed by wind turbines that do not get killed by autos, windows or buildings," says Shawn Smallwood, an ecologist who has worked extensively in Altamont Pass, California, notorious for its expansive wind farms and raptor deaths. Smallwood has found that Altamont blades slay an average of 65 golden eagles a year[2]. "We could lose eagles in this country if we keep on doing this," he says.

Other species at risk include the critically endangered California condors (*Gymnogyps californicus*) — which number only 226 in the wild — and the few hundred remaining whooping cranes (*Grus americanus*), concentrated in the central United States. Biologists can't say whether the increase in wind farms will cause the collapse of these or other bird species, which already face many threats. But waiting for an answer is not an option, says Smallwood. "By the time we do understand the population-level impacts, we might be in a place we don't want to be."

DAMAGE CONTROL

In Cádiz, temporarily shutting down turbines has worked because the biggest threat is to migratory birds, which pass through only occasionally. Similar methods could reduce mortalities along the migratory bottlenecks in Central America, Europe and Asia, says Miguel Ferrer, a conservation biologist at Doñana and a co-author of the Cádiz study.

But that tactic will not work in Altamont Pass, which has both migratory and permanent avian populations. Instead, companies there are making headway by replacing small, ageing turbines with fewer large ones. Choosing sites carefully can help, too. "Raptors do not use the landscape randomly," explains Doug Bell, wildlife programme manager with the East Bay Regional Park District, which manages parklands and monitors wind farms around Altamont.

When the Buena Vista Wind Energy Project at Altamont replaced 179 turbines with 38 taller ones in 2006, Smallwood advised the company to avoid ridge saddles between hills and other hotspots for raptor traffic. Since then, golden eagle fatalities at Buena Vista have dropped by 50% and other raptor deaths by 75%, says Smallwood.

In the eastern United States, Todd Katzner, a biologist at West Virginia University in Morgantown, finds troublesome locations using a tracker designed to fit on golden eagles. "We can identify places where there are wins for both sides," he says. Moving a turbine site by a few hundred metres can substantially reduce the risk of collisions, says Katzner.

Companies say that they have learned from past mistakes. "That there hasn't been another [location like] Altamont Pass for years should be an assurance that the wind industry has gotten better at siting," says Stu Webster, director of permitting and environmental affairs at Iberdrola Renewables, a renewable-energy firm in Portland, Oregon.

Sometimes a slight change in procedures can make a big difference. For example, most turbines are set to turn on when wind speeds reach 4.0 metres per second. But when the Iberdrola Renewables Casselman Wind Project in Pennsylvania increased the threshold to 5.5 metres per second, it slashed deaths of bats — which don't fly as much in high winds — by 93% while shaving just 1% off of power production, says Ed Arnett, who conducted a study there[3] while working at Bat Conservation International in Austin, Texas.

Some wind farms are betting on technology to make a difference. The MERLIN radar system, made by DeTect in Panama City, Florida, scans the skies for up to 6.5 kilometres around and uses algorithms to detect incoming flocks and even individual birds and bats, says Gary Andrews, chief executive of DeTect. Iberdrola Renewables and Pattern Energy, a wind-power company based in San Francisco, California, are using the system at wind farms, as is Torsa Renewables, based in Malaga, Spain.

Some researchers question the effectiveness of the radar. In 2010, a US Fish and Wildlife Service biologist saw a blade hit an American white pelican (*Pelecanus erythrorhynchos*) at Iberdrola's Peñascal wind farm in Texas, which was using MERLIN. But Iberdrola says that the system there is set up to prevent mass mortalities, not to detect individual birds.

According to Iberdrola, birds are most at risk in fog or other periods of low visibility, so Peñascal sometimes shuts down turbines during bad spells, unless the radar reveals that there are no birds around. Generally, however, the radar indicates that birds avoid the turbines by themselves. "We have terabytes' worth of data that are showing us how birds actually react to wind farms," says Webster.

Researchers would love to see such data, but so far they have not been given access. "I haven't seen any results in the published literature," says Arnett, "so in my mind, [the radar] remains untested."

Companies worry that any monitoring data that they release could be used against them in lawsuits by environmental organizations or in political attacks from groups that support the fossil-fuel industries and want to scuttle wind power. The American Wind Wildlife Institute, a coalition of industry and conservation organizations based in Washington DC, is attempting to remedy the situation by creating a limited-access data repository that protects company privacy. The institute expects to complete the pilot phase of the project by mid-summer.

Even as they start to open up, some sectors of the wind industry acknowledge that they should do more to head off problems. "We as an industry need to do a better job of incorporating mitigation strategies into our economics," says John Calaway, director of wind development at Pattern Energy.

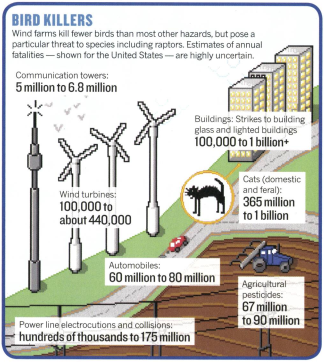

BIRD KILLERS

Wind farms kill fewer birds than most other hazards, but pose a particular threat to species including raptors. Estimates of annual fatalities — shown for the United States — are highly uncertain.

SOURCE: A. MANVILLE, US FISH AND WILDLIFE SERVICE

The strategies seem to be working in Cádiz, but Bechard still frets when he sees vultures on the horizon. "It's always nerve-wracking" wondering whether the turbines will stop in time, he says. When the birds pass safely, he breathes a sigh of relief. But with wind farms popping up around the globe, Bechard worries about what the vultures will encounter as they disappear into the distance. ■

Meera Subramanian *is a freelance writer in Cape Cod, Massachusetts.*

1. de Lucas, M., Ferrer, M., Bechard, M. J. & Muñoz, A. R. *Biol. Conserv.* **147**, 184–189 (2012).
2. Smallwood, K. S. & Karas, B. *J. Wildlife Manage.* **73**, 1062–1071 (2009).
3. Arnett, E. B., Huso, M. M. P. Shirmacher, M. R. & Hayes, S. P. *Front. Ecol. Environ.* **9**, 209–214 (2011).

A BROKEN CONTRACT

AS RESEARCHERS FIND MORE USES FOR DATA, INFORMED CONSENT HAS BECOME A SOURCE OF CONFUSION. SOMETHING HAS TO CHANGE.

BY ERIKA CHECK HAYDEN

Late in May, the direct-to-consumer gene-testing company 23andMe proudly announced the impending award of its first patent. The firm's research on Parkinson's disease, which used data from several thousand customers, had led to a patent on gene sequences that contribute to risk for the disease and might be used to predict its course. Anne Wojcicki, co-founder of the company, which is based in Mountain View, California, wrote in a blog post that the patent would help to move the work "from the realm of academic publishing to the world of impacting lives by preventing, treating or curing disease".

Some customers were less than enthusiastic. Holly Dunsworth, for example, posted a comment two days later, asking: "When we agreed to the terms of service and then when some of us consented to participate in research, were we consenting to that research being used to patent genes? What's the language that covers that use of our data? I can't find it."

The language is there, in both places. To be fair, the terms of service is a bear of a document — the kind one might quickly click past while installing software. But the consent form is compact and carefully worded, and approved by an independent review board to lay out clearly the risks and benefits of participating in research. "If 23andMe develops intellectual property and/or commercializes products or services, directly or indirectly, based on the results of this study, you will not receive any compensation," the document reads.

The example points to a broad problem in research on humans — that informed consent is often not very well informed (see 'Reading between the lines'). Protections for participants have been cobbled together in the wake of past controversies and have always been difficult to uphold. But they are proving even more problematic in the 'big data' era, in which biomedical scientists are gathering more information about more individuals than ever before. Many studies now include the collection of genetic data, and researchers can interrogate those data in a growing number of ways. Several US states, including California, are considering laws that would curtail the way in which researchers, law-enforcement officials and private companies can use a person's DNA.

The research coordinators who develop consent forms cannot predict how such data might be used in the future, nor can they guarantee that the data will remain protected. Many people argue that participants should have more control over how their data are used, and efforts are afoot to give them that control. Researchers, meanwhile, often bristle at the added layers of bureaucracy wrought by the protections, which sometimes provide no real benefits to the participants. The result is a mess of opinions and procedures that sow confusion and risk deterring people from participating in research.

"A lot of times researchers will say, 'Why can't we just go back to the way it was?', which was basically that we take these samples and people do it for altruistic reasons and everything's lovely," says Sharon Terry, president of the patient-advocacy group Genetic Alliance in Washington DC. "That worked in a prior age. I don't think it works today."

The concept of informed consent was first set out in the Nuremberg Code, a set of research-ethics principles adopted in the wake of revelations of torture by Nazi doctors during the Second World War. But in recent years, a series of mishaps over consent have undermined support for research. In 2004, for example, scandal erupted in the United Kingdom after parents found out that from the late 1980s to the mid-1990s doctors and researchers had removed and stored organs and tissues from patients — including infants and children — without parental consent. New laws were passed that required explicit consent for such collections.

Then, in 2010, the Havasupai tribe of Arizona won a US$700,000 settlement against Arizona State University in Phoenix. Individuals believed that they had provided blood for a study on the tribe's high rate of diabetes, but the samples had also been used in mental-illness research and population-genetics studies that called into question the tribe's beliefs about its origins. In the settlement, the university's board of regents said that it wanted to "remedy the wrong that was done".

The cases illustrate the divide between researchers and the public over what people need to know before agreeing to participate in research.

Many of the recent concerns over consent are driven by the rapid growth of genome analysis. Decades ago, researchers weren't able to glean much information from stored tissue; now, they can identify the donor, as well as his or her susceptibilities to many diseases. Researchers try to protect the genetic data through technological and legal mechanisms, but both approaches have weaknesses.

D1Z2
D1S77
D1S49
D1S50
D1S43/D1S47
PND
D1S71
D1S56
ALPL
FUCA1
RH
D1S7
D1S57
MYCL
GLUT1
D1S5
D1Z5
MUC1
SPTA1
CRP
ATP1A2
APOA2
AT3
LAMB2
F13B
D1S53
REN
CR1/CR2/DAF
D1S70
D1S81
D1S48
D1S103
D1S74
D1S8
D1S102
D1S68
cM
300
cM

VIKTOR KOEN

It is not enough to stripping out any information that would identify the donor, such as names and full health records, before the data are stored. In 2008, geneticists showed that they could easily identify individuals within pooled, anonymized data sets if they had a small amount of identified genetic information for reference (N. Homer *et al. PLoS Genet* **4,** e1000167; 2008). And it may become possible to identify a person in a public database from other information collected during a study, such as data on ethnic background, location and medical factors unique to the study participants, or to predict a person's appearance from his or her DNA.

Even legal mechanisms have vulnerabilities. In 2004, Jane Costello, a social psychologist at Duke University in Durham, North Carolina, was forced to go to court to defend the confidentiality of patient records from the Great Smoky Mountains Study. The study, which is just going into its third decade, examines emotional and behavioural problems in a cohort of people who enrolled as adolescents. A participant in the study was testifying against her grandfather, John Trosper 'JT' Bradley, who had been accused of sexual abuse. JT's lawyers subpoenaed the granddaughter's records from the study in hope that the information would undermine her credibility as a witness.

It meant a major crisis of confidence for Costello. "I was telling 1,400-plus people every time we saw them that 'your data are absolutely safe', and now I was in a position where I was told, 'No, that's not true'," she says. After Costello's day in court, in August 2004, the records remained sealed, but mostly because the judge did not believe that they would exonerate JT. The result provided no clarity about patient protections.

BETTER MODELS FOR CONSENT

One solution is to keep genetic information separate from demographic data. The BioVU databank at Vanderbilt University Medical Center in Nashville, Tennessee, for instance, contains DNA samples from patients treated at the hospital — 143,939 people as of 11 June. The DNA is linked to health records in a second database, called a 'synthetic derivative', in which the data are anonymized and scrambled in ways that, its creators say, make it difficult for anyone to work back from the database to verify a patient's identity. Sample-collection dates are altered, for example, and some records are discarded at random, so that it is not possible to know that someone is in the database just because he or she was treated at the hospital. Even researchers who work with the data cannot determine whose data they are using. The databank expects to include as many as 200,000 individuals by 2014, making it one of the largest collections of linked genetic and health records in the world.

But when it comes to consent, BioVU takes a different approach from many other programmes. Patients don't choose to participate; rather they are given the chance to opt out. Patients are asked to sign a 'consent to treat' form every year. It includes a box that they can tick to keep their DNA out of the database. That model helps BioVU to collect many more samples, and much more cheaply, than other projects can.

The opt-out model — which is used in only a few other places — troubles Misha Angrist, a genome policy analyst at Duke University, who says that it risks taking advantage of people when they are ill. "Even a routine visit to the clinic can be a vulnerable moment, and they're saying, 'Would you mind doing this for future generations, to help people just like you?'."

And legal challenges have shown the weaknesses of opt-out policies. Health officials are now destroying millions of blood samples taken from newborn babies in Texas and Minnesota because the families were not adequately informed that the samples, collected to screen for specific inherited disorders, would also be used in research.

Vanderbilt officials and researchers counter that they have run extensive public campaigns to ensure that people in Nashville are aware of BioVU and are comfortable with the way it works. They regularly consult a community advisory board about the project. And Vanderbilt's approach actually goes above and beyond what is required by federal law; because the synthetic derivative includes de-identified

READING BETWEEN THE LINES

Despite the work that goes into making consent forms clear and detailed, some participants say they are confused by the wording.

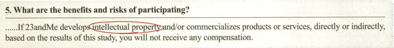

5. What are the benefits and risks of participating?

......If 23andMe develops intellectual property and/or commercializes products or services, directly or indirectly, based on the results of this study, you will not receive any compensation.

23andMe received a patent in May for its work on Parkinson's disease. Some participants did not expect it to seek intellectual-property rights.

From 23andMe's research consent form **www.23andme.com/about/consent/**

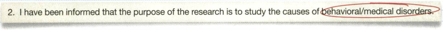

2. I have been informed that the purpose of the research is to study the causes of behavioral/medical disorders.

Many participants in the Medical Genetics at Havasupai study in Arizona in the 1990s were unaware of how broad the research goals were and what kind of studies would be performed.

Courtesy of Pilar Ossorio

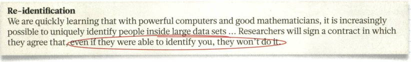

Re-identification

We are quickly learning that with powerful computers and good mathematicians, it is increasingly possible to uniquely identify people inside large data sets ... Researchers will sign a contract in which they agree that, even if they were able to identify you, they won't do it.

In an attempt to be more transparent about privacy risks, the Consent to Research project's 'Portable Legal Consent' essentially states that although anonymity cannot be guaranteed, researchers must pledge to uphold it.

Courtesy of John Wilbanks Consent to Research

data, it doesn't legally require informed consent at all. Last July, the US Department of Health and Human Services signalled that it might be rethinking the rules that exempt de-identified data from the consent requirement, as part of a broad overhaul of research ethics regulations.

Irrespective of the outcome, obliterating patient identities has drawbacks. Researchers can't perform some types of research on the scrambled data. Because dates are changed, studies on the timing of influenza infections, for example, are impossible. And patients can't be told if the research has revealed that they carry individual genetic risks linked to disease.

FULL DISCLOSURE

Returning study results to research participants has been another thorny issue for consent. Doctors might learn about genetic predispositions to disease that are separate from the ailments that led a patient to participate in the research in the first place, but it is not clear what they should do with this information.

UK researchers, for example, are forbidden from sharing genetic results with participants. But US research societies, such as the American College of Medical Genetics and Genomics in Bethesda, Maryland, are moving towards adopting standards that would encourage the practice for some types of findings, such as those that are medically relevant.

Some countries, such as Germany, Austria, Switzerland and Spain, are already feeding back such information. And some clinical sequencing programmes are considering offering patients 'tiered' consent, in which people can decide whether to be told about their data and how much they want to learn.

This is what Han Brunner, a geneticist at the Radboud University Nijmegen Medical Centre in the Netherlands, had hoped to do. Last year, he began a project to sequence the exomes — the protein-coding regions of the genome — of 500 children and adults, looking for the genetic causes of intellectual disabilities, blindness, deafness and other disorders. Brunner proposed allowing participants to choose from three options: they could learn everything that researchers had divined about disease susceptibility; just information relevant to the disease for which their genomes were examined; or no information at all. Ethics reviewers shot down his proposal. "They said that in practice, it would be impossible for people to draw those lines, because people giving consent cannot foresee all the possible outcomes of the study," Brunner says. Instead, everyone participating in the studies must agree to learn all medically relevant information arising from the analysis of their genomes. As a consequence, Brunner recently had to tell the family of a child with a developmental disability that the child also has a genetic predisposition to colon cancer. Not all researchers endorse the idea of informing children about diseases that might affect them as adults. In this case, doctors recommended early screening, and Brunner says, "the family handled it very well; they said, 'This is not what we anticipated, but it's useful information'".

Many of the studies done now ask patients to give consent for research linked to particular investigators or diseases. But that means that researchers cannot pool data from separate studies to tackle different research questions. Many researchers say that the obvious solution is a broad consent document that gives researchers free rein with the data. But many non-scientists think participants should be able to control how their data are used, says lawyer Tim Caulfield of the University of Alberta in Calgary, Canada, who has surveyed patients about this idea. "There's an emerging consensus within the research community about the need to adopt things like broad consent, but that hasn't translated out to the legal community or to the public," he says.

Another solution might be called 'radical honesty'. A US project called Consent to Research, which aims to provide a large pool of user-contributed genomic and health data, has devised what it calls a 'Portable Legal Consent', which allows anyone to upload information about him or herself, such as direct-to-consumer genetic results and lab tests ordered through medical providers, to an interface that strips the data of identifiers. It makes the data widely available to researchers under broad guidelines, but also requires data donors to go through a much more rigorous consent process than most studies do. The Portable Legal Consent specifically informs participants that researchers might be able to determine their identities, but that they are forbidden from doing so under the project's terms of use.

Such approaches could help scientists by giving them access to a trove of data with no restrictions on use. But the participant protections system that is in place might not be ready for such frank dialogues, says Angrist, who serves on one of Duke's institutional review boards.

While reviewing a research proposal for a large biobank, for example, Angrist suggested that the researchers send the participants an annual e-mail explaining how their samples were being used, and thanking them for donating their time and tissue. The review board voted this suggestion down after its chair argued that e-mailing the patients would create a problem in light of the Health Insurance Portability and Accountability Act (HIPAA) — the US law that guarantees the privacy of health records. "The irony is that the HIPAA is supposed to protect people, and what I was hearing was, 'We can't talk to people because we're too busy protecting them'," Angrist says. "Institutions use informed consent to mitigate their own liability and to tell research participants about all the things they cannot have, and all the ways they can't be involved. It borders on farcical."

But as patient data become more precious to researchers, and as advocacy organizations become more involved in driving research agendas and in funding the work, such paternalistic attitudes will probably not survive, says Terry. She adds that technologies that allow research participants to control and track how researchers use their data will soon catch on. These approaches could benefit patients, who gain transparency and control over their data, and researchers, who gain access to richer data sets. "I think we're going to have to get to a place where consenting people becomes customizable easily through technology, and we're not there yet," Terry says. ■ **SEE EDITORIAL P.293**

Erika Check Hayden *writes for* Nature *from San Francisco, California.*

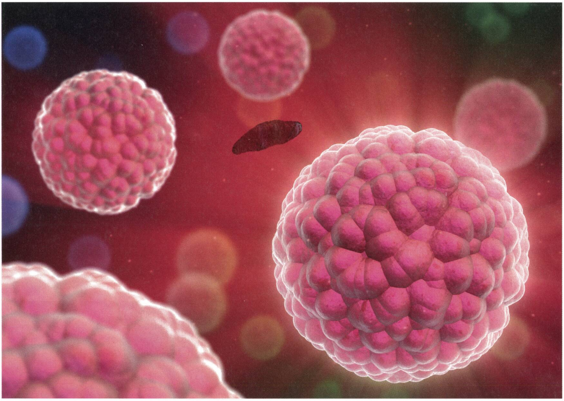

Cell division: The Research Institute of Molecular Pathology researches into the weaknesses of human cancer cells.

Photo: istockphoto

Research for life

Competence in the fight against cancer: the German group Boehringer Ingelheim carries out most of its oncology research in Austria. What makes the business location so attractive.

They are small and unpredictable, aggressive and destructive. Scientists around the world have been searching for their weak spots for decades. Research into cancer cells is a basic feature of the life science sector. A particularly strong business location in this field is Austria. Not only pharmaceutical giants such as Baxter, Sandoz and GlaxoSmithKline, but also small, innovative companies such as AFFiRiS find optimal conditions there. "Customized R&D funding programs as well as a research premium of ten percent are only two ways in which Austria supports the life science sector", says René Siegl, Managing Director of the national investment promotion acgency ABA-Invest in Austria, which consults companies free of charge and provides consulting services for firms setting up business operations in Austria. In addition, Austria offers numerous tax advantages. German companies such as Boehringer Ingelheim are also represented in Austria with research facilities. Boehringer Ingelheim operates its global oncology research center here, and coordinates its entire clinical research for the region of Central and Eastern Europe. For 25 years the company has been the main sponsor of the Research Institute of Molecular Pathology (IMP) at the Campus Vienna Biocenter, where scientists are trying to find the weaknesses of leukemia cells, amongst other things.

SUCCESSFUL CANCER RESEARCH. The objective is to "reprogram" these cells by blocking certain genes. Initial attempts have shown that the approach is successful. An immediate stop to cell division occurs after a specific gene is deactivated. This means that the cancer cells no longer reproduce or even die off. Moreover, researchers also hope to be able to use appropriate drugs in the fight against other types of cancer.

www.investinaustria.at

Investments in research

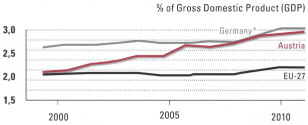

Development of R&D expenditures in Austria, Germany* and the EU-27

Source: Eurostat * 2010 estimate

Join the iCell® Fan Club

i ♥ HUMAN Cells
Use More iCell Neurons
Cellular Dynamics international
Use more iCell Cardiomyocytes

iCell® products are derived from **human iPS cells,** and our biggest fans know that a true human cellular model provides more accurate predictivity.

Quantity: Each vial covers a 96-well plate. Guaranteed.

Quality: Highly consistent and >95% pure with characteristics of native cells.

Easy: Cryopreserved cells + media = convenient kits.

Choice: Ready-made or custom cells available.
- iCell Cardiomyocytes
- iCell Neurons
- iCell Endothelial Cells
- iCell Hepatocytes
- MyCell Custom Services

Cellular Dynamics international

For a growing list of our fans' peer-reviewed, published research on iCell products:

www.cellulardynamics.com/icell

INTRODUCING MyCell™ Custom Services!

© Copyright 2012 Cellular Dynamics International, Inc. iCell and MyCell are trademarks of CDI.

COMMENT

AWARDS Passion and punch-ups in a chronicle of two contested Nobel prizes **p.318**

ECOLOGY A paean to decay charts the life that death provides **p.320**

EXHIBITION London show celebrates Alan Turing's life and legacy **p.321**

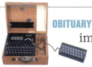

OBITUARY Akira Tonomura, imaging pioneer, remembered **p.324**

S. MAXWELL/ASPEN CENTER FOR PHYSICS

Summer workshops at the Aspen Center for Physics give researchers respite from their academic duties.

Aspen physics turns 50

Michael S. Turner reflects on how mountain serenity has bred big breakthroughs at the Aspen Center for Physics in Colorado.

Theoretical physicists are an odd lot: bad communicators (Niels Bohr and Werner Heisenberg); brilliant showmen (Richard Feynman and George Gamow); the 'strangest man' (Paul Dirac); lots of Hungarians (Leó Szilárd, Edward Teller and Eugene Wigner); bad hair (Albert Einstein); and too few women. They don't need fancy equipment — a pencil and paper will do. But they do like a serene environment, with blackboards and other people of their ilk, in which to come up with big ideas: among them relativity, the Big Bang, quantum mechanics and the atomic bomb.

Over the past 50 years, the Aspen Center for Physics (ACP), nestled in a beautiful valley at 2,400 metres above sea level in the Colorado Rocky Mountains, has provided a 'circle of serenity' during the summer months for 10,000 theoretical physicists, including 53 Nobel laureates, from 65 countries. The centre can lay claim to the string-theory revolution, the birth of the arXiv preprint archive and to setting the agenda for condensed-matter physics. Its history is tied to the revival of a silver-mining town and the American entrepreneurial spirit, and features a fascinating cast of characters, from philosopher Mortimer Adler to journalist Hunter S. Thompson.

The centre's story cannot be separated from that of the town. The 1893 repeal of the Sherman Silver Purchase Act demonetized silver and almost overnight turned Aspen, with a population of about 15,000, into a ghost town. Elizabeth Paepcke, wife of Chicago industrialist Walter Paepcke, visited in 1939, describing it as a place that "had slept since 1893". She found 700 residents, decaying Victorian buildings and wonderful skiing. She persuaded her husband, a devotee of German writer Johann Wolfgang von Goethe, to visit in 1945. Seeing it as the ideal place to bring together the three aspects of life — economic, cultural and physical — he invested millions of dollars in rebuilding it. In 1946, he formed the Aspen Skiing Corporation, which remains the financial engine of the valley.

Aspen's cultural transformation came with the 1949 Goethe bicentennial. Organized by Walter Paepcke (with guidance from Adler and Robert Maynard Hutchins, then chancellor of the University of Chicago in Illinois), the bicentennial aimed to rehabilitate German culture and to revive humanism in the wake of the Second World War and the dawn of the atomic age. Around 2,000 people gathered in a tent designed by architect

▶

▶ Eero Saarinen for the 20-day celebration. They included German–French theologian Albert Schweitzer, pianist Artur Rubinstein, philosopher José Ortega y Gasset and poet Stephen Spender. The event led to the formation of the Aspen Music Festival (now the Aspen Music Festival and School) and, in 1950, of the Aspen Institute for Humanistic Studies (now the Aspen Institute). Just as Paepcke had imagined, today the town brings together culture, wealth and athleticism — and a touch of glitz.

BEGINNINGS

The ACP's origins lie with physicist George Stranahan, heir to the fortunes of the Champion spark-plug company in California and a graduate student at the Carnegie Institute of Technology in Pittsburgh, Pennsylvania. In the late 1950s, he decided that he would rather do his physics during the summer months in the mountains of Colorado, where fishing and hiking provided a more enjoyable backdrop than did an office in steamy Pittsburgh. After a few years, he realized that theoretical physics was best done with others, and set out to draw physicists to Aspen. When he later moved to Colorado, Stranahan became the landlord and close friend of Thompson.

Stranahan got things going with help from Michael Cohen, a condensed-matter theorist at the University of Pennsylvania in Philadelphia, who was one of Feynman's few PhD students, and Robert Craig, executive director of the Aspen Institute. The Stranahan family's Needmor Fund paid for the first building, Stranahan Hall, designed by Bauhaus architect Herbert Bayer, who also planned the Aspen Institute campus. Cohen found the physics talent, and Craig convinced the Aspen Institute to create a physics division.

In spring 1962, a letter was sent out to the physics community tentatively announcing "the possibility of a summer physics institute". The purpose was "to provide a place for physicists to work on their own problems during the summer, in a stimulating physics atmosphere, and in a location with pleasant surroundings and natural beauty". That year, 42 brave souls came to Aspen to "pursue their work with minimal distractions".

The Aspen formula was — and still is — to bring the best theorists together in an informal setting for weeks or months, free from their usual responsibilities of students and teaching, and isolated from distractions. There, they could talk with one another, think big thoughts and come up with game-changing ideas. Physicists were housed two to an office and held discussions on a patio with a small blackboard, often accompanied by beautiful music from the town's music tent. Graduate students were excluded, differentiating Aspen from teaching summer schools. For many years, the buildings had only a handful of public phones. This put a limit on interruptions, but sometimes provided entertainment. I once overheard particle physicist Murray Gell-Mann of the California Institute of Technology quipping, "I don't know the English for it, but the Japanese is …".

An early attempt to bring together physicists and philosophers failed because of Adler's insistence that they agree on "the pyramid of knowledge", which had physics at the bottom and philosophy on top. Because of the clash of cultures and egos, the centre did not stay tied to the Aspen Institute for long and became an independent entity in 1968. Since then, the ACP has been run by physicists who volunteer their time, helped by just two full-time staff. More than 200 top theorists have shaped and guided the centre — including five Nobel laureates and Stephen Hawking.

An early grant from the Sloan Foundation was crucial, and Hans Bethe of Cornell University in New York donated part of his 1967 Nobel prize money. Bethe Hall, built in 1978, was named in his honour. Robert Rathbun Wilson, the first director and builder of Fermilab in Batavia, Illinois, visited Aspen in 1967 and convinced the US Department of Energy to build a large, temporary office building there, where Fermilab's facilities for particle-physics experiments were designed. The construction of Hilbert Hall, named after mathematician David Hilbert, almost tripled the number of physicists that the centre could accommodate.

SOLID FOUNDATIONS

In 1972, the US National Science Foundation became the ACP's main funder, with support from other US science agencies including the Department of Energy and NASA. In the mid-1990s, a $3-million fund-raising campaign led by astrophysicist David Schramm of the University of Chicago financed the final and largest building, Smart Hall.

George Stranahan, Michael Cohen and Robert Craig (left to right): the centre's three founders.

S. MAXWELL/ASPEN CENTER FOR PHYSICS

Contributions came from physicists, friends in the Aspen community and the Smart Family Foundation in Connecticut.

Three figures played a major part in establishing the ACP in the theoretical community: Philip Anderson of Princeton University, Bethe and Gell-Mann. Coincidentally, they all began coming to Aspen two years before receiving a Nobel prize. They set the agenda, served as scientific magnets and gave early legitimacy. Any high-energy theorist would kill to spend three weeks discussing physics with Gell-Mann; Bethe helped to get astrophysics going at the ACP; and Anderson shaped condensed-matter physics there for three decades.

Anderson set the tone for the condensed-matter field with his influential paper 'More is Different' (P. W. Anderson *Science* **177,** 393–396; 1972). Contrary to particle physics, in which scientists pursue a reductionist quest for simplicity at smaller and smaller scales, condensed-matter physics applies the basic rules to discover and study the often unexpected, emergent phenomena that arise in large systems with complicated interactions, such as superconductivity or biological systems. Today, biological physics has emerged as a major activity at the ACP.

Two other condensed-matter theorists played a crucial part: David Pines of the University of Illinois at Urbana–Champaign and Elihu Abrahams of Rutgers University in Piscataway, New Jersey. They pioneered workshops on the latest topics to attract a balance of researchers from universities and from industry (mostly Bell Labs). These workshops brought in young hotshots, keeping the talent pool fresh. One area of scientific focus, strongly correlated electrons in metals, laid the foundations for the current understanding of high-temperature and other unconventional superconductors.

In addition to Bethe's presence, astrophysics at the ACP was jump-started by the discovery in 1967 of pulsars and their identification as neutron stars. The exotic properties of pulsars — rapid rotation, superfluidity and superconductivity — intrigued Pines and other condensed-matter theorists. They brought in astrophysicists with expertise in relativity and nuclear physics, and work done at the centre linked pulsar glitches to superfluidity within neutron stars, advancing both fields. In 1972, NASA started funding an annual workshop, and astrophysics had a foothold in Aspen.

But it was cosmology that caused astrophysics to rise to the same level as particle physics and condensed matter. Around 1980, Schramm and others began to realize that theories of unification in particle physics might revolutionize the sleepy field of cosmology, which had been the province of astronomers since the time of Edwin Hubble. Aspen was the ideal incubator for this

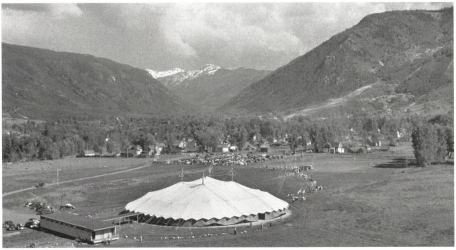

W. EUGENE SMITH/TIME & LIFE PICTURES/GETTY

Aspen's cultural shift started with big-top celebrations for Johann von Goethe's bicentennial in 1949.

young, interdisciplinary field. Workshops brought together astronomers and physicists to discuss the hot topics — Big Bang nucleosynthesis, dark matter, inflation, large-scale structure, the cosmic microwave background and cosmic strings.

HIGH IMPACT

A staggering 10,000 or more papers are attributed to visits to the ACP. But its real impact is the big ideas that originated there. Much of today's consensus cosmology, with its particle dark matter, inflationary origins and dark energy, can trace its roots to the ACP. In his Nobel prize acceptance speech last December, Adam Riess of Johns Hopkins University described how his team, which co-discovered that the expansion of the Universe is speeding up, regularly met at the centre to chart its activities.

Whether or not string theory is the theory of everything, it has changed the course of physics. It began as a way to describe the strong interactions between neutrons, protons and related particles. Supersymmetry, the symmetry between bosons and fermions and a hallmark of today's string theory, traces its origins to theorist Pierre Ramond's first summer in Aspen in 1970, where, as he put it, he "stopped calculating and started thinking". When he got back to Fermilab, he prepared the paper that added supersymmetry to string theory. This has become the pattern: think in Aspen, calculate and write at home.

String theory was declared dead at a 1974 Aspen workshop, having been beaten by quantum chromodynamics as the best description of the strong (colour) interactions between the quark constituents of the hadrons. But John Schwarz of the California Institute of Technology decided to be bold and think bigger, touting strings as the path to unifying the forces of the subatomic world with gravity. For the next ten years, Schwarz, his collaborator Michael Green and a handful of others tried to make good on this promise at the centre. In the summer of 1984, their breakthrough came with a historic paper that showed the mathematical consistency of string theory (technically the cancellation of anomalies), triggering the first string-theory revolution.

The Green–Schwarz discovery was announced immediately in grand fashion during a 'physics cabaret' at Aspen's historic Hotel Jerome. In a skit, Schwarz, playing the role of Gell-Mann, rushed onto the stage to announce that he had discovered the theory of everything — and was eventually carried off the stage by a man in a white coat.

Another revolution, in physics publishing, traces its origin to a chance encounter on an ACP bench in June 1991. Joanne Cohn, a young theorist at the Institute for Advanced Study in Princeton, had been running an informal preprint distribution service, e-mailing papers to hundreds of string theorists who wanted to get the latest results as quickly as possible. Paul Ginsparg, then at the Los Alamos National Laboratory, asked her why she hadn't automated the system. By the next day, Ginsparg had written some scripts, and two months later the Los Alamos arXiv (now residing at Cornell University) was opened for business. Today, more than 1 million articles are downloaded every week.

Physicists have always been attracted to mountains, to hike and to think. ACP cofounder Robert Craig was a world-class mountaineer who scaled some of the toughest and tallest mountains, including K2 in Asia, and many physicists who came to Aspen were serious climbers. A topographical map of the surrounding mountains is displayed prominently in Stranahan Hall. Aspen's combination of challenging hikes, unpredictable mountain weather and crumbling rock means that tragedies are not uncommon.

In 1988, ACP trustee Heinz Pagels, executive director of the New York Academy of Sciences, slipped on a loose stone while climbing on Pyramid Peak in Colorado and fell to his death. A respected popularizer of physics as well as a brilliant theoretical physicist, Pagels' name was given to the centre's summer public lecture series.

Schramm, my mentor, was also an expert climber. One summer, bad weather trapped him and his climbing partner on the face of Colorado's Capitol Peak in freezing rain; they made it back to Aspen two days later, after many had given up hope. Sadly, in December 1997, Schramm died in a plane crash while flying his twin-engine turboprop from Denver to Aspen.

THE FUTURE

Today, the Aspen Center for Physics is thriving on a 1.6-hectare campus, surrounded by a large 'circle of serenity' of open space on the Aspen Meadows. The Aspen Institute, the Aspen Music Festival and School and the ACP are recognized as the town's three major cultural institutions.

Each summer, the ACP's 16-week programme and 10–15 workshops attract more than 500 leading theorists to work on the most important problems in physics. With delight, I note that about 20% of the attendees and members of the governing board are now women, and that the centre now has its first female president — progress for theoretical physics. Discussions fill the offices, halls, alcoves and patios; spontaneous volleyball games occur regularly. New ideas and collaborations made in this informal environment have launched the careers of hundreds of young theorists (myself included) and moved physics forwards.

Will the Aspen formula continue to be as successful as it has been for the past 50 years? Several theoretical-physics institutes now exist — the Isaac Newton Institute in Cambridge, UK, and the Kavli Institutes in Santa Barbara and Beijing. These have longer, more formal programmes, and lack the serenity of Aspen. The bigger challenge comes with the change in the way science is done today. It is more collaborative, more connected and 'more faster'. When the ACP was founded, collaboration required face-to-face interaction. Now, with e-mail and the Internet, many collaborators have never met in person.

Aspen continues to be a place to think, free from the constraints of everyday existence — as Paepcke said, a place for "lifting us out of our usual lives". In today's fast- paced world of science, the need for a circle of serenity is only more acute. ■

Michael S. Turner *is director of the Kavli Institute for Cosmological Physics at the University of Chicago, Illinois 60637, USA. He is chair of the trustees of the Aspen Center for Physics, which he has attended since 1979.*
e-mail: mturner@kicp.uchicago.edu

For more on 50th anniversary events at the Aspen Center for Physics, see go.nature.com/lepwz8.

RUTGERS UNIV. ARCHIVE

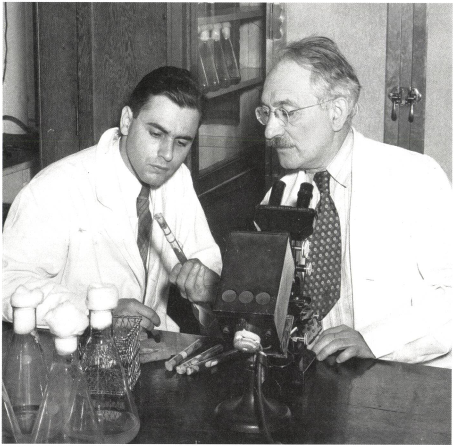

Albert Schatz (left) felt that he deserved a share of the Nobel prize awarded to Selman Waksman (right).

NOBEL PRIZE

A dark edge to the glory

An examination of the battles behind the prestige of top awards grips **Hidde Ploegh**.

Those who enjoy making predictions ahead of each year's Nobel announcements, only to criticize the winners when their choices lose out, may find satisfaction in *Prize Fight*.

Two stories of contested Nobel prizes drive the narrative in this readable book by the distinguished radiologist Morton Meyers. Meyers succeeds in chronicling these events without being overtly partisan, and includes a few vignettes of well-known and not-so-ennobling kerfuffles, with elliptical references to current events. Finally, Meyers discusses the general and fascinating ethical, professional and philosophical issues that arise from the prize fights.

Meyers first tackles biochemist Selman Waksman's 1943 discovery of streptomycin, and the ensuing altercation with Albert Schatz about attribution, intellectual property and commercial exploitation of this early antibiotic. Waksman — who developed soil microbiology and recognized that actinomycetes bacteria are nature's drug store for antibiotics — assigned to Schatz, his graduate student, the search for compounds active against Gram-negative bacteria. Schatz soon came up with *Streptomyces griseus* as a source of streptomycin.

This drug, the lucrative patent for which lists both Schatz and Waksman as its inventors, turned out to be highly active against *Mycobacterium tuberculosis*. It was responsible for remarkable therapeutic successes until the emergence of streptomycin-resistant strains and isoniazid, an antibiotic used in combination therapy, in the early 1950s.

Drawing on historical records and interviews with Schatz's widow, the author lays out a plausible and fascinating story. The failure to communicate and manage expectations led to a painful clash between Schatz and Waksman. A culture that viewed the appropriation of subordinates' discoveries by laboratory chiefs as legitimate deepened the chasm.

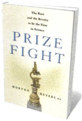

Prize Fight: The Race and the Rivalry to be the First in Science.
MORTON MEYERS
Palgrave Macmillan: 2012. 272 pp. £16.99/$27

Schatz's attempts to redress the perceived injustice — including a lawsuit against Waksman and Rutgers University in New Brunswick, New Jersey, later settled out of court — probably excluded him from academic positions to which he was entitled by talent and previous accomplishment. Reclamations of this type inevitably invite the opprobrium of the larger scientific community, not unlike the fate of many a whistle-blower similarly castigated for attempting to right a wrong. On the fiftieth anniversary of streptomycin's discovery, however, Rutgers finally awarded Schatz its highest decoration: the Rutgers University Medal.

Meyers's second story deals with the development of nuclear magnetic resonance (NMR) imaging as a tool in medical diagnostics, featuring physician Raymond Damadian and his battle with the late Paul Lauterbur, a chemist. This is the livelier portion of the book. Meyers — as a radiologist, effectively gardening in his own backyard — had the added benefit of interviewing both Damadian and Lauterbur.

With physicist Peter Mansfield, Lauterbur in 2003 bested Damadian to Nobel recognition of magnetic resonance imaging (MRI). This outcome prompted the appearance of full-page ads financed by the Friends of Raymond Damadian in a number of newspapers, including *The New York Times*.

As Meyers shows, Damadian was the first to suggest using NMR in imaging to distinguish healthy from cancerous tissues. But he could not claim to have made the essential steps leading to wider practicability of the method. He built a massive machine, 'Indomitable', a prototype of which included a permanent magnet, as well as cardboard and copper foil components. Damadian used this monster to produce a low-resolution image of postdoc Larry Minkoff's chest — which was, indeed, a first. However, many of the financial dividends from Damadian's inventions accrued from patent infringement suits, not from building commercially successful instruments. Lauterbur's and Mansfield's contributions were what ultimately brought the technique to diagnostic practice.

More generally, Meyers uses *Prize Fight* to muse on the obsession with awards and publication in top-flight periodicals, which can ultimately devalue the passion and ingenuity of so many who will never share that limelight. External validation by one's peers is an important, but not the sole, driver of ambition. Taken to pathological extremes, the drive to satisfy this need fuels unethical behaviour and scientific misconduct. Those victimized by it may bear permanent scars or decide to leave science entirely. Milder cases abound. Disagreements and fights over authorship, priority and recognition occur wherever science is practised.

Meyers emphasizes the human nature of scientific pursuit. He reminds us that the individual scientist's contribution is ephemeral: the field moves on. Moreover, every scientist who assembles and leads a team of graduate students, postdocs and technicians has to contend with issues of priority, authorship and, less frequently, assignment of intellectual-property rights. The book has yet to be written that lays out such points of friction for the kinds of research that will never be recognized by the Nobel committee, yet drive entire disciplines relentlessly forward — a category into which most of the science that has a positive impact on society probably falls.

> *"Obsession with awards can devalue the passion and ingenuity of so many who will never share that limelight."*

In the airline industry and medicine, checklists have become an essential step in preventing human error, whether in tightening bolts or measuring drug dosages. In the coda to *Prize Fight*, Meyers provides a checklist of sorts on how to avoid landing oneself in the intellectual and emotional morass that permanently colours the outlook of deserving but unrecognized scientists.

This starts with being aware of the problem, making an effort to be consistent in attribution of authorship, and setting criteria for establishing credit. Easier said than done: these issues are unlikely to disappear any time soon. But we ignore them at the risk of creating toxic working environments. ■

Hidde Ploegh *is professor of biology at the Massachusetts Institute of Technology and the Whitehead Institute for Biomedical Research in Cambridge, Massachusetts.*
e-mail: ploegh@wi.mit.edu

Books in brief

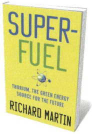

SuperFuel: Thorium, the Green Energy Source for the Future
Richard Martin PALGRAVE MACMILLAN *272 pp. £18.99 (2012)*
Post-Fukushima, uranium-powered plants face being phased out in many countries. But there is a nuclear alternative, argues clean-energy-research analyst Richard Martin: thorium. Less volatile than uranium, four times as abundant, energy-dense and efficient, thorium has major potential, not least because liquid fluoride thorium reactors create no nuclear waste. Martin's investigation reveals how the technology, developed at Oak Ridge National Laboratory in Tennessee, was dropped by President Richard Nixon in 1972 — and how interest is now picking up in China, India and elsewhere.

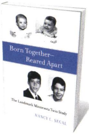

Born Together — Reared Apart
Nancy L. Segal HARVARD UNIVERSITY PRESS *416 pp. £36.95 (2012)*
The 'Jim twins' constituted a watershed in the nature–nurture debate. When Jim Lewis and Jim Springer — twins separated at four months — were reunited at 39, both were found to have loved maths, worked as sheriffs and practised carpentry, among other startling parallels. The case underlined the importance of genetics and led to the Minnesota Study of Twins Reared Apart. In this inclusive overview, Nancy Segal, director of the Twin Studies Center at California State University, Fullerton, examines the study that turned ideas on parenting, teaching, health and sexual orientation upside down.

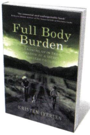

Full Body Burden: Growing Up in the Shadow of a Secret Nuclear Facility
Kristen Iversen HARVILL SECKER *416 pp. £14.99 (2012)*
For years, Kristen Iversen's mother thought that the industrial complex in their small Colorado town manufactured cleaning agents. But this was Rocky Flats — the US government facility where the plutonium 'pits' of nuclear weapons were manufactured. And, as Iversen reveals, it was plagued by safety issues. Among the appalling twists in this tale are high levels of testicular cancer among teenage boys in the area. After an inter-agency raid in 1989, pit production ceased; but Rocky Flats makes for a story with a long half-life.

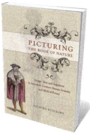

Picturing the Book of Nature: Image, Text, and Argument in Sixteenth-Century Human Anatomy and Medical Botany
Sachiko Kusukawa UNIVERSITY OF CHICAGO PRESS *304 pp. £29 (2012)*
Science historian Sachiko Kusukawa probes the role of illustration in sixteenth-century medical treatises, before the advent of the microscope. Looking at Leonhart Fuch's *De historia stirpium*, Vesalius's *De humani corporis fabrica* and the unpublished *Historia plantarum* of Conrad Gessner, Kusukawa argues that such anatomical and botanic images were not simply records of natural phenomena, but varied visual experiments. His book is studded with illustrative gems, not least John Dee's 'pop-up' pyramids in *Of Euclid's Elements*.

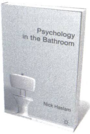

Psychology in the Bathroom
Nick Haslam PALGRAVE MACMILLAN *184 pp. £50 (2012)*
Arcane sexual behaviours are the stuff of cocktail-party chat, whereas the "psychology of flatulence" and incontinence remain taboo. Psychologist Nick Haslam eases open the bathroom door on the many human behaviours associated with excretion. Drawing on clinical research, psychoanalytical theory, language, gender and more, he conducts a fascinating neurogastroenterological journey, from scatological slang and toilet graffiti to the psychological aspects of constipation and diarrhoea. 'Toilet reading' of a high order.

M. GREY/NHPA/PHOTOSHOT

Birds such as golden eagles eat carrion, recycling the nutrients captured during an animal's lifetime.

ANIMAL BEHAVIOUR

Dissecting decay

Clive D. L. Wynne celebrates a lively exploration of the life-and-death cycle in the wild.

Despite focusing on death and decay, *Life Everlasting* is far from morbid; instead, it is life-affirming. Bernd Heinrich, emeritus professor of biology at the University of Vermont in Burlington, does a tremendous job of convincing the reader that physical demise is not an end to life, but an opportunity for renewal.

He was prompted to ponder mortality by an odd request from a friend, who asked if, when he dies, his corpse might be left out for the ravens on Heinrich's land in Maine. That set Heinrich off on a quest to understand the role of death in life. His journey in this book starts and ends in, and often returns to, his beautiful Maine woodland, where nature can be observed at close range, and occasionally friends show up with elderberry wine and guitars.

Heinrich opens with a succession of animal corpses that he watches being buried by beetles, colonized by maggots, hauled off by ravens and vultures, and putrefied by bacteria. He starts small, with a deceased mouse, and proceeds through ever larger bodies: a freshly killed squirrel, a rooster, deer and pig, and finally a massive bull moose. Most of these he places so that he can watch their decay comfortably from a chair in his cabin. Each corpse provides opportunities to describe, in loving detail, the life that death provides.

Beetles with beautiful wings use the dead mouse as a romantic meeting place. Having found each other, they carry the carcass to a safe place for burial. The female lays her eggs in soil close by. When the larvae hatch, the parents feed them regurgitated food from the corpse, staving off decay with antibiotic anal secretions.

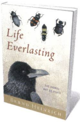

Life Everlasting: The Animal Way of Death
BERND HEINRICH
Houghton Mifflin Harcourt: 2012.
256 pp. £15.99/$25

Maggots prefer the deer carcass. Being larger, it stays warm for longer and encourages bacteria, whose "soupy by-products" provide sustenance for maggots. The maggots quickly colonize the corpse, and, because of their high metabolic rates, actually raise the temperature inside it and accelerate their own growth rate, creating a frenzied positive-feedback loop.

Looking at marine life, Heinrich contemplates the death of salmon and the dismantling of whales. When a whale carcass comes to rest on the ocean floor, it may be kilometres deep, in total darkness and at temperatures very close to freezing. Nonetheless, there is no shortage of specialist scavengers even in these extreme conditions, including sleeper sharks, hagfish and a wealth of tiny crustaceans.

Heinrich also reminisces about his time in Africa during the 1970s. In these time travels he considers the biggest of land beasts — the elephant. This animal's death brings humans into the picture: Heinrich argues that our ancestors were to elephants "what the sleeper sharks and hagfish are to the whales of the ocean depths: the ultimate recyclers".

Discussion of starving people in Zimbabwe today hacking at an elephant carcass segues into consideration of how early humans would have had to learn to cooperate to bring down mammoths, armed only with sharpened sticks and stones. Heinrich suggests that learning to process elephant meat taught us so much that tackling any other animal left us unfazed. He even details the decomposition of elephant dung, recounting with relish the time he watched half a litre of it be colonized by some 3,800 beetles in just 15 minutes.

Heinrich also considers the death of plants. When a tree falls in the forest and no one is around to take the wood away, what becomes of all that timber? In a gripping section on "plant undertakers", he considers how dead plants are broken down and the nutrients captured during their lives recycled. This process is led by sawyer beetles, jewel beetles and bark beetles, followed by horntail wasps, countless other beetles, fungi, birds such as woodpeckers, centipedes, millipedes and, if the tree falls into water, fish. Even other trees may use a rotting log as a base from which to grow.

Heinrich argues passionately that we cannot and should not fight the return of life to life through death. Death is the ultimate recycler. In the United States, most people choose to have their corpse either pumped with toxic formaldehyde and sealed in a steel box, or incinerated. The incineration of bodies in the United States burns enough fuel each year to power 80 trips to the Moon. In this way, we perpetuate in death the exclusion of ourselves from the natural world that many of us also proclaim in life.

Extinction, not death, is the real problem. Heinrich notes that unloved "undertaker" species such as ravens, vultures and condors are especially vulnerable to humans' effects on ecosystems. The largest cause of loss for such species is the complete replacement of large wild animals with farming activities that displace habitat and take away carcasses that nature would have left to return to the earth.

Ultimately, Heinrich is unable to indulge his friend's desire for a "green burial". In the United States, the movement and disposal of dead bodies is tightly bound by legal restrictions. He succeeds, however, in a larger aim. He replaces the inanimate biblical bookends to our lives, 'dust to dust', with what we really are at death: conduits for life. If nature has its way, the real progression is 'life to life'. ■

Clive Wynne *is a professor of psychology at the University of Florida, Gainesville, Florida 32611, USA.*
e-mail: wynne@ufl.edu

MATHEMATICS

A life computed

James Poskett navigates a sophisticated account of Alan Turing's extraordinarily varied intellectual world.

Alan Turing did not invent the computer. During the 1930s, well before the Manchester 'Baby', Pilot ACE or EDVAC machines, thousands were in operation all across Britain. These 'computers' were women, working in teams and each performing a discrete step of a complex mathematical operation.

Employed by the Scientific Computing Service (SCS) in the United Kingdom, these doughty women solved problems in everything from X-ray crystallography to jet-engine design. That world of 'computers before computers' is featured in the opening gallery of *Codebreaker*, the celebration of mathematician Alan Turing's life and legacy at London's Science Museum.

Although the SCS may seem far removed from Turing's world, knowledge of its work can help us to make sense of his seminal 1936 article 'On computable numbers, with an application to the *Entscheidungsproblem*'. This is viewed by some as the origin of the concepts behind the modern computer. But the real story is more complex.

Turing didn't pluck the idea of the modern computer out of thin air. He took the idea of a team of human computers working together and abstracted it, imagining a universal computing machine that could take on all of the individual tasks allocated to the women in the SCS. This was merely a thought experiment for him at first — an aid for approaching David Hilbert's notorious 'decision problem' on the question of whether an algorithm exists for deciding if a given mathematical statement has a proof or not.

Codebreaker — Alan Turing's life and legacy
The Science Museum, London
(21 June 2012–31 July 2013)

Interestingly, although sometimes armed with little more than a pencil and slide rule, the women working for the SCS also used basic calculating machines — one of which sits in the first room of *Codebreaker*. These typewriter-like contraptions, covered in strips of red and white buttons, helped to speed up ballistics calculations crucial to the war effort.

The parade of objects that follows reveals Turing's impact, as well as his influences, leading the visitor through a vast intellectual landscape, from aeronautical design and biochemistry to cryptography and artificial intelligence.

In one gallery, a German Enigma machine, tucked into its neat wooden case, sits among archival photos that evoke the atmosphere of Second World War intelligence. Turing is well known to have worked in wartime cryptanalysis at the Government Code & Cipher School at Bletchley Park, UK. But he did not operate in isolation, collaborating with Gordon Welchman on the design of the electromechanical machines used to crack the code. These devices, each of which could mimic the action of several Enigma machines, in turn originated in the earlier work of Polish cryptanalysts such as Marian Rejewski.

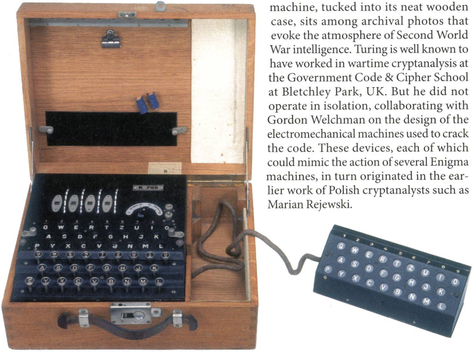

Alan Turing worked on devices to crack the German Enigma machine's code during the Second World War.

SCIENCE & SOCIETY PICTURE LIBRARY

In a nearby gallery, a twisted white metal fuselage serves as a poignant reminder of the part Turing's ideas played in developing safer air travel after the war. In 1954, the world's first commercial jet airliner, the de Havilland Comet registered 'Yoke Peter', exploded in mid-air, killing everyone on board — and prompted the Royal Aircraft Establishment at Farnborough, UK, to find the cause.

By this time, Turing's abstract idea of a universal computing machine had become a reality. The National Physical Laboratory in Teddington, UK, had in 1950 completed the Pilot ACE, an electronic computer designed to one of Turing's first practical specifications. For a short time, this computer was the fastest in the world. The huge rack of wires, relays and coloured transistors is displayed alongside the Yoke Peter wreckage. It helped to process the enormous amounts of data needed to complete detailed analysis of the debris, eventually revealing the point of structural weakness and prompting improvements in the design and manufacture of de Havilland jets.

The exhibition also explores links between the Pilot ACE and Dorothy Hodgkin's work on the structure of vitamin B_{12}. One of her original models of the vitamin, an intricate web of more than 100 red and blue balls, is on show next to the story of her use of computers. Cryptography and X-ray crystallography had much in common at this time: each involved recovering information from a scrambled signal.

Hodgkin's problem was that the images she produced indicated only the amplitudes of the diffracted waves. To establish the correct structure of a molecule, she needed to churn through an enormous number of possible permutations of different wave phases. So she enlisted the help of both the SCS and the Pilot ACE, going on to win the Nobel Prize in Chemistry for her work in 1964.

Turing's relationships with artificial intelligence and developmental biology are also on show through video interviews with contemporary mathematical biologists run next to programmable robotic tortoises. Although Turing didn't work on these machines himself, he was fascinated by the possibility of an artificial mind, coming to London especially to see robots such as these scurry across the floor at the Festival of Britain in 1951.

Codebreaker does an impressive job of bringing these diverse histories together. Turing is rightly celebrated, not as a lone genius, but as an impressive intellect and brilliant collaborator. ■

James Poskett *is a science writer based in Cambridge, UK, specializing in the history and philosophy of science.*
e-mail: james.poskett@cantab.net

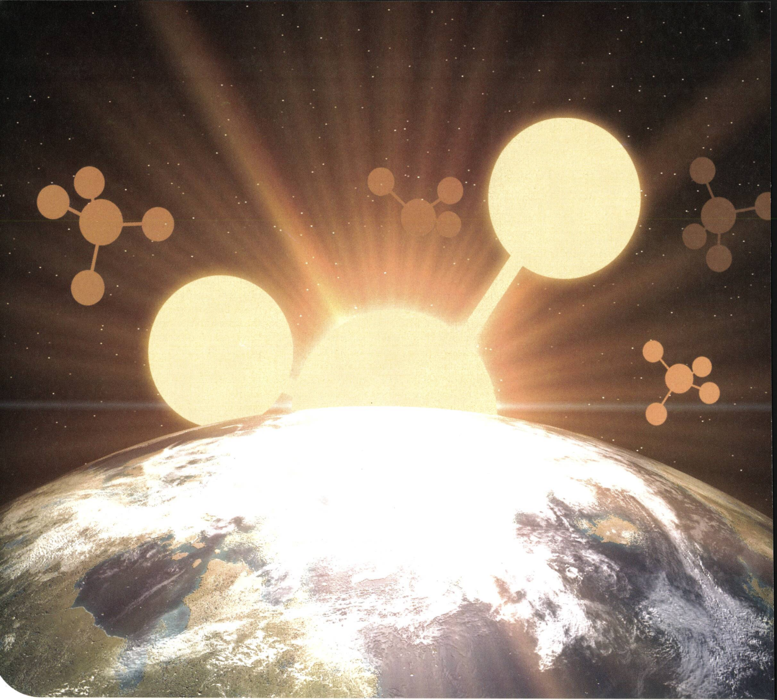

Experience makes a world of difference.

Ash Stevens has provided the industry with contract pharmaceutical manufacturing services for 50 years. This experience includes multiple FDA Fast-Track and Highly Potent API manufacturing approvals.

- Process research, development, and scale-up
- Early-stage to commercial API manufacturing
- Highly potent drug substance development and cGMP manufacturing
- Analytical development and validation
- Comprehensive regulatory support

To see how Ash Stevens can help your drug development program succeed, call or click today.

734-282-3370 ashstevens.com

Ash Stevens®

Correspondence

More ways to govern geoengineering

You call for stronger governance of climate-mitigation strategies that reflect the Sun's energy away from Earth (*Nature* **485,** 415; 2012). We see the scientists' cancellation of a controversial field trial for the UK Stratospheric Particle Injection for Climate Engineering (SPICE) project (*Nature* **485,** 429; 2012) as responsible self-governance in the absence of the governmental oversight that is needed for solar geoengineering research.

The decision to cancel the SPICE balloon experiment can advance norms for research priorities and conditions of research. The underlying governance principles have been articulated by the Bipartisan Policy Center's Task Force on Climate Remediation Research and the Solar Radiation Management Governance Initiative (SRMGI), sponsored by the UK Royal Society, the Environmental Defense Fund and the Academy of Sciences for the Developing World (TWAS).

On the basis of the SPICE example, scientists can now decide — through projects, workshops and professional societies — that there should be no immediate research into deployment methods for geoengineering technologies, and that they will not engage in research that has intellectual-property implications. They can also learn from SPICE about public engagement and ways to make research transparent.

Eventually, legitimate governance must grow out of consultations with diverse constituencies (such as those sponsored by the SRMGI) and needs to come from governmental institutions that are fully accountable to society.

Jane C. S. Long *The Bipartisan Policy Center, Washington DC, USA. janecslong@gmail.com*
Steve Hamburg *Environmental Defense Fund, Washington DC, USA.*
John Shepherd *University of Southampton, UK.*

Use fast reactors to burn plutonium

Frank von Hippel and colleagues review some disposal options for radioactive plutonium waste (*Nature* **485,** 167–168; 2012). Another option is the profitable consumption of plutonium from thermal nuclear plants in a fast-spectrum breeder reactor with fuel recycling.

A prototype Integral Fast Reactor was operated at the Argonne West National Laboratory in Idaho for 30 years until 1994. 'Burning' spent nuclear fuel produces a fraction of the waste of current reactors, and it has low radiotoxicity (W. H. Hannum (ed.) *Prog. Nucl. Energy* **31,** 1–217; 1997).

The reactor's metal fuel (mainly uranium, plutonium and zirconium) and liquid-sodium coolant provide passive safety. An unpressurized pool vessel disperses decay heat by natural convection, even when cooling pumps are inoperable and the heat sink is lost.

The fuel-recycling system generates vast amounts of clean electricity, extending uranium supplies 150-fold — unlike today's once-through-and-throw-away cycle. Its proliferation risk is low because the products are unsuitable for use in fissile weapons.

The company GE Hitachi has designed an integral fast reactor, the 311-megawatt electric Power Reactor Innovative Small Module (PRISM), that is intended for commercial use. A prototype plant is already being considered in the United States, and the company has recommended these plants to the UK government for plutonium disposal (see go.nature.com/dwiqvg).

Barry W. Brook *University of Adelaide, Australia. barry.brook@adelaide.edu.au*
Tom Blees, William H. Hannum *Science Council for Global Initiatives, Woodland, California, USA.*

Spread the risk of antibiotic research

There are commercial as well as scientific barriers to seeking out new antibiotics (*Nature* **485,** 439–440; 2012). These discourage the pharmaceutical industry from investing in further research and clinical development, particularly as current antibiotics are cheap, usually work satisfactorily and generate profits for their manufacturers and distributors.

Producing new antibiotics is costly, particularly at the clinical-trial stage because of concerns over safety and resistance. Intellectual property is an issue in developing new drugs based on established antibiotic classes.

We could wait until the clinical situation becomes severe enough for the private sector to step in with substantial investment, but that would be risky. A mix of private and public investment might work, particularly if the public sector were to take on some of the commercial risk in clinical trials (see *Nature* **472,** 32; 2011). A pragmatic strategy would be to define the clinical profiles of desirable new antibiotics and then to devise commercially viable routes for delivering them to the clinic.

Chris Schofield *University of Oxford, UK. christopher.schofield@chem.ox.ac.uk*

Monitor sea pollution to stop strandings

Hundreds of small cetaceans were stranded along Peru's northern coast earlier this year. While the event is under investigation, Peru's government should be setting up programmes to monitor marine pollution and taking precautions to protect the coastal ecosystem.

The dead animals comprised mainly long-beaked common dolphins (*Delphinus capensis*) and Burmeister's porpoises (*Phocoena spinipinnis*). They had internal trauma and lesions that could have been caused by underwater noise effects (see go.nature.com/tbfi7n). Although military sonar is known to induce cetacean strandings, no naval exercises had been reported in the area. Neither had there been any seismic testing associated with gas and oil exploration, which can also be a contributor.

Persistent pollutants that accumulate in cetaceans could be a factor. These weaken cetacean immune systems, making them more susceptible to infection (P. Ross *Hum. Ecol. Risk Assess.* **8,** 277–292; 2002), exacerbated by food shortages during El Niño episodes and harmful algal blooms.

Juan Jose Alava *Simon Fraser University, Burnaby, Canada. jalavasa@sfu.ca*

China must provide education on HIV

Cultural factors spanning 5,000 years force homosexual men in China to endure huge psychological and social pressures (H. Shang *et al. Nature* **485,** 576–577; 2012). Government authorities need to face up to reality and promote HIV research and public education about transmission of the virus to curb its spread.

Alongside the promotion campaigns of World AIDS Day, China should provide more ways to access up-to-date information on prevention and treatment of HIV infection. Infected people also need proper medical assistance, legal safeguards and humane care.

Jian Zhang, Nan Jiang *South China University of Technology, Guangzhou, China. zhangjian3954@126.com*

Akira Tonomura

(1942–2012)

Physicist who pioneered electron holography.

Akira Tonomura changed the field of fundamental physics through microscopy. Like botanist Robert Brown before him, he opened up a new world to observation. In the nineteenth century, Brown's microscope revealed Brownian motion and the cell nucleus. In the twentieth and twenty-first, Tonomura's has shown us basic principles of the quantum landscape and its applications.

Over decades, Tonomura developed the extremely stable, phase-coherent electron beams needed for good holographic imaging, a technique that enables measurement of both the intensity and the phase of transmitted electrons. This allowed many 'thought experiments' of quantum mechanics to be done in practice, and revealed details of magnetic and electric fields at the nanoscale. Tonomura used electron holography to illuminate the wave–particle duality of electrons and to measure the magnetic fields of superconductors and other quantum effects under challenging conditions, earning him heroic status among electron microscopists. His achievements meant he was tipped several times for a Nobel prize. He died of pancreatic cancer in early May, at the age of 70.

Tonomura spent some of his early childhood in Hiroshima, Japan. Fortunately, his family moved away from the city two months before the fateful morning in early August 1945 when the nuclear bomb was dropped. Soon after graduating in physics from the University of Tokyo in 1965, Tonomura joined the central research laboratory of the Hitachi Corporation in Tokyo and, with crucial encouragement from the distinguished electron microscopist Hiroshi Watanabe, began his long career.

At that time, physicist Dennis Gabor, working at the engineering company British Thomson-Houston, based in London, had already proposed the idea of using holography to increase the resolution of electron microscopes, and the technique had passed some feasibility tests. The most immediate and spectacular applications of holography were in the field of light optics, in which it was used to create stunning three-dimensional images. This led to a Nobel prize for Gabor. Electron holography could advance no further until the invention of the electron biprism (a positively charged filament that causes the electron paths on either side of it to cross) by Gottfried Möllenstedt at the University of Tübingen in Germany, where Tonomura worked briefly in 1973–4. Using this technology, Tonomura created the first practical electron holography microscope for Hitachi in 1978.

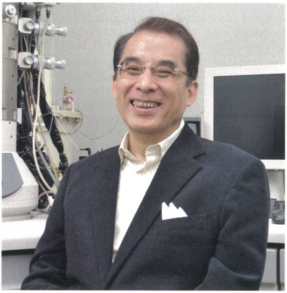

RIKEN

Tonomura's microscope proved crucial in settling a controversy over a bizarre quantum phenomenon. The Aharonov–Bohm (A–B) effect states that the phase of an electron's wavefunction can be shifted by a nearby magnetic field, even if the electron doesn't pass through that field. This idea sits uneasily with the classical theories that were used to develop practical electron optics. Early experiments hinted at confirmation of the A–B effect, but critics argued that stray fields might have caused the observed phase shift. So Tonomura placed a ring magnet inside a superconducting sheath to eliminate any stray magnetic fields, and encased that within a copper layer to stop a passing electron beam from entering the magnetic field region. He then used electron holography to confirm the predicted phase shift between electron paths inside and outside the ring. This conclusive and elegant experiment of 1986 finally silenced the critics, and was immediately recognized beyond the world of electron microscopy as a remarkable tour de force.

Few electron holography microscopes outpaced the resolution of ordinary electron microscopes as Gabor had envisaged, but Tonomura's use of holography to detect electron phases allowed him to pioneer and dominate the technique's practical application. In 1989, he scored a major success by imaging a magnetic vortex emerging from a superconducting film, and built on that with observations of vortices in various metallic and ceramic superconductors. Tonomura and others mapped magnetic fields in small particles, in magnetic tape and, most recently, in the skyrmion lattice — a periodic arrangement of magnetic vortices generated by a complex structure of electron spins. In quantum computing, observations of superconducting vortices are key to investigating the behaviour of these potential 'qubits'.

Tonomura combined stubborn persistence and experimental skill with imagination and excellent communication skills. He presented material with scrupulous care in publications and seminars. In a memorable Royal Institution lecture in 1994, he filled the strictly allotted one-hour time slot almost to the second. His images of magnetic phenomena were so striking that they were often on the cover of major journals. An Internet video of his version of the classic 'double-slit experiment' continues to demonstrate for many the central mystery of quantum mechanics (see go.nature.com/722hph). It shows how electrons travelling through a biprism arrive at a detector one by one, as particles, but over time build up a wave interference pattern.

Tonomura's stellar reputation and powers of persuasion helped to secure financial support from the Japanese government for his ambitious ideas. In 2010, he was awarded the largest grant for an individual research project in the country's history (see *Nature* **464,** 966–967; 2010). He became seriously ill a year later. In the spirit of Gabor's original idea for boosting resolution, the project aims to use high-voltage electron holography to create 3D images of electron wavefunctions. Its future now depends on securing a leader as inspiring as Akira Tonomura. ■

Archie Howie *is a physicist and electron microscopist in the Cavendish Laboratory, University of Cambridge, UK.*
e-mail: ah30@cam.ac.uk

nature OUTLOOK

Produced with support from:

Eat Well, Live Well.
AJINOMOTO®

Making sense of flavour

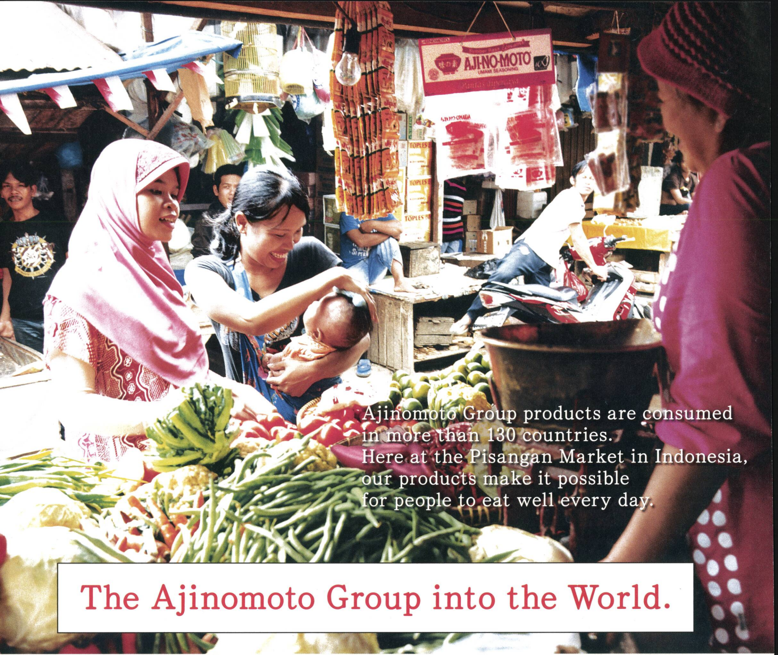

Ajinomoto Group products are consumed
in more than 130 countries.
Here at the Pisangan Market in Indonesia,
our products make it possible
for people to eat well every day.

The Ajinomoto Group into the World.

We all know that food is essential for life. But at the Ajinomoto Group we believe that eating well leads to a healthier life – it is the belief we were founded on, and one that continues to be proven true daily. Every day in more than 130 countries around the globe people use our seasonings, beverages, amino acids and other products to bring out the essential taste inherent in the food they eat. And every day we work hard to bring out the enjoyment of eating for people everywhere. It is precisely because we know that good food is basic to human life that the entire Ajinomoto Group is committed to constantly striving for the food, health, and life of this planet. This is a pledge we make now and for the future.

In the Hoc Mon market in Vietnam, foods featuring our products draw people closer together.

We aim to be "a group of companies that contributes to human health globally".

Eat Well, Live Well.
AJINOMOTO®

http://www.ajinomoto.com/

nature OUTLOOK

TASTE

21 June 2012 / Vol 486 / Issue No 7403

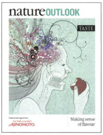

Cover art: Nik Spencer

Editorial
Herb Brody,
Michelle Grayson,
Tony Scully,
Nick Haines

Art & Design
Wes Fernandes,
Nicola Hawes,
Alisdair Macdonald,
Andrea Duffy

Production
Karl Smart,
Susan Gray,
Leonora Dawson-Bowling

Sponsorship
Yuki Fujiwara,
Yvette Smith,
Gerard Preston

Marketing
Elena Woodstock,
Hannah Phipps

Project Manager
Christian Manco

Art Director
Kelly Buckheit Krause

Magazine Editor
Tim Appenzeller

Editor-in-Chief
Philip Campbell

Taste is more than a sensual experience: it is a signal of nutritional value or danger. It has evolved as a vital survival mechanism in mammals (see page S16) and driven epic periods of human history — it was, after all, the quest for spices that helped launch the age of exploration. Yet our understanding of how taste works has lagged behind the other senses.

In the past decade or so, taste science has been on a roll. In 2000, researchers used the newly available human genome data to help identify the receptors that respond to bitterness (S2). Since then, the receptors for sweet, salty, sour and umami (savoury) have also been identified. The exclusive club of basic tastes might be about to admit new members: carbonation, metallic and fattiness.

What's more, taste is revealed to be a whole-body experience; taste receptors are found in the gut, the airways and even on sperm (S7), but the function of many of these sensors remains unclear.

The centrality of flavour to human culture has driven scientists, chefs and the food industry to experiment with new ways of producing familiar and novel tastes (S14) as well as to create a scientific style of experimental cooking (S10). And while the link between smell and taste is well known, studies are showing that the way we experience food is influenced by all five senses (S4). Individual variation in taste tolerances might help explain why some people tend to be obese (S12), although scientists still struggle with the question of whether taste is an inherent attribute of food or a personal psychological construct (S6). However, while much of taste is subjective, tasting technologies aim to define our eating and drinking experiences with machine-like consistency (S18).

We acknowledge the financial support of Ajinomoto Co., Inc. in producing this Outlook. As always, *Nature* has full responsibility for all editorial content.

Herb Brody
Supplements Editor

CONTENTS

S2 GUSTATORY SYSTEM
The finer points of taste
From tongue to brain

S4 SENSORY SCIENCE
Partners in flavour
There's more to tasting than the tongue

S6 PERSPECTIVE
Complexities of flavour
Barry Smith sorts the intrinsic from the subjective

S7 NEUROSCIENCE
Hardwired for taste
What are taste receptors doing throughout the human body?

S10 COOKING
Delicious science
Chef scientists are serving up some stimulating dishes

S12 OBESITY
Insensitive issue
Are some people born preferring fatty foods?

S14 FOOD SCIENCE
Taste bud hackers
Ingenious ways to trick people into liking healthier foods

S16 EVOLUTIONARY BIOLOGY
The lost appetites
What taste sweet to one species is bland to another

S18 TECHNOLOGY
The taste of things to come
Artificial tongues take a sip

Nature Outlooks are sponsored supplements that aim to stimulate interest and debate around a subject of interest to the sponsor, while satisfying the editorial values of *Nature* and our readers' expectations. The boundaries of sponsor involvement are clearly delineated in the Nature Outlook Editorial guidelines available at http://www.nature.com/advertising/resources/pdf/outlook_guidelines.pdf

CITING THE OUTLOOK
Cite as a supplement to *Nature*, for example, *Nature* **Vol XXX**, No. XXXX Suppl, Sxx–Sxx (2012).

VISIT THE OUTLOOK ONLINE
The *Nature Outlook Taste* supplement can be found at http://www.nature.com/nature/outlook/taste It features all newly commissioned content as well as a selection of relevant previously published material.

All featured articles will be freely available for 6 months.

SUBSCRIPTIONS AND CUSTOMER SERVICES
For UK/Europe (excluding Japan): Nature Publishing Group, Subscriptions, Brunel Road, Basingstoke, Hants, RG21 6XS, UK. Tel: +44 (0) 1256 329242. Subscriptions and customer services for Americas – including Canada, Latin America and the Caribbean: Nature Publishing Group, 75 Varick St, 9th floor, New York, NY 10013-1917, USA. Tel: +1 866 363 7860 (US/Canada) or +1 212 726 9223 (outside US/Canada). Japan/China/Korea:Nature Publishing Group — Asia-Pacific, Chiyoda Building 5-6th Floor, 2-37 Ichigaya Tamachi, Shinjuku-ku, Tokyo, 162-0843, Japan. Tel: +81 3 3267 8751.

CUSTOMER SERVICES
Feedback@nature.com

Copyright © 2012 Nature Publishing Group

GUSTATORY SYSTEM

The finer points of taste

As more receptors are defined, researchers will further unlock the mechanics of taste. How the mind perceives these sensory signals is another matter.

BY BIJAL P. TRIVEDI

Take a sip of milk, look in the mirror and stick out your tongue. The tiny pink bumps emerging from the creamy film coating your tongue are the mushroom-shaped, or fungiform, papillae that conceal many of your taste buds. These are the gateway to detecting the sweetness of a cake, the saltiness of a potato crisp, the meatiness of a steak, the bitterness of beer, and the sourness of a lemon.

The four types of papillae that speckle the tongue **(see 'Taste discovery')** give it a rough surface that helps move the food around as we chew. The filiform papillae simply detect texture, whereas the other three — fungiform, foliate and circumvallate — contain onion-shaped taste buds. Each taste bud is packed with taste cells, which are capped with sensors for the five basic tastes (although we may be able to detect other taste qualities too). Contrary to popular belief, every part of the tongue is sensitive to all five taste qualities — the once common 'tongue map' depicting specific regions for each taste was based on a misunderstanding in the early 1900s and is wrong.

In 1931, Arthur Fox, a chemist at US chemical giant DuPont, made a remarkable discovery after accidentally releasing a cloud of fine phenylthiocarbamide (PTC) crystals while transferring the powder to a bottle. A colleague commented that the compound tasted bitter, but Fox, in the midst of the powder cloud, tasted nothing. After testing friends, family and colleagues, Fox found that people are either 'tasters' or 'non-tasters' of PTC (ref. 1). Geneticist L. H. Snyder confirmed Fox's work and found that non-tasting is a recessive Mendelian trait. Later work uncovered a range of PTC sensitivity, suggesting the involvement of more than one gene in perceiving this bitter compound[2].

TASTE TRANSDUCER

It took almost seven decades to pinpoint the genes that encode taste receptors. It was widely believed that each taste cell carried sensors for several, if not all, of the five tastes, with the signals being decoded in the brain. But this made no sense to neuroscientist Charles Zuker, a Howard Hughes Medical Investigator now at Columbia University in New York. He couldn't understand why a cell could carry sensors for both sweet, signalling an energy-rich food, and bitter, which could warn of spoiled or toxic food — a mix-up could be lethal.

➲ NATURE.COM
Why do things taste differently to different people?
go.nature.com/ybgmay

Zuker rejected this 'broad tuning' and assumed that the difference between a sweet and a bitter taste cell, for example, was the collection of receptors on its surface. He joined forces with geneticist Nicholas Ryba of the National Institute of Dental and Craniofacial Research in Bethesda, Maryland, and over the next 12 years they sought to discover the sensors for all five tastes **(see 'Taste discovery')**.

In 2000, using the first draft of the human genome, Zuker and Ryba's team identified the first taste sensors: a family of G-protein-coupled receptors (GPCRs)[3] on chromosome 5. These so-called Taste-2 receptors (T2Rs) can detect bitter tastes from a wide range of different chemical compounds, requiring a collection of sensors. Some T2Rs can detect only one bitter compound, but some can respond to more than 50 natural and synthetic bitter chemicals.

More than five teams were competing to find the sweet receptor.

Each bitter taste cell carries from 4–11 T2Rs — this variety, along with underlying genetic variation, is thought to account for an individual's tolerance of bitter tastes. For example, variation in the gene encoding T2R38 modifies sensitivity to PTC, which correlates with sensitivity to bitter compounds in cabbage or Brussels sprouts[4].

The race was on to find the remaining taste receptors. In 2001, more than five teams were competing to find the sweet receptor and narrowed the candidates to a different family of GPCRs. These T1R receptors have a different structure from the T2Rs, including a bulky extracellular region that interacts with sweet molecules. Zuker and Ryba provided the decisive evidence by transforming a sweet-insensitive mouse into a sugar-loving one, showing that T1R2 and T1R3 combine to detect natural and artificial sweeteners[5]. Barely a year later, they also found that the combination of T1R1 and T1R3 receptors can detect all 20 amino acids found in nature[6], sensing a taste described as umami or savoury (for example, in meat or cheese) that can be chemically distilled into the common food additive monosodium glutamate. The receptors for sweet, bitter and umami all use essentially the same signalling molecules to convey nutrient sensing to the brain.

SOUR SUCCESS

In 2006, Zuker and Ryba discovered the PKD2L1 receptor[7], which detects sourness — a high concentration of hydrogen ions, or acidity, found both unripe and spoiled foods. Sour taste cells also host the Car4 receptor[8], which senses carbon dioxide — block this receptor and a carbonated beverage will taste flat (even though it might still feel bubbly). Finally, in 2010, Zuker and Ryba found that the epithelial sodium channel (ENaC) detects sodium salt[9] (other salts, such as potassium chloride, probably have other receptors). Instead of GPCRs, salt and sour detection uses ion channels — proteins that shuttle sodium and hydrogen ions in and out of cells.

Five basic tastes are generally recognized but there may be others, and the hunt for receptors continues. In 2003, neuroscientist Robert Margolskee, then at the Mount Sinai School of Medicine in New York, showed that mice lacking the T1R3 receptor couldn't taste artificial sweeteners but still had an affinity for sugars, especially glucose, and could also perceive umami[10]. "It said very clearly to us there are two different sweet mechanisms," he says.

But receptors don't tell the whole taste story. Zuker and Ryba are using the taste sensors already discovered to figure out, as Zuker says, "how the brain transforms detection into perception". ■

Bijal P. Trivedi *is a freelance science writer based in Washington, DC.*

1. Fox, A. L. *Science* **73**, 14 (1931).
2. Snyder, L. H. Science **74**, 151–152 (1931)
3 Chandrashekar, J. *et al. Cell* **100**, 703–711 (2000).
4. Boyd, W. C. *Science* **112**, 153 (1950).
5. Nelson, G. *et al. Cell* **106**, 381–390 (2001).
6. Nelson G. *et al. Nature* **416**, 199–202 (2002).
7. Huang, A. L. *et al. Nature* **442**, 934–938 (2006).
8. Chandrashekar J. *et al. Science* **326**, 443–445 (2009).
9. Chandrashekar, J. *et al. Nature* **464**, 297–301 (2010).
10. Damak, S. *et al. Science* **301**, 850–853 (2003).
11. Blakeslee, A. F. & A. L. Fox. *J. Hered.* **23**, 97–107 (1932).
12. Fisher, R. A. *et al. Nature* **144**, 750 (1939).
13. McLaughlin, S. K. *et al. Nature* **357**, 563–569 (1992).
14. Wu, S. V. *et al. Proc. Natl Acad. Sci. USA* **99**, 2392–2397 (2002).
15. Dyer, J. *et al. Biochem. Soc.* **33**, 302–305 (2005).

TASTE DISCOVERY

Study of the basic tastes, and how these are detected by the tongue, is an evolving field.

ORGAN

The tongue contains four types of papillae. Circumvallate, fungiform and foliate papillae contain taste buds, whereas filiform papillae detect only the texture of food.

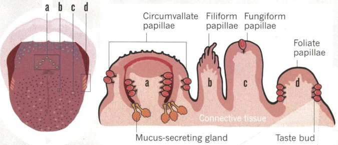
a
b
c
d
Circumvallate papillae
Filiform papillae
Fungiform papillae
Foliate papillae
a
b
c
d
Connective tissue
Mucus-secreting gland
Taste bud

CELLS

Each taste bud is an onion-like structure packed with 50 to 100 taste cells, anatomically classified into four types. Type II cells contain receptors for sweet, bitter, umami and possibly salty tastes; type III for sour; type I are probably supporting cells. Type IV are suspected to be stem cells that supply new taste cells every two weeks.

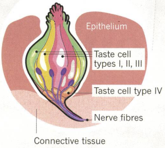
Epithelium
Taste cell types I, II, III
Taste cell type IV
Nerve fibres
Connective tissue

RECEPTORS

Sweet, umami and bitter receptors belong to the superfamily of G-protein coupled receptors. ENaC, the receptor for sodium-salt taste, is an ion channel. Less is known about PKD2L1, but taste cells expressing it respond to the presence of protons (H^+), a breakdown product from acids.

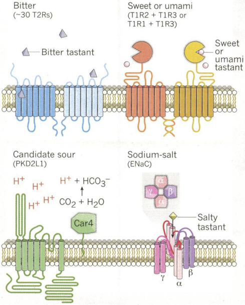
Bitter
(~30 T2Rs)
Bitter tastant
Sweet or umami
(T1R2 + T1R3 or T1R1 + T1R3)
Sweet or umami tastant
Candidate sour
(PKD2L1)
H^+ H^+ $H^+ + HCO_3^-$
H^+ H^+ $CO_2 + H_2O$
Car4
Sodium-salt
(ENaC)
α
γ
β
α
Salty tastant
γ
α
β

MARTIN HARVEY/GETTY IMAGES

350 BC
1900
1910
1920
1930
1940
1950
1960
1970
1980
1990
2000
2010

350 BC

Aristotle writes about the basic tastes, sweet and bitter, which can be modified, he says, by salty and acidic.

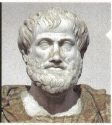

1901

D. Hänig publishes a paper containing data on taste sensitivity in different regions of the tongue. The data are later misinterpreted, giving rise to the myth of the 'tongue map'.

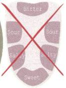
Bitter
Sour
Sour
Salty
Salty
Sweet

1908

Fifth basic taste discovered: savoriness, described as umami, which is conferred by glutamate.

1931–1932

Geneticists confirm findings about sensitivity to bitter tasting PTC and discover non-tasting is a recessive genetic trait [2,11].

1931

Bitter taste sensitivity found to vary among humans[1].

1939

Geneticists show that chimpanzees, like humans, vary in their ability to perceive the bitterness of PTC (see 'The lost appetites', page S16).

1992

Discovery of gustducin, a taste cell-specific G-protein, in the taste buds. Gustducin is later shown to mark bitter, umami and sweet cells[13].

2000 / BITTER

First taste sensors, the T2R bitter receptors, discovered[3].

2001 / SWEET

The sweet receptor is discovered[5]: a combination of T1R2 + T1R3.

2002 / UMAMI

Amino acid detector, T1R1 + T1R3, identified[6].

2006 / SOUR

Cells for sour taste discovered, identified by PKD2L1 (refs 4–7).

2010 / SALTY

ENaC identified as the sodium-salt taste receptor[9].

2002

Bitter taste receptors found[14] in the gastrointestinal tract.

2005

Sweet taste receptor found[15] in the gastro-intestinal tract.

2009

The Car4 receptor, which senses the carbon dioxide in fizzy drinks, is found on sour cells[8].

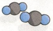

A. INDEN/ CORBIS

SENSORY SCIENCE

Partners in flavour

Our perception of food draws on a combination of taste, smell, feel, sight and sound.

BY NICHOLAS BAKALAR

The way we experience food is not limited to the mouth — odour, vision, hearing and even touch can radically change the taste of food or affect food preference. And it all starts before birth.

Amniotic fluid, the baby's first food, contains glucose, fructose, fatty acids and amino acids, and newborns are born preferring the sweet taste of mother's milk to other flavours. Since the 1970s, researchers have known that the introduction of sweet solutions into the amniotic fluid causes the fetus to swallow more frequently, whereas bitter solutions reduce the rate of swallowing. Similar reactions are seen in babies: they lick their lips and smile when tasting something sweet, and wrinkle their noses and flail their arms in response to a bitter or sour taste, precisely the tastes that warn us to avoid poisons. "A taste for sugar is innate," says Julie Mennella, a biopsychologist at the Monell Chemical Senses Center in Philadelphia, Pennsylvania.

But even in the womb, new tastes can be introduced. The odour of garlic, for example, can be detected in samples of amniotic fluid from women who have eaten garlic pills 45 minutes before. And babies exposed to garlic *in utero* are more apt to like the flavour of garlic in the milk of garlic-eating mothers.

To some extent, a mother can influence her baby's tastes by what she eats during pregnancy and nursing. In one study, babies of mothers who ate more fruit during lactation were more likely to accept peaches than babies fed on formula — but the mothers' consumption of string beans did not have the same effect[1]. The taste for salt, however, is apparently acquired only with age. Babies younger than four months are happy to drink either plain water or water with moderate concentrations of salt, but by the time they are two-and-a-half years old they show a marked preference for salty water.

Researchers have found evidence that pregnant women who consume certain foods — so far they have tested anise, carrot, mint, vanilla and blue cheese — convey a liking for those tastes to their infants[2]. There's a good species-preserving rationale for this behaviour, says Gary Beauchamp, also at the Monell centre: "When a baby begins to eat solid food, the most logical and safest things for it to eat are what its mother ate." Indeed, he adds, this phenomenon suggests a strategy for improving the population's diet generally: "Exposing infants prenatally and postnatally to the flavours of things that people aren't consuming enough of could be a good thing to do."

A SENSORY MILIEU

When taste signals are received, various neural pathways go into action: saliva production increases and stomach secretions are activated. But these pathways do not require food to be in the mouth. The sound of dishes rattling in the kitchen or a picture of a lobster dinner can make the stomach rumble.

Vision provides an essential sensory input for food perception, raising expectations and driving preferences. We unconsciously discriminate between high-calorie and low-calorie foods by sight alone. Kathrin Ohla, a psychologist at

➲ NATURE.COM
The neuroscience of scent and sensibility:
go.nature.com/4nrqbn

the Monell centre, demonstrated that seeing pictures of high- and low-calorie foods provokes responses in different parts of the brain that vary in intensity[3]. Without telling subjects the purpose of the test, Ohla showed them pictures of high-calorie foods, such as lamb chops, salmon, pizza and pastry, alternating with pictures of lower calorie foods, such as beans, watermelon, yogurt and pasta with tomato sauce. After each picture, she applied a weak electric current to the subject's tongue, stimulating the brain's taste function without mimicking any real taste, producing a sensation and metallic taste rather like licking a battery. So the subjects got the food cue from the picture and were immediately given a neutral taste stimulation.

The EEG measurements of brain activity were clear: the electrical current administered after seeing a picture of a high-calorie food stimulated a stronger and, according to the subjects, more pleasant sensation than the same electrical stimulation applied after showing a picture of a low-calorie food.

The neural activity evoked by pictures of high-calorie food was stronger in specific parts of the brain — the bilateral insula and frontal operculum — than when low-calorie foods were viewed. And changes in reported taste pleasantness were correlated with the activation of the medial orbitofrontal cortex.

Even shape can affect taste. David Gal, who studies marketing and consumer behaviour at Northwestern University in Evanston, Illinois, found that after subjects completed an unrelated task that involved sorting geometric figures, a piece of cheese with pointed, rather than rounded corners tasted sharper[4]. Scientists are only beginning to understand the brain mechanisms underlying the connections between the visual and gustatory senses.

SNIFFING A CONNECTION

Odour plays a large role, of course. Chewing releases volatile molecules that travel through the back of the mouth to receptors in the lining of the nasal passages — quite different from taking a sniff through the nose. These receptors allow us to identify the combination of sensations that leads to flavour; that is, to know what we're eating. When you eat a strawberry, it may taste sweet or sour, and you can detect this even while holding your nose. But what disappears is the flavour — the 'strawberriness' of the food. For that, you need a sense of smell.

Smell is much more complex than taste. Humans have only a few different taste receptors: the five that scientists generally agree on (sweet, sour, salty, bitter and umami) and possibly a few others. But there are hundreds of receptors for odours. The possibilities for mixing and matching taste and odour are immense, and lead to the wide variety of flavours we perceive that subjectively bear little resemblance to any of those basic tastes.

Indeed, smell and taste are linked neurologically in a way that no other human senses are.

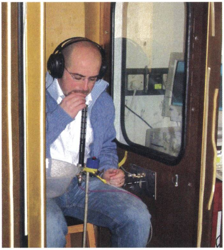

CHARLES SPENCE

Tasty tones: tests have shown that when people hear a crunch, a potato crisp seems fresher.

When we hear and see something at the same time, we are using two senses that have different neural pathways, and we can easily distinguish between them. Not so with smell and taste. Dana Small, a psychologist and neuroscientist at Yale University in New Haven, Connecticut, and the Yale-affiliated John B. Pierce Laboratory, suggests trying what she calls the jelly bean test. Pop a jelly bean into your mouth while you hold your nose — you can sense sweetness, but no flavour. Then let go of your nose, and now you can identify the flavour as well. It seems obvious that the flavour is coming from your nose, even though you can feel the jelly bean in your mouth. It is a very convincing illusion.

Smelling through the nose and smelling through the back of the throat while tasting may be neurologically distinct — and Small has found evidence that they are perceived quite differently. Both orthonasal and retronasal odours arrive via the same pathway, but when they arrive at the same time as taste, then odour and taste are integrated and the flavour perception created. It is only when both taste and odour arrive in the anterior insula that we perceive flavour. In other words, taste and smell have distinct pathways that overlap in the insula

"Taste only happens when molecules bind to receptors on the tongue," she says. "From there, signals go to certain parts of the brain. Smell happens when odour molecules bind to receptors in the nose, and from there signals go to different parts of the brain. They eventually meet up in the anterior insula." It is there, Small says, that we perceive flavour. When taste and smell co-occur, the insula creates flavour. This merging of senses does not happen through simple sniffing of food that's not in the mouth.

FEELING DELICIOUS

We also experience — and differentiate — foods through our physical contact with them. This is especially true of fats — think of the creamy 'mouth feel' of butter and ice-cream, and the oiliness and viscosity of a rich salad dressing. In the orbitofrontal cortex of the brain there is a group of neurons that respond specifically to the texture of fat in the mouth. These neurons respond not only to fatty oils in the mouth, such as vegetable oil, and to foods rich in fat, such as ice-cream and chocolate, but also to non-food substances that have a similarly oily texture, including mineral oil or silicone oil. The taste of a soda is also greatly influenced by feel, in a different way — a flat soda tastes very different from one with carbon dioxide bubbles still rising in it.

Temperature is also a factor. Very cold ice-cream has little flavour, for example, and warming it increases the perceived sweetness. The molecular processes in the taste buds of the tongue that play a key role in the perception of sweet, bitter and umami tastes also regulate sensitivity to temperature[5]. Increasing the temperature of food to between 15 °C and 35 °C enhances the neural response to sweetness. In about 50% of the population, heating or cooling the tongue is by itself enough to cause taste sensations — warming the tongue causes a sweet sensation, and lowering the temperature induces a sour or salty taste.

Sound can also affect taste. In tests conducted by two neuroscientists, Massimiliano Zampini of the University of Trento in Italy and Charles Spence of the University of Oxford, UK, subjects bit into potato crisps and rated their crispness or freshness. The scientists were able to systematically alter their subjects' perceptions: playing a crunching sound when the subjects bit down led to them judging that the crisps were fresher and crisper than when there was no aural cue[6]. In another study, researchers watched a random sample of 15 couples as they drank in a bar on two consecutive Saturday nights, counting the number of drinks they ordered until they left[7]. On the first night, with pop music set at a moderate 75 decibels (dishwasher-level loudness), the men ordered an average of 2.9 drinks and the women 1.5. But on the second night, with the music pumped up to 91 decibels (a motorcycle), the men averaged 4.3 drinks and the women 2.1.

Taste preferences that start in the womb last a lifetime. When people move to another country, they absorb new habits, new language and new styles of clothing. They even accept new kinds of relationships between children and parents. But, says Beauchamp, "one of the last things to change in ethnic groups is food habits. They're the most profound preferences — and one reason is that they're learned very early on." ■

Nicholas Bakalar *is a freelance journalist based in New York City.*

1. Forestell, C. A. & Mennella, J. A. *Pediatrics* **120**, 1247–1254 (2007).
2. Lipchock, S. V. *et al. Clin. Perinatol.* **38**, 627–641 (2011).
3. Ohla, K. *et al. PLoS One* **7**, e32434 (2012).
4. Gal, D. *et al. SSRN eLibrary* http://ssrn.com/abstract=1030197 (2007).
5. Talavera, K. *et al. Nature* **438**, 1022–1025 (2005).
6. Zampini, M. & Spence, *C. Chem. Senses* **3**, 57–67 (2010).
7. Gueguen, N. *et al. Percept. Mot. Skills* **99**, 34–38 (2004).

PERSPECTIVE

Complexities of flavour

Is flavour an intrinsic objective property, or a subjective experience that varies from person to person? **Barry Smith** sorts out the implications.

Although we're all familiar with taste, it is surprisingly complex and puzzling. What we call taste encompasses the combined sensory inputs of taste, touch and smell, as influenced by sight and sound. The tongue and associated receptors in the mouth detect only salty, sweet, sour, bitter, savoury and possibly metallic, yet we can 'taste' such flavours as mango, onion, strawberry, mint, cinnamon and vanilla. Flavours such as these are discovered by the tongue and the nose together, not by either of these organs alone.

We seldom recognize experiences of pure taste. Holding the nose closed reduces our ability to tell the difference between pieces of raw apple and raw potato because it prevents odours in the mouth from reaching the olfactory epithelium at the bridge of the nose. Similarly, people who lose their sense of smell often report that they can't taste anything, even though when tested they can detect salt, sour, bitter and sweet (there is no simple test for the savoury taste, umami).

So the quality we are interested in is not taste *per se*, but flavour. However, trying to define flavour is far from straightforward. For example, in the introduction to the multidisciplinary journal *Flavour*, the editors tell us: "We take flavour to be the experience of eating food as mediated through all the senses." The journal also "emphasizes work that investigates the flavour of real foods". At first, the editors seem to define flavour as an experience, yet those who study the physics and chemistry of flavours in food and wine are not investigating psychological experiences; rather, they are observing and measuring actual physical compounds. To these researchers, flavours reside in the food and drink we consume.What, I think, the editors intend to focus on is the multisensory experiences through which we *perceive* flavours in foods.

> PSYCHOLOGISTS AND NEUROSCIENTISTS TELL US THAT FLAVOUR IS A CONCOCTION OF THE BRAIN

PROPERTY OR EXPERIENCE?

It's not hard to see why people confuse flavour (the objective property) with the subjective experience of flavour. Psychologists and neuroscientists tell us that flavour is a concoction of the brain — the result of the multisensory integration of olfactory, tactile and taste impressions, modulated by the dynamic time course of a tasting event and the location of sensory stimuli in the mouth. According to this view, the flavour of a wine, say, is a psychological construct that will vary from individual to individual as a result of different threshold sensitivities to acid, tannin, sugar, alcohol, carbon dioxide and sulphur. Lighting conditions, mood and even sounds can affect our experience of tasting, and wines can be enhanced or distorted by accompanying foods — all of which suggests that winemakers have little influence over the experience that drinkers of their wines will have.

However, advances in the science of winemaking suggest otherwise, and they are increasingly used to improve the perceptible quality of wines. Winemakers strive to find properties such as 'balance' in a wine — something that drinkers can sense even if they lack the concept of a balanced wine — and winemakers know many of the factors that affect it.

The central question, then, is this: how should we adjudicate between those who say that flavours depend on molecular compounds, and those who stress the varying perceptions of individual eaters and drinkers?

The problem is that analytical chemists struggle to connect the volatile molecules in wines with the varying perceptions of individual tasters. However, this isn't what they should be trying to do. The task is to relate the underlying chemical compounds in a wine to the relatively stable flavours they create, whereas it is the task of psychologists and neuroscientists to chart the complex relationship between flavours and flavour experiences — explaining why the latter can vary as a result of conditions internal and external to the taster. Only by recognizing flavours as intermediaries between the chemical compounds in a wine and our individual reactions to it can we hope to bridge the two.

FINDING THE FLAVOUR

The right way to view flavours is as configurations of sapid, odorous and textural properties of foods or liquids that we track using a combination of our senses. The flavour of menthol, for example, comprises a minty aroma, a slightly bitter taste, and a cool sensation in the mouth resulting from irritation of the trigeminal nerve (which also causes the hot sensation when we eat mustard or chillies). For single flavours, such as strawberry, mint and mango, which are easy to detect, there is little variation between tasters. But for more complex products, like wines, we don't always detect all their flavours. Our individual flavour experiences, like our other perceptions, are not always exact guides to reality. Tasting is hard — it requires experience, practise and knowledge to identify what one is tasting.

Studying the multisensory nature of flavour perception helps us understand how perceptions can vary across individuals, and within individuals over time, as a result of a variety of factors that affect our ability to taste. If a wine remains unchanged, we should see these variations as different ways of perceiving the same flavour, rather than claiming that there are as many flavours as there are tasters. Where the flavours of a wine evolve in the glass or the bottle, the task of an experienced taster is to assess its changing flavour profile from the series of snapshots that individual perceptions provide. Psychology and neuroscience are beginning to show us just how many factors are involved in individual perception, and with luck we will be able to work out the conditions that not only diminish, but also improve, our access to the real flavours in our food and drink. ■

Barry Smith *is director of the Institute of Philosophy at the University of London's School of Advanced Study.*
e-mail: barry.smith@sas.ac.uk

SOPHIE CASSON/THREE IN A BOX

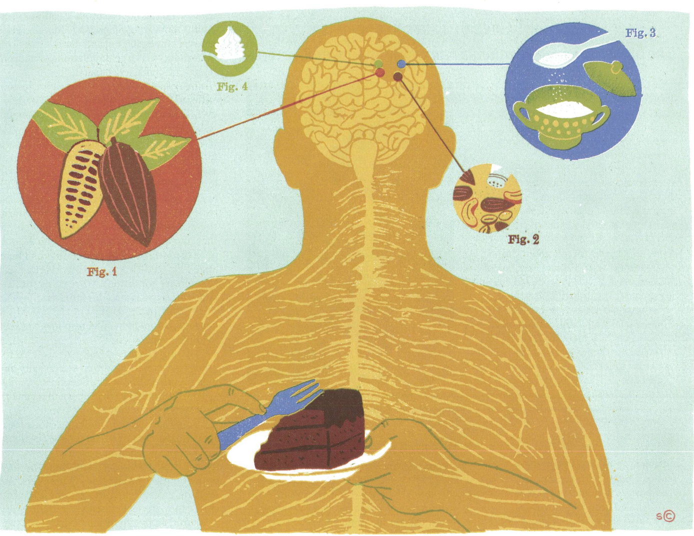

NEUROSCIENCE

Hardwired for taste

Research into human taste receptors extends beyond the tongue to some unexpected places.

BY BIJAL P. TRIVEDI

A mouthful of bittersweet chocolate cake with a molten centre can trigger potent memories of pleasure, lust and even love. But all it takes is one bad oyster to make you steer clear of this mollusc for life. Neuroscientists who study taste are just beginning to understand how and why the interaction of a few molecules on your tongue can trigger innate behaviours or intense memories.

The sensors in our mouths that detect basic tastes — sweet, salty, bitter, sour and umami, and arguably a few others — are only the start of the story (see 'The finer points of taste', page S2). The way the brain represents these tastes is just as important. Researchers have recently developed a 'gustotopic map' based on the idea that, just as each taste bud on the tongue responds to a single taste, so there are regions of the brain that are similarly dedicated[1].

The other recent revelation in taste research is that the receptors that detect bitter, sweet and umami are not restricted to the tongue. They are distributed throughout the stomach, intestine and pancreas, where they aid the digestive process by influencing appetite and regulating insulin production. They have also been found in the airways, where they have an impact on respiration, and even on sperm, where they affect maturation. A better understanding of what they do and how they work could have implications for treating conditions ranging from diabetes to infertility.

BRAIN MAP

After discovering the sensors for the five basic tastes, Charles Zuker, a Howard Hughes Medical Investigator now at Columbia University, New York, and geneticist Nicholas Ryba, of the National Institute of Dental and Craniofacial Research in Bethesda, Maryland, embarked on a logical follow-on project. Their goal, Zuker says, was to determine how the brain "transforms detection into perception".

Results of previous studies into taste representation in the brain "have been confusing", says Ryba. One of the leading theories was that the gustatory cortex — the primary brain region responsible for taste perception — was 'broadly tuned', with each neuron responding particularly well to one taste but still able to respond to others. Moreover, the neurons were thought to be distributed evenly. This model seemed to be consistent with smell, the other chemical sense,

➲ NATURE.COM
The network and the principles of food pairing:
go.nature.com/bw66nx

which produces no recognizable patterns in the brain. Odour recognition is a matter of combinatorial processing: small differences in firing patterns across large populations of neurons represent a characteristic smell.

The research that led to these conclusions suffered from poor spatial resolution, however. To address this shortcoming, Zuker and Ryba's team used functional brain-imaging techniques to investigate how individual taste qualities stimulate neural activity in the gustatory cortex on a fine scale. Their tools included two-photon calcium imaging, which reveals processes deeper inside the brain, and with greater spatial resolution, than conventional single-photon methods. They found that dropping any of several bitter liquids onto the tongue of an animal that had been anaesthetized (both for convenience and to replicate conditions in previous studies) consistently activated the same small group of neurons in the gustatory cortex. These neurons did not light up in response to sweet, savoury or salty liquids.

The team ran the same experiment for the other tastes and found that sweet, salty and umami each had its own distinct cluster, or hotspot, of neurons. The only hotspot they couldn't locate was for sour tastes.

These findings contradict previous ideas about how the brain processes taste. Seeing the first hotspot was "stunning", recalls Ryba. "On the one hand it was very surprising: at the level of the tongue, the sweet and bitter cells and receptors are intermingled, yet at the level of the cortex they are separated by 2.5 millimetres" — a surprisingly large distance that could span hundreds of neurons. On the other hand, Ryba can see the logic of this organization: separating the bitter hotspot from the sweet, for example, means that bitterness can be wired to a brain area that drives aversion, whereas sweetness can be wired to attraction.

So far the gustatory map is sparse, with just four identified hotspots. But other areas nearby might also be used for taste coding, possibly involving other senses, speculates Ryba. These areas might represent mixtures of tastes or perception of flavour.

Finding these hotspots is "a breakthrough" that provides a "basic underlying principle of how the cortex is organized", says Susan Travers, a neuroscientist at Ohio State University in Columbus. Nevertheless, Travers thinks the new map is oversimplified. Previous experiments found that a neuron "doesn't respond to just one stimulus", she says. For example, "you would expect the sweet hotspot to have some smaller responses to other stimuli", such as salt or umami.

Sidney Simon, a neuroscientist at Duke University in Durham, North Carolina, who specializes in gustatory physiology, says that Ryba and Zuker's experiments are "technically spectacular" — but he also has concerns. He says it is strange that they didn't find a sour hotspot, and recommends that they explore whether it

THE SECRET LIVES OF TASTE RECEPTORS

The ability to sense chemicals has whole-body applications

Taste receptors promote survival by detecting nutritious foods and helping us avoid toxic ones. But these receptors exist beyond the tongue and digestive system. How do they contribute to the survival of the species?

In a bid to find out, Thomas Finger, a neurobiologist and co-director of the University of Colorado's Rocky Mountain Taste and Smell Center in Aurora, has been studying solitary chemoreceptor cells (SCCs). In 2003, he discovered SCCs in the nasal cavities of rats and mice; more recently, he and others have found SCCs expressing taste receptors in the human nose. The rodent SCCs contain T2Rs (bitter receptors) and all the rest of the cellular machinery found in bitter taste cells on the tongue. In 2010, Finger and colleagues showed[5] that bitter compounds that tickle these receptors trigger apnoea: "they stop breathing, they cough and sneeze," he says. The receptors, which are exposed to harmful irritants in the air as well as to compounds produced by bacteria growing in the nasal cavity, transmit their signal to the trigeminal nerve, which temporarily inhibits breathing. This response, he hypothesizes, is to stop the irritant from being inhaled deep into the lungs.

It's not only the T2Rs that are found in hard-to-explain places. The T1Rs, responsible for sensing sweet and umami, exist in the airways too, although what they do there remains unknown. "It is easier to understand the T2Rs than the T1Rs," says Finger, "T2Rs always seem to be present in the context of detecting toxins. The T1Rs seem to have other functions here that are unclear."

Collections of bitter receptors are also found on tiny finger-like projections called cilia on human airway epithelium cells. When the researchers stimulated the receptors using bitter compounds, such as nicotine or quinine, the cilia waved back and forth vigorously, helping to clear the airways of irritating compounds.

Researchers at the University of Maryland School of Medicine in Baltimore discovered T2Rs on smooth muscle cells in the human airway[6]. Exposure to bitter compounds caused these cells to relax. Testing this effect in asthmatic mice, where smooth-muscle contraction narrows the airways and obstructs breathing, had the same effect: bitter compounds relaxed the smooth muscle and improved breathing.

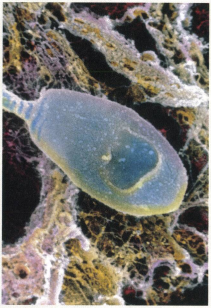

A sperm trying to fertilize an egg. Umami receptors, found on the sperm's surface, are thought to help control the release of DNA.

PROF. P. MOTTA/DEPT. OF ANATOMY/UNIVERSITY "LA SAPIENZA", ROME/SCIENCE PHOTO LIBRARY

There are many more locations where the presence of taste receptors is enigmatic. A team of researchers led by Ingrid Boekhoff of the Walther Straub Institut for Pharmacology and Toxicology in Munich, Germany, recently found[7] that mouse and human spermatozoa express T1R1 and T1R3, the umami receptor. Murine sperm that lack T1R1 had an increased rate of spontaneous acrosome reaction — a disgorging of DNA that normally only happens when the sperm meets an egg. The mutant sperm also had higher levels of calcium and a second messenger molecule called cAMP. Boekhoff and her colleagues suggest that the umami receptor somehow keeps the sperm in a quiet state by controlling calcium ions and cAMP — which are known to influence the acrosome reaction — until it reaches an egg.

The bitter receptor T2R5 is also found in the testes[8]; deleting these cells leads to smaller testes and a huge reduction in the number of mature sperm. According to Robert Margolskee, associate director of the Monell Chemical Senses Center in Philadelphia, Pennsylvania, it is not clear what the bitter or umami receptors are doing in these locations. "But we have the tools to start figuring it out," he says. "Check back in five years and we'll have a pretty good idea." — **B.T.**

lies in a different area or whether sour detection is dispersed throughout the brain. He adds that these experiments should be performed on conscious animals, which, in terms of smell at least, respond differently from anaesthetized ones.

Zuker takes the criticisms in his stride. He's not perturbed by the lack of a sour hotspot and explains that, unlike the other four tastes, sour — or acid detection — is also involved with pain. "When you put a drop of acid on your finger it burns, you aren't getting a sour lemony taste," he says. So the cortical representation is likely to be more complicated than a single hotspot. Other tastes don't have this type of conflict, he adds.

As for Travers' comment that the hotspots appear to be too specialized, Zuker concedes that there may be some sensory crossover, with some cells in the bitter hotspot, for example, also responding to other tastes. The key, he stresses, is that there is overall topographic segregation, and that the vast majority of neurons within a hotspot are selective for just one taste.

TASTE CIRCUITS

Cells with taste receptors are found throughout the body (shown in green)[9]. Along the digestive tract, their presence is probably related to food. But in bile ducts — that carry only secretions produced by the body — their purpose is more enigmatic.

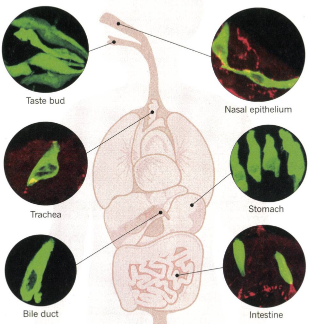

DR. MARCO TIZZANO OF UNIV. COLORADO MEDICAL SCHOOL

Zuker and Ryba now plan to explore how taste mixtures are encoded, and then how sweet and bitter tastes, after being detected by their corresponding cortical fields, can trigger such exquisite behaviours — from attraction to aversion, from pleasure to rejection.

OUT OF THE MOUTH

While Zuker and Ryba use receptors to explore how taste relates to emotion, memory and learning, other researchers hope to explain what taste receptors are doing in other parts of the body.

If taste receptors seem out of place anywhere other than the mouth, this is only because they were first found in taste buds on the tongue, says neurobiologist Thomas Finger, co-director of the University of Colorado's Rocky Mountain Taste and Smell Center in Aurora. Taste buds are simply a way of sensing chemicals, so they can have functions unrelated to detecting the flavour of food. And they are surprisingly common in the body (see 'The secret lives of taste receptors'), although their presence is sometimes baffling. "We don't know the function of these receptors in more places than we do know them," says Finger.

It is not surprising that some of the better-understood examples are in the digestive system. The T1R2/T1R3 sweet receptor is found on K- and L-type enteroendocrine cells in the intestine. These cells secrete hormones called incretins, which in turn stimulate insulin production. The sweet receptors neatly explain a phenomenon that had mystified physiologists for more than 50 years: that eating glucose triggers significantly more insulin than injecting it directly into the bloodstream. Neuroscientist Robert Margolskee, now associate director of the Monell Chemical Senses Center in Philadelphia, Pennsylvania, realized that if there were receptors in the intestine that could detect glucose and trigger the release of hormones, this would provide the missing link for the so-called incretin effect. In 2007, his hypothesis proved correct as his team found the sweet receptor on L cells in the human duodenum[2] and showed that these cells produce the gastrointestinal incretin hormone GLP-1, which stimulates insulin production and sends a satiety signal to the brain. Blocking or deleting these sweet receptors decreases insulin release.

In a further study in mice, Margolskee's team showed that when sweet receptors detect glucose, the L cells manufacture a glucose transporter that draws the sugar into the cells lining the intestine. Artificial sweeteners also trigger the glucose transporter and lead to a spike in insulin — this is a concern, but is unlikely to cause clinical hypoglycaemia (low blood glucose), Margolskee says.

"Sweet receptors, traditionally associated with just the mouth, were in the gut and essentially 'tasting' the sugar a second time," says Anthony Sclafani, a behavioural neuroscientist at the City University of New York. This 'second tasting' triggers glucose transport into the cells and bloodstream, and the faster this happens, the more insulin will be released. "It's an incredibly important finding for the control of blood sugar," he says, adding that it was surprising that artificial sweeteners, which were thought to influence only the tongue, also trigger changes in the gut.

Other T1R receptors in the digestive system also play a role in appetite and blood sugar control. In the stomach, cells carrying the T1R3 receptor, which aids detection of both sugar and amino acids, secrete the hunger hormone ghrelin when they encounter carbohydrates and protein, encouraging eating when important nutrients are available.

For bitter tastes, however, the T2R receptors in the digestive system seem to have contradictory functions. In 2011, Belgian researchers showed that bitter-tasting compounds that reach the stomach of mice initially trigger the release of ghrelin, stimulating eating as usual[3]. But after 30 minutes, food intake decreased, as did gastric emptying, keeping the food in the stomach. This curbs the appetite by prolonging the sense of fullness and satiety — perhaps to prevent the ingestion of toxic food.

"It's too early to know whether this is a normal satiety response or this is mimicking a response to a toxin," says Roger Cone, a biophysicist at Vanderbilt University in Nashville, Tennessee. It seems counter-intuitive that eating a bitter compound, which is thought to signal a toxin, actually stimulates the appetite. Yet this is an effect that has been known about for centuries. Indeed, the Romans drank wine infused with bitter herbs to prime the appetite and prevent overeating. And, the authors speculate, stimulating bitter receptors in the gut could potentially be used to treat certain eating disorders.

Bitter receptors are also present in the large intestine. In 2009, researchers at the University of Shizuoka in Japan showed that activation of T2Rs in the colon of humans and rats stimulates the secretion of anions, inducing water to enter and causing diarrhoea[4]. The authors suggest that this acts as a defence against dangerous organisms and irritants.

Investigating the function of the taste receptors distributed throughout the body could help clinicians tackle diseases ranging from eating disorders to diabetes. Digesting all this information will take time, but it is clear that the function of taste receptors goes far beyond the pleasure of eating chocolate cake. ■

Bijal P. Trivedi *is a freelance science writer based in Washington DC.*

1. Chen, X. *et al. Science* **333**, 1262–1266 (2011).
2. Jang, H. J. *et al. Proc. Natl Acad. Sci. USA* **104**, 15069–15074 (2007).
3. Janssen, S. *et al. Proc. Natl Acad. Sci. USA* **108**, 2094–2099 (2011).
4. Kaji, I. *et al. Am. J. Physiol. Gastrointest. Liver Physiol.* **296**, G971–G981 (2009).
5. Tizzano, M. *et al. Proc. Natl Acad. Sci. USA* **107**, 3210–3215 (2010).
6. Deshpande, D. A. *et al. Nature Med.* **16**, 1299–1304 (2010).
7. Meyer, D. *et al. PLoS One* **7**, e32354 (2012).
8. Li, F. & Zhou, M. *Mol. Hum. Reprod.* **18**, 289–297 (2012).
9. Finger, T. E. & Kinnamon, S. C. *Biol. Rep.* **3**, 20 (2011).

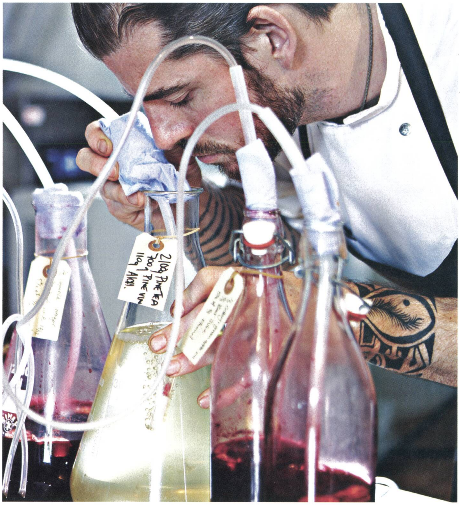

Lars Williams, head of research at Nordic Food Lab, part of Noma, inspects a variety of vinegar concoctions.

CLAUS BECH-POULSEN

COOKING

Delicious science

Chefs are teaming up with researchers to create avant-garde dishes. Is 'molecular gastronomy' more than a fad?

BY COURTNEY HUMPHRIES

Food science has often focused on nutrition or industrial-scale food and flavour production. But over the past two decades, a discipline that blends science and cooking has made its way into universities, restaurants and even home kitchens. Collaborations between scientists and chefs have made advances in the study of gastronomy and spurred culinary innovations that are opening up fresh ways of studying something we often take for granted: the enjoyment of a good meal.

This field is often called 'molecular gastronomy', although both scientists and chefs have objected to the term (see 'Name that cuisine'). Hervé This, a chemist at the French National Institute for Agricultural Research in Paris, who coined the term in 1988, wanted to establish a new field that uses science to understand what happens to food when it is cooked.

This conjunction of cooking and science has spawned several developments. First, researchers have turned the kitchen into a place for serious scientific study, with a growing number of papers and books detailing the physical and chemical transformations involved in cooking. At the same time, collaborations between scientists and chefs have helped bring scientific knowledge and technological innovations into fine restaurants and even homes. And finally, the field has spurred an interest among both scientists and chefs in moving beyond the physical properties of foods to understanding the psychology and neuroscience of perceiving and enjoying food.

THE SCIENCE OF COOKING

The chemical and physical transformations that take place during cooking are complex. The browning of meat, for example, involves molecular changes produced in a complex set of cascading chemical interactions known as Maillard reactions. Analyses of foods undergoing Maillard reactions have shown that the process releases hundreds of compounds, some of which have been harnessed by the flavour industry to create processed foods that taste better — compounds that contain the amino acid cysteine provide a meaty smell, for example, and compounds with methionine enhance the flavour of potatoes.

Many researchers are trying to understand what makes some cooking methods work better than others. In 2010, Pia Snitkjaer, a PhD student at the University of Copenhagen, described the investigation of the perceived flavour and chemical composition of meat stock as it is cooked[1]. Most of the traditional ways of cooking have been passed down through the generations without any systematic testing, and molecular gastronomy can pinpoint those that do not yield the best flavour. Hervé This has debunked the myth that adding hot vinegar to mayonnaise prevents its decomposition, for example, and that eggs can only be whipped once. Such explorations are also taking place in restaurant test kitchens and other informal settings, as documented by a six-volume cookbook *Modernist Cuisine* (go. nature/ymtjuj) published in 2011 by a team led by Nathan Myhrvold, formerly chief technologist at Microsoft and now chief executive of the patent licensing firm Intellectual Ventures, based in Bellevue, Washington. In addition to recipes, the book details the basic science of cooking, from the properties of water to the principles of heat transfer in pans (it turns out that copper pans don't transfer heat any better than aluminium ones).

As well as the growing number of scientists interested in studying cooking, many famous chefs have embraced a scientific approach to creating new dishes. Restaurants such as the recently closed elBulli in Roses, Spain, The Fat Duck in Bray, UK, Alinea in Chicago, Illinois, and Noma in Copenhagen, Denmark, have made their reputations through their development kitchens. Chefs at these establishments have experimented with new methods to create some surprising dishes — and have sometimes joined scientists as co-authors in published research.

Ferran Adrià was one of the first to take this approach, playing with the physical properties of food. At elBulli, he used methods such as spherification, in which liquid ingredients are mixed with sodium alginate and submerged in a

➲ NATURE.COM
Chew on this, a review of the Edible exhibition:
go.nature.com/q76bjv

calcium bath, resulting in caviar-like spheres that burst in the mouth. A similar technique creates balls from alcoholic liquids, like the carbonated mojito spheres created by chef José Andrés for his restaurant Minibar in Washington DC. "We used to cook only by repeating what we saw without really having a deep understanding of why it was happening," says Andrés. Now, he says, the application of scientific principles to cooking has fuelled culinary innovation. Andrés visited the Fluid Dynamics Laboratory led by John Bush at the Massachusetts Institute of Technology (MIT), who was mimicking the hydrodynamic properties of aquatic flowers to create flexible petal-shaped films that, when pulled out of water, enclose a small amount of water. Andrés and his team have recently developed similar petal-like sheets made of gelatin, which will enable them to create an edible snack with liquid inside.

Such inventions have stimulated new interest in the science of cooking, and a wave of science-focused cookbooks, TV shows and websites bringing these ideas into home kitchens. Amateur cooks can now buy sous vide machines (which use a temperature-controlled water bath to cook food slowly in sealed plastic bags), air pumps to make foams, and ingredients such as sodium alginate and xanthum gum to alter the textures and properties of food.

THE PLEASURE PRINCIPLE

For some scientists, the most interesting questions in gastronomy lie not in the chemistry and physics of food, but in the brain. Peter Barham, a physicist at the University of Bristol, UK, and co-editor of the new journal *Flavour,* says that much of what people call molecular gastronomy is simply the application of scientific knowledge about the physics and chemistry of food that has been known for some time. "What is not well researched is the link between the food that goes into our mouth and what we think of it," he says. Barham is one of the authors of a paper[2] published in *Chemical Reviews* in 2010 arguing for a broad definition of molecular gastronomy as "the scientific study of why some food tastes terrible, some is mediocre, some good, and occasionally some absolutely delicious".

The study of the nature of flavour perception, eating and enjoyment or 'neurogastronomy' is making many new discoveries, says Barham. It is becoming increasingly clear, for example, that what we taste depends on the information coming from our other senses (see 'Partners in taste', page S4). Chefs who appreciate this phenomenon realize that that they can make meals taste better by paying attention to the other sensory inputs their customers receive. Heston Blumenthal and his chefs at The Fat Duck have spent several years collaborating with Charles Spence, an experimental psychologist who heads the Crossmodal Research Laboratory at the University of Oxford, UK, who has shown that factors such as background music, plate colour and the materials used for the cutlery can affect how a dish tastes. After finding that the sound of ocean waves made a seafood dish taste better, The Fat Duck serves a 'Sound of the Sea' dish that is accompanied by an iPod playing ocean sounds.

How do flavours come together? Per Møller, a sensory scientist at the University of Copenhagen in Denmark and Barham's co-editor at *Flavour*, says that cooking presents a wealth of scientific puzzles — such as the basis of food pairings. "What makes most people click when you mix gin and tonic?" he asks. One hypothesis proposed by chefs is that foods that go well together have certain flavours in common — a company called Sense for Taste in Brugge, Belgium, has created a food-pairing database on this premise — but Møller says this hasn't been fully investigated by scientists. A 2011 study of more than 50,000 recipes found that Western recipes choose ingredients with shared flavour compounds, whereas East Asian recipes tend to avoid them[3].

> ***"What makes most people click when you mix gin and tonic?"***

The ultimate question is why we enjoy certain meals. The components of a recipe matter, but they must be perceived in the right way by the brain. Molecular gastronomy as a discipline can explain how food preferences, cravings, reward systems, satiety and even expectations affect the eating experience. A 2008 study by researchers from Stanford University in California and the California Institute of Technology in Pasadena, for instance, found that people thought the same wine tasted better when it was labelled as expensive — and functional magnetic resonance imaging scans revealed that they derived more pleasure from drinking it[4].

Barham believes that the current fad for science-based cuisine will run its course in the next few years, at least at the top restaurants that made it famous. But even so, he says, "there are aspects of what we're doing that are going to outlast the fads in the kitchen". Education is one such area. Barham argues that cooking offers an engaging — and safe — way to run a classroom chemistry experiment. "If you can do that, you can also encourage more people to cook at home," he says, a skill that he hopes will combat unhealthy eating among young people. But leaving aside such virtuous aims, studies that integrate cooking, chemistry and nutrition also give an added emphasis to an aspect of food that ought not be overlooked: pleasure. ■

Courtney Humphries *is a freelance science writer based in Boston, Massachusetts.*

1. Snitkjær, P. *et al. Food Chem.* **122**, 645–655 (2010).
2. Barham, P. *et al. Chem. Rev.* **110**, 2313–2365 (2010).
3. Ahn, Y.-Y. *et al. Nature Sci. Rep.* doi: 10.1038/srep00196 (2011).
4. Plassmann, H. *et al. Proc. Natl Acad. Sci. USA* **105**, 1050–1054 (2008).

GETTY IMAGES

NAME THAT CUISINE

Scientists and chefs find fault with 'molecular gastronomy'

Science has had a big influence on cooking, and cooking has made its way into many laboratories and journals. But what should we call this hybrid field? In 1992, French chemist Hervé This and Hungarian physicist Nicholas Kurti organized the International Workshop on Molecular and Physical Gastronomy in Erice, Italy, which was attended by chefs and scientists from around the world. The idea was to launch a scientific discipline devoted to investigating 'culinary transformations'.

Hervé This later dubbed the field 'molecular gastronomy', a term that has become linked with unusual and technically innovative dishes served at top restaurants. He has argued that such work should be called 'molecular cuisine', and avoid the term gastronomy, because it represents the application of science rather than true scientific investigation.

Many chefs also eschew the term 'molecular gastronomy'. In a 2006 open letter published in the UK newspaper *The Observer*, for example, food writer Harold McGee joined cooking pioneer Ferran Adrià and several other chefs to explain that the workshop "did not influence our approach, and the term 'molecular gastronomy' does not describe our cooking, or indeed any style of cooking." — **C.H.**

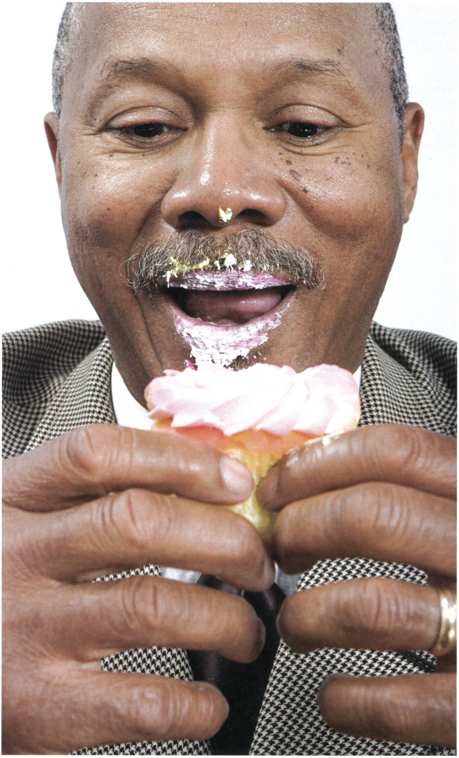

IMAGE SOURCE/ GETTY IMAGES

OBESITY

Insensitive issue

It is becoming clear that links between taste preferences and obesity go beyond simply having a sweet tooth.

BY JAMES MITCHELL CROW

What does chocolate ice-cream taste like? A simple enough question, you might think: sweet and creamy, with a slightly bitter cocoa kick. Delve a bit deeper, though, and the exercise becomes impossibly subjective, because what you taste when you eat ice-cream is not the same as the next person's experience. Your tongue and your taste buds are unique, and a sweet taste that seems strong to you might be almost undetectable to someone else.

Perhaps more importantly, individuals also vary greatly in how pleasurable and satiating they find ice-cream, or any number of other foods. Could someone's taste perceptions and preferences be a major influence on their weight?

The emergence of obesity as the world's largest preventable health disorder gives urgency to this question. Although the drivers of obesity are far more complex than simply a sweet tooth, study after study suggests that shifting taste preferences are a big part of the puzzle. The latest findings are forcing us to fundamentally re-examine our understanding of taste perception itself.

EXPANDING RESEARCH

Research into a link between an appreciation for sweetness and body weight goes back at least to the 1950s. And almost from the start, the evidence has been contradictory. A landmark 2006 review[1] by Linda Bartoshuk, a sensory scientist at the University of Florida in Gainesville, offered an explanation for why the results have been so mixed. Bartoshuk argued that a taste described as "extremely sweet" by a lean person might not seem so sweet to someone overweight, because their food experiences are different — and ignoring this divide masks the difference in their taste preferences. "We discovered something that should have been obvious — that if you're fat, you like sweet and fat better — that's part of what keeps you fat," she says.

Although studies such as Bartoshuk's point to a slight preference for sweet foods among obese people, the link becomes much stronger when a food's fat content is also considered. "There's a relatively clear link between sweet and fat together — obese people tend to like sweet fatty foods," says Lucy Donaldson, who studies taste perception and ill health at the University of Bristol, UK. "But they also tend to like fatty savoury things," she adds.

Recent research into links between obesity and savoury preferences has not revealed any clear relationship with salt or umami taste perception, however. Only one link seems to hold firm. "What is strongly associated with obesity is not the consumption of carbohydrates or sweets — it is the consumption of fat," says Yanina Pepino, who studies taste perception and disease at Washington University in St

➲ NATURE.COM
Neural circuit mediates appetite and body weight:
go.nature.com/wyolnn

D. HURST / ALAMY

Louis, Missouri. "The obese crave more fat."

Fat is not one of the established five tastes (sweet, sour, salty, umami and bitter). However, a growing group of researchers suspect that the sense of taste is implicated (see 'Hardwired for taste', page S7). For one thing, the tongue has taste receptors for two of the three macronutrients we need in our food: sweet corresponds to carbohydrates, and umami indicates protein. "It makes logical sense that we have some form of taste response to the other macronutrient: fat," says Russell Keast, a sensory scientist at Deakin University in Melbourne, Australia. Fat content affects not only a food's taste, but also its appearance, texture and perhaps even smell. Keast and his colleagues have devised tests to assess whether people can detect fatty acid in custard when all sensory cues apart from taste are removed. "The sense of smell and any textural effects are minimized, and everything is under red light just in case there are any visual differences," he says.

Could insensitive taste receptors be to blame when you reach for that extra doughnut?

Just as carbohydrates and protein are revealed by the taste of their breakdown products, Keast thinks we can taste the breakdown products of fat — fatty acids. And intriguingly, the obese and overweight seem to be less sensitive at detecting them[2]. Last year, using their 'sensory-matched custards', Keast and his colleagues showed that people with low sensitivity for fatty acids tended to consume significantly more fat in their diet, and have a higher body mass index (BMI), than people with high sensitivity for flavour[3].

Pepino is also researching fatty tastes. "We still cannot claim that fat is a basic taste, but within the limitations that we do know, the relationship between taste perception and obesity is strongest with fat," she says.

RICH TASTE

The prime candidate for the fatty acid taste receptor is a protein called CD36. The initial evidence came from rodents: mice genetically engineered to lack CD36, for example, lose their natural preference for fat, whereas their affinity for other tastes remains unaffected[4]. Pepino is investigating similar patterns in people with natural genetic variants that lead to either over— or under — expression of CD36. "We hypothesized that if you are in the group with the higher expression level then you will be more sensitive to detect fat at very small concentrations. And that's exactly what we found," she says.

Even so, the idea that a 'fat taste' even exists is not universally accepted. Bartoshuk, for example, questions how fatty acid detection could play a role in sensing dietary fat in the mouth. "Fat doesn't usually break down until it gets to the stomach," she says. "And if you taste fatty acids in their pure form, they are bitter — really nasty. So how is something nasty, that's barely detectable, going to help you regulate fat at all?"

Keast argues that the explanation lies in the fact that fatty foods naturally contain low levels of free fatty acids alongside the fat itself. "As the fat level rises, so do the levels of naturally free fatty acids," he says.

What's more, the unpleasant taste of fatty acids doesn't become apparent until their concentration is much higher than our threshold detection level — which is quite low, he adds. As food degrades naturally, the level of free fatty acids increases "until they can be recognized. This is unpleasant and indicates the food is past its best." It's a similar story for other tastes, he adds — too much salt, for example, turns an enjoyable flavour into something unpleasant.

CAUSE OR EFFECT?

Now the correlation is emerging, the next big question pertains to causation. Does a reduced ability to taste fat tip someone towards eating an excess of fatty food, or does eating a fat-filled diet depress our sensitivity to fatty tastes?

The answer probably lies in the middle, with a balance of genetics and environment. "Whether you like fat depends on many different things, starting with what you're exposed to *in utero* and as a neonate, which sets quite a lot of your preferences," says Donaldson (see 'Partners in flavour', page S4). But some studies have shown that these preferences are still malleable after childhood. Change your diet, and your preferences can be partly reset — for better or worse.

> *"If you're fat, you like sweet and fat better — that's part of what keeps you fat."*

The early work on dietary malleability was carried out with salt. Consuming too much salt has long been associated with high blood pressure and hence an elevated risk of cardiovascular disease. Reducing salt intake over a period of time diminishes someone's desire for salty food. Donaldson and colleagues have recently shown with sugar that things can also swing the other way[5]. A group of young adults were asked to consume two sweet sports drinks a day for a month in addition to their regular diet. "We wanted to know if you could change sweet preference in a relatively short period of time — and we were quite surprised when we did," Donaldson says. "The people who didn't prefer sweet things at the beginning preferred sweet things at the end."

Keast is starting to see similar shifts with fat taste perception[6]. "If we go on a low-fat diet, our sensitivity to fats increases," he says. In one experiment, "both lean and obese people responded to a very-low-fat four-week diet, becoming orally more sensitive to fat". Keast is now beginning longer-term trials to assess whether this increased sensitivity can be translated into a decreased preference for — and hence consumption of — fatty food.

Obesity is a multifaceted disease with no simple, single cause. But for Pepino, one take-home message is already becoming clear. "Promoting a healthy diet and a healthy lifestyle should always be the first line of treatment for obesity," she says. "For people who want to reduce their fat intake, they just have to persevere and it will become easier." ■

James Mitchell Crow *is a freelance science writer based in Melbourne, Australia.*

1. Bartoshuk, L. M. *et al. Phil. Trans. R. Soc. Lond. B* **361**, 1137–1148 (2006).
2. Tucker, R. M. & Mattes, R. D. *J. Food Sci.* **77**, S148–S151 (2011).
3. Stewart, J. E., Newman, L. P. & Keast, R. S. *J. Clin. Nutr.* **30**, 838–844 (2011).
4. Pepino, M. Y. *et al. J. Lipid Res.* **53**, 561–566 (2012).
5. Sartor, F. *et al. Appetite* **57**, 237–246 (2011).
6. Stewart, J. E. & Keast, R. S. *J. Int. J. Obesity* doi: 10.1038/ijo.2011.155 (2011).

METTLER TOLEDO
Excellence
MENU R&D
Pioneer
OHAUS
4.9228
CDN

CHRIS LOSS

The combined hot and cold sensations of chilli and peppercorn might make a tasty substitute to salt.

FOOD SCIENCE

Taste bud hackers

Scientists and psychologists are trying to trick our mouths and minds into enjoying foods that are better for us.

BY LAUREN GRAVITZ

Tucked away in a biotechnology park in North Brunswick, New Jersey, researchers at Chromocell are trying to make us change the contents of our kitchen cupboards. They are screening hundreds of thousands of molecules to find ones that can enhance certain tastes, such as sweet or salty, with the hope of concocting foods that are kind to our waistlines but still excite our palates.

The business of creating taste enhancers and ingredient substitutes for high-sugar, high-salt and high-fat foods is decades old. Artificial sweeteners such as saccharin have been in widespread use since the mid-1900s, for example. But such products have had only modest success. Diet soda, for example, still makes up only 30% of the overall soda market. And potato crisps fried in olestra, a fat substitute with molecules too large to be absorbed by the gut, have fewer calories but prevent the body from absorbing vitamins and nutrients. Consumers complained that these crisps caused unpleasant side effects.

People don't derive as much pleasure from most low-fat, low-sodium or low-calorie foods as they do from more indulgent chocolate mousses and French fries. "Fat has a taste and a smell, it can change an item's taste and smell, it has a texture and it changes texture. It's a really tricky little thing," says Jeannine Delwiche, who leads research into reducing salt, sugar and fat at multinational PepsiCo based in Purchase, New York,. "So when you start to talk about changing fat in a food, you're going to be changing all of those things." Which means, she says, it's very difficult to create a product that gets it all right. The food industry is hoping that an updated understanding of taste and its underlying biology will yield flavoursome formulations that are better for us than the products on the shelves today.

FISHING FOR FLAVOURS

One of the major steps forward in taste science in recent decades has been the discovery and exploration of distinct taste receptors on the human tongue. Our taste buds have separate receptors for, at the very least, five basic tastes: sweet, salty, sour, bitter and umami (savoury). Of these, the receptors for sweet, bitter and umami are all members of a family of proteins called G-protein-coupled receptors (GPCRs). And because GPCRs are well understood, they provide numerous opportunities for scientists looking for molecules that might trigger them.

Enter Chromocell and Senomyx, based in San Diego, California. These companies have adapted high-throughput screening systems developed by the pharmaceutical industry to find potential drug candidates against GPCRs, to identify molecules that interact with taste cells. "The whole idea of using molecular biology to trick or tweak your taste buds is kind of novel for the food industry," says Beverly Tepper, a taste researcher at Rutgers University in New Brunswick, New Jersey.

The screening systems work by running a slew of molecules past a panel of taste receptors to see what sticks. To find new sweeteners, for instance, researchers take the protein that taste cells recognize as sweet and express it in a stable cell line. "Then we use this as a fishing net to run thousands of different compounds against that cell," says Rudy Fritsch, who leads Chromocell's flavours and nutrition research. When the instruments indicate that one of the molecules has stuck to a receptor — much like a key in a lock — then the molecule is worth further investigation.

Senomyx and Chromocell use slightly different systems and maintain slightly different research goals. Senomyx was the first company to use a high-throughput screening approach to taste research and is concentrating on synthetic chemicals. Two of its sweet enhancers are already found in products being sold in test markets in China, Africa, North America and elsewhere.

Chromocell is taking a different tack. Rather than synthesizing potential taste enhancers in the lab, its researchers are putting more emphasis on using their high-throughput fishing net to catch natural compounds. This is an approach with popular appeal — a growing proportion of the public views artificial sweeteners and fat substitutes with suspicion, so many companies are looking instead for natural products.

Not all researchers believe that taste enhancement needs to come from new molecules isolated in a lab. Scientists in flavour houses (companies that develop chemicals for the food and drink industry), food companies and academic institutions are also seeking fresh combinations of existing tastes and flavours, or are tweaking the properties of existing ingredients, to improve a food's health profile while maintaining its appeal. They're looking for tastes and aromas that can elicit either physical or psychological reactions to help enhance flavour.

Playing around with the shape and size of salt crystals, for instance, can help lower sodium intake but maintain saltiness. Smaller crystals, or those produced in the shape of a pyramid, have more surface area and pack a bigger punch to the palate. But such crystals are only effective for solid foods, not in soup or mixtures where the salt is dissolved.

"Scientists and flavour chemists are going to be searching every blade of grass and every leaf in the Amazon for something that might potentiate taste. And there just aren't many things out there like that that have been found," says Chris Loss, a chef and culinary scientist at the Culinary Institute of America in Hyde Park, New York. Rather than looking for something that tastes precisely like foods higher in sugar or salt, industry researchers are instead aiming to concoct healthier combinations that are just as tasty.

Because the brain associates salt with savoury, umami flavourings such as monosodium glutamate (MSG) — a salt of a non-essential amino acid that is found in many everyday foods, such as cheese and tomatoes — can enhance a food's taste so effectively that less sodium is needed to achieve the desired effect. And adding flavours that the brain associates with sugary items, such as vanilla, can trick us into thinking a food is sweeter than it really is.

Loss has been toying with different combinations that might trick the tongue into thinking it is tasting salt. "Every taste bud is surrounded by chemosensory receptors that pick up on the capsaicin in peppers or the cooling effect from menthol," he says. Because these receptors are in such close proximity to the ones that sense taste, he wondered if "you could tickle them a little bit", stimulating the taste receptors without the actual molecular match.

Along with Szechuan cuisine expert Shirley Cheng, Loss has used a combination of chilli peppers and a uniquely numbing type of Szechuan peppercorn to create an alternating combination of heating (chilli) and cooling (peppercorn) effects. He tried to find a combination of these ingredients that would allow him to reduce a dish's added salt. "We did a sensory test and, while we didn't find any increase in perceived saltiness, we found that people liked it equally well," Loss says.

The renaissance in taste enhancement is not limited to processed and prepared foods. Some scientists are trying to restore taste and nutrition to foods that have gradually had the flavour bred out of them in favour of other traits, such as high yield and resilience to long-distance travel. "If we can make produce taste better, people will eat more of it," says Harry Klee, a horticultural scientist at the University of Florida in Gainesville.

Working with other researchers at the same institute — Linda Bartoshuk, who studies taste and olfaction and Charlie Sims, who runs sensory testin — Klee has developed chemical profiles of nearly 200 different varieties of heirloom tomato. Those with the most diverse range of sugars, acids and volatile chemicals were presented to panels of 100 consumers. These taste testers noted down which ones they liked and how strong their preferences were, allowing the researchers to determine which properties of the fruits confer the most (and least) desirable flavours. By analysing the highest- and lowest-ranked tomatoes, the researchers determined which compounds contributed to overall taste[1]. "We could then use that data to extract the ideal recipe of the perfect tomato, which we've done," Klee says. "Now, we can rescue the genetics of what's in the good ones and try to reincorporate those into commercial tomatoes."

SCENTS AND SENSIBILITY

During the taster panels, Klee and his colleagues also discovered that the smell tests used to assess a food's appeal had been going about it the wrong way. It was generally assumed that a food's odour, sniffed before it was put in the mouth, was enough to determine its impact on taste — the food industry has been operating on that assumption for decades. Indeed other research has shown that when we eat something, the odours that go up to our olfactory bulb from the back of the mouth are processed in a different part of the brain to the odours taken in when we put our nose near something and sniff.

"In previous years, people used the wrong volatiles," Bartoshuk says. So she, Klee and Sims used a different method. By sorting the tomatoes according to taste-tester preference, the researchers were able to pinpoint the volatile compounds that actually elicited a response. They used volatiles not just to make a food smell fantastic, but also to taste fantastic — endpoints not as closely linked as had been thought. "Now we know what to look for, we've done it in tomatoes and strawberries, and we're going to do it in blueberries too," Bartoshuk says.

Fundamentally, the Florida researchers are working towards the same goal as their counterparts in industry. "We've tried to educate people about how to eat healthier diets, but none of us do it," Bartoshuk says. "I know perfectly well I have no business eating spare ribs but I eat them anyway because I like them. And one way to get people to eat healthier is to make [healthy] foods that they like." ■

Lauren Gravitz *is a science writer based in Los Angeles, California.*

SWEET DISCOVERIES

1880
1890
1990
1910
1920
1930
1940
1950
1960
1970
1980
1990
2000

1879 / SACCHARINE

400x SWEETER THAN SUGAR

Discovered by accident by researchers at Johns Hopkins University in Maryland, saccharin became popular during sugar rationing. (TRADE NAMES INCLUDE:)
Sweet'N Low, Sweet Twin

1931 / STEVIA

350x

Derived from a plant, *Stevia rebaudiana*, that has been used by the Guarani people of South America for more than 1,000 years. Isolated by two French chemists in 1931, but not approved in US until 2008.
Stevia, Only Sweet, SweetLeaf, Truvia

1937 / CYCLAMATE

30x

Discovered by accident by a researcher at the University of Illinois, it was initially marketed as an alternative sweetener for use by diabetics. A controversial study linked cyclamate with cancer, and the FDA banned it in 1969. Cyclamate, as Sucaryl, is still available outside the United States.

1965 / ASPARTAME

200x

Discovered accidentally by a chemist at Searle laboratories in Illinois. Controversy over its safety and allergenicity means it is one of the most studied food additives.
NutraSweet, Equal, Canderel

1967 / ACESULFAME POTASSIUM

200x

Discovered accidentally by scientists at Hoechst in Germany, "Ace K" is often blended with other sweeteners to help mask after tastes.
Sweet One and Sunett

1976 / SUCRALOSE

600x

Discovered by scientists from sugar manufacturer Tate & Lyle and at Queen Elizabeth college in London. Sucralose is derived from sugar: 3 chlorine atoms replace 3 hydroxyl groups.
Splenda and others

1996 / NEOTAME

8,000x

Discovered by researchers at Monsanto in France who were looking for molecules similar to aspartame but without the allergenicity.
Neotame is not yet marketed

---

1. Tieman, D. *et al. Current Biol.* **22**, 1035–1039 (2012).

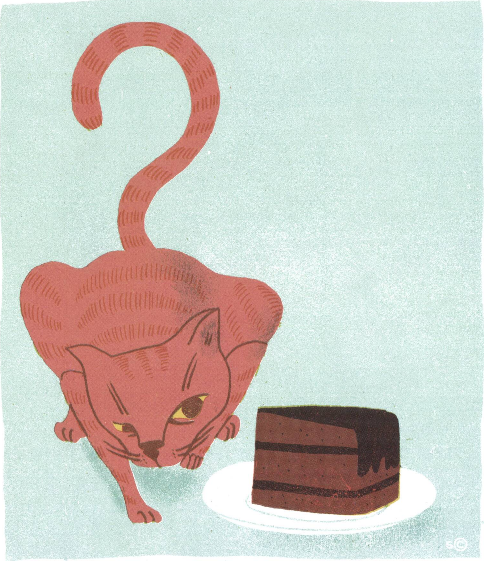

SOPHIE CASSON /THREE IN A BOX

EVOLUTIONARY BIOLOGY

The lost appetites

Many vertebrates can detect the same five basic tastes that humans can, but there are exceptions. Are the differences caused by a change in diet?

BY EWEN CALLAWAY

Ronald Fisher must have been relieved when a chimpanzee at Edinburgh Zoo took a sip of water, looked him in the eye and spat at him.

It was August 1939, and Fisher was testing whether chimps could taste water laced with a chemical called phenylthiocarbamide (PTC) that some humans find nauseatingly bitter and others can't taste. Fisher and his colleagues Edmund Ford and Julian Huxley had been worried that the apes wouldn't make their preferences known, rendering the experiment pointless.

Instead, about three-quarters of the chimps they tested expressed their displeasure with PTC. Fisher's team speculated that the variation in sensitivity to bitter tastes was caused by a genetic mutation shared by humans and chimps, and that natural selection had maintained this diversity in both species. "Wherein the selective advantages lie, it would at present be useless to conjecture," the trio wrote[1] in a letter to *Nature*.

More than 70 years later, biologists are still trying to figure it out. The availability of different animal genomes has given scientists more insight, culminating in the startling discovery that, for many creatures, some tastes have no evolutionary benefit at all. Kurt Schwenk, a biologist at the University of Connecticut in Storrs who studies chemical sensing in lizards and snakes, says: "The whole story of the evolution of taste is really the evolution of loss of taste."

The most obvious explanation for the changes is lifestyle. At some point in evolutionary history, a shift in diet removed the need to sense certain chemicals in food. Evolution is a game of 'use it or lose it', and genes that do not aid an animal's survival or reproduction are liable to build up random mutations that destroy their ability to make a working protein. Gary Beauchamp, a geneticist at the Monell Chemical Senses Center in Philadelphia, Pennsylvania, likens the situation to that of sight in cave-dwelling fish. A life of darkness eliminated the usefulness of vision, so the fish collected mutations in genes involved in eye development and eventually lost their sight altogether.

Another example of taste loss lies closer to home: cats cannot taste sweet substances. Beauchamp noticed this quirk in the 1970s, and in 2005 his team finally found out why[2]. All cats share a mutation that disables one of the two genes that build a working sweet receptor, whether for the tongue, intestine or any other part of the body. Because all felines — from domestic cats to lions — have an identical mutation, it is likely that the sweet-receptor gene became inactive in their common evolutionary ancestor. Beauchamp speculates that this ancestral animal moved to a diet composed of protein-rich meat, devoid of sugary plants, negating the need for a sweet receptor.

Beauchamp's team recently discovered that the inability to taste sweetness is more widespread. They analysed 12 non-feline species belonging to the order Carnivora, including sea-lions, otters and hyenas, and identified crippling mutations in the sweet-receptor gene in 7 of them[3]. What's more, six species carried unique mutations, suggesting that the ability to taste sweetness had been lost repeatedly over the course of evolution. Presumably the mutations appeared after each species or its ancestors switched to a meat-only diet, Beauchamp says. This interpretation is supported by the team's finding that an omnivorous member of Carnivora, the spectacled bear, still has a working sweet receptor.

There may be other reasons why tastes are so dispensable. As well as lacking sweet receptors, dolphins also lack the ability to build working umami (which sense amino acids in proteins) and bitter taste receptors. One theory posits that because dolphins swallow their food whole, moderating their intake is irrelevant. However, this theory applies only to the ability to taste food, and ignores the role of these receptors in other parts of the body (see 'Hardwired for taste', page S7). There is no evidence that losing taste genes confers any advantages to an animal, although Schwenk is happy to speculate. "Most carnivores are scavengers as well as predators," he says. "They eat a lot of rotting flesh, so it might be good to not taste it so well."

Pandas, a largely vegetarian member of Carnivora, also lack umami receptors. The pandas' bamboo-only diet gives them little need to detect proteins, says Jianzhi Zhang, an evolutionary geneticist at the University of Michigan in Ann Arbor, who reported this lack of receptors in 2010. His team also discovered that vampire bats have no sweet receptor, and that all bats, including insectivorous species, lack umami receptors[4]. Zhang's team has also been unable to find working sweet-receptor genes in several species of birds, grass-eating horses and omnivorous pigs — a pattern he finds puzzling.

DEVONIAN TASTES

The sense of taste must have carried an evolutionary advantage to have evolved in the first place. Beauchamp says that taste-sensing systems in the mouth perform two essential tasks: umami and sweet detection help animals find energy-dense nutrients, and bitter detection helps them avoid toxic substances. Scientists know far less about the biology and evolution of sour and salt tastes. One theory is that detecting salts helps an animal control its levels of sodium and other ions, whereas sour tastes help it avoid the acids in unripe fruit and spoiled foods.

All vertebrates have some ability to avoid toxic chemicals and seek out nutrients. By comparing animals from different branches of the evolutionary tree, scientists have inferred that taste probably evolved more than 500 million years ago — before land vertebrates, bony fish, sharks and lampreys diverged — when their common ancestor, a primitive fish, developed a new kind of cell.

Taste buds have been repeatedly tweaked over time to suit various animals' dietary needs, says Thomas Finger, co-director of the University of Colorado's Rocky Mountain Taste and Smell Center in Aurora. Many fish are covered with taste buds. "The super-tasters among the animal world are goldfish," says Finger. "Goldfish and catfish have way more taste buds than anybody else." They have poor vision, and their taste buds, including those on their whiskers, could help them sense their way to a meal in murky water, he adds.

The evidence suggests that umami receptors were the first to develop. In 2008, Zhang's team reported the discovery of genes, similar to those that encode receptors used by humans and mice to sense the amino acid glutamate, in the genome of the elephant shark, a species that branched off from other fish 400 million years ago. Sharks lack bitter taste receptors, suggesting that these genes evolved more recently.

➲ NATURE.COM
Ever craved soil? Evolutionary theory might explain why:
go.nature.com/1duag4

The super-tasters among the animal world are goldfish.

Bitter is perhaps the taste that most intrigues evolutionary biologists. It is the 'Darwin's finch' of taste, elaborated and customized to suit a species' ecological niche. Humans have 24 or 25 (depending on the person) different bitter receptors, each recognizing unique combinations of chemicals.

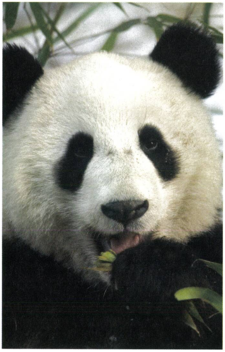

KEREN SU/ GETTY IMAGES

A strict bamboo diet might have stripped the panda of the umami and sweet taste receptors.

Toxic bitter compounds come in all shapes and sizes, so it makes sense that the receptors that recognize them are diverse, says Beauchamp. Bitterness is code for danger, but many bitter compounds also provide important nutrients. For example, during the lean winter months, the Japanese macaque supplements its diet by eating willow trees. The bark of the willow contains salicin, which tastes bitter to many animals. A recent study of the bitter receptor T2R16, which is common to all primates, reported that the macaque version is the least responsive to salicin[5].

Bitter taste evolution, then, is also about distinguishing between different chemicals. "If you go out into the real vegetable world, what you'll find is that almost everything is bitter," says Beauchamp. "An animal that rejects everything that's bitter would be in trouble."

This principle could explain Fisher's discovery that some individuals, among both humans and chimps, are unable to taste PTC. Seven decades later, researchers finally identified the gene responsible for PTC sensitivity, called *T2R38*, and confirmed that different versions of the gene largely explain why not everyone can taste the chemical (see 'Finer points of taste', page S2).

Recent studies have refined Fisher's ideas about how the variations in PTC sensitivity evolved. A team led by Stephen Wooding, an evolutionary biologist at the University of Texas Southwestern Medical Center in Dallas, repeated Fisher's experiments[6] using apples spiked with PTC, instead of water solutions (perhaps to avoid being spat at). Chimps still differed in their ability to taste the bitter chemical, but DNA sequencing revealed that chimpanzees that cannot taste PTC have an entirely different mutation in *T2R38* from human non-tasters — their insensitivity evolved independently.

One of the compounds that T2R38 recognizes, goitrin, is abundant in cruciferous vegetables, such as broccoli and Brussels sprouts. Goitrin can prevent hyperthyroidism, a condition caused by low iodine intake. Perhaps a reduced sensitivity to PTC and goitrin persists in the population because it helps iodine-starved individuals avoid hyperthyroidism, Wooding speculates.

Diet is not the only driver of change in bitter-tasting ability, however. Geneticist Sarah Tishkoff's team at the University of Pennsylvania in Philadelphia recently tested[7] hundreds of individuals from 57 human populations in Central and West Africa. They found both PTC tasters and non-tasters, but there was no obvious correlation with their different diets.

In the past decade, scientists have discovered sweet receptors in the gut that influence insulin levels, and bitter receptors in the lungs that can clear inhaled substances. Tishkoff's team suggests that roles such as these, and not diet, might explain the evolutionary differences in PTC tasting. Zhang also thinks there is more to the evolution of taste than just flavour. He suggests that researchers use model organisms, such as mice lacking various taste genes, to understand the roles of these receptors. "We're finding a lot of mismatches between feeding ecology and taste-receptor evolution," he says. "Perhaps we still do not have a complete understanding of the functions of those genes — or of taste." ■

Ewen Callaway *is a news reporter for* Nature *in London.*

1. Fisher, R. A., Ford, E. B. & Huxley, J. *Nature* **144**, 750 (1939).
2. Li, X. *et al. PLoS Genet.* **1**, e3 (2005).
3. Jiang, P. *et al. Proc. Natl Acad. Sci. USA* **109**, 4956-4961 (2012).
4. Zhao, H. *et al. Genome Biol. Evol.* **4**, 73–79 (2011).
5. Imai, H. *et al. Biol. Lett.* doi: 10.1098/rsbl.2011.1251 (2012).
6. Wooding, S. *et al. Nature* **440**, 930–934 (2006).
7. Campell, M. C. *et al. Mol. Biol. Evol.* Doi: 10.1093/molbev/msr293 (2011).

1/64
1/32
3/64
1/16
5/64
3/32
7/64
1/8
·0156
·0313
·0469
·0625
·0781
·0938
·1094
·1250
0,40
0,79
1,19
1,58
1,98
2,38
2,78
3,17
33/64
17/32
35/64
9/16
37/64
19/32
39/64
5/8
·5156
·5313
·5469
·5625
·5781
·5938
·6094
·6250
13,10
13,49
13,89
14,29
14,68
15,08
15,48
15,87
·1406
·1563
·1719
·1875
·2031
·2188
·2344
·2500
ON
OFF
s©

SOPHIE CASSON / THREE IN A BOX

TECHNOLOGY

The taste of things to come

Artificial tongues that mimic the human sensory experience could aid the development of better and more consistently flavoured foods.

BY NEIL SAVAGE

Imagine a food wholesaler in London deciding whether to buy a new batch of coffee from a farmer in Brazil. She'd like to taste a sample to see if it will appeal to her customers. So she links to the supplier over the Internet, makes a selection, turns to a machine on her desk, and voilà! — she's sipping coffee on another continent.

This scenario — replicating the flavour of not only coffee but a wide variety of food and drink — isn't all that far fetched, says physicist Seunghun Hong of Seoul National University in South Korea. "You can actually reproduce those smells or tastes using very cheap chemicals," he says.

What's lacking for such a device is not the technology to recreate flavours and aromas, but the data about the specifics of such sensations that could be transmitted from the Brazilian grower to the British buyer. "We don't have those kinds of quantitative numbers to evaluate your smell and taste. That's why you cannot say that this coffee tastes the same as coffee ten years ago," Hong explains.

But he and other researchers are working to change that, developing artificial tongues that can respond to flavours in ways analogous to the human tongue. Such sensors could provide quality control in food and agriculture, record information about taste in ways that are not now possible, aid the development of new flavours and artificial sweeteners, and help make medicines more palatable.

ELECTRONIC TONGUES

There are well-established technologies for measuring and reproducing three of the five human senses — sight, sound and touch — but mimicking our two chemical senses, taste and smell, has proved more challenging. Kenneth Suslick, a chemist and materials scientist at the University of Illinois at Urbana-Champaign, says that artificial versions of these senses would have practical applications and also provide an aid to understanding another aspect of human biology.

Suslick works on both artificial tongues and artificial noses: the noses deal with gases, whereas the tongues handle liquids (and solids that have been liquefied, which is what happens when we eat). Human noses, and the devices that mimic them, contain hundreds of different receptors capable of identifying the complex patterns of thousands of smells. Taste, by contrast, is made up of just a handful of components — the exact number is disputed, but researchers have agreed on at least five (see 'Hardwired for taste', page S8).

Taste lends itself to automation because it is fundamentally a chemical process. Sweetness sensors react to sugar molecules. Sourness is a measure of pH. Saltiness is a measure of the positively charged ions of alkali metals, notably sodium. And umami, the savoury or meaty taste, is detected by a receptor for glutamate. Only the fifth major taste, bitterness, is poorly defined, and may be a catch-all term for several different chemical reactions, Suslick says.

Artificial tongues often rely on measuring changes in electrical potential or current caused by the target molecule reacting with a receptor. These devices are therefore often called electronic tongues, or e-tongues, and work in a similar way to the real thing. In the human tongue, various molecules in food bind to proteins in the taste buds, producing a pattern of electrical signals that the brain interprets as a particular flavour. Although it might be possible to build a device that would break down a food into its component chemicals and measure their relative quantities, creating such a set of instructions for say chocolate ice-cream wouldn't be practical, because a single food item might contain more than 1,000 different chemical substances. And that's not how people identify tastes anyway, says Kiyoshi Toko, professor of information science and electrical engineering at Kyushu University in Fukuoka, Japan.

"Humans don't discriminate each chemical substance," he says, but rather classify a discrete set of tastes. He believes there are two additional tastes beyond those widely accepted. One he calls astringency, which is a form of bitterness caused by tannins. The other he calls pungency — that's the sting from foods such as hot peppers, and in humans is experienced by receptors for heat and pain.

Toko has developed an e-tongue that consists of a series of polymer membranes, each coated with a different lipid, fitted onto a plastic tube and connected to an electrode. When the tube is immersed in a sample liquid, the taste molecules in the liquid interact with the lipids and change the electrical potential of the membranes in a characteristic way. The result is a readout that corresponds to taste.

A company founded to market his technology — Intelligent Sensor Technology of Kanagawa, Japan — has sold about 300 taste sensing machines in the past five years. The system can examine foods such as soy sauce, soup and sake for six taste qualities —the five standard ones plus astringency. The same sensors also produce readings for five aftertastes, mostly variations of bitterness as well as the 'richness' evoked by umami. He says he doesn't know how to make a sensor to detect pungency, but he's working on it.

Hong has a device that works in a similar way. He built a transistor using carbon nanotubes, which are highly sensitive to electrical changes, and coated the surface of the nanotubes with a protein — one that detects bitterness, for example. When substances in the sample bind to the protein, they send a signal through the transistor, and a change in electrical conductance registers the bitterness. This technique mimics the human response more closely than some other approaches, he says, because the proteins he uses are those actually found in human taste buds, which makes them highly selective for the molecules to be tasted. He produces the proteins by inserting human genes into *Escherichia coli* bacteria. "Our device has exactly the same response as the human taste system," he says.

Suslick's system, by contrast, relies on colour-changing dyes, rather than electrical changes. His sensors are designed to measure sweetness. He originally printed an array of commercially available reagents on an acetate membrane, measuring about 2.5 cm by 4 cm. The sensor can simply be dipped into a sample liquid, where various substances react with the different pigments and change colour. A computer compares images of the array taken before and after dipping, and produces a 'difference map' that shows how much each spot has changed.

KENNETH S. SUSLICK

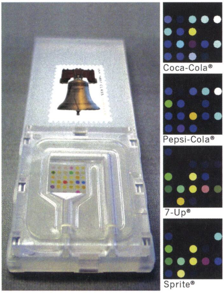

Disposable chips produce flavour 'fingerprints'.

He tested his sensor on 14 different natural and artificial sweeteners. Each array produced a pattern of colours unique to the particular sweetener, providing visible fingerprints for substances including aspartame, saccharin and fructose. The cheap, disposable sensors gave results in about two minutes, speed that could be attractive to a beverage company that wants to use the sensors for quality control. Combining this 'taste chip' with other arrays for sour, bitter, salt and umami tastes might provide a reasonable mimic of the human tongue, Suslick says.

A FLAVOUR SENSATION

However, neither e-tongues nor colour matrices can completely reproduce the experience of flavour. "An awfully large fraction of what we call taste is actually smell," Suslick points out. "Anyone who's ever had a head cold knows that." The whole taste experience is based on a complex interaction of responses by numerous receptors. Each receptor can respond to more than one chemical, and its response can affect how the brain interprets the responses from other receptors. The result, whether in the brain or an artificial system, is a complicated feedback pattern. Researchers use statistical methods from the field of artificial intelligence to map out the complex response patterns from an array of sensors. Suslick says it's not yet clear how many points such a map must include to describe an approximation of someone's reaction to taste.

"Ultimately, we would like to take the patterns and see if they can be predictive of human response," says chemist Eric Anslyn of the University of Texas at Austin. With a colleague who studies wine-making at the University of California, Davis, Anslyn has developed a sensor that can identify different wine varieties. His device can distinguish between a Pinot Noir and a Merlot, for instance, but it cannot yet discern nuances, such as whether the drink is oaky or fruity.

A crucial part of developing an artificial tasting system is calibrating its results to real human responses. In Denmark, chemist Anders Malmendal of the University of Aarhus is trying to do this by using what he calls a 'magnetic tongue'. His technique relies on readings from nuclear magnetic resonance (NMR) spectroscopy, a common laboratory analytical technique for identifying chemical composition and concentrations. Often used in metabolomics, which screens biological samples for the by-products of metabolic activity, NMR is a good way to detect toxic effects of new drugs. Malmendal, along with colleagues from the University of Naples Federico II in Italy, used NMR spectroscopy to identify different brands of canned tomatoes. The researchers bought 18 cans at stores around Naples and used NMR to obtain their chemical signatures, each consisting of 870 variables.

To match these signatures to subjective human taste, Malmendal and colleagues turned to a panel of 12 human experts. These tasters provided detailed descriptions of flavour, odour and texture, according to an accepted set of food industry standards. Malmendal's team then matched the NMR data to the panellists' assessments, so they could use the chemical signature to say what a particular tomato would taste like to people.

With a large enough library of reference samples, food producers could test a sample and predict how consumers would react to it. One company, Bruker Biospin of Cologne, Germany, sells a juice screener that uses NMR spectroscopy and a library of more than 3,000 reference samples of 30 types of fruit from 50 countries. Quality controllers can tell if the juice is fresh or from concentrate, whether there's added sugar, and whether cheaper mandarin juice is mixed in with the orange juice — in some cases they even can tell roughly where the oranges originated. In March 2012, the company introduced a similar system for wine.

Any technique that can consistently distinguish one food sample from another can be used this way. Build up a library of human assessments of various instances of different foods, and you can predict the taste of new samples based on how well they match. But Suslick points out two problems with this approach. Paying experts to assess every variety of every food would be prohibitively expensive. And in the end, no matter how sophisticated the gadgetry, taste remains a stubbornly subjective experience. "Can we distinguish between coffees? Yes," Suslick says. "Can I tell you what the best coffee is? No." ■

Neil Savage *is a freelance science writer based in Lowell, Massachusetts.*

Eat Well, Live Well.
AJINOMOTO®

Umami taste research and beyond: the challenge for Ajinomoto Co., Inc.

Authors
Ana San Gabriel[1], Masanori Kohmura[2], Hisayuki Uneyama[3], Eiichiro Kimura[4], Tohru Kouda[3], Yasufumi Furuhata[5] & Takeshi Kimura[6]

[1]Public Communications Department, Ajinomoto Co., Inc., 15-1 Kyobashi 1-chome, Chuo-ku, 104-8315 Tokyo, Japan.

[2]Quality Assurance & External Scientific Affairs Department, Ajinomoto Co., Inc., 15-1 Kyobashi 1-chome, Chuo-ku, 104-8315 Tokyo, Japan.

[3]Institute for Innovation, Ajinomoto Co., Inc., 1-1 Suzuki-cho, Kawasaki-shi, 210-8681 Japan.

[4]Ajinomoto North America, Inc., 400 Kelby Street, Fort Lee, New Jersey 07024, USA.

[5]Institute of Food Science and Technologies, Ajinomoto Co., Inc., 1-1 Suzuki-cho, Kawasaki-shi, 210-8681 Japan.

[6]R&D Planning Department, Ajinomoto Co., Inc., 15-1 Kyobashi 1-chome, Chuo-ku, 104-8315 Tokyo, Japan.

Growth through innovation

Founded over a century ago as a business venture based on collaboration between academia and industry to create a new seasoning, Ajinomoto Co. is still a top seasoning provider today. It also leads the world in the production of pharmaceutical-grade amino acids, and was rated as the number one innovator in the US food beverage and tobacco sector by the US Patent Board in 2011.

Ajinomoto Co. has contributed to advances in taste physiology and the safety and efficacy of amino acids through both internal research and funding of academic research. The company strives to improve lives globally by contributing to significant advances in food science and human and animal health. Ajinomoto Co. strongly believes that solutions to future challenges must be based on science and technology.

Early history

The early history of Ajinomoto Co., Inc. is synonymous with the history of umami. The founding of the company was based on the discovery of umami, the fifth basic taste. Umami has a pleasurable meat-like quality that enhances other flavours in foods.

In 1908, Kikunae Ikeda, a chemistry professor at the Tokyo Imperial University, identified glutamate as the key substance in traditional Japanese soup stock or 'dashi', made with dried kelp called 'kombu'. Ikeda was convinced that the taste of glutamate was a discrete basic taste separate from sweet, salty, sour and bitter. At that time there was no word to describe this unique taste that was more than simply savoury, so he chose the combination of the Japanese words 'uma' — delicious — and 'mi' — taste — to create the word, umami. Ikeda later patented a method to produce monosodium glutamate (MSG) as a seasoning.

Ikeda had studied in Germany and was surprised by the strong and tall physique of the Germans compared to that of the Japanese. This fostered a desire in him to improve the nutrition of the Japanese people, and he believed that a seasoning to improve the taste of the then poor Japanese diet would benefit the nutritional health of the population and help him accomplish his goal. Ikeda's vision became the basis of our corporate mission today: 'Eat Well, Live Well'.

Ikeda was approached by Saburosuke Suzuki II, who owned a business that produced iodine from seaweed. Suzuki launched a business venture to begin selling MSG as AJI-NO-MOTO®, the world's first umami seasoning, in 1909.

MSG sales started in Taiwan and Korea in 1910. A Shanghai office opened in 1917. After the Second World War, the US military became interested in the use of MSG because they found Japanese military rations appetizing. This interest led to pioneering symposia on MSG by the Quartermaster Food Institute (Chicago) in 1948 and 1958.

Glutamate was first produced industrially by acid hydrolysis of wheat gluten, and later soy. In 1956, a competitor developed a method to produce glutamate by fermentation of *Corynebacterium*. This spurred research into new manufacturing technologies, which, after the 1970s, led to the production of MSG by companies around the world, using fermentation, chemical synthesis and extraction from plant materials. Since then, owing to cost competitiveness and public acceptance issues, fermentation technology has become dominant in the production of glutamate and most other amino acids. Thus, Ajinomoto Co. has adopted fermentation as their main method of production.

Assessment of MSG safety

Since 1909, MSG has been used safely as a food ingredient in many countries. In the 1950s, the Joint FAO/WHO Expert Committee on Food Additives (JECFA) was established to evaluate the safety of food additives on an international level. Several countries also established independent regulations to control the use of food additives. In the US, Food

Additive amendments were added to the Federal Food, Drug, and Cosmetic Act to enable the evaluation of substances added to food. MSG was classified as a generally recognized as safe (GRAS) substance because it had a long history of safe usage and the glutamate intake from added MSG was much lower than the total glutamate intake from foods.

In the late 1960s, two publications cast doubt on the safety of MSG. One was a study using neonatal mice that showed brain damage after the injection of large amounts of MSG. The other was a Letter to the Editor of a prestigious medical journal in which the author suggested that MSG could potentially be responsible for the adverse symptoms he experienced after eating Chinese meals (the so-called Chinese restaurant syndrome (CRS)). Following these reports, JECFA evaluated the safety of MSG in 1970. The Expert Committee concluded that glutamate as an additive in the diet could not cause brain damage.

Ajinomoto Co. felt it had a responsibility to evaluate the safety of MSG and believed that evidence should be based on sound science, so it began its own rigorous research on MSG. The company also sought objective scientific counsel and encouraged the involvement of renowned scientific institutions around the world.

JECFA re-evaluated MSG in 1987 and assigned MSG to 'ADI not specified' (ADI, acceptable daily intake), which is the safest category for a food additive[1]. Many rigorous experiments have now demonstrated that the ingestion of MSG in food is not associated with adverse reactions or CRS[2]. Indeed, MSG is one of the most studied food ingredients and its safety has undergone scrupulous review by scientific risk assessment bodies from organizations and governments worldwide, including the FAO, WHO, the European Commission, the US, Australia and New Zealand.

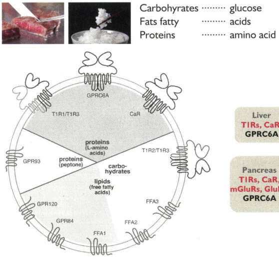

Figure 1a

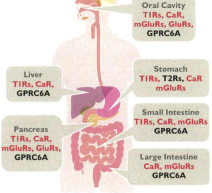

Figure 1b

Possible Physiological Actions		
Taste Information	Taste Sensation	Appetite/Food Palatability Recognition of umami taste
	Cephalic Phase Digestive Response	Food Ingestion Aid Saliva/Swallowing Reflexes
		Food Digestion Preperation Gastric/pancreatic juices GI hormones GI motility
Visceral Information	Post-ingestive effects	Appitite/Food Palatability Satiety Signaling
	Gastrointestinal Phase Digestive Responses	Triggering of Food Digestion Gut digestive enzymes GI hormones GI motility
		Mucosal Defense Mucus/bicarbonate

Figure 1c

Figure 1 | Physiological significance of nutrient signalling in the GI tract.
(a) Molecular pharmacology of promiscuous seven transmembrane receptors sensing organic nutrients (Wellendorph, P, Johansen, L. D. & Bräuner-Osborne, *H. Mol. Pharmacol.* **76**, 453–465 (2009). Taste-receptor candidates for recognition of the three major macronutrients. (b) Peripheral distribution of taste receptor candidates in the GI system and related organs. (c) Possible physiological activities mediated by nutrient chemical sensing during a meal.

History of research and development diversification

While the original seasonings business has expanded globally and remains a core concern for Ajinomoto Co., changes in production technology and competition have driven the company's diversification into multiple technological areas. The use of soy as a starting material in the early days of glutamate production led to the establishment of an edible oils business and eventually to diversification into the processed and frozen foods business. Furthermore, following the development of the first glutamate-producing *Corynebacterium* strain, other amino-acid-producing bacterial strains were developed. This has led to Ajinomoto Co. becoming the premier supplier of pharmaceutical-grade amino acids, as well as a major supplier of amino acids for feed. Nowadays, with the utilization of metabolic engineering, other targets are being pursued vigorously. The development of a *Corynebacterium* system for protein production is enabling Ajinomoto Co. to move into protein producing business, Corynex®[3] for the pharmaceutical industry.

Ajinomoto Co. has also invested in other life science areas, resulting in the 1981 establishment of its pharmaceutical business, which specializes in products for enteral and parenteral nutrition. This research has resulted in the creation of a biomarker business, AminoIndex® based on the generation of multiple component amino acid indices that can identify specific disease and physiological states[4].

The discontinuation of the chemical process for glutamate led to the creation of innovative products such as insulating films for layer build-up in microprocessors, with The Ajinomoto Build-up Film (ABF) becoming the de facto standard in microprocessor manufacturing. The recent development of a novel technology to manufacture high quality peptides has led to a peptide synthesis business, AJIPHASE®[5].

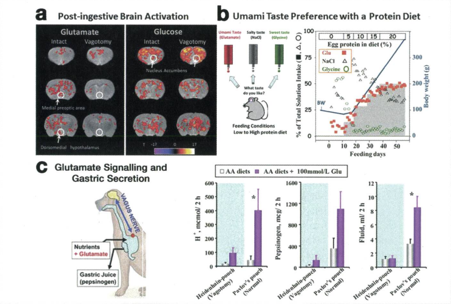

Figure 2 | **Glutamate signalling in the GI tract as a key mechanism for post-ingestive effects.**
(a) Brain activation after glutamate or glucose gavage. Intragastric glutamate stimulates different centres from those stimulated by glucose. The reward centre — the nucleus accumbens — only lit up with glucose, not with glutamate. Brain recognition of luminal glutamate is dependent on vagus nerve activation.
(b) Protein intake and taste preference. Rats prefer salty and sweet tastes with a low-protein diet, whereas they prefer umami taste with a high-protein diet.
(c) Effects of dietary glutamate on gastric exocrine secretion.
Levels of pepsinogen increased after direct administration of glutamate into the stomach.
The vagus nerve is intact in Pavlov-pouched dogs but dissected in Heidenhein pouched dogs[11].

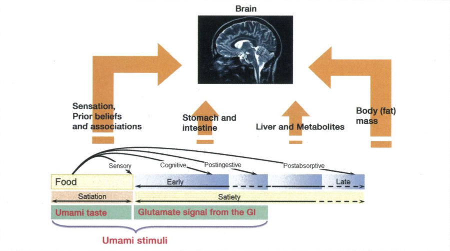

Figure 3 | **Possible mechanisms of food-intake regulation by umami stimuli.**
This cascade represents the effect of umami taste stimuli in satiation and satiety, which act via physiological signals to control the suppression of appetite after eating. *Modified from Dr. John Blundell (Blundell, J. E., Food Acceptance and Nutrition, Academic Press, London, 1987)*

Development of umami taste research

It is not surprising that, having been founded based on the discovery of umami, Ajinomoto Co. would pursue research on umami taste. Japanese researchers have played an important part in establishing umami as the fifth basic taste[6]. Many taste researchers believe that basic tastes reflect biological needs. That is, sweet taste signals energy (glucose and glycogenetic amino acids), salty taste is the signal for minerals (sodium and potassium), sour taste is the signal for organic acids, bitter taste is the signal for poisons and pharmacologically active compounds (plant alkaloids), and umami taste is the signal for protein (amino acids). Recently, a wide variety of taste receptors has been discovered. These receptors recognize components from the major macronutrients, such as carbohydrates and amino acids (Fig. 1a), and they have been found not only in the oral cavity, but also in other parts of the digestive tract. Researchers from Ajinomoto Co. and from other institutions have identified taste receptors on the mucosa of the digestive or gastrointestinal (GI) tract, such as the stomach and intestine, which appear to mediate the chemical perception of nutrients[7]. These data suggest that chemical sensing by taste receptors may help to regulate food digestion, nutrient utilization, and nutrient intake through modulation of the gut–brain axis[8]. Ajinomoto Co. researchers believe that further advances in understanding taste receptor physiology may provide therapeutic targets useful in treating pathologies such as overeating and anorexia. Such knowledge could help prevent lifestyle-related diseases including obesity and hypertension.

Discovery of glutamate-signalling mechanisms in the GI tract

Free glutamate, a major component of umami taste, is a well-known excitatory neurotransmitter in the brain. Consequently, neuroscience research dominated the field of glutamate receptors until the discovery of umami taste receptors at the beginning of the twenty-first century. After scientists identified the widespread peripheral distribution of these receptors, especially in the GI system, glutamate receptor research broadened to include peripheral chemical sensing (Fig. 1b). Chemical sensing of glutamate in the GI tract sends nutrient information via the abdominal vagus nerve from the stomach and intestine to the brain (afferent) and in turn relays physiological responses from the brain to the visceral organs (efferent) (Fig. 1c). The electrophysiologist Akira Niijima at Niigata University demonstrated that the vagus nerve responds to luminal application of free glutamate.

Subsequently, in collaboration with scientists from Ajinomoto Co., he found that coeliac afferents, the intestinal fibres that respond to nutrients, recognize each of the 20 amino acids, whereas gastric afferents respond only to free glutamate[9]. These data indicate that the intestinal mucosa is able to recognize all individual amino acids, whereas the gastric mucosa can only detect free glutamate.

More recent studies using functional magnetic resonance imaging (fMRI) have clarified the substrates of gut glutamate signalling[10]. They suggest that intragastric glutamate can activate the dorsal nucleus of the vagus nerve and the nucleus of the solitary tract, which are the output and input pathways of the vagus nerve, respectively. Other activated areas include the insula cortex, which integrates taste and visceral information, and the hypothalamus, a homeostatic control centre (Fig. 2a). Almost all nuclear activation disappears after abdominal vagotomy, strongly suggesting that glutamate sensing input to the brain is transmitted via the vagus nerve. This direct neural gastric–central nervous system afferent transmission is unique compared to those of other nutrients such as glucose or fat, for which information is transmitted by mechanisms independent of the vagus (that is, humoral factors).

Umami taste and its connection to protein appetite

Worldwide, collaborators with Ajinomoto Co. have helped to elucidate the connection between umami taste and glutamate signalling to the brain. About 30 years ago, Kunio Torii at Ajinomoto Co. demonstrated that rats fed a protein-rich diet prefer a solution with free glutamate[8] (Fig. 2b). Thereafter, physiologists from the Pavlov Institute of Physiology demonstrated that glutamate in the stomach lumen enhances acid and pepsin secretion induced by proteins, and that this is dependent on vagus nerve activation (Fig. 2c). Data were interpreted as suggesting that the GI system digests and absorbs proteins more effectively when accompanied by free glutamate[11]. Moreover, in addition to promoting protein digestion, physiologists from the University of California, Los Angeles (UCLA) revealed that glutamate in the gut also enhances mucosal defence mechanisms against the harmful effects of gastric juice by inducing the secretion of mucin and hydrogen bicarbonate[12].

On the basis of this evidence, it has been concluded that glutamate signalling plays an important part in enhancing protein digestion in the stomach. Visceral information from glutamate signalling may elicit the post-ingestive feeling of 'satiety' or 'satiation', characteristic of protein-rich foods. These functions give biological significance to the chemical sensing of free glutamate and may explain the reason why we have evolved a preference for umami taste, as glutamate is the most abundant amino acid in nature.

Benefits of umami seasoning in controlling eating behaviour

Because stimulation of the vagus nerve by glutamate may activate brain regions associated with energy homeostasis[8], the neuronal and hormonal pathways that are activated by umami taste may also influence appetite. The potential signalling mechanisms involved in the glutamate satiety cascade are illustrated in Fig. 3. This cascade indicates the effect of glutamate stimuli on satiation (which brings a meal to an end) and satiety (which maintains the inhibition of eating). Glutamate acts via physiological signals that modulate the suppression of appetite after eating.

The physiological responses that result from the taste of food are not only important in food palatability but are also believed to be implicated in the recent obesity epidemic. Compared to the number of publications there have been on the role of sweet taste and the regulation of appetite, few published human psychophysical studies have investigated the relationship between umami taste perception and body weight.

In a double-blind crossover study to investigate the effects of umami and sweet taste on satiation and food intake in women, umami taste had a stronger effect on modulating food choice than either sweet or bland tastes. Preloading subjects with an umami taste solution has the potential to reduce preference for high-fat foods in a subsequent meal. One possible implication of this result is that umami taste helps to preserve normal appetite.

Appetite regulation and satiety

Human milk is rich in free amino acids, among which glutamate is the most abundant. It is also higher in glutamate than for most mammals, with the exception of closely related primates. Glutamate levels are low in colostrum, but increase progressively during lactation until about the sixth month when infants often begin eating solid foods. Breast-fed infants are the gold standard for normative weight gain. Relative to breast-fed infants, infants fed a regular cow-milk infant formula show accelerated weight gain during the first 12 months of life. This accelerated gain has been reported to increase the risk for later obesity. Recent studies have found that free glutamate plays a role in satiation in infants[13]. Therefore, it is possible that free glutamate in breast milk is important in the regulation of infant food intake and body weight gain.

In normal-weight women between 20 and 40 years of age, a preload of chicken broth with MSG significantly decreases the subsequent sensation of hunger and desire to snack in comparison with a control group given a preload without MSG. This suggests that MSG can promote satiety in adults as well as infants.

Reducing dietary sodium

Dietary recommendations urge consumers to reduce their sodium intake because high sodium is a risk factor for the development of hypertension. Ajinomoto Co. has long had an interest in the properties of umami taste that may help to lower the salt content of foods. MSG and calcium di-glutamate (CDG) can enhance palatability in soups with low sodium levels. Indeed, they may partly replace sodium chloride without compromising the pleasantness of low-sodium chicken broth[14]. The Institute of Medicine Committee on Strategies to Reduce Sodium Intake in the US identified added MSG as one potential strategy to lower overall levels of sodium in food intake.

Flavour substance discovery and innovation

We cook using many kinds of seasonings that include many flavour ingredients. The discovery of new flavour substances contributes to our quality of life, allowing us to cook in different styles with similar food ingredients.

Major advances in understanding the basic mechanisms of taste perception in the last decade have led to the discovery of novel flavour substances. Ajinomoto Co. is now in the process of establishing screening systems for the discovery of new taste-modifying substances based on the calcium sensing receptor (CaSR), together with sensory evaluation studies. CaSR is thought to be involved in taste modification because it localizes in taste tissues and binds to glutathione and related peptides[15]. Glutathione and other peptides identified from foodstuffs are reported to enhance sweet, salty and umami taste. These substances particularly contribute to the oral sensation of thickness, continuity and mouthfulness, which are also given with umami substance, in foods. Which are also given with umami substance. Such modifying characteristics have been described by the Japanese term 'kokumi'[16].

Ajinomoto Co. scientists have identified several CaSR agonists, and they all have 'kokumi' properties. Several of the compounds have a higher activity than glutathione and they are now on the FEMA list of GRAS substances. One example is gamma Glu-Val-Gly (gEVG). This peptide, naturally present in foods, does not have any taste itself but provides a preferable 'kokumi' flavour at parts per million (p.p.m.) levels.

CaSR agonists such as gEVG[17] are thought to modify tastes through its receptor cells different from the ones that process sweet or umami taste. Research is on-going to try to elucidate the mechanisms of 'kokumi'

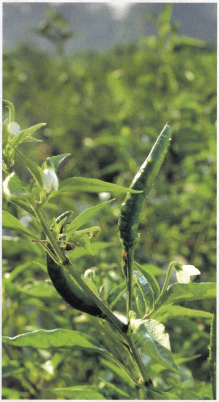

Figure 4 | Picture of CH-19 Sweet, the source of capsinoids.

Potential thermogenesis of 'hot' food

Besides the five basic tastes, trigeminal somatosensory stimuli are also important in the overall perception of foods. Many plant-derived irritants such as capsaicin, the active compound of chilli peppers, impart a sense of hotness to foods and drinks. The hotness or spiciness of capsaicin comes from activation of the transient receptor potential vanilloid receptor 1 (TRPV1) which is found in trigeminal neurons from the oral cavity.

Interestingly, the feeling of pungency from substances in spices seems to affect not only our preferences for food, but also thermogenesis. In fact, capsaicin has been reported to increase thermtogenesis mainly through activation of the central nervous system. In clinical trials, consumption of capsaicin with a meal immediately increased diet-induced energy expenditure. Although this trait may seem to have potential for controlling energy balance, long-term use of capsaicin can be limited by its strong irritant quality. Researchers at Ajinomoto Co. and collaborators have identified a possible solution with a capsinoid analogue from CH-19 Sweet, a less pungent chilli pepper (Fig. 4). This capsinoid is equipotent in thermogenesis but is much less pungent orally than capsaicin. The thermogenic effect of capsinoids also involves activation of TRPV1 receptors of vagal afferent neurons in the GI system. This in turn leads to activation of sympathetic efferent fibres that up-regulate uncoupling proteins[18], which is believed to be the mechanism by which an oral daily intake of 6 mg of capsinoids induced abdominal fat loss. More importantly, this increase in postprandial thermogenesis and an increase in fat oxidation were observed in obese patients consuming a calorie-restricted, high-protein diet supplemented with capsinoids[19].

Future directions

If the global population continues to grow at the current rate, it is predicted that food resources may become scarce. At the same time, insufficient, excess and/or unbalanced nutrition that leads to malnutrition, obesity and lifestyle-related diseases are also worldwide problems. Ajinomoto Co., with its strength in scientific innovation, can contribute to enhancing human health and the sustainability of food resources by providing healthier foods and ingredients with greater palatability, allowing the use of basic foodstuffs that are both easier to grow and more affordable.

The Ajinomoto Group will continue to pursue research and development in three main interacting areas: (1) food; (2) bioscience products and fine chemicals, and (3) pharmaceuticals and health. Our overall goal is to contribute to solving critical issues that will benefit human society by optimizing human health and environmental sustainability.

References

1.Walker, R. & Lupien, J. R. The safety evaluation of monosodium glutamate. *J. Nutr.* **130**, 1049S–1052S (2000).

2. Williams, A. N. & Woessner, K. M. Monosodium glutamate 'allergy': menace or myth? *Clin. Exp. Allergy* **39**, 640–646 (2009).

3. Yoshimi, K. *et al*. TatABC overexpression improves Corynebacterium glutamicum Tat-dependent protein secretion. *Appl. Environ. Microbiol*. **75**, 603–607 (2009).

4. Yohei, M. *et al*. Plasma free amino acid profiling of five types of cancer patients and its application for early detection. PLoS ONE **6**, e24143 (2011).

5. Daisuke, T. *et al*. Development of an efficient liquid-phase peptide synthesis protocol using a novel fluorine-derived anchor support compound with Fmoc chemistry; AJIPHASE®. *Tetrahedron Lett*. **53**, 1936–1939 (2012).

6. Yamaguchi, S. Basic properties of umami and its effects on food flavor. *Food Rev. Int*. **14**, 139–176 (1998).

7. San Gabriel, A. *et al*. mGluR1 in the fundic glands of rat stomach. *FEBS Lett*. **581**, 1119–1123 (2007).

8. Kondoh, T. *et al*. Activation of the gut-brain axis by dietary glutamate and physiologic significance in energy homeostasis. *Am. J. Clin. Nutr*. **90**, 832S–837S (2009).

9. Uneyama, H. *et al*. Luminal amino acid sensing in the rat gastric mucosa. *Am. J. Physiol. Gastrointest. Liver Physiol*. **291**, G1163–G1170 (2006).

10. Tsurugizawa, T. *et al*. Mechanisms of neuronal responses to gastrointestinal nutritive stimuli: the gut-brain axis. *Gastroenterology* **137**, 262–273 (2009).

11. Zolotarev, V. *et al*. Effect of free dietary glutamate on gastric secretion in dogs. Ann. N. Y. Acad. Sci. **1170**, 87–90 (2009).

12. Akiba, Y *et al*. Luminal L-glutamate enhances duodenal mucosal defense mechanisms via multiple glutamate receptors in rats. *Am. J. Physiol. Gastrointest. Liver Physiol*. **297**, G781–G91 (2009).

13. Ventura, A. *et al*. Infant regulation of intake: the effect of free glutamate content in infant formulas. *Am. J. Clin. Nutr*. **95**, 875–881 (2012).

14. Carter, B. E. *et al*. The sensory optimum of chicken broths supplemented with calcium-di-glutamate: a possibility for reducing sodium while maintaining taste. *Food Qual. Prefer.* **22**, 699–703 (2011).

15. Ohsu, T. *et al*. Involvement of the calcium-sensing receptor in human taste perception. *J. Biol. Chem*. **285**, 1016–1022 (2010).

16. Ueda, Y. *et al*. Characteristic flavor constituents in water extract of garlic. *Agric. Biol. Chem*. **54**, 163–169 (1990).

17. Maruyama, Y. *et al*. *Kokumi* substances enhancers of basic tastes induce responses in calcium-sensing receptor expressing taste cells. *PLoS ONE* **7**, e34489 (2012).

18. Watanabe, T. *et al*. Capsaicin, a pungent principle of hot red pepper, evokes catecholamine secretion from the adrenal medulla of anesthetized rats. *Biochem. Biophys. Res. Commun*. **142**, 259–264 (1987).

19. Lee, T. A. *et al*. Effects of dehydrocapsiate on adaptative and diet-induced thermogenesis with a high protein very low calorie diet: a randomized control trial. *Nutr. Metab*. **7**, 78–83 (2010).

nature.com/scientificreports

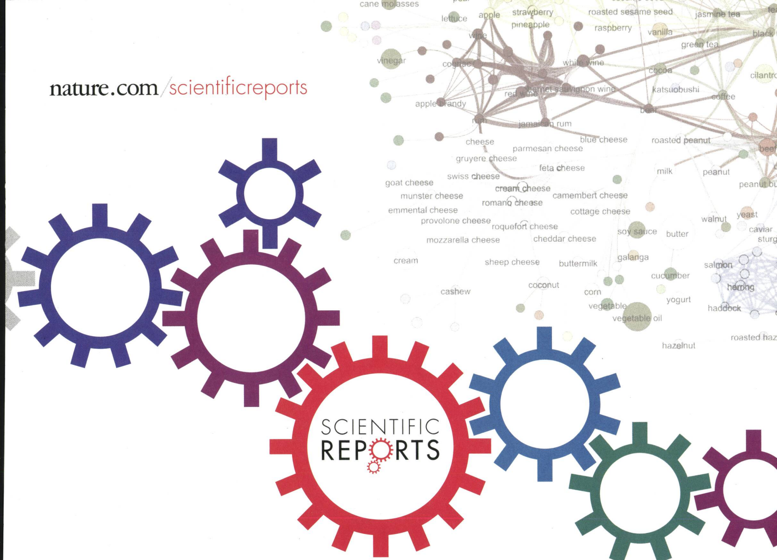
cane molasses
lettuce
apple
strawberry
pineapple
roasted sesame seed
raspberry
vanilla
jasmine tea
green tea
vinegar
cognac
white wine
cocoa
cilantro
red wine
cabernet sauvignon wine
katsuobushi
coffee
apple brandy
rum
jamaican rum
beer
cheese
parmesan cheese
blue cheese
roasted peanut
gruyere cheese
feta cheese
milk
peanut
swiss cheese
goat cheese
cream cheese
munster cheese
romano cheese
camembert cheese
emmental cheese
cottage cheese
walnut
yeast
provolone cheese
roquefort cheese
mozzarella cheese
cheddar cheese
soy sauce
butter
caviar
cream
sheep cheese
buttermilk
galanga
salmon
cashew
coconut
corn
cucumber
herring
yogurt
vegetable
vegetable oil
haddock
hazelnut
SCIENTIFIC REPORTS

Make your paper seen
Make your paper open
Submit to *Scientific Reports*

Flavor network and the principles of food pairing

- Viewed over 144,000 times
- Freely accessible online less than 9 weeks from submission after full peer review
- Covered in various media outlets including NPR, *Globe and Mail* and *Daily Mail*

Published in *Scientific Reports*

Submit your next paper to *Scientific Reports*

nature.com/scientificreports

nature publishing group npg

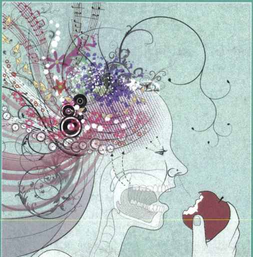

nature

http://www.nature.com/nature/outlook/taste

RESEARCH

NEW ONLINE

Papers published this week at Nature.com/nature

NEWS & VIEWS Genome-wide analyses of breast tumours suggest new drug targets **p.328**

PERSPECTIVE The prickly topic of human adaptation of avian H5N1 viruses **p.335**

LETTER With gigapixel digital photography, every snap is a torrent of data **p.386**

PUBLISHED 17 JUNE 2012

GENETICS

X chromosomes under control

In both eutherian (placental) and metatherian (marsupial) females, one of the two X chromosomes is inactivated to ensure that they have the same dose of X-linked genes as XY males. In eutherians, the inactivation is initiated by the non-coding RNA *Xist*, but *Xist* is not conserved in metatherians, so the mechanism underlying inactivation in these mammals has been unclear. Here, Jennifer Grant *et al.* identify a non-coding RNA, *Rsx*, with properties consistent with X-inactivation in a marsupial.

Rsx **is a metatherian RNA with** ***Xist*****-like properties in X-chromosome inactivation**
J Grant *et al.*
doi:10.1038/nature11171

NEUROSCIENCE

Primate neural circuits grasped

Dexterous hand movement in primates requires direct connections between the motor cortex, the part of the brain that controls movement, and spinal neurons. Tadashi Isa and colleagues establish a role for a conserved, 'evolutionarily older' indirect pathway that involves spinal interneurons in hand dexterity in macaques. The technique they used — selective and reversible blockade of synaptic transmission by double infection of viral vectors to control expression of GFP-tagged tetanus neurotoxin — should be useful for dissection of circuit function in other primates.

Genetic dissection of the circuit for hand dexterity in primates
M Kinoshita *et al.*
doi:10.1038/nature11206

BIOCHEMISTRY

Heterogeneous pathways and timing of factor departure during translation initiation
A Tsai *et al.*
doi:10.1038/nature11172

PUBLISHED 20 JUNE 2012

ASTRONOMY

In pursuit of the first stars

Rennan Barkana and colleagues report simulations of the distribution of the first stars at a red-shift of $z = 20$, a cosmic age of about 180 million years. The model takes account of a recent suggestion that star formation was suppressed in some regions by the velocity differences between dark matter and baryonic gas. The simulations suggest that such suppression would cause a signal in the 21-cm spectral emission line of neutral hydrogen — the dominant element in the early epochs — several times larger than previously estimated. That's within the observational capabilities of current large radio telescopes — if they were designed to observe 50–100 megahertz frequencies.

The signature of the first stars in atomic hydrogen at redshift 20
E Visbal *et al.*
doi:10.1038/nature11177

➲ YOUNG INVESTIGATOR AWARD

The 2012 Eppendorf Young European Investigator Award goes to Elizabeth Murchison (Wellcome Trust Sanger Institute, Cambridge, UK) for work on the cancer threatening the Tasmanian devil with extinction. Elizabeth talks about her work here:
www.nature.com/nature/awards/eppendorf

ECOLOGY

Ecosystem responses

At subcellular and individual levels, the relationship between respiration and temperature is exponential, but this is modified at the ecosystem level by community structure and species abundances. This study takes data from nine types of ecosystem to construct a global database of seasonal temperature dependence of ecosystem respiration. The data reveal that short-term (daily) temperature dependence is identical across all ecosystems and that long-term (annual) dependence is stronger in aquatic than terrestrial environments, which indicates that aquatic ecosystems will be more sensitive to global warming.

Reconciling the temperature dependence of respiration across timescales and ecosystem types
G Yvon-Durocher *et al.*
doi:10.1038/nature11205

CANCER

Novel mutations target distinct subgroups of medulloblastoma
G Robinson *et al.*
doi:10.1038/nature11213

ECOLOGY

Disentangling nestedness from models of ecological complexity
A James *et al.*
doi:10.1038/nature11214

MATERIALS

Graphene useful for plasmonics

Plasmonic devices that exploit surface plasmons (electromagnetic waves that propagate along the surface of metals) offer the possibility of controlling light at sub-wavelength scales. Graphene is a promising plasmonics platform as it can interact strongly with light and host surface plasmons in the infrared range. Two independent groups report that plasmons can be directly launched in graphene, and observed with near-field optical microscopy. Wavelengths and amplitudes of the plasmons can be tuned by a gate voltage, a promising capability for the development of on-chip graphene photonics for use in telecommunications and information processing.

Gate-tuning of graphene plasmons revealed by infrared nano-imaging
Z Fei *et al.*
doi:10.1038/nature11253

Optical nano-imaging of gate-tunable graphene plasmons
J Chen *et al.*
doi:10.1038/nature11254

BRIEF COMMUNICATIONS ARISING

Arising from 'Light echoes reveal an unexpectedly cool η Carinae during its nineteenth-century Great Eruption' by A Rest et al. *Nature* ***482,*** *375–378 (2012)*

The Great Eruption of η Carinae
K Davidson & R M Humphreys
doi:10.1038/nature11166

Reply **—** A Rest *et al.*
doi:10.1038/nature11167

NEWS & VIEWS

DRUG DISCOVERY

Computer model predicts side effects

Drug candidates are usually found to be unsafe only late in the drug discovery process. A method for predicting the many biological targets of a given molecule might allow drug safety to be considered much earlier. SEE ARTICLE P.361

KYLE KOLAJA

Creating safe, effective drugs is not for the faint hearted. Pharmaceutical companies screen up to millions of compounds to find the handful that are suitable for clinical development. The process typically begins with analogues of biologically active compounds being made to find those that interact potently and selectively with the drug target of interest. Attention then shifts to other properties of the compounds that could affect their use as drugs, including their safety profile. Unfortunately, predicting compound toxicity — let alone adverse side effects in patients — in preclinical studies is an onerous task. But on page 361 of this issue, Lounkine *et al.*[1] report a computational approach for predicting side effects that might help to streamline drug discovery*.

Identifying the mechanisms behind adverse drug effects remains inherently difficult, despite major investment in predictive tools by pharmaceutical and biotechnology companies (Fig. 1). The challenge is often magnified by the limited availability of many compounds, the need to identify toxicity risks in a short space of time and the difficulty in identifying the biological targets that mediate any observed toxicity[2]. Side effects can result from the intended action of a drug (such as the bleeding associated with medications that prevent blood clots) or because of unintended 'off-target' activity (such as the increase in blood pressure caused by torcetrapib, a compound that was designed to raise levels of 'good' cholesterol in the blood[3]). Any method that can rapidly and reliably identify the off-target activities of a compound, and the associated commercial liabilities, early in the drug-discovery process would be a powerful, must-have tool for a toxicologist.

Lounkine and colleagues use two steps to determine the biological targets for which a molecule may have affinity. The structural similarity of known ligand molecules for a given biological target is first calculated and the structural relationship of the group of ligands with a test compound is then assessed. This approach helps to reveal associations between compounds that would not be obvious from more conventional analyses of chemical structures or the amino-acid sequences of receptors. This mathematical method for predicting 'guilt by association' doesn't require any compound material to generate testable hypotheses, making it a neat way to rapidly interpret observations of toxicity.

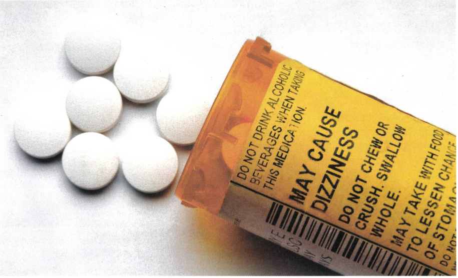

LAMB/ALAMY

Figure 1 | Assessing the risks. The adverse side effects of drugs are difficult to foresee. Lounkine and colleagues' computational method[1] for predicting such effects opens up a fresh approach for safety assessment in drug discovery.

To test their computational approach, Lounkine *et al.* used it to estimate the binding affinities of a comprehensive set of 656 approved drugs for 73 biological targets. They identified 1,644 possible drug–target interactions, of which 403 were already recorded in ChEMBL, a publicly available database of biologically active compounds. However, because the authors had used this database as a training set for their model, these predictions were not really indicative of the model's effectiveness, and so were not considered further.

A further 348 of the remaining 1,241 predictions were found in other databases (which the authors hadn't used as training sets), leaving 893 predictions, 694 of which were then tested experimentally. The authors found that 151 of these predicted drug–target interactions were genuine. So, of the 1,241 predictions not in ChEMBL, 499 were true; 543 were false; and 199 remain to be tested. Many of the newly discovered drug–target interactions would not have been predicted using conventional computational methods that calculate the strength of drug–target binding interactions based on the structures of the ligand and of the target's binding site.

The authors built on their results by identifying adverse side effects associated with a particular chemical structural fingerprint, again using a guilt-by-association mathematical approach. Their model predicted an impressive 247 new drug–target–side effect associations, shedding light onto previously unappreciated possible mechanisms of side effects. For example, it suggested that prenylamine (a drug that widens blood vessels) causes sedation by acting at the histamine H_1 receptor. And it predicted that the anti-allergy drug diphenhydramine causes tremors by acting not only at a known off-target receptor (the sodium channel SCN10A), but also at a dopamine transporter protein, SLC6A3, for which the drug was not previously known to be a ligand.

Lounkine *et al.* went on to provide strong experimental evidence of a previously unrecognized mechanism for the upper abdominal pain caused by chlorotrianisene, a drug used to treat symptoms of menopause and deficiencies in ovary function. Their computational method predicted that chlorotrianisene has potent affinity towards the COX-1 enzyme; COX-1 is a target of non-steroidal anti-inflammatory drugs, a class of molecules that has long been associated with adverse gastrointestinal events[4]. The authors found that chlorotrianisene potently inhibits platelet aggregation in samples of human blood, which is a widely accepted biomarker of the *in vivo* effects of COX-1 inhibition and connects chlorotrianisene's adverse effect to a plausible mechanism. This example demonstrates how rapidly Lounkine and colleagues' computational predictions can glean information about the off-target toxicology of drugs.

---

*This article and the paper[1] under discussion were published online on 10 June 2012.

Although the authors' computational approach is highly informative, it does have some deficiencies. Roughly half of its predictions of adverse drug activity are false, which could prompt unnecessary biological experimentation in drug-discovery programmes, or even stop a safe compound from being developed further as a drug. And, as with any test, Loukine and colleagues' approach will overlook certain drug activities — although such false negatives are less disconcerting at the early stages of drug discovery because thorough testing of on- and off-target effects will subsequently be conducted as a matter of course. It is also worth noting that the authors' assessment of their technique's performance is based on a retrospective training set; prospective use will be required to fine-tune the model and to discover how well it truly performs.

Nonetheless, a computational method for predicting which biological sites are likely to be targeted by compounds provides a new way to improve safety assessment in drug discovery. Because Lounkine and colleagues' approach doesn't require compounds to be synthesized or wet-lab experiments to be conducted, it will be useful very early in the discovery process to predict the potential for off-target binding of drug candidates, and so to prioritize which compounds should be made by medicinal chemists. The ability to associate side effects with predicted off-target activity means that chemists can be guided not only by the efficacy of compounds, but also by safety concerns, as soon as a drug-discovery programme is initiated. ■

Kyle Kolaja *is in the Department of Nonclinical Safety, Hoffman-La Roche, Nutley, New Jersey 07110, USA.*
e-mail: kyle.kolaja@roche.com

1. Lounkine, E. *et al. Nature* **486,** 361–367 (2012).
2. Sasseville, V. G. *et al. Chem. Biol. Interact.* **150,** 9–25 (2004).
3. Schwartz, G. G. *Curr. Atheroscler. Rep.* **14,** 41–48 (2012).
4. Park, S. C., Chun, H. J., Kang, C. D. & Sul, D. *World J. Gastroenterol.* **17,** 4647–4653 (2011).

MATERIALS CHEMISTRY

Carbon origami

A reaction that folds up large aromatic molecules and fixes them into bowl shapes expands opportunities for making nanometre-scale objects from single sheets of carbon. Such objects have potential applications in electronics.

JAY S. SIEGEL

Single layers of carbon atoms, known as graphene sheets, have been fêted as the material of choice for future generations of electronic devices. But carbon can form a broad range of networks besides the hexagonal 'chicken-wire' arrangement of atoms found in graphene. For example, networks formed from combinations of rings of five, six or seven carbon atoms can result in bowl, tube and saddle morphologies[1] that have diverse physical and electronic properties of use in applications ranging from structural engineering to light-energy conversion. Although they may form spuriously in nature, their selective preparation is difficult, requiring a high level of expertise in the crafts of molecular design and chemical synthesis. Reporting in *Angewandte Chemie*, Amsharov *et al.*[2] describe a practical method for preparing bowl-shaped carbon structures (buckybowls) in high yields, offering the tantalizing prospect that other extended, non-planar networks of carbon atoms will be accessible in the future.

The authors start from polynuclear aromatic compounds (Fig. 1), which can be thought of as small graphene fragments. Transformation of these fragments into buckybowls can be achieved by forming carbon–carbon (C–C) bonds exclusively across 'cove' regions in the molecules — regions in which the carbon skeleton of the molecule curves inwards like the coastline around a cove. These reactions result in the formation of five-membered rings that induce the curvature found in carbon bowls and tubes; however, selectively forming C–C bonds across cove regions is easier said than done.

Amsharov *et al.* offer a solution to this problem by heating a polynuclear aromatic compound that bears a fluorine atom in the cove region with an alumina catalyst (Al_2O_3). This is a remarkable approach because carbon–fluorine bonds are generally regarded as being very strong, and therefore unreactive. The authors observed that only fluorine atoms in cove regions take part in the transformation — when they performed their reactions on starting materials containing fluorine atoms at non-cove regions, these atoms remained unaltered in the product.

The transformation occurs at temperatures substantially lower than those required by alternative methods for making carbon networks, such as flash vacuum pyrolysis[3] (FVP), in which the reactant is rapidly heated in a vacuum, or chemical vapour deposition[4], in which starting materials react on the surface of a substrate to make a thin film. What's more, the method works well with solid substrates in the absence of a solvent, affording well-characterized products in good yields. This is handy, because many of the substrates that are likely to be used in the reaction are insoluble in most solvents. The authors also report that, in compounds that have several cove regions bearing a fluorine atom, C–C bonds can form at multiple regions.

Amsharov and colleagues' reaction is one of several transformations[5] that create new C–C bonds between aromatic rings, starting from aryl halides — compounds in which an aromatic ring is attached through a carbon atom to a halogen, typically chlorine, bromine or iodine. For example, FVP is known to effect intramolecular reactions of this sort by eliminating hydrogen halide molecules (HX, where X is a halogen) from aryl halides. These FVP processes involve highly reactive intermediates, such as free radicals, carbenes or benzyne. Aryl halides can also react on certain metal surfaces to form ribbons or star-shaped junctions of graphene[6]; catalysis by the metal makes the reaction possible.

Most such reactions of aryl halides work best with starting materials that bear weak carbon–halogen bonds: carbon–iodine bonds are generally the weakest, then carbon–bromine bonds, followed by carbon–chlorine bonds. Carbon–fluorine bonds are typically even stronger than carbon–chlorine bonds, and so Amsharov and colleagues' use of these in C–C bond-formation reactions is unusual, with few other examples known[7,8].

The development of strategies to manufacture graphene and related carbon-based materials that have designed shapes and symmetries[9] is one of the foremost challenges in materials chemistry. Similarly, the race to find an industrial method for producing graphene sheets of decimetre-to-metre dimensions is hotly contested. Recent developments, such

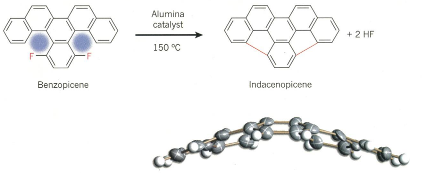

Figure 1 | Bent into shape. Amsharov *et al.*[2] report a method for making buckybowls — nanometre-scale objects that can be thought of as a single layer of carbon atoms bent into a bowl shape. They used a reaction in which a carbon–carbon bond forms across the 'cove' regions (blue areas) of polynuclear aromatic compounds, such as the benzopicene molecule in this example. The reaction requires an alumina (Al_2O_3) catalyst and occurs only where fluorine atoms are present at cove regions. The fluorine atoms in the starting material, and the bonds formed during the reaction, are shown in red. The structure shown beneath the reaction is the X-ray crystal structure of the buckybowl product, indacenopicene.

as kilogram-scale processes for preparing the archetypal buckybowl, corannulene[10], will help by increasing the commercial availability of building blocks for carbon nanotubes and graphene fragments.

To understand one way in which such fragments could be used, consider the example of a fullerene — a 'buckyball' of carbon atoms, in which the atoms form the vertices of a network of polygons that makes up a spherical surface. Imagine cutting the network open. Depending on where you cut, various two-dimensional projections can be obtained[11,12] that can be folded back into the ball. If polynuclear aromatic compounds are available that correspond to such projections, then synthetic methods such as that of Amsharov *et al.* could be used to fold up the molecules and 'glue' the edges together.

The synthesis of specific projections is therefore a fashionable strategy for preparing designer fullerenes[13]. Compounds such as corannulene are good starting points for many such projections, so having a readily available supply opens up opportunities to make these materials[14]. In the same way, the synthesis of molecules that can be thought of as cross-sections of carbon nanotubes has become something of an art form[15,16], with one idea being that these could be stacked up and joined together to make nanotubes.

It is worth noting that, although many aspects of chemical synthesis may be thought of as having the character of engineering, chemical methods are not generally transferable to every synthetic problem — unlike universal engineering tools, which can be used transferably to make almost anything. The optimal construction of molecular targets often requires finding exactly the right tool for each job. Nevertheless, seemingly specialized synthetic methods do evolve into everyday tools used by chemists around the world and, ultimately, into scalable processes for industrial chemical production. In this way, Amsharov and colleagues' findings, and those of others aiming to make similar materials, are vital because they reveal new types of efficient chemical transformation that might some day form the basis of the manufacture of graphenic materials tailored to a variety of applications. ■

Jay S. Siegel *is at the Organic Chemistry Institute, University of Zurich, Zurich CH-8057, Switzerland.*
e-mail: jss@oci.uzh.ch

1. Ebbesen, T. W. *Phys. Today* **49** (June), 26–32 (1996).
2. Amsharov, K. Y., Kabdulov, M. A. & Jansen, M. *Angew. Chem. Int. Edn* **51,** 4594–4597 (2012).
3. Brown, R. F. C. *Pyrolytic Methods in Organic Chemistry: Application of Flow and Flash Vacuum Pyrolytic Techniques* (Academic, 1980).
4. Bae, S. *et al. Nature Nanotechnol.* **5,** 574–578 (2010).
5. Hassan, J., Sévignon, M., Gozzi, C., Schulz, E. & Lemaire, M. *Chem. Rev.* **102,** 1359–1469 (2002).
6. Cai, J. *et al. Nature* **466,** 470–473 (2010).
7. Allemann, O., Duttwyler, S., Romanato, P., Baldridge, K. K. & Siegel, J. S. *Science* **332,** 574–577 (2011).
8. Douvris, C. & Ozerov, O. V. *Science* **321,** 1188–1190 (2008).
9. Simpson, C. D. *et al. J. Am. Chem. Soc.* **126,** 3139–3147 (2004).
10. Butterfield, A. M, Gilomen, B. & Siegel, J. S. *Org. Proc. Res. Dev.* **16,** 664–676 (2012).
11. Scott, L. T. *et al. Science* **295,** 1500–1503 (2002).
12. Otero, G. *et al. Nature* **454,** 865–868 (2008).
13. Scott, L. T. *Angew. Chem. Int. Edn* **48,** 436–437 (2009).
14. Scott, L. T. *et al. J. Am. Chem. Soc.* **134,** 107–110 (2012).
15. Omachi, H., Segawa, Y. & Itami, K. *Acc. Chem. Res.* http://dx.doi.org/10.1021/ar300055x (2012).
16. Jasti, R., Bhattacharjee, J., Neaton, J. B. & Bertozzi, C. R. *J. Am. Chem. Soc.* **130,** 17646–17647 (2008).

GENOMICS

The breast cancer landscape

Whole-genome sequencing of breast cancers is exposing the scope of tumour diversity and helping to pinpoint avenues for precise diagnostics and targeted therapy. SEE ARTICLES P.346 & P.353, LETTERS P.395, P.400 & P.405

JOE GRAY & BRIAN DRUKER

The information-generating power of genome-analysis technologies is increasing at a rate that surpasses even the doubling in computer performance that is achieved every 18 months by the semiconductor industry[1]. Genome-analysis methods are now sufficiently powerful, fast and reliable that they are underpinning efforts to elucidate the molecular architecture of human cancers[2,3] and, in some cases, can be used in routine clinical practice[4]. Five papers[5–9] published in this issue present whole-genome analyses of a range of different breast cancers, providing a comprehensive picture of breast cancer's genetic diversity and suggesting refined tumour-classification strategies and new lines of therapeutic attack.

Genome-analysis techniques allow detection of various genetic abnormalities, including DNA sequence changes, structural changes (such as translocations) that alter the order in which DNA segments occur in the genome, and copy-number variants, in which whole segments of DNA are deleted, duplicated or amplified. These techniques can also provide information about the transcriptome — the complement of RNA molecules that are transcribed from DNA — at a particular time or in a particular tissue. Furthermore, they can give an indication of epigenetic modifications, which are chemical modifications to DNA and associated proteins that regulate gene transcription rates without changing the nucleotide sequence.

Early transcriptome-wide studies of patients with breast cancer demonstrated that the tumours could be organized into subtypes on the basis of patterns of gene expression that differed in clinical outcome[10]. This advance led to the development of clinical assays that are now used to identify patients at sufficiently low risk of cancer recurrence to warrant surveillance in lieu of chemotherapy[11,12]. Genome-wide measurements of DNA sequence, copy number, structure and gene-expression levels during the past decade have revealed remarkably diverse derangement in individual breast tumours, among different tumours and during various stages of tumour development. These aberrations involve many genes, including several implicated in cancer[13–15].

Expanding on these analyses are genome-wide functional studies[16], which have begun to identify aberrant genes that contribute to the changes in physiological processes that occur in breast cancer, in the hope that these might yield to therapeutic attack. These studies were inspired by the development of therapies that effectively treat tumours in which the gene *ERBB2* is amplified[17]. In parallel, *in vitro* systems that model aspects of breast-cancer diversity are being used to identify molecular features that predict therapeutic responses[18,19]. These efforts are now being stimulated by the development of high-resolution and high-throughput techniques, including microarray analysis and massively parallel DNA and RNA sequencing, that provide detailed information about the nature of cancer-causing aberrations[20].

The five papers in this issue describe the application of these techniques to a range of breast cancers. Curtis *et al.*[5] (page 346) analysed copy number, sequence changes known as single nucleotide polymorphisms, and gene-transcription rates in approximately 2,000 breast cancers encompassing all known types. They defined 45 regions of sequence amplification or deletion that deregulate genes that are likely to be involved in the pathophysiology of breast cancer. These regions are now sufficiently well defined for researchers to commence studies of the driver genes expected to lie therein. Curtis and colleagues also integrated their measurements of copy number and gene expression to define new breast-cancer subtypes that are associated with different patient outcomes, although these associations are not yet strong enough to be applied in the clinic.

Triple-negative breast cancers are those in which the tumours express neither *ERBB2* nor the genes that encode the receptors for oestrogen or progesterone. Shah *et al.*[6] (page 395) assessed mutations, copy number and gene expression in triple-negative breast cancers and found that the frequencies of copy-number abnormalities and mutations vary markedly between and within the tumours, which indicates that mutations can arise at multiple stages of tumour progression. Their study also suggests that three genes, *TP53*, *PIK3CA* and *PTEN*, are involved in the early stages of breast-cancer development. Interestingly, only one-third of the low-prevalence mutated genes that the authors identified were transcribed into RNA, which suggests that they may be chance mutations unrelated to the cancer and/or that the mutations involved genes with tumour-suppressive activity.

Stephens *et al.*[7] (page 400) analysed somatic mutations and copy-number variants in 100 breast cancers and discovered numerous aberrations, including nine new cancer genes that were mutated rarely but more frequently than would be expected by chance, indicating that they have functional roles in the cancers in which they arise. Many of these mutations are predicted to lead to the expression of truncated proteins, which implies that the proteins, in their normal forms, are likely to have tumour-suppressor roles. The authors also report that certain DNA-base substitutions are strongly associated with the age of the patient in tumours that do not overexpress the ostrogen receptor (oestrogen-receptor-negative tumours), but not in oestrogen-receptor-positive (overexpressing) ones, suggesting an important difference in the dynamics of mutation accumulation in these two tumour types.

> ***"The data in these five manuscripts are a remarkable testament to the power of genomic technologies."***

Ellis and colleagues[8] (page 353) focused on oestrogen-receptor-positive breast cancers. They assessed the genomes of tumours from patients participating in pre-operative clinical evaluation of their response to a class of drugs called aromatase inhibitors. The researchers showed that tumours that have a high frequency of cells expressing a protein, Ki67, which is associated with resistance to aromatase inhibitors, contained an elevated frequency of somatic mutations (those that arise during tumour progression, rather than being inherited) and genome-structure changes compared with tumours with a low frequency of Ki67-positive cells. This finding implicates genetic changes that lead to deregulation of DNA replication and repair processes in this drug resistance. However, a single 'smoking gun' predictor of resistance did not emerge from this study.

Finally, Banerji and colleagues[9] (page 405) examined somatic mutations in diverse breast cancers and report a rate of non-silent mutations (those that change the amino-acid sequence of a protein) of around one mutation per million DNA base pairs. Their study also added three aberrations to the list of those implicated in breast cancer — mutations in the genes *CBFB* and *RUNX1*, and the *MAGI3–AKT3* gene fusion.

The data in these five papers are a remarkable testament to the power of genomic technologies to define the landscape of a complex disease state, and they give us the most thorough view yet of the molecular underpinnings of breast cancers. However, much remains to be accomplished to move this information into routine clinical practice. These studies, and those that preceded them, show that individual breast cancers typically carry a few consistent and functionally characterized abnormalities, along with tens to thousands of other changes that are rare or unique to the individual tumour and about which little is known. We need to understand which of these genes contribute to tumorigenesis or tumour progression and how this ensemble of aberrations collaborates, changes during tumour evolution and interacts with the tumour microenvironment — and thereby how it regulates each tumour's behaviour and response to therapy. Understanding such deregulated biology should facilitate the development of therapeutic approaches targeting specific cellular pathways, including combination therapies, which are likely to be needed to achieve more durable patient responses.

However, therapeutic-strategy development will require target validation, tumour-genome analysis (especially of tumours that respond to treatment), and the organization and analysis of clinical metadata on a scale that has not yet been attempted. Although this is a daunting prospect, the promise still remains that the precision with which breast cancers are diagnosed and managed will be improved by the identification of new drug targets and by the ability to assign cancers to molecular subtypes that are associated with effective treatments. This is being made possible only by the remarkable advances in measurement science and computational capability. ■

Joe Gray *and* **Brian Druker** *are at the Knight Cancer Institute, Oregon Health and Science University, Portland, Oregon 97239, USA.*
e-mails: grayjo@ohsu.edu; drukerb@ohsu.edu

1. www.genome.gov/sequencingcosts
2. Collins, F. S. & Barker, A. D. *Sci. Am.* **296,** 50–57 (2007).
3. Hudson, T. J. *et al. Nature* **464,** 993–998 (2010).
4. Corless, C. L. *Science* **334,** 1217–1218 (2011).
5. Curtis, C. *et al. Nature* **486,** 346–352 (2012).
6. Shah, S. P. *et al. Nature* **486,** 395–399 (2012).
7. Stephens, P. J. *et al. Nature* **486,** 400–404 (2012).
8. Ellis, M. J. *et al. Nature* **486,** 353–360 (2012).
9. Banerji, S. *et al. Nature* **486,** 405–409 (2012).
10. Perou, C. M. *et al. Nature* **406,** 747–752 (2000).
11. Paik, S. *et al. N. Eng. J. Med.* **351,** 2817–2826 (2004).
12. van 't Veer, L. J. *et al. Nature* **415,** 530–536 (2002).
13. Gray, J. W. & Chin, L. *Nature* **452,** 553–563 (2008).
14. Meyerson, M. *et al. Nature Rev. Genet.* **11,** 685–696 (2010).
15. Kristensen, V. N. *et al. Proc. Natl Acad. Sci. USA* **109,** 2802–2807 (2012).
16. Sims, D. *et al. Genome Biol.* **12,** R104 (2011).
17. Slamon, D. *et al. N. Engl. J. Med.* **365,** 1273–1283 (2011).
18. Heiser, L. M. *et al. Proc. Natl Acad. Sci. USA* **109,** 2724–2729 (2012).
19. Barretina, J. *et al. Nature* **483,** 603–607 (2012).
20. Mardis, E. R. *Nature* **470,** 198–203 (2011).

NUCLEAR PHYSICS

Symmetrical tin

The tin isotope ^{100}Sn is the heaviest 'doubly magic nucleus' that has an equal number of protons and neutrons. It is now finally starting to give up its secrets, thanks to the persistent efforts of nuclear physicists. SEE ARTICLE P.341

DANIEL BAZIN

On page 341 of this issue, Hinke *et al.*[1] report how, after years of endeavour, they have achieved a significant leap forward in the study of the heaviest 'symmetrical doubly magic' nucleus — the tin isotope ^{100}Sn. Composed of 50 protons and 50 neutrons, this nucleus is drawing the attention of nuclear physicists around the globe because of its unique location in the nuclear landscape.

Nuclei are complex and challenging quantum objects. In contrast to the structure of atoms, for which the fundamental interaction between the electrons and the nucleus — the electromagnetic force — is known with great precision, the interaction between the constituents of a nucleus, the strong nuclear force, is not so well known. This is due in part to the composite nature of the nuclear constituents, or nucleons, and the nature of the fundamental forces that bind nucleons together (quantum chromodynamics and the electroweak force).

As far as we know, nuclei are the smallest objects that can be split up into their constituents. They are therefore the smallest entities in which emergent properties — patterns that arise from complexity — can be studied. Nuclear scientists study these emergent phenomena and are using them to decipher the nature of the nuclear force. Magic numbers are numbers of protons or neutrons that form full shells in an atomic nucleus, and are perhaps the foremost emergent property of nuclei. Thought to have first been coined by the physicist Eugene Wigner, the term reflects the unexpected shell structure of nuclei, as opposed to the liquid-like behaviour expected for such densely packed and strongly interacting objects. In fact, the independent particle model used to describe atoms, in which electrons (the particles) are assumed to move independently of each other, also works remarkably well for nuclei. The model has been able to explain — at least for stable nuclei[2] — the observed sequence of magic numbers: 2, 8, 20, 28, 50, 82 and 126, all of which, by virtue of their 'magic' nature, correspond to increased stability.

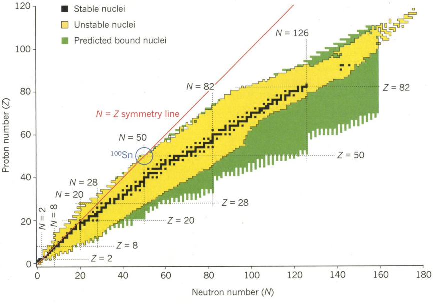

Figure 1 | Nuclear landscape. The chart shows the location of all nuclei as a function of their neutron number (*N*) and proton number (*Z*). Dashed lines represent magic numbers, which correspond to full shells of protons or neutrons. Doubly magic nuclei lie at the intersections of magic-number lines. Symmetrical nuclei have an equal number of protons and neutrons. Hinke *et al.*[1] have produced and studied ^{100}Sn, the heaviest symmetrical doubly magic nucleus. Note that the calculation used to predict bound nuclei in this chart is limited to those with *N* less than 160.

In recent years, however, as physicists have expanded their reach across the nuclear landscape, a different picture has emerged. The magic numbers observed in stable nuclei seem to be either vanishing or evolving, especially on the neutron-rich side of the nuclide chart[3,4], which plots proton number against neutron number (Fig. 1).

Nuclei that have a magic number of neutrons or protons are more tightly bound than their non-magic counterparts, and their intrinsic simplicity makes them prime candidates for testing proposed models of nuclear structure. Particularly interesting are nuclei in which the number of both protons and neutrons reaches one of the magic numbers. These doubly magic nuclei have even greater binding energy than singly magic nuclei.

One would expect that symmetrical doubly magic nuclei, which have an equal magic number of protons and neutrons, would follow the magic number sequence, and this is indeed the case for light nuclei: those of helium (^{4}He), oxygen (^{16}O) and calcium (^{40}Ca). However, because of the repulsion between protons, the line of stable nuclei in the nuclide chart veers away from the symmetry line, as ever more neutrons are required to bind heavier nuclei (Fig. 1). As a result, the only two other nuclei that follow the magic sequence are the nickel nucleus ^{56}Ni and ^{100}Sn. These nuclei are bound but unstable: they undergo β-decay, in which a positron (the antiparticle of an electron) is emitted to produce a daughter nucleus.

Although ^{56}Ni is not too far from being a stable nucleus (^{58}Ni is stable), ^{100}Sn is very close to the edge of nuclear stability, where the nuclear force between nucleons can no longer bind them into a nucleus. The nucleus ^{100}Sn has 12 neutrons fewer than the lightest stable isotope of tin, ^{112}Sn. Therein lies the particular attraction of ^{100}Sn: it is at the same time doubly magic and at the edge of the nuclear landscape. Many long-standing questions about this oddball are now beginning to be answered. For example, is it really doubly magic and simple in structure? How is the strength of its β-decay distributed across the energy levels of its daughter nucleus, indium-100? Does it have isomeric (metastable) states? The study of its β-decay is particularly interesting because of the large energy gap between the ground state of ^{100}Sn and that of its daughter, a characteristic of nuclei that are close to the limits of nuclear binding.

Unfortunately, what makes this nucleus attractive is also what makes it difficult to study. It is so far away from stable isotopes that it is extremely difficult to produce. Two types of nuclear reaction have typically been used to attempt this feat. One, called fusion–evaporation[5], is a bottom-up approach, in which two nuclei are fused together with minimum excitation energy, so as to minimize the subsequent loss of protons or α-particles (^{4}He nuclei). The other reaction, called projectile fragmentation[6], is more brutal but at present more effective. In this approach, a high-energy projectile that is heavier than ^{100}Sn — the xenon nucleus ^{124}Xe, at 1 gigaelectronvolt per atomic mass unit in Hinke and colleagues' experiment[1] — is sheared by making it collide with a target, leaving a residue that is composed of 50 protons and 50 neutrons. The chance of ending up with the desired nucleus is greater in the former approach than in the latter, but because of the underlying high energy involved, the latter method is more efficient at finding the 'needle in the haystack', and the experiment is actually feasible. To give a sense of the filtering (isolating the desired nuclei from the multitude of other species produced by the nuclear reaction) needed to pull this off, consider that, out of the 1.2×10^{15} ^{124}Xe projectiles accelerated during Hinke and colleagues' experiment at the GSI Helmholtz Centre for Heavy Ion Research in Darmstadt, Germany, only 259 ^{100}Sn nuclei were identified.

The results of the authors' experiment represent a giant step compared with previous attempts to study ^{100}Sn. Not only have the experimenters greatly improved the precision of the half-life measurement of this isotope, but they have, for the first time, also determined the end point of the energy spectrum of β-decay (the maximum energy of the emitted positrons) and have observed γ-ray transitions, which correspond to decays between states of the daughter nucleus. Their deductions are stunning: ^{100}Sn seems to have the highest-known β-decay strength of all nuclei, and has been classified as a 'superallowed Gamow–Teller decay' (Gamow–Teller transitions allow the spin to change by 0 or ± 1 between the initial state of the parent and the final states of the daughter). Usually, this label is reserved for Fermi decays (transitions that occur between states of the same spin), because they typically have the largest strengths.

As always happens with scientists, once they have been given a taste of a new delicacy, they crave more. Other laboratories have joined the race and are working to improve on the GSI ^{100}Sn production rates. They include: the Radioactive Isotope Beam Factory in Wako, part of Japan's RIKEN national network of labs, which has recently synthesized ^{100}Sn nuclei; SPIRAL2 at the heavy-ion accelerator GANIL in France; and the Facility for Rare Isotope Beams at Michigan State University. These facilities will produce this remarkable nucleus, as well as many others, in even larger quantities. Deciphering the emergent properties of ^{100}Sn, and of other nuclei located far from the stability line on the nuclide chart, should lead scientists towards a fuller understanding of the nuclear force. ■

Daniel Bazin *is at the National Superconducting Cyclotron Laboratory, Michigan State University, East Lansing, Michigan 48824–1321, USA.*
e-mail: bazin@nscl.msu.edu

1. Hinke, C. B. *et al. Nature* **486,** 341–345 (2012).
2. Mayer, M. G. *Phys. Rev.* **74,** 235–239 (1948).
3. Mayer, M. G. & Jensen, J. H. D. *Elementary Theory of Nuclear Shell Structure* (Wiley, 1955).
4. Sorlin, O. & Porquet, M.-G. *Prog. Part. Nucl. Phys.* **61,** 602–673 (2008).
5. Seweryniak, D. *et al. Phys. Rev. Lett.* **99,** 022504 (2007).
6. Morrissey, D. J. & Sherrill, B. M. *Phil. Trans. R. Soc. Lond. A* **356,** 1985–2006 (1998).

PLANETARY SCIENCE

Early start for rocky planets

The chemical composition of stars that host small planets seems to be more varied than that of large planets. This finding may push back the clock for the start of rocky planets and of life around stars other than the Sun. SEE LETTER P.375

DEBRA FISCHER

On page 375 of this issue, Buchhave *et al.*[1] describe a spectroscopic analysis of the chemical composition of stars hosting planet candidates that have been detected by NASA's Kepler mission. The authors have focused on 152 stars harbouring planet candidates that are a similar size to Neptune or smaller. The key result of this work is that small planets — those with a radius up to four times that of Earth — form under a broader range of environmental conditions than do gas-giant planets. This is an important finding, as it shows that the formation of small planets is a less constrained process than is the formation of large planets. It also implies that small, rocky planets formed at an earlier epoch in the Universe's history than gas giants*.

To appreciate this result, flash back to only a few hundred million years after the Big Bang, when the first stars in the Universe had just formed; the Universe today is approximately 14 billion years old. Those stars were composed of only hydrogen and helium, because heavier elements did not yet exist. Metals — defined by astronomers as all elements that are heavier than helium — are manufactured by the fusion of lighter elements in the 'pressure-cooker' cores of stars. When stars explode at the end of their lifetimes, their repositories of metals are cast into space, where they seed molecular clouds to produce new generations of stars that are enriched in heavy elements. Thus powered by the life cycle of stars, the chemical composition of the Universe has evolved from a simple mixture of hydrogen and helium gases to its current state replete with all of the elements in the periodic table.

The chemical evolution of the Universe has profound implications for the formation of planets. Planets are born in 'protoplanetary' disks around nascent stars; both the star and the protoplanetary disk inherit the chemical composition of the parent molecular cloud. A star that consists of only hydrogen and helium will have a disk with that same composition. This makes it unlikely that the first stars in the Universe formed with planetary companions or life; the elements from which planets and our bodies are made did not exist. Even if exotic gas-giant planets composed of hydrogen and helium existed, they could not have harboured pools of liquid water or a veneer of prebiotic chemistry. Therefore, planets that could have acted as platforms for biology did not populate the early Universe.

Fast-forward 13.6 billion years to the present time and the situation is markedly different. Ground-based surveys, a hallmark of the past two decades, have detected hundreds of planets orbiting nearby stars. As the first of these planets were discovered, an interesting correlation was immediately noted: a large fraction of gas-giant planets was being detected around metal-rich stars[2–4]. Conversely, gas-giant planets were rarely detected around stars that had metallicities (metal abundances) lower than that of the Sun[5]. The general interpretation of this planet–metallicity correlation was that the presence of heavy elements is an environmental condition that increases the density of the protoplanetary disk and therefore the efficiency of planet formation. In the past few years, however,

> ***"This result is exciting because it illuminates the history of the environmental requirements for planet formation."***

---

*This article and the paper[1] under discussion were published online on 13 June 2012.

ground-based surveys have also detected super-Earths — planets that have masses from a few to ten times the mass of Earth. Interestingly, the host stars of these low-mass planets do not seem to exhibit the same high metal content as do hosts of gas-giant planets.

NASA's Kepler mission has revolutionized exoplanet science by virtue of its vast number of planet detections — more than 2,000 planet candidates to date. Buchhave and colleagues' analysis is the first comprehensive assessment of host-star metallicity for the super-Earth- and Neptune-sized planets detected by Kepler, and it elevates the trend inferred by ground-based surveys[6] to a solid statistical result: small planets can form around stars that have a lower metal content than do the host stars of gas-giant planets. The authors obtained the element composition of Kepler stars by matching observed spectra to reference spectra.

This result is exciting because it illuminates the history of the environmental requirements for planet formation. In the beginning, stars formed in isolation, without planets or life. As the chemical evolution of the Universe proceeded, protoplanetary disks developed with a sufficient inventory of heavy elements to build the cores of planets, whether rocky or gaseous. However, for a gas-giant planet to form, there is a race against time: the core needs to reach a critical mass before the gas-rich material dissipates from the disk, which occurs within about 5 million years[7,8]. If the core reaches the critical mass before the gas is lost, runaway gas accretion occurs. High metallicity helps the core to win this race. Small, rocky planets can accrete dust and rocky material long after the volatile gas has dissipated from the disk. They then acquire tenuous atmospheres by releasing light, volatile elements as gas or by accreting trace amounts of gas from the disk. This process can continue for 50 million to 100 million years[9–11].

Unfortunately, it is difficult to use knowledge of metallicity to pinpoint the beginning of the 'age of planet formation', because the chemical enrichment of the Universe is not a monotonic process — some regions inside galaxies may have developed high metallicity rapidly whereas other regions are still metal-poor today. However, knowing that the formation of rocky planets can occur in environments of lower metallicity than those of gas giants implies that there could be some places in the Universe where rocky planets and life got an earlier start than did Earthlings. ■

Debra Fischer *is in the Department of Astronomy, Yale University, New Haven, Connecticut 06511, USA.*
e-mail: debra.fischer@yale.edu

1. Buchhave, L. A. *et al. Nature* **486,** 375–377 (2012).
2. Gonzalez, G. *Mon. Not. R. Astron. Soc.* **285,** 403–412 (1997).
3. Santos, N. C., Israelian, G. & Mayor, M. *Astron. Astrophys.* **415,** 1153–1166 (2004).
4. Fischer, D. A. & Valenti, J. *Astrophys. J.* **622,** 1102–1117 (2005).
5. Mortier, A. *et al. Astron. Astrophys.* (in the press); preprint at http://arxiv.org/abs/1205.3723 (2012).
6. Mayor, M. *et al.* preprint at http://arxiv.org/abs/1109.2497 (2011).
7. Haisch, K. E. Jr, Lada, E. A. & Lada, C. J. *Astrophys. J.* **553,** L153–L156 (2001).
8. Pascucci, I. & Tachibana, S. *Protoplanetary Dust: Astrophysical and Cosmochemical Perspectives* (eds Apai, D. & Lauretta, D. S.) 263–298 (Cambridge Univ. Press, 2010).
9. Lissauer, J. J. *Icarus* **69,** 249–265 (1987).
10. Raymond, S. N., Quinn, T. & Lunine, J. I. *Icarus* **168,** 1–17 (2004).
11. Raymond, S. N., O'Brien, D. P., Morbidelli, A. & Kaib, N. A. *Icarus* **203,** 644–662 (2009).

VIROLOGY

Bird flu in mammals

An engineered influenza virus based on a haemagglutinin protein from H5N1 avian influenza, with just four mutations, can be transmitted between ferrets, emphasizing the potential for a human pandemic to emerge from birds. SEE LETTER P.420

HUI-LING YEN &
JOSEPH SRIYAL MALIK PEIRIS

Influenza pandemics in humans arise from animal influenza viruses, yet the molecular changes required for an animal virus to be transmitted efficiently between humans are poorly understood. Highly pathogenic H5N1 avian flu viruses have circulated in poultry for more than 16 years, only rarely resulting in human infections. But when people do catch H5N1 bird flu, their disease is of unusual severity, raising concerns that a human H5N1 pandemic might have a catastrophic impact on public health. However, an H5N1 virus that can be efficiently transmitted from human to human has not yet emerged, leading some researchers to question whether these viruses are inherently incapable of acquiring this capacity. On page 420 of this issue, Imai *et al.*[1] demonstrate that H5N1 viruses do have the potential to cause a human pandemic. The authors identify mutations in the avian virus that permit viral transmission between ferrets by means of respiratory droplets — the best available model for influenza transmission in humans*.

Imai *et al.* focused on the haemagglutinin (HA) protein of a highly pathogenic H5N1 influenza virus, which is involved in binding and fusion of the virus to the cells that it infects; the HA type is used in the viral nomenclature, together with the other influenza surface glycoprotein involved, a neuraminidase (NA). The HA of H5N1 viruses preferentially binds sialic acids in receptors on the surface of avian cells (Siaα2,3), whereas cells of the human upper airway predominantly have another type of sialic acid (Siaα2,6), which is recognized by human influenza viruses. The researchers introduced random mutations into the globular head of the HA molecule, where the receptor-binding domain is located, and searched for mutated viruses that exhibited enhanced binding to Siaα2,6. Using reverse genetics, a technique that allows genetic manipulation of the virus genome, they then made a 'hybrid' H5N1 virus in which the gene encoding one of these mutated H5 HA proteins replaced the HA gene in the H1N1 virus that caused a human pandemic in 2009.

The researchers infected ferrets with this hybrid H5N1 virus and, following multiple rounds of infection, isolation of the virus from the upper respiratory tract of the infected animals, and reinfection in animals not previously exposed to the virus, they obtained a virus that can be transmitted efficiently between the animals. Four key amino-acid changes in the HA are associated with ferret respiratory-droplet transmissibility in the authors' virus (Fig. 1a). Three of the mutations (N158D, N224K and Q226L) contribute to Siaα2,6 specificity. The fourth (T318I) lowers the pH at which the protein undergoes a structural change that allows it to release its genetic material into the cytoplasm of an infected cell by fusion of the viral envelope with intracellular membranes.

There have been many previous attempts to determine whether H5N1 can acquire transmission capacity in ferrets. Two studies[2,3] assessed H5N1 and H3N2 hybrid viruses, and another study[4] introduced mutations into the H5N1 HA that are known to increase Siaα2,6 binding in H2 and H3 haemagglutinin — but neither approach conferred transmissibility by respiratory droplets. One study achieved partial transmissibility by introducing three HA mutations (Q196R, Q226L and G228S) into an H5N1 virus and combining this with the NA protein of a human seasonal H3N2 virus (Fig. 1b). It is interesting that the two H5 HAs that demonstrate transmissibility among ferrets[1,5] (Fig. 1a,b) contain similar mutations: one at amino-acid residues 158–160, which removes an *N*-linked glycosylation site of the globular head[6], and the other at residues 221–228, which alters the structure of the loop of the receptor-binding domain[6].

Another research group previously produced a transmissible H9N2 hybrid virus[7] using the HA and NA of a low-pathogenic avian virus

---

*This article and the paper[1] under discussion were published online on 2 May 2012.

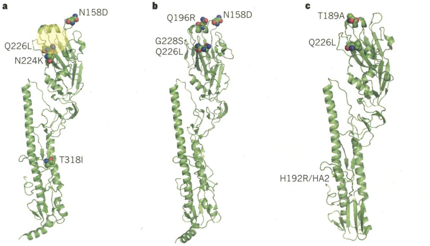

A/Vietnam/1203/2004 (H5N1)

A/Egret/Egypt/1162/2006 (H5N1)

A/Ferret/Maryland/P10-UMD/2008 (H9N2)

Figure 1 | Avian haemagglutinins transmissible in mammals. The haemagglutinin (HA) protein of influenza determines the type of target cell that the virus can infect. By mutating the site of the HA that binds to sialic acids in receptors on target cells, which differ between avian and mammalian cells, and other protein regions that determine the pH at which virus–cell fusion can occur, researchers have generated viruses that have avian HA proteins that can be transmitted from mammal to mammal. **a**, Imai *et al.*[1] identify four mutations (N158D, N224K, Q226L and T318I) in the HA of a highly pathogenic avian influenza virus, H5N1, that allow a virus with this HA to be transmitted by respiratory droplets between ferrets. The receptor-binding site of the HA is shaded in yellow. **b**, Chen *et al.*[5] also created a virus with an H5N1 HA that can be partially transmitted between ferrets, by introducing three mutations (Q196R, Q226L and G228S) into the H5 HA. The virus used as the basis for this hybrid already contained the N158D mutation that Imai and colleagues also identified in their mutated HA. **c**, Sorrell *et al.*[7] used the HA protein from a low-pathogenic H9N2 avian virus to achieve similar transmissibility. The Q226L mutation was already present in this virus, and two additional mutations (T189A and H192R/HA2) were acquired during ferret infection studies. The H192R/HA2 mutation cannot be shown because the protein is cleaved at a site that lies in front of this amino-acid residue. Full virus names and their subtypes are given below each structure. Mutated amino-acid residues are indicated by red and blue spheres.

and other genes from a human seasonal H3N2 virus. The HA of this hybrid contains a Q226L mutation, which confers human-like Siaα2,6 binding[7] (Fig. 1c). During the 10 rounds of infection that were needed for this H9N2 virus to acquire transmissibility, it accumulated two additional HA mutations, one located at residue 189 of HA1 (close to the receptor-binding domain) and the other at residue 192 of HA2 (close to the membrane-fusion domain), as well as one NA mutation located in the transmembrane domain. Together, these studies demonstrate that mutations that increase Siaα2,6 binding[1,5,7], as well as those that stabilize HA structure[1,7], seem to be functionalities required for the HA of viruses that are transmissible among mammals.

Thus, Imai and colleagues' generation of a respiratory-droplet-transmissible H5N1 virus represents the culmination of a sustained effort by numerous groups to better understand the mechanisms that can confer mammalian transmissibility in avian influenza viruses. However, it is likely that different combinations of HA mutations can achieve the same effects, and further studies are needed to explore this possibility. Furthermore, although transmission of influenza A virus among humans is already known[8,9] to involve the virus HA, NA and basic polymerase protein 2, it is possible that other viral proteins, not explored by Imai and colleagues, also contribute to mammalian transmissibility.

It is intriguing that, although the parent H5N1 virus strain (A/Vietnam/1203/2004) used by Imai *et al.* causes lethal disease in ferrets when they are directly infected, infection with the ferret-transmissible H5N1 virus does not kill the animals. It is possible that the change in receptor binding from Siaα2,3, which is present on alveolar epithelial cells in ferret and human lungs, to Siaα2,6, found on cells of the upper respiratory tract, may change the virus from one that causes alveolar infection, likely to result in more severe disease, to one targeting the upper airways, which is associated with milder symptoms. However, Imai and colleagues did not find that the two viruses differ markedly in their targeting of the upper or lower respiratory regions.

Imai and colleagues' H1N1 virus with an H5 HA is a laboratory creation, but it should not be considered an experimental artefact. Natural emergence of an H5N1–H1N1 hybrid virus is plausible. Some H1N1 and H5N1 viruses readily swap genes with one another *in vitro*[10,11], generating hybrid viruses. Furthermore, pandemic H1N1 viruses are established in pigs in many parts of the world, and H5N1 viruses have been isolated from pigs[12], suggesting that opportunities exist for the viruses to combine in these animals.

However, these findings do not only provide further indication that such a virus may arise naturally; they also pave the way for improved influenza surveillance and pandemic preparedness. For example, one of the four mutations reported by Imai *et al.*, N158D, results in a loss of *N*-linked glycosylation, and loss of glycosylation at this residue is increasingly seen among naturally occurring H5N1 isolates. Although the other three mutations have only very rarely been seen in H5N1 isolates from the field, mutations in HA that change the virus from binding Siaα2,3 to binding both Siaα2,3 and Siaα2,6 have been reported in both birds and humans[13]. These findings reinforce the need for focusing even greater attention on H5N1 infections in humans and other mammals (including pigs). Influenza viruses exist as genetic variants termed quasi-species even within a single clinical specimen, but such genetic diversity may not be fully assessed by conventional sequencing methods. Investigation of mammalian clinical specimens using new deep sequencing methods for these mutations, and for other mutations that confer similar functionality, will allow us to evaluate the extent of H5N1 adaptation that is occurring in mammalian hosts. More broadly, understanding the mutations that confer mammalian transmission of avian influenza viruses will allow better risk assessment of the animal viruses that represent a pandemic threat, and help to select virus strains against which pre-pandemic vaccines should be generated. ■

Hui-Ling Yen *and* **Joseph Sriyal Malik Peiris** *are at the School of Public Health and the Centre of Influenza Research, LKS Faculty of Medicine, The University of Hong Kong, and the HKU-Pasteur Research Centre, Pokfulam, Hong Kong.*
e-mails: malik@hku.hk; hyen@hku.hk

1. Imai, M. *et al. Nature* **486,** 420–428 (2012).
2. Jackson, S. *et al. J. Virol.* **83,** 8131–8140 (2009).
3. Maines, T. R. *et al. Proc. Natl Acad. Sci. USA* **103,** 12121–12126 (2006).
4. Maines, T. R. *et al. Virology* **413,** 139–147 (2011).
5. Chen, L.-M. *et al. Virology* **422,** 105–113 (2012).
6. Stevens, J. *et al. J. Mol. Biol.* **381,** 1382–1934 (2008).
7. Sorrell, E. M., Wan, H., Araya, Y., Song, H. & Perez, D. R. *Proc. Natl Acad. Sci. USA* **106,** 7565–7570 (2009).
8. Belser, J. A., Maines, T. R., Tumpey, T. M. & Katz, J. M. *Expert Rev. Mol. Med.* **12,** e39 (2010).
9. Sorrell, E. *et al. Curr. Opin. Virol.* **1,** 635–642 (2011).
10. Cline, T. D. *et al. J. Virol.* **85,** 12262–12270 (2011).
11. Octaviani, C. P., Ozawa, M., Yamada, S., Goto, H. & Kawaoka, Y. *J. Virol.* **84,** 10918–10922 (2010).
12. Nidom, C. A. *et al. Emerg. Infect. Dis.* **16,** 1515–1523 (2010).
13. Yamada, S. *et al. Nature* **444,** 378–382 (2006).

nature

21 June 2012 / Vol 486 / Issue No. 7403

Publication policies, author guidelines and information

This is a summary of *Nature*'s guide to authors, publication policies and other author information, available in full on the web via our main author information page at www.nature.com/nature/authors.

Getting published in *Nature*

Please read www.nature.com/nature/authors/get_published before finalizing any original scientific research manuscripts you intend to submit. This section explains *Nature*'s editorial criteria, and how manuscripts are handled by the editors after submission and before acceptance for publication.

Formatting guide

Please read www.nature.com/nature/authors/gta before finalizing and submitting your contribution. This section provides instructions for preparing, formatting and writing all types of contribution published by *Nature*.

Publication policies

This section, at www.nature.com/authors, describes *Nature*'s conditions of publication, including policies on authorship; competing financial interests; duplicate publication; prepublicity and embargoes; materials and data availability; research on animal (including human) subjects; referees; corrections, retractions, errata and addenda to published papers; the complaints procedure and refutations; and copyright/licence to publish. All contributions, for whatever section of the journal, are considered for publication and published on the condition that authors agree to these policies.

Submissions

These sections, at www.nature.com/nature/authors/submissions, contain our online service for presubmission enquiries and submission and tracking of Articles, Letters and Review-type manuscripts. Authors should read the formatting guide before using this service. Authors who cannot submit online can submit by post, but *Nature* strongly recommends the online service. **Authors must not submit by both methods.** Authors experiencing operational difficulty in using the online submission service can send an enquiry to mtshelp@nature.com, with a brief explanation of the problem.

Editorial contacts and author services

This section, at www.nature.com/nature/about/contact, provides the addresses of *Nature*'s editorial offices; names of editorial staff; and contact details for advice, reprints, permissions, press office (press@nature.com), and other author-related contact information, including postal addresses for mailed submissions. Short biographies of editors are also available at www.nature.com/nature/about/editors.

Final submissions

This section, at www.nature.com/nature/authors/submissions/final, applies only if an Article or Letter has been accepted in principle for publication and the author has been asked by the editor for a final version. Authors will need to upload electronic files of the text, production-quality figures and supplementary information (if any) to our database. Authors must include a completed manuscript checklist and all relevant signed forms and declarations as requested by the editor.

Short version of guide to authors

See www.nature.com/nature/authors for full version. Contributors not used to *Nature*'s format are advised to read some papers in published issues before submission, to familiarize themselves with *Nature*'s style. *Nature*'s main formats for original research are Articles and Letters.

ARTICLES are original reports whose conclusions represent a substantial advance in understanding of an important problem and have immediate, far-reaching implications. They do not normally exceed **5 pages** of *Nature* and have **no more than 50** references. (One page of undiluted text is about 1,300 words.)

Articles have a summary for readers outside the discipline, separate from the main text and containing no references, of up to 150 words. The summary does not contain numbers, abbreviations, acronyms or measurements unless essential. It contains a brief account of the background and rationale of the work, followed by a statement of the main conclusions, introduced by the phrase 'Here we show' or its equivalent.

The Article itself typically has about 3,000 words of text, beginning with up to 500 words of referenced text expanding on the background to the work, followed by a concise, focused account of the findings, and ending with one or two short paragraphs of discussion. The text can contain a few short subheadings consisting of about 20 but no more than 40 characters (including spaces) each.

LETTERS are short reports of original research focused on an outstanding finding whose importance means that it will be of interest to scientists in other fields. They do not normally exceed **4 pages** of *Nature*, and have **no more than 30** references. They begin with a **fully referenced paragraph** of not more than 300 words, aimed at readers in other disciplines. This paragraph contains a summary of the background and rationale for the work, followed by a one-sentence statement of the main conclusions introduced by the phrase 'Here we show' or its equivalent, and ending with two to three sentences describing the implications in context.

The main text which follows is typically up to 1,500 words long. This text can, if the author requires, start with a further brief paragraph of introductory material. A description of the research then follows. Any discussion at the end of the text should be as succinct as possible.

FIGURES in both Articles and Letters are as small as possible: Articles typically have 5 or 6 figures, Letters typically have 3 or 4 figures. Legends and/or methods are additional to the main text. Methods Summaries (which are published in print only) are no longer than 300 words; Methods sections (which are published online) can be up to 1,000 words; legends should not exceed 100 words each and start with a one-sentence title for the figure, followed by a brief explanation of the parts and symbols.

See www.nature.com/nature/authors/gta/others.html for details of other types of contribution to *Nature*, including Brief Communications Arising; Reviews and Perspectives (presubmission enquiries to reviewsandinsights@nature.com); and Correspondence (submit to corres@nature.com).

See Authors and Referees @ NPG (www.nature.com/authors) for details of Nature journals' publication policies, author and referee services, author benefits and for links to Nautilus and Peer to Peer blogs.

doi:10.1038/nature11170

Engineering H5N1 avian influenza viruses to study human adaptation

David M. Morens[1], Kanta Subbarao[1] & Jeffery K. Taubenberger[1]

Two studies of H5N1 avian influenza viruses that had been genetically engineered to render them transmissible between ferrets have proved highly controversial. Divergent opinions exist about the importance of these studies of influenza transmission and about potential 'dual use' research implications. No consensus has developed yet about how to balance these concerns. After not recommending immediate full publication of earlier, less complete versions of the studies, the United States National Science Advisory Board for Biosecurity subsequently recommended full publication of more complete manuscripts; however, controversy about this and similar research remains.

Knowledgeable observers operating within a legitimate framework for the public good have expressed divergent opinions about the importance and public safety implications of two papers, one recently published[1] and one soon-to-be published[2], describing the production of ferret-transmissible H5N1 influenza viruses, and about related influenza transmission and pathogenesis research[3–7]. Some have emphasized that understanding the underlying principles of influenza virus host adaptation and transmission can lead to better prevention and control of viruses that arise naturally, whereas others have drawn attention to 'dual use' implications—that is, bioterrorism—or to accidental release of potentially deadly viruses. The most commonly mentioned public safety concerns relate to three assumptions: (1) H5N1 viruses are currently highly lethal to humans but are poorly transmissible; (2) genetic manipulation of H5N1 viruses to increase transmissibility in mammals such as ferrets will create variant viruses that remain highly pathogenic and that become transmissible in humans; and (3) if accidentally or intentionally released, such a virus could precipitate a historically severe influenza pandemic. How do these assumptions hold up against scientific data? In this perspective, we address research evidence related to the epidemic/pandemic potential of genetically engineered H5N1 viruses, and discuss limitations in understanding how influenza viruses become pathogenic, transmissible and potentially pandemic in humans.

Background

Influenza is among the leading global infectious causes of death, periodically causing pandemics that can kill millions of people. Countless influenza A viruses circulate globally in a reservoir that consists of hundreds of avian species. Rarely, one of these viruses undergoes changes that enable it to switch hosts to infect mammals, including humans, although it is not clear whether human transmission can result directly from adaptation of an avian influenza virus (this has not been documented to occur), or only indirectly via further adaptation of pre-existing human or mammalian-adapted viruses, the mechanism that has been associated with all known pandemic and seasonal viruses after 1918. The factors underlying all such emergences are poorly understood[8]. In the past 80 years of influenza virology, three pandemics have resulted from reassortments of pre-existing human-adapted or mammalian-adapted viruses with one or more avian-influenza-derived genes, but no purely avian influenza virus has emerged to cause a pandemic or human outbreak, or has even become stably adapted to humans. However, because avian influenza viruses have adapted to other mammals, it is considered plausible that such an emergence could occur in humans.

Among many other important research areas related to influenza, it is therefore critical to study the mechanisms by which influenza viruses emerge from birds to become adapted to mammals and ultimately humans, and to learn how the phenotypic properties of such evolving viruses may be associated with human transmission and disease. Among the many subtypes and strains of avian influenza A viruses that exist in nature, those that have at least occasionally infected mammals (for example, H5N1, H7N7 and H9N2) are of interest because they might theoretically be more likely than other influenza A viruses to adapt directly or indirectly to humans. Highly pathogenic avian influenza (HPAI) H5N1 viruses have been of particular interest with respect to theoretical pandemic potential because they have been unusually pathogenic in domestic poultry and have infected and killed several hundred people over a 15-year period.

In seeking to understand such influenza viruses, a research approach used widely in virology is to engineer specific genetic mutations into naturally occurring viruses, and then study the resulting viral phenotypic properties in animals, including infectivity, cell tropism, viral replication, pathogenicity and transmissibility. These types of experiments can potentially provide clues about whether and how a virus might adapt to humans, and what prevention and control options might be useful if that virus did emerge. Much H5N1 research of this type has already been published, including viral genetic engineering to evaluate properties such as pathogenicity and transmissibility in ferrets and other animal models. In the context of this published research literature, we comment on questions relevant to the two papers under discussion[1,2].

H5N1 infectivity for humans

The ongoing HPAI H5N1 enzootic continues to cause 'spill-over' human infections. World Health Organization (WHO) data indicate that since 2003, HPAI H5N1 viruses have infected 603 people and killed 356 (ref. 9). Technically, the term 'highly pathogenic' refers only to the effects of certain H5 and H7 influenza viruses in poultry, not in humans or other mammals; most such viruses either cannot infect, or are relatively harmless in, humans. HPAI H5 and H7 phenotypes are both associated with mutations in the haemagglutinin (HA) gene that usually result from insertion of a sequence of codons encoding multiple basic amino acids at the location where the two linked protein domains comprising the

---

[1] National Institute of Allergy and Infectious Diseases, National Institutes of Health, Bethesda, Maryland 20892, USA.

mature HA are cleaved during infection[10]. This cleavage site change leads to disseminated viral replication in multiple organs of avian species, resulting in high mortality. However, in humans, who cannot be easily infected with most low pathogenicity or HPAI viruses, if they can be infected at all, efficient replication outside the respiratory tract generally does not occur. Therefore, despite the current unusual situation with H5N1 viruses in humans since 2003 (see below), neither H5N1 nor other HPAI viruses would necessarily replicate systemically or cause extreme pathogenicity should human adaptation occur. Although the basis of HPAI H5N1 viral pathogenicity in severe and fatal human cases remains unknown, there is no evidence suggesting that it results from changes known to be associated with viral adaptation to gallinaceous poultry; in fact, no human-adapted or pandemic influenza virus contains genetic changes indicative of prior poultry adaptation.

Solely on the basis of publicly available information about pathogenicity of intranasally inoculated H5N1 virus (the model for natural human and animal infection), the laboratory-derived H5N1 viruses produced in the two papers under discussion[1,11–15] do not have enhanced pathogenicity in ferrets compared to the 2009 pandemic H1N1 virus, which is considered to be mildly pathogenic for humans[14,15]. An apparent misconception has nevertheless arisen in recent public discussions of these studies, namely that the engineered, ferret-transmissible H5N1 viruses were extremely pathogenic in ferrets after intranasal inoculation or aerosol transmission. This notion seems to have resulted in part from misunderstandings about a technique—intratracheal inoculation—used in a separate sub-study reported in the manuscript by the Fouchier group[14,15], a method that is not directly relevant to viral transmissibility or natural pathogenesis. As documented since the 1940s[16], intratracheal inoculation of influenza viruses is not a 'model' for natural viral pathogenicity; influenza viruses that are otherwise considered to be of low pathogenicity often induce severe and even fatal disease in animals when administered by this route, including the 2009 pandemic H1N1 virus[15]. The presentation of transmissibility studies alongside high-dose intratracheal inoculation pathogenesis studies in the Fouchier manuscript seems to have suggested (incorrectly) to some that the engineered transmissible H5N1 virus is deadly after intranasal inoculation or aerosol transmission between ferrets and, by extension, might be both transmissible and deadly for humans, that is, a virus of deadly pandemic potential. No evidence has yet been presented to support this, although the possibility that additional unspecified genetic changes might do so cannot be excluded.

Potential for human adaptation of H5N1 viruses

It is questionable to what extent HPAI H5N1 is adapted to, or capable of adapting to, humans. It is not clear why one evolving lineage of avian HPAI H5N1 viruses, out of a large and genetically divergent pool of H5 and other avian influenza viruses that rarely infect humans (much less cause severe human disease), has recently infected hundreds or perhaps thousands of people. It may be that the human cases are a result of unusual high-dose exposures or rare individual genetic susceptibilities. Alternatively, H5N1 viruses may be beginning to do something no other HPAI virus has ever been documented to do—adapt directly to humans. And if H5N1 did adapt, could it cause a pandemic?

No HPAI virus in the historic record has ever been efficiently transmitted between humans, let alone caused a pandemic. Even when avian influenza virus genes have been imported by reassortment into existing human influenza viruses, as happened for example in 1957 with H2N2 influenza and in 1968 with H3N2 influenza, the sources seem to have been circulating low-pathogenicity avian viruses, not poultry-adapted viruses such as HPAI viruses[10]. Conceivably, the considerable host-switching mutations associated with adaptation of wild bird viruses to gallinaceous poultry, or at least of wild viruses to HPAI poultry viruses, represent an evolutionary pathway divergent from those pathways associated with mammalian adaptation, seemingly presenting an additional challenge for poultry-adapted influenza viruses to achieve efficient mammalian adaptation[17]. After 15 years of high-density enzootic circulation in domestic poultry around the world, no human-adapted H5N1 virus has emerged from a natural reservoir, suggesting the existence of unknown biological barriers.

Despite circulation of influenza A viruses of 16 HA subtypes in billions of birds over a very long time span, the four pandemics in the last century have been restricted to influenza viruses bearing HA subtypes H1, H2 or H3. Decades ago, many experts predicted that influenza pandemics could be explained by 'recycling' of a small number of HAs in new human generations; more recently, this belief has been expanded to posit that the other HA subtypes (including H5) are fundamentally incapable of adapting to humans, being selected against by biological constraints or unappreciated selection pressures[18–20]. Despite widespread influenza virus circulation and dynamic evolution at the human–animal interface, with many billions of quasispecies, mutations and gene constellations circulating, only four influenza pandemics have occurred in the last century, and in the three of those with a known viral origin the viruses resulted from reassortment of pre-existing human or swine viruses[21], not by mutation or adaptation of existing avian viruses.

This suggests that *de novo* emergence of a human pandemic influenza virus is an extremely rare event that is not easily achieved in nature[10], and presumably would not be easily achieved by engineering a small number of laboratory mutations. As some of the key engineered H5N1 mutations in the two studies occur spontaneously during normal laboratory passage[22], or have been found singly or in combination in natural H5N1 and in other influenza viruses[23–26], including strains from wild birds, it remains unclear whether or how the engineered viruses in question create or increase the risk of a pandemic.

Engineering H5N1 phenotypic changes

Serial passage of a virus in intact animals or in tissues derived from a particular species often results in enhanced species-specific virulence, which can be applied to establish an animal model with measurable morbidity and/or mortality outcomes useful for evaluating antiviral therapeutics, passive immunization and vaccines. Influenza viruses, SARS coronavirus and Ebola virus have all been passaged in mice to enhance virulence; the resulting host-adapted viruses have been studied biologically and used to evaluate strategies for control and prevention. However, adaptational mutations resulting from serial passage tend to be host-specific and may not produce the same outcomes in other species. For example, the classical swine influenza virus, A/swine/Iowa/1930 (H1N1), is very pathogenic in ferrets and mice but poses no threat to humans[27]. Another example is mouse-adapted Ebola virus, which is lethal for mice and guinea pigs but attenuated for nonhuman primates[28,29]. Ferrets are susceptible to a wide range of viruses including influenza viruses, SARS coronavirus, canine distemper virus and some parvoviruses, many of which do not infect humans or other mammals. A number of influenza viruses that replicate efficiently in ferrets[30–33] seem poorly able, or unable, to infect humans, even after experimental challenge[34]. Thus, pathogenicity and transmissibility of any influenza virus in ferrets cannot be used directly to predict what type and severity of disease the same virus might produce in humans and human populations.

Predicting human transmissibility

It is unclear whether genetic manipulation of an H5N1 virus to achieve transmissibility in a particular mammal such as a ferret can predict human transmissibility. Because natural history and viral challenge studies cannot always be performed in humans, they have been conducted in experimental animals including mice, guinea pigs, ferrets, non-human primates and various other mammals. Unfortunately, there is no perfect animal model capable of reproducing all of the important variables involved in human influenza infection, although each animal model may be useful in understanding some aspect of influenza biology. Unlike most other mammals, ferrets generally can be infected with many or most avian, mammalian and human influenza viruses without prior viral adaptation, and often transmit efficiently between them[35], providing useful general information about the viral genetic basis of phenotypic properties such as infectivity, pathogenicity, transmissibility and immune responses[35], even though the findings cannot necessarily be directly applied to human infections[36–38]. Furthermore, in decades of research, using a large number of different avian and mammalian influenza viruses, severe or fatal disease has not often been observed in ferrets following intranasal inoculation or aerosol exposure.

These useful traits of easy infectability and mildly symptomatic infection have rendered the ferret a 'permissive' influenza model. Specifically, many naturally occurring influenza viruses that infect, and often transmit between, ferrets are not known to infect people or cause human disease[27,30–33,39,40]. Ferrets are thus an imperfect model for predicting human infectivity or transmissibility, let alone the high level of transmissibility characteristic of pandemic spread. On the basis of public presentations by the senior authors of the two studies in question, neither of the engineered H5N1 viruses was as efficiently transmissible in ferrets as the human-adapted 2009 pandemic H1N1 virus[14,15]. Phenotypic properties such as replication, pathogenicity and transmissibility are likely to be polygenic traits driven by mutations that are independent and possibly competing[10,41]. Transmissibility is a complex phenotype that probably requires cooperative changes in more than one gene segment, and these may differ greatly between different viruses that become transmissible. Mutations that confer transmissibility in a ferret may be species-specific and irrelevant to other hosts[42]. There are probably multiple unique virus-specific pathways to transmissibility for particular viruses infecting particular hosts[43]. For example, transmissibility of the 1918 pandemic H1N1 virus has been linked to changes in the genes encoding HA and PB2 proteins[36,37], whereas transmissibility of the 2009 pandemic H1N1 virus, which has a closely related HA, has been linked to gene segments encoding the neuraminidase and matrix proteins[44].

Moreover, because determinants of viral pathogenicity may be lost upon adaptation to a new host, H5N1 viruses, whether or not transmissible, do not always cause severe disease in ferrets or non-human primates[45–47]. For these reasons viral phenotypes observed in animal models like the ferret may not predict what would happen in humans. Indeed, given that many influenza viruses that are non-pathogenic for humans easily transmit and may cause illness in ferrets, the 'ferret model' does not reliably predict human transmissibility or pathogenicity, although the model remains valuable for understanding the principles and dynamics of infection.

In addition to data from experiments in mammals, it is noteworthy that of the many mammalian-adapted influenza viruses that infect and transmit explosively among pigs, among horses and among dogs, few infect humans and none are transmitted between them[48]. Although swine influenza viruses caused sporadic human infections before 2009[49,50], and caused the 2009 H1N1 pandemic[21], outbreaks associated with human influenza viruses are rare in pigs. It is even conceivable that H5N1 viruses have already become adapted to mammals without causing severe disease or onward transmission to humans. Evidence from China's Qinghai Lake, for example, shows 13.4% H5N1 seropositivity and 3.4% active infection in apparently healthy, live-caught rodents called pikas[51]. Clearly, adaptation of an influenza virus to a specific mammalian host does not necessarily predict its infectiousness, pathogenicity or transmissibility in other mammals, even though valuable insights into mechanisms of disease, host responses, and prevention and treatment may be obtained by studying these particular animals. Such insights can provide valuable clues in designing countermeasures against deadly epidemics and pandemics.

H5N1 case-fatality rate

Belief that an H5N1 virus could produce a 59% pandemic case-fatality rate is the most frightening aspect of the current controversy surrounding aerosol transmission of H5N1 virus in ferrets. In 500 years of observation, no influenza pandemic is believed to have caused a case-fatality rate over about 2% (ref. 52); pandemic and seasonal circulation of H1, H2 and H3 influenza viruses over the past century have all produced lower overall mortality rates[53]. The widely cited 59% figure is not a mortality rate but a case-fatality rate computed from cumulative cases reported to WHO since 2003[9]. (Case fatality refers to fatal cases divided by all fatal plus non-fatal cases combined.) By general consensus, the WHO figure probably overestimates actual mortality. Among other concerns common to epidemiological data, the WHO case definition[54] features diagnostic severity criteria (evidence of an acute pneumonia on chest radiograph plus evidence of respiratory failure) that constitute a self-fulfilling prophecy for fatality; as with many illnesses studied epidemiologically, severe diseases are more likely to receive optimal diagnostic work-up ('detection bias'); and most H5N1 cases have been reported from countries with limited resources for identifying milder cases, if they occurred. These factors together could combine to erroneously inflate case-fatality calculations by over-counting severe cases and under-counting mild cases[55].

However, potentially more important clues to actual H5N1 pathogenicity and human case-fatality rates come from epidemiological studies, which taken together suggest to us that H5N1 may not be highly lethal except in people with rare susceptibilities. Forty-six published H5N1 seroprevalence studies of various exposure categories (household contacts, healthcare workers, poultry workers, and so on) show generally low H5N1 seroprevalence (mean, 1.7% of 21,435 persons examined in all 46 studies combined (a bibliography of these studies is available from the authors on request)). Given intense poultry and other exposures in many study areas, these low rates at first seem perplexing, especially when compared to the much higher seroprevalence rates in humans for other avian influenza viruses such as H9N2 (ref. 56). When such information is considered in light of statistically significant clustering of non-human-transmitted (that is, presumably avian-acquired) household cases in genetically related versus unrelated persons[57,58], a reasonable explanation seems to us to be that H5N1 is so poorly adapted to humans that exposure does not normally lead to infection or even the development of a detectable immune response[57,59], except in persons with specific but undefined genetic susceptibilities, many of whom become cases[60–62]. There are few data on what the basis of such genetic susceptibilities may be, although recent evidence has linked severe human influenza to a minor *IFITM3* allele[63], supporting the suspicion that genetic determinants of influenza infection and replication in humans do exist.

A published meta-analysis of selected seroprevalence studies implies that the actual H5N1 case-fatality rate may be far below 1% (ref. 56), and thus probably far below the case-fatality rates for seasonal influenza. This has been disputed because it has been difficult to find mild cases, and because of the possibility that some low-level antibody titres (<1:80) might be false positives[5]. On the other hand, rapid disappearance of human H5N1 vaccine-induced antibody[64] suggests that the opposite problem of false negatives could be occurring and, if so, might be especially problematic in cross-sectional studies in which the time since infection is not known, and which could in some cases be long enough for antibody titres to wane to sub-threshold or undetectable levels.

Given such confusing information, there has been little agreement so far on the important question of asymptomatic and undetected H5N1 infections. But whatever the case, unless healthy seropositive people detected in seroprevalence studies temporally and geographically associated with H5N1 cases are all falsely seropositive, their addition to exposure denominators greatly decreases case-fatality determinations. For example, the 1997 Hong Kong H5N1 outbreak case-fatality rate of 33.3% (ref. 65) drops to around 3% with the addition of exposed seropositive persons detected in the related seroprevalence studies. Similar recalculations of other data would yield far lower rates, and wider seroprevalence studies would undoubtedly lower case-fatality rates even further.

Thus, an explanation for the apparent case-fatality rate/seroprevalence paradox may not be purely one of missing cases. Like other poorly adapted viruses that rarely infect humans[34], the H5N1 virus may simply be productively infecting too few of the people exposed to it, even in situations of widespread human contact, leaving minimal immunological evidence of exposure at the population level, while at the same time 'finding' and infecting those occasional persons with unusual susceptibilities to it; that is, cases[59]. Even so, it should be remembered that limited spread of a deadly H5N1 virus, or pandemic H5N1 spread associated with a far lower case-fatality rate, would still be of public health concern.

The dangers of information release

Owing to global concern over a possible H5N1 influenza pandemic, the pathogenicity, immunogenicity and transmissibility of naturally occurring and laboratory-derived H5N1 viruses have been examined extensively and safely using high-containment facilities and appropriate regulatory and safety oversight (see later). The two H5N1 studies under discussion[1,2] build upon and are the logical extensions of dozens of similar published studies performed in the wake of the 1997 Hong Kong H5N1 outbreak. This research includes another published study in which genetic engineering of the H5N1 virus was able to newly create transmissibility in ferrets[66], a similar study in which increased ferret transmissibility was not documented[67], and a study in which transmissibility was restored and arguably increased in guinea pigs[68]. None of these publications, including the prior publication of engineered H5N1 transmissibility in ferrets, led to concern among scientists, federal agencies or the public.

Such studies feature numerous pathogenicity-associated, and sometimes transmissibility-associated, mutations affecting the HA-receptor-binding site, including changes that enhance receptor affinity for α2-6-linked sialic acid receptors, thought to be important for human adaptation[25,69–71]. Other studies have examined mutations associated with changing antigenicity[72,73], changes associated with fusion[25,74], changes associated with the polybasic HA cleavage site[75–77], and virulence factors in the polymerase proteins, crucial for viral replication[24,68], and in the non-structural protein (NS1), involved in antagonizing host type I interferon responses[78–80]. This widely available body of published research complicates determination of what to do with these two and with similar research manuscripts that seem likely to continue to appear. Withholding or redacting them does not prevent anyone from piecing together the basic information that they contain. Most of this information is generally known and relatively obvious, has already been published, and is now being widely publicized and discussed as a result of increased attention[11,13,14,81,82].

Some would argue that even this background research should not have been done, or should henceforth be classified and made available only to 'approved' scientists who would be vetted by yet-to-be-determined mechanisms[83,84]. But had these former studies not been made available in the open literature, the field of influenza research would have been considerably impeded and our current state of knowledge and readiness for responding to future outbreaks and/or pandemics would be lessened. Some proposed that 'censoring' this information actually increases the risk of bioterrorism[85]. The two studies under discussion[1,2] can help augment surveillance to detect naturally emerging viruses with pandemic potential and expand our knowledge of the principles underlying host adaptation. Although the dangers of 'information release' in the case of these two studies is probably small or nil—because all or most of the critical information is widely available anyway—it nevertheless remains important to rethink larger questions about balancing safety (accidental or deliberate release of an influenza virus or any dangerous pathogen) with the need to study such viruses to learn enough of their biology to prevent and control them. These are important issues that should be discussed broadly among scientists, policy makers and the public.

Biosafety and biosecurity concerns

As novel pathogens emerge, scientists must be able to continue to work with them safely and appropriately in teams using the talents of many highly trained researchers. Numerous layers of robust biosafety and biosecurity protection and oversight are in place to safeguard the scientists and the public alike, including rigorous safety training, biocontainment practices, regulations and oversight, select agent rules, background investigations and biosurety oversight[86]. The H5N1 studies under discussion[1,2] were both performed in high containment laboratories with rigorous and appropriate oversight and biosecurity measures[15], as is the case for all such research in the US.

Few disagree that it is crucial to continue research with H5N1 and other emerging infections, including investigation of how emerging pathogens adapt to new hosts and cause disease. However, it is important to ask whether some types of infectious diseases research should not be done, or not published openly. If so, we need criteria to identify such research in advance, and processes to balance the importance of the research knowledge with the importance of preventing adverse consequences of the research[87]. Even with the eventual publication of the two H5N1 studies, questions about how such research should be approved, evaluated and made public remain unanswered[83,84]. The biomedical field is built on more than a century of openness and full publication/broad discussion of all findings; it is unclear how redacted publications of future scientific data can be accomplished, and what effect such a system would have on science and scientific progress.

These complex questions have been asked and answered in the past[87], and are being asked again in the context of these two papers. Continued discussion and decisions about how to deal with this research will be of importance to scientific progress and public health. We believe that it is important to consider the broader context of research aimed at understanding how influenza viruses adapt to humans. H5N1 is only one of many avian influenza viruses. If, as we believe existing data suggest, pathways to human adaptation are many, virus-specific, and with few common denominators, it will be important to study not just H5N1 but a wide range of avian and mammalian- and human-adapted viruses, including studies that feature backward genetic engineering to remove phenotypic determinants of adaptation, studies in nonhuman primates and, when safe and appropriate to do so, in human challenge studies[88].

Future directions

The H5N1 controversy underscores how little is known about determinants of human influenza pathogenicity and transmissibility, which are among the most fundamentally important questions in infectious disease research because of the huge burden of influenza.

In the past two decades the question of pursuing and publishing potential 'dual use' infectious disease research has always been decided in favour of conducting and publishing the research; for example, delineating the genomes of smallpox[89] and SARS viruses[90], defining the pathogenicity of neuraminidase-inhibitor-resistant influenza viruses[91,92], genetically altering and making ferret transmissible both a more pathogenic pandemic H2N2 influenza virus[93] and an H9N2 avian influenza virus[40], and resurrecting from RNA fragments, recreating and studying *in vivo* the 1918 pandemic influenza virus[94–96]. In the latter case, important findings already have markedly enhanced our understanding of the emergence, transmissibility and pathogenicity of that important virus, helping us to prepare for and respond to the emergence of other influenza viruses. Examples include using the 1918 HA crystal structure in vaccine design[97], investigating the role of the host immune response in disease[98,99], identification of mutations associated with pathogenicity and host adaptation[36,100,101], understanding influenza evolution[21], and helping guide and target the response to the 2009 H1N1 pandemic[53,102]. All of this work has been done safely with appropriate oversight, and without negative consequences.

In considering the threat of bioterrorism or accidental release of genetically engineered viruses, it is worth remembering that nature is the ultimate bioterrorist. Indeed, H5N1 mutations, including some of those made in the two studies under discussion[1,2], occur spontaneously in nature, probably at a high rate, although they have not yet led to a pandemic. Given the relative rarity of pandemics caused by newly emerging influenza viruses, their explosive transmissibility may result from unique and virus-specific mutational changes that arise at very low frequency. For past pandemics, we have had limited ability to detect such changes by surveillance or by animal model experimentation. Thus, our best hope in preventing and controlling the microbial agents that continually challenge us is to increase fundamental knowledge about the mechanisms by which they emerge, spread and cause disease, so that we can develop countermeasures such as enhanced surveillance, better diagnostics, vaccines and drug therapies. In moving forward we need to be safety conscious and to have consensus safety measures and policies in place, while at the same time using all available tools to seek broad understanding about the complex relationships between viruses and hosts. It is only this knowledge that stands between us and the devastation of future influenza pandemics. In reconsidering the proper balance between progress and safety, the critical importance of advancing scientific knowledge needs to be kept front and centre.

1. Imai, M. *et al.* Experimental adaptation of an influenza H5 HA confers respiratory droplet transmission to a reassortant H5 HA/H1N1 virus in ferrets. *Nature* http://dx.doi.org/10.1038/nature10831 (this issue).
2. Herfst, S. *et al.* Aerosol transmission of avian influenza A/H5N1 virus. *Science* (22 June 2012).
3. Doherty, P. C. & Thomas, P. G. Dangerous for ferrets: lethal for humans? *BMC Biol.* **10,** 10 (2012).
4. Fouchier, R. *et al.* Preventing pandemics: the fight over flu. *Nature* **481,** 257–259 (2012).
5. Osterholm, M. T. & Kelley, N. S. Mammalian-transmissible H5N1 influenza: facts and perspective. *MBio* **3,** 2 (2012).
6. Palese, P. Don't censor life-saving science. *Nature* **481,** 115 (2012).
7. Webster, R. G. Mammalian-transmissible H5N1 influenza: the dilemma of dual-use research. *MBio* **3,** 1 (2012).
8. Parrish, C. R. *et al.* Cross-species virus transmission and the emergence of new epidemic diseases. *Microbiol. Mol. Biol. Rev.* **72,** 457–470 (2008).
   Authors review data on viral host-switch events.
9. WHO. Cumulative number of confirmed human cases of avian influenza A(H5N1) reported to WHO. http://www.who.int/influenza/human_animal_interface/H5N1_cumulative_table_archives/en/index.html (2012).
10. Taubenberger, J. K. & Kash, J. C. Influenza virus evolution, host adaptation, and pandemic formation. *Cell Host Microbe* **7,** 440–451 (2010).
    A review of influenza host adaptation and pandemic formation.
11. Brown, T. H5N1 research discussed in special session at ASM. http://www.medscape.com/viewarticle/759465 (2012).
12. Fouchier, R. A. *et al.* Pause on avian flu transmission research. *Science* **335,** 400–401 (2012).
13. Kawaoka, Y. H5N1: Flu transmission work is urgent. *Nature* **482,** 155 (2012).
14. Osterholm, M. T., Fauci, A. S., Alberts, B. & Fouchier, R. A. M. Discussion of NSABB's publication recommendations for the NIH-funded research on the transmissibility of H5N1. http://www.asmbiodefense.org/index.php/program-information/nsabbs-recommendations-for-h5n1-research (2012).
15. Kawaoka, Y. & Fouchier, R. A. Royal Society meeting. H5N1 research: biosafety, biosecurity and bioethics. http://royalsociety.org/events/2012/viruses/ (2012).
16. Wilson, H. E., Saslaw, S., Doan, C. A., Woolpert, O. C. & Schwab, J. L. Reactions of monkeys to experimental mixed influenza and *Streptococcus* infections: an analysis of the relative roles of humoral and cellular immunity, with the description of an intercurrent nephritic syndrome. *J. Exp. Med.* **85,** 199–215 (1947).
17. Swayne, D. E. Understanding the complex pathobiology of high pathogenicity avian influenza viruses in birds. *Avian Dis.* **51,** 242–249 (2007).
    A review of highly pathogenic avian influenza viruses.
18. Francis, T. Jr. Influenza: the new acquayantance. *Ann. Intern. Med.* **39,** 203–221 (1953).
19. Masurel, N. & Marine, W. M. Recycling of Asian and Hong Kong influenza A virus hemagglutinins in man. *Am. J. Epidemiol.* **97,** 44–49 (1973).
20. Hilleman, M. R. Realities and enigmas of human viral influenza: pathogenesis, epidemiology and control. *Vaccine* **20,** 3068–3087 (2002).
21. Morens, D. M., Taubenberger, J. K. & Fauci, A. S. The persistent legacy of the 1918 influenza virus. *N. Engl. J. Med.* **361,** 225–229 (2009).
22. Bogs, J. *et al.* Reversion of PB2-627E to -627K during replication of an H5N1 Clade 2.2 virus in mammalian hosts depends on the origin of the nucleoprotein. *J. Virol.* **85,** 10691–10698 (2011).
23. Chen, H. *et al.* Properties and dissemination of H5N1 viruses isolated during an influenza outbreak in migratory waterfowl in western China. *J. Virol.* **80,** 5976–5983 (2006).
24. Hatta, M., Gao, P., Halfmann, P. & Kawaoka, Y. Molecular basis for high virulence of Hong Kong H5N1 influenza A viruses. *Science* **293,** 1840–1842 (2001).
    A study showing the key role that changes in a viral polymerase gene has in H5N1 virulence in a mammalian model.
25. Stevens, J. *et al.* Structure and receptor specificity of the hemagglutinin from an H5N1 influenza virus. *Science* **312,** 404–410 (2006).
    A study describing the haemagglutinin crystal structure of an H5N1 influenza virus and studies of mutations associated with receptor-binding specificity.
26. Yen, H. L. *et al.* Inefficient transmission of H5N1 influenza viruses in a ferret contact model. *J. Virol.* **81,** 6890–6898 (2007).
27. Memoli, M. J. *et al.* An early 'classical' swine H1N1 influenza virus shows similar pathogenicity to the 1918 pandemic virus in ferrets and mice. *Virology* **393,** 338–345 (2009).
28. Bray, M., Davis, K., Geisbert, T., Schmaljohn, C. & Huggins, J. A mouse model for evaluation of prophylaxis and therapy of Ebola hemorrhagic fever. *J. Infect. Dis.* **178,** 651–661 (1998).
29. Bray, M., Hatfill, S., Hensley, L. & Huggins, J. W. Haematological, biochemical and coagulation changes in mice, guinea-pigs and monkeys infected with a mouse-adapted variant of Ebola Zaire virus. *J. Comp. Pathol.* **125,** 243–253 (2001).
30. Chen, G. L. *et al.* Evaluation of replication and cross-reactive antibody responses of H2 subtype influenza viruses in mice and ferrets. *J. Virol.* **84,** 7695–7702 (2010).
31. Hinshaw, V. S., Webster, R. G., Easterday, B. C. & Bean, W. J. Jr. Replication of avian influenza A viruses in mammals. *Infect. Immun.* **34,** 354–361 (1981).
32. Joseph, T. *et al.* Evaluation of replication and pathogenicity of avian influenza a H7 subtype viruses in a mouse model. *J. Virol.* **81,** 10558–10566 (2007).
33. Song, H., Wan, H., Araya, Y. & Perez, D. R. Partial direct contact transmission in ferrets of a mallard H7N3 influenza virus with typical avian-like receptor specificity. *Virol. J.* **6,** 126 (2009).
34. Beare, A. S. & Webster, R. G. Replication of avian influenza viruses in humans. *Arch. Virol.* **119,** 37–42 (1991).
35. Belser, J. A., Katz, J. M. & Tumpey, T. M. The ferret as a model organism to study influenza A virus infection. *Dis. Model Mech.* **4,** 575–579 (2011).
    A review of the ferret as a model organism in influenza virus pathogenicity studies.
36. Tumpey, T. M. *et al.* A two-amino acid change in the hemagglutinin of the 1918 influenza virus abolishes transmission. *Science* **315,** 655–659 (2007).
    A study elucidating the importance of the haemagglutinin-receptor-binding region in conferring ferret transmissibility in the 1918 pandemic influenza virus.
37. Van Hoeven, N. *et al.* Human HA and polymerase subunit PB2 proteins confer transmission of an avian influenza virus through the air. *Proc. Natl Acad. Sci. USA* **106,** 3366–3371 (2009).
    A study describing the importance of both the 1918 haemagglutinin and polymerase PB2 genes in conferring ferret transmissibility in viruses expressing 1918 pandemic influenza virus genes.
38. Watanabe, T. *et al.* Viral RNA polymerase complex promotes optimal growth of 1918 virus in the lower respiratory tract of ferrets. *Proc. Natl Acad. Sci. USA* **106,** 588–592 (2009).
39. Kimble, J. B., Sorrell, E., Shao, H., Martin, P. L. & Perez, D. R. Compatibility of H9N2 avian influenza surface genes and 2009 pandemic H1N1 internal genes for transmission in the ferret model. *Proc. Natl Acad. Sci. USA* **108,** 12084–12088 (2011).
40. Sorrell, E. M., Wan, H., Araya, Y., Song, H. & Perez, D. R. Minimal molecular constraints for respiratory droplet transmission of an avian-human H9N2 influenza A virus. *Proc. Natl Acad. Sci. USA* **106,** 7565–7570 (2009).
41. Koster, F. *et al.* Exhaled aerosol transmission of pandemic and seasonal H1N1 influenza viruses in the ferret. *PLoS ONE* **7,** e33118 (2012).
42. Yamanaka, T. *et al.* No evidence of horizontal infection in horses kept in close contact with dogs experimentally infected with canine influenza A virus (H3N8). *Acta Vet. Scand.* **54,** 25 (2012).
43. Mänz, B., Brunotte, L., Reuther, P. & Schwemmle, M. Adaptive mutations in NEP compensate for defective H5N1 RNA replication in cultured human cells. *Nature Commun.* **3,** 802 (2012).
44. Lakdawala, S. S. *et al.* Eurasian-origin gene segments contribute to the transmissibility, aerosol release, and morphology of the 2009 pandemic H1N1 influenza virus. *PLoS Pathog.* **7,** e1002443 (2011).
45. Chen, Y. *et al.* Pathological lesions and viral localization of influenza A (H5N1) virus in experimentally infected Chinese rhesus macaques: implications for pathogenesis and viral transmission. *Arch. Virol.* **154,** 227–233 (2009).
46. Govorkova, E. A. *et al.* Lethality to ferrets of H5N1 influenza viruses isolated from humans and poultry in 2004. *J. Virol.* **79,** 2191–2198 (2005).
47. Maines, T. R. *et al.* Avian influenza (H5N1) viruses isolated from humans in Asia in 2004 exhibit increased virulence in mammals. *J. Virol.* **79,** 11788–11800 (2005).
48. Morens, D. M. & Taubenberger, J. K. Historical thoughts on influenza viral ecosystems, or behold a pale horse, dead dogs, failing fowl, and sick swine. *Influenza Other Respir. Viruses* **4,** 327–337 (2010).
49. Myers, K. P., Olsen, C. W. & Gray, G. C. Cases of swine influenza in humans: a review of the literature. *Clin. Infect. Dis.* **44,** 1084–1088 (2007).
50. Shinde, V. *et al.* Triple-reassortant swine influenza A (H1) in humans in the United States, 2005–2009. *N. Engl. J. Med.* **360,** 2616–2625 (2009).
51. Zhou, J. *et al.* Characterization of the H5N1 highly pathogenic avian influenza virus derived from wild pikas in China. *J. Virol.* **83,** 8957–8964 (2009).
52. Morens, D. M. & Taubenberger, J. K. Pandemic influenza: certain uncertainties. *Rev. Med. Virol.* **21,** 262–284 (2011).
    A historical review of influenza pandemics.
53. Morens, D. M., Taubenberger, J. K. & Fauci, A. S. The 2009 H1N1 pandemic influenza virus: what next? *MBio* **1,** 4 (2010).
54. WHO. WHO case definitions for human infections with influenza A(H5N1) virus. http://www.who.int/influenza/resources/documents/case_definition2006_08_29/en/index.html (2006).
55. Palese, P. & Wang, T. T. H5N1 influenza viruses: facts, not fear. *Proc. Natl Acad. Sci. USA* **109,** 2211–2213 (2012).
56. Wang, T. T., Parides, M. K. & Palese, P. Seroevidence for H5N1 influenza infections in humans: meta-analysis. *Science* **335,** 1463 (2012).

57. Aditama, T. Y. *et al.* Risk factors for cluster outbreaks of avian influenza A H5N1 infection, Indonesia. *Clin. Infect. Dis.* **53,** 1237–1244 (2011).
A study describing human H5N1 case clusters in Indonesia.
58. Aditama, T. Y. *et al.* Avian influenza H5N1 transmission in households, Indonesia. *PLoS ONE* **7,** e29971 (2012).
59. Roos, R. No sign of missed H5N1 cases in Bangladesh study. http://www.cidrap.umn.edu/cidrap/content/influenza/avianflu/news/mar1312seroprev.html (2012).
60. Horby, P. *et al.* What is the evidence of a role for host genetics in susceptibility to influenza A/H5N1? *Epidemiol. Infect.* **138,** 1550–1558 (2010).
61. Trammell, R. A. & Toth, L. A. Genetic susceptibility and resistance to influenza infection and disease in humans and mice. *Expert Rev. Mol. Diagn.* **8,** 515–529 (2008).
62. Zhang, L., Katz, J. M., Gwinn, M., Dowling, N. F. & Khoury, M. J. Systems-based candidate genes for human response to influenza infection. *Infect. Genet. Evol.* **9,** 1148–1157 (2009).
63. Everitt, A. R. *et al.* IFITM3 restricts the morbidity and mortality associated with influenza. *Nature* **484,** 519–523 (2012).
64. Brady, R. C. *et al.* Safety and immunogenicity of a subvirion inactivated influenza A/H5N1 vaccine with or without aluminum hydroxide among healthy elderly adults. *Vaccine* **27,** 5091–5095 (2009).
65. Katz, J. M. *et al.* Antibody response in individuals infected with avian influenza A (H5N1) viruses and detection of anti-H5 antibody among household and social contacts. *J. Infect. Dis.* **180,** 1763–1770 (1999).
66. Chen, L. M. *et al. In vitro* evolution of H5N1 avian influenza virus toward human-type receptor specificity. *Virology* **422,** 105–113 (2012).
67. Maines, T. R. *et al.* Effect of receptor binding domain mutations on receptor binding and transmissibility of avian influenza H5N1 viruses. *Virology* **413,** 139–147 (2011).
68. Steel, J., Lowen, A. C., Mubareka, S. & Palese, P. Transmission of influenza virus in a mammalian host is increased by PB2 amino acids 627K or 627E/701N. *PLoS Pathog.* **5,** e1000252 (2009).
69. Ilyushina, N. A., Govorkova, E. A., Gray, T. E., Bovin, N. V. & Webster, R. G. Human-like receptor specificity does not affect the neuraminidase-inhibitor susceptibility of H5N1 influenza viruses. *PLoS Pathog.* **4,** e1000043 (2008).
70. Yamada, S. *et al.* Haemagglutinin mutations responsible for the binding of H5N1 influenza A viruses to human-type receptors. *Nature* **444,** 378–382 (2006).
71. Yen, H. L. *et al.* Changes in H5N1 influenza virus hemagglutinin receptor binding domain affect systemic spread. *Proc. Natl Acad. Sci. USA* **106,** 286–291 (2009).
72. Rudneva, I. A. *et al.* Antigenic epitopes in the hemagglutinin of Qinghai-type influenza H5N1 virus. *Viral Immunol.* **23,** 181–187 (2010).
73. Wang, W. *et al.* Glycosylation at 158N of the hemagglutinin protein and receptor binding specificity synergistically affect the antigenicity and immunogenicity of a live attenuated H5N1 A/Vietnam/1203/2004 vaccine virus in ferrets. *J. Virol.* **84,** 6570–6577 (2010).
74. Sui, J. *et al.* Structural and functional bases for broad-spectrum neutralization of avian and human influenza A viruses. *Nature Struct. Mol. Biol.* **16,** 265–273 (2009).
75. Bogs, J. *et al.* Highly pathogenic H5N1 influenza viruses carry virulence determinants beyond the polybasic hemagglutinin cleavage site. *PLoS ONE* **5,** e11826 (2010).
76. Gohrbandt, S. *et al.* Amino acids adjacent to the haemagglutinin cleavage site are relevant for virulence of avian influenza viruses of subtype H5. *J. Gen. Virol.* **92,** 51–59 (2011).
77. Suguitan, A. L. Jr *et al.* The multibasic cleavage site of the hemagglutinin of highly pathogenic A/Vietnam/1203/2004 (H5N1) avian influenza virus acts as a virulence factor in a host-specific manner in mammals. *J. Virol.* **86,** 2706–2714 (2012).
78. Seo, S. H., Hoffmann, E. & Webster, R. G. Lethal H5N1 influenza viruses escape host anti-viral cytokine responses. *Nature Med.* **8,** 950–954 (2002).
79. Spesock, A. *et al.* The virulence of 1997 H5N1 influenza viruses in the mouse model is increased by correcting a defect in their NS1 proteins. *J. Virol.* **85,** 7048–7058 (2011).
80. Zielecki, F. *et al.* Virulence determinants of avian H5N1 influenza A virus in mammalian and avian hosts: role of the C-terminal ESEV motif in the viral NS1 protein. *J. Virol.* **84,** 10708–10718 (2010).
81. MacKenzie, D. Five easy mutations to make bird flu a lethal pandemic. *New Sci.* http://www.newscientist.com/article/mg21128314.600-five-easy-mutations-to-make-bird-flu-a-lethal-pandemic.html (2011).
82. WHO. Public health, influenza experts agree H5N1 research critical, but extend delay. http://www.who.int/mediacentre/news/releases/2012/h5n1_research_20120217/en/index.html (2012).
83. NSABB. National Science Advisory Board for Biosecurity Findings and Recommendations March 29–30, 2012. http://oba.od.nih.gov/biosecurity/biosecurity_documents.html (NSABB, 2012).
84. WHO. Report on technical consultation on H5N1 research issues. http://www.who.int/influenza/human_animal_interface/consensus_points/en/index.html (2012).
85. MacKenzie, D. Censoring flu data could raise bioterror threat. *New Sci.* http://www.newscientist.com/article/dn21675-censoring-flu-data-could-raise-bioterror-threat.html (2012).
86. CDC in *Biosafety in Microbiological and Biomedical Laboratories (BMBL)* (eds Chosewood, L. C. & Wilson, D. E.) Ch. 8 (Government Printing Office, 2009).
87. National Research Council in *Science and Security in a Post 9/11 World: A Report Based on Regional Discussions Between the Science and Security Communities* Ch. 4, 57–68 (NAS, 2007).
88. Killingley, B. *et al.* Potential role of human challenge studies for investigation of influenza transmission. *Lancet Infect. Dis.* **11,** 879–886 (2011).
89. Massung, R. F. *et al.* Potential virulence determinants in terminal regions of variola smallpox virus genome. *Nature* **366,** 748–751 (1993).
90. Marra, M. A. *et al.* The genome sequence of the SARS-associated coronavirus. *Science* **300,** 1399–1404 (2003).
91. Herlocher, M. L. *et al.* Influenza viruses resistant to the antiviral drug oseltamivir: transmission studies in ferrets. *J. Infect. Dis.* **190,** 1627–1630 (2004).
92. Memoli, M. J. *et al.* Multidrug-resistant 2009 pandemic influenza A(H1N1) viruses maintain fitness and transmissibility in ferrets. *J. Infect. Dis.* **203,** 348–357 (2011).
93. Pappas, C. *et al.* Receptor specificity and transmission of H2N2 subtype viruses isolated from the pandemic of 1957. *PLoS ONE* **5,** e11158 (2010).
94. Taubenberger, J. K. & Kash, J. C. Insights on influenza pathogenesis from the grave. *Virus Res.* **162,** 2–7 (2011).
95. Taubenberger, J. K. *et al.* Characterization of the 1918 influenza virus polymerase genes. *Nature* **437,** 889–893 (2005).
96. Tumpey, T. M. *et al.* Characterization of the reconstructed 1918 Spanish influenza pandemic virus. *Science* **310,** 77–80 (2005).
97. Fleishman, S. J. *et al.* Computational design of proteins targeting the conserved stem region of influenza hemagglutinin. *Science* **332,** 816–821 (2011).
98. Kash, J. C. *et al.* Genomic analysis of increased host immune and cell death responses induced by 1918 influenza virus. *Nature* **443,** 578–581 (2006).
99. Kobasa, D. *et al.* Aberrant innate immune response in lethal infection of macaques with the 1918 influenza virus. *Nature* **445,** 319–323 (2007).
100. Pappas, C. *et al.* Single gene reassortants identify a critical role for PB1, HA, and NA in the high virulence of the 1918 pandemic influenza virus. *Proc. Natl Acad. Sci. USA* **105,** 3064–3069 (2008).
101. Qi, L. *et al.* The ability of pandemic influenza virus hemagglutinins to induce lower respiratory pathology is associated with decreased surfactant protein D binding. *Virology* **412,** 426–434 (2011).
102. Morens, D. M., Taubenberger, J. K., Harvey, H. A. & Memoli, M. J. The 1918 influenza pandemic: lessons for 2009 and the future. *Crit. Care Med.* **38,** e10–e20 (2010).

Acknowledgements This work was supported by the National Institutes of Health and the National Institute of Allergy and Infectious Diseases. The authors declare no competing financial interests. We thank L. Qi for translation and discussion of a Chinese language publication.

Author Contributions D.M.M., K.S. and J.K.T. jointly co-authored this manuscript.

Author Information Reprints and permissions information is available at www.nature.com/reprints. The authors declare no competing financial interests. Readers are welcome to comment on the online version of this article at www.nature.com/nature. Correspondence and requests for materials should be addressed to D.M.M. (dm270q@nih.gov).

doi:10.1038/nature11116

Superallowed Gamow–Teller decay of the doubly magic nucleus ^{100}Sn

C. B. Hinke[1], M. Böhmer[1], P. Boutachkov[2], T. Faestermann[1], H. Geissel[2], J. Gerl[2], R. Gernhäuser[1], M. Górska[2], A. Gottardo[3], H. Grawe[2], J. L. Grębosz[4], R. Krücken[1,5], N. Kurz[2], Z. Liu[6], L. Maier[1], F. Nowacki[7], S. Pietri[2], Zs. Podolyák[8], K. Sieja[7], K. Steiger[1], K. Straub[1], H. Weick[2], H.-J. Wollersheim[2], P. J. Woods[6], N. Al-Dahan[8], N. Alkhomashi[8], A. Ataç[9], A. Blazhev[10], N. F. Braun[10], I. T. Čeliković[11], T. Davinson[6], I. Dillmann[2], C. Domingo-Pardo[12], P. C. Doornenbal[13], G. de France[14], G. F. Farrelly[8], F. Farinon[2], N. Goel[2], T. C. Habermann[2], R. Hoischen[2], R. Janik[15], M. Karny[16], A. Kaşkaş[9], I. M. Kojouharov[2], Th. Kröll[17], Y. Litvinov[2], S. Myalski[4], F. Nebel[1], S. Nishimura[13], C. Nociforo[2], J. Nyberg[18], A. R. Parikh[19], A. Procházka[2], P. H. Regan[8], C. Rigollet[20], H. Schaffner[2], C. Scheidenberger[2], S. Schwertel[1], P.-A. Söderström[13], S. J. Steer[8], A. Stolz[21] & P. Strmeň[15]

The shell structure of atomic nuclei is associated with 'magic numbers' and originates in the nearly independent motion of neutrons and protons in a mean potential generated by all nucleons. During β^+-decay, a proton transforms into a neutron in a previously not fully occupied orbital, emitting a positron–neutrino pair with either parallel or antiparallel spins, in a Gamow–Teller or Fermi transition, respectively. The transition probability, or strength, of a Gamow–Teller transition depends sensitively on the underlying shell structure and is usually distributed among many states in the neighbouring nucleus. Here we report measurements of the half-life and decay energy for the decay of ^{100}Sn, the heaviest doubly magic nucleus with equal numbers of protons and neutrons. In the β-decay of ^{100}Sn, a large fraction of the strength is observable because of the large decay energy. We determine the largest Gamow–Teller strength so far measured in allowed nuclear β-decay, establishing the 'superallowed' nature of this Gamow–Teller transition. The large strength and the low-energy states in the daughter nucleus, ^{100}In, are well reproduced by modern, large-scale shell model calculations.

Gamow–Teller transitions, in which a proton is transformed into a neutron or vice versa, while possibly flipping its spin, represent an important spin–isospin degree of freedom in atomic nuclei. They are important in many astrophysical processes: they govern, for example, electron capture during the core collapse of supernovae. Furthermore, a detailed understanding of Gamow–Teller transitions will provide an essential constraint on the neutrino mass, in the event that neutrinoless double β-decay is ever observed. Most of the Gamow–Teller strength is found in the collective Gamow–Teller giant resonance (GTGR) of the neighbouring nucleus, which is typically a broad structure composed of many states. Whereas in charge-exchange reactions in stable nuclei the full GTGR is accessible, the Gamow–Teller strength in unstable nuclei can, so far, only be studied through β-decay. However, β-decay studies can observe only the fraction of the total Gamow–Teller strength within the decay energy window. Towards more proton-rich nuclei, this window becomes larger. Nevertheless, it is still experimentally challenging to detect all small components of the Gamow–Teller strength[1,2]. Thus, in most nuclei, measuring the full Gamow–Teller strength is difficult because it is fragmented and only partly accessible in β-decays.

^{100}Sn has $N = 50$ neutrons and $Z = 50$ protons, and as a result has completely occupied shells. It is therefore called 'doubly magic' and is particularly suited both experimentally and theoretically to the study of Gamow–Teller transitions. The closed $N = Z = 50$ shells reduce the effect of long-range correlations, thus decreasing the amount of fragmentation of the GTGR. Theoretical predictions suggest that a single state is dominantly populated in this decay. At the same time, the energy window for β-decay is ~7.4 MeV (ref. 3), and most of the GTGR is therefore accessible. Such a situation for a doubly magic system is realized nowhere else in the Segrè chart (a two-dimensional lattice in which all known nuclei are arranged with N and Z on the x and y axes, respectively): ^{16}O and ^{40}Ca are stable nuclei; ^{56}Ni has too small a Q_{EC} value (the energy available for β^+-decay or electron-capture decay) to make the Gamow–Teller resonance observable in β-decay; and doubly magic nuclei with $N = Z$ that are heavier than ^{100}Sn are unbound. Also, a recent experiment shows that ^{56}Ni has a much more fragmented Gamow–Teller strength[4] as a result of a less robust $N = Z = 28$ doubly magic shell closure as well as subtle differences in the shell structure (Methods Summary and Supplementary Information).

In an extreme, pure single-particle picture, the only possible Gamow–Teller transition of ^{100}Sn is the decay of a proton in the completely filled $g_{9/2}$ shell to a neutron in the empty $g_{7/2}$ shell because the $g_{9/2}$ neutron orbital is filled and no levels above $Z = 50$ are occupied. The large energy separation (shell gap) between these spin-parallel ($g_{9/2}$) and spin-antiparallel ($g_{7/2}$) orbitals, for which the orbital angular momentum is $L = 4$, is responsible for 50 being a magic number. The β-decay of ^{100}Sn is supposed to be enhanced as a result of the large

---

[1] Physik Department E12, Technische Universität München, D-85748 Garching, Germany. [2] GSI Helmholtzzentrum für Schwerionenforschung GmbH, D-64291 Darmstadt, Germany. [3] Istituto Nazionale di Fisica Nucleare, Laboratori Nazionali di Legnaro, 35020 Legnaro, Italy. [4] The Henryk Niewodniczanski Institute of Nuclear Physics (IFJ PAN), 31-342 Krakow, Poland. [5] TRIUMF, Vancouver, British Columbia V6T 2A3, Canada. [6] School of Physics & Astronomy, The University of Edinburgh, Edinburgh EH9 3JZ, UK. [7] Université de Strasbourg, IPHC, 67037 Strasbourg Cedex, France. [8] Department of Physics, University of Surrey, Guildford GU2 7XH, UK. [9] Physics Department, Faculty of Science, Ankara University, 06100 Tandogan, Ankara, Turkey. [10] Institute of Nuclear Physics, University of Cologne, D-50937 Köln, Germany. [11] Institute Vinca, University of Belgrade, 11000 Belgrade, Serbia. [12] IFIC, CSIC-University of Valencia, E-46071 Valencia, Spain. [13] RIKEN Nishina Center, Wako, Saitama 351-0198, Japan. [14] Grand Accélérateur National d'Ions Lourds, CEA/DSM-CNRS/IN2P3, 14076 Caen, France. [15] Comenius University, 818 06 Bratislava 16, Slovakia. [16] Institute of Experimental Physics, University of Warsaw, PL-00681 Warsaw, Poland. [17] Institut für Kernphysik, Technische Universität Darmstadt, D-64289 Darmstadt, Germany. [18] Department of Physics & Astronomy, Uppsala University, SE-75120 Uppsala, Sweden. [19] Departamento de Fisica i Enginyeria Nuclear, Universitat Politecnica de Catalunya (EUETIB), E-08036 Barcelona, Spain. [20] KVI, University of Groningen, 9747AA Groningen, The Netherlands. [21] National Superconducting Cyclotron Laboratory, Michigan State University, East Lansing, Michigan 48824-1321, USA.

number of protons occupying the $g_{9/2}$ shell, which can decay to the mostly empty neutron $g_{7/2}$ shell. This would lead to a GTGR consisting of only a single $I^{\pi} = 1^{+}$ level (I, spin; π, parity) with a large Gamow–Teller strength of about $B_{\mathrm{GT}} = 10$, taking into account the standard renormalization factor (0.75) of the Gamow–Teller matrix element due to configurations outside the model space[5]. This unique situation has been termed 'superallowed' Gamow–Teller decay[6]. Even in more realistic models, including particle–hole correlations, the Gamow–Teller decay of the ground state of ^{100}Sn is predicted to populate with more than 95% probability a single 1^{+} state in ^{100}In at an excitation energy of about 3 MeV. In these calculations, a Gamow–Teller strength of around 8–14 is obtained[7–10], leading to renormalized predictions of 5–7 (refs 8, 10). These theoretical results are summarized in Methods Summary and Supplementary Information.

The production of ^{100}Sn, and the study of its decay properties, has been the aim of several experiments[11–16], but in these only a few ^{100}Sn nuclei were uniquely identified. Here we report a new measurement of the half-life and Q_{EC} value from 259 identified ^{100}Sn nuclei, which yields the smallest log(ft) value of any known β-decay (here t is the half-life and f is a phase space factor that takes into account the trivial decay energy dependence of the half-life). The Gamow–Teller strength is inversely proportional to ft and thus is greatest for the ^{100}Sn decay establishing the robustness of $N = Z = 50$ shell closures. The experimentally observed Gamow–Teller strength is well described in modern, large-scale shell model (LSSM) calculations, which are able to handle an unprecedentedly large degree of configuration mixing in the case of ^{100}Sn. This ^{100}Sn doubly magic shell closure is the benchmark for various topics currently discussed in this mass region, such as spin-aligned pairing in $N = Z$ nuclei, alpha clustering and quadrupole collectivity in the Sn isotopic chain.

Experimental details

The experiment was performed at the GSI Helmholtzzentrum für Schwerionenforschung, Germany. A ^{124}Xe beam with a kinetic energy of 1.0A GeV (A, nucleon number) and 1-s-long spills of 3×10^{9} ions every 3 s was directed onto a beryllium target placed in front of the fragment separator[17]. Neutron-deficient nuclei were produced through relativistic projectile fragmentation, transmitted to the final focal plane of the fragment separator, and identified event by event (Fig. 1). The correct identification was verified by observing the γ-radiation depopulating known isomers, for example the 8^{+} isomer in ^{98}Cd. In total, 259 ^{100}Sn nuclei were unambiguously identified. This corresponds to a production rate of 0.75 per hour and a cross-section of 5.8 ± 2.1 pb. All uncertainties correspond to one standard deviation.

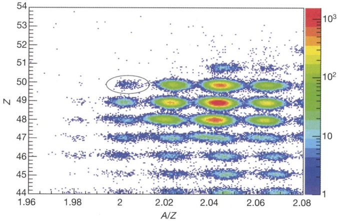

Figure 1 | Particle identification plot. Events are plotted with respect to Z and the mass-to-charge ratio, A/Z, for the full statistics of the ^{100}Sn fragment separator setting. In total, 259 ^{100}Sn nuclei (those indicated in the figure) were unambiguously identified. Resolutions (full-widths at half-maximum) in mass of $\Delta A = 0.32$ ($A = N + Z$) and in nuclear charge of $\Delta Z = 0.25$ were obtained. The colours indicate the number of events per bin in a logarithmic scale as indicated on the right-hand side.

The ions were implanted into a stack of highly segmented silicon strip detectors surrounded by the RISING array, which consists of 105 germanium detectors arranged in the stopped-beam configuration[18] to detect γ-rays with high efficiency. Of the 259 identified ^{100}Sn nuclei, 163 were stopped in the 2.1-mm-thick implantation layer.

Analysis and results

Following a ^{100}Sn implantation in a pixel of the implantation zone of the silicon detector, all decay events were recorded that occurred within 15 s in that pixel or in the directly neighbouring ones. During this correlation time, it was possible to assign 126 decay chains to the 163 ^{100}Sn implantations. A maximum-likelihood (MLH) analysis with a maximum of three decay events during the correlation time was used to analyse these decay chains. The half-life of ^{100}Sn was deduced to be 1.16 ± 0.20 s in the MLH analysis using established values for the lifetimes of the daughter nuclei. The measurement is much more precise than previous experiments yielding $0.94^{+0.54}_{-0.27}$ s (ref. 14) and $0.55^{+0.70}_{-0.31}$ s (ref. 16). In Fig. 2, we show the decay curve for ^{100}Sn.

Figure 3 shows the γ-ray spectrum observed in coincidence with decay events following ^{100}Sn implantations. Notably, discrete γ-transitions from the ^{100}Sn decay could be observed. The five transitions denoted in Fig. 3 are associated with the depopulation of excited states in the daughter nucleus ^{100}In.

The statistics were sufficient only to establish a coincidence between the 436-keV and 96-keV transitions, and it is thus impossible to deduce an unambiguous level scheme for ^{100}In. Within the uncertainties, the transitions could have the same intensity, which would allow for a single cascade of five transitions from the excited 1^{+} state to the ground state. However, this would lead to an excitation energy of more than 4 MeV, which is higher than the value of about 2.5 MeV predicted with realistic shell model calculations (see, for example, refs 19, 20). The large uncertainties in the observed intensities also allow for two parallel cascades originating from this 1^{+} state.

Figure 4 shows the relevant level scheme for ^{100}In obtained from LSSM calculations. In this approach, ^{100}Sn is not treated as an inert, doubly magic core but instead excitations across the $N = Z = 50$ shell closures were allowed within the fifth ($4\hbar\omega$) harmonic oscillator shell (Methods Summary and Supplementary Information).

The states of two multiplets that are relevant for the decay are shown. The states originate in the coupling of proton (π) holes in the $g_{9/2}$ orbital either to neutron (ν) particles in the $g_{7/2}$ orbital ($\pi g_{9/2}^{-1} \otimes \nu g_{7/2}^{1}$) with total spin and parity $I^{\pi} = 1^{+}$–8^{+} or to neutron

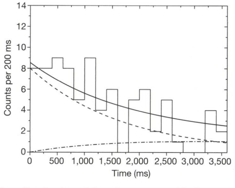

Figure 2 | Time distribution of first decay events. The histogram shows the observed time distribution of all first decay events in the nearest-neighbouring pixels after implantation of ^{100}Sn nuclei. Decay curves resulting from the MLH analysis are shown individually for ^{100}Sn (dashed) and its daughter nucleus ^{100}In (dash–dot). The solid line shows the sum of these decay curves and takes into account a small amount of random background.

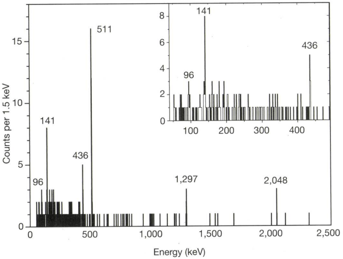

Figure 3 | Spectrum of γ-radiation. Energy distribution of the γ-radiation observed within 4 s after implantation of ^{100}Sn. With 65% probability these are directly following the ^{100}Sn decay. The other contributions are uncorrelated background decays and daughter decays of ^{100}In. None of the observed lines corresponds to known transitions from these minor contributions. The line at 511 keV is due to positron annihilation radiation. The measured absolute numbers of transitions of the five lines with the energies 96, 141, 436, 1,297 and 2,048 keV are respectively 79 ± 40, 100 ± 31, 59 ± 22, 72 ± 26 and 53 ± 26 corrected for electron conversion assuming M1 (magnetic dipole) transitions. Inset, enlarged view of the energy range up to 500 keV.

particles in the $d_{5/2}$ orbital ($\pi g_{9/2}^{-1} \otimes \nu d_{5/2}^{1}$) with $I^{\pi} = 2^{+}$–7^{+}. The predictions reflect the observed γ-ray transitions well if the high-energy, 2,048-keV, transition populates the lowest 2^{+} state, this then decays to lower-lying states via the 436-, 141- and 96-keV transitions, and the decay chain ends either in the 6^{+} ground state or a low-lying isomeric state with unobserved decay. In this picture, the second 2^{+} state is populated by the 1,297-keV transition and decays to the lower-lying 2^{+} and 3^{+} states. This may lead to a fragmentation of the intensities, making it impossible to observe these transitions in the present experiment. This picture is supported by three experimental facts: the measurement of the total γ-ray energy ($E^{*}_{1+} = 2.76 \pm 0.43$ MeV) in a previous experiment with a bismuth germanate detector[14]; the known mass difference between ^{100}Sn and ^{100}In[13], combined with our measured β-decay end-point energy ($E^{*}_{1+} = 2.6 \pm 1.0$ MeV); and our observation of a single event of β-delayed proton emission ($E^{*}_{1+} = 2.93 \pm 0.34$ MeV). It is fully consistent with the expectation that a single 1^{+} state is dominantly populated in the decay. Further details are given in Methods Summary and Supplementary Information.

As a key feature of this experiment, we measured the kinetic energy of the decay positrons fully absorbed in the compact silicon detector array. The spectrum resulting from the summed energies deposited by a β-particle in the pixels of the calorimeter up to 3 s after a ^{100}Sn implantation is shown in Fig. 5. It was fitted using a MLH analysis based on a single-component β-decay phase space function to determine the end-point energy in the decay of ^{100}Sn. For the fit of the end-point energy, only data in the energy region between 400 and 2,600 keV were used. In the analysis, corrections were applied to account for the emission of conversion electrons instead of low-energy γ-rays during the de-excitation of the daughter nucleus ^{100}In, for bremsstrahlung emitted when the positrons are slowed down and for the annihilation of positrons in flight before the deposition of their total kinetic energy. The end-point energy of the β-decay, if populating a single final state in the daughter nucleus ^{100}In, was determined to be 3.29 ± 0.20 MeV. The corresponding fraction of electron-capture decays is 13% of all ^{100}Sn decays.

Discussion

Using the measured half-life and the end-point energy, we calculated a log(*ft*) value of $2.62^{+0.13}_{-0.11}$, which is the smallest such value found so far for any nuclear β-decay. Thus, the Gamow–Teller decay of ^{100}Sn has a much larger strength than the known $0^{+} \rightarrow 0^{+}$ superallowed Fermi decays of $N = Z$ nuclei and can indeed be considered a superallowed Gamow–Teller decay[21]. This finding is also illustrated in Fig. 6, which shows the distribution of log(*ft*) values for allowed Gamow–Teller and Fermi transitions.

The extracted Gamow–Teller strength of the ^{100}Sn ground-state decay to the single excited 1^{+} state in ^{100}In is $B_{\mathrm{GT}} = 9.1^{+2.6}_{-3.0}$. The measured value is extraordinarily large but consistent with the value of $B_{\mathrm{GT}} = 5.8^{+5.5}_{-3.2}$ deduced from previous results for Q_{EC} and half-life[22], within the large error bars of the earlier measurement. The uncertainty in the new B_{GT} value is dominated by the uncertainty in the β-decay end-point energy. The extraction of the strength was done under the assumption that the Gamow–Teller decay was into only one final 1^{+}

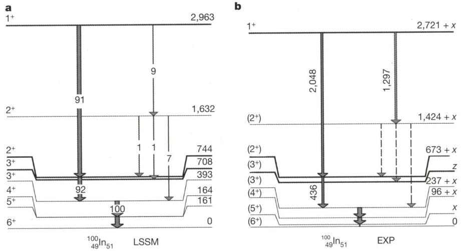

Figure 4 | Tentative level scheme of ^{100}In. **a**, LSSM calculation of the low-lying excited states in ^{100}In. Spin and parity (I^{π}) are shown on the left and energy (keV) is shown on the right. Populated levels with an almost pure $\pi g_{9/2}^{-1} \otimes \nu g_{7/2}^{1}$ configuration are indicated with bold lines, and the remaining levels are part of the $\pi g_{9/2}^{-1} \otimes \nu d_{5/2}^{1}$ multiplet. Gamma-transitions with their relative intensities (in per cent and indicated by arrow width) are shown for selected transitions. **b**, Most likely level scheme for the five observed γ-transitions in ^{100}In (three with energies (keV) shown). Because one low-energy transition might have been missed, the energy of the levels might have a systematic shift of up to $x = 80$ keV. The dashed transitions and level *z* were not observed. The assignment of spin and parity is certain only for the 1^{+} state; the others are tentative assignments based on theory.

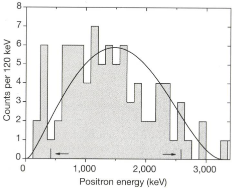

Figure 5 | Distribution of the positron energies emitted in the β-decay of ^{100}Sn. The spectrum contains only decay events that can be assigned to ^{100}Sn decays with a probability of at least 75%. The MLH fit was applied to the region between 400 and 2,600 keV, which is indicated with markers. The solid curve illustrates the shape of the best-fitting single-component β-decay phase space function determined by MLH analysis.

state in ^{100}In. However, if 1^+ states at excitation energies above the observed state were also populated, the summed Gamow–Teller strength would increase while the strength of the decay into the first excited 1^+ state would decrease. It would have been difficult to observe such higher-energy states because the reduced phase space for lower-energy β^+-particles would have led to a strongly reduced population.

The LSSM calculations, which within the *gds* harmonic oscillator shell take into account most of the long-range correlations across the $N = Z = 50$ doubly magic shell closure and include up to five particle–hole excitations (Methods Summary and Supplementary Information), yield a total summed Gamow–Teller strength of $B_{\mathrm{GT}} = 8.19$ for all possible final states in the daughter nucleus up to 60 MeV. The standard renormalization due to correlations beyond the 0*g*, 1*d*, 2*s* model space has been applied[5]. The distribution of strength up to an excitation energy of 10 MeV is shown in Methods Summary and Supplementary Fig. 1.

A Gamow–Teller strength of $B_{\mathrm{GT}} = 7.82$ is predicted in the experimental Q_{EC} window of 7.03(20) MeV. This corresponds to a reduction in the total renormalized Gamow–Teller strength of the extreme single-particle estimate ($B_{\mathrm{GT,ESPM}} \approx 10$) by 18% for excitation energies up to 60 MeV and by 22% in the Q_{EC} window. It is due to mixing in the *gds* harmonic oscillator shell, that is, emptying of the proton $g_{9/2}$ orbital, pre-filling of the neutron $g_{7/2}$ orbital and destructive interference of the four possible combinations of Gamow–Teller transitions within the *g* orbital ($L = 4$). The occupation numbers of the two orbitals that are linked by the Gamow–Teller operator, which acts on spin and isospin but does not change *L*, directly influence the strength of the transition matrix element.

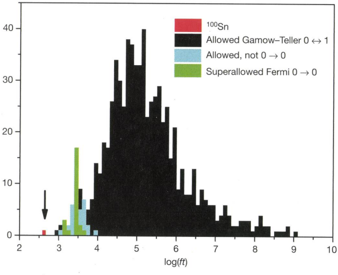

Figure 6 | Log(*ft*) values of allowed nuclear β-decays. Number distribution of log(*ft*) values for allowed β-transitions (obeying the selection rules). The data are from ref. 26. The values are for generally allowed Gamow–Teller transitions between 0^+ and 1^+ states (black), mixed Fermi/Gamow–Teller transitions (blue) and the well-established pure, superallowed Fermi transitions from 0^+ to 0^+ states (green). The decay of ^{100}Sn is unique because it has the smallest known log(*ft*) value (red) of any nuclear β-decay.

The calculation predicts that the largest fraction of the strength remains located in the first excited 1^+ state, in agreement with earlier calculations[7,21]. Nevertheless, according to our LSSM calculations it is reasonable to consider that several 1^+ states in ^{100}In are populated in the decay of ^{100}Sn. If, as an exercise, we take from the LSSM calculation the four lowest 1^+ states in ^{100}In with their energy splittings and relative Gamow–Teller strengths (Methods Summary and Supplementary Information), the value of $B_{\mathrm{GT}}(1_1^+) = 9.1^{+2.6}_{-3.0}$ (assuming a single 1^+ state) would be reduced to $B_{\mathrm{GT}}(1_1^+) = 7.6^{+2.2}_{-2.5}$ for the first excited 1^+ state using the experimental half-life and β-spectrum. The corresponding summed Gamow–Teller strength would be $\sum_{i=1}^{4} B_{\mathrm{GT}}(1_i^+) = 9.9^{+2.8}_{-3.2}$. Because this exercise served only to gauge the effect of branching on the experimental B_{GT} value, no error for the branching ratios is included.

The LSSM result of $B_{\mathrm{GT}} = 5.7$ for this first excited 1^+ state agrees within the statistical uncertainty with the value, $B_{\mathrm{GT}} = 7.6^{+2.2}_{-2.5}$, extracted from the experimental log(*ft*) value under the above assumptions. The experimental concentration of most of the Gamow–Teller strength in the first excited 1^+ state clearly classifies the ^{100}Sn Gamow–Teller decay as superallowed. This large experimental Gamow–Teller strength of the transition to the first excited 1^+ state proves that both the ^{100}Sn ground state and the first excited 1^+ state in ^{100}In have relatively pure wavefunctions. As expected, the LSSM calculation reveals that the respective wavefunctions consist predominantly of the $\pi g_{9/2}^{10} \otimes \nu g_{7/2}^{0}$ (82% probability) and $\pi g_{9/2}^{9} \otimes \nu g_{7/2}^{1}$ (54% probability) components. The high purity of the wavefunctions within the *gds* model space establishes the simultaneous robustness of the $Z = 50$ and $N = 50$ shell closures in ^{100}Sn, which is only ~3 MeV from the proton drip line, corroborating for $N = 50$ the results of refs 23, 24, and excludes the need for explicitly treating the unbound proton orbits as continuum states.

The LSSM calculations allow enough configuration mixing in the *gds* shell that convergent results are obtained, leading to meaningful conclusions in this exotic region far from the valley of stability. This indicates that it should be possible to obtain reliable, more accurate results for nuclei in the neighbourhood of ^{100}Sn, especially close to the proton drip line.

The underlying shell structures of nuclei in the vicinity of ^{100}Sn have to be determined with the highest possible accuracy to address the important issues in nuclear structure, such as the possibility of a new coupling scheme developing in the $N = Z$ nuclei in the vicinity of ^{100}Sn (ref. 25). The present measurement is a stringent test for LSSM calculations, in which the realistic character of such a coupling scheme still needs to be probed.

A better understanding of the nuclear structure is of major importance for modelling weak interaction rates in nuclei, which depend on the underlying shell structure and are important in many astrophysical processes. For example, Gamow–Teller transitions govern electron capture during the core collapse of supernovae. Also, Gamow–Teller transitions are an essential constraint on the theoretical calculations of neutrino-less double-β-decay matrix elements, the knowledge of which is necessary to relate the neutrino mass to the rate of this yet undiscovered process. Further interest in the decay rates of nuclei around ^{100}Sn comes from the study of certain astrophysical processes, as this region has been considered the end of the rapid proton capture process due to the Sn-Sb-Te cycle.

METHODS SUMMARY

^{100}Sn and neighbouring nuclei were produced by fragmentation of a $1.0A$-GeV ^{124}Xe beam from the GSI accelerators, separated in the fragment separator and identified by multiple energy-loss, magnetic rigidity and time-of-flight measurements. The nuclei were stopped in an implantation detector with high spatial resolution to correlate implantations with succeeding decays. The device was surrounded by the stopped-beam RISING array of 15 × 7 germanium detectors in close geometry. In this configuration, the set-up enabled us to do nearly 4π spectroscopy of the emitted γ-radiation and particle-decay radiation. With a photopeak efficiency of about 10% (1 MeV) for γ-ray detection and nearly 100% for full energy detection of decay particles up to 5 MeV, this high-resolution set-up allowed for a maximum use of the secondary beam.

The ^{100}Sn half-life and the β-decay end-point energy were calculated in the framework of a MLH analysis applied respectively to the time distribution of β-decays after implantation and the energy distribution of emitted positrons. This analysis also considered the daughter decays and the presence of uncorrelated random background decays from previous implantations.

To interpret the measured Gamow–Teller strength and the observed γ-rays emitted from ^{100}In, we carried out LSSM calculations. The valence space used in the LSSM consists of the fifth ($4\hbar\omega$) harmonic oscillator shell, that is, proton and neutron $\pi\nu(g,d,s)$ orbitals outside the ^{80}Zr core. The calculations included up to five particle–hole excitations from the $g_{9/2}$ proton and neutron orbitals to the rest of the shell, which made it possible for us to obtain convergent results for excitation spectra and the Gamow–Teller strength.

Received 28 October 2011; accepted 2 April 2012.

1. Ichimura, M., Sakai, H. & Wakasa, T. Spin-isospin responses via (p,n) and (n,p) reactions. *Prog. Part. Nucl. Phys.* **56,** 446–531 (2006).
2. Hardy, J. C., Carraz, L. C., Jonson, B. & Hansen, P. G. The essential decay of pandemonium: a demonstration of errors in complex beta-decay schemes. *Phys. Lett. B* **71,** 307–310 (1977).
3. Audi, G., Wapstra, A. H. & Thibault, C. The Ame2003 atomic mass evaluation: (II). Tables, graphs and references. *Nucl. Phys. A* **729,** 337–676 (2003).
4. Sasano, M. *et al.* Gamow-Teller transition strengths from ^{56}Ni. *Phys. Rev. Lett.* **107,** 202501 (2011).
5. Caurier, E., Martínez-Pinedo, G., Nowacki, F., Poves, A. & Zuker, P. A. The shell model as a unified view of nuclear structure. *Rev. Mod. Phys.* **77,** 427–488 (2005).
6. Brown, B. A. The nuclear shell model towards the drip lines. *Prog. Part. Nucl. Phys.* **47,** 517–599 (2001).
7. Brown, B. A. & Rykaczewski, K. Gamow-Teller strength in the region of ^{100}Sn. *Phys. Rev. C* **50,** R2270–R2273 (1994).
8. Dean, D. J., Koonin, S. E., Kuo, T. T. S., Langanke, K. & Radha, P. B. Complete $0\hbar\omega$ shell model Monte Carlo calculations of ^{94}Ru, ^{96}Pd, ^{96,98}Cd and ^{100}Sn. *Phys. Lett. B* **367,** 17–20 (1996).
9. Bobyk, A., Kaminski, W. & Borzov, I. N. Gamow-Teller beta-decay strengths of neutron-deficient tin isotopes: comparison of FFST and pnBCS+QRPA results. *Acta Phys. Pol. B* **31,** 953–963 (2000).
10. Batist, L. *et al.* Systematics of Gamow-Teller beta decay "Southeast" of ^{100}Sn. *Eur. Phys. J. A* **46,** 45–53 (2010).
11. Schneider, R. *et al.* Production and identification of ^{100}Sn. *Z. Phys. A* **348,** 241–242 (1994).
12. Lewitowicz, M. *et al.* Identification of the doubly-magic nucleus ^{100}Sn in the reaction ^{112}Sn+$^{\mathrm{nat}}$Ni at 63 MeV/nucleon. *Phys. Lett. B* **332,** 20–24 (1994).
13. Chartier, M. *et al.* Mass measurement of ^{100}Sn. *Phys. Rev. Lett.* **77,** 2400–2403 (1996).
14. Sümmerer, K. *et al.* Identification and decay spectroscopy of ^{100}Sn at the GSI projectile fragment separator FRS. *Nucl. Phys. A* **616,** 341–345 (1997).
15. Stolz, A. *et al.* Projectile fragmentation of ^{112}Sn at $E_{\mathrm{lab}} = 1$A GeV. *Phys. Rev. C* **65,** 064603 (2002).
16. Bazin, D. *et al.* Production and beta-decay of rp-process nuclei ^{96}Cd, ^{98}In, and ^{100}Sn. *Phys. Rev. Lett.* **101,** 252501 (2008).
17. Geissel, H. *et al.* The GSI projectile fragment separator (FRS): a versatile magnetic system for relativistic heavy ions. *Nucl. Instrum. Methods B* **70,** 286–297 (1992).
18. Pietri, S. *et al.* Recent results in fragmentation isomer spectroscopy with rising. *Nucl. Instrum. Methods B* **261,** 1079–1083 (2007).
19. Plettner, C. *et al.* Beta decay of ^{100}In. *Phys. Rev. C* **66,** 044319 (2002).
20. Coraggio, L., Covello, A., Gargano, A. & Itaco, N. Structure of particle-hole nuclei around ^{100}Sn. *Phys. Rev. C* **70,** 034310 (2004).
21. Hamamoto, I. & Sagawa, H. Gamow-Teller beta decay and isospin impurity in nuclei near the proton drip line. *Phys. Rev. C* **48,** R960–R963 (1993).
22. Faestermann, T. *et al.* Decay studies of N ≈ Z nuclei from ^{75}Sr to ^{102}Sn. *Eur. Phys. J. A* **15,** 185–188 (2002).
23. Blazhev, A. *et al.* Observation of a core-excited E4 isomer in ^{98}Cd. *Phys. Rev. C* **69,** 064304 (2004).
24. Boutachkov, P. *et al.* High-spin isomers in ^{96}Ag: excitations across the Z = 38 and Z = 50, N = 50 closed shells. *Phys. Rev. C* **84,** 044311 (2011).
25. Cederwall, B. *et al.* Evidence for a spin-aligned neutron–proton paired phase from the level structure of ^{92}Pd. *Nature* **469,** 68–71 (2011).
26. Singh, B., Rodriguez, J. L., Wong, S. S. M. & Tuli, J. K. Review of log*ft* values in β-decay. *Nucl. Data Sheets (N.Y. N.Y.)* **84,** 487–563 (1998).

Supplementary Information is linked to the online version of the paper at www.nature.com/nature.

Acknowledgements We thank the staff of the GSI ion source and accelerator for the preparation of a stable, high-intensity ^{124}Xe beam, and we thank the fragment separator technicians for setting up the beamline detectors. We acknowledge discussions with G. Martínez-Pinedo, K. Langanke and A. Zuker. We are also grateful to the EUROBALL Owners Committee for the use of the Euroball Cluster Detectors. This work was supported by the BMBF under contracts 06MT238, 06MT9156, 06KY205I and 06KY9136I; by the GSI; by the DFG Cluster of Excellence 153 'Origin and Structure of the Universe'; by the EC within the FP6 through I3-EURONS (contract no. RII3-CT-2004-506065); and by the Swedish Research Council.

Author Contributions Fragment separator: H.W., P.B., H. Geissel, M.G., Zs.P. and C.N.; particle detectors: C.B.H., K. Straub, R.G., T.F., L.M. and F. Nebel; RISING γ-array: P.B., M.G., S.P., J.G., I.M.K. and H.-J.W.; data acquisition and analysis software: M.B., R.G., J.L.G., N.K. and L.M.; data analysis and interpretation: C.B.H., K. Straub, T.F., M.G., H. Grawe, R.K., K. Steiger, F. Nowacki and K. Sieja; shell model calculations: F. Nowacki and K. Sieja; writing of manuscript: C.B.H., T.F., R.G., H. Grawe, R.K., F. Nowacki and K. Sieja. All authors except H. Grawe, F. Nowacki and K. Sieja took part in the preparation and the experiments, and all authors commented on the final paper.

Author Information Reprints and permissions information is available at www.nature.com/reprints. The authors declare no competing financial interests. Readers are welcome to comment on the online version of this article at www.nature.com/nature. Correspondence and requests for materials should be addressed to T.F. (thomas.faestermann@ph.tum.de).

doi:10.1038/nature10983

The genomic and transcriptomic architecture of 2,000 breast tumours reveals novel subgroups

Christina Curtis[1,2]†*, Sohrab P. Shah[3,4]*, Suet-Feung Chin[1,2]*, Gulisa Turashvili[3,4]*, Oscar M. Rueda[1,2], Mark J. Dunning[2], Doug Speed[2,5]†, Andy G. Lynch[1,2], Shamith Samarajiwa[1,2], Yinyin Yuan[1,2], Stefan Gräf[1,2], Gavin Ha[3], Gholamreza Haffari[3], Ali Bashashati[3], Roslin Russell[2], Steven McKinney[3,4], METABRIC Group‡, Anita Langerød[6], Andrew Green[7], Elena Provenzano[8], Gordon Wishart[8], Sarah Pinder[9], Peter Watson[3,4,10], Florian Markowetz[1,2], Leigh Murphy[10], Ian Ellis[7], Arnie Purushotham[9,11], Anne-Lise Børresen-Dale[6,12], James D. Brenton[2,13], Simon Tavaré[1,2,5,14], Carlos Caldas[1,2,8,13] & Samuel Aparicio[3,4]

The elucidation of breast cancer subgroups and their molecular drivers requires integrated views of the genome and transcriptome from representative numbers of patients. We present an integrated analysis of copy number and gene expression in a discovery and validation set of 997 and 995 primary breast tumours, respectively, with long-term clinical follow-up. Inherited variants (copy number variants and single nucleotide polymorphisms) and acquired somatic copy number aberrations (CNAs) were associated with expression in ~40% of genes, with the landscape dominated by *cis*- and *trans*-acting CNAs. By delineating expression outlier genes driven in *cis* by CNAs, we identified putative cancer genes, including deletions in *PPP2R2A*, *MTAP* and *MAP2K4*. Unsupervised analysis of paired DNA–RNA profiles revealed novel subgroups with distinct clinical outcomes, which reproduced in the validation cohort. These include a high-risk, oestrogen-receptor-positive 11q13/14 *cis*-acting subgroup and a favourable prognosis subgroup devoid of CNAs. *Trans*-acting aberration hotspots were found to modulate subgroup-specific gene networks, including a TCR deletion-mediated adaptive immune response in the 'CNA-devoid' subgroup and a basal-specific chromosome 5 deletion-associated mitotic network. Our results provide a novel molecular stratification of the breast cancer population, derived from the impact of somatic CNAs on the transcriptome.

Inherited genetic variation and acquired genomic aberrations contribute to breast cancer initiation and progression. Although somatically acquired CNAs are the dominant feature of sporadic breast cancers, the driver events that are selected for during tumorigenesis are difficult to elucidate as they co-occur alongside a much larger landscape of random non-pathogenic passenger alterations[1,2] and germline copy number variants (CNVs). Attempts to define subtypes of breast cancer and to discern possible somatic drivers are still in their relative infancy[3–6], in part because breast cancer represents multiple diseases, implying that large numbers (many hundreds or thousands) of patients must be studied. Here we describe an integrated genomic/transcriptomic analysis of breast cancers with long-term clinical outcomes composed of a discovery set of 997 primary tumours and a validation set of 995 tumours from METABRIC (Molecular Taxonomy of Breast Cancer International Consortium).

A breast cancer population genomic resource

We assembled a collection of over 2,000 clinically annotated primary fresh-frozen breast cancer specimens from tumour banks in the UK and Canada (Supplementary Tables 1–3). Nearly all oestrogen receptor (ER)-positive and/or lymph node (LN)-negative patients did not receive chemotherapy, whereas ER-negative and LN-positive patients did. Additionally, none of the HER2^{+} patients received trastuzumab. As such, the treatments were homogeneous with respect to clinically relevant groupings. An initial set of 997 tumours was analysed as a discovery group and a further set of 995 tumours, for which complete data later became available, was used to test the reproducibility of the integrative clusters (described below). An overview of the main analytical approaches is provided in Supplementary Fig. 1. Details concerning expression and copy number profiling, including sample assignment to the PAM50 intrinsic subtypes[3,4,7] (Supplementary Fig. 2), copy number analysis (Supplementary Tables 4–8) and validation (Supplementary Figs 3 and 4 and Supplementary Tables 9–11), and *TP53* mutational profiling (Supplementary Fig. 5) are described in the Supplementary Information.

Genome variation affects tumour expression architecture

Genomic variants are considered to act in *cis* when a variant at a locus has an impact on its own expression, or in *trans* when it is associated

---

[1] Department of Oncology, University of Cambridge, Hills Road, Cambridge CB2 2XZ, UK. [2] Cancer Research UK, Cambridge Research Institute, Li Ka Shing Centre, Robinson Way, Cambridge CB2 0RE, UK. [3] Department of Pathology and Laboratory Medicine, University of British Columbia, Vancouver, British Columbia V6T 2B5, Canada. [4] Molecular Oncology, British Columbia Cancer Research Centre, Vancouver, British Columbia V5Z 1L3, Canada. [5] Department of Applied Mathematics and Theoretical Physics, University of Cambridge, Centre for Mathematical Sciences, Cambridge CB3 0WA, UK. [6] Department of Genetics, Institute for Cancer Research, Oslo University Hospital Radiumhospitalet, Montebello, 0310 Oslo, Norway. [7] Department of Histopathology, School of Molecular Medical Sciences, University of Nottingham, Nottingham NG5 1PB, UK. [8] Cambridge Breast Unit, Addenbrooke's Hospital, Cambridge University Hospital NHS Foundation Trust and NIHR Cambridge Biomedical Research Centre, Cambridge CB2 2QQ, UK. [9] King's College London, Breakthrough Breast Cancer Research Unit, London WC2R 2LS, UK. [10] Manitoba Institute of Cell Biology, University of Manitoba, Manitoba R3E 0V9, Canada. [11] NIHR Comprehensive Biomedical Research Centre at Guy's and St Thomas' NHS Foundation Trust and King's College London, London WC2R 2LS, UK. [12] Institute for Clinical Medicine, Faculty of Medicine, University of Oslo, 0316 Oslo, Norway. [13] Cambridge Experimental Cancer Medicine Centre, Cambridge CB2 0RE, UK. [14] Molecular and Computational Biology Program, University of Southern California, Los Angeles, California 90089, USA. †Present addresses: Department of Preventive Medicine, Keck School of Medicine, University of Southern California, Los Angeles, California 90033, USA (Ch.C.); University College London, Genetics Institute, WC1E 6BT, UK (D.S.).

*These authors contributed equally to this work.

‡Lists of participants and affiliations appear at the end of the paper.

with genes at other sites in the genome. We generated a map of CNAs, CNVs (Supplementary Fig. 6, Supplementary Tables 12–15) and single nucleotide polymorphisms (SNPs) in the breast cancer genome to distinguish germline from somatic variants (see Methods), and to examine the impact of each of these variants on the expression landscape. Previous studies[8] have shown that most heritable gene expression traits are governed by a combination of *cis* (proximal) loci, defined here as those within a 3-megabase (Mb) window surrounding the gene of interest, and *trans* (distal) loci, defined here as those outside that window. We assessed the relative influence of SNPs, CNVs and CNAs on tumour expression architecture, using each of these variants as a predictor (see Methods) to elucidate expression quantitative trait loci (eQTLs) among patients.

Both germline variants and somatic aberrations were found to influence tumour expression architecture, having an impact on $>$39% (11,198/28,609) of expression probes genome-wide based on analysis of variance (ANOVA; see Methods), with roughly equal numbers of genes associated in *cis* and *trans*. CNAs were associated with the greatest number of expression profiles (Fig. 1, Supplementary Figs 7–13 and Supplementary Tables 16–20), but were rivalled by SNPs to explain a greater proportion of expression variation on a per-gene basis genome-wide, whereas the contribution from CNVs was more moderate (Fig. 1b and Supplementary Table 21). The true ratio of putative *trans* versus *cis* eQTLs is hard to estimate[9]; however, the large sample size used here allowed the detection of small effects, with 5,401 and 5,462 CNAs significantly (Šidák adjusted P value <0.0001) associated in *cis* or in *trans*, respectively. Whereas *cis*-associations tended to be stronger, the *trans*-acting loci modulated a larger number of messenger RNAs, as described below.

Expression outliers refine the breast cancer landscape

As shown above, $\sim$20% of loci exhibit CNA-expression associations in *cis* (Supplementary Fig. 14). To refine this landscape further and identify the putative driver genes, we used profiles of outlying expression (see Methods and ref. 10) and the high resolution and sensitivity of the Affymetrix SNP 6.0 platform to delineate candidate regions. This approach markedly reduces the complexity of the landscape to 45 regions (frequency > 5, Fig. 2) and narrows the focus, highlighting novel regions that modulate expression. The full enumeration of regions delineated by this approach and their subtype-specific associations (Supplementary Figs 15 and 16 and Supplementary Tables 22–24) includes both known drivers (for example, *ZNF703* (ref. 11), *PTEN* (ref. 12), *MYC*, *CCND1*, *MDM2*, *ERBB2*, *CCNE1* (ref. 13)) and putative driver aberrations (for example, *MDM1*, *MDM4*, *CDK3*, *CDK4*, *CAMK1D*, *PI4KB*, *NCOR1*).

The deletion landscape of breast cancer has been poorly explored, with the exception of *PTEN*. We illustrate three additional regions of significance centred on *PPP2R2A* (8p21, Fig. 2, region 11), *MTAP* (9p21, Fig. 2, region 15) and *MAP2K4* (17p11, Fig. 2, region 33), which exhibit heterozygous and homozygous deletions (Supplementary Figs 15, 17–19 and Supplementary Table 24) that drive expression of these loci. We observe breast cancer subtype-specific (enriched in mitotic ER-positive cancers) loss of transcript expression in *PPP2R2A*, a B-regulatory subunit of the PP2A mitotic exit holoenzyme complex. Somatic mutations in *PPP2R1A* have recently been reported in clear cell ovarian cancers and endometrioid cancers[14,15], and methylation silencing of *PPP2R2B* has also been observed in colorectal cancers[16]. Thus, dysregulation of specific PPP2R2A functions in luminal B breast cancers adds a significant pathophysiology to this subtype.

MTAP (9p21, a component of methyladenosine salvage) is frequently co-deleted with the *CDKN2A* and *CDKN2B* tumour suppressor genes in a variety of cancers[17] as we observe here (Supplementary Figs 17c and 18). The third deletion encompasses *MAP2K4* (also called *MKK4*) (17p11), a p38/Jun dual specificity serine/threonine protein kinase. *MAP2K4* has been proposed as a recessive cancer gene[18], with mutations noted in cell lines[19]. We show, for the first time, the recurrent deletion of *MAP2K4* (Supplementary Figs 17d and 19) concomitant with outlying expression (Supplementary Fig. 15) in predominantly ER-positive cases, and verify homozygous deletions (Supplementary Table 9) in primary tumours, strengthening the evidence for *MAP2K4* as a tumour suppressor in breast cancer.

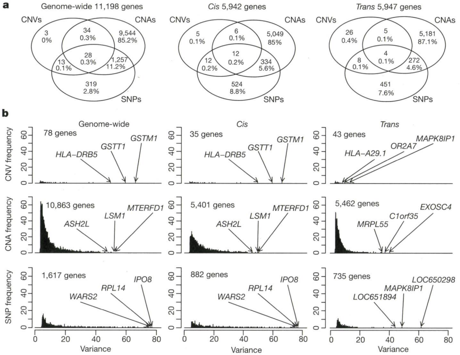

Figure 1 | Germline and somatic variants influence tumour expression architecture. a, Venn diagrams depict the relative contribution of SNPs, CNVs and CNAs to genome-wide, *cis* and *trans* tumour expression variation for significant expression associations (Šidák adjusted P-value ≤ 0.0001). **b,** Histograms illustrate the proportion of variance explained by the most significantly associated predictor for each predictor type, where several of the top associations are indicated.

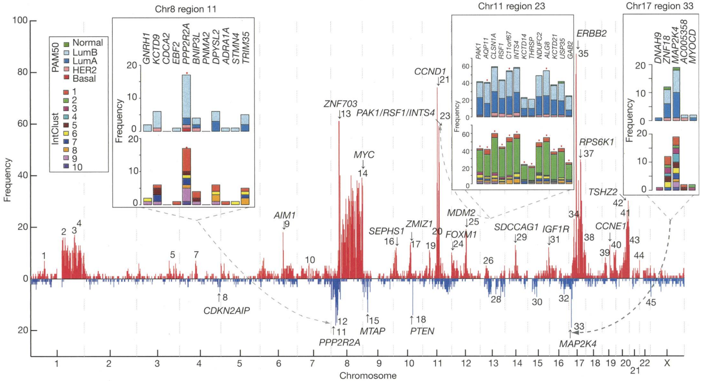

Figure 2 | Patterns of *cis* outlying expression refine putative breast cancer drivers. A genome-wide view of outlying expression coincident with extreme copy number events in the CNA landscape highlights putative driver genes, as indicated by the arrows and numbered regions. The frequency (absolute count) of cases exhibiting an outlying expression profile at regions across the genome is shown, as is the distribution across subgroups for several regions in the insets. High-level amplifications are indicated in red and homozygous deletions in blue. Red asterisks above the bar plots indicate significantly different observed distributions than expected based on the overall population frequency (χ^2 test, $P < 0.0001$).

Trans-acting associations reveal distinct modules

We next asked how *trans*-associated expression profiles are distributed across the genome. We mapped these in the expression landscape by examining the matrices of CNA–expression associations (see Methods). This revealed strong off-diagonal patterns at loci on chromosomes 1q, 7p, 8, 11q, 14q, 16, 17q and 20q (Fig. 3a), including both positive and negative associations, as well as numerous *trans*-acting aberration hotspots (defined as CNAs associated with >30 mRNAs). Importantly, these aberration hotspots can be grouped into pathway modules, which highlight known driver loci such as *ERBB2* and *MYC*, as well as novel loci associated with large *trans* expression modules (Supplementary Tables 25 and 26). The T-cell-receptor (TCR) loci on chromosomes 7 (*TRG*) and 14 (*TRA*) represent two such hotspots that modulated 381 and 153 unique mRNAs, respectively, as well as 19 dually regulated genes (Supplementary Fig. 20). These cognate mRNAs were highly enriched for T-cell activation and proliferation, dendritic cell presentation, and leukocyte activation, which indicate the induction of an adaptive immune response associated with tumour-infiltrating lymphocytes (Fig. 3b, Supplementary Fig. 20 and Supplementary Tables 27 and 28), as described later.

In a second approach, we examined the genome-wide patterns of linear correlation between copy number and expression features (see Methods), and noted the alignment of several off-diagonal signals, including those on chromosome 1q, 8q, 11q, 14q and 16 (Supplementary Fig. 21). Additionally, a broad signal on chromosome 5 localizing to a deletion event restricted to the basal-like tumours was observed (Supplementary Fig. 21), but was not detected with the eQTL framework, where discrete (as opposed to continuous) copy number values were used. This basal-specific *trans* module is enriched for transcriptional changes involving cell cycle, DNA damage repair and apoptosis (Supplementary Table 29), reflecting the high mitotic index typically associated with basal-like tumours, described in detail below.

Integrative clustering reveals novel subgroups

Using the discovery set of 997 breast cancers, we next asked whether novel biological subgroups could be found by joint clustering of copy number and gene expression data. On the basis of our finding that *cis*-acting CNAs dominated the expression landscape, the top 1,000 *cis*-associated genes across all subtypes (Supplementary Table 30) were used as features for input to a joint latent variable framework for integrative clustering[20] (see Methods). Cluster analysis suggested 10 groups (based on Dunn's index) (see Methods and Supplementary Figs 22 and 23), but for completeness, this result was compared with the results for alternative numbers of clusters and clustering schemes (see Methods, Supplementary Figs 23–27 and Supplementary Tables 31–33). The 10 integrative clusters (labelled IntClust 1–10) were typified by well-defined copy number aberrations (Fig. 4, Supplementary Figs 22, 28–30 and Supplementary Tables 34–39), and split many of the intrinsic subtypes (Supplementary Figs 31–33). Kaplan–Meier plots of disease-specific survival and Cox proportional hazards models indicate subgroups with distinct clinical outcomes (Fig. 5, Supplementary Figs 34, 35 and Supplementary Tables 40 and 41). To validate these results, we trained a classifier (754 features) for the integrative subtypes in the discovery set using the nearest shrunken centroids approach[21] (see Methods and Supplementary Tables 42 and 43), and then classified the independent validation set of 995 cases into the 10 groups (Supplementary Table 44). The reproducibility of the clusters in the validation set is shown in three ways. First, classification of the validation set resulted in the assignment of a similar proportion of cases to the 10 subgroups, each of which exhibited nearly identical copy number profiles (Fig. 4). Second, the groups have substantially similar hazard ratios (Fig. 5b, Supplementary Fig. 35 and Supplementary Table 40). Third, the quality of the clusters in the validation set is emphasized by the in-group proportions (IGP) measure[22] (Fig. 4).

Among the integrative clusters, we first note an ER-positive subgroup composed of 11q13/14 *cis*-acting luminal tumours (IntClust 2,

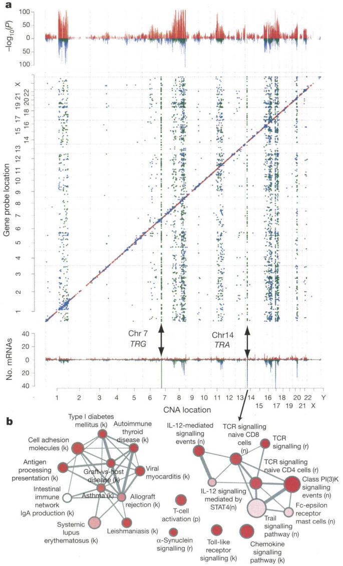

Figure 3 | *Trans*-acting aberration hotspots modulate concerted molecular pathways. **a**, Manhattan plot illustrating *cis* and *trans* expression-associated copy number aberrations from the eQTL analysis (top panel). The matrix of significant predictor–expression associations (adjusted P-value ≤ 0.0001) exhibits strong off-diagonal patterns (middle panel), and the frequency of mRNAs associated with a particular copy number aberration further illuminates these *trans*-acting aberration hotspots (bottom panel). The directionality of the associations is indicated as follows: *cis*: positive, red; negative, pink; *trans*: positive, blue; negative, green. **b**, Enrichment map of immune response modules in the *trans*-associated TRA network, where letters in parentheses represent the source database as follows: b, NCI-PID BioCarta; c, cancer cell map; k, KEGG; n, NCI-PID curated pathways; p, PANTHER; r, Reactome.

$n = 45$) that harbour other common alterations. This subgroup exhibited a steep mortality trajectory with elevated hazard ratios (discovery set: 3.620, 95% confidence interval (1.905–6.878); validation set: 3.353, 95% confidence interval (1.381–8.141)), indicating that it represents a particularly high-risk subgroup. Several known and putative driver genes reside in this region, namely *CCND1* (11q13.3), *EMSY* (11q13.5), *PAK1* (11q14.1) and *RSF1* (11q14.1), which have been previously linked to breast[13,23] or ovarian cancer[24]. Both the copy number (Fig. 4) and expression outlier landscapes (Fig. 2) suggest at least two separate amplicons at 11q13/14, one at *CCND1* (11q13.3) and a separate peak from 11q13.5-11q14.1 spanning *UVRAG–GAB2*, centred around *PAK1*, *RSF1*, *C11orf67* and *INTS4*, where it is more challenging to distinguish the driver[24]. Notably, the expression outlier profiles for this region are enriched for samples belonging to IntClust 2 (Fig. 2, inset region 23) and all 45 members of this subgroup harboured amplifications of these genes, with high frequencies of amplification also observed for *CCND1* ($n = 39$) and *EMSY* ($n = 34$). In light of these observations, the 11q13/14 amplicon may be driven by a cassette of genes rather than a single oncogene.

Second, we note the existence of two subgroups marked by a paucity of copy number and *cis*-acting alterations. These subgroups cannot be explained by low cellularity tumours (see Methods). One subgroup (IntClust3, $n = 156$) with low genomic instability (Fig. 4 and Supplementary Fig. 22) was composed predominantly of luminal A cases, and was enriched for histotypes that typically have good prognosis, including invasive lobular and tubular carcinomas. The other subgroup (IntClust 4, $n = 167$) was also composed of favourable outcome cases, but included both ER-positive and ER-negative cases and varied intrinsic subtypes, and had an essentially flat copy number landscape, hence termed the 'CNA-devoid' subgroup. A significant proportion of cases within this subgroup exhibit extensive lymphocytic infiltration (Supplementary Table 45).

Third, several intermediate prognosis groups of predominantly ER-positive cancers were identified, including a 17q23/20q *cis*-acting luminal B subgroup (IntClust 1, $n = 76$), an 8p12 *cis*-acting luminal subgroup (IntClust 6, $n = 44$), as well as an 8q *cis*-acting/20q-amplified mixed subgroup (IntClust 9, $n = 67$). Two luminal A subgroups with similar CNA profiles and favourable outcome were noted. One subgroup is characterized by the classical 1q gain/16q loss (IntClust 8, $n = 143$), which corresponds to a common translocation event[25], and the other lacks the 1q alteration, while maintaining the 16p gain/16q loss with higher frequencies of 8q amplification (IntClust 7, $n = 109$). We also noted that the majority of basal-like tumours formed a stable, mostly high-genomic instability subgroup (IntClust 10, $n = 96$). This subgroup had relatively good long-term outcomes (after 5 years), consistent with ref. 26, and characteristic *cis*-acting alterations (5 loss/8q gain/10p gain/12p gain).

The *ERBB2*-amplified cancers composed of HER2-enriched (ER-negative) cases and luminal (ER-positive) cases appear as IntClust 5 ($n = 94$), thus refining the ERBB2 intrinsic subtype by grouping additional patients that might benefit from targeted therapy. Patients in this study were enrolled before the general availability of trastuzumab, and as expected this subgroup exhibits the worst disease-specific survival at both 5 and 15 years and elevated hazard ratios (discovery set: 3.899, 95% confidence interval (2.234–6.804); validation set: 4.447, 95% confidence interval (2.284–8.661)).

Pathway deregulation in the integrative subgroups

Finally, we projected the molecular profiles of the integrative subgroups onto pathways to examine possible biological themes among breast cancer subgroups (Supplementary Tables 46 and 47) and the relative impact of *cis* and *trans* expression modules on the pathways. The CNA-devoid (IntClust 4) group exhibits a strong immune and inflammation signature involving the antigen presentation pathway, OX40 signalling, and cytotoxic T-lymphocyte-mediated apoptosis (Supplementary Fig. 36). Given that *trans*-acting deletion hotspots were localized to the *TRG* and *TRA* loci and were associated with an adaptive immune response module, we asked whether these deletions contribute to alterations in this pathway. The CNA-devoid subgroup (IntClust 4) was found to exhibit nearly twice as many deletions (typically heterozygous loss) at the *TRG* and *TRA* loci (~20% of cases) as compared to the other subtypes (with the exception of IntClust 10), and deletions of both TCR loci were significantly associated with severe lymphocytic infiltration (χ^2 test, $P < 10^{-9}$ and $P < 10^{-8}$, respectively). Notably, these *trans*-associated mRNAs were significantly enriched in the immune response signature of the CNA-devoid subgroup (Supplementary Fig. 36) as well as among genes differentially expressed in CNA-devoid cases with severe lymphocytic infiltration (Supplementary Fig. 37). We conclude that genomic copy number loss

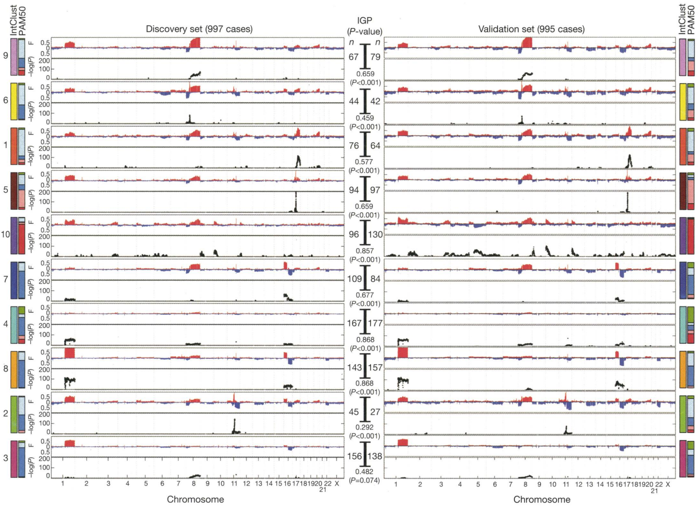

Figure 4 | The integrative subgroups have distinct copy number profiles. Genome-wide frequencies (F, proportion of cases) of somatic CNAs (y-axis, upper plot) and the subtype-specific association ($-\log_{10}$ P-value) of aberrations (y-axis, bottom plot) based on a χ^2 test of independence are shown for each of the 10 integrative clusters. Regions of copy number gain are indicated in red and regions of loss in blue in the frequency plot (upper plot). Subgroups were ordered by hierarchical clustering of their copy number profiles in the discovery cohort ($n = 997$). For the validation cohort ($n = 995$), samples were classified into each of the integrative clusters as described in the text. The number of cases in each subgroup (n) is indicated as is the in-group proportion (IGP) and associated P-value, as well as the distribution of PAM50 subtypes within each cluster.

at the TCR loci drives a *trans*-acting immune response module that associates with lymphocytic infiltration, and characterizes an otherwise genomically quiescent subgroup of ER-positive and ER-negative patients with good prognosis. These observations suggest the presence of mature T lymphocytes (with rearranged TCR loci), which may explain an immunological response to the cancer. In line with these findings, a recent study[27] demonstrated the association between $CD8^+$ lymphocytes and favourable prognosis.

Also among the *trans*-influenced groups is IntClust 10 (basal-like cancer enriched subgroup), which harbours chromosome 5q deletions (Supplementary Fig. 21). Numerous signalling molecules, transcription factors and cell division genes were associated in *trans* with this deletion event in the basal cancers, including alterations in *AURKB*, *BCL2*, *BUB1*, *CDCA3*, *CDCA4*, *CDC20*, *CDC45*, *CHEK1*, *FOXM1*, *HDAC2*, *IGF1R*, *KIF2C*, *KIFC1*, *MTHFD1L*, *RAD51AP1*, *TTK* and *UBE2C* (Supplementary Fig. 38). Notably, *TTK* (*MPS1*), a dual specificity kinase that assists *AURKB* in chromosome alignment during mitosis, and recently reported to promote aneuploidy in breast cancer[28], was upregulated. These results indicate that 5q deletions modulate the coordinate transcriptional control of genomic and chromosomal instability and cell cycle regulation within this subgroup.

In contrast to these subtype-specific *trans*-associated signatures, the high-risk 11q13/14 subgroup was characterized by strong *cis*-acting associations. Like the basal cancers, this subgroup also exhibited alterations in key cell-cycle-related genes (Supplementary Fig. 39), which probably have a role in its aggressive pathophysiology, but the nature of the signature differs. In particular, the regulation of the G1/S transition by BTG family proteins, which include CCND1, PPP2R1B and E2F2, was significantly enriched in the 11q13/14 *cis*-acting subgroup, but not the basal cancers, and this is consistent with *CCND1* and the *PPP2R* subunit representing subtype-specific drivers in these tumours.

Discussion

We have generated a robust, population-based molecular subgrouping of breast cancer based on multiple genomic views. The size and nature of this cohort made it amenable to eQTL analyses, which can aid the identification of loci that contribute to the disease phenotype[29]. CNAs and SNPs influenced expression variation, with CNAs dominating the landscape in *cis* and *trans*. The joint clustering of CNAs and gene expression profiles further resolves the considerable heterogeneity of the expression-only subgroups, and highlights a high-risk 11q13/14 *cis*-acting subgroup as well as several other strong *cis*-acting clusters and a genomically quiescent group. The reproducibility of subgroups with these molecular and clinical features in a validation cohort of 995 tumours suggests that by integrating multiple genomic

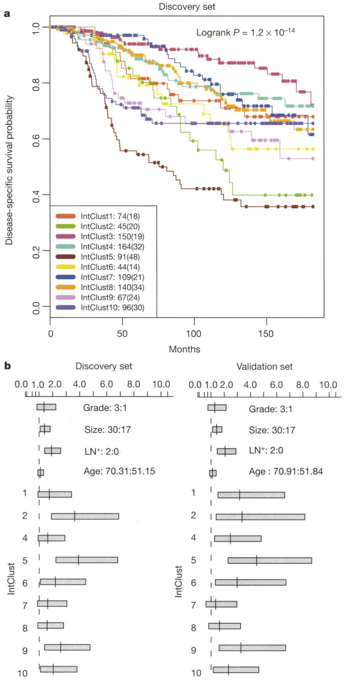

Figure 5 | The integrative subgroups have distinct clinical outcomes. **a**, Kaplan–Meier plot of disease-specific survival (truncated at 15 years) for the integrative subgroups in the discovery cohort. For each cluster, the number of samples at risk is indicated as well as the total number of deaths (in parentheses). **b**, 95% confidence intervals for the Cox proportional hazard ratios are illustrated for the discovery and validation cohort for selected values of key covariates, where each subgroup was compared against IntClust 3.

features it may be possible to derive more robust patient classifiers. We show here, for the first time, that subtype-specific *trans*-acting aberrations modulate concerted transcriptional changes, such as the TCR deletion-mediated adaptive immune response that characterizes the CNA-devoid subgroup and the chromosome 5 deletion-associated cell cycle program in the basal cancers.

The integrated CNA-expression landscape highlights a limited number of genomic regions that probably contain driver genes, including *ZNF703*, which we recently described as a luminal B specific driver[11], as well as somatic deletion events affecting key subunits of the PP2A holoenzyme complex and *MTAP*, which have previously been under-explored in breast cancer. The CNA-expression landscape also illuminates rare but potentially significant events, including *IGF1R*, *KRAS* and *EGFR* amplifications and *CDKN2B*, *BRCA2*, *RB1*, *ATM*, *SMAD4*, *NCOR1* and *UTX* homozygous deletions. Although some of these events have low overall frequencies ($<1\%$ patients) (Figs 2, Supplementary Fig. 15 and Supplementary Tables 22–24), they may have implications for understanding therapeutic responses to targeted agents, particularly those targeting tyrosine kinases or phosphatases.

Finally, because the integrative subgroups occur at different frequencies in the overall population, focusing sequencing efforts on representative numbers from these groups will help to establish a comprehensive breast cancer somatic landscape at sequence-level resolution. For example, a significant number ($\sim 17\%$, $n = 167$ in the discovery cohort) of breast cancers are devoid of somatic CNAs, and are ripe for mutational profiling. Our work provides a definitive framework for understanding how gene copy number aberrations affect gene expression in breast cancer and reveals novel subgroups that should be the target of future investigation.

METHODS SUMMARY

All patient specimens were obtained with appropriate consent from the relevant institutional review board. DNA and RNA were isolated from samples and hybridized to the Affymetrix SNP 6.0 and Illumina HT-12 v3 platforms for genomic and transcriptional profiling, respectively. A detailed description of the experimental assays and analytical methods used to analyse these data are available in the Supplementary Information.

Received 24 April 2011; accepted 22 February 2012.

Published online 18 April; corrected 20 June 2012 (see full-text HTML version for details).

1. Leary, R. J. *et al.* Integrated analysis of homozygous deletions, focal amplifications, and sequence alterations in breast and colorectal cancers. *Proc. Natl Acad. Sci. USA* **105,** 16224–16229 (2008).
2. Bignell, G. R. *et al.* Signatures of mutation and selection in the cancer genome. *Nature* **463,** 893–898 (2010).
3. Perou, C. M. *et al.* Molecular portraits of human breast tumours. *Nature* **406,** 747–752 (2000).
4. Sørlie, T. *et al.* Gene expression patterns of breast carcinomas distinguish tumor subclasses with clinical implications. *Proc. Natl Acad. Sci. USA* **98,** 10869–10874 (2001).
5. Chin, K. *et al.* Genomic and transcriptional aberrations linked to breast cancer pathophysiologies. *Cancer Cell* **10,** 529–541 (2006).
6. Chin, S. F. *et al.* High-resolution aCGH and expression profiling identifies a novel genomic subtype of ER negative breast cancer. *Genome Biol.* **8,** R215 (2007).
7. Parker, J. S. *et al.* Supervised risk predictor of breast cancer based on intrinsic subtypes. *J. Clin. Oncol.* **27,** 1160–1167 (2009).
8. Stranger, B. E. *et al.* Genome-wide associations of gene expression variation in humans. *PLoS Genet.* **1,** e78 (2005).
9. Gilad, Y., Rifkin, S. A. & Pritchard, J. K. Revealing the architecture of gene regulation: the promise of eQTL studies. *Trends Genet.* **24,** 408–415 (2008).
10. Teschendorff, A. E., Naderi, A., Barbosa-Morais, N. L. & Caldas, C. PACK: Profile analysis using clustering and kurtosis to find molecular classifiers in cancer. *Bioinformatics* **22,** 2269–2275 (2006).
11. Holland, D. *et al.* ZNF703 is a common Luminal B breast cancer oncogene that differentially regulates luminal and basal progenitors in human mammary epithelium. *EMBO Mol. Med.* **3,** 167–180 (2011).
12. Li, J. *et al.* PTEN, a putative protein tyrosine phosphatase gene mutated in human brain, breast, and prostate cancer. *Science* **275,** 1943–1947 (1997).
13. Santarius, T., Shiply, J., Brewer, D., Stratton, M. R. & Cooper, C. S. A census of amplified and overexpressed human cancer genes. *Nature Rev. Cancer* **10,** 59–64 (2010).
14. Jones, S. *et al.* Frequent mutations of chromatin remodeling gene ARID1A in ovarian clear cell carcinoma. *Science* **330,** 228–231 (2010).
15. McConechy, M. K. *et al.* Subtype-specific mutation of PPP2R1A in endometrial and ovarian carcinomas. *J. Pathol.* **223,** 567–573 (2011).
16. Tan, J. *et al.* B55β-associated PP2A complex controls PDK1-directed MYC signaling and modulates rapamycin sensitivity in colorectal cancer. *Cancer Cell* **18,** 459–471 (2010).
17. Christopher, S. A., Diegelman, P., Porter, C. W. & Kruger, W. D. Methylthioadenosine phosphorylase, a gene frequently codeleted with p16 (CDKN2A/ARF), acts as a tumor suppressor in a breast cancer cell line. *Cancer Res.* **62,** 6639–6644 (2002).
18. Teng, D. H. *et al.* Human mitogen-activated protein kinase kinase 4 as a candidate tumor suppressor. *Cancer Res.* **57,** 4177–4182 (1997).
19. Hollestelle, A. *et al.* Distinct gene mutation profiles among luminal-type and basal-type breast cancer cell lines. *Breast Cancer Res. Treat.* **121,** 53–64 (2010).

20. Shen, R., Olshen, A. B. & Ladanyi, M. Integrative clustering of multiple genomic data types using a joint latent variable model with application to breast and lung cancer subtype analysis. *Bioinformatics* **25,** 2906–2912 (2009).
21. Tibshirani, R., Hastie, T., Narasimhan, B. & Chu, G. Diagnosis of multiple cancer types by shrunken centroids of gene expression. *Proc. Natl Acad. Sci. USA* **99,** 6567–6572 (2002).
22. Kapp, A. V. & Tibshirani, R. Are clusters found in one dataset present in another dataset? *Biostatistics* **8,** 9–31 (2007).
23. Hughes-Davies, L. *et al.* EMSY links the BRCA2 pathway to sporadic breast and ovarian cancer. *Cell* **115,** 523–535 (2003).
24. Brown, L. A. *et al.* Amplification of 11q13 in ovarian carcinoma. *Genes Chromosom. Cancer* **47,** 481–489 (2008).
25. Russnes, H. G. *et al.* Genomic architecture characterizes tumor progression paths and fate in breast cancer patients. *Sci. Transl. Med.* **2,** 38ra47 (2010).
26. Blows, F. M. *et al.* Subtyping of breast cancer by immunohistochemistry to investigate a relationship between subtype and short and long term survival: a collaborative analysis of data for 10,159 cases from 12 studies. *PLoS Med.* **7,** e1000279 (2010).
27. Mahmoud, S. M. A. *et al.* Tumor-infiltrating $CD8^+$ lymphocytes predict clinical outcome in breast cancer. *J. Clin. Oncol.* **29,** 1949–1955 (2011).
28. Daniel, J., Coulter, J., Woo, J.-H., Wilsbach, K. & Gabrielson, E. High levels of the Mps1 checkpoint protein are protective of aneuploidy in breast cancer cells. *Proc. Natl Acad. Sci. USA* **108,** 5384–5389 (2011).
29. Chen, Y. *et al.* Variations in DNA elucidate molecular networks that cause disease. *Nature* **452,** 429–435 (2008).

Supplementary Information is linked to the online version of the paper at www.nature.com/nature.

Acknowledgements The METABRIC project was funded by Cancer Research UK, the British Columbia Cancer Foundation and Canadian Breast Cancer Foundation BC/Yukon. The authors also acknowledge the support of the University of Cambridge, Hutchinson Whampoa, the NIHR Cambridge Biomedical Research Centre, the Cambridge Experimental Cancer Medicine Centre, the Centre for Translational Genomics (CTAG) Vancouver and the BCCA Breast Cancer Outcomes Unit. S.P.S. is a Michael Smith Foundation for Health Research fellow. S.A. is supported by a Canada Research Chair. This work was supported by the National Institutes of Health Centers of Excellence in Genomics Science grant P50 HG02790 (S.T.). The authors thank C. Perou and J. Parker for discussions on the use of the PAM50 centroids. They also acknowledge the patients who donated tissue and the associated pseudo-anonymized clinical data for this project.

Author Contributions Ch.C. led the analysis, designed experiments and wrote the manuscript. S.P.S. led the HMM-based analyses, expression outlier and *TP53* analyses, and contributed to manuscript preparation. S.-F.C. generated data, designed and performed experiments. G.T. generated data, provided histopathology expertise and analysed *TP53* sequence data. O.M.R., M.J.D., D.S., A.G.L., S.S., Y.Y., S.G., Ga.H., Gh.H., A.B., R.R., S.M. and F.M. performed analyses. G.T., A.G., E.P., S.P. and I.E. provided histopathology expertise. A.L. performed *TP53* sequencing. A.-L.B.-D. oversaw *TP53* sequencing. S.P., P.W., L.M., G.W., I.E., A.P., Ca.C. and S.A. contributed to sample selection. J.D.B. and S.T. contributed to study design. S.T. provided statistical expertise. The METABRIC Group contributed collectively to this study. Ca.C. and S.A. co-conceived and oversaw the study, and contributed to manuscript preparation and were responsible for final editing. Ca.C. and S.A. are joint senior authors and project co-leaders.

Author Information The associated genotype and expression data have been deposited at the European Genome-Phenome Archive (http://www.ebi.ac.uk/ega/), which is hosted by the European Bioinformatics Institute, under accession number EGAS00000000083. Reprints and permissions information is available at www.nature.com/reprints. The authors declare no competing financial interests. Readers are welcome to comment on the online version of this article at www.nature.com/nature. Correspondence and requests for materials should be addressed to Ca.C. (carlos.caldas@cancer.org.uk) or S.A. (saparicio@bccrc.ca).

METABRIC Group

Co-chairs Carlos Caldas[1,2], Samuel Aparicio[3,4]

Writing committee Christina Curtis[1,2]†, Sohrab P. Shah[3,4], Carlos Caldas[1,2], Samuel Aparicio[3,4]

Steering committee James D. Brenton[1,2], Ian Ellis[5], David Huntsman[3,4], Sarah Pinder[6], Arnie Purushotham[6], Leigh Murphy[7], Carlos Caldas[1,2], Samuel Aparicio[3,4]

Tissue and clinical data source sites: University of Cambridge/Cancer Research UK Cambridge Research Institute Carlos Caldas (Principal Investigator)[1,2]; Helen Bardwell[2], Suet-Feung Chin[1,2], Christina Curtis[1,2]†, Zhihao Ding[2], Stefan Gräf[1,2], Linda Jones[8], Bin Liu[1,2], Andy G. Lynch[1,2], Irene Papatheodorou[1,2], Stephen J. Sammut[9], Gordon Wishart[9]; **British Columbia Cancer Agency** Samuel Aparicio (Principal Investigator)[3,4], Steven Chia[4], Karen Gelmon[4], David Huntsman[3,4], Steven McKinney[3,4], Caroline Speers[4], Gulisa Turashvili[3,4], Peter Watson[3,4,7]; **University of Nottingham:** Ian Ellis (Principal Investigator)[5], Roger Blamey[5], Andrew Green[5], Douglas Macmillan[5], Emad Rakha[5]; **King's College London** Arnie Purushotham (Principal Investigator)[6], Cheryl Gillett[6], Anita Grigoriadis[6], Sarah Pinder[6], Emanuele de Rinaldis[6], Andy Tutt[6]; **Manitoba Institute of Cell Biology** Leigh Murphy (Principal Investigator)[7], Michelle Parisien[7], Sandra Troup[7]

Cancer genome/transcriptome characterization centres: University of Cambridge/Cancer Research UK Cambridge Research Institute Carlos Caldas (Principal Investigator)[1,2], Suet-Feung Chin (Team Leader)[1,2], Derek Chan[1], Claire Fielding[2], Ana-Teresa Maia[1,2], Sarah McGuire[2], Michelle Osborne[2], Sara M. Sayalero[2], Inmaculada Spiteri[2], James Hadfield[2]; **British Columbia Cancer Agency** Samuel Aparicio (Principal Investigator)[3,4], Gulisa Turashvili (Team Leader)[3,4], Lynda Bell[4], Katie Chow[4], Nadia Gale[4], David Huntsman[3,4], Maria Kovalik[4], Ying Ng[4], Leah Prentice[4]

Data analysis subgroup: University of Cambridge/Cancer Research UK Cambridge Research Institute Carlos Caldas (Principal Investigator)[1,2], Simon Tavaré (Principal Investigator)[1,2,10,11], Christina Curtis (Team Leader)[1,2]†, Mark J. Dunning[2], Stefan Gräf[1,2], Andy G. Lynch[1,2], Oscar M. Rueda[1,2], Roslin Russell[2], Shamith Samarajiwa[1,2], Doug Speed[2,10]; Florian Markowetz (Principal Investigator)[1,2], Yinyin Yuan[1,2]; James D. Brenton (Principal Investigator)[1,2]; **British Columbia Cancer Agency** Samuel Aparicio (Principal Investigator)[3,4], Sohrab P. Shah (Team Leader)[3,4], Ali Bashashati[3], Gavin Ha[3], Gholamreza Haffari[3] & Steven McKinney[3,4]

[1]Department of Oncology, University of Cambridge, Hills Road, Cambridge CB2 2XZ, UK. [2]Cancer Research UK, Cambridge Research Institute, Li Ka Shing Centre, Robinson Way, Cambridge CB2 0RE, UK. [3]Department of Pathology and Laboratory Medicine, University of British Columbia, Vancouver, British Columbia V6T 2B5, Canada. [4]Molecular Oncology, British Columbia Cancer Research Centre, Vancouver, British Columbia V5Z 1L3, Canada. [5]Department of Histopathology, School of Molecular Medical Sciences, University of Nottingham, Nottingham NG5 1PB, UK. [6]King's College London, Breakthrough Breast Cancer Research Unit, London, WC2R 2LS, UK. [7]Manitoba Institute of Cell Biology, University of Manitoba, Manitoba R3E 0V9, Canada. [8]Cambridge Experimental Cancer Medicine Centre, Cambridge CB2 0RE, UK. [9]Cambridge Breast Unit, Addenbrooke's Hospital, Cambridge University Hospital NHS Foundation Trust and NIHR Cambridge Biomedical Research Centre, Cambridge CB2 2QQ, UK. [10]Department of Applied Mathematics and Theoretical Physics, University of Cambridge, Centre for Mathematical Sciences, Cambridge CB3 0WA, UK. [11]Molecular and Computational Biology Program, University of Southern California, Los Angeles, California 90089, USA. †Present address: Department of Preventive Medicine, Keck School of Medicine, University of Southern California, Los Angeles, California 90033, USA.

doi:10.1038/nature11143

Whole-genome analysis informs breast cancer response to aromatase inhibition

Matthew J. Ellis[1,2,3]*, Li Ding[4,5]*, Dong Shen[4,5]*, Jingqin Luo[3,6], Vera J. Suman[7], John W. Wallis[4,5], Brian A. Van Tine[1], Jeremy Hoog[1], Reece J. Goiffon[8,9,10], Theodore C. Goldstein[11], Sam Ng[11], Li Lin[1], Robert Crowder[1], Jacqueline Snider[1], Karla Ballman[7], Jason Weber[1,8,12], Ken Chen[13], Daniel C. Koboldt[4,5], Cyriac Kandoth[4,5], William S. Schierding[4,5], Joshua F. McMichael[4,5], Christopher A. Miller[4,5], Charles Lu[4,5], Christopher C. Harris[4,5], Michael D. McLellan[4,5], Michael C. Wendl[4,5], Katherine DeSchryver[1], D. Craig Allred[3,14], Laura Esserman[15], Gary Unzeitig[16], Julie Margenthaler[2], G. V. Babiera[13], P. Kelly Marcom[17], J. M. Guenther[18], Marilyn Leitch[19], Kelly Hunt[13], John Olson[17], Yu Tao[6], Christopher A. Maher[1,4], Lucinda L. Fulton[4,5], Robert S. Fulton[4,5], Michelle Harrison[4,5], Ben Oberkfell[4,5], Feiyu Du[4,5], Ryan Demeter[4,5], Tammi L. Vickery[4,5], Adnan Elhammali[8,9,10], Helen Piwnica-Worms[8,12,20,21], Sandra McDonald[2,22], Mark Watson[6,14,22], David J. Dooling[4,5], David Ota[23], Li-Wei Chang[3,14], Ron Bose[2,3], Timothy J. Ley[1,2,4], David Piwnica-Worms[8,9,10,12,24], Joshua M. Stuart[11], Richard K. Wilson[2,4,5] & Elaine R. Mardis[2,4,5]

To correlate the variable clinical features of oestrogen-receptor-positive breast cancer with somatic alterations, we studied pretreatment tumour biopsies accrued from patients in two studies of neoadjuvant aromatase inhibitor therapy by massively parallel sequencing and analysis. Eighteen significantly mutated genes were identified, including five genes (*RUNX1*, *CBFB*, *MYH9*, *MLL3* and *SF3B1*) previously linked to haematopoietic disorders. Mutant MAP3K1 was associated with luminal A status, low-grade histology and low proliferation rates, whereas mutant TP53 was associated with the opposite pattern. Moreover, mutant *GATA3* correlated with suppression of proliferation upon aromatase inhibitor treatment. Pathway analysis demonstrated that mutations in *MAP2K4*, a MAP3K1 substrate, produced similar perturbations as MAP3K1 loss. Distinct phenotypes in oestrogen-receptor-positive breast cancer are associated with specific patterns of somatic mutations that map into cellular pathways linked to tumour biology, but most recurrent mutations are relatively infrequent. Prospective clinical trials based on these findings will require comprehensive genome sequencing.

Oestrogen-receptor-positive breast cancer exhibits highly variable prognosis, histological growth patterns and treatment outcomes. Neoadjuvant aromatase inhibitor treatment trials provide an opportunity to document oestrogen-receptor-positive breast cancer phenotypes in a setting where sample acquisition is easy, prospective consent for genomic analysis can be obtained and responsiveness to oestrogen deprivation therapy is documented[1]. We therefore conducted massively parallel sequencing (MPS) on 77 samples accrued from two neoadjuvant aromatase inhibitor clinical trials[2,3]. Forty-six cases underwent whole-genome sequencing (WGS) and 31 cases underwent exome sequencing, followed by extensive analysis for somatic alterations and their association with aromatase inhibitor response. Case selection for discovery was based on the levels of the tumour proliferation marker Ki67 in the surgical specimen, because high cellular proliferation despite aromatase inhibitor treatment identifies poor prognosis tumours exhibiting oestrogen-independent growth[4] (Supplementary Fig. 1). Twenty-nine samples had Ki67 levels above 10% ('aromatase-inhibitor-resistant tumours', median Ki67 21%, range 10.3–80%) and 48 were at or below 10% ('aromatase-inhibitor-sensitive tumours', median Ki67 1.2%, range 0–8%). Cases were also classified as luminal A or B by gene expression profiling[3]. We subsequently examined interactions between Ki67 biomarker change, histological categories, intrinsic subtype and mutation status in selected recurrently mutated genes in 310 cases overall. Pathway analysis was applied to contrast the signalling perturbations in aromatase-inhibitor-sensitive versus aromatase-inhibitor-resistant tumours.

Results

The mutation landscape of luminal-type breast cancer

Using paired-end MPS, 46 tumour and normal genomes were sequenced to at least 30-fold and 25-fold haploid coverage, respectively, with diploid coverage of at least 95% based on concordance with SNP array data (Supplementary Table 1). Candidate somatic events were identified using multiple algorithms[5,6], and were then verified by hybridization capture-based validation that targeted all putative somatic single-nucleotide variants (SNVs) and small insertions/deletions (indels) that

---

[1]Department of Internal Medicine, Division of Oncology, Washington University, St Louis, Missouri, USA. [2]Siteman Cancer Center, Washington University, St Louis, Missouri 63110, USA. [3]Breast Cancer Program, Washington University, St Louis, Missouri 63110, USA. [4]The Genome Institute, Washington University, St Louis, Missouri 63108, USA. [5]Department of Genetics, Washington University, St Louis, Missouri 63108, USA. [6]Division of Biostatistics, Washington University, St Louis, Missouri 63110, USA. [7]ACOSOG Statistical Center, Mayo Clinic, Rochester, Minnesota 55905, USA. [8]BRIGHT Institute, Washington University School of Medicine, St Louis, Missouri 63110, USA. [9]Molecular Imaging Center, Washington University, St Louis, Missouri 63110, USA. [10]Malinckrodt Institute of Radiology, Washington University, St Louis, Missouri 63110, USA. [11]Department of Biomolecular Engineering, University of California, Santa Cruz, California 95064, USA. [12]Department of Cell Biology and Physiology, Washington University, St Louis, Missouri 63110, USA. [13]M. D. Anderson Cancer Center, Houston, Texas 77030, USA. [14]Department of Pathology and Immunology, Washington University, St Louis, Missouri 63110, USA. [15]Helen Diller Cancer Center, University of California, San Francisco, California 94143, USA. [16]Doctors Hospital of Laredo, Laredo, Texas 78045, USA. [17]Duke University Cancer Center, Durham, North Carolina 27705, USA. [18]Good Samaritan Hospital, Cincinnati, Ohio 45406, USA. [19]Simmons Cancer Center, University of Texas Southwestern, Dallas, Texas 75390, USA. [20]Department of Internal Medicine, Washington University, St Louis, Missouri 63110, USA. [21]Howard Hughes Medical Institute, Chevy Chase, Maryland 20815, USA. [22]ACOSOG Central Specimen Bank, Washington University, St Louis, Missouri 63110, USA. [23]ACOSOG Operations Center, Duke University, Durham, North Carolina 27705, USA. [24]Department of Developmental Biology, Washington University, St Louis, Missouri 63110, USA.

*These authors contributed equally to this work.

overlap coding exons, splice sites and RNA genes (tier 1), high-confidence SNVs and indels in non-coding conserved or regulatory regions (tier 2), as well as non-repetitive regions of the human genome (tier 3). In addition, somatic structural variants and germline structural variants that potentially affect coding sequences (Supplementary Information) were assessed. Digital sequencing data from captured target DNAs from the 46 tumour and normal pairs (Supplementary Table 2 and Supplementary Information) confirmed 81,858 mutations (point mutations and indels) and 773 somatic structural variants. The average numbers of somatic mutations and structural variants were 1,780 (range 44–11,619) and 16.8 (range 0–178) per case, respectively (Supplementary Table 3). Tier 1 point mutations and small indels predicted for all 46 cases also were validated using both 454 and Illumina sequencing (Supplementary Information). BRC25 was a clear outlier with only 44 validated tiers 1–3 mutations, all at low allele frequencies (ranging from 5% to 26.8%). This sample probably had low tumour content despite histopathology assessment, but the data are included to avoid bias.

The overall mutation rate was 1.18 validated mutations per megabase (Mb) (tier 1: 1.05; tier 2: 1.14; tier 3: 1.20). The mutation rate for tier 1 was higher than that observed for acute myeloid leukaemia (0.18–0.23)[6,7], but lower than that reported for hepatocellular carcinoma (1.85)[8], malignant melanoma (6.65)[9] and lung cancers (3.05–8.93)[10,11] (Supplementary Table 4). The background mutation rate (BMR) across the 21 aromatase-inhibitor-resistant tumours was 1.62 per Mb, nearly twice that of the 25 aromatase-inhibitor-sensitive tumours at 0.824 per Mb ($P = 0.02$, one-sided t-test). A trend for more somatic structural variations in the aromatase-inhibitor-resistant group was also observed, as the validated somatic structural variation frequency in the 21 aromatase-inhibitor-resistant tumour genomes was 21.69 versus an average of 12.76 in 25 aromatase-inhibitor-sensitive tumours ($P = 0.16$, one-sided t-test) (Fig. 1). If ten *TP53* mutated cases were excluded, the background mutation rate still tended to be higher in the aromatase-inhibitor-resistant group ($P = 0.08$). To demonstrate that a single-tumour core biopsy produced representative genomic data, whole-genome sequencing of two pre-treatment biopsies was conducted for 5 of the 46 cases. The frequency of mutations in the paired specimens showed high concordance in all cases (correlation coefficiency ranged from 0.74 to 0.95) (Supplementary Fig. 2) and a somatic mutation was infrequently detected in only one of the two samples (4.65% overall).

Significantly mutated genes in luminal breast cancer

The discovery effort was extended by studying 31 additional cases by exome sequencing, producing an additional 1,371 tier 1 mutations. In total the 77 cases yielded 3,355 tier 1 somatic mutations, including 3,208 point mutations, 1 dinucleotide mutation and 146 indels, ranging from 1 to 28 nucleotides. The point mutations included 733 silent, 2,145 missense, 178 nonsense, 6 read-through, 69 splice-site mutations and 77 in RNA genes (Supplementary Table 5). Of 2,145 missense mutations, 1,551 were predicted to be deleterious by SIFT[12] and/or PolyPhen[13]. The MuSiC package[45] was applied to determine the significance of the difference between observed versus expected mutation events in each gene, on the basis of the background mutation rate. This identified 18 significantly mutated genes with a convolution false discovery rate (FDR) < 0.26 (Table 1 and Supplementary Table 6). The list contains genes previously identified as mutated in breast cancer (*PIK3CA*[14], *TP53*[15], *GATA3*[12], *CDH1*[13], *RB1*[16], *MLL3*[17], *MAP3K1*[18] and *CDKN1B*[19]) as well as genes not previously observed in clinical breast cancer samples, including *TBX3*, *RUNX1*, *LDLRAP1*, *STNM2*, *MYH9*, *AGTR2*, *STMN2*, *SF3B1* and *CBFB*.

Thirteen mutations (3 nonsense, 6 frame-shift indels, 2 in-frame deletions and 2 missense) were identified in *MAP3K1* (Table 1 and Fig. 2), a serine/threonine kinase that activates the ERK and JNK kinase pathways through phosphorylation of *MAP2K1* and *MAP2K4* (ref. 20). Of interest, a missense (S184L) and a splice-region mutation (e2+3 probably affecting splicing) in *MAP2K4* were observed in two tumours with no *MAP3K1* mutation (Fig. 2). Single nonsynonymous mutations in *MAP3K12*, *MAP3K4*, *MAP4K3*, *MAP4K4*, *MAPK15* and *MAPK3* were also detected (Supplementary Table 5). *TBX3* harboured three small indels (one insertion and two deletions). *TBX3* affects expansion of breast cancer stem-like cells through regulation of FGFR[21]. Two truncating mutations in the tumour suppressor *CDKN1B* were

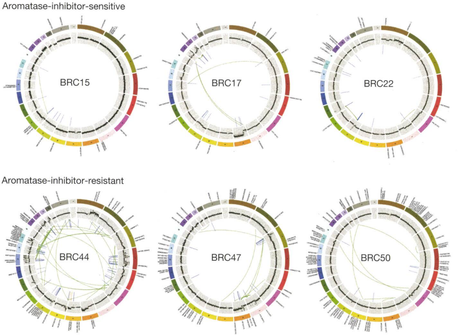

Figure 1 | Genome-wide somatic mutations. Circos plots[44] indicate validated somatic mutations comprising tier 1 point mutations and indels, genome-wide copy number alterations, and structural rearrangements in six representative genomes. Three on-treatment Ki67 less than or at 10% (top panel: BRC15, BRC17 and BRC22) and three on-treatment Ki67 greater than 10% (bottom panel: BRC44, BRC47 and BRC50) cases are shown. Significantly mutated genes are highlighted in red. No purity-based copy number corrections were used for plotting copy number.

Table 1 | Significantly mutated genes identified in 46 whole genomes and 31 exomes sequenced in luminal breast cancer patients

Gene	Total	MS	NS	Indel	SS	**P value**	FDR
MAP3K1	13	2	3	8	0	0	0
PIK3CA	45	44	0	1	0	0	0
TP53	18	13	1	1	1	0	0
GATA3	8	1	0	4	3	1.15×10^{-19}	7.41×10^{-16}
CDH1	8	1	1	5	1	3.07×10^{-15}	1.59×10^{-11}
TBX3	3	0	0	3	0	2.58×10^{-6}	0.011
ATR	6	6	0	0	0	3.73×10^{-6}	0.014
RUNX1	4	4	0	0	0	6.59×10^{-6}	0.021
ENSG00000212670*	2	2	0	0	0	2.31×10^{-5}	0.066
RB1	4	2	1	0	1	2.76×10^{-5}	0.071
LDLRAP1	2	1	1	0	0	4.27×10^{-5}	0.092
STMN2	2	1	0	1	0	4.15×10^{-5}	0.092
MYH9	4	1	1	2	0	8.96×10^{-5}	0.178
MLL3	5	1	1	3	0	1.04×10^{-4}	0.191
CDKN1B	2	0	1	1	0	1.39×10^{-4}	0.240
AGTR2	2	2	0	0	0	1.71×10^{-4}	0.256
SF3B1	3	3	0	0	0	1.79×10^{-4}	0.256
CBFB	2	1	1	0	0	1.70×10^{-4}	0.256

* ENSG00000212670 is not in RefSeq release 50.
MS, Missense; NS, nonsense; SS, splice site.

identified[19]. Four missense *RUNX1* mutations were observed, with three in the RUNT domain clustered within the 8 amino acid putative ATP-binding site (R166Q, G168E and R169K). *RUNX1* is a transcription factor affected by mutation and translocation in the M2 subtype of acute myeloid leukaemia[22] and is implicated in tethering the oestrogen receptor to promoters independently of oestrogen response elements[23]. Two mutations (N104S and N140*) were also identified in *CBFB*, the binding partner of *RUNX1*. Additional mutations included 3 missense (2 K700E and 1 K666Q), in *SF3B1*, a splicing factor implicated in myelodysplasia[24] and chronic lymphocytic leukaemia[25]. One missense mutation, one nonsense mutation and two indels were found in the *MYH9* gene, involved in hereditary macrothrombocytopenia[26] as well as being observed in an ALK translocation in anaplastic large cell lymphoma[27].

We also identified three significantly mutated genes (*LDLRAP1*, *AGTR2* and *STMN2*) not previously implicated in cancer. A missense and a nonsense mutation were observed in *LDLRAP1*, a gene associated with familial hypercholesterolaemia[28]. *AGTR2*, angiotensin II receptor type 2, harboured two missense mutations (V184I and R251H). Angiotensin signalling and oestrogen receptor intersect in models of tissue fibrosis[29]. *STMN2*, a gene activated by JNK family kinases[30,31] and therefore regulated by *MAP3K1* and *MAP2K4*, harboured one frameshift deletion and one missense mutation. Three deletions and one point mutation (Supplementary Fig. 3) were identified in a large, infrequently spliced non-coding (lnc) RNA gene, *MALAT1* (metastasis associated lung adenocarcinoma transcript 1), that regulates alternative splicing by modulating the phosphorylation of SR splicing factor[32]. Translocations and point mutations of *MALAT1* have been reported in sarcoma[33] and colorectal cancer cell lines[34]. Five additional MALAT1 mutations were found in the recurrent screening set (Supplementary Table 5d). The locations of these mutations clustered in a region of species homology (F1 and 2 domains) that could mediate interactions with SRSF1 (ref. 32, Supplementary Fig. 4). Non-coding mutation clusters were found in *ATR*, *GPR126* and *NRG3* (Supplementary Information and Supplementary Table 7).

Correlating mutations with clinical data

To study clinical correlations, mutation recurrence screening was conducted on an additional 240 cases (Supplementary Table 8 and Supplementary Fig. 1). By combining WGS, exome and recurrence screening data, we determined the mutation frequency in *PIK3CA* to be 41.3% (131 of 317 tumours) (Supplementary Table 5a–d and Supplementary Fig. 3). *TP53* was mutated in 51 of 317 tumours (16.1%) (Supplementary Table 5a–d and Supplementary Fig. 3). Additionally, 52 nonsynonymous *MAP3K1* mutations in 39 tumours and 10 mutations in its substrate *MAP2K4* were observed, representing a combined case frequency of 15.5% (Supplementary Table 5a–d and Fig. 3). Of note, 52 of the 62 non-silent mutations in *MAP3K1* and *MAP2K4* were scattered indels or other protein-truncating events strongly suggesting functional inactivation. In addition, 13 tumours harboured two non-silent *MAP3K1* mutations, indicative of bi-allelic loss and reinforcing the conclusion that this gene is a tumour suppressor. Twenty nine tumours harboured a total of 30 mutations in *GATA3*, consisting of 25 truncation events, one in-frame insertion, and 4 missense mutations including 3 recurrent mutations at M294K (Supplementary Table 5a–d and Supplementary Fig. 3). BRC8 harboured a chromosome 10 deletion that includes *GATA3*. *CDH1* mutation data were available for 169 samples and, as expected, its mutation status was strongly associated with lobular breast cancer[13] (Table 2a). We applied a permutation-based approach in MuSiC[45] to ascertain relationships between mutated genes. Negative correlations were found between mutations in gene pairs such as *GATA3* and *PIK3CA* ($P = 0.0026$), *CDH1* and *GATA3* ($P = 0.015$), and *CDH1* and *TP53* ($P = 0.022$). *MAP3K1* and *MAP2K4* mutations were mutually exclusive, albeit without reaching statistical significance ($P = 0.3$). In contrast, a positive correlation between *MAP3K1*/*MAP2K4* and *PIK3CA* mutations was highly significant ($P = 0.0002$) (Supplementary Table 9).

Two independent mutation data sets, designated 'Set 1' (discovery cohort) and 'Set 2' (validation cohort), from these clinical trial samples were analysed separately and then in combination, with a false discovery rate (FDR)-corrected *P* value to gauge the overall strength and

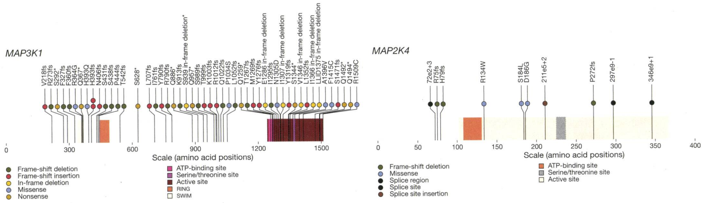
MAP3K1
V218fs
R273fs
S292*
F327fs
F360fs
R364G
Q367*
H393Q
H393fs
N406fs
S431fs
S438fs
P444fs
T542fs
S628*
L707fs
I761fs
Y790fs
R790fs
Q886*
K913fs
S939 in-frame deletion*
Q957*
S989fs
T999fs
K1003fs
R1012fs
Q1022fs
P1034S
L1052fs
Q1259*
T1267fs
M1269fs
Y1276fs
E1286 in-frame deletion
I1295fs
N1305D
I1307 in-frame deletion
Y1319fs
S1344*
V1346 in-frame deletion
L1352fs
I1366 in-frame deletion
LLID1375 in-frame deletion
A1396V
F1415C
S1471fs
Q1492*
Q1494*
R1509C
0
300
600
900
1200
1500
Scale (amino acid positions)
● Frame-shift deletion
● Frame-shift insertion
● In-frame deletion
● Missense
● Nonsense
■ ATP-binding site
■ Serine/threonine site
■ Active site
■ RING
☐ SWIM
MAP2K4
72e2+3
R75fs
H79fs
R134W
S184L
D186G
211e5+2
P272fs
297e9-1
346e9+1
0
50
100
150
200
250
300
350
400
Scale (amino acid positions)
● Frame-shift deletion
● Missense
● Splice region
● Splice site
● Splice site insertion
■ ATP-binding site
■ Serine/threonine site
☐ Active site

Figure 2 | *MAP3K1* and *MAP2K4* mutations observed in 317 samples. Somatic status of all mutations was obtained by Sanger sequencing of PCR products or Illumina sequencing of targeted capture products. The locations of conserved protein domains are highlighted. Each nonsynonymous substitution, splice site mutation or indel is designated with a circle at the representative protein position with colour to indicate translation effects of the mutation. Asterisk, nonsense mutations that cause truncation of the open reading frame.

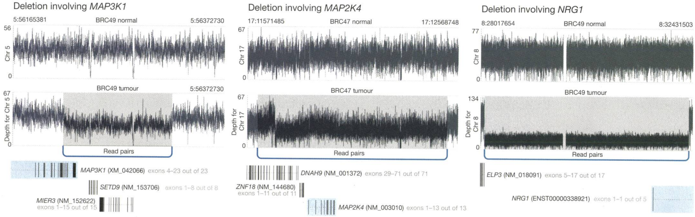

Figure 3 | Structural variants in significantly mutated or frequently deleted genes. One *MAP3K1* deletion in BRC49 and one *MAP2K4* deletion in BRC47, and one *ELP3-NRG1* fusion in BRC49 identified using Illumina paired-end reads from whole-genome sequence data. Arcs represent multiple breakpoint-spanning read pairs with sequence coverage depth plotted in black across the region. Chr, chromosome.

consistency of genotype–phenotype relationships (Table 2a, b and Supplementary Fig. 1). *TP53* mutations in both data sets correlated with significantly higher Ki67 levels, both at baseline ($P = 0.0003$) and at surgery ($P = 0.001$). Furthermore, *TP53* mutations were significantly enriched in luminal B tumours ($P = 0.04$) and in higher histological grade tumours ($P = 0.02$). In contrast, *MAP3K1* mutations were more frequent in luminal A tumours ($P = 0.02$), in grade 1 tumours ($P = 0.005$) and in tumours with lower Ki67 at baseline ($P = 0.001$) with consistent findings across both data sets. *GATA3* mutation did not influence baseline Ki67 levels but was enriched in samples exhibiting greater percentage Ki67 decline ($P = 0.01$). This finding requires further verification because it was significant in Set 1 (uncorrected P value 0.003) but was a marginal finding in Set 2 ($P = 0.08$). However, it suggests *GATA3* mutation may be a positive predictive marker for aromatase inhibitor response.

Structural variation and DNA repair mechanisms

Analysis of copy number alterations (CNAs) revealed arm-level gains for 1q, 5p, 8q, 16p, 17q, 20p and 20q and arm-level losses for 1p, 8p, 16q, and 17p in the 46 WGS tumour genomes (Supplementary Fig. 5). A total of 773 structural variants (579 deletions, 189 translocations and 5 inversions) identified by WGS were validated as somatic in 46 breast cancer genomes by capture validation. No recurrent translocations were detected but six in-frame fusion genes were validated by reverse transcription followed by PCR (Supplementary Information and Supplementary Tables 10–13). Seven tumours had multiple complex translocations with breakpoints suggestive of a catastrophic mitotic event ('chromothripsis'; Supplementary Table 11). Analysis of the structural variant genomic breakpoints shows the spectra of putative chromothripsis-related events are the same as seen for other somatic events, with the majority of structural variants arising from non-homologous end-joining. We classified somatic (mitotic) and germline (meiotic) structural variants into four groups: variable number tandem repeat (VNTR), non-allelic homologous recombination (NAHR), microhomology-mediated end joining (MMEJ), and non-homologous end joining (NHEJ), according to criteria described in Supplementary Information. The fraction of each classification is shown for germline and somatic (mitotic) events (Supplementary Table 14). There were significantly more somatic NHEJ events in tumour genomes than the other three types ($P < 2.2 \times 10^{-16}$).

Pathways relevant to aromatase inhibitor response

Pathscan[35] analysis (Supplementary Table 15 and Supplementary Information) indicated that somatic mutations detected in the 77 discovery cases affect a number of pathways, including caspase cascade/apoptosis, ErbB signalling, Akt/PI3K/mTOR signalling, TP53/RB signalling and MAPK/JNK pathways (Fig. 4a). To discern the pathways relevant to aromatase inhibitor sensitivity, we conducted separate pathway analyses for aromatase-inhibitor-sensitive versus aromatase-inhibitor-resistant tumours. Whereas the majority of top altered pathways (FDR ≤ 0.15) in each group are shared, several pathways were enriched in the aromatase-inhibitor-resistant group, including the TP53 signalling pathway, DNA replication, and mismatch repair. Specifically, 38% of the aromatase-inhibitor-resistant group (11 of 29 tumours) have mutations in the TP53 pathway with three having double or triple hits involving *TP53*, *ATR*, *APAF1* or *THBS1*. In contrast, only 16.6% (8 of 48 tumours) of the Ki67 low group had mutations in the TP53 signalling pathway, each with only a single hit in genes *TP53*, *ATR*, *CCNE2* or *IGF1*. (Supplementary Table 16).

GeneGo pathway analysis of MetaCore interacting network objects was used to identify genes in the 77 luminal breast cancers with low-frequency mutations that cluster into pathway maps. Eight networks assembled from significant maps encompassed mutations from 71 (92%) of the tumours (Fig. 4b). Many of the network objects shared pathways with significantly mutated genes such as *TP53*, *MAP3K1*, *PIK3CA* and *CDH1*. GeneGo analysis also revealed that several genes with low-frequency mutations were actually subunits of complexes, resulting in higher mutation rates for that object, for example, the condensin complex (4 mutations in 4 genes) and the MRN complex (4 mutations in 3 genes). Several pathways without multiple significantly mutated genes, such as the apoptotic cascade, calcium/phospholipase signalling and G-protein-coupled receptors, were significantly affected by low-frequency mutations. Grouping tumours by significantly mutated genes and pathway mutation status showed that whereas 55 (71%) of the tumours contained significantly mutated genes in significant pathways, an additional 16 (21%) contained only non-significantly mutated genes in these pathways. Thus, tumours without a given significantly mutated gene often had other mutations in the same relevant pathway (Fig. 4b, Supplementary Fig. 6, Supplementary Table 17 and Supplementary Information).

We also applied PARADIGM[36] to infer pathway-informed gene activities using gene expression and copy-number data to identify several 'hubs' of activity (Supplementary Fig. 7, Supplementary Fig. 8 and Supplementary Information). As expected, *ESR1* and *FOXA1* were among the hubs activated cohort-wide while other hubs exhibited high but differential changes in aromatase-inhibitor-resistant tumours including *MYC*, *FOXM1* and *MYB* (Supplementary Fig. 8). The concordance among the 104 MetaCore maps from GeneGo analysis described above is significant, with 75 (72%) matching one of the

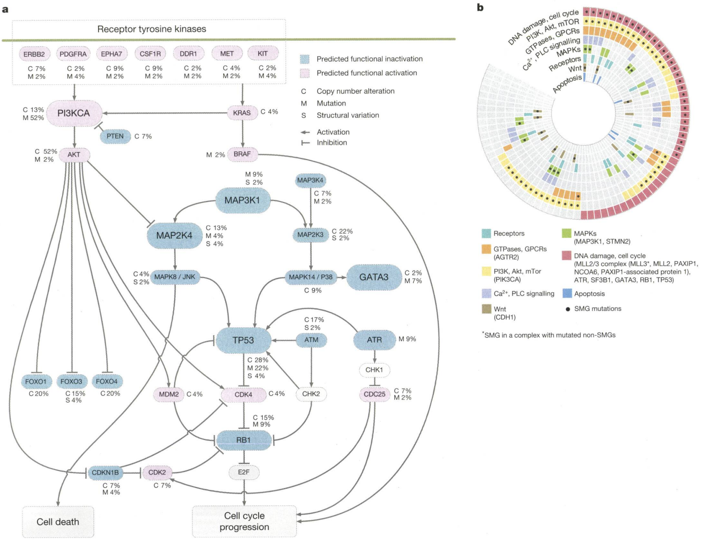
a
Receptor tyrosine kinases
ERBB2
C 7%
M 2%
PDGFRA
C 2%
M 4%
EPHA7
C 9%
M 2%
CSF1R
C 9%
M 2%
DDR1
C 2%
M 2%
MET
C 4%
M 2%
KIT
C 2%
M 4%
🟦 Predicted functional inactivation
🟪 Predicted functional activation
C Copy number alteration
M Mutation
S Structural variation
Activation
Inhibition
C 13%
M 52%
PI3KCA
KRAS
C 4%
PTEN
C 7%
C 52%
M 2%
AKT
M 2%
BRAF
M 9%
S 2%
MAP3K1
MAP3K4
C 7%
M 2%
MAP2K4
C 13%
M 4%
S 4%
MAP2K3
C 22%
S 2%
C 4%
S 2%
MAPK8 / JNK
MAPK14 / P38
C 9%
GATA3
C 2%
M 7%
C 17%
S 2%
TP53
ATM
ATR
M 9%
C 28%
M 22%
S 4%
CHK1
FOXO1
C 20%
FOXO3
C 15%
S 4%
FOXO4
C 20%
MDM2
C 4%
CDK4
C 4%
CHK2
CDC25
C 7%
M 2%
C 15%
M 9%
RB1
E2F
CDKN1B
C 7%
M 4%
CDK2
C 7%
Cell death
Cell cycle progression
b
DNA damage, cell cycle
PI3K, Akt, mTOR
GTPases, GPCRs
Ca²⁺, PLC signalling
MAPKs
Receptors
Wnt
Apoptosis
Receptors
GTPases, GPCRs (AGTR2)
PI3K, Akt, mTor (PIK3CA)
Ca²⁺, PLC signalling
Wnt (CDH1)
MAPKs (MAP3K1, STMN2)
DNA damage, cell cycle (MLL2/3 complex (MLL3*, MLL2, PAXIP1, NCOA6, PAXIP1-associated protein 1), ATR, SF3B1, GATA3, RB1, TP53)
Apoptosis
● SMG mutations
*SMG in a complex with mutated non-SMGs

Figure 4 | Key cancer pathway components altered in luminal breast tumours. **a**, Only genetic alterations identified in 46 WGS cases are shown. Alterations were discovered in key genes in the *TP53/RB*, *MAPK*, *PI3K/AKT/mTOR* pathways. Genes coloured blue and red are predicted to be functionally inactivated and activated, respectively, through focused mutations including point mutations and small indels (M), copy number deletions (C), or other structural changes (S) that affect the gene. The inter-connectedness of this network (several pathways) shows that there are many different ways to perturb a pathway. **b**, Eight interaction networks from canonical maps are significantly over-represented by mutations in 77 luminal breast tumours (46 WGS and 31 exome cases). In the concentric circle diagram, tumours are arranged as radial spokes and categorized by their mutation status in each network (concentric ring colour) and significantly mutated gene mutation status (black dots). Tumour classification by pathway analysis shows many tumours unaffected by a given significantly mutated gene often harbour other mutations in the same network. For full annotation, see Supplementary Information and Supplementary Fig. 6. PLC, phospholipase C; SMG, significantly mutated gene.

PARADIGM subnetworks at the 0.05 significance level after multiple test correction ($P < 4.4 \times 10^{-6}$; Bonferroni-adjusted hypergeometric test) (Supplementary Fig. 9). We identified significant subnetworks associated with Ki67 biomarker status (Supplementary Fig. 10 and Supplementary Information) involving transcription factors controlling large regulons.

The PARADIGM-inferred pathway signatures were further used to derive a map of the genetic mechanisms that may underlie treatment response. A subnetwork was constructed in which interactions were retained only if they connected two features with higher than average absolute association with Ki67 biomarker status (Supplementary Figs 10 and 11 and Supplementary Information). Consistent with the PathScan results, among the largest of the hubs in the identified network were a central DNA damage hub with the second highest connectivity (55 regulatory interactions; 1% of the network) and *TP53* with the 14th highest connectivity (26 connections; 0.5% of the network). Additional highly connected hubs identified in order of connectivity were *MYC* with 79 connections (1.4%), *FYN* with 45 (0.8%), *MAPK3* with 43, *JUN* with 40, *HDAC1* with 40, *SHC1* with 39, and *HIF1A/ARNT* complex with 39 (Supplementary Fig. 11).

To identify higher-level connections between mutations and clinical features, we compared the samples on the basis of pathway-derived signatures. For each clinical attribute and each significantly mutated gene, we dichotomized the discovery samples into a positive and a negative group to derive pathway signatures that discriminated between the groups (see details in Supplementary Information). We then computed all pair-wise Pearson correlations between pathway signatures and clustered the resulting correlations (Fig. 5). The entire process was repeated using validated mutations and signatures derived from the validation set (Supplementary Fig. 12). In line with expectation, *PIK3CA*, *MAP3K1*, *MAP2K4*, and low risk preoperative endocrine prognostic index (PEPI) scores (PEPI is an index of recurrence risk post neoadjuvant aromatase inhibitor therapy[4]) cluster with the luminal A subtypes and with each other, and are supported by the validation set analysis. The luminal B-like signatures included *TP53*, *RB1*, *RUNX1* and *MALAT1*, which also associated

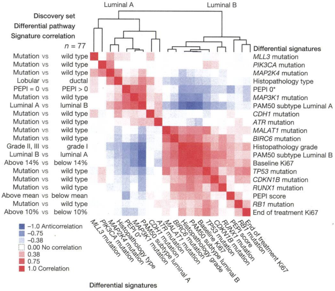

Figure 5 | Pathway signatures reveal connections between mutations and clinical outcomes. PARADIGM-based pathway signatures were derived for tumour feature dichotomies including mutation driven gene signatures (mutant versus non-mutant), histopathology type (lobular versus ductal), preoperative endocrine prognostic index (PEPI) score (PEPI = 0 favourable versus PEPI >0 unfavourable), PAM50 (50-gene intrinsic breast cancer subtype classifier) luminal A subtype (luminal A versus luminal B) and the reverse (luminal B versus luminal A), histopathology grade (grades II and III versus I), baseline Ki67 levels ($\geq 14\%$ versus $< 14\%$), and end-of-treatment Ki67 levels ($\geq 10\%$ versus $< 10\%$) and overall PEPI score (higher than mean unfavourable versus lower than mean favourable). Pearson correlations were computed between all pair-wise signatures; positive correlations, red; negative correlations, blue; column features ordered identically as rows. Correlation analysis on the 77 samples in the discovery set is shown. Asterisk: Ki67 < 2.7%, oestrogen-receptor-positive, node negative and tumour size $\leq$ 5 cm.

with other poor outcome features such as high baseline and surgical Ki67 levels, high grade histology and high PEPI scores. The *TP53* and *MALAT1* associations in the discovery set also were supported by the validation set analysis.

Druggable gene analysis

We defined mutations in druggable tyrosine kinase domains including in *ERBB2* (a V777L and a 755–759$^{\mathrm{LRENT}}$ in-frame deletion homologous to gefitinib-sensitizing *EGFR* mutations in lung cancer[37]), as well as in *DDR1* (A829V, R611C), *DDR2* (E583D), *CSF1R* (D735H, M875L), and *PDGFRA* (E924K). In addition, pleckstrin homology domain mutations were observed in *AKT1* (C77F) and *AKT2* (S11F) and a kinase domain mutation was identified in *RPS6KB1* (S375F) (Supplementary Table 18).

Discussion

The low frequency of many significantly mutated genes presents an enormous challenge for correlative analysis, but several statistically significant patterns were identified, including the relationship between *MAP3K1* mutation, luminal A subtype, low tumour grade and low Ki67 proliferation index. On this basis, for patients with *MAP3K1* mutant luminal tumours, neoadjuvant aromatase inhibitor could provide a favourable option. In contrast, tumours with *TP53* mutations, which are mostly aromatase inhibitor resistant, would be more appropriately treated with other modalities. MAP3K1 activates the ERK family, thus, loss of ERK signalling could explain the indolent nature of MAP3K1-deficient tumours[20]. However, MAP3K1 also activates JNK through MAP2K4, which also can be mutated[38]. Loss of JNK signalling produces a defect in apoptosis in response to stress, which would hypothetically explain why these mutations accumulate[39,40]. *PIK3CA* harboured the most mutations (41.3%) but was neither associated with clinical nor Ki67 response, confirming our earlier report[41]. However, the positive association between *MAP3K1*/*MAP2K4* mutations and *PIK3CA* mutation at both the mutation and pathway levels suggests cooperativity (Fig. 4a).

The finding of multiple significantly mutated genes linked previously to benign and malignant haematopoietic disorders suggests that breast cancer, like leukaemia, can be viewed as a stem-cell disorder

Table 2 | Correlations between mutations and clinical features

a Luminal subtype and histology grade

Gene	Expression/histo-pathology variable	Mutation frequency*	Set1 *P*†	Set2 *P*†	Whole set FDR *P*‡
TP53	Luminal subtype A	9.3% (13/140)	0.001	0.46	0.041
	Luminal subtype B	21.5% (38/177)			
TP53	Histological grade I	4.5% (3/66)	0.05	0.067	0.02
	Histological grade II/III	19.2% (48/250)			
MAP3K1	Luminal subtype A	20.0% (28/140)	0.018	0.028	0.005
	Luminal subtype B	6.2% (11/177)			
MAP3K1	Histological grade I	25.8% (17/66)	0.061	0.011	0.005
	Histological grade II/III	8.8% (22/250)			
CDH1	Histological type ductal	5.9% (10/169)	0.41§	2.8×10^{-11}	3.9×10^{-10}
	Histological type lobular	50.0% (20/40)			

b Mutation and Ki67 index

Gene	Ki67 variable	Wild type mean‖	Mutant mean‖	Set1 *P*¶	Set2 *P*¶	Whole set FDR *P*‡
TP53	Baseline	13.1	25.1	3.7×10^{-5}	0.012	0.0003
	Surgery	1.4	4	0.0002	0.014	0.001
	% change	−89.2	−84.3	0.09	0.28	0.24
MAP3K1	Baseline	15.8	8.1	0.049	0.001	0.002
	Surgery	1.86	0.75	0.11	0.1	0.05
	% change	−88.3	−90.5	0.49	0.65	0.55
GATA3	Baseline	14.8	11.5	0.13	0.95	0.56
	Surgery	1.95	0.38	0.001	0.23	0.012
	% change	−86.8	−96.9	0.003	0.08	0.012

* Mutation percentage (mutant cases/total cases in a category), counts are based on all cases (Set 1 and Set 2 combined).

† Unadjusted *P* value from Fisher's exact test or Chi-square test as appropriate.

‡ Benjamini–Hochberg false discovery rate (FDR)-adjusted *P* value using all cases (Set1 and Set2 combined).

§ Only 77 cases in Set1 had CDH1 sequencing results.

‖ Geometric means are based on all cases (Set1 and Set2 combined).

¶ Unadjusted *P* value from Wilcoxon rank sum test.

that produces indolent or aggressive tumours that display varying phenotypes depending on differentiation blocks generated by different mutation repertoires[42]. Whereas only *MLL3* showed statistical significance in the analysis of 46 WGS cases, multiple mutations in genes related to histone modification and chromatin remodelling are worth noting (Supplementary Table 19). An array of coding mutations and structural variations was discovered in methyltransferases (*MLL2, MLL3, MLL4* and *MLL5*), demethyltransferases (*KDM6A, KDM4A, KDM5B* and *KDM5C*), and acetyltransferases (*MYST1, MYST3* and *MYST4*). Furthermore, our analysis identified several adenine-thymine (AT)-rich interactive domain-containing protein genes (*ARID1A, ARID2, ARID3B* and *ARID4B*) that harboured mutations and large deletions, reinforcing the role of members from the SNF/SWI family in breast cancer.

Pathway analysis enables the evaluation of mutations with low recurrence frequency where statistical comparisons are conventionally underpowered. For example, the eight samples with *MAP2K4* mutations were sufficient to derive a reliable pathway-based gene signature in PARADIGM that aligns with *MAP3K1*. This approach also pointed to a putative connection between *MALAT1* and the *TP53* pathway. Finally, we provide evidence that transcriptional associations to Ki67 response reside in a connected network under the control of several key 'hub' genes including *MYC, FYN* and *MAP* kinases, among others. Targeting these hubs in resistant tumours could produce therapeutic advances. In conclusion, the genomic information derived from unbiased sequencing is a logical new starting point for clinical investigation, where the mutation status of an individual patient is determined in advance and treatment decisions are driven by therapeutic hypotheses that stem from knowledge of the genomic sequence and its possible consequences. However, the accrual of large numbers of patients and the use of comprehensive sequencing and gene expression approaches will be required because of the extreme genomic heterogeneity documented by this investigation.

METHODS SUMMARY

Clinical trial samples were accessed from the preoperative letrozole phase 2 study (NCT00084396)[2] that investigated the effect of letrozole for 16 to 24 weeks on surgical outcomes and from the American College of Surgeons Oncology Group (ACOSOG) Z1031 study (NCT00265759)[3] that compared anastrozole with exemestane or letrozole for 16 to 18 weeks before surgery (REMARK flow charts, Supplementary Fig. 1). Baseline snap-frozen biopsy samples with greater than 70% tumour content (by nuclei) underwent DNA extraction and were paired with a peripheral blood DNA sample. Two formalin-fixed biopsies were obtained at baseline and at surgery, and were used to conduct oestrogen receptor and Ki67 immunohistochemistry as previously published[4]. Paired end Illumina reads from tumours and normal samples were aligned to NCBI build36 using BWA. Somatic point mutations were identified using SomaticSniper[43], and indels were identified by combining results from a modified version of the Samtools indel caller (http://samtools.sourceforge.net/), GATK and Pindel. Structural variations were identified using BreakDancer[5] and SquareDancer (unpublished). All putative somatic events found in 46 cases were validated by targeted custom capture arrays (Nimblegen)/Illumina sequencing and all tier 1 mutations for 46 WGS cases also were validated using PCR/454 sequencing. All statistical analyses, including significantly mutated gene, mutation relation and clinical correlation were done using the MuSiC package[45] and/or by standard statistical tests (Supplementary Information). Pathway analysis was performed with PathScan, GeneGo Metacore (http://www.genego.com/metacore.php) and PARADIGM. A complete description of the materials and methods used to generate this data set and results is provided in the Supplementary Methods section.

Received 16 June 2011; accepted 12 April 2012.

Published online 10 June 2012.

1. Chia, Y. H., Ellis, M. J. & Ma, C. X. Neoadjuvant endocrine therapy in primary breast cancer: indications and use as a research tool. *Br. J. Cancer* **103,** 759–764 (2010).
2. Olson, J. A. Jr *et al.* Improved surgical outcomes for breast cancer patients receiving neoadjuvant aromatase inhibitor therapy: results from a multicenter phase II trial. *J. Am. Coll. Surg.* 208, 906–914; discussion 915–906 (2009).
3. Ellis, M. J. *et al.* Randomized phase II neoadjuvant comparison between letrozole, anastrozole, and exemestane for postmenopausal women with estrogen receptor-rich stage 2 to 3 breast cancer: clinical and biomarker outcomes and predictive value of the baseline PAM50-based intrinsic subtype—ACOSOG Z1031. *J. Clin. Oncol.* **29,** 2342–2349 (2011).
4. Ellis, M. J. *et al.* Outcome prediction for estrogen receptor-positive breast cancer based on postneoadjuvant endocrine therapy tumor characteristics. *J. Natl. Cancer Inst.* **100,** 1380–1388 (2008).
5. Chen, K. *et al.* BreakDancer: an algorithm for high-resolution mapping of genomic structural variation. *Nature Methods* **6,** 677–681 (2009).
6. Mardis, E. R. *et al.* Recurring mutations found by sequencing an acute myeloid leukemia genome. *N. Engl. J. Med.* **361,** 1058–1066 (2009).
7. Ley, T. J. *et al.* DNA sequencing of a cytogenetically normal acute myeloid leukaemia genome. *Nature* **456,** 66–72 (2008).
8. Totoki, Y. *et al.* High-resolution characterization of a hepatocellular carcinoma genome. *Nature Genet.* **43,** 464–469 (2011).
9. Pleasance, E. D. *et al.* A comprehensive catalogue of somatic mutations from a human cancer genome. *Nature* **463,** 191–196 (2010).
10. Pleasance, E. D. *et al.* A small-cell lung cancer genome with complex signatures of tobacco exposure. *Nature* **463,** 184–190 (2010).
11. Lee, W. *et al.* The mutation spectrum revealed by paired genome sequences from a lung cancer patient. *Nature* **465,** 473–477 (2010).
12. Usary, J. *et al.* Mutation of *GATA3* in human breast tumors. *Oncogene* **23,** 7669–7678 (2004).
13. Berx, G. *et al.* E-cadherin is a tumour/invasion suppressor gene mutated in human lobular breast cancers. *EMBO J.* **14,** 6107–6115 (1995).
14. Samuels, Y. *et al.* High frequency of mutations of the *PIK3CA* gene in human cancers. *Science* **304,** 554 (2004).
15. Prosser, J., Thompson, A. M., Cranston, G. & Evans, H. J. Evidence that p53 behaves as a tumour suppressor gene in sporadic breast tumours. *Oncogene* **5,** 1573–1579 (1990).
16. T'Ang, A., Varley, J. M., Chakraborty, S., Murphree, A. L. & Fung, Y. K. Structural rearrangement of the retinoblastoma gene in human breast carcinoma. *Science* **242,** 263–266 (1988).
17. Wang, X. X. *et al.* Somatic mutations of the mixed-lineage leukemia 3 (*MLL3*) gene in primary breast cancers. *Pathol. Oncol. Res.* **17,** 429–433 (2011).
18. Kan, Z. *et al.* Diverse somatic mutation patterns and pathway alterations in human cancers. *Nature* **466,** 869–873 (2010).
19. Spirin, K. S. *et al. p27/Kip1* mutation found in breast cancer. *Cancer Res.* **56,** 2400–2404 (1996).
20. Fanger, G. R., Johnson, N. L. & Johnson, G. L. MEK kinases are regulated by EGF and selectively interact with Rac/Cdc42. *EMBO J.* **16,** 4961–4972 (1997).
21. Fillmore, C. M. *et al.* Estrogen expands breast cancer stem-like cells through paracrine FGF/Tbx3 signaling. *Proc. Natl Acad. Sci. USA* **107,** 21737–21742 (2010).
22. Mao, S., Frank, R. C., Zhang, J., Miyazaki, Y. & Nimer, S. D. Functional and physical interactions between AML1 proteins and an ETS protein, MEF: implications for the pathogenesis of t(8;21)-positive leukemias. *Mol. Cell. Biol.* **19,** 3635–3644 (1999).
23. Stender, J. D. *et al.* Genome-wide analysis of estrogen receptor α DNA binding and tethering mechanisms identifies Runx1 as a novel tethering factor in receptor-mediated transcriptional activation. *Mol. Cell. Biol.* **30,** 3943–3955 (2010).
24. Papaemmanuil, E. *et al.* Somatic *SF3B1* mutation in myelodysplasia with ring sideroblasts. *N. Engl. J. Med.* **365,** 1384–1395 (2011).
25. Wang, L. *et al. SF3B1* and other novel cancer genes in chronic lymphocytic leukemia. *N. Engl. J. Med.* **365,** 2497–2506 (2011).
26. Chen, Z. *et al.* The May-Hegglin anomaly gene *MYH9* is a negative regulator of platelet biogenesis modulated by the Rho-ROCK pathway. *Blood* **110,** 171–179 (2007).
27. Lamant, L. *et al.* Non-muscle myosin heavy chain (*MYH9*): a new partner fused to *ALK* in anaplastic large cell lymphoma. *Genes Chromosom. Cancer* **37,** 427–432 (2003).
28. Wilund, K. R. *et al.* Molecular mechanisms of autosomal recessive hypercholesterolemia. *Hum. Mol. Genet.* **11,** 3019–3030 (2002).
29. Dellê, H. *et al.* Antifibrotic effect of tamoxifen in a model of progressive renal disease. *J. Am. Soc. Nephrol.* **23,** 37–48 (2012).
30. Tararuk, T. *et al.* JNK1 phosphorylation of SCG10 determines microtubule dynamics and axodendritic length. *J. Cell Biol.* **173,** 265–277 (2006).
31. Westerlund, N. *et al.* Phosphorylation of SCG10/stathmin-2 determines multipolar stage exit and neuronal migration rate. *Nature Neurosci.* **14,** 305–313 (2011).
32. Tripathi, V. *et al.* The nuclear-retained noncoding RNA MALAT1 regulates alternative splicing by modulating SR splicing factor phosphorylation. *Mol. Cell* **39,** 925–938 (2010).
33. Rajaram, V., Knezevich, S., Bove, K. E., Perry, A. & Pfeifer, J. D. DNA sequence of the translocation breakpoints in undifferentiated embryonal sarcoma arising in mesenchymal hamartoma of the liver harboring the t(11;19)(q11;q13.4) translocation. *Genes Chromosom. Cancer* **46,** 508–513 (2007).
34. Xu, C., Yang, M., Tian, J., Wang, X. & Li, Z. MALAT-1: a long non-coding RNA and its important 3′ end functional motif in colorectal cancer metastasis. *Int. J. Oncol.* **39,** 169–175 (2011).
35. Wendl, M. C. *et al.* PathScan: a tool for discerning mutational significance in groups of putative cancer genes. *Bioinformatics* **27,** 1595–1602 (2011).
36. Vaske, C. J. *et al.* Inference of patient-specific pathway activities from multi-dimensional cancer genomics data using PARADIGM. *Bioinformatics* **26,** i237–i245 (2010).
37. Lynch, T. J. *et al.* Activating mutations in the epidermal growth factor receptor underlying responsiveness of non-small-cell lung cancer to gefitinib. *N. Engl. J. Med.* **350,** 2129–2139 (2004).

38. Johnson, G. L. & Lapadat, R. Mitogen-activated protein kinase pathways mediated by ERK, JNK, and p38 protein kinases. *Science* **298,** 1911–1912 (2002).
39. Widmann, C., Johnson, N. L., Gardner, A. M., Smith, R. J. & Johnson, G. L. Potentiation of apoptosis by low dose stress stimuli in cells expressing activated MEK kinase 1. *Oncogene* **15,** 2439–2447 (1997).
40. Wagner, E. F. & Nebreda, A. R. Signal integration by JNK and p38 MAPK pathways in cancer development. *Nature Rev. Cancer* **9,** 537–549 (2009).
41. Ellis, M. J. *et al.* Phosphatidyl-inositol-3-kinase alpha catalytic subunit mutation and response to neoadjuvant endocrine therapy for estrogen receptor positive breast cancer. *Breast Cancer Res. Treat.* **119,** 379–390 (2010).
42. Prat, A. & Perou, C. M. Mammary development meets cancer genomics. *Nature Med.* **15,** 842–844 (2009).
43. Larson, D. E. *et al.* SomaticSniper: identification of somatic point mutations in whole genome sequencing data. *Bioinformatics* **28,** 311–317 (2011).
44. Krzywinski, M. *et al.* Circos: an information aesthetic for comparative genomics. *Genome Res.* **19,** 1639–1645 (2009).
45. Dees, N. *et al.* MuSiC: Identifying mutational significance in cancer genomes. *Genome Res.* (in the press).

Supplementary Information is linked to the online version of the paper at www.nature.com/nature.

Acknowledgements This article is dedicated to the memory of Evelyn Lauder in recognition of her efforts to eradicate breast cancer. We would like to thank the participating patients and their families, clinical investigators and their support staffs, and J. A. Zujewski and the Cancer Therapy Evaluation Program at the US National Cancer Institute. We would like to acknowledge the efforts of the following people and groups at The Genome Institute for their contributions to this manuscript: the Analysis Pipeline group for developing the automated analysis pipelines that generated alignments and somatic variants; the LIMS group for developing tools to manage validation array ordering, capture and sequencing, and J. Veizer and H. Schmidt for structural variant and recurrent screening analyses. We thank the many members of the Siteman Cancer Center at Washington University in St Louis for support, and the committed members of the American College of Surgeons Oncology Group and their patients for contributing samples to the Z1031 trial. This work was funded by grants to R.K.W. from the National Human Genome Research Institute (NHGRI U54 HG003079), grants to M.J.E. from the National Cancer Institute (NCI R01 CA095614, NCI U01 CA114722), the Susan G. Komen Breast Cancer Foundation (BCTR0707808), and the Fashion Footwear Charitable Foundation, Inc., grant awards to ACOSOG included NCI U10 CA076001, the Breast Cancer Research Foundation, and clinical trial support from Novartis and Pfizer, and a Center grant (NCI P50 CA94056) to D.P.-W. We also acknowledge institutional support in the form of the Washington University Cancer Genome Initiative (R.K.W.), and a productive partnership with Illumina, Inc. The tissue procurement core was supported by an NCI core grant to the Siteman Cancer Center (NCI 3P50 CA68438). The BRIGHT Institute is supported in part by an ATT/Emerson gift to the Siteman Cancer Center.

Author Contributions M.J.E. led the clinical investigations, biomarker analysis and chip-based genomics. E.R.M., M.J.E., L.D., R.S.F., T.J.L. and R.K.W. designed the experiments. L.D. and M.J.E. led data analysis. D.S., J.W.W., D.C.K., C.C.H., M.D.M., K.C., C.A.Mi., F.D., W.S.S., M.C.W., R.C. and C.K. performed data analysis. D.S., C.A.Ma., J.W.W., J.F.M., C.L. and L.D. prepared figures and tables. R.S.F., L.L.F., R.D., M.H., T.L.V., J.H., L.L., R.C. and J.S. performed laboratory experiments. L.E., G.U., J.M., G.V.B., P.K.M., J.M.G., M.L., K.H. and J.O. provided samples and clinical data. V.J.S., K.B., J.L., Y.T. and C.K. provided statistical and clinical correlation analysis. D.O. oversees the ACOSOG Operations Center that provides oversight and tracking for ACOSOG clinical trials. K.D., S.McD., D.C.A. and M.W. provided pathology analysis. B.A.V.T., J.W., R.J.G., A.E., D.P.-W., H.P.-W., J.M.S., T.C.G., S.N., C.K. and M.C.W. performed pathway analysis. L.-W.C. and R.B. analysed the druggable target mutation data. D.J.D. and B.O. provided informatics support. L.D., M.J.E. and E.R.M. wrote the manuscript. T.J.L., M.C.W. and R.K.W. critically read and commented on the manuscript.

Author Information DNA sequence data are deposited in the restricted access portal at dbGaP, accession number phs000472.v1.p1. Gene expression array data used in the Paradigm training set is deposited in GEO, accession number GSE29442, and a Superseries that covers both the Agilent gene expression data and the Agilent array CGH data used for the Paradigm test set is deposited in GEO, accession number GSE35191 . Reprints and permissions information is available at www.nature.com/reprints. This paper is distributed under the terms of the Creative Commons Attribution-Non-Commercial-Share Alike licence, and is freely available to all readers at www.nature.com/nature. The authors declare no competing financial interests. Readers are welcome to comment on the online version of this article at www.nature.com/nature. Correspondence and requests for materials should be addressed to M.J.E., L.D. and E.R.M.

ARTICLE

doi:10.1038/nature11159

Large-scale prediction and testing of drug activity on side-effect targets

Eugen Lounkine[1]*, Michael J. Keiser[2,3]*, Steven Whitebread[1], Dmitri Mikhailov[1], Jacques Hamon[4], Jeremy L. Jenkins[1], Paul Lavan[4], Eckhard Weber[4], Allison K. Doak[3], Serge Côté[4], Brian K. Shoichet[3] & Laszlo Urban[1]

Discovering the unintended 'off-targets' that predict adverse drug reactions is daunting by empirical methods alone. Drugs can act on several protein targets, some of which can be unrelated by conventional molecular metrics, and hundreds of proteins have been implicated in side effects. Here we use a computational strategy to predict the activity of 656 marketed drugs on 73 unintended 'side-effect' targets. Approximately half of the predictions were confirmed, either from proprietary databases unknown to the method or by new experimental assays. Affinities for these new off-targets ranged from 1 nM to 30 μM. To explore relevance, we developed an association metric to prioritize those new off-targets that explained side effects better than any known target of a given drug, creating a drug–target–adverse drug reaction network. Among these new associations was the prediction that the abdominal pain side effect of the synthetic oestrogen chlorotrianisene was mediated through its newly discovered inhibition of the enzyme cyclooxygenase-1. The clinical relevance of this inhibition was borne out in whole human blood platelet aggregation assays. This approach may have wide application to de-risking toxicological liabilities in drug discovery.

Adverse drug reactions (ADRs) can limit the use of otherwise effective drugs. Next to lack of efficacy, they are the leading cause for attrition in clinical trials of new drugs[1–3] and are more prominent still in the failure of molecules to advance from pre-clinical research into human trials[4]. Some ADRs are caused by modulation of the primary target of a drug[5], others result from non-specific interactions of reactive metabolites[6]. In many cases, however, ADRs are caused by unintended activity at off-targets. Notorious examples of off-target toxicity include that of the appetite suppressant fenfluramine–phentermine (fen-phen), which was withdrawn from the market after numerous patient deaths. These owed to the activation of the 5-hydroxytryptamine-2B (5-HT_{2B}) receptor by one of its metabolites, norfenfluramine, leading to proliferative valvular heart disease[7]. Similarly, well-known drugs, such as the antihistamine terfenadine, have been withdrawn because they caused arrhythmias and death, which have been attributed to their off-target inhibition of the human *ether-à-go-go*-related gene potassium channel (hERG, also known as KCNH2)[8,9]. Prediction of unknown off-target drug interactions might prevent such disastrous drug toxicities, which are often detected only after fatalities in the clinic, and might allow safer molecules to be prioritized for pre-clinical development. Methods to systematically predict off-targets, and associate these with side effects, have thus attracted intense interest[10–16], frequently in the form of either chemical genomics[17,18] or informatics[19–26] approaches.

Whereas the informatics methods have never been tested systematically on a large scale, in principle they can be deployed against thousands of targets. Here we present a large-scale, prospective evaluation of safety target prediction using one such method, the similarity ensemble approach (SEA)[25–27]. SEA calculates whether a molecule will bind to a target based on the chemical features it shares with those of known ligands, using a statistical model to control for random similarity. Because SEA relies only on chemical similarity, it can be applied systematically and, for those targets that have known ligands, comprehensively. For 656 drugs approved for human use (Supplementary Table 1), targets were predicted from among 73 proteins (Supplementary Table 2 and Methods) with established association of ADRs[22,28], for which assays were available at Novartis. Encouragingly, many of the predictions were confirmed, often at pharmacologically relevant concentrations. This motivated us to develop a guilt-by-association metric that linked the new targets to the ADRs of those drugs for which they are the primary or well-known off-targets, creating a drug–target–ADR network. The applicability and the limitations of this approach will be considered.

Testing the predictions

The 656 drugs were computationally screened for their likelihood to bind to 73 targets (Supplementary Table 2) using SEA[25–27]. The targets belong to the Novartis *in vitro* safety panels based on their association with ADRs[22,28]. Here we insisted that they also be described in the ChEMBL database[29], enabling correspondence with SEA predictions (Supplementary Table 2). ChEMBL annotates more than 285,000 ligands modulating more than 1,500 different human targets with affinities better than 30 μM. SEA calculated the similarity of each drug versus each set of ligands for the 73 targets, comparing the overall set similarity to a model of such expected at random. For instance, the sodium channel blocker aprindine loosely resembled the set of histamine H_1 ligands; although no single H_1 ligand was strongly similar to the drug (Table 1), the overall similarity of the set was much greater than expected at random, leading to a highly significant SEA expectation value (*E* value) of 5×10^{-26} between aprinidine and H_1 receptor ligands. Only 1,644 of the more than 47,000 possible drug–target pairs had significant *E* values. Of these, 403 were already known in ChEMBL and so were trivially confirmed; we do not consider these further. Of the remaining 1,241 predictions, 348 (28%) were unknown to ChEMBL, but could be found in proprietary ligand–target databases that were unavailable to SEA (see Methods). The remaining

---

[1]Novartis Institutes for Biomedical Research, Cambridge, Massachusetts 02139, USA. [2]SeaChange Pharmaceuticals Inc, 409 Illinois Street, San Francisco, California 94158, USA. [3]Department of Pharmaceutical Chemistry, University of California, San Francisco, 1700 4th Street, Byers Hall Suite 508D, California 94158-2550, USA. [4]Novartis Institutes for Biomedical Research, 4056 Basel, Switzerland.

*These authors contributed equally to this work.

Table 1 | New drug-off-target predictions confirmed by *in vitro* experiment

Drug	Closest chEMBL molecule	Tc value	Target	SEA *E* value	IC_{50} (μM)	Closest known target	BLAST *E* value
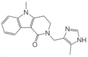 Alosetron	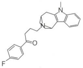	0.25	HTR2B	10.6×10^{-17}	0.02	KCNH7	3.6×10^{2}
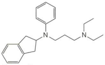 Aprindine	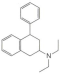	0.38	HRH1	5.0×10^{-26}	0.78	SCN5A	3.3×10^{-1}
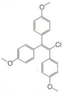 Chlorotrianisene	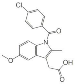	0.31	COX-1	1.9×10^{-17}	0.16	ESR1	9.0×10^{2}
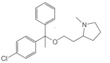 Clemastine	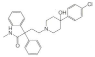	0.31	SLC6A4	1.1×10^{-14}	0.42	KCNH2	6.1×10^{1}
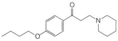 Dyclonine	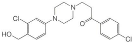	0.36	DRD4	1.5×10^{-17}	4.1	SLC6A3	2.3×10^{2}
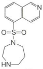 Fasudil	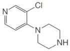	0.37	ADRA2A	1.1×10^{-7}	4.0	CCR2	1.5×10^{-9}
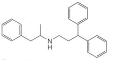 Prenylamine	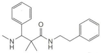	0.31	OPRM1	1.1×10^{-8}	1.8	CACNA1G	3.5×10^{0}
	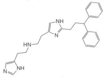	0.30	HRH1	3.2×10^{-66}	7.9	SCN5A	3.3×10^{-1}
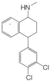 Sertraline	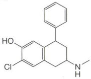	0.33	HRH2	5.1×10^{-45}	1.4	HTR4	6.8×10^{-51}
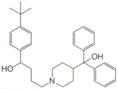 Terfenadine	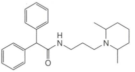	0.24	SCN5A	8.9×10^{-8}	7.1	CYP2D6	5.9×10^{1}

Representative, confirmed predictions are shown. Tc values determined using ECFP_4-based molecular similarity to the closest ChEMBL reference molecule in the target set. The closest known target is a known target of the drug that has highest sequence similarity to the predicted target. The BLAST *E* value is based on the sequence identity of the predicted target to the closest known target; values greater than 10^{-5} represent unrelated proteins.

893 predictions represented previously unexplored drug–target associations.

Of these predictions, 694 were tested at Novartis. For 478, activity was less than 25% at 30 μM; these were considered disproved. For another 65 predictions, activity was between 25 and 50% at 30 μM; these were considered ambiguous. Finally, for 151 of the new drug–target predictions, half-maximum inhibitory concentration (IC_{50}) values of less (better) than 30 μM were measured in concentration–response curves (Fig. 1a and Supplementary Fig. 1). In 125 cases, the drugs had an IC_{50} value better than 10 μM, and in 48 cases activities were sub-micromolar (Table 1, Supplementary Table 3 and Supplementary Fig. 1). In summary, of the 1,042 predictions that were tested (694 by assay,

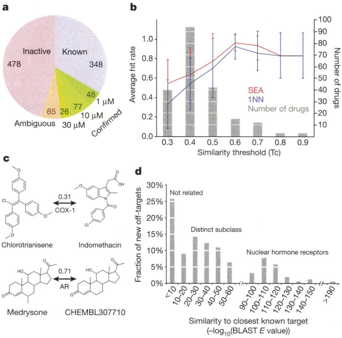

Figure 1 | Predicting off-targets, and their novelty. a, Success of SEA predictions. Known: predicted off-targets confirmed by proprietary databases. Confirmed: predictions tested *in vitro* achieving $IC_{50} < 30\,\mu M$. Ambiguous: predictions with 25–50% activity at 30 μM. Inactive: <25% activity. **b**, SEA enriched for non-trivial similarity. Drugs were binned (grey) by lowest Tc values yielding valid SEA predictions. Hit rates of SEA (red) and 1NN (blue) are shown. Error bars denote s.d. **c**, Non-intuitive (chlorotrianisene) and straightforward (medrysone) SEA predictions, with Tc values to closest references shown. Chlorotrianisene is only marginally similar to indomethacin, but is (correctly) predicted for COX-1. AR, androgen receptor. **d**, Sequence similarities of each confirmed drug off-target to the closest known target of the drug.

348 by databases), 48% were confirmed either in proprietary databases, unknown to the method and to those undertaking the SEA calculation, or in Novartis assays in full concentration responses, and just under 46% were disproved (Fig. 1a).

In assessing these results, one would like to compare the true predictions with the false-positive and the false-negative predictions. Whereas this work offers guidance on false-positive predictions, we can only address false negatives for a few compounds (Supplementary Results). Among these was astemizole, which had affinities ranging from 0.1 to 9 μM on the 5-HT_{2A}, 5-HT_{2B} and 5-HT_{2C} serotonin receptors and the histamine H_2 and dopamine D_2 receptors, as measured in other projects at Novartis. These targets were missed owing to a charge post-filter, separate from SEA itself, which excluded compounds with net charge dissimilar from the reference ligands[30]. Astemizole was improperly assigned[31] a charge of +2, wrongly differentiating it from the known ligands; the SEA E values linking astemizole to these targets were themselves between 10^{-25} to 10^{-27}. Other failures could be attributed to SEA itself. For instance, promazine bound to the histamine H_1 and H_2 receptors with low to mid-nanomolar affinities, but the SEA E values at 10^{-4} to 10^{-3} were below our significance cut-off. This work was undertaken with ChEMBL_2 as a source of ligand–target association; had we used the more recent ChEMBL_10, the H_1 receptor would have been predicted with an E value of 10^{-9} (see http://sea.bkslab.org), and had we used ChEMBL_12 and a newer version of SEA, both targets would have been predicted. Clearly, with its reliance on topology and on inference from known ligand–target associations, SEA will have false negatives.

A key question is whether the new predictions were in any way surprising. One way to evaluate this is to compare the similarity of drugs predicted for new targets with the closest previously known ligand for that target. We used Tanimoto coefficients (Tc), which compare the groups in common between two molecules, here represented by ECFP_4 fingerprints. Tc values between nearest molecules were small, often less than 0.4 (ref. 32); visual inspection of these pairs confirms the dissimilarity suggested by the low Tc values (Table 1). More systematically, SEA may be compared with a method that predicts targets based only on the one-nearest neighbour (1NN) model (Fig. 1b). For close analogues (Tc values > 0.7; Fig. 1c), the fraction of true positives was comparable between 1NN and SEA approaches (Fig. 1b). But across most similarity thresholds, SEA substantially outperformed 1NN, and by nearly twofold in the low similarity range. Thus, for the Rho kinase inhibitor fasudil, SEA predicted only the adrenergic α_{2A} receptor, with an E value of 1.1×10^{-7}, which was experimentally confirmed ($IC_{50} = 4\,\mu M$). This occurred despite the low similarity of the closest known α_2 ligand, which had a Tc value of 0.37 to fasudil. Conversely, at this similarity threshold the 1NN model predicted nine targets, only three of which were confirmed (Supplementary Table 4). For chlorotrianisene, two of the three targets predicted by SEA were confirmed; conversely, at its 0.31 Tc for cyclooxygenase-1 (COX-1, also known as PTGS1) the 1NN model predicted ten targets, only two of which were confirmed.

We also investigated how often the new off-target would have been obvious based on sequence similarity of the targets[25,26,33]. We calculated the BLAST sequence similarity of predicted targets to any known target of a drug (Table 1 and Supplementary Table 3). Of the 151 new off-target predictions, 39 (26%) had BLAST E values greater (worse) than 10^{-5}, suggesting the previously known targets shared no sequence similarity with the new off-targets (Table 1, Supplementary Table 3 and Fig. 1d). For example, the anaesthetic dyclonine was shown to bind the histamine H_2 receptor (HRH2), whereas the closest known target was the $Na_v1.8$ channel (SCN10A), which has no significant sequence similarity (BLAST E value > 1) and is functionally unrelated to the H_2 receptor. Similarly, the anti-nausea drug alosetron antagonized the 5-HT_{2B} receptor with an IC_{50} of 18 nM, although 5-HT_{2B} has no sequence similarity to the ion channel targets of this drug (Table 1). Chlorotrianisene potently inhibits the enzyme COX-1, which is unrelated by sequence to the primary nuclear hormone receptor of this drug, the oestrogen receptor (Table 1).

Associating *in vitro* targets with ADRs

To assess the potential clinical relevance of the discovered targets systematically, we developed a quantitative score that associated *in vitro* activity with patient ADRs. We enumerated all possible target–ADR pairs for 2,760 drugs with available adverse event annotations, expressing as an enrichment score the co-occurrence of pairs that were more common than expected by chance (Supplementary Table 5). For example, 'abdominal pain upper' has been reported for 45 drugs that interact with COX-1. The ADR abdominal pain upper was linked with 6,046 drug–target pairs, whereas COX-1 was linked with 2,188 drug–ADR pairs; there were a total of 681,797 target–ADR pairs overall. Thus the pair abdominal pain upper–COX-1 was enriched 2.3-fold above random (Methods), with a χ^2 P value of 9.9×10^{-9}. A total of 3,257 significant target–ADR associations were identified (Supplementary Table 5).

Having identified new off-targets for the drugs, and linked these with observed ADRs, we sought drug–target–ADR connections that illuminate the clinical relevance of the predictions. Of the 151 confirmed new drug–target associations tested at Novartis, 82 were significantly associated with one or more ADR, resulting in a total of 247 drug–target–ADR links. In 116 cases, the enrichment factor (EF) of the new drug–target–ADR link was stronger than that for any previously known target (Table 2 and Supplementary Table 6). For example, prenylamine was found to bind the histamine H_1 receptor (HRH1), which we associate with a sedation ADR (EF = 4.9). By contrast, none of the known targets of prenylamine was associated

Table 2 | Characteristic new, confirmed targets associated with ADRs of the drugs

Drug name	Target	Activity (μM) (median)	AUC (μM h)	C_{max} (μM)	Adverse event	EF ratio	Alternative target	Comparable drug
Chlorotrianisene	COX-1	0.16	NA	NA	Abdominal pain upper	2.32	None	None
					Rash	1.79	None	None
Clemastine	SLC6A4	0.42	NA	NA	Sleep disorder	2.15	None	None
Cyclobenzaprine	HRH1	0.02	0.16–4.10 (0.69)	0.01–0.13 (0.06)	Ataxia	1.73	None	**Desipramine**
					Somnolence	1.49	None	**Aripiprazole**
Diphenhydramine	SLC6A3	4.33	2.57–3.42 (3.00)	0.26–0.26 (0.26)	Tremor	2.02/1.90	SCN10A	**Citalopram**
Loxapine	CHRM2	1.12	0.03–0.43 (0.21)	0.02–0.41 (0.14)	Tachycardia	2.08/1.97	CHRM1	Sibutramine
Methylprednisolone	PGR	1.30	0.09–10.76 (1.28)	0.06–2.11 (0.31)	Depression	3.87/2.49	NR3C1	Flutamide
Prenylamine	HRH1	7.87	0.12–0.12 (0.12)	1.20–1.20 (1.20)	Sedation	4.94	None	None
Ranitidine	CHRM2	5.56	5.66–121.90 (9.67)	1.14–9.11 (2.12)	Constipation	1.63	None	Haloperidol
Ritodrine	OPRM1	9.18	0.03–0.32 (0.11)	0.01–0.15 (0.04)	Hyperhidrosis	3.21	None	**Oxycodone**

ADRs are listed that are more strongly associated with the predicted target than any known target, together with pharmacokinetic data (AUC and C_{max}), where available. Numbers in parentheses denote the median value, and the range denotes the minimal and maximal reported value. Where pharmacokinetics (PK) and pharmacodynamic activity (PD) were available, drugs have been identified that behave comparably to the predicted drug and also cause the adverse event. The EF ratio is the ADR–target enrichment for the predicted/best alternative known target ratio. Comparable drugs are those that are known to bind the predicted target (bold denotes predicted target is the primary target), share the ADR and behave similarly in terms of PK and PD (see Methods). NA, not available.

with this side effect. For other cases, known targets represented an alternative explanation for an ADR. For instance, we found that diphenhydramine binds to the dopamine transporter (SLC6A3; Table 2), which is associated with tremor[34]. Although tremor was also associated with one of the known targets of diphenhydramine, sodium channel SCN10A (EF = 1.9)[35], its association with the dopamine transporter was higher (EF = 2.02), indicating a possible mechanistic link with the new off-target. Conversely, the 'dry mouth' side effect of diphenhydramine was better explained by its known antagonism of the M_3 muscarinic receptor (CHRM3; EF = 2.45, Supplementary Table 5).

We asked whether the affinity of a drug for its predicted ADR–target was relevant given its pharmacology, comparing the predictions against other drugs with similar pharmacodynamics and pharmacokinetics (Table 2). This was possible for 36 drug–target–ADR links (Supplementary Table 6). For instance, cyclobenzaprine was shown to bind to the histamine H_1 receptor at 21 nM, whereas its median maximal plasma concentration (C_{max}) was 61 nM; nine other drugs binding the H_1 receptor in the nanomolar range with comparable C_{max} values were found (Table 2). Although some of the measured drug–target affinities were moderate, the pharmacokinetic data often confirmed that they were nevertheless relevant. For instance, the affinity of ranitidine (Zantac) for the M_2 muscarinic receptor, which we associate with its constipation ADR, is only 5.6 μM. Nevertheless, with an area under the curve (AUC) value of 5.7 to 122 μM h (minimal and maximal reported values) in plasma, this association seems plausible. Similarly, diphenhydramine has an IC_{50} value of only 4.3 μM against the dopamine transporter, a target that we associate with the tremor side effect of the drug. Nevertheless, the AUC value of diphenhydramine of 2.6 to 3.4 μM h supports the relevance of its modest IC_{50} value.

Drug–target–ADR networks

Network graphs help to visualize the new and known drug–target links, and the adverse events with which they are associated (Fig. 2a–c). For example, the oestrogen receptor (ESR1) modulator chlorotrianisene was found to inhibit COX-1, with an affinity substantially better than its affinity for ESR1. Drugs that modulate the two proteins can share two of the adverse reactions of chlorotrianisene ('erythema multiforme' and 'oedema'), but 'rash' and 'abdominal pain upper' link only to drugs inhibiting COX-1, and these are both associated with chlorotrianisene almost uniquely among the oestrogen receptor modulators (Fig. 2c and Supplementary Table 5). For prenylamine, a new G-protein-coupled receptor (GPCR) cluster (HRH1, OPRM1 and ADRB2) emerges that is unrelated to the primary ion channel activity of the drug, but uniquely link to its sedative and myocardial infarction ADRs (Fig. 2b). For domperidone, its known activity at dopamine receptors is associated with a Parkinsonism-like phenotype ('hyperprolactinaemia' and 'extrapyramidal disorder'), whereas 'somnolence' associates only with the newly discovered opioid activity (Fig. 2a).

Several of the drug–target–ADR associations that emerged were surprising. Among them were the association of the muscle relaxant cyclobenzaprine with somnolence, the H_2 antagonist ranitidine with constipation, and chlorotrianisene with upper abdominal pain (Table 2). Cyclobenzaprine caught our attention because even its mechanism of action target for muscle relaxation has not been characterized, and its association with the off-target discovered here, the H_1 receptor (IC_{50} = 20 nM), precedes the identification of its primary target. The central nervous system H_1 receptor is strongly associated with somnolence, consistent with the ADR of the drug, and supported by its pharmacokinetics. Similarly, the constipation effect of ranitidine is consistent with its activity on the M_2 muscarinic receptor. Although its affinity for M_2 is moderate at 5.5 μM, the pharmacokinetics make this affinity relevant to this ADR.

Perhaps the most compelling demonstration of a drug–target–ADR association is one *in vivo*, or in an accepted *in vivo* biomarker. The observation that chlorotrianisene was a potent COX-1 inhibitor seemed a reasonable explanation for the upper abdominal pain (epigastralgia) side effect provoked by the drug, and one that lent itself to direct testing in an accepted biomarker. Epigastralgia is a well-known ADR of non-steroidal anti-inflammatory drugs (NSAIDs), which inhibit the cyclooxygenase enzymes COX-1 and COX-2. COX-1 has housekeeping effects in the gastric mucosa[36], and its inhibition can lead to mucosal thinning and gastroduodenal ulceration, leading to upper gastric pain and the thousands of annual hospitalizations that are associated with NSAID use[37]. NSAIDs also inhibit platelet aggregation by direct inhibition of their endogenous COX-1 enzyme[38]. Intriguingly, this effect is unreported for other synthetic oestrogens, which, to the contrary, are more likely to promote platelet aggregation[39,40]. A widely accepted model for platelet aggregation may be run *ex vivo*, in whole blood, allowing one to test for target engagement of COX-1 in this effect.

Accordingly, collagen-induced platelet aggregation was measured in freshly drawn human blood from six healthy volunteer donors. Acetylsalicylic acid, the active ingredient in aspirin, inhibited platelet aggregation by 42–48% at 250 μM. The more potent NSAID indomethacin inhibited platelet aggregation by 50% at 50 μM. Chlorotrianisene inhibited platelet aggregation in whole blood with a potency almost indistinguishable from that of indomethacin, and more potently than acetylsalicylic acid (Fig. 2d). These results are consistent with an *in vivo* inhibitory activity of chlorotrianisene on COX-1, and with the epigastralgia that is among its common side effects.

Drug and target promiscuity

To investigate overall patterns of drug and target promiscuity, we integrated the experimental results from this and other Novartis studies. The most promiscuous target was the voltage-gated sodium channel

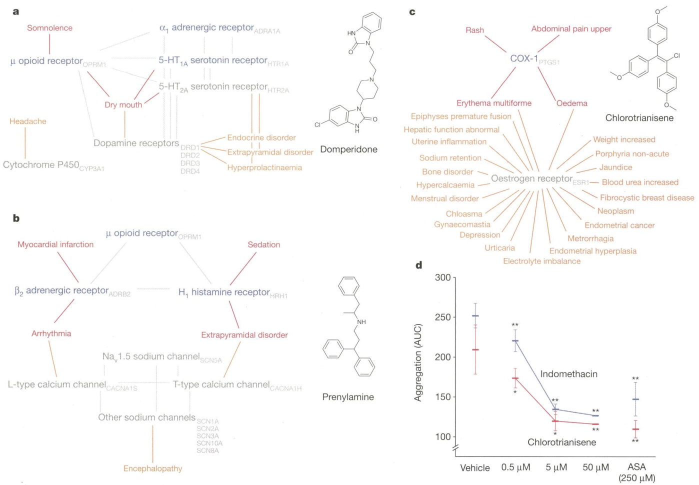
a
Somnolence
α1 adrenergic receptor ADRA1A
μ opioid receptor OPRM1
5-HT1A serotonin receptor HTR1A
5-HT2A serotonin receptor HTR2A
Dry mouth
Headache
Dopamine receptors DRD1 DRD2 DRD3 DRD4
Endocrine disorder
Extrapyramidal disorder
Hyperprolactinaemia
Cytochrome P450 CYP3A1
Domperidone
b
μ opioid receptor OPRM1
Myocardial infarction
Sedation
β2 adrenergic receptor ADRB2
H1 histamine receptor HRH1
Arrhythmia
Extrapyramidal disorder
Nav1.5 sodium channel SCN5A
L-type calcium channel CACNA1S
T-type calcium channel CACNA1H
Other sodium channels SCN1A SCN2A SCN3A SCN10A SCN8A
Encephalopathy
Prenylamine
c
Rash
Abdominal pain upper
COX-1 PTGS1
Erythema multiforme
Oedema
Chlorotrianisene
Epiphyses premature fusion
Hepatic function abnormal
Uterine inflammation
Sodium retention
Bone disorder
Hypercalcaemia
Menstrual disorder
Chloasma
Gynaecomastia
Depression
Urticaria
Electrolyte imbalance
Oestrogen receptor ESR1
Weight increased
Porphyria non-acute
Jaundice
Blood urea increased
Fibrocystic breast disease
Neoplasm
Endometrial cancer
Metrorrhagia
Endometrial hyperplasia
d
Aggregation (AUC)
300
250
200
150
100
Indomethacin
Chlorotrianisene
Vehicle
0.5 μM
5 μM
50 μM
ASA (250 μM)
**
*

Figure 2 | Off-target networks. a–c, Off-target networks for three drugs. Known targets of the drugs are grey, whereas newly predicted targets are blue; the adverse events associated with each are orange and red, respectively. Red adverse events are significantly (EF > 1, *q* value < 0.05) associated with the new off-targets. Targets related by sequence are connected by grey edges. **d**, Chlorotrianisene inhibits platelet aggregation. Two independent experiments (red and blue) are shown for chlorotrianisene and indomethacin, respectively. ASA, acetylsalicylic acid (positive control); vehicle denotes negative control. $*P < 0.05$, $**P < 0.01$ (paired Student's *t*-test differences compared with vehicle control). Error bars denote s.d.

(SCN5A), to which 70 out of 126 (56%) tested drugs bound (Fig. 3a). From a target family standpoint, however, this was an exception, as most other promiscuous targets were small molecule-recognizing GPCRs; of non-GPCRs, only SCN5A and the ion channel hERG were targeted more than average (>13% of drugs tested). Transporters had mid-range promiscuity; enzymes, nuclear receptors and ligand-gated ion channels were less promiscuous, whereas peptide-recognizing receptors were hit least of all (Supplementary Tables 2 and 7).

Inverting this analysis, the most promiscuous drug, chlorhexidine, hit 34 out of 54 (64%) targets against which it was tested, and another nine drugs were active on more than 50% of their tested targets (Fig. 3b and Supplementary Table 8). Twenty-five drugs bound to proteins from among all major target classes. Highly promiscuous drugs were often lipophilic and cationic at physiological pH (Fig. 3b)[41,42].

Predicting off-targets and adverse events

This study begins to quantify drug polypharmacology at scale: the 656 drugs considered here each modulated an average of seven safety targets, sometimes across several classes, and more than 10% of the drugs acted on nearly half (45%) of the 73 targets (Fig. 3b). It is sobering that this promiscuity is observed for approved human drugs, which have typically already been optimized to minimize toxicity. For lead molecules that are progressing towards the clinic, this level of off-target promiscuity might be higher still[28]. Anticipating these off-targets is difficult, as they can be unrelated in sequence and structure to the primary targets of a drug, and even known target–ADR associations are not always straightforward. Two results of this study begin to address these challenges. First, of the 1,042 predicted drug–target associations that were tested, 48% were confirmed (Fig. 1a). With 46% of the predictions disproved, the method remains imperfect, but this rate may nevertheless be high enough to prioritize compound classes and targets for testing. Second, a guilt-by-association metric can link off-targets with ADRs. A three-way association between drugs, molecular targets and ADRs may be systematically calculated and interpreted (Fig. 2a–c).

Surprisingly, drugs often modulated off-targets unrelated to their primary target. Of the 151 off-targets that were confirmed by new experiment, 39 were unrelated by sequence to any of the known drug targets (Fig. 1d). For example, the antitussive clemastine and the antihistamine diphenhydramine (an active ingredient in products such as Tylenol PM), both of which act on the histamine H_1 GPCR, also modulate the serotonin transporter (5-HTT, also known as SLC6A4), to which the primary target is unrelated by sequence or structure. Conversely, the serotonin transporter inhibitor sertraline acts on the histamine H_2 GPCR. The activity of drugs on targets that are unrelated by sequence or structure to their primary targets can seem capricious and certainly makes prioritization of likely targets more difficult. A ligand-based approach offers an orthogonal view of target relationships and so can illuminate similarities that are opaque from a molecular biology perspective. The converse is also true, and the two views will often be complementary.

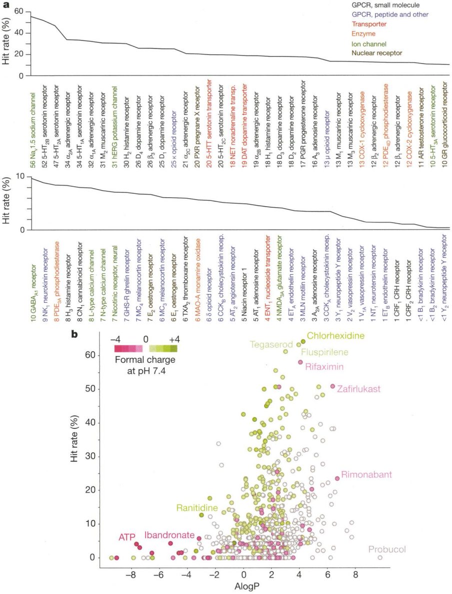

Figure 3 | Target and drug promiscuity. **a**, Target promiscuity. Targets are sorted based on the percentage of drugs hitting the target below 30 μM (indicated by numbers next to target names). Colours code for seven distinct target classes. **b**, Promiscuous drugs are often hydrophobic and cationic. Each point represents one drug. Ionization at pH 7.4 and AlogP (calculated octanol–water partitioning coefficient) values were calculated from drug structures. Hit rate denotes the percentage of targets the drug binds below 30 μM.

The association between chlorotrianisene, COX-1 and epigastralgia illustrates the potential of the approach. The therapeutic target of chlorotrianisene, the oestrogen nuclear hormone receptor, bears no sequence or structural similarity to the COX-1 enzyme, but the likelihood of cross-activity between the two targets is articulated by ligand similarity (Table 1). Correspondingly, the linking of abdominal pain and COX-1 only emerges when one quantitatively compares the ADRs of known COX-1 inhibitors to what one would expect at random. The potent inhibition of platelet aggregation by chlorotrianisene in whole blood (Fig. 2d) is consistent with the systemic, *in vivo* activity of this drug at relevant concentrations on COX-1.

Certain shortcomings of the method should not escape the reader's attention. Almost 46% of the predicted drug–target associations were disproved, and the method, which is inference-based, undoubtedly has important false negatives. As such, SEA cannot replace compound-target testing. What it can do is identify compounds early in development for possible liabilities that would ordinarily be identified only much later in drug progression. Similarly, the guilt-by-association method is inference-based and mechanism-naive, and so will miss some target–ADR associations and make others that are invalid. Also, only some side effects fall into the remit of this approach, which assumes an off-target mechanism. Side effects, like other pharmacological events, have a strong exposure component, and can result from complex interactions with regulatory networks[43]. Thus, topical drugs such as econazole or chlorhexidine, although promiscuous *in vitro*, have fewer ADRs than expected because they never achieve sufficient systemic exposure *in vivo*. Conversely, a drug such as tacrolimus might be relatively selective *in vitro*, but is associated with several side effects owing to its broad immunosuppressant effects.

These caveats should not obscure the potential of this approach to predict and understand drug side effects. The method was used automatically at scale, without human intervention. Whereas its predictions were sometimes disproved, they were just as often confirmed. If some of the targets it suggested required no imaginative leap—as when a steroid was predicted for a new nuclear hormone receptor—a quarter of the confirmed targets were unrelated by sequence or structure to any of the known targets of the drugs (Fig. 1c, d, Table 1 and Supplementary Table 2). Pragmatically, the ability to calculate drug–target–ADR networks provides a tool to anticipate liabilities among candidate drugs being advanced towards the clinic, or yet earlier, for prioritization of chemotypes in preclinical series. If such networks cannot replace direct experimentation, they can usefully prioritize off-targets for consideration. As we struggle to develop new therapeutics, this and related approaches[11,19,21–24,44,45] can identify molecules with liabilities early in their development, and so focus effort on those candidates that are least subject to them.

METHODS SUMMARY

A collection of on-hand 656 US Food and Drug Administration-approved drugs was computationally screened against a panel of 339 molecular targets representing the species-specific expansion of 73 target assays used in Novartis safety panels. Each of the 339 target proteins was represented by its set of known ligands, as extracted from the ChEMBL_2 database. The two-dimensional structural similarity of a drug to the ligand set of a target was quantified as an E value using the SEA, then subjected to a molecular charge filter. Predictions were tested retrospectively using proprietary databases including GeneGo Metabase, Thompson Reuters Integrity, Drugbank and GVKBio; new predictions were tested prospectively in Novartis *in vitro* assays. Binding assays, and, when available, functional assays were performed including scintillation proximity, fluorometric imaging, filtration, fluorescence polarization, patch clamp, time-resolved fluorescence resonance energy transfer, and homogenous time-resolved fluorescence assays. Concentration-response curves were calculated using XLfit (v.2 or v.4, IDBS) or corresponding in-house software. All curves were redrawn using GraphPad PRISM v.5. Adverse drug reaction data were extracted from the World Drug Index and encoded using the medicinal dictionary for regulatory affairs (MedDRA). Using target annotations from GeneGo Metabase, Integrity, Drugbank, ChEMBL and GVKBio, target–ADR pairs for all drugs were enumerated. Disproportionality analysis in conjunction with a chi-squared test for association was carried out for all drug–target pairs. The false discovery rate was controlled using the Benjamini–Hochberg correction for multiple hypothesis testing. Pharmacokinetic data were extracted from Integrity. For target and drug promiscuity analysis, combined external and internal target annotations were used. The computational workflow apart from SEA was implemented in Pipeline Pilot version 8 and statistical analyses were performed in R. Platelet aggregometry was performed in human blood for chlorotrianisene and indomethacin, with acetylsalicylic acid as a positive control.

Full Methods and any associated references are available in the online version of the paper at www.nature.com/nature.

Received 14 October 2011; accepted 25 April 2012.
Published online 10 June 2012.

1. Giacomini, K. M. *et al.* When good drugs go bad. *Nature* **446,** 975–977 (2007).
2. Arrowsmith, J. Trial watch: phase III and submission failures: 2007–2010. *Nature Rev. Drug Discov.* **10,** 87 (2011).
3. Arrowsmith, J. Trial watch: phase II failures: 2008–2010. *Nature Rev. Drug Discov.* **10,** 328–329 (2011).
4. Boyer, S. The use of computer models in pharmaceutical safety evaluation. *Altern. Lab. Anim.* **37,** 467–475 (2009).
5. Wong, D., Wang, M., Cheng, Y. & Fitzgerald, G. A. Cardiovascular hazard and non-steroidal anti-inflammatory drugs. *Curr. Opin. Pharmacol.* **5,** 204–210 (2005).
6. Antunes, A. M. M. *et al.* Protein adducts as prospective biomarkers of nevirapine toxicity. *Chem. Res. Toxicol.* **23,** 1714–1725 (2010).
7. Rothman, R. B. *et al.* Evidence for possible involvement of 5-HT$_{2B}$ receptors in the cardiac valvulopathy associated with fenfluramine and other serotonergic medications. *Circulation* **102,** 2836–2841 (2000).
8. Roy, M., Dumaine, R. & Brown, A. M. HERG, a primary human ventricular target of the nonsedating antihistamine terfenadine. *Circulation* **94,** 817–823 (1996).
9. Curran, M. E. *et al.* A molecular basis for cardiac arrhythmia: HERG mutations cause long QT syndrome. *Cell* **80,** 795–803 (1995).
10. Ji, Z. L. *et al.* Drug Adverse Reaction Target Database (DART): proteins related to adverse drug reactions. *Drug Saf.* **26,** 685–690 (2003).
11. Kuhn, M., Campillos, M., Letunic, I., Jensen, L. J. & Bork, P. A side effect resource to capture phenotypic effects of drugs. *Mol. Syst. Biol.* **6,** 343 (2010).
12. Matthews, E. J. & Frid, A. A. Prediction of drug-related cardiac adverse effects in humans–A: Creation of a database of effects and identification of factors affecting their occurrence. *Regul. Toxicol. Pharmacol.* **56,** 247–275 (2010).
13. Yang, X. *et al.* Kinase inhibition-related adverse events predicted from *in vitro* kinome and clinical trial data. *J. Biomed. Inform.* **43,** 376–384 (2010).
14. Hopkins, A. L. Network pharmacology: the next paradigm in drug discovery. *Nature Chem. Biol.* **4,** 682–690 (2008).
15. Zhang, J.-X. *et al.* DITOP: drug-induced toxicity related protein database. *Bioinformatics* **23,** 1710–1712 (2007).
16. Yang, L., Luo, H., Chen, J., Xing, Q. & He, L. SePreSA: a server for the prediction of populations susceptible to serious adverse drug reactions implementing the methodology of a chemical-protein interactome. *Nucleic Acids Res.* **37,** W406–W412 (2009).
17. Lee, S., Lee, K. H., Song, M. & Lee, D. Building the process-drug-side effect network to discover the relationship between biological processes and side effects. *BMC Bioinformatics* **12** (suppl. 2), S2 (2011).
18. Schreiber, G. & Keating, A. E. Protein binding specificity versus promiscuity. *Curr. Opin. Struct. Biol.* **21,** 50–61 (2011).
19. Oprea, T. I. *et al.* Associating drugs, targets and clinical outcomes into an integrated network affords a new platform for computer-aided drug repurposing. *Mol. Inform.* **30,** 100–111 (2011).
20. Paolini, G. V., Shapland, R. H. B., van Hoorn, W. P., Mason, J. S. & Hopkins, A. L. Global mapping of pharmacological space. *Nature Biotechnol.* **24,** 805–815 (2006).
21. Scheiber, J. *et al.* Mapping adverse drug reactions in chemical space. *J. Med. Chem.* **52,** 3103–3107 (2009).
22. Bender, A. *et al.* Analysis of pharmacology data and the prediction of adverse drug reactions and off-target effects from chemical structure. *ChemMedChem* **2,** 861–873 (2007).
23. Campillos, M., Kuhn, M., Gavin, A.-C., Jensen, L. J. & Bork, P. Drug target identification using side-effect similarity. *Science* **321,** 263–266 (2008).
24. Tatonetti, N. P. *et al.* Detecting drug interactions from adverse-event reports: interaction between paroxetine and pravastatin increases blood glucose levels. *Clin. Pharmacol. Ther.* **90,** 133–142 (2011).
25. Keiser, M. J. *et al.* Predicting new molecular targets for known drugs. *Nature* **462,** 175–181 (2009).
26. Keiser, M. J. *et al.* Relating protein pharmacology by ligand chemistry. *Nature Biotechnol.* **25,** 197–206 (2007).
27. Hert, J., Keiser, M. J., Irwin, J. J., Oprea, T. I. & Shoichet, B. K. Quantifying the relationships among drug classes. *J. Chem. Inf. Model.* **48,** 755–765 (2008).
28. Azzaoui, K. *et al.* Modeling promiscuity based on *in vitro* safety pharmacology profiling data. *ChemMedChem* **2,** 874–880 (2007).
29. Gaulton, A. *et al.* ChEMBL: a large-scale bioactivity database for drug discovery. *Nucleic Acids Res.* 40, D1100–D1107 10.1093/nar/gkr777 (2012).
30. Laggner, C. *et al.* Chemical informatics and target identification in a zebrafish phenotypic screen. *Nature Chem. Biol.* **8,** 144–146 (2012).
31. Shelley, J. C. *et al.* Epik: a software program for pK$_a$ prediction and protonation state generation for drug-like molecules. *J. Comput. Aided Mol. Des.* **21,** 681–691 (2007).
32. Muchmore, S. W. *et al.* Application of belief theory to similarity data fusion for use in analog searching and lead hopping. *J. Chem. Inf. Model.* **48,** 941–948 (2008).
33. Yıldırım, M. A., Goh, K.-I., Cusick, M. E., Barabási, A.-L. & Vidal, M. Drug–target network. *Nature Biotechnol.* **25,** 1119–1126 (2007).
34. Marshall, V. & Grosset, D. G. Role of dopamine transporter imaging in the diagnosis of atypical tremor disorders. *Mov. Disord.* **18** (suppl. 7), S22–S27 (2003).
35. Kuo, C. C., Huang, R. C. & Lou, B. S. Inhibition of Na$^+$ current by diphenhydramine and other diphenyl compounds: molecular determinants of selective binding to the inactivated channels. *Mol. Pharmacol.* **57,** 135–143 (2000).
36. Schoen, R. T. & Vender, R. J. Mechanisms of nonsteroidal anti-inflammatory drug-induced gastric damage. *Am. J. Med.* **86,** 449–458 (1989).
37. Kong, S. X., Hatoum, H. T., Zhao, S. Z., Agrawal, N. M. & Geis, S. G. Prevalence and cost of hospitalization for gastrointestinal complications related to peptic ulcers with bleeding or perforation: comparison of two national databases. *Am. J. Manag. Care* **4,** 399–409 (1998).
38. G., Perrone, M., Scilimati, A., Simone, L. & Vitale, P. Selective COX-1 inhibition: A therapeutic target to be reconsidered. *Curr. Med. Chem.* **17,** 3769–3805 (2010).
39. Akarasereenont, P., Tripatara, P., Chotewuttakorn, S., Palo, T. & Thaworn, A. The effects of estrone, estradiol and estriol on platelet aggregation induced by adrenaline and adenosine diphosphate. *Platelets* **17,** 441–447 (2006).
40. Norris, L. A. & Bonnar, J. Effect of oestrogen dose on whole blood platelet activation in women taking new low dose oral contraceptives. *Thromb. Haemost.* **72,** 926–930 (1994).
41. Leeson, P. D. & Springthorpe, B. The influence of drug-like concepts on decision-making in medicinal chemistry. *Nature Rev. Drug Discov.* **6,** 881–890 (2007).
42. Peters, J.-U., Schnider, P., Mattei, P. & Kansy, M. Pharmacological promiscuity: dependence on compound properties and target specificity in a set of recent Roche compounds. *ChemMedChem* **4,** 680–686 (2009).
43. Cosgrove, B. D. *et al.* Cytokine-associated drug toxicity in human hepatocytes is associated with signaling network dysregulation. *Mol. Biosyst.* **6,** 1195–1206 (2010).
44. Mestres, J., Gregori-Puigjané, E., Valverde, S. & Solé, R. V. Data completeness–the Achilles heel of drug-target networks. *Nature Biotechnol.* **26,** 983–984 (2008).
45. Mestres, J., Gregori-Puigjané, E., Valverde, S. & Solé, R. V. The topology of drug-target interaction networks: implicit dependence on drug properties and target families. *Mol. Biosyst.* **5,** 1051–1057 (2009).

Supplementary Information is linked to the online version of the paper at www.nature.com/nature.

Acknowledgements E.L. is a presidential postdoctoral fellow supported by the Education Office of the Novartis Institutes for Biomedical Research (co-mentors L.U. and B.K.S.). Supported by US National Institutes of Health grants GM71896 (to B.K.S. and J. Irwin), AG002132 (to S. Prusiner and B.K.S.), and GM93456 (to M.J.K.), and by QB3 Rogers Family Foundation 'Bridging-the-Gap' Award (to M.J.K.).

Author Contributions SEA calculations were undertaken by M.J.K. Target–ADR associations, networks and promiscuity analysis were by E.L. *In vitro* assays were directed by S.W., J.H. and L.U. PK and PD experiments were conducted by E.W. and P.L. Platelet aggregation study was designed and carried out by L.U. and S.C. Chlorotrianisene solubility and aggregation were conducted by A.K.D. The project was conceived and planned by B.K.S., J.J., D.M. and L.U. Overall analysis and writing was largely by E.L., M.J.K., B.K.S. and L.U. All authors contributed to the manuscript.

Author Information Reprints and permissions information is available at www.nature.com/reprints. The authors declare competing financial interests: details accompany the full-text HTML version of the paper at www.nature.com/nature. Readers are welcome to comment on the online version of this article at www.nature.com/nature. Correspondence and requests for materials should be addressed to J.J. (jeremy.jenkins@novartis.com), B.K.S. (shoichet@cgl.ucsf.edu) or L.U. (laszlo.urban@novartis.com).

doi:10.1038/nature11211

Structure of yeast Argonaute with guide RNA

Kotaro Nakanishi[1]*, David E. Weinberg[2,3]*, David P. Bartel[2,3] & Dinshaw J. Patel[1]

The RNA-induced silencing complex, comprising Argonaute and guide RNA, mediates RNA interference. Here we report the 3.2 Å crystal structure of *Kluyveromyces polysporus* Argonaute (KpAGO) fortuitously complexed with guide RNA originating from small-RNA duplexes autonomously loaded and processed by recombinant KpAGO. Despite their diverse sequences, guide-RNA nucleotides 1–8 are positioned similarly, with sequence-independent contacts to bases, phosphates and 2′-hydroxyl groups pre-organizing the backbone of nucleotides 2–8 in a near-A-form conformation. Compared with prokaryotic Argonautes, KpAGO has numerous surface-exposed insertion segments, with a cluster of conserved insertions repositioning the N domain to enable full propagation of guide–target pairing. Compared with Argonautes in inactive conformations, KpAGO has a hydrogen-bond network that stabilizes an expanded and repositioned loop, which inserts an invariant glutamate into the catalytic pocket. Mutation analyses and analogies to ribonuclease H indicate that insertion of this glutamate finger completes a universally conserved catalytic tetrad, thereby activating Argonaute for RNA cleavage.

RNA interference (RNAi) is a eukaryote-specific gene-silencing pathway triggered by double-stranded RNA (dsRNA)[1–3]. In this pathway, the ribonuclease (RNase) III enzyme Dicer first cleaves the dsRNA trigger into small interfering RNAs (siRNAs), which have 5′-monophosphates and pair to each other with two-nucleotide 3′ overhangs[4–6]. The siRNA duplex is incorporated into the effector protein Argonaute (AGO), at which point one of the strands (designated the passenger strand) is cleaved[7–9]. After the cleaved passenger strand is discarded, the resulting ribonucleoprotein complex (the RNA-induced silencing complex, or RISC) uses the remaining siRNA strand (designated the guide strand) to specify interactions with target RNAs[10,11]. If sequence complementarity between guide and target is extensive, AGO again catalyses cleavage, resulting in 'slicing' of the target RNA[12].

The first structures of full-length AGOs were of prokaryotic proteins from *Pyrococcus furiosus*[12] and *Aquifex aeolicus*[13]. Early structures revealed that the PIWI domain adopts an RNase H-like fold, thereby implicating AGO as the 'slicer' enzyme that mediates RNAi[12,14,15]. Because these prokaryotic enzymes bind 5′-phosphorylated guide DNAs rather than RNAs[13,16], subsequent structures featured the binary complex of *Thermus thermophilus* Ago (TtAGO) with guide DNA[17] and ternary complexes with target RNAs of varying length[18,19]. These studies shed light on the nucleation, propagation and cleavage steps of the AGO catalytic cycle[19,20]. However, the physiological role of prokaryotic AGOs is enigmatic; the origin of the guide DNA is unknown, and bacteria lack recognizable components of the RNAi pathway[21]. Therefore, attention has turned to eukaryotic AGOs, which use RNA guides and have protein-binding partners absent in bacteria[22]. Eukaryotic AGOs are also larger than prokaryotic AGOs because of insertion elements of unknown structure and function. Structures of individual domains and the MID-PIWI lobe within eukaryotic AGO have been determined[23–28], but structural characterization of the entire protein has remained a challenge.

Although *Saccharomyces cerevisiae* lacks RNAi, some closely related budding-yeast species were recently shown to have retained RNAi, thereby offering fresh possibilities for the study of the eukaryotic pathway[29]. We previously determined the structure and mechanism of Dicer from the budding yeast *Kluyveromyces polysporus*[30] and thus turned our attention to the AGO of this species.

Cleavage activity of budding-yeast AGO

K. polysporus AGO (Ago1) has the four conserved domains (N, PAZ, MID, PIWI) and two linker regions (L1, L2) found in other AGOs (Fig. 1a). It also has an amino-terminal extension, predicted to be disordered, which we removed to facilitate crystallization. The resulting protein, KpAGO, can substitute for the full-length protein when reconstituting RNAi in *S. cerevisiae* (Fig. 1b).

KpAGO and other budding-yeast AGOs have acidic side chains at the three positions corresponding to active-site residues in slicing-competent AGOs[31] (Supplementary Fig. 1), which suggested that KpAGO might also cleave target RNAs. Indeed, after incubation with a single-stranded guide RNA, recombinant KpAGO cleaved a matched target RNA at the expected position (Fig. 1c). To examine whether slicing occurs *in vivo*, we performed degradome sequencing from a related RNAi-containing yeast, *Saccharomyces castellii*. This procedure identifies polyadenylated RNAs containing 5′-monophosphates, including products of AGO-catalysed slicing[32,33]. Many *AGO1*-dependent degradome tags mapped to Y′-element transcripts (major targets of *S. castellii* RNAi[29]), and these tended to pair to endogenous siRNAs in the register that implicated cleavage across from positions 10–11 of the guide RNA, which was diagnostic of slicing[34] (Supplementary Fig. 2). These results indicate that budding-yeast AGO functions as a slicer during endogenous RNAi, and with the *in vitro* results establish KpAGO as a eukaryotic slicer suitable for structure–function analyses.

Structural architecture of eukaryotic AGO

We crystallized recombinant KpAGO purified from *Escherichia coli*. Extensive screening identified several crystals that were free of twinning, one of which diffracted to 3.2 Å resolution. A crystal of selenomethionine-substituted KpAGO yielded reflections suitable

---

[1]Structural Biology Program, Memorial Sloan-Kettering Cancer Center, New York, New York 10065, USA. [2]Whitehead Institute for Biomedical Research, 9 Cambridge Center, Cambridge, Massachusetts 02142, USA. [3]Howard Hughes Medical Institute and Department of Biology, Massachusetts Institute of Technology, Cambridge, Massachusetts 02139, USA.
*These authors contributed equally to this work.

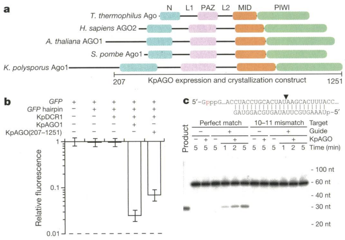

Figure 1 | **Cleavage activity of budding-yeast AGO. a**, Domain architectures of AGO proteins from *T. thermophilus*, *Homo sapiens*, *Arabidopsis thaliana*, *Schizosaccharomyces pombe* and *K. polysporus*. **b**, RNAi reconstituted in *S. cerevisiae* using *K. polysporus* genes. Median green fluorescent protein (GFP) intensity is plotted as a fraction of GFP-only control. Error bars, quartiles; dashed line, background fluorescence. **c**, Cleavage activity of KpAGO. RNAs labelled at a cap phosphate (red) and matching the guide (either perfectly or with mismatches to positions 10–11) were incubated with/without (+/−) KpAGO that had been pre-incubated in the presence/absence (+/−) of synthetic guide RNA. Product was resolved on a denaturing polyacrylamide gel alongside cap-labelled synthetic product (left) and RNA standards (migration shown on right; nt, nucleotide).

for phasing by single-wavelength anomalous dispersion (Supplementary Table 1; representative electron density is shown in Supplementary Fig. 3).

The overall structure of KpAGO resembles the bilobal architecture of its prokaryotic counterparts, but with expansions throughout the protein (Fig. 2a and Supplementary Fig. 4). Of the 19 insertion segments not found in prokaryotic AGOs[12,13,17], 11 were conserved segments (cS) found in all eukaryotic AGOs, albeit with some differences in secondary structure and length, whereas the remaining eight were variable segments (vS) found in only some eukaryotic AGOs (Supplementary Fig. 1). All insertion segments are external, generating new surfaces for potential interactions with AGO-binding proteins.

Autonomously loaded guide RNA

After modelling the KpAGO protein, the $F_o - F_c$ map revealed continuous residual electron density lying along the nucleic-acid-binding channel (Fig. 2b). This unanticipated density resembled that of an oligonucleotide and could be fit well with an RNA octamer (Fig. 2c and Supplementary Fig. 5a). Analysis of end-labelled polynucleotides extracted from soluble and crystalline KpAGO confirmed the presence of small RNAs (Fig. 2d and Supplementary Fig. 5b), the high-throughput sequencing of which identified a diverse population with a bimodal length distribution centring at 12 and 17 nucleotides (Supplementary Table 2 and Supplementary Fig. 5c, d).

The location of the copurifying RNAs suggested that they might represent functional guide RNAs. Supporting this interpretation, they had two features of budding-yeast guide RNAs: 5′ uridine enrichment (Fig. 2e) and the presence of 5′ monophosphate, indicated by both electron density (Fig. 2c) and a phosphatase-sensitive block of 5′-end labelling (Supplementary Fig. 5e)[29]. Moreover, the KpAGO preparation sliced an RNA containing a site complementary to a copurifying 17-nucleotide RNA comprising approximately 0.1% of our sequencing reads (Fig. 2f and Supplementary Fig. 5c). Slicing was at the anticipated linkage and sensitive to mismatches to guide nucleotides 10–11. Reactions showed initial burst kinetics, as observed previously

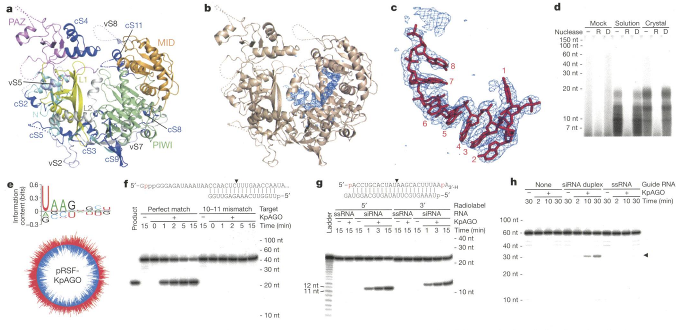
a
PAZ
cS4
vS8
cS11
MID
L1
vS5
cS2
N
L2
cS5
cS8
cS3
vS7
PIWI
vS2
cS9
b
c
8
7
1
6
5
4
3
2
d
Mock
Solution
Crystal
Nuclease
R
D
150 nt -
100 nt -
60 nt -
40 nt -
30 nt -
20 nt -
10 nt -
7 nt -
e
Information content (bits)
0.6
0.3
0
−0.3
pRSF-KpAGO
f
5′-GpppGGGAGAUAAAUAACCAACUCUUUGAACCAAUA...
GGUUGAGAAACUUGGUUp-5′
Perfect match
10–11 mismatch
Target
KpAGO
Time (min)
Product
- 100 nt
- 60 nt
- 40 nt
- 30 nt
- 20 nt
- 10 nt
g
5′-pACCUGCACUAUAAGCACUUUAApA3′-H
GAUGGACGUGAUAUUCGUGAAAUp-5′
5′
3′
Radiolabel
ssRNA
siRNA
RNA
KpAGO
Time (min)
Ladder
12 nt
11 nt
- 40 nt
- 30 nt
- 20 nt
- 10 nt
h
None
siRNA duplex
ssRNA
Guide RNA
KpAGO
Time (min)
100 nt -
60 nt -
40 nt -
30 nt -
20 nt -
10 nt -

Figure 2 | **KpAGO architecture and copurifying RNA. a**, KpAGO protein structure, with N (cyan), linker L1 (yellow), PAZ (violet), linker L2 (grey), MID (orange), and PIWI (green) domains in ribbon representation. Constant (cS) and variable (vS) insertion segments, blue and slate, respectively; disordered regions, dotted lines. **b**, $F_o - F_c$ map (blue) contoured at 2.8σ before modelling RNA. **c**, Simulated-annealing omit map (blue) contoured at 3.5σ around final RNA model (red). **d**, Nuclease sensitivity of copurifying nucleic acid. End-labelled polynucleotides extracted from the indicated KpAGO samples were either untreated (−) or incubated with RNase (R) or DNase (D) before analysis on a denaturing gel. **e**, Nucleotide composition and origin of copurifying RNA. Sequences were analysed for enriched or depleted nucleotides (positive or negative bits, respectively) at each of the first eight positions (top). Numbers of sequencing reads mapping along each strand of the KpAGO expression plasmid are indicated (bottom, log scale). **f**, Cleavage activity guided by copurifying RNA. As in Fig. 1c, except labelled RNAs were designed to match the indicated copurifying RNA. **g**, Autonomous duplex loading and passenger-strand cleavage. Labelled single-stranded RNA (ssRNA) or siRNA duplex was incubated with or without KpAGO. **h**, Autonomous duplex loading and target cleavage. As in Fig. 1c, except KpAGO and RNA concentrations were reduced by 90% and 99.95%, respectively.

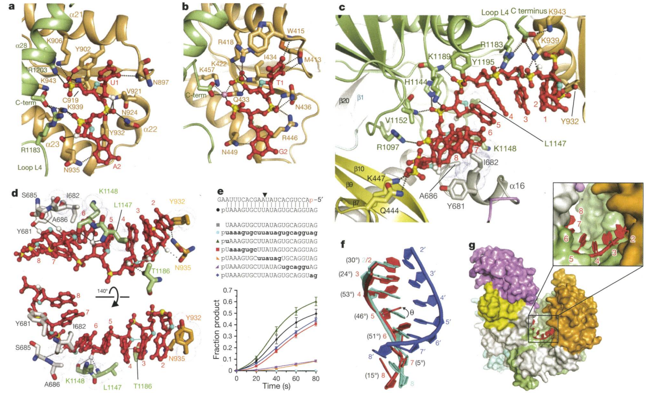
a
α21
α28
K906
Y902
R1203
K943
C-term
C919
K939
U1
N897
V921
N924
Y932
α22
R1183
α23
Loop L4
N935
A2
b
W415
R418
I434
M413
K422
K457
C-term
T1
Q433
N436
R446
N449
G2
c
Loop L4 C terminus K943
R1183
K939
K1189
Y1195
H1144
β20
β1
V1152
4
3
1
Y932
2
5
6
L1147
R1097
7
K1148
8
I682
β10
K447
β9
β7
A686
α16
Y681
Q444
d
S685
I682
K1148
L1147
2
Y932
6
3
A686
5
4
Y681
8
7
T1186
N935
140°
8
Y681
7
I682
6
5
Y932
S685
4
3
2
N935
A686
K1148
L1147
T1186
e
GAAUUUCACGAAUAUCACGUCCAp–5′
● pUAAAGUGCUUAUAGUGCAGGUAG
■ UAAAGUGCUUAUAGUGCAGGUAG
● p**uaaagugcuuauagugcagguag**
▲ p**u**AAAGUGCUUAUAGUGCAGGUAG
■ pU**aaagugc**UUAUAGUGCAGGUAG
◣ pUAAAGUGC**uuauag**UGCAGGUAG
◢ pUAAAGUGCUUAUAG**ugcaggu**AG
◆ pUAAAGUGCUUAUAGUGCAGGU**ag**
Fraction product
0.7
0.6
0.5
0.4
0.3
0.2
0.1
0
0
20
40
60
80
Time (s)
f
2′
(30°) 2/2
(24°) 3
3′
(53°) 4
4′
(46°) 5
θ
5′
(51°) 6
6′
7′
8′
7 (5°)
(15°) 8
8
g
8
7
6
2
3
5
4

Figure 3 | Organization of the guide RNA. a, b, The 5′-nucleotide-binding pockets of KpAGO (**a**) and TtAGO[17] (**b**). Colours, as in Fig. 2a; protein, ribbon representation; highlighted residues and RNA, stick representation; O2′, O4′ and phosphate, white, cyan and yellow, respectively; hydrogen bonds, dotted lines. **c, d,** Interactions involving bases and either phosphates (**c**) or 2′-OH groups (**d**) of the seed region. Intermolecular (black) and intramolecular (blue) hydrogen bonds, dotted lines; hydrophobic interactions, van der Waals radii. **e,** Effects of guide-strand modifications on duplex loading and passenger-strand cleavage. KpAGO was incubated with siRNA duplexes with the indicated guide strands; p, 5′ monophosphate; upper case, 2′-OH; lower case bold, 2′-deoxy. The fraction of labelled passenger strand cleaved is plotted (average of three independent replicates; error bars, standard deviations; points connected by smooth curves). **f,** Superposition of guide-RNA nucleotides 2–8 (red) on A-form RNA (cyan and blue). Dihedral angles (θ) between guide-RNA bases and those of A-form RNA are in parentheses. **g,** Solvent-exposed seed nucleotides (red). KpAGO surface is rendered, domains coloured as in Fig. 2a.

for metazoan AGOs[31,35–38], although addition of Triton enabled sustained product formation (Supplementary Fig. 5f), perhaps by facilitating a conformational change that promotes product release.

Most copurifying RNAs mapped to the KpAGO expression plasmid (Fig. 2e and Supplementary Fig. 6) in a manner suggesting origins from siRNA-like duplexes loaded into KpAGO with subsequent passenger-strand cleavage (Supplementary Fig. 7). For this to occur, KpAGO must be able to load siRNA duplexes in the absence of RISC-loading factors. Indeed, purified KpAGO incubated with an siRNA duplex generated products diagnostic of passenger-strand cleavage (Fig. 2g) and formed active RISC able to slice cognate target RNA (Fig. 2h). Loading was more efficient with duplex than with single-stranded guide and occurred asymmetrically in a manner consistent with preference for 5′ uridine on the guide strand (Fig. 2h and Supplementary Fig. 8a–c).

We conclude that KpAGO can autonomously load an siRNA duplex, lose the passenger strand and then slice targets. This conclusion counters the prevailing view that loading of siRNA duplexes to form functional RISC requires RISC-loading factors[11]. We suspect that other AGOs might also autonomously load siRNA duplexes and that reports to the contrary resulted from assaying target-RNA slicing under conditions in which AGO retained inhibitory passenger-strand fragments. Autonomous loading explains how KpAGO RISC fortuitously formed in the absence of other RNAi proteins. In contrast to previous preparations of AGO complexes used for structural studies, the formation of KpAGO RISC through loading of a duplex resembles the physiological RISC-assembly pathway. From this perspective, the KpAGO structure reflects the natural state of eukaryotic RISC.

Organization of the guide RNA

Electron density corresponding to the base of nucleotide 1 was smaller than that corresponding to most other positions (Supplementary Fig. 9), which agreed with our sequencing results showing that KpAGO-bound RNAs were diverse but enriched for a 5′ uridine (Fig. 2e). Therefore, we modelled the first nucleotide as uridine and the next seven as adenine (the generic nucleotide used to minimize bias during refinement[39]) and refined the final structure as a KpAGO–pUAAAAAAAp binary complex (Supplementary Table 1 and Supplementary Fig. 10).

The guide-strand nucleotides 2–8 run along the nucleic-acid-binding channel, from the MID domain to the L2 domain. These nucleotides, including their bases, have electron-density quality resembling that of the KpAGO protein, even though this density represents a composite of thousands of different RNAs. Thus, for this segment of the guide RNA, known as the seed region, diverse RNA sequences are all presented in essentially the same orientation. The electron density disappeared after the ninth nucleotide (Fig. 2b, c), even though most copurifying RNAs were longer than nine nucleotides (Supplementary Fig. 5d). This density loss indicates that guide-RNA 3′ halves are either disordered or adopt diverse sequence-specific conformations. In addition, the PAZ domain is not well ordered, as observed in TtAGO complexes in which the PAZ domain has released the 3′ end of the guide[19], consistent with the idea that KpAGO holds the guide RNA without assistance from the PAZ domain.

Like prokaryotic AGOs[15,17–19,40], KpAGO recognizes the 5′ phosphate of the guide, the notable difference being that KpAGO uses the ammonium group of Lys 939 rather than a divalent cation (despite Mn^{2+} in the crystallization buffer) to neutralize the negative charge resulting from the close juxtaposition of the C-terminal carboxylate and phosphates 1 and 3 (Fig. 3a, b). The inserted carboxy terminus is anchored by Lys 939 and Lys 943 (Fig. 3a), with mutation of either residue impeding guide-RNA binding in *Drosophila* AGO1 (ref. 28). Another distinct facet involves Arg 1183, which hydrogen bonds with the C-terminal carboxylate and phosphate 4 (Fig. 3c). In the free *Neurospora crassa* QDE-2 (NcQDE-2) MID-PIWI structure[28] the analogous arginine is in a disordered loop, suggesting that guide RNA recruits Arg 1183 to the 5′-phosphate–binding pocket. Notably, conservation of Lys 939 and Arg 1183 is restricted to eukaryotic AGOs (Supplementary Fig. 1).

The Asn 897 main-chain amide interacts with the O2 carbonyl of the uridine at position 1 (Fig. 3a). Because analogous interactions with O2 of cytidine and N3 of purines would be isosteric, this hydrogen bond cannot explain the preference for a 5′ uridine. The preference might instead be attributed to the relatively weak stacking and pairing of uridine, which would facilitate the requisite flipping out of nucleotide 1 during siRNA loading[16,40].

KpAGO interacts with phosphates of the seed region primarily using contacts homologous to those observed in prokaryotic AGO complexes[16–19,40] (Fig. 3c). Structures of prokaryotic complexes, however, have not revealed intermolecular contacts to the guide-RNA 2′-OH groups. We find that KpAGO forms hydrogen bonds with most 2′-OH groups of the seed, using main-chain atoms at positions 2, 5 and 6 and hydroxyl groups of Thr 1186 and Tyr 681 at positions 4 and 7, respectively (Fig. 3d). We also observe an intra-RNA hydrogen bond between the 2′-OH group at position 3 and O4′ at position 4, a type of interaction proposed to facilitate base-pair fluctuations in A-form RNA helices[41]. A second intra-RNA hydrogen bond involves the 2′-OH group at position 1 and a non-bridging oxygen of phosphate 2, as previously observed in *Archaeoglobus fulgidus* PIWI–siRNA complex structures[16,40].

To examine the contributions of guide-strand 5′ phosphate and 2′-OH groups, we monitored autonomous loading and passenger-strand cleavage of modified siRNA duplexes. Removing the monophosphate or substituting all guide-strand 2′-OH groups with 2′-H (deoxy) greatly impaired activity (Fig. 3e and Supplementary Fig. 11), consistent with observations in transfected human cells[42,43]. To learn more about the 2′-OH groups contributing to this effect, we compared guide RNAs with deoxy substitutions at positions 1, 2–8, 9–14, 15–21 and 22–23. Substitution of the 2′-OH group at position 1 enhanced activity (perhaps by facilitating flipping out of nucleotide 1), whereas substitutions in all other regions impaired activity (Fig. 3e and Supplementary Fig. 11). Deoxy substitution at positions 2–8 impaired activity to a similar degree as at positions 22–23, which are presumably recognized by the PAZ domain[23–25]. Thus, the 2′-OH groups within the seed region contribute to duplex loading or passenger-strand cleavage. Nonetheless, greater effects were observed at positions 9–14 and 15–21, the understanding of which will require structural studies of additional states along the eukaryotic RISC-assembly pathway.

Together, contacts to the phosphate and 2′-OH groups maintain the sugar–phosphate backbone of the single-stranded guide-RNA seed in a near-A-form conformation resembling that of the siRNA duplex (Fig. 3f). Maintaining this conformation pre-organizes the seed backbone for pairing to the target, as anticipated from studies of microRNA targeting[1] and supported by structural and biophysical studies[16,40,44]. Also as anticipated, the bases of the seed nucleotides are stacked, with Watson–Crick faces (particularly those of nucleotides 2–4) displayed to solvent and accessible to nucleate pairing to target RNA (Fig. 3g).

The surprising feature of the guide-RNA conformation was the tilting of the bases away from the orientation required for helical pairing (Fig. 3f). KpAGO makes hydrophobic contacts with the bases at positions 2, 5 and 6 while anchoring the sugar–phosphate backbone (Fig. 3c, d). Base 2 packs against Tyr 932 (Fig. 3d), which is conserved as Tyr or Thr in eukaryotic AGOs (Supplementary Fig. 1) and thus might represent a conserved hydrophobic interaction that facilitates the flipping out of nucleotide 1 by preventing its stacking on base 2. As observed in structures of prokaryotic AGO complexes[16–19,40], base 2 is recognized at N3 (purines) or O2 (pyrimidines) by the side chain of Asn 935 (Fig. 3d), which is conserved throughout all AGOs. Bases 5 and 6 are surrounded by a hydrophobic pocket comprising Ile 682, Ala 686, Leu 1147 and Lys 1148 (Fig. 3d). Bases 3 and 4 make no contact with KpAGO but are nonetheless tilted because of continuous stacking of the seed bases (Fig. 3c, d). Untilting of the seed stack, which would accompany nucleation of target pairing at positions 2–4, might disfavour contacts to Ile 682 and neighbouring residues, thereby facilitating repositioning of α16, a helix that would otherwise block full seed pairing. Such changes in base tilting and α16 might communicate the presence of target RNA.

Potentially unobstructed guide–target pairing

To compare the architectures of eukaryotic and prokaryotic AGOs, we structurally aligned each domain of KpAGO on its TtAGO counterpart. Except for the N domain, each of the domains superimposed well (Supplementary Fig. 12). The structural difference between the N domains is attributed to cS1, cS3 and vS2 (Fig. 4a, b). cS1 and cS3 cluster together with cS7 and cS10 (Supplementary Fig. 13a) such that they bury a space observed in prokaryotic AGO structures and concomitantly lengthen the nucleic-acid-binding channel[12,13,17–19] (Fig. 4c, d). These insertion segments interact with the L2-linker and PIWI domains through a hydrogen-bond network involving residues that are conserved throughout eukaryotic AGOs (Supplementary Figs 1 and 13a), which indicates that an extended nucleic-acid-binding channel is a general feature of eukaryotic AGOs.

In all crystallized conformations of TtAGO, the N domain blocks the channel and prevents propagation of guide–target pairing beyond position 16 (ref 19) (Fig. 4c and Supplementary Fig. 13c, d). In addition to lengthening the nucleic-acid-binding channel, the cS1/3/10 cluster positions the KpAGO N domain such that a slight widening of the channel would allow pairing to propagate to the 3′ end of the guide RNA (Fig. 4d and Supplementary Fig. 13b). The potential for unobstructed propagation of guide–target pairing is consistent with the prevalence of pairing throughout the 3′ region of plant small RNAs that guide target cleavage[45] and the contribution of such pairing to the stability of guide–target association *in vitro*[35,37].

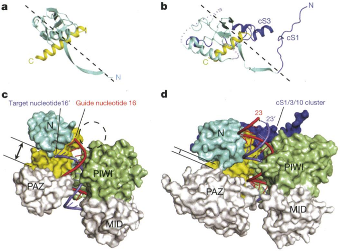

Figure 4 | An extended, potentially unobstructed nucleic-acid-binding channel in KpAGO. **a**, **b**, Position of N domain (cyan) relative to L1-linker domain (yellow) in TtAGO[19] (**a**) and KpAGO (**b**). Domains are oriented based on their N-terminal beta strands (dashed line connects strand termini). Colours, as in Fig. 2a. **c**, **d**, Channels of TtAGO ternary complex[19] (**c**) and KpAGO with modelled A-form duplex (**d**). Protein surfaces are rendered, highlighting distances between the N and PAZ domains (parallel lines) and the cS1/3/10 cluster (blue), which fills a cavity (dashed circle).

Glu 1013 completes a catalytic tetrad

When comparing the structures of KpAGO and the free NcQDE-2 MID-PIWI lobe[28], we observed notable differences in loops L1 and L2 (Supplementary Table 3). In KpAGO, loop L2 expands by partial unfolding of α25 (Fig. 5a) and packs into a cavity, such that the invariant Glu 1013 side chain inserts into the catalytic pocket, near the three Asp residues of the active site (Fig. 5b). This conformation is enabled by the movement of loop L1, which otherwise blocks access to the catalytic pocket (Fig. 5c). Opening of the loop L1 gate in KpAGO is accompanied by a conformational transition of cS11 and hydrophobic packing between aliphatic side chains on loop L1 and cS11. Notably, deletion of cS11 from *Drosophila* AGO1 inhibits guide-RNA binding and abolishes silencing activity[28].

The plugged-in conformation, in which the Glu 1013 finger is inserted into the catalytic pocket, is stabilized by an extensive hydrogen-bond network, with Glu 1013 bridging His 977 and Arg 1045, and loop L2 main-chain atoms interacting with Arg 1045 and Glu 1060 (Fig. 5b). These four residues are conserved throughout eukaryotic AGOs (and even most of the PIWI clade; Supplementary Fig. 1). Glu 1013, Arg 1045 and Glu 1060 are also conserved throughout prokaryotic AGOs, prompting a search for a similar plugged-in conformation in the available structures[12,13,17–19,28]. We found both plugged-in and unplugged conformations of TtAGO, with striking parallels to the eukaryotic hydrogen-bond network and correlated loop movements (Fig. 5a–f). The plugged-in conformation was observed only in complexes in which the PAZ domain released the 3′ end of the guide and TtAGO assumed its catalytically active state (Supplementary Table 3). In contrast, the inactive states—either those of the apo proteins or complexes in which the PAZ domain engages the guide 3′ end—resembled the unplugged conformation. These observations indicate that the plugged-in conformation of loop L2 is correlated with release of the 3′ end of the guide and formation of active RISC. Supporting the functional importance of the plugged-in conformation, mutation of any of the four residues of the KpAGO hydrogen-bond network impaired RNAi (Fig. 5g).

The structures of ternary TtAGO complexes in the plugged-in conformation show the position of loop L2 in the context of guide and target strands. TtAGO loop L2 interacts with the guide DNA at positions 11–15 (Supplementary Table 3)[19]. Moreover, the carboxyl group of the glutamate finger approaches both the 2′-OH of the nucleotide adjacent to the scissile phosphate and one of the two active-site divalent metal ions (Fig. 5h), which indicates that the glutamate finger might act as a catalytic residue. Indeed, simultaneous coordination of the analogous 2′-OH and metal ion is the role of Glu 109 in the 'DEDD' catalytic tetrad at the active site of *Bacillus halodurans* RNase H1 (ref. 46). Although the PIWI domain of AGO has an RNase H fold, only a conserved 'DDX' catalytic triad (where 'X' is generally Asp or His) had been recognized in AGOs with slicer

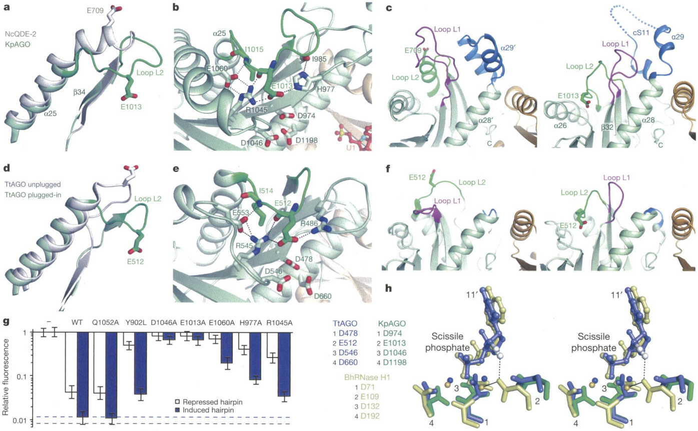
a
E709
NcQDE-2
KpAGO
Loop L2
β34
α25
E1013
b
α25
I1015
I985
E1060
E1013
H977
R1045
D974
D1046
D1198
U1
c
Loop L1
E709
α29′
Loop L2
α28′
C
cS11
α29
Loop L1
Loop L2
E1013
α26
β32
α28
C
d
TtAGO unplugged
TtAGO plugged-in
Loop L2
E512
e
I514
E512
E553
R486
R545
D478
D546
D660
f
E512
Loop L2
Loop L1
Loop L1
Loop L2
E512
g
–
WT
Q1052A
Y902L
D1046A
E1013A
E1060A
H977A
R1045A
Relative fluorescence
1
0.1
0.01
Repressed hairpin
Induced hairpin
TtAGO
1 D478
2 E512
3 D546
4 D660
KpAGO
1 D974
2 E1013
3 D1046
4 D1198
BhRNase H1
1 D71
2 E109
3 D132
4 D192
h
11′
Scissile phosphate
3
2
4
1
11′
Scissile phosphate
3
2
4
1

Figure 5 | A plugged-in glutamate finger at the active site. **a**, Superposition of α25 and β34 of KpAGO (green) on counterparts of NcQDE-2 MID-PIWI lobe (grey), highlighting the extended loop L2 (dark green). **b**, Hydrogen-bond network stabilizing the plugged-in loop L2. Loop L2, dark green; otherwise, as in Fig. 3a. **c**, Closed (left) and open (right) configurations of the loop L1 gate (purple) in NcQDE-2 MID-PIWI lobe and KpAGO, respectively. cS11, blue; otherwise, as in panel **b**. **d**, Superposition of the region flanking loop L2 in the unplugged (grey) and plugged-in (green) conformations of TtAGO, depicted as in panel **a**. **e**, Hydrogen-bond network stabilizing the plugged-in loop L2 in TtAGO, depicted as in panel **b**. **f**, Closed and open configurations of the loop L1 gate in the unplugged and plugged-in conformations of TtAGO, respectively, depicted as in panel **c**. **g**, RNAi reconstituted in *S. cerevisiae* using wild-type (WT) *K. polysporus AGO1* or genes with the indicated substitutions. Silencing was monitored under either permissive (induced hairpin, blue bars) or stringent (repressed hairpin, open bars) conditions. Q1052 and Y902, conserved residues insensitive and sensitive to substitution, respectively[28], were included as controls. Dashed lines (blue and black), background fluorescence (permissive and stringent conditions, respectively); otherwise, as in Fig. 1b. **h**, Stereoview of KpAGO catalytic residues (green) superpositioned with catalytic residues, divalent cations, scissile phosphate and adjacent nucleoside in TtAGO (blue) and *B. halodurans* RNase H1 (BhRNase H1, yellow) ternary complexes.

activity[47,48]. On the basis of analogy to RNase H, a fourth catalytic residue had been suspected, but previous searches for this missing component had focused on the residues corresponding to Arg 1045 and Glu 1060 (refs 12, 13, 31, 46 and 47), whose conservation and proximity to the catalytic pocket are now explained instead by their roles in stabilizing the plugged-in conformation (Fig. 5b). In support of the glutamate finger as the missing catalytic residue that helps to coordinate an active-site metal ion (either directly or through outer-sphere contacts), the putative DEDD catalytic tetrads in the plugged-in conformations of both TtAGO and KpAGO are nearly isosteric with the RNase H DEDD tetrad (Fig. 5h). Moreover, when we assayed RNAi, only mutation of Glu 1013 abrogated RNAi to the extent observed for mutation of Asp 1046, a previously identified active-site residue (Fig. 5g). Thus, we propose that the glutamate finger constitutes the second residue of a universally conserved RNase-H-like DEDX catalytic tetrad at the active site of slicing AGOs.

Our new insights suggest the following model for AGO loading and catalysis. The apo protein in the unplugged conformation binds the siRNA duplex, in part using contacts between the two-nucleotide overhang of the guide strand and the PAZ domain. As the duplex loads and the 3′ end of the guide stand is released from the PAZ domain, the glutamate finger inserts into the active site, thereby completing the DEDX catalytic tetrad to enable cleavage of the passenger strand. After discarding the passenger-strand fragments, the resulting RISC remains in a plugged-in conformation resembling that of the current structure and is competent to bind and cleave suitably paired target RNAs.

While our manuscript was in review, a structure of human AGO2 (HsAGO2; also known as EIF2C2) with RNA of unknown biochemical origin and function was reported[49]. The authors noted many contacts to the RNA 5′ monophosphate and sugar–phosphate backbone analogous to those of KpAGO. Our inspection of the HsAGO2 structure further revealed that it also has an extended nucleic-acid-binding channel, an N domain positioned to allow unobstructed guide–target pairing, and a plugged-in glutamate finger that completes a DEDH catalytic tetrad (Supplementary Fig. 14). These similarities indicate that the HsAGO2 structure (for which conserved residues were mutated to improve diffraction) has features of active RISC and that studies of KpAGO will continue to provide insights relevant to metazoan AGOs.

In contrast to RNase H, which forms its active site during initial folding, AGO requires a conformational change to form its active site. What might explain this difference between these two related RNases? The constitutive active site of RNase H is well-suited to its role in nonspecifically cleaving RNA–DNA hybrids, whereas proper AGO function requires high specificity. Coupling siRNA duplex loading (in part through recognition by the PAZ domain) with active-site formation imparts specificity to AGO, thereby preventing it from cleaving any base-paired RNA. After passenger-strand cleavage and removal, activity of the licensed AGO is restricted by its guide RNA. In this way, AGO activity is tightly controlled and spurious endonucleolytic cleavage is prevented. The previous view was that among proteins adopting the RNase H fold, RNase H enzymes were unique in having a catalytic tetrad, whereas the related endonucleases of this protein superfamily (including AGO) were missing the active-site residue corresponding to Glu 1013 (ref. 48). Our findings revising this view imply that some other proteins for which only a catalytic triad has hitherto been identified (for example, bacterial UvrC DNA repair protein) might also use the conditional insertion of a ‘missing’ catalytic residue to impart specificity.

METHODS SUMMARY

KpAGO was overexpressed in *Escherichia coli* as a His–SUMO-tagged fusion. Native and SeMet-substituted crystals were obtained by sitting-drop vapour diffusion at 20 °C. The phase was determined by the single-wavelength anomalous dispersion method with selenium anomalous signals. Cleavage assays were performed with synthetic or transcribed RNA in 30 mM Tris-HCl pH 7.5, 130 mM KCl, 10 mM NaCl, 1.1 mM MgCl$_2$, 0.1 mM EDTA, 1.3 mM dithiothreitol (DTT) and 5% glycerol, including 0.1% Triton X-100 where indicated. Yeast manipulations, *in vivo* assays and high-throughput sequencing were essentially as described previously[29,32]. Details of all procedures are listed in Methods.

Full Methods and any associated references are available in the online version of the paper at www.nature.com/nature.

Received 23 April; accepted 11 May 2012.
Published online 18 May 2012.

1. Bartel, D. P. MicroRNAs: genomics, biogenesis, mechanism, and function. *Cell* **116,** 281–297 (2004).
2. Meister, G. & Tuschl, T. Mechanisms of gene silencing by double-stranded RNA. *Nature* **431,** 343–349 (2004).
3. Malone, C. D. & Hannon, G. J. Small RNAs as guardians of the genome. *Cell* **136,** 656–668 (2009).
4. Bernstein, E., Caudy, A. A., Hammond, S. M. & Hannon, G. J. Role for a bidentate ribonuclease in the initiation step of RNA interference. *Nature* **409,** 363–366 (2001).
5. Elbashir, S. M., Lendeckel, W. & Tuschl, T. RNA interference is mediated by 21- and 22-nucleotide RNAs. *Genes Dev.* **15,** 188–200 (2001).
6. Hutvágner, G. *et al.* A cellular function for the RNA-interference enzyme Dicer in the maturation of the *let-7* small temporal RNA. *Science* **293,** 834–838 (2001).
7. Matranga, C., Tomari, Y., Shin, C., Bartel, D. P. & Zamore, P. D. Passenger-strand cleavage facilitates assembly of siRNA into Ago2-containing RNAi enzyme complexes. *Cell* **123,** 607–620 (2005).
8. Miyoshi, K., Tsukumo, H., Nagami, T., Siomi, H. & Siomi, M. C. Slicer function of *Drosophila* Argonautes and its involvement in RISC formation. *Genes Dev.* **19,** 2837–2848 (2005).
9. Rand, T. A., Petersen, S., Du, F. & Wang, X. Argonaute2 cleaves the anti-guide strand of siRNA during RISC activation. *Cell* **123,** 621–629 (2005).
10. Tomari, Y. & Zamore, P. D. Perspective: machines for RNAi. *Genes Dev.* **19,** 517–529 (2005).
11. Carthew, R. W. & Sontheimer, E. J. Origins and mechanisms of miRNAs and siRNAs. *Cell* **136,** 642–655 (2009).
12. Song, J. J., Smith, S. K., Hannon, G. J. & Joshua-Tor, L. Crystal structure of Argonaute and its implications for RISC slicer activity. *Science* **305,** 1434–1437 (2004).
13. Yuan, Y. R. *et al.* Crystal structure of *A. aeolicus* argonaute, a site-specific DNA-guided endoribonuclease, provides insights into RISC-mediated mRNA cleavage. *Mol. Cell* **19,** 405–419 (2005).
14. Liu, J. *et al.* Argonaute2 is the catalytic engine of mammalian RNAi. *Science* **305,** 1437–1441 (2004).
15. Parker, J. S., Roe, S. M. & Barford, D. Crystal structure of a PIWI protein suggests mechanisms for siRNA recognition and slicer activity. *EMBO J.* **23,** 4727–4737 (2004).
16. Ma, J. B. *et al.* Structural basis for 5′-end-specific recognition of guide RNA by the *A. fulgidus* Piwi protein. *Nature* **434,** 666–670 (2005).
17. Wang, Y., Sheng, G., Juranek, S., Tuschl, T. & Patel, D. J. Structure of the guide-strand-containing argonaute silencing complex. *Nature* **456,** 209–213 (2008).
18. Wang, Y. *et al.* Structure of an argonaute silencing complex with a seed-containing guide DNA and target RNA duplex. *Nature* **456,** 921–926 (2008).
19. Wang, Y. *et al.* Nucleation, propagation and cleavage of target RNAs in Ago silencing complexes. *Nature* **461,** 754–761 (2009).
20. Parker, J. S. How to slice: snapshots of Argonaute in action. *Silence* **1,** 3 (2010).
21. Makarova, K. S., Wolf, Y. I., van der Oost, J. & Koonin, E. V. Prokaryotic homologs of Argonaute proteins are predicted to function as key components of a novel system of defense against mobile genetic elements. *Biol. Direct* **4,** 29 (2009).
22. Meister, G. *et al.* Identification of novel argonaute-associated proteins. *Curr. Biol.* **15,** 2149–2155 (2005).
23. Lingel, A., Simon, B., Izaurralde, E. & Sattler, M. Structure and nucleic-acid binding of the *Drosophila* Argonaute 2 PAZ domain. *Nature* **426,** 465–469 (2003).
24. Yan, K. S. *et al.* Structure and conserved RNA binding of the PAZ domain. *Nature* **426,** 468–474 (2003).
25. Ma, J. B., Ye, K. & Patel, D. J. Structural basis for overhang-specific small interfering RNA recognition by the PAZ domain. *Nature* **429,** 318–322 (2004).
26. Boland, A., Tritschler, F., Heimstadt, S., Izaurralde, E. & Weichenrieder, O. Crystal structure and ligand binding of the MID domain of a eukaryotic Argonaute protein. *EMBO Rep.* **11,** 522–527 (2010).
27. Frank, F., Sonenberg, N. & Nagar, B. Structural basis for 5′-nucleotide base-specific recognition of guide RNA by human AGO2. *Nature* **465,** 818–822 (2010).
28. Boland, A., Huntzinger, E., Schmidt, S., Izaurralde, E. & Weichenrieder, O. Crystal structure of the MID-PIWI lobe of a eukaryotic Argonaute protein. *Proc. Natl Acad. Sci. USA* **108,** 10466–10471 (2011).
29. Drinnenberg, I. A. *et al.* RNAi in budding yeast. *Science* **326,** 544–550 (2009).
30. Weinberg, D. E., Nakanishi, K., Patel, D. J. & Bartel, D. P. The inside-out mechanism of Dicers from budding yeasts. *Cell* **146,** 262–276 (2011).
31. Rivas, F. V. *et al.* Purified Argonaute2 and an siRNA form recombinant human RISC. *Nature Struct. Mol. Biol.* **12,** 340–349 (2005).
32. Addo-Quaye, C., Eshoo, T. W., Bartel, D. P. & Axtell, M. J. Endogenous siRNA and miRNA targets identified by sequencing of the *Arabidopsis* degradome. *Curr. Biol.* **18,** 758–762 (2008).
33. German, M. A. *et al.* Global identification of microRNA-target RNA pairs by parallel analysis of RNA ends. *Nature Biotechnol.* **26,** 941–946 (2008).

34. Elbashir, S. M., Martinez, J., Patkaniowska, A., Lendeckel, W. & Tuschl, T. Functional anatomy of siRNAs for mediating efficient RNAi in *Drosophila melanogaster* embryo lysate. *EMBO J.* **20,** 6877–6888 (2001).
35. Haley, B. & Zamore, P. D. Kinetic analysis of the RNAi enzyme complex. *Nature Struct. Mol. Biol.* **11,** 599–606 (2004).
36. Martinez, J. & Tuschl, T. RISC is a 5′ phosphomonoester-producing RNA endonuclease. *Genes Dev.* **18,** 975–980 (2004).
37. Ameres, S. L., Martinez, J. & Schroeder, R. Molecular basis for target RNA recognition and cleavage by human RISC. *Cell* **130,** 101–112 (2007).
38. Förstemann, K., Horwich, M. D., Wee, L., Tomari, Y. & Zamore, P. D. *Drosophila* microRNAs are sorted into functionally distinct argonaute complexes after production by dicer-1. *Cell* **130,** 287–297 (2007).
39. Frazão, C. *et al.* Unravelling the dynamics of RNA degradation by ribonuclease II and its RNA-bound complex. *Nature* **443,** 110–114 (2006).
40. Parker, J. S., Roe, S. M. & Barford, D. Structural insights into mRNA recognition from a PIWI domain-siRNA guide complex. *Nature* **434,** 663–666 (2005).
41. Pan, Y. & MacKerell, A. D. Jr. Altered structural fluctuations in duplex RNA versus DNA: a conformational switch involving base pair opening. *Nucleic Acids Res.* **31,** 7131–7140 (2003).
42. Schwarz, D. S., Hutvágner, G., Haley, B. & Zamore, P. D. Evidence that siRNAs function as guides, not primers, in the *Drosophila* and human RNAi pathways. *Mol. Cell* **10,** 537–548 (2002).
43. Chiu, Y. L. & Rana, T. M. siRNA function in RNAi: a chemical modification analysis. *RNA* **9,** 1034–1048 (2003).
44. Parker, J. S., Parizotto, E. A., Wang, M., Roe, S. M. & Barford, D. Enhancement of the seed-target recognition step in RNA silencing by a PIWI/MID domain protein. *Mol. Cell* **33,** 204–214 (2009).
45. Mallory, A. C. *et al.* MicroRNA control of *PHABULOSA* in leaf development: importance of pairing to the microRNA 5′ region. *EMBO J.* **23,** 3356–3364 (2004).
46. Nowotny, M., Gaidamakov, S. A., Crouch, R. J. & Yang, W. Crystal structures of RNase H bound to an RNA/DNA hybrid: substrate specificity and metal-dependent catalysis. *Cell* **121,** 1005–1016 (2005).
47. Hall, T. M. Structure and function of argonaute proteins. *Structure* **13,** 1403–1408 (2005).
48. Nowotny, M. Retroviral integrase superfamily: the structural perspective. *EMBO Rep.* **10,** 144–151 (2009).
49. Schirle, N. T. & Macrae, I. J. The crystal structure of human Argonaute2. *Science* http://dx.doi.org/10.1126/science.1221551 (26 April 2012).

Supplementary Information is linked to the online version of the paper at www.nature.com/nature.

Acknowledgements We thank K. Rajashankar for data processing and phasing, V. Auyeung and D. Shechner for discussions, the Whitehead Genome Technology Core for high-throughput sequencing, and the NE-CAT beamline at the Advanced Photon Source. This work was supported by National Institutes of Health grants AI068776 (D.J.P.) and GM61835 (D.P.B.), a Human Frontier Science Program Long-term Fellowship (K.N.), a fellowship from the Japan Society for the Promotion of Science for Research Abroad (K.N.), and a National Science Foundation graduate research fellowship (D.E.W.). D.P.B. is an Investigator of the Howard Hughes Medical Institute.

Author Contributions All authors designed the study and wrote the manuscript. Structural experiments were performed by K.N. under the supervision of D.J.P. Biochemical experiments were performed by D.E.W. under the supervision of D.P.B.

Author Information The structural coordinates of KpAGO have been deposited in the Protein Data Bank (http://www.rcsb.org/pdb) under accession code 4F1N. RNA-sequencing data have been deposited in the Gene Expression Omnibus (http://www.ncbi.nlm.nih.gov/geo) under accession number GSE37725. Reprints and permissions information is available at www.nature.com/reprints. The authors declare no competing financial interests. Readers are welcome to comment on the online version of this article at www.nature.com/nature. Correspondence and requests for materials should be addressed to D.J.P. (pateld@mskcc.org) or D.P.B. (dbartel@wi.mit.edu).

LETTER

doi:10.1038/nature11121

An abundance of small exoplanets around stars with a wide range of metallicities

Lars A. Buchhave[1,2], David W. Latham[3], Anders Johansen[4], Martin Bizzarro[2], Guillermo Torres[3], Jason F. Rowe[5], Natalie M. Batalha[6], William J. Borucki[7], Erik Brugamyer[8], Caroline Caldwell[8], Stephen T. Bryson[7], David R. Ciardi[9], William D. Cochran[8], Michael Endl[8], Gilbert A. Esquerdo[3], Eric B. Ford[10], John C. Geary[3], Ronald L. Gilliland[11], Terese Hansen[1], Howard Isaacson[12], John B. Laird[13], Philip W. Lucas[14], Geoffrey W. Marcy[12], Jon A. Morse[15], Paul Robertson[8], Avi Shporer[16,17], Robert P. Stefanik[3], Martin Still[18] & Samuel N. Quinn[3]

The abundance of heavy elements (metallicity) in the photospheres of stars similar to the Sun provides a 'fossil' record of the chemical composition of the initial protoplanetary disk. Metal-rich stars are much more likely to harbour gas giant planets[1–4], supporting the model that planets form by accumulation of dust and ice particles[5]. Recent ground-based surveys suggest that this correlation is weakened for Neptunian-sized planets[4,6–9]. However, how the relationship between size and metallicity extends into the regime of terrestrial-sized exoplanets is unknown. Here we report spectroscopic metallicities of the host stars of 226 small exoplanet candidates discovered by NASA's Kepler mission[10], including objects that are comparable in size to the terrestrial planets in the Solar System. We find that planets with radii less than four Earth radii form around host stars with a wide range of metallicities (but on average a metallicity close to that of the Sun), whereas large planets preferentially form around stars with higher metallicities. This observation suggests that terrestrial planets may be widespread in the disk of the Galaxy, with no special requirement of enhanced metallicity for their formation.

In February 2011, the Kepler mission[10] announced its discovery of 1,235 planet candidates, of which more than half have radii smaller than that of Neptune[11]: $R_P < 4R_\oplus$, where $R_\oplus$ is the Earth radius. We used reconnaissance spectra obtained by the Kepler Follow-up Observing Program (FOP) to derive metallicities for several hundred of the brighter planet candidates, and used the results to explore the relationship between planet size and host-star metallicity. Metallicity, denoted [m/H], is defined as the proportion of a star's outer layers made up of chemical elements other than hydrogen and helium and expressed on a logarithmic scale where zero is the Sun's metallicity. Thousands of spectra have been gathered by the Kepler FOP, but the majority of the spectra have signal-to-noise ratios too low to extract precise stellar parameters using traditional methods. To take full advantage of this large observational effort, we have developed a tool (stellar parameter classification (SPC); see Supplementary Information) that uses a library of synthetic spectra to determine stellar parameters from spectra with modest signal-to-noise ratios (signal-to-noise per pixel >15). Using this approach, we derived metallicities in a consistent and homogeneous manner for the entire sample of Kepler FOP spectra, thus avoiding the systematic differences that can occur when comparing metallicities derived by different techniques. Only the most robust classifications are presented here (Supplementary Information), yielding precise stellar parameters for 152 stars harbouring 226 planet candidates mostly in orbits within 0.5 AU of the host star. We used the stellar parameters from SPC and the Yonsei–Yale stellar evolutionary models[12] to estimate the radii of the host stars, which we couple with the photometric data from the Kepler mission[11] to infer the planet radii (Supplementary Information).

Previous studies[4,6–9] have suggested that the observed correlation between metallicity and the likelihood that solar-type stars host gas giants is weaker for Neptunian-sized planets. However, it is unclear whether this correlation extends into the regime of terrestrial-sized planets, which is important for a better understanding of planet-formation processes. The number of host stars with planets smaller than Neptune in our sample (175 planets) is significantly larger than in earlier studies and includes much smaller planets (as small as Earth). This allows us to compare a statistically significant sample of homogenously derived spectroscopic metallicities of solar-type stars hosting small and large planets. By contrast, a recent study used metallicity indicators based on photometry[13]. In Fig. 1, we show that the average metallicity of stars hosting planets with radii smaller than that of Neptune ($R_P < 4.0R_\oplus$) is lower ($[\mathrm{m/H}] = -0.01 \pm 0.02$) than that of the stars harbouring gas giant planets ($[\mathrm{m/H}] = +0.15 \pm 0.03$). We find that smaller planets are observed at a wide range of host-star metallicities ($-0.6 < [\mathrm{m/H}] < +0.5$), whereas larger planets are detected preferentially around stars with higher metallicity (Figs 2 and 3). To investigate the statistical significance of the difference in metallicity, we perform the two-sample Kolmogorov–Smirnov test of the two subsamples of host stars and find the probability that the two distributions are not drawn randomly from the same parent population is 99.96% (over 3.5σ). An F-test shows that fitting the data in Fig. 3 with a metallicity that increases linearly, as opposed to being constant, as a function of radius yields a better fit with a confidence level of 99.99995% ($\sim 5\sigma$).

Figures 2 and 3 reveal that the population of small planets has a wide range of host-star metallicities, but on average the metallicity of the stars hosting the smaller planets is lower than that of the larger planets. The Kepler-11 system[14] demonstrates that small planets can possess a wide range of mean densities, much like their Jupiter-sized counterparts, and the low mean density of exoplanets Kepler-11d, e and f implies that these planets formed before the gas in the system dissipated completely. The metallicity of the protoplanetary disk may have a key role in how quickly planetary cores can form and, thus, in whether they are able to accrete a gaseous envelope before the gas in the system dissipates. However, additional data, including dynamical masses, are

---

[1] Niels Bohr Institute, University of Copenhagen, DK-2100 Copenhagen, Denmark. [2] Centre for Star and Planet Formation, Natural History Museum of Denmark, University of Copenhagen, DK-1350 Copenhagen, Denmark. [3] Harvard-Smithsonian Center for Astrophysics, Cambridge, Massachusetts 02138, USA. [4] Lund Observatory, Lund University, Box 43, 221 00 Lund, Sweden. [5] SETI Institute/NASA Ames Research Center, Moffett Field, California 94035, USA. [6] San Jose State University, San Jose, California 95192, USA. [7] NASA Ames Research Center, Moffett Field, California 94035, USA. [8] University of Texas, Austin, Texas 78712, USA. [9] NASA Exoplanet Science Institute/California Institute of Technology, Pasadena, California 91109, USA. [10] University of Florida, 211 Bryant Space Sciences Center, Gainesville, Florida 32611, USA. [11] Space Telescope Science Institute, Baltimore, Maryland 21218, USA. [12] University of California, Berkeley, California 94720, USA. [13] Bowling Green State University, Bowling Green, Ohio 43403, USA. [14] Centre for Astrophysics, University of Hertfordshire, College Lane, Hatfield AL10 9AB, UK. [15] Department of Physics, Applied Physics and Astronomy, Rensselaer Polytechnic Institute, CII 9015, 110 8th Street, Troy, New York 12180, USA. [16] Las Cumbres Observatory, Global Telescope Network, Santa Barbara, California 93117, USA. [17] Department of Physics, University of California, Santa Barbara, California 93106, USA. [18] Bay Area Environmental Research Institute/NASA Ames Research Center, Moffett Field, California 94035, USA.

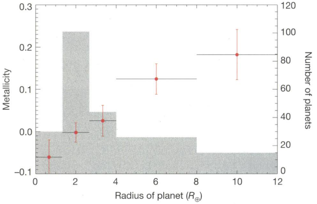

Figure 1 | Average host-star metallicities. Stellar metallicity is defined as $[\mathrm{m/H}] = \log_{10}(N_{\mathrm{m}}/N_{\mathrm{H}})_{\mathrm{star}} - \log_{10}(N_{\mathrm{m}}/N_{\mathrm{H}})_{\mathrm{Sun}}$, where N_{m} and N_{H} are respectively the number densities of metal atoms (all elements more massive than helium) and hydrogen atoms. Red points represent the average metallicity of the host stars with planets of different radii grouped in $1.33R_\oplus$ and $4R_\oplus$ bins. The bin size is indicated by the length of the horizontal line and the uncertainty in the average metallicity is given by the standard error. The shaded grey histogram shows the number of planets in each bin, and illustrates the large number of small planets in the Kepler sample. The average metallicity of host stars with smaller planets ($R_{\mathrm{P}} < 4R_\oplus$) is lower ($[\mathrm{m/H}] = -0.01 \pm 0.02$) than that of host stars with larger planets ($[\mathrm{m/H}] = +0.15 \pm 0.03$). Some of the planetary candidates in the Kepler sample are expected to be false positives that do not turn out to be transiting planets, such as occurs when the reduced signal from a background eclipsing binary is by chance contained within the photometric aperture of the foreground target star. The false-positive rate of the candidates that pass the standard vetting procedures applied by the Kepler team has been estimated to be less than 10% (ref. 26). Therefore, such a low false-positive rate is not expected to impact our results and interpretation. We have thus ignored possible contamination by false positives. We do not derive absolute probabilities or occurrence rates of planets and therefore do not attempt to eliminate the many strong bias and selection effects that, for example, completeness studies (for example ref. 27) must take into account. We have explored the possibility that correlations between planet size and parameters such as orbital semi-major axis are the source of the apparent dependence on metallicity, but find no evidence for such an effect (Supplementary Information).

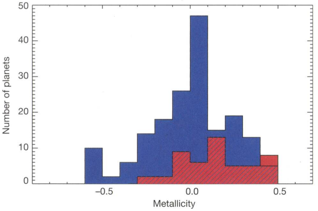

Figure 2 | Comparison of host-star metallicities for small and large planets. The histograms compare the metallicities of two samples of stars hosting planets by dividing the sample at $R_{\mathrm{P}} = 4R_\oplus$. The host stars of the gas giant planets ($R_{\mathrm{P}} \geq 4R_\oplus$; red histogram) are clearly more metal rich than those of the smaller planets ($R_{\mathrm{P}} < 4R_\oplus$; blue histogram), which have a much wider range of metallicities. The hatched area represents the area where the histograms overlap. A Kolmogorov–Smirnov test shows that the probability that the two distributions are not drawn randomly from the same parent population is greater than 99.96%; that is, the two distributions differ by more than 3.5σ. The average metallicity of the stars with small planets ($[\mathrm{m/H}] = -0.01 \pm 0.02$; blue histogram) differs by almost 5σ from that of the larger planets ($[\mathrm{m/H}] = +0.15 \pm 0.03$; red histogram).

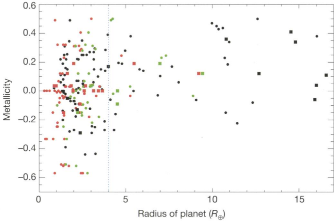

Figure 3 | Individual host-star metallicity as a function of planet radius. The black dots represent single-planet systems, whereas the green dots represent the largest planet and the red dots represent all the smaller planets in multiple-planet systems. The confirmed, published Kepler planets in our samples are plotted as squares with the same colour code as the dots. Planet candidates in multiple systems are each added to the sample with the same host-star metallicity. In Supplementary Information, we consider systems of planets as opposed to individual planets by neglecting all but the largest planet in each system. The vertical dotted line indicates the division of the sample at $R_{\mathrm{P}} = 4.0R_\oplus$. The data show that Kepler detects small planets around stars with a wide range of metallicities ($-0.6 < [\mathrm{m/H}] < 0.5$), and that larger planets are found preferentially around stars with solar metallicity or higher. The average uncertainty in the individual measurements in metallicity is 0.08 dex and that in planetary radius is 12%.

needed better to understand the seemingly diverse regime of small planets.

Our data show that the well-established correlation between metallicity and occurrence of giant planets[1–3] does not extend into the smaller planet regime below $R_{\mathrm{P}} < 4R_\oplus$, where the host stars instead have a wide range of metallicities. This observation implies that, by contrast with smaller planets, gas giants require exceptional conditions to trigger their formation. Our findings agree well with the core accretion theory for planet formation, whereby high-metallicity environments allow planetary cores to grow rapidly to reach approximately ten times the mass of the Earth, continue to accrete a gaseous envelope and evolve to gas giants of several hundred Earth masses[5]. Gas disks around young stars are observed to dissipate within a few million years[15], requiring the cores of their planets to reach ten Earth masses within that time if they are to become gas giants. Planets forming in low-metallicity environments, however, may not reach large enough core masses before the dissipation of the gas disk, which could explain why we find very few gas giants around low-metallicity stars. Planetary accretion cannot compete with gas dissipation around low-metallicity stars because the number density of planetesimals is low[16–18] and gas disks dissipate sooner around low-metallicity stars[19,20].

The semi-major axes of the orbits of the majority of the Kepler planets analysed in this work are less than 0.5 AU, so the detected gas giants in our sample were probably brought into orbits within 1 AU by migration[21]. A decreased efficiency of migration in low-metallicity disks could partly explain the observed deficiency of gas giants around the low-metallicity stars. The formation of gas giants late in the lifetime of the protoplanetary gas disk would reduce their subsequent migration because the gas disk is diluted at that stage. This could partly explain why we observe so few gas giants in close orbits. However, late planet formation will in itself suppress formation of gas giants because some cores are formed after the disappearance of the gas disk. Hence, migration cannot be the only reason for the small number of gas giants that we observe around low-metallicity stars.

During the initial stages of planet formation, dust grains collide to form planetesimals, which represent the kilometre-sized building blocks of planets. In some models, planetesimal formation is only possible in disks with metallicities greater than the solar value[17,18]. However, our results show that small planets are present around stars with a wide range of metallicities. The formation of planetesimals in low-metallicity environments can occur if the metallicity is enhanced by preferential evaporation of gas in the disk, for example by photo-evaporation processes associated with the central star or, alternatively, by external sources such as nearby massive stars. In both cases, the removal of gas by photo-evaporation is expected to occur early in the lifetime of the disk, possibly within one million years[22,23]. Such short timescales are consistent with radiometric age dating of meteorites suggesting that, in the Solar System, planetesimal accretion may have begun as early as a few hundred thousand years following formation of the Sun[24].

Finally, we note that some studies have proposed that a metallicity of at least half that of the Sun is required for the formation of terrestrial planets[25]. However, our analysis based on the Kepler planet candidates indicates that terrestrial planets can form at a wide range of metallicities, including metallicities almost four times lower than that of the Sun ($[\mathrm{m/H}] \approx -0.6$). In addition, we find that the frequency of occurrence of small planets ($R_P < 4.0R_\oplus$) relative to that of large planets ($R_P > 4.0R_\oplus$) is $\sim$2.7:1 for stars of metallicity greater than that of the Sun but increases to $\sim$5.9:1 for stars of metallicity less than that of the Sun. Therefore, the formation of small, terrestrial planets does not require a metal-rich environment, suggesting that their existence might be widespread in the disk of the Galaxy.

Received 23 December 2011; accepted 5 April 2012.

Published online 13 June 2012.

1. Santos, N. C., Israelian, G. & Mayor, M. Spectroscopic [Fe/H] for 98 extra-solar planet-host stars. Exploring the probability of planet formation. *Astron. Astrophys.* **415,** 1153–1166 (2004).
2. Fischer, D. A. & Valenti, J. The planet-metallicity correlation. *Astrophys. J.* **622,** 1102–1117 (2005).
3. Johnson, J. A., Aller, K. M., Howard, A. W. & Crepp, J. R. Giant planet occurrence in the stellar mass-metallicity plane. *Publ. Astron. Soc. Pacif.* **122,** 905–915 (2010).
4. Sousa, S. G., Santos, N. C., Israelian, G., Mayor, M. & Udry, S. Spectroscopic stellar parameters for 582 FGK stars in the HARPS volume-limited sample. Revising the metallicity-planet correlation. *Astron. Astrophys.* **533,** A141 (2011).
5. Pollack, J. B. *et al.* Formation of the giant planets by concurrent accretion of solids and gas. *Icarus* **124,** 62–85 (1996).
6. Udry, S. *et al.* The HARPS search for southern extra-solar planets. V. A 14 Earth-masses planet orbiting HD 4308. *Astron. Astrophys.* **447,** 361–367 (2006).
7. Sousa, S. G. *et al.* Spectroscopic parameters for 451 stars in the HARPS GTO planet search program. Stellar [Fe/H] and the frequency of exo-Neptunes. *Astron. Astrophys.* **487,** 373–381 (2008).
8. Ghezzi, L. *et al.* Stellar parameters and metallicities of stars hosting Jovian and Neptunian mass planets: a possible dependence of planetary mass on metallicity. *Astrophys. J.* **720,** 1290–1302 (2010).
9. Mayor, M. *et al.* The HARPS search for southern extra-solar planets XXXIV. Occurrence, mass distribution and orbital properties of super-Earths and Neptune-mass planets. Preprint at http://arxiv.org/abs/1109.2497 (2011).
10. Borucki, W. J. *et al.* Kepler planet-detection mission: introduction and first results. *Science* **327,** 977–980 (2010).
11. Borucki, W. J. *et al.* Characteristics of planetary candidates observed by Kepler. II. Analysis of the first four months of data. *Astrophys. J.* **736,** 19–41 (2011).
12. Yi, S. *et al.* Toward better age estimates for stellar populations: the Y2 isochrones for solar mixture. *Astrophys. J. Suppl. Ser.* **136,** 417–437 (2001).
13. Schlaufman, K. C. & Laughlin, G. Kepler exoplanet candidate host stars are preferentially metal rich. *Astrophys. J.* **738,** 177–186 (2011).
14. Lissauer, J. J. *et al.* A closely packed system of low-mass, low-density planets transiting Kepler-11. *Nature* **470,** 53–58 (2011).
15. Haisch, K. E., Lada, E. A. & Lada, C. J. Disk frequencies and lifetimes in young clusters. *Astrophys. J.* **553,** L153–L156 (2001).
16. Ida, S. & Lin, D. N. C. Toward a deterministic model of planetary formation. II. The formation and retention of gas giant planets around stars with a range of metallicities. *Astrophys. J.* **616,** 567–572 (2004).
17. Throop, H. B. & Bally, J. Can photoevaporation trigger planetesimal formation? *Astrophys. J.* **623,** L149–L152 (2005).
18. Johansen, A., Youdin, A. & Mac Low, M.-M. Particle clumping and planetesimal formation depend strongly on metallicity. *Astrophys. J.* **704,** L75–L79 (2009).
19. Ercolano, B. & Clarke, C. J. Metallicity, planet formation and disc lifetimes. *Mon. Not. R. Astron. Soc.* **402,** 2735–2743 (2010).
20. Yasui, C., Kobayashi, N., Tokunaga, A. T., Saito, M. & Tokoku, C. Short lifetime of protoplanetary disks in low-metallicity environments. *Astrophys. J.* **723,** L113–L116 (2010).
21. Lin, D. N. C., Bodenheimer, P. & Richardson, D. C. Orbital migration of the planetary companion of 51 Pegasi to its present location. *Nature* **380,** 606–607 (1996).
22. Gorti, U. & Hollenbach, D. Photoevaporation of circumstellar disks by far-ultraviolet, extreme-ultraviolet and X-ray radiation from the central star. *Astrophys. J.* **690,** 1539–1552 (2009).
23. Hester, J. J., Desch, S. J., Healy, K. R. & Leshin, L. A. The cradle of the Solar System. *Science* **304,** 1116–1117 (2004).
24. Schiller, M. *et al.* Rapid timescales for magma ocean crystallization on the howardite-eucrite-diogenite parent body. *Astrophys. J.* **740,** L22–L28 (2011).
25. Gonzalez, G., Brownlee, D. & Ward, P. The galactic habitable zone: galactic chemical evolution. *Icarus* **152,** 185–200 (2001).
26. Morton, T. D. & Johnson, J. A. On the low false positive probabilities of Kepler planet candidates. *Astrophys. J.* **738,** 170–182 (2011).
27. Howard, A. W. *et al.* Planet occurrence within 0.25 AU of Solar-type stars from Kepler. Preprint at http://arxiv.org/abs/1103.2541 (2011).

Supplementary Information is linked to the online version of the paper at www.nature.com/nature.

Acknowledgements The Kepler mission was competitively selected as the tenth NASA Discovery mission. Funding for this mission is provided by NASA's Science Mission Directorate. The Centre for Star and Planet Formation is funded by the Danish National Research Foundation. L.A.B. was funded by the Carlsberg Foundation. A.J. was partially funded by the European Research Council under ERC Starting Grant agreement 278675-PEBBLE2PLANET.

Author Contributions L.A.B. led the project and developed the classification tools for the metallicity analysis. D.W.L., A.J. and M.B. contributed to the discussion of the theoretical implications of the data. G.T. supplied the isochrone fitting tools. J.F.R. provided the planet radii from the Kepler photometry. D.W.L., C.C., W.D.C., G.A.E., E.B., M.E., J.C.G., T.H., G.W.M., P.R., R.P.S. and S.N.Q. worked on gathering the spectroscopic observations. D.W.L., W.J.B., S.T.B., N.M.B., D.R.C., W.D.C., R.L.G., P.W.L., G.W.M., A.S., M.S., H.I., E.B.F. and S.N.Q. worked on identifying the Kepler planets and eliminating false positives. W.J.B. led the Kepler mission. J.B.L., J.A.M. and D.W.L. worked on the synthetic stellar model library. All authors discussed the results and commented on the manuscript. L.A.B. wrote the paper with equal input from D.W.L., A.J. and M.B.

Author Information Reprints and permissions information is available at www.nature.com/reprints. The authors declare no competing financial interests. Readers are welcome to comment on the online version of this article at www.nature.com/nature. Correspondence and requests for materials should be addressed to L.A.B. (buchhave@astro.ku.dk).

LETTER

doi:10.1038/nature11216

Constraints on the volatile distribution within Shackleton crater at the lunar south pole

Maria T. Zuber[1], James W. Head[2], David E. Smith[1], Gregory A. Neumann[3], Erwan Mazarico[1], Mark H. Torrence[4], Oded Aharonson[5], Alexander R. Tye[2], Caleb I. Fassett[2], Margaret A. Rosenburg[5] & H. Jay Melosh[6]

Shackleton crater is nearly coincident with the Moon's south pole. Its interior receives almost no direct sunlight and is a perennial cold trap[1,2], making Shackleton a promising candidate location in which to seek sequestered volatiles[3]. However, previous orbital and Earth-based radar mapping[4–8] and orbital optical imaging[9] have yielded conflicting interpretations about the existence of volatiles. Here we present observations from the Lunar Orbiter Laser Altimeter on board the Lunar Reconnaissance Orbiter, revealing Shackleton to be an ancient, unusually well-preserved simple crater whose interior walls are fresher than its floor and rim. Shackleton floor deposits are nearly the same age as the rim, suggesting that little floor deposition has occurred since the crater formed more than three billion years ago. At a wavelength of 1,064 nanometres, the floor of Shackleton is brighter than the surrounding terrain and the interiors of nearby craters, but not as bright as the interior walls. The combined observations are explicable primarily by downslope movement of regolith on the walls exposing fresher underlying material. The relatively brighter crater floor is most simply explained by decreased space weathering due to shadowing, but a one-micrometre-thick layer containing about 20 per cent surficial ice is an alternative possibility.

Detailed study of the topography of Shackleton (Fig. 1a) offers the opportunity to improve understanding of processes that operate in permanently shadowed regions (Fig. 1b). Crater geometry, age and preservation state are relevant for understanding the accumulation and preservation of volatiles as well as the processes that modify the lunar surface over geologic timescales.

Our analysis uses observations from the Lunar Orbiter Laser Altimeter (LOLA)[10], an instrument on NASA's Lunar Reconnaissance Orbiter (LRO) mission. LOLA is a five-beam laser altimeter that operates at a wavelength of 1,064.4 nm with a 28-Hz pulse repetition rate. From LRO's mapping orbit at ~50 km altitude, the instrument illuminates 5-m-diameter spots on the lunar surface, returning up to 140 measurements of elevation per second; the five profiles enable characterization of bi-directional slopes over various baselines, and roughness from averaging of pulse elevations. In addition, from the spreading of backscattered laser pulses, LOLA obtains the root-mean-square (RMS) roughness of the surface within laser footprints. Finally, from the ratio of received to transmitted laser energy, LOLA measures the reflectance of the lunar surface at zero phase angle at the laser wavelength within laser spots.

As of 1 December 2011, the LOLA instrument has accumulated more than 5.1 billion elevation measurements[11]. Because Shackleton lies nearly at a pole, where the LOLA coverage is densest, it is possible to construct a digital elevation model of unprecedented spatial resolution and radial accuracy. More than 5,000 LOLA tracks, referenced to the Moon's centre of mass via precision orbits determined from radio tracking[12] aided by Earth-based laser tracking[13,14], were converted to topography. Track segments within the area of interest were geometrically corrected at orbit crossover points[15].

Figure 1a shows the topography of Shackleton crater sampled at 10-m spatial resolution; individual measurements have an accuracy of ~1 m with respect to the Moon's centre of mass. The 40 km × 40 km topographic model of Shackleton is derived from 5.358 million elevation measurements with an average of 0.34 altimeter measurements in each 10-m square area; the resolution is comparable to or better than other studies of Shackleton's interior by images[9], Earth-based radar[6] and orbital synthetic aperture radar[16]. The topography reveals the near-axisymmetric bowl-shaped nature of the crater, in which the crater rim and interior walls are well preserved. The depth/diameter ratio of the crater is 0.195 ± 0.025 (Table 1), which is consistent with other fresh simple craters[17].

Figure 1c shows bi-directional surface slopes over 10-m baselines that quantify the uniform, steep inner walls; slopes approach the angle of repose. Slopes are greatest in the mid-levels of walls, which is in contrast to many crater walls on Mars, where near-vertically oriented cliffs of outwardly dipping coherent cap rock are exposed in the upper walls[18].

Surface roughness at a scale of 20–50 m is shown in Fig. 1d. These data indicate that crater walls are smoother, within bounds of measurement uncertainty, at this spatial scale than the floor or rim, especially portions of lower walls aligned with mounds on the crater floor. Table 1 lists estimated roughness values of various crater components. Similarly, the average RMS roughness derived from spreading of individual laser footprints (Supplementary Information) is lower on the crater walls. Pulses returned from the steep walls of Shackleton are spread in time by >10 ns, but after correcting for the effect of local slope on a longer baseline, the pulse spreading due to surface roughness is somewhat less than on the crater floor or surrounding terrain. The floor can be divided into two regions, a flat portion and an elevated terrain. The roughness of the mound unit increases at the largest scales due to its hummocky character, but it is smoother than the flat region at smaller scales, due to its paucity of craters.

Figure 2 shows a more detailed view of the topography of Shackleton's floor, which highlights the irregularly distributed deposits and numerous small craters (see also Fig. 1e). The largest mound of material has a relief of ~210 m (Table 1) and the highest-local slope of any of the floor deposits is ~25°, which is below the angle of repose. Two areas of the floor show fan-shaped structures consisting of material that has been transported downslope from the interior walls in a manner commonly observed in craters of this size range[17]. The limited fan material around the margins of the crater floor, combined with the asymmetric distribution and slope properties of deposits, suggest that the predominant contribution to the fill is ejecta fallback with a secondary contribution from slumped wall deposits.

---

[1]Department of Earth, Atmospheric and Planetary Sciences, Massachusetts Institute of Technology, Cambridge, Massachusetts 02139, USA. [2]Department of Geological Sciences, Brown University, Providence, Rhode Island 02912, USA. [3]Solar System Exploration Division, NASA/Goddard Space Flight Center, Greenbelt, Maryland 20771, USA. [4]Stinger Ghaffarian Technologies, Greenbelt, Maryland 20770, USA. [5]Division of Geological and Planetary Sciences, California Institute of Technology, Pasadena, California 91125, USA. [6]Department of Earth and Atmospheric Sciences, Purdue University, West Lafayette, Indiana 47907, USA.

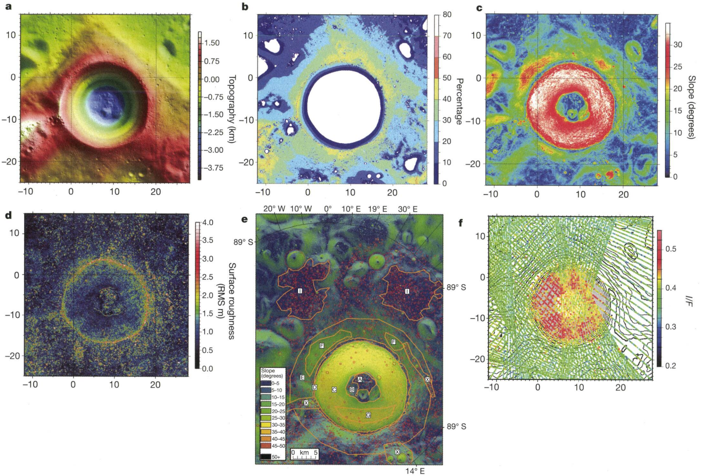

Figure 1 | Detailed characterization of Shackleton crater. **a**, Topography in km; **b**, percentage of time illuminated; **c**, 10-m baseline slopes in degrees; **d**, surface roughness shown as RMS residual in m; **e**, locations of crater counts used to determine relative ages; and **f**, zero-phase, 1,064-nm reflectance shown as *I*/*F*. Topography, slopes and roughness are based on a 10-m spatial resolution grid of all available LOLA profiles. In **a**–**d** and **f**, *x* and *y* axes indicate spatial scale, where (0, 0) is the lunar south pole and colour scales show magnitude of plotted quantity. White regions in **b** correspond to zero illumination. Panel **e** shows locations of craters counted to estimate relative age, plotted over 10-m slopes (colour coded as in inset). Crater regions in **e** correspond to: A, flat region of crater floor; A/B, entire crater floor; C, crater wall; D, crater rim crest; E/F, inner rim annulus (~5.5 km); E, inner rim annulus excluding steep region (F); F, steep rim region within annulus; G, crater wall section; I, Shackleton crater deposits north of rim in flat areas; and X, secondary crater chains and clusters (removed from analysis). In **f**, reflectance is expressed as a radiance factor (*I*/*F*), which is defined as the ratio of the measured radiance *I* to the radiance *F* of an ideal diffusive surface in vacuum with 100% reflectance under the same illumination. Each dot represents a 0.4 × 0.4 km pixel median average of LOLA's spot 3 reflectance. Contours show topography at 0.2 km intervals. The grey annulus shows the 17-km diameter of the steepest portion of the walls and the 7-km diameter of the floor.

Table 1 | Parameters describing Shackleton crater

Parameter	Value
Areocentric latitude of centre of rim (degrees)	−89.655
Areocentric longitude of centre of rim (degrees)	129.174
Lunar radius at floor centre (km)	1,734.63
Mean crater diameter at rim (km)	21
Mean depth, rim to floor (km)	4.1 ± 0.05
Mean rim height above datum (km)	1.3
Range of floor topography (km)	~0.210
Area of crater at rim (km^2)	~346
Area of crater floor (km^2)	~38
Estimated fill depth (km)	~0.75
Crater volume (km^3)	640 ± 10
Fill volume, including mounds (km^3)	12 ± 1
Maximum wall slope (degrees)	35
Average wall slope (degrees)	30.5
RMS roughness* of crater exterior (m)	~1
RMS roughness* of crater walls (m)	<1
RMS roughness* of crater floor (m)	~1
RMS roughness* of crater rim (m)	~1
I/*F* of crater exterior	0.32 ± 0.04
I/*F* of interior walls	0.46 ± 0.03
I/*F* of interior floor	0.43 ± 0.02
Ratio of average depth/average rim diameter, *d*/*D*	0.195 ± 0.025

See Fig. l legend for definition of *I*/*F*.

* Within 5-m spots.

Shackleton was previously assigned an Eratosthenian age[19] (middle lunar history; in the approximate interval 1–3.2 Gyr before present) on the basis of its relatively fresh morphology, its lack of rays, and counts of superposed craters[3] using AMIE image data (50 m per pixel) and Arecibo radar data (20 m per pixel). Craters were counted within a crater diameter (~20 km) of the rim crest, avoiding obvious secondary craters. This analysis was subsequently revisited and resulted in an older, Imbrian age[3] (in the approximate interval 3.2–3.8 Gyr before present).

Here we use a LOLA shaded relief map to advance previous work by individually dating different parts of the crater (see Fig. 1e and Supplementary Information) to investigate the processes that have operated since crater formation. LOLA observations permit dating of shadowed regions in the crater interior and allow spatially unbiased measurements of crater density due to uniformity in illumination conditions. In addition, illumination can be varied over the topographic model to enhance crater detection. On the basis of comparison of the several different areas of the rim of the crater, it is clear that the variable slopes of the rough crater rim have an influence on crater retention. For example, two areas of very flat terrain on the Shackleton flank within one crater diameter of the rim crest (I; Fig. 1e) yield modelled crater ages of ~3.69 Gyr, whereas areas closer to the rim crest (within ~5.5 km)

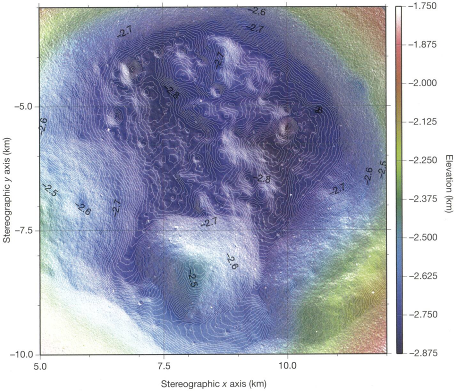

Figure 2 | High-resolution elevation map in stereographic projection of the floor of Shackleton. Elevations are contoured at 5-m intervals with colours indicating elevation with respect to 1,737.4 km. The axes indicate spatial scales.

yield ages of ~1.21 Gyr (F, steeper slopes; Fig. 1e) and ~2.91 Gyr (E, fewer steep slopes; Fig. 1e). The flat areas of the Shackleton crater deposit (I; Fig. 1e) indicate an age of ~3.69 Gyr (Supplementary Table 1), older than the originally estimated age of 1.3–3.3 Gyr (ref. 19) but close to the Upper Imbrian age of ~3.6 Gyr estimated subsequently[3]. Determination of ages of these individual regions permits quantitative investigation of how the crater has been modified.

A critical question is the age of the permanently shadowed portions of the interior walls and floor of Shackleton. Analysis indicates that the lunar spin axis has been at its approximate current orientation for ~2 Gyr (ref. 20). If the crater had been accumulating volatiles in the permanently shadowed areas over a period of this order, it is reasonable to hypothesize that its interior was resurfaced, covering and burying craters and thus producing a younger relative age. Examination of the steep crater wall (C; Fig. 1e) yields a much younger crater retention age of ~1.44 Gyr, which could be consistent with either volatile mantling or downslope mass wasting (Fig. 1c)[21]. Examination of the permanently shadowed parts of the crater floor (A; Fig. 1e), the area where volatiles plausibly accumulated, reveals a crater retention age of ~3.60 Gyr, essentially identical to the flat areas of the crater rim. Including the rougher parts of the crater floor (B; Fig. 1e) produces an age of ~3.29 Gyr, which almost certainly reflects the influence of downslope transport, as observed on the inner part of the Shackleton rim, on the retention of craters. The similar age of the Shackleton crater exterior and floor (~3.69 and 3.60 Gyr) is evidence that if volatiles accumulated in this cold trap for ~10^9 years, they were not in sufficient quantity to alter in a statistically significant sense the size–frequency distribution of superposed craters in the size range counted.

Knowledge of the crater size–frequency distribution (Supplementary Fig. 1) permits an assessment of the minimum amount of deposition that could occur without disrupting this distribution. The craters counted on Shackleton's floor ranged from ~250 m up to ~500 m in diameter, representing a range of fresh crater depths of ~50–100 m (ref. 22). Accumulation of volatiles to thicknesses in excess of 20–50 m would significantly alter the crater size–frequency distribution and should be observed in terms of a deficit in the number of small craters. A rollover in the curve at small crater diameters is observed, but is very similar to that seen outside the crater (I; Fig 1e and Supplementary Fig. 1), and thus is more likely to be due to the typical destruction effects of superposed craters and other diffusive processes (such as micrometeorite bombardment or seismic shaking associated with moonquakes triggered by stresses associated with impacts or tides) at these diameters. On the other hand, if volatiles were cold-trapped by vapour diffusion into the regolith, as opposed to deposition in surface layers, then muting of superposed craters may not have been as significant.

Figure 1f shows profiles of 1,064-nm reflectance of Shackleton crater and its surroundings. A previous study[9] obtained images of the floor of Shackleton from the Kaguya Terrain Camera at the time of maximum scattering illumination at the lunar south pole and observed no evidence for brightening; results were interpreted to indicate an absence of pure ice deposits on the crater floor. In the current study, LOLA profiles assembled from numerous orbital passes at the most favourable conditions for obtaining reliable measurements of reflectance show that the crater walls are anomalously bright relative to the surrounding terrain. Similarly to other impact craters in this size range, this brightness could be due to downslope movement of material caused by micrometeorite and small projectile bombardment on steep slopes, or by seismic shaking. The cascading of regolith material downslope exposes optically less mature surfaces than those developed and retained on lower slopes.

At a wavelength of 1,064 nm, the floor of Shackleton crater is darker than its interior walls, but both floors and walls are considerably brighter than the surrounding terrain, including the interiors of nearby craters that are both shadowed and sunlit. The relative brightness of the floor relative to surroundings requires explanation. Micrometeorite bombardment and impingement of the solar wind produce 'space weathering' of exposed geologic materials that reddens and darkens their surfaces[23]. The former (bombardment) would be less significant in the shadowed interior of Shackleton than in the surrounding region because the interior of the crater has not been exposed to the Sun for more than 2 Gyr (ref. 20), whereas the latter (solar wind impingement) might be enhanced in permanently shadowed craters[24]. Thus the floor brightness enhancement could be explained by a dearth of space weathering by micrometeorite bombardment.

Volatile deposition is an alternative possibility. Under the conservative assumption that water ice has a 1,064-nm reflectance twice that of the lunar regolith[25] and that both are observed at zero phase, the measured reflectance of the floor can be explained by a micrometre-thick surface layer (the depth over which the laser backscatter measurement is sensitive) of 22% ice mixed with rock[26]. Greater ice contents distributed throughout a thicker layer are possible but cannot be constrained from LOLA's reflectivity measurement. For comparison, far-ultraviolet reflectance of permanently shadowed regions from the LRO Lyman Alpha Mapping Project (LAMP) is consistent with ~1–2% surface water frost[27].

Results from the LRO Mini-RF orbital radar for the interior of Shackleton[16] provide additional insight. Regions with thick ice deposits are expected to have circular polarization ratios (CPR) >1, but such high ratios can also be explained by surface roughness. High-resolution images from ground-based radar[6] show that some areas with high CPR lie inside the rim of Shackleton. Mini-RF data[16] reveal that CPR values decrease with depth within the crater, and CPR values on the floor of Shackleton crater are predominantly <1. The pixels with CPR values in excess of unity are distributed heterogeneously throughout the crater walls, correlate generally with regions of high roughness observed by LOLA (Fig. 1d) and include some sunlit areas (Fig. 1b). Although some contribution to high CPR values from volatiles is possible, and would imply a process in which volatile deposition operates very rapidly in comparison to the rate of removal, the combined data suggest that the higher floor reflectance is due primarily to the dearth of space weathering in this shadowed environment.

In considering why Shackleton's interior walls have a higher reflectance than its floor, it is instructive to note that wall brightening is not restricted to areas that are continuously shadowed but extends to the upper illuminated portions. Consequently, a higher concentration of surface volatiles on the walls than present on the floor is an unlikely explanation. More likely is downslope movement of regolith material on the steep crater walls that has exposed brighter underlying material; downslope movement is consistent with the observed slopes near the angle of repose and the roughness and morphology of Shackleton's interior walls (Fig. 1c, d), as well as with Earth-based radar backscatter[6] and Mini-RF[16] measurements.

METHODS SUMMARY

LOLA, an instrument on board the LRO spacecraft, outputs five beams per laser pulse that are backscattered from the lunar surface and detected in the instrument's receiver. The relevant measurement is the time of flight of each individual laser pulse, which can be converted to a range of the spacecraft to the lunar surface given knowledge of the position of the spacecraft with respect to the Moon's centre of mass. Radial range errors were minimized by geometric adjustment of altimetric tracks within the study area. In practice, profiles of one-way range from the LOLA instrument to the lunar surface along the spacecraft ground track were converted to lunar radius at each bounce point using the reconstructed orbit of LRO. Topography was determined by subtracting a sphere of 1,737.4 km from each radius measurement.

Slopes were calculated from a two-laser-spot fit at 20–50-m length scales, and RMS roughness represents a standard deviation about a plane fitted by least-squares to two laser shots along-track, from which at least four valid spots are returned out of a possible total of ten. The plane has dimensions of 90–100 m in the longest axis and 10–40 m in the shortest axis, depending on the positions of the spots returned.

The ratio of returned to transmitted pulse energy is a measure of surface reflectance at the laser wavelength. The transmitted and returned pulse energies were measured by integrating the area under the pulses. Observations of 1,064-nm reflectance were derived from LOLA tracks crossing Shackleton for days 130–149 in 2010.

Full Methods and any associated references are available in the online version of the paper at www.nature.com/nature.

Received 23 December 2011; accepted 4 May 2012.

1. Watson, K., Murray, B. C. & Brown, H. The behavior of volatiles on the lunar surface. *J. Geophys. Res.* **66,** 3033–3045 (1961).
2. Arnold, J. R. Ice in the lunar polar regions. *J. Geophys. Res.* **84,** 5659–5668 (1979).
3. Spudis, P. D., Plescia, J., Josset, J.-L. & Beauvivre, S. Geology of Shackleton Crater and the south pole of the Moon. *Geophys. Res. Lett.* 36, L14201, http://dx.doi.org/10.1029/2008GL034468 (2008).
4. Nozette, S. *et al.* The Clementine bistatic radar experiment. *Science* **274,** 1495–1498 (1996).
5. Stacy, N. J. S., Campbell, D. B. & Ford, P. G. Arecibo radar mapping of the lunar poles: a search for ice deposits. *Science* **276,** 1527–1530 (1997).
6. Campbell, D. B., Campbell, B. A., Carter, L. M., Margot, J.-L. & Stacy, N. J. S. No evidence for thick deposits of ice at the lunar south pole. *Nature* **443,** 835–837 (2006).
7. Simpson, R. & Tyler, G. L. Reanalysis of Clementine bistatic radar data from the lunar south pole. *J. Geophys. Res.* **104,** 3845–3862 (1999).
8. Nozette, S. *et al.* Integration of lunar polar remote-sensing data sets: evidence for ice at the lunar south pole. *J. Geophys. Res.* **106** (E10), 23253–23266 (2001).
9. Haruyama, J. *et al.* Lack of exposed ice inside lunar south pole Shackleton crater. *Science* **322,** 938–939 (2008).
10. Smith, D. E. *et al.* The Lunar Orbiter Laser Altimeter investigation on the Lunar Reconnaissance Orbiter mission. *Space Sci. Rev.* **150,** 209–241 (2010).
11. Smith, D. E. *et al.* Results from the Lunar Orbiter Laser Altimeter (LOLA): global, high resolution topographic mapping of the Moon. *Lunar Planet. Sci. Conf.* **XLII,** 2350 (2011).
12. Mazarico, E. *et al.* Orbit determination of the Lunar Reconnaissance Orbiter. *J. Geod.* **86,** 193–207 (2012).
13. Sun, X. *et al. The Laser Ranging Subsystem on the Lunar Reconnaissance Orbiter*. Report No. GSC-15884-1 (NASA New Technology Report, Washington DC, 2009).
14. Zuber, M. T. *et al.* The Lunar Reconnaissance Orbiter laser ranging investigation. *Space Sci. Rev.* **150,** 63–80 (2010).
15. Neumann, G. A., Rowlands, D. D., Lemoine, F. G., Smith, D. E. & Zuber, M. T. Crossover analysis of MOLA altimetric data. *J. Geophys. Res.* **106** (E10), 23753–23768 (2001).
16. Thomson, B. J. *et al.* The interior of Shackleton crater as revealed by Mini-RF orbital radar. *Lunar Planet. Sci. Conf.* **XLII,** 1626 (2011).
17. Pike, R. J. in *Impact and Explosion Cratering* (eds Roddy, D. J., Pepin, R. O. & Merrill, R. B.) 489–509 (Pergamon, 1977).
18. Squyres, S. W. *et al.* Exploration of Victoria crater by the Mars Rover Opportunity. *Science* **324,** 1058–1061 (2009).
19. Wilhelms, D. E., Howard, K. A. & Wilshire, H. G. *Geologic Map of the South Side of the Moon* (Map I-1162, US Geological Survey, 1979).
20. Ward, W. R. Past orientation of the lunar spin axis. *Science* **189,** 377–379 (1975).
21. Howard, K. A. Fresh lunar impact craters — review of variations with size. In *Proc. 5th Lunar Sci. Conf.* 61–69 (Pergamon, 1974).
22. Pike, R. J. Depth/diameter relations of fresh lunar craters: revision from spacecraft data. *Geophys. Res. Lett.* **1,** 291–294 (1974).
23. Hapke, B. Space weathering from Mercury to the asteroid belt. *J. Geophys. Res.* **106** (E5), 10039–10073 (2001).
24. Zimmerman, M. I. Farrell, W. M., Stubbs, T. J., Halekas, J. S. & Jackson, T. L. Solar wind access to polar craters: feedback between surface charging and plasma expansion. *Geophys. Res. Lett.* 38, L19202, http://dx.doi.org/10.1029/2011GL048880 (2011).
25. Kwok, R., Cunningham, G. F., Zwally, H. J. & Yi, D. ICESat over Arctic sea ice: Interpretation of altimetric and reflectivity profiles. *J. Geophys. Res.* 111, C06006, http://dx.doi.org/10.1029/2005JC003175 (2006).
26. Pieters, C. M. *et al.* Character and spatial distribution of OH/H_2O on the surface of the Moon seen by M3 on Chandrayaan-1. *Science* **326,** 568–572 (2009).
27. Gladstone, G. R. *et al.* Far-ultraviolet reflectance properties of the Moon's permanently shadowed regions. *J. Geophys. Res.* 117, E00H04, http://dx.doi.org/10.1029/2011JE003913 (2012).

Supplementary Information is linked to the online version of the paper at www.nature.com/nature.

Acknowledgements The LOLA investigation is supported by the Lunar Reconnaissance Orbiter Mission under the auspices of NASA's Exploration Systems Mission Directorate and Science Mission Directorate. We thank T. Perron for discussions.

Author Contributions M.T.Z. led and participated in all aspects of the analysis and wrote the paper. J.W.H. oversaw the relative age dating analysis and participated in geologic interpretation of topography, slopes and roughness. D.E.S. led the acquisition and correction of the LOLA observations. G.A.N. led the slope and roughness analysis and contributed to the development of the topographic grid. E.M. performed refined orbit adjustments and led the analysis of illumination. A.R.T. and C.I.F. performed the crater counts used in the relative age date analysis. O.A. and M.A.R. contributed to the analysis and interpretation of slopes and roughness. H.J.M. contributed to the interpretation of the crater morphology in the context of Shackleton's geological history and volatile sequestration.

Author Information Reprints and permissions information is available at www.nature.com/reprints. The authors declare no competing financial interests. Readers are welcome to comment on the online version of this article at www.nature.com/nature. Correspondence and requests for materials should be addressed to M.T.Z. (zuber@mit.edu).

doi:10.1038/nature11178

Electronic nematicity above the structural and superconducting transition in $BaFe_2(As_{1-x}P_x)_2$

S. Kasahara[1,2], H. J. Shi[1], K. Hashimoto[1]†, S. Tonegawa[1], Y. Mizukami[1], T. Shibauchi[1], K. Sugimoto[3,4], T. Fukuda[5,6,7], T. Terashima[2], Andriy H. Nevidomskyy[8] & Y. Matsuda[1]

Electronic nematicity, a unidirectional self-organized state that breaks the rotational symmetry of the underlying lattice[1,2], has been observed in the iron pnictide[3–7] and copper oxide[8–11] high-temperature superconductors. Whether nematicity plays an equally important role in these two systems is highly controversial. In iron pnictides, the nematicity has usually been associated with the tetragonal-to-orthorhombic structural transition at temperature T_s. Although recent experiments[3–7] have provided hints of nematicity, they were performed either in the low-temperature orthorhombic phase[3,5] or in the tetragonal phase under uniaxial strain[4,6,7], both of which break the 90° rotational C_4 symmetry. Therefore, the question remains open whether the nematicity can exist above T_s without an external driving force. Here we report magnetic torque measurements of the isovalent-doping system $BaFe_2(As_{1-x}P_x)_2$, showing that the nematicity develops well above T_s and, moreover, persists to the non-magnetic superconducting regime, resulting in a phase diagram similar to the pseudogap phase diagram of the copper oxides[8,12]. By combining these results with synchrotron X-ray measurements, we identify two distinct temperatures—one at T^*, signifying a true nematic transition, and the other at T_s ($<T^*$), which we show not to be a true phase transition, but rather what we refer to as a 'meta-nematic transition', in analogy to the well-known meta-magnetic transition in the theory of magnetism.

Magnetic torque measurements provide a stringent test of nematicity for systems with tetragonal symmetry[13]. The torque $\boldsymbol{\tau} = \mu_0 V\mathbf{M} \times \mathbf{H}$ is a thermodynamic quantity, a differential of the free energy with respect to angular displacement. Here μ_0 is the permeability of vacuum, V is the sample volume, and $\mathbf{M}$ is the magnetization induced in the magnetic field $\mathbf{H}$. When $\mathbf{H}$ is rotated within the tetragonal a–b plane (Fig. 1a, b), τ is a periodic function of 2ϕ, where ϕ is the azimuthal angle measured from the a axis:

$$\tau_{2\phi} = \frac{1}{2}\mu_0 H^2 V[(\chi_{aa} - \chi_{bb})\sin 2\phi - 2\chi_{ab}\cos 2\phi] \qquad (1)$$

where the susceptibility tensor χ_{ij} is defined by $M_i = \Sigma_j \chi_{ij} H_j$. In a system maintaining tetragonal symmetry, $\tau_{2\phi}$ should be zero, because $\chi_{aa} = \chi_{bb}$ and $\chi_{ab} = 0$. Finite values of $\tau_{2\phi}$ appear if a new electronic or magnetic state emerges that breaks the C_4 tetragonal symmetry. In such a case, rotational symmetry breaking is revealed by $\chi_{aa} \neq \chi_{bb}$ and/or $\chi_{ab} \neq 0$, depending on the direction of the nematicity.

$BaFe_2(As_{1-x}P_x)_2$ is a prototypical family of iron pnictides[14–18], whose phase diagram is displayed in Fig. 1c. The temperature evolution of the torque $\tau(\phi)$ for the optimally doped compound ($x = 0.33$) is depicted in the upper panels of Fig. 1d. The two- and four-fold oscillations, $\tau_{2\phi}$ and $\tau_{4\phi}$, obtained from the Fourier analysis are shown respectively in the middle and lower panels of Fig. 1d. The distinct two-fold oscillations appear at low temperatures, whereas they are absent at high temperatures

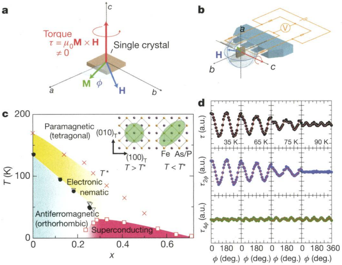

Figure 1 | Torque magnetometry and the doping–temperature phase diagram of $BaFe_2(As_{1-x}P_x)_2$. a, b, Schematic representations of the experimental configuration for torque measurements under in-plane field rotation. In a nematic state, domain formation with different preferred directions in the a–b plane ('twinning') will occur. We used very small single crystals with typical size ~70 μm × 70 μm × 30 μm, in which a significant difference in volume between the two types of domains enables the observation of uncompensated $\tau_{2\phi}$ signals. The equation given in the figure for τ assumes unit volume; see text for details. A single-crystalline sample (brown block) is mounted on the piezo-resistive lever which is attached to the base (blue block) and forms an electrical bridge circuit (orange lines) with the neighbouring reference lever. A magnetic field **H** can be rotated relative to the sample, as illustrated by a blue arrow on a sphere. In this experiment, the field is precisely applied in the a–b plane. **c**, Phase diagram of $BaFe_2(As_{1-x}P_x)_2$. This system is clean and homogeneous[14,16,17], as demonstrated by the quantum oscillations observed over a wide x range[16]. The antiferromagnetic transition at T_N (filled circles)[15] coincides or is preceded by the structural transition at T_s (open triangles)[18]. The superconducting dome extends over a doping range $0.2 < x < 0.7$ (open squares), with maximum $T_c = 31$ K. Crosses indicate the nematic transition temperature T^* determined by the torque and synchrotron X-ray diffraction measurements. The insets illustrate the tetragonal FeAs/P layer. $\chi_{ab} = 0$ above T^* yielding an isotropic torque signal (green-shaded circle), whereas $\chi_{ab} \neq 0$ below T^*, indicating the appearance of the nematicity along the $[110]_T$ (Fe–Fe bond) direction, illustrated with the green-shaded ellipse. **d**, The upper panels depict the temperature evolution of the raw torque $\tau(\phi)$ at $\mu_0 H = 4$ T for $BaFe_2(As_{0.67}P_{0.33})_2$ ($T_c = 30$ K). All torque curves are reversible with respect to the field rotation. $\tau(\phi)$ can be decomposed as $\tau(\phi) = \tau_{2\phi} + \tau_{4\phi} + \tau_{6\phi} + \cdots$, where $\tau_{2n\phi} = A_{2n\phi}\sin 2n(\phi - \phi_0)$ has $2n$-fold symmetry with integer n. The middle and lower panels display the two- and four-fold components obtained from Fourier analysis. The four-fold oscillations $\tau_{4\phi}$ (and higher-order terms) arise primarily from the nonlinear susceptibilities[13]. a.u., arbitrary units.

---

[1]Department of Physics, Kyoto University, Kyoto 606-8502, Japan. [2]Research Center for Low Temperature and Materials Sciences, Kyoto University, Kyoto 606-8501, Japan. [3]Research and Utilization Division, JASRI SPring-8, Sayo, Hyogo 679-5198, Japan. [4]Structural Materials Science Laboratory, RIKEN SPring-8, Sayo, Hyogo 679-5148, Japan. [5]Quantum Beam Science Directorate, JAEA SPring-8, Sayo, Hyogo 679-5148, Japan. [6]Materials Dynamics Laboratory, RIKEN SPring-8, Sayo, Hyogo 679-5148, Japan. [7]JST, Transformative Research-Project on Iron Pnictides (TRIP), Chiyoda, Tokyo 102-0075, Japan. [8]Department of Physics and Astronomy, Rice University, 6100 Main Street, Houston, Texas 77005, USA. †Present address: Institute for Materials Research, Tohoku University, Sendai 980-8577, Japan.

(middle panels of Fig. 1d). As shown in the upper panel of Fig. 2a, the amplitude of the two-fold oscillation $|A_{2\phi}|$ is nearly zero at high temperatures, and grows rapidly below $T^* \approx 85$ K. These results clearly indicate that the tetragonal C_4 symmetry, which is preserved at high temperatures, is broken below T^*, demonstrating the formation of the electronic nematic phase at T^*. The two-fold oscillations below T^* follow the functional form $\tau_{2\phi} = A_{2\phi}\cos 2\phi$, meaning that $\chi_{aa} = \chi_{bb}$ and $\chi_{ab} \neq 0$, which indicates the nematicity along the tetragonal [110] direction, that is, the Fe–Fe bond direction (Fig. 1c, inset). Anomalies at T^* can also be seen in the synchrotron X-ray diffraction measurements (middle panel of Fig. 2a), in which the full-width at half-maximum (FWHM) of the high-order Bragg peaks at $T < T^*$ (Fig. 2a, red circles) grows more quickly as temperature is reduced than does the linear extrapolation from above T^*, and is accompanied by the suppression of the peak intensity (green circles). This indicates a broadening (or small splitting) of the Bragg peak below T^*, implying domain formation due to the nematicity which, to some extent, couples to the orthorhombic lattice distortion (as discussed later).

Figure 2b–e shows the results for the lower-concentration samples ($x = 0.27, 0.23, 0.14, 0$) exhibiting both the tetragonal-to-orthorhombic and magnetic transitions. In these crystals, $|A_{2\phi}|$ is finite even at 200 K (grey circles in upper panels), and initially increases with decreasing temperature, exhibiting a cusp-like peak at T^*. We attribute T^* to the electronic nematic transition temperature for the following reasons. Similarly to the optimally doped compound, the X-ray FWHM and intensity change their slope at T^* (middle panels in Fig. 2b–e). Moreover, the two-fold term in these compounds can be clearly separated into two components (see Supplementary Information) as $\tau_{2\phi} = A_{2\phi}^{\mathrm{nem}} \cos 2\phi + A_{2\phi}^{\mathrm{ext}} \sin 2(\phi - \phi_{\mathrm{ext}})$, in which ϕ_{ext} is temperature independent and $A_{2\phi}^{\mathrm{ext}}$ has a smooth temperature dependence with the phase ϕ_{ext} that is sample dependent. This demonstrates that the observed two-fold oscillations contain the [110] nematic term $A_{2\phi}^{\mathrm{nem}}\cos 2\phi$ in addition to some other, extrinsic two-fold term. The obtained nematic amplitude $A_{2\phi}^{\mathrm{nem}}(T)$ appears below T^* (blue circles in upper panels); this behaviour is well reproduced for different crystals of the same composition (Fig. 2b and Supplementary Fig. 3). The origin of the non-zero two-fold signal at temperatures above T^* is not clear, but the sample-dependent phase ϕ_{ext} points to the possibility of impurity-induced in-plane magnetic anisotropy[19]. In contrast to previous experiments, the present measurements have been performed in the absence of uniaxial stress, providing thermodynamic evidence for the electronic nematic transition at T^*, well above the structural lattice transition temperature T_s. The continuous doping dependence of $T^*(x)$ displayed in Fig. 1c indicates that nematicity persists over a wide range of doping, covering the non-magnetic superconducting regime.

Clearly, there cannot be two nematic phase transitions at both T_s and T^*, because the C_4 rotational symmetry can only be broken once. Our measurements show that the temperature T^* ($>T_s$) marks the onset of the true phase transition, accompanied by the nematic two-fold torque component $A_{2\phi} \neq 0$. This raises the question as to what happens at the structural transition temperature, T_s. This question can be answered straightforwardly if one considers the Landau free energy expansion in terms of two order parameters, the orthorhombic lattice distortion $\delta = (a-b)/(a+b)$ and the phenomenological electronic nematic parameter ψ (proportional to the measured torque amplitude $A_{2\phi}$), which can be written as follows:

$$F[\delta,\psi] = \left[t_s\delta^2 - u\delta^4 + v\delta^6\right] + \left[t_p\psi^2 + w\psi^4 + \mathcal{O}(\psi^6)\right] - g\psi\delta \quad (2)$$

with the terms in the first set of square brackets on the right-hand side describing the first-order structural phase transition and the second bracket responsible for the (second-order) nematic phase transition.

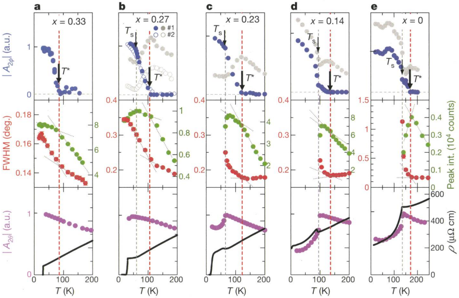

Figure 2 | Nematic and meta-nematic transitions. Temperature dependence of the two-fold oscillation amplitude $|A_{2\phi}|$ of the torque (blue circles in upper panels), the FWHM and peak intensity (red and green circles in middle panels, respectively) of the synchrotron X-ray Bragg reflection, the in-plane resistivity ρ (black lines in lower panels), and the torque amplitude for polar-angle rotation (pink circles in lower panels) are shown for x values of 0.33 (**a**), 0.27 (**b**), 0.23 (**c**), 0.14 (**d**) and 0 (**e**). The nematic transition temperature T^* and the meta-nematic transition temperature T_s are defined by red and grey vertical dashed lines, respectively, as well as by arrows in the upper panels. For underdoped ($x \leq 0.27$) and parent ($x = 0$) crystals, the intrinsic nematic signal for $|A_{2\phi}|$ is extracted from the raw data (grey circles in upper panels) with subtraction of the smooth background of the two-fold oscillations, $A_{2\phi}{}^{\mathrm{ext}}\sin 2(\phi - \phi_{\mathrm{ext}})$, above T^* (Supplementary Fig. 2). For $x = 0.27$, the sample dependence is also shown. The X-ray data have been analysed for several Bragg peaks in the following tetragonal directions of the reciprocal space: $[10,0,0]_{\mathrm{T}}$ (**a**), $[7,7,0]_{\mathrm{T}}$ (**b**, **e**) or $[8,8,0]_{\mathrm{T}}$ (**c**, **d**). For $x \leq 0.23$ a clear splitting of the Bragg peaks is observed below T_s (Supplementary Fig. 5). The dotted lines are guides to the eye. For $x = 0$, 0.27 and 0.33, the same crystal has been used for the torque and X-ray measurements. We find no clear anomaly in the resistivity $\rho(T)$ and the torque signal $|A_{2\theta}|$ for polar-angle rotation (which would detect the a–c anisotropy of susceptibility; lower panel), indicating that the anomalies are associated only with the in-plane nematicity. The magnitude of $|A_{2\phi}|$ has only a weak field dependence (Supplementary Fig. 4), implying that the nematic anisotropy prevails in the zero-field limit, which is consistent with the X-ray results taken at zero field.

Here u, v and w are phenomenological Landau coefficients describing these transitions, and g is the coupling strength between the two order parameters. The temperature-dependent coefficients $t_s = \left(T - T_s^{(0)}\right)/T_s^{(0)}$ and $t_p = \left(T - T_p^{(0)}\right)/T_p^{(0)}$ were chosen such that in the absence of the coupling between the two order parameters, the structural transition occurs at lower temperature $T_s^{(0)} \left(< T_p^{(0)}\right)$. Thanks to the linear coupling between the two order parameters, as expressed in the last term in equation (2), both ψ and δ develop non-zero values below the nematic transition temperature T^* (Fig. 3a, b). On the other hand, T_s ceases to be a true phase transition, since the C_4 symmetry is already broken on either side of T_s, and the lattice distortion δ is non-zero over the entire temperature range (Fig. 3a). Instead, both δ and ψ undergo a finite jump at T_s, as illustrated in Fig. 3. We call this a 'meta-nematic transition', in analogy to the meta-magnetic transition in the theory of magnetism, where the magnetization undergoes a jump as a function of temperature or applied magnetic field, but remains non-zero on both sides of the transition. The analysis of the free energy below T^* shows that it exhibits a maximum at $\psi = 0$ and a single minimum at finite ψ, as in the second-order Landau phase transition (Supplementary Fig. 6).

To quantify the lattice distortion δ experimentally, we have analysed the X-ray data using a two-peak fitting procedure (Supplementary Fig. 5), which reveals that the data in the region $T_s < T < T^*$ can be fitted with very small but finite δ. The results, $\delta(T)$, can be well reproduced within the framework of equation (2), as Fig. 3a demonstrates. Moreover, the same set of Landau parameters also fits the temperature dependence of the nematic order parameter $\psi \propto A_{2\phi}$ well, except below the Néel temperature T_N, where additional effects of antiferromagnetism may enter the magnetic torque anisotropy (Fig. 3b). We have thus established that the true thermodynamic transition occurs at $T = T^*$, and is accompanied by the development of non-zero values of both the nematic order parameter ψ and the lattice distortion δ. We note that similarly small but non-zero values of δ have been recently reported[20] in the powder diffraction measurements of $SmFeAs(O_{1-x}F_x)$.

Under applied uniaxial strain, the lattice distortion δ is expected to develop a non-zero value even above the tetragonal-to-orthorhombic structural transition temperature, and by virtue of linear coupling to the nematic order parameter in equation (2), this will lead to an increase in the value of the electronic anisotropy ψ. This reasoning is consistent with the observation of resistivity anisotropy in the detwinned samples above the structural transition[6,7].

We note that the above explanation in terms of coupling between the electronic and lattice degrees of freedom is very generic, and does not depend on the precise microscopic nature of the nematic order parameter ψ, be it caused by Z_2 spin-nematic ordering[21–24], or by orbital ordering[25–29]. In fact, both mechanisms can cooperate to break the C_4 symmetry spontaneously. In the spin-nematic scenario, the instability is driven by thermal spin fluctuations above the antiferromagnetically ordered phase[24], potentially applicable to the $x \lesssim 0.30$ regime in $BaFe_2(As_{1-x}P_x)_2$ (ref. 15). In the absence of long-range magnetic ordering ($x > 0.30$), quantum spin fluctuations can in principle still drive the instability; however, the fact that the nematic transition at T^* occurs even for superconducting samples far away from the antiferromagnetic phase (see Fig. 1c) indicates that a different mechanism may be at play. In particular, orbital ordering may turn out to be more important, where the electronic nematic transition naturally occurs as a result of orbital polarization between the Fe d_{xz} and d_{yz} orbitals[29], $\psi \propto (n_{xz} - n_{yz})$, where n_{xz} (n_{yz}) denotes the occupation of the iron d_{xz} (d_{yz}) orbital. This mechanism of nematicity is supported by the recent angle-resolved photoemission spectroscopy (ARPES)[4] and quadrupolar resonance measurements[30].

There is a growing body of evidence that entanglement of the spin and orbital degrees of freedom leads to emergent novel electronic phases in the iron pnictides. The present temperature-doping phase diagram bears a resemblance to that of the high-transition-temperature (high-T_c) copper oxides, in that the suppression of the antiferromagnetic ground state leads to the emergence of high-T_c superconductivity, and the electronic nematic instability occurs well above the magnetic and superconducting transitions. Recent infrared studies of charge dynamics report the formation of a pseudogap in the excitation spectrum of optimally doped $BaFe_2(As_{1-x}P_x)_2$ below ~100 K (S. J. Moon *et al.*, unpublished results). Further studies are therefore needed to clarify how the nematic transition we report here is related to the pseudogap formation in the iron pnictides.

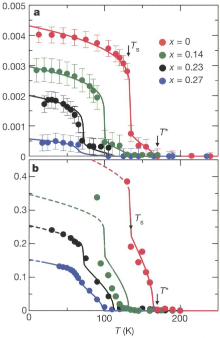

Figure 3 | Temperature dependence of the nematic order parameter and lattice distortion. **a**, Lattice distortion δ ($= (a - b)/(a + b)$) and **b**, the nematic order parameter ψ, proportional to measured $A_{2\phi}$ component of the torque in the paramagnetic temperature region, are fitted to the theory (lines) based on the Landau free energy expansion (equation (2)) using the same set of parameters (Supplementary Information). For the parent compound ($x = 0$, red): $u = 3.28$, $v = 4.08$, $w = 4.52$, $g = 1.91$, $T_s^{(0)} = 52$ K, $T_p^{(0)} = 117$ K; for $x = 0.14$ (green): $u = 9.48$, $v = 31.4$, $w = 31.5$, $g = 2.72$, $T_s^{(0)} = 35$ K, $T_p^{(0)} = 79$ K; for $x = 0.23$ (black): $u = 8.57$, $v = 27.3$, $w = 22.4$, $g = 2.34$, $T_s^{(0)} = 26$ K, $T_p^{(0)} = 79$ K; and for $x = 0.27$ (blue): $u = 4.37$, $v = 10.07$, $w = 42.58$, $g = 3.11$, $T_s^{(0)} = 24$ K, $T_p^{(0)} = 56$ K. Note that because of the coupling between the order parameters, both T_s and T^* get renormalized compared to their initial values $T_s^{(0)}$ and $T_p^{(0)}$. The experimental errors in **a** (error bars, s.e.m.) are estimated in the two-peak fitting procedure from the width of the Bragg peaks (Supplementary Information). In the antiferromagnetic phase below T_N, the amplitude $A_{2\phi}(T)$ shows deviations from $\psi(T)$ (dashed lines in **b**) for $x \leq 0.14$, where effects of the antiferromagnetic moment on torque may be large.

Received 1 November 2011; accepted 1 May 2012.

1. Kivelson, S. A., Fradkin, E. & Emery, V. J. Electronic liquid-crystal phases of a doped Mott insulator. *Nature* **393,** 550–553 (1998).
2. Fradkin, E., Kivelson, S. A., Lawler, M. J., Eisenstein, J. P. & Mackenzie, A. P. Nematic Fermi fluids in condensed matter physics. *Annu. Rev. Condens. Matter Phys.* **1,** 153–178 (2010).
3. Zhao, J. *et al.* Spin waves and magnetic exchange interactions in $CaFe_2As_2$. *Nature Phys.* **5,** 555–560 (2009).
4. Yi, M. *et al.* Symmetry-breaking orbital anisotropy observed for detwinned $Ba(Fe_{1-x}Co_x)_2As_2$ above the spin density wave transition. *Proc. Natl Acad. Sci. USA* **108,** 6878–6883 (2011).
5. Chuang, T.-M. *et al.* Nematic electronic structure in the "parent" state of the iron-based superconductor $Ca(Fe_{1-x}Co_x)_2As_2$. *Science* **327,** 181–184 (2010).
6. Chu, J.-H. *et al.* In-plane resistivity anisotropy in an underdoped iron arsenide superconductor. *Science* **329,** 824–826 (2010).
7. Tanatar, M. *et al.* Uniaxial-strain mechanical detwinning of $CaFe_2As_2$ and $BaFe_2As_2$ crystals: optical and transport study. *Phys. Rev. B* **81,** 184508 (2010).
8. Lawler, M. J. *et al.* Intra-unit-cell electronic nematicity of the high-T_c copper-oxide pseudogap states. *Nature* **466,** 347–351 (2010).

9. Hinkov, V. *et al.* Electronic liquid crystal state in the high-temperature superconductor $YBa_2Cu_3O_{6.45}$. *Science* **319,** 597–600 (2008).
10. Ando, Y., Segawa, K., Komiya, S. & Lavrov, A. N. Electrical resistivity anisotropy from self-organized one dimensionality in high-temperature superconductors. *Phys. Rev. Lett.* **88,** 137005 (2002).
11. Daou, R. *et al.* Broken rotational symmetry in the pseudogap phase of a high-T_c superconductor. *Nature* **463,** 519–522 (2010).
12. Damascelli, A., Hussain, Z. & Shen, Z.-X. Angle-resolved photoemission studies of the cuprate superconductors. *Rev. Mod. Phys.* **75,** 473–541 (2003).
13. Okazaki, R. *et al.* Rotational symmetry breaking in the hidden-order phase of URu_2Si_2. *Science* **331,** 439–442 (2011).
14. Kasahara, S. *et al.* Evolution from non-Fermi- to Fermi-liquid transport via isovalent doping in $BaFe_2(As_{1-x}P_x)_2$ superconductors. *Phys. Rev. B* **81,** 184519 (2010).
15. Nakai, Y. *et al.* Unconventional superconductivity and antiferromagnetic quantum critical behavior in the isovalent-doped $BaFe_2(As_{1-x}P_x)_2$. *Phys. Rev. Lett.* **105,** 107003 (2010).
16. Shishido, H. *et al.* Evolution of the Fermi surface of $BaFe_2(As_{1-x}P_x)_2$ on entering the superconducting dome. *Phys. Rev. Lett.* **104,** 057008 (2010).
17. Hashimoto, K. *et al.* Line nodes in the energy gap of superconducting $BaFe_2(As_{1-x}P_x)_2$ single crystals as seen via penetration depth and thermal conductivity. *Phys. Rev. B* **81,** 220501(R) (2010).
18. Böhmer, A. E. *et al.* Thermodynamic phase diagram and phase competition in $BaFe_2(As_{1-x}P_x)_2$ studied by thermal expansion. Preprint at http://arxiv.org/abs/1203.2119 (2012).
19. Inoue, Y., Yamakawa, Y. & Kontani, H. Impurity-induced electronic nematic state in iron-pnictide superconductors. Preprint at ⟨http://arxiv.org/abs/1110.2401⟩ (2011).
20. Martinelli, A. *et al.* Retention of the tetragonal to orthorhombic structural transition in F-substituted SmFeAsO: a new phase diagram for $SmFeAs(O_{1-x}F_x)$. *Phys. Rev. Lett.* **106,** 227001 (2011).
21. Fang, C., Yao, H., Tsai, W.-F., Hu, J. & Kivelson, S. A. Theory of electron nematic order in LaFeAsO. *Phys. Rev. B* **77,** 224509 (2008).
22. Xu, C., Müller, M. & Sachdev, S. Ising and spin orders in the iron-based superconductors. *Phys. Rev. B* **78,** 020501(R) (2008).
23. Fernandes, R. M. *et al.* Effects of nematic fluctuations on the elastic properties of iron arsenide superconductors. *Phys. Rev. Lett.* **105,** 157003 (2010).
24. Fernandes, R. M., Chubukov, A. V., Knolle, J., Eremin, I. & Schmalian, J. Preemptive nematic order, pseudogap, and orbital order in the iron pnictides. *Phys. Rev. B* **85,** 024534 (2012).
25. Singh, R. R. P. Exchange constants and neutron spectra of iron pnictide materials. Preprint at http://arxiv.org/abs/0903.4408 (2009).
26. Lee, C.-C., Yin, W.-G. & Ku, W. Ferro-orbital order and strong magnetic anisotropy in the parent compounds of iron-pnictide superconductors. *Phys. Rev. Lett.* **103,** 267001 (2009).
27. Lv, W., Wu, J. & Phillips, P. Orbital ordering induces structural phase transition and the resistivity anomaly in iron pnictides. *Phys. Rev. B* **80,** 224506 (2009).
28. Chen, C.-C. *et al.* Orbital order and spontaneous orthorhombicity in iron pnictides. *Phys. Rev. B* **82,** 100504 (2010).
29. Nevidomskyy, A. H. Interplay of orbital and spin ordering in the iron pnictides. Preprint at http://arxiv.org/abs/1104.1747 (2011).
30. Lang, G. *et al.* Nanoscale electronic order in iron pnictides. *Phys. Rev. Lett.* **104,** 097001 (2010).

Supplementary Information is linked to the online version of the paper at www.nature.com/nature.

Acknowledgements We thank J. G. Analytis, A. Q. R. Baron, E. Bascones, A. Carrington, A. V. Chubukov, R. M. Fernandes, I. Fischer, H. Ikeda, H. Kontani, R. Okazaki and J. Schmalian for discussions. This research was supported by a Grant-in-Aid for the Global COE programme 'The Next Generation of Physics, Spun from Universality and Emergence' from MEXT of Japan, and by the KAKENHI programme from JSPS. A.H.N. and Y.M. acknowledge the hospitality of the Aspen Center for Physics. The synchrotron radiation experiments were performed at the BL02B1 of SPring-8 with the approval of the Japan Synchrotron Radiation Research Institute (JASRI).

Author Contributions S.K. and H.J.S. performed magnetic torque measurements. S.K., H.J.S., K.H., S.T., Y. Mizukami, T.S., K.S. and T.F. contributed to the synchrotron X-ray measurements. S.K. grew the single crystals and performed transport measurements. A.H.N. carried out theoretical modelling and calculations. T.S. and Y. Matsuda conceived and designed the project. T.S., A.H.N. and Y. Matsuda wrote the manuscript with input from all authors.

Author Information Reprints and permissions information is available at www.nature.com/reprints. The authors declare no competing financial interests. Readers are welcome to comment on the online version of this article at www.nature.com/nature. Correspondence and requests for materials should be addressed to Y. Matsuda (matsuda@scphys.kyoto-u.ac.jp) or T.S. (shibauchi@scphys.kyoto-u.ac.jp).

LETTER

doi:10.1038/nature11150

Multiscale gigapixel photography

D. J. Brady[1], M. E. Gehm[2], R. A. Stack[3], D. L. Marks[1], D. S. Kittle[1], D. R. Golish[2], E. M. Vera[2] & S. D. Feller[1]

Pixel count is the ratio of the solid angle within a camera's field of view to the solid angle covered by a single detector element. Because the size of the smallest resolvable pixel is proportional to aperture diameter and the maximum field of view is scale independent, the diffraction-limited pixel count is proportional to aperture area. At present, digital cameras operate near the fundamental limit of 1–10 megapixels for millimetre-scale apertures, but few approach the corresponding limits of 1–100 gigapixels for centimetre-scale apertures. Barriers to high-pixel-count imaging include scale-dependent geometric aberrations, the cost and complexity of gigapixel sensor arrays, and the computational and communications challenge of gigapixel image management. Here we describe the AWARE-2 camera, which uses a 16-mm entrance aperture to capture snapshot, one-gigapixel images at three frames per minute. AWARE-2 uses a parallel array of microcameras to reduce the problems of gigapixel imaging to those of megapixel imaging, which are more tractable. In cameras of conventional design, lens speed and field of view decrease as lens scale increases[1], but with the experimental system described here we confirm previous theoretical results[2–6] suggesting that lens speed and field of view can be scale independent in microcamera-based imagers resolving up to 50 gigapixels. Ubiquitous gigapixel cameras may transform the central challenge of photography from the question of where to point the camera to that of how to mine the data.

AWARE-2 is a monocentric, multiscale camera with 120°-by-50° field of view (FOV) and a 38-μrad instantaneous FOV (the angular extent of a single pixel). A monocentric, multiscale camera consists of a spherically symmetric objective lens[3] surrounded by an array of secondary microcameras[2,4,6–9]. AWARE-2 includes 98 microcameras, each with a 14-megapixel sensor. It was constructed as part of the US Defense Advanced Research Projects Agency AWARE programme, which focuses on creating a microcamera platform for scalable, 1–100-gigapixel cameras. Just as the microprocessor is a platform for scalable parallel computing, the microcamera is a platform for scalable parallel cameras with diverse applications in wide-field microscopy, event capture, persistent surveillance and space awareness. As with microprocessors, the designer of microcameras must address granularity and performance trade-offs in selecting aperture and focal plane size, materials and components, and interconnection and processing architecture. Details of the AWARE-2 system design are presented in Supplementary Information, sections 2 and 3. In this Letter, we compare AWARE-2 with previous gigapixel-scale imaging systems, illustrate the capture of a large-scale dynamic event, demonstrate the capacity for high-dynamic-range (HDR) imaging in microcamera systems and analyse the camera's optical resolution.

A gigapixel camera requires a lens system capable of resolving more than 10^9 elements and detectors containing more than 10^9 elements. Designs that address these challenges may be segmented into terrestrial cameras with horizontal 90–120° FOVs (AWARE[4] and Asymmagon; see http://www.gigapxl.org/), airborne surveillance cameras with cylindrical 60–70° FOVs (ARGUS-IS[10] and the multilens array[11]) and astronomical systems with cylindrical 3–4° FOVs (LSST[12] and Pan-STARRS[13]). Design metrics for these systems are provided in Supplementary Table 1.1. Lens design strategies differ between arrays of narrow-field cameras (the multilens array) and single objectives with curved focal planes. Although arbitrarily large pixel counts may be obtained using arrays of conventional cameras, design comparisons confirm, as predicted[1], that the volume of a system with a flat focal plane scales much faster than does that of a design with a curved focal plane. Multiscale design captures the advantage of camera arrays (off-the-shelf focal plane arrays) while avoiding the disadvantage (cost and volume of multiple objective lenses). AWARE uses microcamera arrays to create a large virtual-focal-plane array, in place of precision-mosaicked sensor arrays as used in ARGUS, LSST and Pan-STARRS. The most important points of comparison are that the AWARE design is scalable to larger pixel counts, as illustrated by the AWARE-40 design[4], and that AWARE provides operational advantages over the comparison systems because the focus, gain and exposure of each microcamera can be independently controlled. The disadvantage of the AWARE approach is that a stop must be introduced in the microcamera to balance relative illumination and modulation transfer, thereby increasing system *f* number (the ratio of lens focal length to effective aperture, which is a measure of lens speed) and volume[4,9]. Bare mosaicked arrays may be preferred for fixed-focus, cost-insensitive airborne and astronomical systems. Multiscale design, however, uniquely makes possible compact, low-cost, terrestrial imaging systems focused at finite range.

The potential for novel science using AWARE-2 is illustrated in Fig. 1, which is a gigapixel snapshot of tundra swans on Pungo Lake in the Pocosin Lakes National Wildlife Refuge, USA. Microcamera data was registered and stitched onto a rectangular grid with 38-μrad instantaneous FOV, to produce a 0.96-gigapixel version of Fig. 1. Nonuniformity correction and logarithmic scaling were applied to improve visual display. Figure 1 is downsampled to 4 megapixels for publication. Raw microcamera images of Fig. 1 regions a, b, c, d and e are shown in Fig. 2. The gigapixel snapshot provides information, such as exactly how many swans are on Pungo Lake (656) or in the air above it (27) at the instant the snapshot was taken, that would be unobtainable using a scanned panoramic camera shooting from the same position. Also, the image and image sequences can be mined to analyse signalling behaviour across the flock and to track individual birds. AWARE-2 microcamera control modules use custom electronic modules (Supplementary Information, section 3) to buffer approximately ten image frames locally and to capture asynchronously and transfer individual microcamera images at up to ten frames per second.

An example HDR image is shown in Fig. 3. The brightness of this scene varies from regions of fully sunlit flat surfaces and bright sky to areas of deep shadow. An auto-exposure algorithm adjusts the exposure time for each individual microcamera to maximize the usage of the 8-bit dynamic range in each sensor. When the images are composited into the final scene, knowledge of the exposure setting is combined with the measured pixel values to estimate the source radiance with a global 32-bit dynamic range. Displays are typically limited to 8-bit output, so this HDR result must be mapped onto this smaller dynamic range. Figure 3 was generated by tone-mapping the HDR image.

---

[1]Fitzpatrick Institute for Photonics, Duke University, PO Box 90291, Durham, North Carolina 27708, USA. [2]ECE Department, University of Arizona, PO Box 210104, Tucson, Arizona 85721, USA. [3]Distant Focus Corporation, PO Box 7857, Champaign, Illinois 61826, USA.

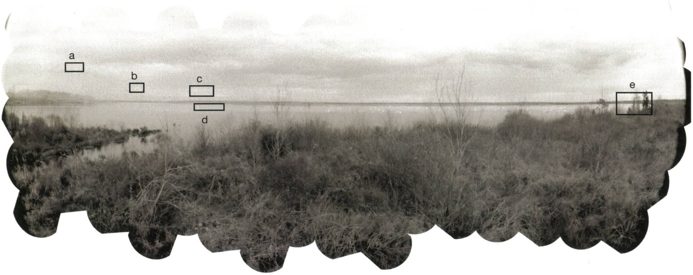

Figure 1 | Pungo Lake as captured using AWARE-2. The total FOV is 120° by 50° and the composite image here consists of 0.96 gigapixels, where each pixel has an instantaneous FOV of 38 μrad. The measured values are logarithmically mapped to make better use of the display dynamic range. The relative responsivities of the individual microcameras were adjusted iteratively to minimize variation across sub-image boundaries. The labelled regions are referred to in Fig. 2.

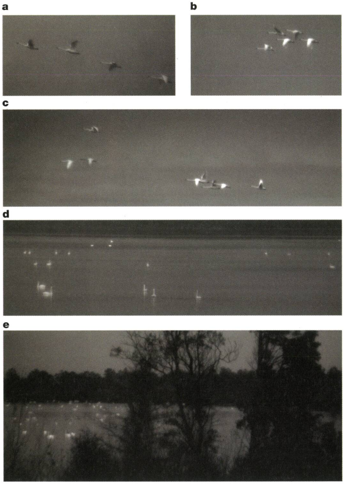

Figure 2 | Details of Fig. 1. a–e, Labelled regions in Fig. 1. The swans in **c** are 114 pixels long and are 310–350 m from AWARE-2. Each pixel corresponds to 13 mm at the position of the swans. In **d**, the most distant bird is 17 pixels long and the closest is 70 pixels long. The limited depth of focus of the camera is illustrated in **e**, where regions of the foreground foliage are in sharpest focus.

Tone mapping creates an individual 32-bit/8-bit conversion for each pixel in the scene, but ensures that the mappings vary smoothly from pixel to pixel[14]. The majority of the display dynamic range is used on shadows and highlights, with mid-tones compressed. The tone-mapped image more accurately matches human visual processing because our vision is foveated and our pupils adjust as we examine different regions of a wide field. More details on the compositing process are provided in Supplementary Information.

The maximum pixel count for an imager with aperture diameter A and the mean operating wavelength λ is $S = \pi A^2 \sin^2(\mathrm{FOV}/2)/\lambda^2$ (ref. 2). For AWARE-2, FOV = 120° and $A = 16$ mm, corresponding to a limit of two gigapixels at an operating wavelength of 550 nm. At its design capacity of 220 microcameras, a fully populated AWARE-2 would capture three gigapixels but the estimated field would decrease to two gigapixels after sensor regions with limited illumination had been removed and overlapping regions had been merged. AWARE-2's resolution is illustrated by the star field shown in Fig. 4, which shows details of a gigapixel sky survey with an exposure time of 1.85 s. Faint stars in this image illuminate two to four pixels after median filtering to remove hot pixels and logarithmic intensity mapping to fill the display dynamic range. We anticipate that higher-resolution multiscale systems with terrestrial motion compensation and microcamera adaptive optics to remove atmospheric blur may be developed for space situational awareness.

As shown in systematic resolution images and modulation transfer function measurements presented in Supplementary Information, section 4b, most of the blur in the star field image is due to defects in AWARE-2's microcamera lenses. To allow low-cost gigapixel array integration, AWARE-2 uses injection-moulded plastic relay optics. These lenses may be moulded with aspheric surfaces, requiring fewer elements and consequently less volume and mass than a spherical glass-element camera with similar performance. However, birefringence in the fabricated optics due to residual stresses introduced during moulding degrades AWARE-2's image quality and resolution relative to fundamental limits. We expect newer high-index plastics that minimize birefringence to enable the camera to approach these theoretical limits. We have also built glass microcamera lenses and, as shown in Supplementary Information, section 4c, AWARE-2 achieves pixel-limited optical resolution with these lenses.

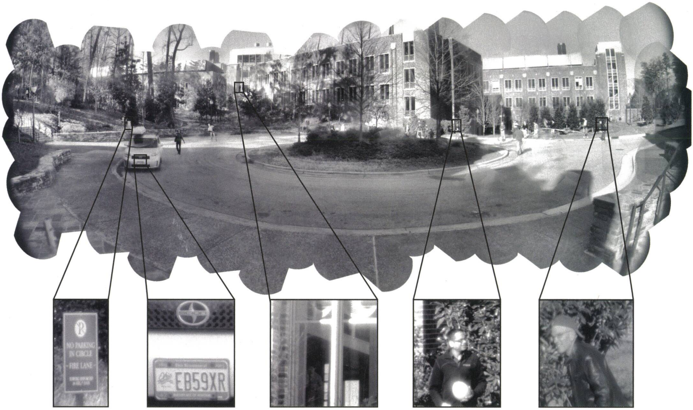
NO PARKING
IN CIRCLE
FIRE LANE
EB59XR

Figure 3 | Traffic circle captured using AWARE-2. Insets are digitally magnified by a factor of 13. Distances to the inset regions range from 15 m ('no parking' sign; first from left) to 92 m (detail of building; third from left). The exposure time for each microcamera was set independently of the others, and a tone-mapping algorithm was used to convert the resulting HDR image for display. Global distortion associated with mapping the 120° horizontal field onto a flat image is apparent.

AWARE-2 demonstrates that the age of ever-increasing pixel count is far from over. Although development of high-performance, low-cost microcamera optics and optomechanics have been the main challenge in the present stage of multiscale camera development, integrated circuits, rather than optics, remain the primary barrier to ubiquitous high-pixel-count imaging. To accommodate the electronics and allow for heat dissipation (the camera expends 430 W during image acquisition), AWARE-2 is mounted in a $0.75\,\mathrm{m} \times 0.75\,\mathrm{m} \times 0.5\,\mathrm{m}$ frame. The optical system occupies less than 3% of the system volume. The size of the camera is dictated both by the size of the electronic control boards and the need to cool them effectively. As more efficient and compact electronics are developed, hand-held gigapixel photography may become an everyday reality.

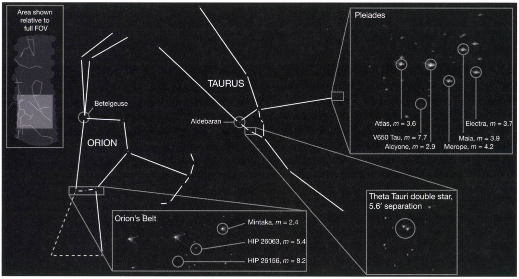
Area shown relative to full FOV
TAURUS
Betelgeuse
ORION
Aldebaran
Pleiades
Atlas, m = 3.6
Electra, m = 3.7
V650 Tau, m = 7.7
Maia, m = 3.9
Alcyone, m = 2.9
Merope, m = 4.2
Theta Tauri double star, 5.6′ separation
Orion's Belt
Mintaka, m = 2.4
HIP 26063, m = 5.4
HIP 26156, m = 8.2

Figure 4 | Details of a star field captured using AWARE-2 with a 1.85-s exposure time. Image data was logarithmically mapped to display values to make better use of the available display dynamic range. Stars with apparent magnitudes of $m < 8.2$ mag are visible in the image. However, those with $m \leq 3.5$ mag saturate the detector at this exposure time.

METHODS SUMMARY

In Figs 1 and 2, all microcameras were set to focus at infinity and had a fixed exposure time of 232 μs. The image was captured on 5 December 2011 at 10:43. Figure 3 was captured using independent auto-exposure and auto-focus in each microcamera. The image shows the Fitzpatrick Center at Duke University on 18 January 2012. In Fig. 4, all microcameras were set to focus at infinity and had a fixed exposure time of 1.85 s. The camera was pointed at a right ascension of 4 h 59 min 2 s and a declination of $37^\circ\ 05'\ 45''$ and was located at $36^\circ\ 00'\ 50.24''$ N, $79^\circ\ 00'\ 13.38''$ W. Cloud cover was near zero. The typical sky brightness at this location is 19.50–18.38 mag arcsec^{-2} in the V band (Bortle scale of approximately 6). The image was captured on 15 January 2012 at 21:44:54 local time.

Auto-exposure initialization requires several seconds and updates in every third frame thereafter. The algorithm steps exposure up and down in logarithmically spaced increments until 1–3% of the pixels are saturated. After exposure is set, the focus motor is stepped in fixed increments. The focus metric is the soft-thresholded sum of the absolute value of the horizontal and vertical gradients independently evaluated over a region of interest, typically a 1,024 × 1,024-pixel image centre. Soft-thresholding sets gradient values below a fixed bias to zero, thus emphasizing sharper features. The step direction reverses when the metric at the present position exceeds the metric at the last position. Focal adjustment stops when reverses occur in three subsequent steps or when eight reverses occur in total. Focus resumes if the metric exceeds 30% of the stored minimum value. If the number of saturated pixels leaves the 1–3% target range, auto-exposure and focus reset.

AWARE-2 was pointed at clear sky with a diffuse plastic dome over the gigagon lens location, to calibrate each pixel's gain and illumination. In all figures shown, variable pixel gain and illumination was removed by 'flat-field correction'.

Received 2 January; accepted 17 April 2012.

1. Lohmann, A. W. Scaling laws for lens systems. *Appl. Opt.* **28,** 4996–4998 (1989).
2. Brady, D. J. & Hagen, N. Multiscale lens design. *Opt. Express* **17,** 10659–10674 (2009).
3. Marks, D. L. & Brady, D. J. in *Imaging Systems 2010*, paper ITuC2 (Optical Society of America, 2010).
4. Marks, D. L., Tremblay, E. J., Ford, J. E. & Brady, D. J. Microcamera aperture scale in monocentric gigapixel cameras. *Appl. Opt.* **50,** 5824–5833 (2011).
5. Son, H. S., Marks, D. L., Hahn, J., Kim, J. & Brady, D. J. Design of a spherical focal surface using close-packed relay optics. *Opt. Express* **19,** 16132–16138 (2011).
6. Tremblay, E. J., Marks, D. L., Brady, D. J. & Ford, J. E. Design and scaling of monocentric multiscale imagers. *Appl. Opt.* (in the press).
7. Cossairt, O., Miau, D. & Nayar, S. K. in *Proc. IEEE Internat. Conf. Comput. Photogr.* http://dx.doi.org/10.1109/ICCPHOT.2011.5753115 (IEEE, 2011).
8. Ford, J. E. & Tremblay, E. in *Imaging Systems 2010*, paper IMC2 (Optical Society of America, 2010).
9. Marks, D. L. & Brady, D. J. Close-up imaging using microcamera arrays for focal plane synthesis. *Opt. Eng.* **50,** 033205–033209 (2011).
10. Leininger, B. *et al.* Autonomous real-time ground ubiquitous surveillance-imaging system (ARGUS-IS). *Proc. SPIE* **6981,** 69810H (2008).
11. Pollock, D. B. *et al.* Multi-lens array system and method. US patent application 11/456 745 (2006).
12. Kahn, S. M. *et al.* Design and development of the 3.2 gigapixel camera for the Large Synoptic Survey Telescope. *Proc. SPIE* **7735,** 77350J (2010).
13. Kaiser, N. Pan-STARRS: a wide-field optical survey telescope array. *Proc. SPIE* **5489,** 11–22 (2004).
14. Reinhard, E., Ward, G., Pattanaik, S. & Debevec, P. *High Dynamic Range Imaging: Acquisition, Display, and Image-Based Lighting* 187–191 (Morgan Kaufmann, 2006).

Supplementary Information is linked to the online version of the paper at www.nature.com/nature.

Acknowledgements The AWARE programme is supported by the Defense Advanced Research Projects Agency (DARPA) contract HR0011-10-C-0073. The project was initiated at DARPA by D. Healy and is managed by N. Dhar. The AWARE-2 microcamera optics design team includes D. Marks, E. Tremblay and J. Ford. Microcamera optics were fabricated by Rochester Photonics Corporation under the management of P. McLaughlin. P. Jansen, J. Hughes and S. Gewalt developed the parallel processing framework, data routing and hardware interface. H. Son and J. Kim developed the optomechanical layout.

Author Contributions D.J.B. and M.E.G. wrote the paper. M.E.G. wrote Supplementary Information, section 1. D.L.M. wrote Supplementary Information, section 2. R.A.S. and M.E.G. wrote Supplementary Information, section 3. D.S.K., D.L.M. and D.J.B. wrote Supplementary Information, section 4. D.S.K., D.L.M. and S.D.F. collected resolution test images and modulation transfer function data. D.S.K. and D.J.B. collected the images shown in Figs 1, 2 and 4. D.S.K. and S.D.F. collected the image shown in Fig. 3. D.R.G., E.M.V. and M.E.G. formed composite images for Figs 1, 3 and 4.

Author Information Reprints and permissions information is available at www.nature.com/reprints. The authors declare no competing financial interests. Readers are welcome to comment on the online version of this article at www.nature.com/nature. Correspondence and requests for materials should be addressed to D.J.B. (dbrady@duke.edu).

LETTER

doi:10.1038/nature11186

First dairying in green Saharan Africa in the fifth millennium BC

Julie Dunne[1], Richard P. Evershed[1], Mélanie Salque[1], Lucy Cramp[1], Silvia Bruni[2], Kathleen Ryan[3], Stefano Biagetti[4] & Savino di Lernia[4,5]

In the prehistoric green Sahara of Holocene North Africa—in contrast to the Neolithic of Europe and Eurasia—a reliance on cattle, sheep and goats emerged as a stable and widespread way of life, long before the first evidence for domesticated plants or settled village farming communities[1–3]. The remarkable rock art found widely across the region depicts cattle herding among early Saharan pastoral groups, and includes rare scenes of milking; however, these images can rarely be reliably dated[4]. Although the faunal evidence provides further confirmation of the importance of cattle and other domesticates[5], the scarcity of cattle bones makes it impossible to ascertain herd structures via kill-off patterns, thereby precluding interpretations of whether dairying was practiced. Because pottery production begins early in northern Africa[6] the potential exists to investigate diet and subsistence practices using molecular and isotopic analyses of absorbed food residues[7]. This approach has been successful in determining the chronology of dairying beginning in the 'Fertile Crescent' of the Near East and its spread across Europe[8–11]. Here we report the first unequivocal chemical evidence, based on the δ^{13}C and Δ^{13}C values of the major alkanoic acids of milk fat, for the adoption of dairying practices by prehistoric Saharan African people in the fifth millennium BC. Interpretations are supported by a new database of modern ruminant animal fats collected from Africa. These findings confirm the importance of 'lifetime products', such as milk, in early Saharan pastoralism, and provide an evolutionary context for the emergence of lactase persistence in Africa.

It is widely accepted that African pastoralism with cattle, sheep and goats emerged long before plant domestication[2], in contrast to the process of 'neolithization' in the Near East, characterized by the transition from a mobile hunter-gatherer lifestyle to an increasingly settled, agricultural way of life. In Saharan Africa, during the Early Holocene, largely sedentary and pottery-producing hunters, fishers and gatherers became nomadic cattle herders[3], dynamically adapting to, and exploiting, different environments and resources.

Today, it seems impossible that cattle could survive in such a hostile environment as the arid desert land of the Sahara, but this region enjoyed vastly more favourable climatic and environmental conditions[12] during the Holocene African Humid Period, which began around 10,000 years ago[13]. Here, faunal evidence demonstrates that by the early sixth millennium BC, cattle, sheep and goats were found together across the savannas of what is now the Sahara[1,5]. This suggests that the inception of dairying practices in North Africa and an early and independent 'secondary products' economy[14] seems plausible given what we now know of the first appearance of milking in the Near East[8].

Compelling evidence of prehistoric cattle herding in northern Africa comes from the remarkable rock paintings and engravings of the Sahara (Fig. 1), possibly the world's largest concentration of prehistoric art, long known for their rich and vivid portrayal of scenes from everyday life[4,15,16]. The extensive rock art demonstrates that cattle played an important part in the lives and ideology of ancient human groups living in this region during the Holocene. This pictorial record contains countless scenes with representations of cattle, some emphasizing the female's full udders and, in a few cases, depictions of the actual milking of a cow, such as at Wadi Teshuinat II[15] in the Acacus or Wadi Tiksatin in the Messak[16]. However, reliable dates for this rock art can rarely be ascertained[4].

Faunal remains from securely dated contexts indicate that domesticated animals (cattle, sheep or goats) were present in the area from the early sixth millennium BC, becoming much more common in the fifth millennium BC. Unfortunately, these remains are highly fragmented and poorly preserved, precluding herd reconstructions, and thus even indirect evidence of dairying is missing[5].

Direct evidence for the practice of dairying, beginning in the seventh millennium BC in northwestern Anatolia[8], appearing in the sixth millennium BC in eastern Europe[11] and reaching Britain in the fourth millennium BC[9,10], has been established through the compound-specific stable carbon isotope analysis of animal fat residues preserved in archaeological pottery. Notably, this research on the antiquity of dairying practices has largely been confined to Europe, the Near East and Eurasia, with no attempt yet being made to identify the inception of dairying practices in the African continent.

Here we present direct chemical evidence for early dairying practices within the central Sahara through the use of gas chromatography (GC), gas chromatography–mass spectrometry (GC–MS) and gas chromatography–combustion–isotope ratio mass spectrometry (GC–C–IRMS) analyses carried out on organic residues extracted from archaeological pottery sampled from the Takarkori rock shelter located in the southwest Fezzan, Libyan Sahara, an area licensed to Sapienza University of Rome (Supplementary Fig. 1). Four seasons of fieldwork identified evidence of Late Acacus (hunter-gatherer) occupation followed by Early, Middle and Late Pastoral remains (Supplementary Fig. 2), dating between approximately 8100 and 2600 BC (Supplementary Table 1). This long Pastoral period, between approximately 6000 and 2600 BC, denotes the adoption of cattle together with sheep and goats, combined with intensive exploitation of wild cereals[17,18].

Analyses of absorbed organic residues focused on 81 potsherds (Supplementary Table 2), covering a wide range of decorative techniques and motifs found on Saharan ceramics[18,19] (Supplementary Fig. 3). These vessels were mainly excavated from securely dated Middle Pastoral ($n = 56$) levels (approximately 5200–3800 BC), with a small number originating from the Late Acacus ($n = 8$) and Early ($n = 14$) and Late Pastoral ($n = 3$) periods. The lipids were extracted using established protocols[8–10]. Many potsherds demonstrated extraordinary preservation of lipids, containing concentrations of up to 6 mg g^{-1} (mean 1.2 mg g^{-1}), with one particular potsherd (TAK

---

[1]Organic Geochemistry Unit, School of Chemistry, University of Bristol, Cantock's Close, Bristol BS8 1TS, UK. [2]Dipartimento di Chimica Inorganica, Metallorganica e Analitica "Lamberto Malatesta", Università degli Studi di Milano - Via G. Venezian 21, 20133 Milano, Italy. [3]African Section, University of Pennsylvania Museum of Archaeology and Anthropology, 3260 South Street, Philadelphia, Pennsylvania 19104-6324, USA. [4]Dipartimento di Scienze dell'Antichità, Sapienza, Università di Roma, Via Palestro, 63 - 00185 Roma, Italy. [5]School of Geography, Archaeology & Environmental Sciences, University of the Witwatersrand, Johannesburg, Private Bag 3, Wits 2050, South Africa.

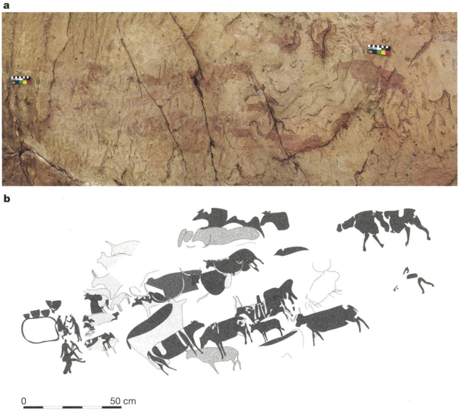

Figure 1 | Rock art image and tracing from Teshuinat II rock shelter, South West Libya. a, b, Rock art image (**a**) and tracing (**b**) showing Saharan pastoralists with their pots and cattle (adapted with permission from ref. 15).

443) having a concentration of 17 mg g^{-1}. It is noteworthy that lipids were observed in every potsherd, in contrast to European archaeological sites, where generally <40% of potsherds contain extractable lipids with mean concentrations of approximately 0.1 mg g^{-1} (refs 10, 20). This remarkable preservation is likely to be related to the extremely arid conditions prevailing in the region.

Lipid biomarker analyses by GC–MS showed that residues fall into three broad categories (Fig. 2). The most common distribution (Fig. 2a) was dominated by high abundances of the $C_{16:0}$ and $C_{18:0}$ fatty acids, which derive from degraded animal fats. Also abundant were branched-chain fatty acids, C_{13} to C_{18}, components of bacterial origin diagnostic of ruminant animal fats[21]. The second most common type of residue (Fig. 2c) contained a relatively low abundance of the $C_{18:0}$ alkanoic acid, with several extracts showing high abundances of C_{12} and C_{14} homologues. Such distributions have rarely been seen in European pottery and are more diagnostic of plant oils[22]. Also present, and again rarely seen in European prehistoric ceramics, are a homologous series of long-chain *n*-alkanes from C_{16}–C_{33} (odd-over-even carbon number predominance), usually maximising at C_{25}, regarded as originating from epicuticular waxes of vascular plants[23]. A third, intermediate category of residue (Fig. 2b) is characterized by a series of α,ω-dicarboxylic acids (diacids), in the C_5 to C_{18} carbon-chain-length range (Fig. 2a, b) with C_9 (azelaic acid) the most abundant homologue, the latter commonly deriving from the 'drying reaction' of plant oils[24]. Such residues also contained long-chain alkyl lipids of plant origin. Together such mixtures probably reflect either processing of both plant and animal products in the vessels or the multi-use of vessels.

Of the 81 potsherds, only those residues unambiguously assigned as degraded animal fats (Table 1)—that is, those dominated by palmitic ($C_{16:0}$) and stearic ($C_{18:0}$) alkanoic acids (for example, Fig. 2a)—were selected for GC–C–IRMS analysis to determine the $\delta^{13}C$ values for $C_{16:0}$ and $C_{18:0}$, with the aim of establishing their origins. Differences in the $\delta^{13}C$ values of $C_{16:0}$ and $C_{18:0}$ alkanoic acids are due to the differential routing of dietary carbon and fatty acids during the synthesis of adipose and dairy fats in ruminant animals, thus allowing ruminant milk fatty acids to be distinguished from carcass fats by calculating $\boldsymbol{\Delta}^{13}C$ values ($\delta^{13}C_{18:0}$–$\delta^{13}C_{16:0}$) and plotting that against the $\delta^{13}C$ value of the $C_{16:0}$ alkanoic acid. Previous research has shown that by plotting $\boldsymbol{\Delta}^{13}C$ values, variations in C_3 versus C_4 plant consumption are removed, thereby emphasizing biosynthetic and metabolic characteristics of the fat source[9,10]. We have now confirmed this through the GC–C–IRMS of a new reference collection of modern ruminant animal fats from Africa collected to encompass the range of carbon isoscapes[25] likely to have been encountered by early Saharan pastoralists. The $\delta^{13}C$ values of the $C_{16:0}$ and $C_{18:0}$ components of these modern fats, presented in Fig. 3, show $\delta^{13}C$ values of goat dairy fats from the Acacus region, Libya ($n = 9$), together with cattle dairy fats and cattle, sheep and goat adipose fats ($n = 9$, 12, 7 and 12, respectively) from Kenya. The $\delta^{13}C_{16.0}$ values for the $C_{16:0}$ alkanoic acids of the African reference fats plot in the range from −35 to −15‰, indicating diets ranging from predominantly C_3 to C_4. These results confirm the global applicability of the $\boldsymbol{\Delta}^{13}C$ proxy.

Of the 29 animal fat residues selected for GC–C–IRMS analyses, 22 originate from Middle Pastoral levels, 3 from the Late Acacus, 2 from the Early Pastoral and the remaining 2 from the Late Pastoral period (Table 1). The comparison of the $\boldsymbol{\Delta}^{13}C$ values of the modern reference animal fats with those of the archaeological pottery residues from the Middle Pastoral period (approximately 5200–3800 BC) show that 50% of these plot within, or on the edge of, the isotopic ranges for dairy fats, with a further 33% falling within the range for ruminant adipose fats and the remainder corresponding to non-ruminant carcass fats (Fig. 3). Notably, the residues originating from earlier periods do not contain dairy fats, and plot in the non-ruminant fat range, probably deriving from wild fauna found locally. The unambiguous conclusion is that the appearance of dairy fats in pottery correlates with the more abundant presence of cattle bones in the cave deposits, suggesting

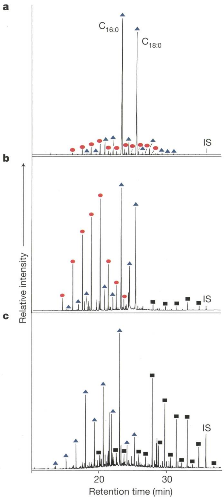

Figure 2 | Partial gas chromatograms displaying the trimethylsilylated lipid extract from potsherds excavated from Middle Pastoral levels in the Takarkori rock shelter. **a–c**, The distributions are characteristic of degraded animal fat (**a**), a mixture of animal and plant fats (**b**) and plant material (**c**). Chromatographic peak identities denoted by filled triangles comprise straight-chain fatty acids in the carbon chain range $C_{9:0}$ to $C_{29:0}$, maximizing at $C_{16:0}$; filled squares represent *n*-alkanes in the carbon-chain range $C_{20:0}$ to $C_{35:0}$; and filled circles indicate α,ω-dicarboxylic acids (diacids) in the carbon-chain range $C_{5:0}$ to $C_{16:0}$. IS, internal standard, C_{34} *n*-tetratriacontane.

a full pastoral economy as the cattle were intensively exploited for their secondary products.

Of particular note is the wide range of $\delta^{13}C$ values exhibited by the alkanoic acids, plotting across the range −25‰ to −10‰, which is broader even than the reference fats range (maximum −15‰). This suggests that the animals giving rise to these fats had subsisted on an extensive range of different forages either composed completely of C_3 plants, varying combinations of C_3 and C_4 plants, or a diet comprising wholly C_4 plants. The wide range of alkanoic acid $\delta^{13}C$ values found for these African potsherds is unprecedented and points to differing pastoral modes of subsistence (such as vertical transhumance, which is still practised today) by these prehistoric Saharan groups. This is supported by their settlement pattern based on summer sites in the lowland sand seas and winter sites (such as Takarkori) in the mountains[3], which was probably in response to seasonal weather patterns.

Our findings provide unequivocal evidence for extensive processing of dairy products in pottery vessels in the Libyan Sahara during the Middle Pastoral period (approximately 5200–3800 BC), confirming that milk played an important part in the diet of these prehistoric pastoral people. The findings are notable for three other reasons: (1) they confirm that domesticated cattle, used as part of a dairying economy, were present in North Africa during the fifth millennium BC, thus supporting the idea of an earlier ingression into the central Sahara[1–3] and suggesting a local process of pastoral development, based on the exploitation of secondary products; (2) the finding of dairy fat residues in pottery is consistent with milk being processed, thereby

Table 1 | Subset of potsherds selected for isotopic analyses

Potsherd number	Laboratory code	Period	Wall decoration technique	Diameter at mouth (cm)	Part of vessel	Lipid concentration ($\mu g\,g^{-1}$)	$\delta^{13}C_{16:0}$	$\delta^{13}C_{18:0}$	$\Delta^{13}C$	Classification
21	TAK21A	Middle Pastoral	Plain edge fishnet	Not known	Wall + base	5,830.6	−14.7	−20.5	−5.8	Dairy
26	TAK1	Middle Pastoral	APS return	20	Rim + wall	760.7	−14.2	−15.0	−0.9	Ruminant adipose
45	TAK45	Middle Pastoral	APS return	Not known	Wall	639.8	−21.9	−24.1	−2.1	Ruminant adipose
120	TAK120	Middle Pastoral	APS return	Not known	Wall	5,592.7	−15.2	−18.7	−3.5	Dairy
124	TAK124	Middle Pastoral	Ridged APS return	Not known	Wall	1,615.5	−18.1	−20.1	−2.0	Ruminant adipose
197	TAK197	Middle Pastoral	APS return	Not known	Wall	151.5	−20.9	−21.1	−0.2	Non-ruminant adipose
420	TAK420	Middle Pastoral	APS return, triangles	Not known	Wall	1,119.3	−18.3	−21.5	−3.2	Dairy
443	TAK443	Middle Pastoral	APS return	Not known	Wall	17,217.6	−16.9	−23.7	−6.8	Dairy
576	TAK6	Middle Pastoral	Ridged plain edge	30	Rim + wall	800.2	−22.0	−21.7	0.3	Non-ruminant adipose
748	TAK9	Middle Pastoral	Ridged APS return	22	Rim + wall	5,650.5	−13.7	−19.0	−5.2	Dairy
824	TAK11	Late Pastoral	Continuous plain edge and impressed dashes	Not known	Wall + base	4,994.2	−20.5	−24.9	−4.4	Dairy
873	TAK873	Middle Pastoral	APS return	Not known	Wall	71.8	−18.5	−17.7	0.8	Non-ruminant adipose
896	TAK896	Middle Pastoral	APS return	Not known	Wall	218.0	−23.6	−25.0	−1.5	Ruminant adipose
987	TAK987	Middle Pastoral	APS return	Not known	Rim + wall	4,442.6	−13.6	−19.3	−5.7	Dairy
997	TAK15	Middle Pastoral	APS return	16	Rim + wall	1,117.4	−13.3	−17.4	−4.1	Dairy
1009	TAK1009	Middle Pastoral	APS paired lines, banded	Not known	Wall	1,555.7	−11.0	−11.0	0.0	Non-ruminant adipose
1012	TAK1012	Middle Pastoral	Irregular APS return	Not known	Wall	3,591.2	−14.9	−16.5	−1.7	Ruminant adipose
1572	TAK1572	Middle Pastoral	APS return	Not known	Wall	3,148.5	−23.7	−28.2	−4.5	Dairy
1693	TAK21	Late Acacus	Undecorated	Not known	Rim + wall	20.1	−23.1	−19.8	3.3	Non-ruminant adipose
1797	TAK24	Early Pastoral	Combined plain edge with semilunar-motif impressed dots	30	Rim + wall	1,674.6	−21.9	−21.0	0.9	Non-ruminant adipose
1846	TAK25	Middle Pastoral	Plain edge continuous	Not known	Wall + base	819.2	−15.6	−19.7	−4.1	Dairy
1863	TAK26	Middle Pastoral	Ridged APS return	16	Rim + wall	175.0	−22.3	−26.2	−4.0	Dairy
1903	TAK27	Early Pastoral	Cord impression	20	Rim + wall	308.5	−22.8	−21.7	1.1	Non-ruminant adipose
2028	TAK2028	Middle Pastoral	APS, paired lines of dashes	Not known	Wall + base	1,931.0	−24.5	−28.9	−4.4	Dairy
2251	TAK28	Middle Pastoral	APS (row of impressed dots)	14	Rim	96.9	−21.5	−24.0	−2.5	Ruminant adipose
2523	TAK29	Late Pastoral	Undecorated	Not known	Rim + wall	445.6	−18.5	−19.7	−1.2	Ruminant adipose
2588	TAK30	Late Acacus	UNCL (impressed dots)	30	Rim + wall	823.3	−13.9	−13.8	0.1	Non-ruminant adipose
2817	TAK32	Late Acacus	Rocker packed	Not known	Rim	6,882.8	−19.3	−17.5	1.8	Non-ruminant adipose
2857	TAK35	Middle Pastoral	APS return continuous, triangles	Not known	Rim + wall	238.3	−20.1	−22.9	−2.8	Ruminant adipose

APS, alternately pivoting stamp.

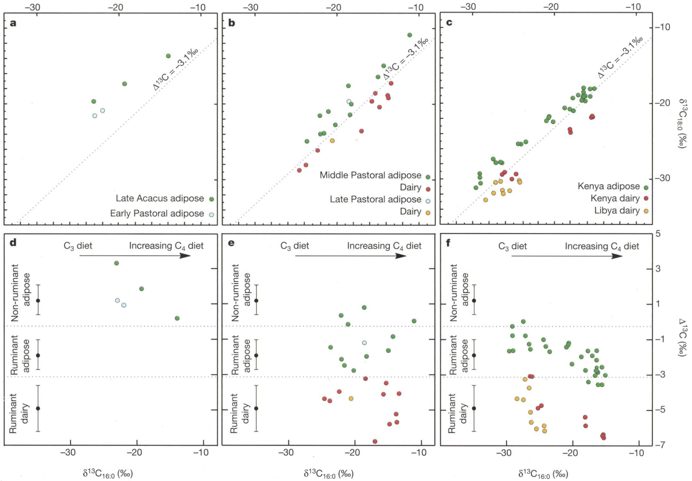

Figure 3 | Plots of $\delta^{13}C$ values and $\Delta^{13}C$ values of alkanoic acids in modern reference ruminant fats and archaeological animal fat residues in prehistoric Saharan pottery. a–c, Plots of the $\delta^{13}C_{16:0}$ and $\delta^{13}C_{18:0}$ values for archaeological animal fat residues in Late Acacus (hunter-gatherer) and Early Pastoral (Neolithic) pottery (**a**), archaeological animal fat residues in Middle and Late Pastoral Neolithic pottery (**b**), and modern reference animal fats collected from Libya and Kenya (**c**). **d–f**, Plots denote $\Delta^{13}C$ values for the archaeological fat residues (Late Acacus/Early Pastoral) (**d**) and Middle/Late Pastoral (**e**) and modern reference animal fats (**f**). Notably, the residues originating from the Late Acacus and Early Pastoral periods (**d**) do not contain dairy fats, and plot in the non-ruminant range, probably deriving from wild fauna. **e**, The extensive processing of dairy products in pottery vessels from this region begins in the Middle Pastoral period approximately 5200–3800 BC. The broad array of values suggests that the animals giving rise to these ruminant fats subsisted on an extensive range of different diets either composed completely of C_3 plants, varying amounts of C_3 and C_4 plants or, for some of the archaeological samples, a diet comprising wholly C_4 plants. The ranges shown here represent the mean ± 1 standard deviation of the $\Delta^{13}C$ values for a global database comprising modern reference ruminant animal fats from Africa, the UK (animals raised on a pure C_3 diet)[10], Kazakhstan[28], Switzerland[29] and the Near East[30], published elsewhere.

providing an explanation of how, in spite of lactose intolerance, milk products could be consumed by these people with the practice being adopted quickly; (3) they are consistent with the finding of the $-13910*T$ allele, associated with the lactase persistence trait in Europeans, across some Central African groups such as the Fulbe from northern Cameroon[26], supporting arguments for some movement of people, together with their cattle, from the Near East into eastern Africa in the Early to Middle Holocene; and (4) they provide a context for understanding the origins and spread of other, independently arising LP-associated gene variants in sub-Saharan Africa[27].

METHODS SUMMARY

A total of 81 potsherds were sampled from the Takarkori rock shelter, Tadrart Acacus Mountains, Libyan Sahara, of which 56 were excavated from the Middle Pastoral period and the remainder originated from the Late Acacus ($n = 8$), and Early ($n = 14$) and Late Pastoral ($n = 3$) periods (Supplementary Table 2). Of the 81 potsherds analysed, 29 were selected for GC–C–IRMS analysis; of these, 18 showed clear evidence of pure animal fat origin, with the remaining 11 comprising lipid profiles suggestive of the mixing of animal and plant fats.

Lipid analysis and interpretations were performed using established protocols described in detail in earlier publications[8–10]. Briefly, ~2 g of potsherd was sampled and surfaces were cleaned with a modelling drill to remove any exogenous lipids. The potsherds were then ground to a powder, an internal standard was added, and solvent was extracted by ultrasonication (chloroform/methanol 2:1 v/v, 2 × 10 ml). The solvent was evaporated under a gentle stream of nitrogen to obtain the total lipid extract (TLE). Aliquots of the TLE were trimethylsilylated (*N*,*O*-bis(trimethylsilyl)trifluoroacetamide 80 μl, 70 °C, 60 min), and submitted to analysis by GC and GC–MS. Further aliquots of the TLE were treated with $NaOH/H_2O$ (9:1 w/v) in methanol (5% v/v, 70 °C, 1 h). Following neutralization, lipids were extracted into chloroform and the excess solvent was evaporated under a gentle stream of nitrogen. Fatty acid methyl esters (FAMEs) were prepared by reaction with BF_3-methanol (14% w/v, 70 °C, 1 h). The FAMEs were extracted with chloroform and the solvent removed under nitrogen. The FAMEs were re-dissolved into hexane for analysis by GC and GC–C–IRMS.

FAMEs of freeze-dried reference fats (typically using 5 mg of TLEs) were prepared exactly as above.

Received 16 March; accepted 8 May 2012.

1. Gifford-Gonzalez, D. & Hanotte, O. Domesticating animals in Africa: implications of genetic and archaeological findings. *J. World Prehist.* **24,** 1–23 (2011).
2. Marshall, F. & Hildebrand, E. Cattle before crops: the beginnings of food production in Africa. *J. World Prehist.* **16,** 99–143 (2002).

3. di Lernia, S. in *Droughts, Food and Culture: Ecological Change and Food Security in Africa's Later Prehistory* (ed. Hassan, F. A.) 225–250 (Kluwer Academic/Plenum, 2002).
4. di Lernia, S. & Gallinaro, M. The date and context of Neolithic rock art in the Sahara: engravings and ceremonial monuments from Messak Settafet (south-west Libya). *Antiquity* **84,** 954–975 (2010).
5. Gautier, A. in *Droughts, Food and Culture: Ecological Change and Food Security in Africa's Later Prehistory* (ed. Hassan, F. A.) 195–208 (Kluwer Academic/Plenum, 2002).
6. Huysecom, E. *et al.* The emergence of pottery in Africa during the tenth millennium cal BC: new evidence from Ounjougou (Mali). *Antiquity* **83,** 905–917 (2009).
7. Evershed, R. P. Organic residue analysis in archaeology: the archaeological biomarker revolution. *Archaeometry* **50,** 895–924 (2008).
8. Evershed, R. P. *et al.* Earliest date for milk use in the Near East and southeastern Europe linked to cattle herding. *Nature* **455,** 528–531 (2008).
9. Copley, M. S. *et al.* Direct chemical evidence for widespread dairying in prehistoric Britain. *Proc. Natl Acad. Sci. USA* **100,** 1524–1529 (2003).
10. Dudd, S. N. & Evershed, R. P. Direct demonstration of milk as an element of archaeological economies. *Science* **282,** 1478–1481 (1998).
11. Craig, O. E. *et al.* Did the first farmers of central and eastern Europe produce dairy foods? *Antiquity* **79,** 882–894 (2005).
12. Cremaschi, M., Zerboni, A., Spötl, C. & Felletti, F. The calcareous tufa in the Tadrart Acacus Mt. (SW Fezzan, Libya) An early Holocene palaeoclimate archive in the central Sahara. *Palaeogeogr. Palaeoclimatol. Palaeoecol.* **287,** 81–94 (2010).
13. deMenocal, P. *et al.* Abrupt onset and termination of the African Humid Period: rapid climate responses to gradual insolation forcing. *Quat. Sci. Rev.* **19,** 347–361 (2000).
14. Sherratt, A. The secondary exploitation of animals in the Old World. *World Archaeol.* **15,** 90–104 (1983).
15. Gallinaro, M. *et al.* in *La Memoria dell'arte. Le pitture rupestri dell'Acacus tra passato e futuro* (eds di Lernia, S. & Zampetti, D.) 73–255 (All'Insegna del Giglio, 2008).
16. Lutz, R. & Lutz, G. *The Secret of the Desert: the Rock Art of the Messak Settafet and Messak Mellet, Libya* (Golf, 1995).
17. Biagetti, S. & di Lernia, S. in *On Shelter's Ledge: Histories, Theories and Methods of Rockshelter Research* (eds Kornfeld, M., Vasil'ev, S. & Miotti, L.) 125–132 (British Archaeological Reports S1655, Archaeopress, 2007).
18. Biagetti, S., Merighi, F. & di Lernia, S. Decoding an Early Holocene Saharan stratified site. Ceramic dispersion and site formation processes in the Takarkori rock-shelter, Acacus Mountains, Libya. *J. Afric. Archaeol.* **2,** 3–21 (2004).
19. Caneva, I. in *Archaeology and Environment in the Libyan Sahara. The Excavations in the Tadrart Acacus, 1978–1983* (ed. Barich, B.) 231–254 (British Archaeological Reports S368, Archaeopress, 1987).
20. Charters, S. *et al.* Quantification and distribution of lipid in archaeological ceramics: implications for sampling potsherds for organic residue analysis. *Archaeometry* **35,** 211–223 (1993).
21. Christie, W. W. *Lipid Metabolism in Ruminant Animals* (Pergamon, 1981).
22. Copley, M. S. *et al.* Detection of palm fruit lipids in archaeological pottery from Qasr Ibrim, Egyptian Nubia. *Proc. R. Soc. Lond. B* **268,** 593–597 (2001).
23. Tulloch, A. P. in *Chemistry and Biochemistry of Natural Waxes* (ed. Kolattukudy, P. E.) 235–287 (Elsevier, 1976).
24. Mills, J. S. & White, R. *The Organic Chemistry of Museum Objects* 2nd edn (Elsevier, 1987).
25. West, J. B., Bowen, G. J., Dawson, T. E. & Tu, K. P. *Isoscapes: Understanding Movement, Pattern and Process on Earth through Isotope Mapping* (Springer, 2010).
26. Mulcare, C. A. *et al.* The T allele of a single-nucleotide polymorphism 13.9 kb upstream of the lactase gene (*LCT*) (*C−13.9kbT*) does not predict or cause the lactase-persistence phenotype in Africans. *Am. J. Hum. Genet.* **74,** 1102–1110 (2004).
27. Itan, Y., Jones, B. L., Ingram, C. J., Swallow, D. M. & Thomas, M. G. A worldwide correlation of lactase persistence phenotype and genotypes. *BMC Evol. Biol.* **10,** 36 (2010).
28. Outram, A. K. *et al.* The earliest horse harnessing and milking. *Science* **323,** 1332–1335 (2009).
29. Spangenberg, J. E., Jacomet, S. & Schibler, J. Chemical analyses of organic residues in archaeological pottery from Arbon Bleiche 3, Switzerland—evidence for dairying in the late Neolithic. *J. Archaeol. Sci.* **33,** 1–13 (2006).
30. Gregg, M. W., Banning, E. B., Gibbs, K. & Slater, G. F. Subsistence practices and pottery use in Neolithic Jordan: molecular and isotopic evidence. *J. Archaeol. Sci.* **36,** 937–946 (2009).

Supplementary Information is linked to the online version of the paper at www.nature.com/nature.

Acknowledgements We thank the UK Natural Environment Research Council for a PhD studentship to J. D. and the Life Science Mass Spectrometry Facility. Sapienza, University of Rome (Grandi Scavi di Ateneo) and The Minister of Foreign Affairs (DGSP) are thanked for funding for the Italian Archaeological Mission in the Sahara. Our Libyan colleagues in the Departments of Archaeology in Tripoli and Ghat, in particular S. Agab, are also thanked. The USA National Science Foundation and The Royal Society are further thanked for funding.

Author Contributions R.P.E. and S.d.L. conceived and planned the project. J.D., R.P.E. and S.d.L. wrote the paper. J.D., M.S., L.C. and S.B. performed analytical work and data analysis, and S.d.L. and K.R. directed sampling of archaeological materials and reference fats. All other authors either directed excavations or provided expertise in relation to pottery together with essential insights into the study region and sites. M.S. and L.C. contributed to revising the article. All authors read and approved the final manuscript.

Author Information Reprints and permissions information is available at www.nature.com/reprints. The authors declare no competing financial interests. Readers are welcome to comment on the online version of this article at www.nature.com/nature. Correspondence and requests for materials should be addressed to R.P.E. (r.p.evershed@bristol.ac.uk) or S.d.L. (Savino.Dilernia@uniroma1.it).

doi:10.1038/nature10933

The clonal and mutational evolution spectrum of primary triple-negative breast cancers

Sohrab P. Shah[1,2], Andrew Roth[1,2]*, Rodrigo Goya[3]*, Arusha Oloumi[1,2]*, Gavin Ha[1,2]*, Yongjun Zhao[3]*, Gulisa Turashvili[1,2]*, Jiarui Ding[1,2]*, Kane Tse[3]*, Gholamreza Haffari[1,2]*, Ali Bashashati[1,2]*, Leah M. Prentice[1,2], Jaswinder Khattra[1,2], Angela Burleigh[1,2], Damian Yap[1,2], Virginie Bernard[4], Andrew McPherson[1,2], Karey Shumansky[1,2], Anamaria Crisan[1,2], Ryan Giuliany[1,2], Alireza Heravi-Moussavi[1,2], Jamie Rosner[1,2], Daniel Lai[1,2], Inanc Birol[3], Richard Varhol[3], Angela Tam[3], Noreen Dhalla[3], Thomas Zeng[3], Kevin Ma[3], Simon K. Chan[3], Malachi Griffith[3], Annie Moradian[3], S.-W. Grace Cheng[3], Gregg B. Morin[3,5], Peter Watson[1,6], Karen Gelmon[6], Stephen Chia[6], Suet-Feung Chin[7,8], Christina Curtis[7,8,9], Oscar M. Rueda[7,8], Paul D. Pharoah[7], Sambasivarao Damaraju[10], John Mackey[10], Kelly Hoon[11], Timothy Harkins[11], Vasisht Tadigotla[11], Mahvash Sigaroudinia[12], Philippe Gascard[12], Thea Tlsty[12], Joseph F. Costello[13], Irmtraud M. Meyer[5,14,15], Connie J. Eaves[16], Wyeth W. Wasserman[4,5], Steven Jones[3,5,17], David Huntsman[1,2,18], Martin Hirst[3,15,19], Carlos Caldas[7,8,20,21], Marco A. Marra[3,5] & Samuel Aparicio[1,2]

Primary triple-negative breast cancers (TNBCs), a tumour type defined by lack of oestrogen receptor, progesterone receptor and *ERBB2* gene amplification, represent approximately 16% of all breast cancers[1]. Here we show in 104 TNBC cases that at the time of diagnosis these cancers exhibit a wide and continuous spectrum of genomic evolution, with some having only a handful of coding somatic aberrations in a few pathways, whereas others contain hundreds of coding somatic mutations. High-throughput RNA sequencing (RNA-seq) revealed that only approximately 36% of mutations are expressed. Using deep re-sequencing measurements of allelic abundance for 2,414 somatic mutations, we determine for the first time—to our knowledge—in an epithelial tumour subtype, the relative abundance of clonal frequencies among cases representative of the population. We show that TNBCs vary widely in their clonal frequencies at the time of diagnosis, with the basal subtype of TNBC[2,3] showing more variation than non-basal TNBC. Although *p53* (also known as *TP53*), *PIK3CA* and *PTEN* somatic mutations seem to be clonally dominant compared to other genes, in some tumours their clonal frequencies are incompatible with founder status. Mutations in cytoskeletal, cell shape and motility proteins occurred at lower clonal frequencies, suggesting that they occurred later during tumour progression. Taken together, our results show that understanding the biology and therapeutic responses of patients with TNBC will require the determination of individual tumour clonal genotypes.

To understand the patterns of somatic mutation in TNBC, we enumerated genome aberrations at all scales from 104 cases of primary TNBC (Affymetrix SNP6.0, 104 cases; RNA-seq, 80 cases; genome/exome sequencing, 65 cases: 54 exomes, 15 genomes with 4 overlapping) (Supplementary Table 1 and Supplementary Fig. 1), annotated with clinical information (Supplementary Table 2). We revalidated 2,414 somatic single nucleotide variants[4,5] (SNVs) (Supplementary Table 3) with targeted deep sequencing to a median of 20,000× coverage, including 43 non-coding splice site dinucleotide mutations (Supplementary Table 4) and 104 genes with 107 indels (Supplementary Table 5 and Supplementary Methods). Notably, the distribution of somatic mutation abundance varies in a continuous distribution among tumours (Fig. 1a) and seems to be unrelated to the proportion of the genome altered by copy number alterations (CNAs) (Fig. 1b) or tumour cellularity (Supplementary Fig. 2b). Although this distribution could be partially explained by a false-negative rate in mutation discovery, others have noted similar distributions in epithelial cancers[6], suggesting that the total mutation content of individual tumours may be shaped by biological processes or differential exposure to mutagenic influences in the population.

The overall pattern (Supplementary Fig. 3a, b) of CNA abundance appears similar (Supplementary Fig. 4) to that seen in a larger, independent series of ~2,000 SNP6.0 profiled breast tumours[7]. Among the most frequently observed CNA events (Supplementary Table 6) are the tumour suppressor and oncogenes *PARK2* (6%), *RB1* (5%), *PTEN* (3%) and *EGFR* (5%). Here we report intragenic deletions (Supplementary Fig. 5) in the *PARK2* tumour suppressor[8,9], specifically linking *PARK2* with TNBC for the first time. Consistent with previous reports in breast cancer[10], we did not observe frequent recurrent structural rearrangements (Supplementary Fig. 3d and Supplementary Table 7), although we revalidated many individual fusion events involving known oncogenes or tumour suppressors (for example, *KRAS*, *RB1*, *IDH1*, *ETV6*) (Supplementary Tables 8–10).

A comparison of RNA-seq data with genomes/exomes data revealed that only 36% of validated somatic SNVs were observed in the transcriptome sequence (Supplementary Table 3 and Supplementary Fig. 2b). In a recent lymphoma study, similar proportions were observed (137 of 329 somatic mutations expressed in RNA-seq)[11]. As expected, the proportion of low-abundance somatic SNVs observed in RNA is reflected in the distribution of wild-type, heterozygous and homozygous expressed mutations (Supplementary Fig. 2b), consistent with the notion that

---

[1]Department of Pathology and Laboratory Medicine, University of British Columbia, Vancouver, British Columbia V6T 2B5, Canada. [2]Molecular Oncology, British Columbia Cancer Research Centre, Vancouver, British Columbia V5Z 1L3, Canada. [3]Canada's Michael Smith Genome Sciences Centre, Vancouver, British Columbia V5Z 1L3, Canada. [4]Centre for Molecular Medicine and Therapeutics, 950 West 28th Avenue, Vancouver, British Columbia V5Z 4H4, Canada. [5]Department of Medical Genetics, University of British Columbia, Vancouver, British Columbia V6T 1Z3, Canada. [6]British Columbia Cancer Agency, 600 West 10th Avenue, Vancouver, British Columbia V5Z 4E6, Canada. [7]Cancer Research UK, Cambridge Research Institute, Li Ka Shing Centre, Robinson Way, Cambridge CB2 0RE, UK. [8]Department of Oncology, University of Cambridge, Hills Road, Cambridge CB2 2XZ, UK. [9]Department of Preventive Medicine, Keck School of Medicine, University of Southern California, Los Angeles, California 90033, USA. [10]Departments of Oncology and Laboratory Medicine and Pathology, University of Alberta, 11560 University Avenue, Cross Cancer Institute, Edmonton, Alberta T6G 1Z2, Canada. [11]Life Technologies, 101 Lincoln Centre Dr., Foster City, California 94404, USA. [12]Department of Pathology and Helen Diller Family Comprehensive Cancer Center, University of California, San Francisco, California 94143, USA. [13]Brain Tumor Research Center, Department of Neurosurgery, Helen Diller Family Comprehensive Cancer Center, University of California San Francisco, San Francisco, California 94143, USA. [14]Department of Computer Science, University of British Columbia, Vancouver, British Columbia V6T 1Z4, Canada. [15]Centre for High-Throughput Biology, University of British Columbia, Vancouver, British Columbia V6T 1Z4, Canada. [16]Terry Fox Laboratory, BC Cancer Agency, 675 W 10th Avenue, Vancouver, British Columbia V5Z 1L3, Canada. [17]Department of Molecular Biology and Biochemistry, Simon Fraser University, 8888 University Dr., Burnaby, British Columbia V5A1S6, Canada. [18]Centre for Translational and Applied Genomics, BC Cancer Agency, 600 West 10th Ave, Vancouver, British Columbia V5Z 4E6, Canada. [19]Department of Microbiology and Immunology, University of British Columbia, Vancouver, British Columbia V6T 1Z3, Canada. [20]Cambridge Breast Unit, Addenbrookes Hospital, Cambridge University Hospital NHS Foundation Trust and NIHR Cambridge Biomedical Research Centre, Cambridge CB2 2QQ, UK. [21]Cambridge Experimental Cancer Medicine Centre (ECMC), Cambridge CB2 0RE, UK.

*These authors contributed equally to this work.

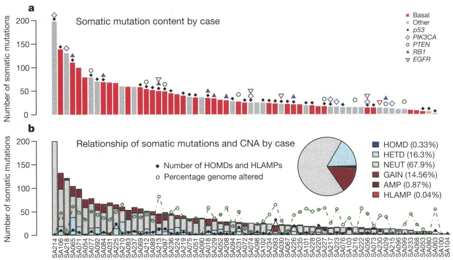

Figure 1 | Distribution of number of validated somatic mutations by case over 65 cases. **a**, Mutation frequency (basal, red; other, grey). Patients harbouring known driver gene mutations are indicated. **b**, Case-specific and overall (inset) distributions of mutations in CNA classes. AMP, amplification; GAIN, single copy gain; HETD, hemizygous deletion; HLAMP, high-level amplification; HOMD, homozygous deletion; NEUT, no copy number change. The number of (HOMD, HLAMP) CNAs (black diamonds) and percentage genome altered (green circles) are indicated.

low-abundance alleles may represent rarer clones in the primary tumour. We found 43 splice junction mutations with evidence for an impact on splicing patterns (Supplementary Table 4), encompassing several known tumour suppressors (*p53*, *PIK3R1*; Supplementary Fig. 6) as well as many genes not yet implicated in carcinogenesis. Analysis of 72 somatic mutations in the non-coding space of experimentally determined human regulatory regions[12] showed (Supplementary Table 11) a significant overrepresentation (31.9% versus expected 2.5%, Fisher exact test $P = 2 \times 10^{19}$) of mutations within retinoblastoma-associated protein (RB)-binding sites. Six mutations were predicted to be damaging to RB binding (Supplementary Methods and Supplementary Fig. 7). This is consistent with observations of frequent functional disruption of the RB-regulated cell cycle network[13] in TNBC.

We next searched for mutation enrichment patterns in three ways: by single gene mutation frequency over multiple cases; by the mutation frequency over multiple members of a gene family; and by correlating mutation status with expression networks. First, similar to other studies[14,15], *p53* is the most frequently mutated gene (Supplementary Table 12) with 62% of basal TNBC (determined by gene expression classification with PAM50 (ref. 16) analysis on RNA-seq expression profiles) and 43% of non-basal TNBC cases harbouring a validated somatic mutation. We also observed frequent mutations in *PIK3CA* at 10.2% (7/65), *USH2A* (Usher syndrome gene, implicated in actin cytoskeletal functions) at 9.2% (6/65), *MYO3A* at 9.2%, *PTEN* and *RB1* at 7.7% (5/65) and a further eight genes (including *ATR*, *UBR5* (also known as *EDD1*), *COL6A3*) at 6.2% (4/65) of cases in the cohort (Fig. 2a). Considering background mutation rates[17], *p53*, *PIK3CA*, *RB1*, *PTEN*, *MYO3A* and *GH1* showed evidence of single gene selection ($q < 0.1$) (Supplementary Table 13). Additional recurrent mutations of note occurred in the synuclein genes (*SYNE1* and *SYNE2*, 9.2% 6/65, recently implicated in squamous head and neck cancers[18,19]), *BRCA2* (three cases), and several other well known oncogenes (*BRAF*, *NRAS*, *ERBB2* and *ERBB3*) with mutations in two cases each. Approximately 20% of cases contained examples of potentially 'clinically actionable' somatic aberrations, including *BRAF* V600E, high-level *EGFR* amplifications and *ERBB2* and *ERBB3* mutations.

In the second approach we searched for statistically overrepresented gene families and protein functions using the Reactome functional protein interaction database[20] (Supplementary Methods). This analysis quantifies gene family involvement through sparse mutation patterns in functionally connected genes, which would be statistically underrepresented by single gene recurrent mutation analysis. The overrepresented pathways (false discovery rate (FDR) < 0.001) included *p53*-related pathways along with chromatin remodelling, PIK3 signalling, ERBB signalling, integrin signalling and focal adhesion, WNT/cadherin signalling, growth hormone and nuclear receptor co-activators, and ATM/RB-related pathways (Fig. 3a and Supplementary Table 14). We note that the candidate 'driver' *MYO3A*, a cytoskeleton motor protein involved in cell shape and motility, relates to several pathways upstream and downstream of integrin signalling. The mutated genes include extracellular matrix (ECM) interactions (laminins, collagens), ECM receptors (integrins), several proteins

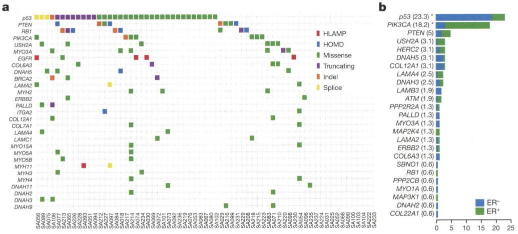

Figure 2 | Population patterns of co-occurrence and mutual exclusion of genomic aberrations in TNBC. **a**, Case-specific mutations in known driver genes, plus genes from integrin signalling and ECM-related proteins (laminins, collagens, integrins, myosins and dynein) derived from all aberration types: high-level amplifications (HLAMP), homozygous deletions (HOMD), missense, truncating, splice site and indel somatic mutations are depicted in genes with at least two aberrations in the population. **b**, Distribution of somatic mutations in 25 genes across all exons of 159 additional breast cancers (relative proportion of ER$^+$ cases in green, and ER$^-$ in blue), shown as a percentage of cases (in parentheses) with one or more mutations. *$P < 0.05$.

regulating actin cytoskeleton dynamics (usherin, palladin, multiple myosins) and microtubule motor proteins (kinesins) (Fig. 2a). All of these contribute to cellular processes that have been functionally implicated in cancer progression; however, a signature of somatic mutation associated with these proteins has not been previously noted in TNBC.

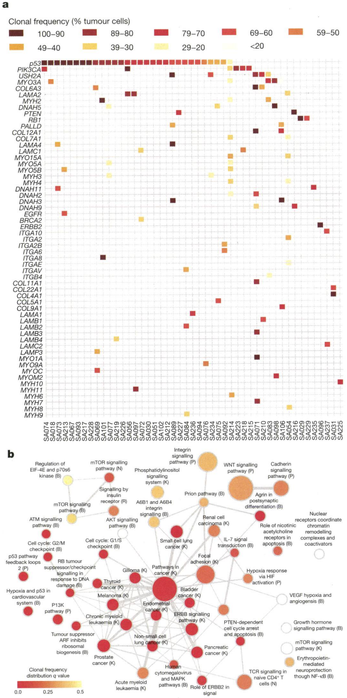

Figure 3 | Network analysis of 254 recurrently mutated genes by somatic point mutations and indels. a, Case-specific mutations shaded according to clonal frequencies in known driver genes, plus genes from integrin signalling and ECM-related proteins (laminins, collagens, integrins, myosins and dyneins). **b**, Significantly overrepresented pathways (FDR < 0.001) from recurrently mutated genes (see Supplementary Methods). Node shading encodes the adjusted *P* value (*q* value) of the comparison of the distribution of clonal frequencies of mutations in a given pathway to the overall distribution of clonal frequencies. A spectrum of higher (red) and lower (yellow) clonal frequencies is evident. Letters in parentheses indicate database sources.

To confirm the mutational spectrum in the general breast cancer population we re-sequenced all exons of 29 genes in an additional 159 breast cancers (82 oestrogen receptor $(\mathrm{ER})^+$ and 77 ER^-, tumour and matched normal) (Fig. 2b), and confirmed that many of the genes found in the discovery cohort were recurrently mutated in an additional population. Whether this pattern of mutation represents the occurrence of disease-modifying mutations, or possibly selection from other processes (for example, transcription-related hypermutation) is unknown. Interestingly, the enrichment of cytoskeletal functions in the somatic aberration landscape is also evident from the copy number and alternative splicing landscapes (Supplementary Fig. 8).

Third, we integrated both the CNA and mutation data with expression data to reveal genomic events associated with extreme changes in the transcription of interacting genes[20] (Table 1), using a bipartite graph-based method (driverNet; Supplementary Methods). The somatic aberrations showing statistically significant association with extreme expression in this analysis ($P < 0.05$) (Table 1 and Supplementary Table 15) implicate well known oncogenes and tumour suppressors (*TP53*, *PIK3CA*, *NRAS*, *EGFR*, *RB1*, *ATM*) and suggest several new genes of interest, including *PRPS2* (a nucleotide biosynthesis enzyme, rank 7), harbouring homozygous deletions in three cases, *NRC31* (a glucocorticoid receptor, rank 10) with SNVs in three cases, four PKC-related genes, *PRKCZ*, *PRKCQ*, *PRKG1* and *PRKCE*. The gene networks show a partial overlap with driverNet applied to the TCGA ovarian high-grade serous data[21] (Supplementary Table 16).

Having identified candidate driver genes and significantly overrepresented pathways, we asked how these are distributed among individual tumours by clustering a pathway–patient-mutation matrix (Supplementary Fig. 9). The abundance of implicated pathways can be

Table 1 | Analysis of the top somatically aberrated genes influencing expression

Rank	Gene	gband	SNV or indel	HLAMP	HOMD	Events	*P* value
1	*TP53*	17p13.1	35	0	0	2242	0
2	*PIK3CA*	3q26.32	7	0	0	441	1×10^{-4}
3	*NRAS*	1p13.2	2	0	0	271	4×10^{-4}
4	*EGFR*	7p11.2	1	5	0	220	4×10^{-4}
5	*RB1*	13q14.2	5	0	5	184	5×10^{-4}
6	*PGM2*	4p14	1	0	1	172	5×10^{-4}
7	*PRPS2*	23p22.2	0	0	3	171	5×10^{-4}
8	*PTEN*	10q23.31	5	0	3	150	5×10^{-4}
9	*PRKCE*	2p21	0	0	1	136	7×10^{-4}
10	*NR3C1*	5q31.3	3	0	0	130	7×10^{-4}
11	*CREBBP*	16p13.3	1	0	1	119	8×10^{-4}
12	*CS*	12q13.2	1	0	0	108	0.0011
13	*MAN2A2*	15q26.1	2	0	1	104	0.0012
14	*HMGCS2*	1p12	1	2	0	100	0.0013
15	*HEXA*	15q24.1	2	1	0	97	0.0013
16	*ADCY9*	16p13.3	2	1	0	91	0.0017
17	*OR4N4*	15q11.2	0	0	5	90	0.0017
18	*LCLAT1*	2p23.1	0	0	1	85	0.002
19	*DGKI*	7q33	2	0	0	82	0.0022
20	*CYP2A6*	19q13.2	1	0	0	80	0.0024
21	*JAK1*	1p31.3	1	0	0	78	0.0026
22	*POLR1A*	2p11.2	2	0	0	78	0.0026
23	*PLD1*	3q26.31	1	0	0	69	0.0038
24	*IDH3B*	20p13	1	0	1	68	0.004
25	*PAPSS2*	10q23.2	0	0	3	67	0.0041
26	*PRKX*	23p22.33	0	0	2	65	0.0046
27	*TPH2*	12q21.1	1	0	0	65	0.0046
28	*UGT2B17*	4q13.2	0	0	1	63	0.0053
29	*RRM2*	2p25.1	1	0	0	57	0.0072
30	*ATM*	11q22.3	1	0	0	55	0.0084
31	*CLCA1*	1p22.3	2	0	0	54	0.009
32	*PRKCZ*	1p36.33	1	0	0	53	0.0095

Rank, derived by the driverNet algorithm (see Supplementary Methods); gene, somatically aberrated gene; gband, chromosomal band containing gene; SNV or indel, the number of cases harbouring an SNV or indel in the gene; HLAMP, the number of cases harbouring a predicted high-level amplification; HOMD, the number of cases harbouring a predicted homozygous deletion; events, number of gene expression outliers (see Supplementary Methods) coincident with a genomic aberration and where the outlying gene is connected to the aberrated gene; *P* value, statistical significance based on a randomly generated background distribution (Supplementary Methods).

seen to be only partially related to the total number of mutations in a case, groups 1 and 2 having on average fewer mutations per case. The frequent involvement of pathways with *p53*, *PTEN* and *PIK3CA* as members, is noted (Supplementary Fig. 9); however, the case groupings also vary by the progressive inclusion of additional pathways (for example, WNT signalling, integrin signalling, ERBB signalling, hypoxia and PI3K). More than two thirds of cases contained one or more mutations in the actin/cytoskeletal functions group of genes (Supplementary Fig. 9). Some 12% of cases did not contain somatic aberrations in any of the frequent drivers or cytoskeletal genes (Supplementary Table 12). This suggests that primary TNBCs are mutationally heterogenous from the outset, with some patients' tumours having a small number of implicated pathways and few mutations, whereas other patients present with tumours containing extensive mutation burdens and multiple pathway involvement.

Motivated by the observation that early primary TNBCs show a wide variation of mutation content, we asked whether the clonal composition of these primary cancers is similarly varied. We and others have shown[22,23] how deep-frequency measurements of allelic abundance can be used to study tumour clonal evolution. Clonal mutation frequency, a compound measure of clonal complexity, (Fig. 4a) can be estimated from allele abundance, once the influence of copy number states, regional loss of heterozygosity (LOH state) and tumour cellularity have been considered (although we note that approximately 68% of SNVs in this study are in diploid, neutral regions). To extend allelic abundance measurements to estimation of clonal frequencies, we implemented a Dirichlet process clustering model (pyclone; Supplementary Methods and Supplementary Fig. 10) that simultaneously estimates the genotype and clonal frequency given a list of deeply sequenced mutations and their local copy number and heterozygosity contexts.

Using the set of deeply sequenced (median 20,000×), validated SNVs, our analysis revealed (Fig. 4b) that groups of mutations within individual cases have different clonal frequencies, indicative of distinct clonal genotypes. Remarkably, the tumours exhibit a wide spectrum of modes over clonal frequencies (Fig. 4b and Supplementary Fig. 11), with some cases showing only one or two frequency modes (Fig. 4b), indicating a smaller number of clonal genotypes, whereas other tumours exhibit multiple clonal frequency modes, indicating more extensive clonal evolution. Consistent with early 'driver gene' status, mutations in known tumour suppressors such as p53 tend to occur in the highest clonal frequency group in most tumours. However, in some cases (for example, SA219, SA236; Fig. 4b, Supplementary Fig. 11) p53 resides in lower-abundance clonal frequency groups (Supplementary Fig. 12 and Fig. 3a), suggesting that it was not the founding event. Although the number of clonal frequency modes tends to increase with the number of mutations, the relationship is not strictly linear (Fig. 4c). To determine whether basal and non-basal cancers differ in their clonality, we compared the distribution of clonal modes (clusters) by case and as an overall distribution, and note that basal TNBCs have more clonal frequency modes than non-basal TNBCs (Fig. 4c). Both of these distributions emphasize a key observation; namely, that at the time of diagnosis TNBCs already display a widely varying clonal evolution that mirrors the variation in mutational evolution.

Finally, we asked where key pathways appear in the distribution of clonal frequency groups. We examined the clonal frequency of genes in each pathway and ascertained if there was a deviation away from the distribution of clonal frequency for all mutations. As expected, pathways involving p53 and *PIK3CA* showed significantly skewed distributions (Wilcoxon, $q < 0.01$; Fig. 3b and Supplementary Fig. 12) towards higher clonal frequencies, consistent with their roles in early tumorigenesis (Fig. 3a and Supplementary Table 17). Intriguingly, pathways with cytoskeletal genes such as myosins, laminins, collagens and integrins tend to have lower median clonal frequencies, suggesting that somatic mutations in these genes are acquired much later (Fig. 3b). Notably, the median clonal frequency for Reactome pathway 'p53 pathway feedback loops', including 46 mutations in *ATM*, *ATR*, *NRAS*, *PIK3CA*, *PTEN*, *SIAH1* and *p53*,was 73% (Wilcoxon, $q = 0.0007$), whereas 'integrin cell surface interactions', including 23 mutations in integrin, laminin and collagen genes, had a median clonal frequency of 42% (Wilcoxon, $q = 0.9569$).

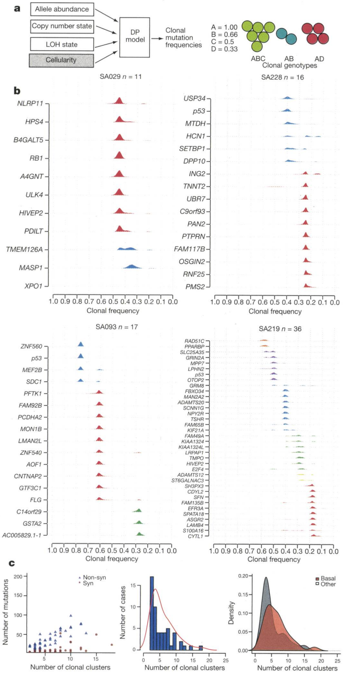

Figure 4 | Clonal evolution in TNBC. **a**, Schematic representation of integration of CNA, LOH, allelic abundance measurements and normal cell contamination for clonal frequency estimation using a Dirichlet process (DP) model (left). Example of a mixture of three clonal genotypes composed of four mutations (A, B, C, D) and their resulting clonal frequencies. **b**, Estimated clonal frequencies for four cases are shown as the distribution of posterior probabilities from the pyclone model (Supplementary Methods). Clonal frequency distributions are coloured by their frequency group membership. **c**, Left, relationship of mutation abundance (synonymous (Syn) and non-synonymous (Non-syn)) and the inferred number of clonal clusters. Middle, distribution and kernel density (red line) of the number of inferred clonal clusters over 54 TNBCs. Right, kernel density distribution of clonal clusters for basal (red) and non-basal (grey) tumours.

Primary TNBCs are still treated as if they were a single disease entity, yet it is clear they do not behave as a single entity in response to current therapies. Here we show for the first time, using next-generation sequencing mutational profiling methods, that treatment-naive TNBCs display a complete spectrum of mutational and clonal evolution, with some patients' tumours showing only a few somatic coding sequence point mutations with a limited number of molecular pathways implicated, whereas other patients' tumours exhibit considerable additional mutational involvement. Moreover, the clonal heterogeneity of these cancers is also a continuum, with some patients presenting with low-clonality cancers and other cases exhibiting more extensive clonal evolution at diagnosis. In this respect, the basal expression subtype of TNBCs also tends to show higher clonality at diagnosis, although the relationship is not exact.

In clonally evolving tumours, identification of genes by single gene mutation frequency measurements will probably favour early driver genes, because the subsequent involvement of multiple additional pathways during tumour progression is unlikely to be observed as a frequent single gene mutation. The clonality analysis emphasizes this point: known drivers such as *p53*, *PIK3CA* and *PTEN* have among the highest clonal frequencies, whereas mutations in cell shape/motility and ECM-signalling genes appear in the lower clonal frequency groups, distributed over many genes. Although p53 somatic mutations are clearly early events, the clonal frequencies observed in some TNBC suggest that they are not always the first event, raising a question about what drives early clonal expansion in some of these cancers. Our findings suggest that each TNBC at the time of primary diagnosis may be at a very different phase of molecular progression, with possible implications for approaches to the biology of low clonality versus high clonality primary tumours.

METHODS SUMMARY

The genomes and transcriptomes of 104 TNBCs were profiled with Affymetrix SNP6.0 arrays (all cases), RNA-seq (80 cases; Illumina GAII), and whole exome/genome sequencing (65 cases; tumour and normal DNA). Exomes were obtained using Agilent's Human All Exon SureSelect Target Enrichment System v.1 followed by Illumina GAII sequencing, and whole genomes were sequenced using Life Technologies SOLiD system. Data were analysed using computational approaches to detect somatic SNVs[4,5], indels, copy number alterations, gene fusions and gene expression patterns. Predictions were then validated using orthogonal experimental assays, including targeted ultra-deep amplicon sequencing of SNVs to $\sim$20,000× redundancy. We determined single genes under selection using a statistical approach that considers patient-specific background mutation and transition/transversion rates. Mutations predicted to alter transcriptional profiles were determined using an integrated bipartite graph-based method (driverNet) that associates genomic aberrations with outlying expression patterns informed by predefined pathway gene sets. Disrupted pathways were determined using the Reactome FI Cytoscape plugin. Clonal analysis was performed (cases with >10 mutations) using a Dirichlet process statistical model that simultaneously estimates clonal frequencies and mutation genotype given deeply sequenced somatic SNVs and copy number estimates. Experimental assays and analytical methodology are detailed in the Supplementary Information.

Received 16 June 2011; accepted 15 February 2012.
Published online 4 April 2012.

1. Blows, F. M. *et al.* Subtyping of breast cancer by immunohistochemistry to investigate a relationship between subtype and short and long term survival: a collaborative analysis of data for 10,159 cases from 12 studies. *PLoS Med.* **7,** e1000279 (2010).
2. Perou, C. M. *et al.* Molecular portraits of human breast tumours. *Nature* **406,** 747–752 (2000).
3. Sørlie, T. Gene expression patterns of breast carcinomas distinguish tumor subclasses with clinical implications. *Proc. Natl Acad. Sci. USA* **98,** 10869–10874 (2001).
4. Roth, A. *et al.* JointSNVmix: A probabilistic model for accurate detection of somatic mutations in normal/tumour paired next generation sequencing data. *Bioinformatics* http://dx.doi.org/10.1093/bioinformatics/bts053 (27 January 2012).
5. Ding, J. *et al.* Feature-based classifiers for somatic mutation detection in tumour—normal paired sequencing data. *Bioinformatics* **28,** 167–175 (2012).
6. Ding, L. *et al.* Somatic mutations affect key pathways in lung adenocarcinoma. *Nature* **455,** 1069–1075 (2008).
7. Curtis, C. *et al.* The genomic and transcriptomic architecture of 2,000 breast tumours reveals novel subgroups. *Nature* http://dx.doi.org/10.1038/nature10983 (this issue).
8. Poulogiannis, G. *et al.* *PARK2* deletions occur frequently in sporadic colorectal cancer and accelerate adenoma development in *Apc* mutant mice. *Proc. Natl Acad. Sci. USA* **107,** 15145–15150 (2010).
9. Bignell, G. R. *et al.* Signatures of mutation and selection in the cancer genome. *Nature* **463,** 893–898 (2010).
10. Stephens, P. J. *et al.* Complex landscapes of somatic rearrangement in human breast cancer genomes. *Nature* **462,** 1005–1010 (2009).
11. Morin, R. D. *et al.* Frequent mutation of histone-modifying genes in non-Hodgkin lymphoma. *Nature* **476,** 298–303 (2011).
12. Chicas, A. *et al.* Dissecting the unique role of the retinoblastoma tumor suppressor during cellular senescence. *Cancer Cell* **17,** 376–387 (2010).
13. Herschkowitz, J. I., He, X., Fan, C. & Perou, C. M. The functional loss of the retinoblastoma tumour suppressor is a common event in basal-like and luminal B breast carcinomas. *Breast Cancer Res.* **10,** R75 (2008).
14. Langerød, A. *et al.* TP53 mutation status and gene expression profiles are powerful prognostic markers of breast cancer. *Breast Cancer Res.* **9,** R30 (2007).
15. Børresen-Dale, A.-L. TP53 and breast cancer. *Hum. Mutat.* **21,** 292–300 (2003).
16. Parker, J. S. *et al.* Supervised risk predictor of breast cancer based on intrinsic subtypes. *J. Clin. Oncol.* **27,** 1160–1167 (2009).
17. Youn, A. & Simon, R. Identifying cancer driver genes in tumor genome sequencing studies. *Bioinformatics* **27,** 175–181 (2011).
18. Agrawal, N. *et al.* Exome sequencing of head and neck squamous cell carcinoma reveals inactivating mutations in NOTCH1. *Science* **333,** 1154–1157 (2011).
19. Stransky, N. *et al.* The mutational landscape of head and neck squamous cell carcinoma. *Science* **333,** 1157–1160 (2011).
20. Wu, G., Feng, X. & Stein, L. A human functional protein interaction network and its application to cancer data analysis. *Genome Biol.* **11,** R53 (2010).
21. Cancer Genome Atlas Research Network. Integrated genomic analyses of ovarian carcinoma. *Nature* **474,** 609–615 (2011).
22. Shah, S. P. *et al.* Mutational evolution in a lobular breast tumour profiled at single nucleotide resolution. *Nature* **461,** 809–813 (2009).
23. Ding, L. *et al.* Genome remodelling in a basal-like breast cancer metastasis and xenograft. *Nature* **464,** 999–1005 (2010).

Supplementary Information is linked to the online version of the paper at www.nature.com/nature.

Acknowledgements The support of the BC Cancer Agency Tumour Bank, CBCF Breast Tumour Bank Alberta and the Addenbrookes Tumour bank (supported by NIHR and ECMC) is acknowledged. Technical support is acknowledged from the Centre for Translational Genomics, the Michael Smith Genome Sciences Centre technical group, the BCCA Flow Cytometry Core Facility in the Terry Fox Laboratory and the Cancer Research UK Cambridge Research Institute. Supported by the BC Cancer Foundation, US Department of Defense CDMRP program, Canadian Breast Cancer Foundation (BC Yukon) (to S.A. and S.S.), Michael Smith Foundation for Health Research (to S.S.), US National Institutes of Health (NIH) Roadmap Epigenomics Program, NIH grant 5U01ES017154-02 (to M.H., M.A.M., J.C. and T.T.), Cancer Research UK (to C. Caldas and P.D.P.) and the National Institute of General Medical Sciences (R01GM084875 to W.W.W.), the Canadian Breast Cancer Research Alliance and the Canadian Cancer Society (to S.A. and C.E.). We thank B. Reva, Y. Antipin and C. Sander (Memorial Sloan Kettering Cancer Center) for assistance with MutationAssessor, and G. Wu (Ontario Institute for Cancer Research) for assistance with Reactome.

Author Contributions S.A., S.P.S., C. Caldas and M.A.M. designed and implemented the research plan and wrote the manuscript. S.P.S., A.R., R. Goya, G. Ha, J.D., G. Haffari, A. Bashashati, A. McPherson, K.S., A.C., R. Giuliany, A.H.-M., J.R., D.L., I.B., R.V., S.W.C., M.G., I.M.M., S.J., C. Curtis, O.M.R., P.D.P., V.B. and W.W.W. conducted bioinformatic analyses of the data and/or gave advice on analytic methodology. G.T. conducted histopathological review and immunohistochemistry. A.O., Y.Z., G.T., K.T., L.M.P., J.K., A.B., D.Y., A.T., N.D., T.Z., S.-F.C., K.M. and M.H. conducted sequencing or experimental validation of somatic aberrations. D.Y., A. Moradian, S.-W.G.C. and G.B.M. conducted proteome validation of splicing. P.W., K.G., S.C., S.-F.C., G.T., J.M., C. Caldas, P.D.P. and D.H. collected and interpreted clinical data. S.D., J.F.C., T.T., M.S., P.G. and C.J.E. contributed materials or reagents. K.H., V.T., T.H., M.H. and M.A.M. generated sequence data.

Author Information Aligned exome/genome sequence data, RNA-seq data and Affymetrix SNP6.0 data sets are available at the European Genome-phenome Archive (http://www.ebi.ac.uk/ega/) under study accession number EGAS00001000132. Normal reference RNA-seq datasets are available at the NCBI Short Read Archive (http://www.ncbi.nlm.nih.gov/Traces) under study accession number SRP000930. Reprints and permissions information is available at www.nature.com/reprints. The authors declare no competing financial interests. Readers are welcome to comment on the online version of this article at www.nature.com/nature. Correspondence and requests for materials should be addressed to S.A. (saparicio@bccrc.ca), C. Caldas (carlos.caldas@cancer.org.uk), S.P.S. (sshah@bccrc.ca) or M.M. (mmarra@bcgsc.ca).

LETTER

doi:10.1038/nature11017

The landscape of cancer genes and mutational processes in breast cancer

Philip J. Stephens[1]*, Patrick S. Tarpey[1]*, Helen Davies[1], Peter Van Loo[1,2], Chris Greenman[1,3,4], David C. Wedge[1], Serena Nik-Zainal[1], Sancha Martin[1], Ignacio Varela[1], Graham R. Bignell[1], Lucy R. Yates[1,5,6], Elli Papaemmanuil[1], David Beare[1], Adam Butler[1], Angela Cheverton[1], John Gamble[1], Jonathan Hinton[1], Mingming Jia[1], Alagu Jayakumar[1], David Jones[1], Calli Latimer[1], King Wai Lau[1], Stuart McLaren[1], David J. McBride[1], Andrew Menzies[1], Laura Mudie[1], Keiran Raine[1], Roland Rad[1], Michael Spencer Chapman[1], Jon Teague[1], Douglas Easton[7,8], Anita Langerød[9], OSBREAC†, Ming Ta Michael Lee[10], Chen-Yang Shen[10], Benita Tan Kiat Tee[11], Bernice Wong Huimin[12], Annegien Broeks[13], Ana Cristina Vargas[14], Gulisa Turashvili[15,16], John Martens[17], Aquila Fatima[18], Penelope Miron[18], Suet-Feung Chin[19], Gilles Thomas[20], Sandrine Boyault[20], Odette Mariani[21], Sunil R. Lakhani[14,22,23], Marc van de Vijver[24], Laura van 't Veer[13], John Foekens[17], Christine Desmedt[25], Christos Sotiriou[25], Andrew Tutt[5], Carlos Caldas[19,26], Jorge S. Reis-Filho[27], Samuel A. J. R. Aparicio[15,16], Anne Vincent Salomon[21,28], Anne-Lise Børresen-Dale[9,29], Andrea L. Richardson[18,30], Peter J. Campbell[1,31,32], P. Andrew Futreal[1] & Michael R. Stratton[1]

All cancers carry somatic mutations in their genomes. A subset, known as driver mutations, confer clonal selective advantage on cancer cells and are causally implicated in oncogenesis[1], and the remainder are passenger mutations. The driver mutations and mutational processes operative in breast cancer have not yet been comprehensively explored. Here we examine the genomes of 100 tumours for somatic copy number changes and mutations in the coding exons of protein-coding genes. The number of somatic mutations varied markedly between individual tumours. We found strong correlations between mutation number, age at which cancer was diagnosed and cancer histological grade, and observed multiple mutational signatures, including one present in about ten per cent of tumours characterized by numerous mutations of cytosine at TpC dinucleotides. Driver mutations were identified in several new cancer genes including *AKT2*, *ARID1B*, *CASP8*, *CDKN1B*, *MAP3K1*, *MAP3K13*, *NCOR1*, *SMARCD1* and *TBX3*. Among the 100 tumours, we found driver mutations in at least 40 cancer genes and 73 different combinations of mutated cancer genes. The results highlight the substantial genetic diversity underlying this common disease.

The coding exons of 21,416 protein coding genes and 1,664 microRNAs were sequenced and copy number changes examined in 100 primary breast cancers, 79 of which were oestrogen receptor positive (ER+) and 21 of which were oestrogen receptor negative (ER−) (Supplementary Table 1). We sequenced normal DNAs from the same individuals to exclude inherited sequence variation. We identified 7,241 somatic point mutations: 6,964 were single-base substitutions, of which 4,737 were predicted to generate missense; 422, nonsense; 158, an essential splice site; 8, stop codon read-through; and 1,637, silent changes in protein sequence. Two substitutions were found in microRNAs. There were 277 small insertions or deletions (71 and 206, respectively), of which 231 introduced translational frameshifts and 46 were in-frame (Supplementary Table 2). Analyses of copy number yielded 1,712 homozygous deletions and 1,751 regions of increased copy number (amplification) (Supplementary Table 3).

Somatic driver substitutions and small insertions/deletions (indels) were identified in cancer genes previously implicated in breast cancer development, including *AKT1*, *BRCA1*, *CDH1*, *GATA3*, *PIK3CA*, *PTEN*, *RB1* and *TP53* (Supplementary Table 4; see also http://www.sanger.ac.uk/genetics/CGP/Census). Likely drivers were also found in cancer genes involved in other cancer types, including *APC*, *ARID1A*, *ARID2*, *ASXL1*, *BAP1*, *KRAS*, *MAP2K4*, *MLL2*, *MLL3*, *NF1*, *SETD2*, *SF3B1*, *SMAD4* and *STK11*.

To identify new cancer genes, we searched for non-random clustering of somatic mutations in each of the 21,416 protein-coding genes[2,3] and sequenced a subset of genes highlighted by this analysis in a follow-up series of 250 breast cancers (Supplementary Tables 5 and 6). Persuasive evidence was found for nine new cancer genes (Fig. 1a and Supplementary Fig. 1). Of these *ARID1B*, *CASP8*, *MAP3K1*, *MAP3K13*, *NCOR1*, *SMARCD1* and *CDKN1B* had the truncating

---

[1]Cancer Genome Project, Wellcome Trust Sanger Institute, Wellcome Trust Genome Campus, Hinxton CB10 1SA, UK. [2]Human Genome Laboratory, Department of Human Genetics, VIB and University of Leuven, Herestraat 49 Box 602, B-3000 Leuven, Belgium. [3]School of Computing Sciences, University of East Anglia, Norwich NR4 7TJ, UK. [4]The Genome Analysis Centre, Norwich Research Park, Norwich NR4 7UH, UK. [5]Breakthrough Breast Cancer Research Unit, Research Oncology, 3rd Floor Bermondsey Wing, Guy's Hospital Campus, Kings College London School of Medicine, London SE1 9RT, UK. [6]Department of Clinical Oncology, Ground floor, Lambeth Wing, Guys and St Thomas' NHS Trust, Westminster Bridge Road, London SE1 7EH, UK. [7]Centre for Cancer Genetic Epidemiology, Department of Oncology, Strangeways Research Laboratory, Cambridge CB1 8RN, UK. [8]Centre for Cancer Genetic Epidemiology, Department of Public Health and Primary Care, Strangeways Research Laboratory, Cambridge CB1 8RN, UK. [9]Department of Genetics, Institute for Cancer Research, The Norwegian Radium Hospital, Oslo University Hospital, 0310 Oslo, Norway. [10]National Genotyping Center, Institute of Biomedical Sciences, Academia Sinica, 128 Academia Road, Sec 2, Nankang, Taipei 115, Taiwan, China. [11]Department of General Surgery, Singapore General Hospital, 169608, Singapore. [12]NCCS-VARI Translational Research Laboratory, National Cancer Centre Singapore, 11 Hospital Drive, 169610, Singapore. [13]Department Experimental Therapy, The Netherlands Cancer Institute, Plesmanlaan 121, 1066 CX Amsterdam, The Netherlands. [14]The University of Queensland Centre for Clinical Research, The Royal Brisbane & Women's Hospital, Herston, Brisbane, Queensland 4029, Australia. [15]Department of Pathology and Laboratory Medicine, University of British Columbia, Vancouver, British Columbia V6T 2B5, Canada. [16]Molecular Oncology, British Columbia Cancer Research Centre, Vancouver, British Columbia V5Z 1L3, Canada. [17]Department of Medical Oncology, Erasmus University Medical Center, Daniel den Hoed Cancer Center and Cancer Genomics Center, Postbus 2040, 3000 CA Rotterdam, Netherlands. [18]Department of Cancer Biology, Dana-Farber Cancer Institute, 450 Brookline Avenue, Boston, Massachusetts 02215, USA. [19]Department of Oncology, University of Cambridge and Cancer Research UK Cambridge Research Institute, Li Ka Shin Centre, Cambridge CB2 0RE, UK. [20]Universite Lyon 1, INCa-Synergie, Centre Leon Berard, 28 rue Laennec, Lyon CEDEX 08, France. [21]Institut Curie, Department of Tumor Biology, 26 rue d'Ulm, 75248 Paris CEDEX 05, France. [22]The University of Queensland School of Medicine, Herston Road, Herston, Brisbane, Queensland 4006, Australia. [23]Anatomical Pathology, Pathology Queensland, The Royal Brisbane and Women's Hospital, Herston, Brisbane, Queensland 4029, Australia. [24]Department of Pathology, Academic Medical Center, Meibergdreef 9, 1105 AZ Amsterdam, The Netherlands. [25]Breast Cancer Translational Laboratory, Université Libre de Bruxelles, Jules Bordet Institute, Boulevard de Waterloo 121, 1000 Brussels, Belgium. [26]NIHR Cambridge Biomedical Research Centre and Cambridge Experimental Cancer Medicine Centre, Cambridge University Hospitals NHS Foundation Trust, Cambridge CB2 2QQ, UK. [27]The Breakthrough Breast Cancer Research Centre, Institute of Cancer Research, London SW3 6JB, UK. [28]Institut Curie, INSERM Unit 830, 26 rue d'Ulm, 75248 Paris CEDEX 05, France. [29]K.G. Jebsen Center for Breast Cancer Research, Institute for Clinical Medicine, Faculty of Medicine, University of Oslo, 0318 Oslo, Norway. [30]Department of Pathology, Brigham and Women's Hospital, Harvard Medical School, 75 Francis St, Boston, Massachusetts 02115, USA. [31]Department of Haematology, Addenbrooke's Hospital, Cambridge CB2 0QQ, UK. [32]Department of Haematology, University of Cambridge, Hills Road, Cambridge CB2 2XY, UK.

*These authors contributed equally to this work.

†Lists of participants and their affiliations appear at the end of the paper.

mutations and often biallelic inactivation characteristic of inactivated, potentially recessive cancer genes (Supplementary Table 4). *AKT2* is probably an activated, dominantly acting cancer gene. The effects of *TBX3* mutations on its function are unclear.

MAP3K1 encodes a serine/threonine protein kinase that regulates the activity of the ERK MAP kinase (the extracellular signal-regulated mitogen-activated protein kinase), JUN kinase and p38 signalling pathways implicated in control of cell proliferation and death[4]. Somatic mutations in *MAP3K1* were observed in 6% of breast cancers, predominantly in ER+ cases. Most were protein truncating. MAP3K1 phosphorylates and activates the protein encoded by *MAP2K4*, a known recessive cancer gene with inactivating mutations in breast and other cancers[5]. In turn, MAP2K4 phosphorylates and activates the JUN kinases MAPK8 (also known as JNK1) and MAPK9 (also known as JNK2), which phosphorylate JUN, TP53 and other transcription factors mediating cellular responses to stress[4]. Truncating mutations and other non-synonymous mutations were also found in *MAP3K13*, which encodes a kinase that phosphorylates and activates MAP2K7. MAP2K7 phosphorylates and activates MAPK8 and MAPK9 (ref. 4). Thus, in breast cancer, inactivating mutations in *MAP3K1*, *MAP2K4* and *MAP3K13* are predicted to abrogate signalling pathways that activate JUN kinases (Fig. 1b).

In the serine/threonine kinase gene *AKT2*, we identified a single somatic missense mutation, Glu 17 Lys, that is identical to the recurrent, activating mutation in *AKT1* previously reported in breast cancer[6]. Thus, *AKT2* is also probably a cancer gene, albeit one infrequently implicated in breast cancer development. Because AKT phosphorylates and inhibits MAP2K4 (ref. 7) and mutations in *PIK3CA* and *PTEN* can result in AKT activation[8], about half of breast cancers may have abrogation of JUN kinase signalling (Fig. 1b). The biological consequences of the reduction in JUN kinase activity are likely to be diverse and complex, but may include destabilization and consequent inactivation of TP53 with disruption of pro-apoptotic cellular signalling in response to stress[9].

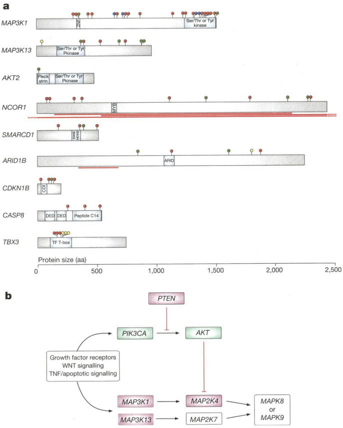

Figure 1 | New cancer genes established in this study and involvement of the JUN kinase signalling pathway. a, Representations of the protein-coding sequences and major domains in cancer genes established in this study. Somatic mutations are shown as circles: truncating (red), essential splice site (blue), missense (green) and in-frame indel (yellow). The red lines indicate the positions of large homozygous deletions. aa, amino acids. **b**, Pathways regulating the JUN kinases MAP2K7 and MAP2K8, indicating genes with mutations in this series. Genes in green are activated by mutations, whereas genes in red are inactivated.

We observed truncating mutations and homozygous deletions of *NCOR1*. In addition to mediating repression of thyroid-hormone and retinoic-acid receptors by promoting chromatin condensation and preventing access of the transcription machinery[10], NCOR1 participates in ligand-dependent transcriptional repression by oestrogen receptor alpha[11]. We also identified inactivating mutations in *SMARCD1* and *ARID1B*, further implicating aberrant chromatin regulation. The encoded proteins of both are components of the SWI/SNF chromatin modelling complex, which incorporates the products of several established recessive cancer genes, including *PBRM1*, *ARID1A*, *SMARCB1* and *SMARCA4* (refs 3, 12–14).

We found three truncating mutations and a missense mutation in *CDKN1B*. Two truncating mutations in *CDKN1B* in cancer have previously been reported[15,16], and collectively the results confirm that *CDKN1B* is a cancer gene. CDKN1B (also known as p27 or KIP1) normally inhibits activation of cyclin E/CDK2 and cyclin D/CDK4 complexes, thus preventing cell cycle progression at phase G1[17].

Three truncating mutations were observed in *CASP8*. CASP8 is a member of the cysteine/aspartic acid protease family that forms a complex with the FAS cell surface receptor to promote programmed cell death. Inactivation of CASP8 in these cancers is therefore predicted to abrogate apoptosis in response to a variety of signals.

Six tumours had mutations in *TBX3*, which encodes a T-box transcription factor that regulates stem cell pluripotency-associated and reprogramming factors and is involved in normal breast development[18,19]. Constitutional inactivating mutations in *TBX3* cause ulnar-mammary syndrome, in which there is failure of breast and apocrine development coupled with abnormalities of limb morphogenesis[20]. Three breast cancers had in-frame deletions, one of Thr 210 and the other two of Asn 212, a residue through which the T-box domain binds to DNA. Despite the presence of truncating mutations in three further cases, the recurrent and clustered in-frame deletions and the finding that all mutations were heterozygous suggests that they may not simply result in loss of function. Indeed, recent reports suggest that increased activity of TBX3 is likely to contribute to oncogenesis. The proportion of stem-like cells in breast cancers is increased by oestrogen-dependent activation of the TBX3 pathway[21]. Moreover, TBX3 overexpression increases the efficiency of the derivation of induced pluripotent stem cells[18] and the ability of cancer cells to form tumours[21].

Further supporting their role in oncogenesis, three of the nine newly identified somatically mutated cancer genes, *MAP3K1*, *CASP8* and *TBX3*, carry inherited common variants, identified by genome-wide association studies, that confer small increased risks of breast cancer[22,23]. Several additional genes showed truncating mutations and are biologically plausible candidate cancer genes contributing infrequently to breast cancer development. Some, including *ASXL2*, *ARID5B*, *KDM3A*, *SETD1A*, *CHD1*, *NCOR2*, *HDAC9* and *CTCF*, encode proteins that regulate chromatin structure, whereas others, including *FANCA* and *ATR*, are involved in DNA repair.

Cancers arise through successive waves of clonal expansion dependent on the sequential acquisition of driver mutations. A central parameter of cancer development is therefore the number of driver mutations required for conversion of a normal cell into a symptomatic cancer. Estimates based on cancer age–incidence curves have indicated that approximately five rate-limiting steps underlie the development of common adult solid tumours[24]. Experimental studies have similarly indicated that a limited number of key genetic changes are required for

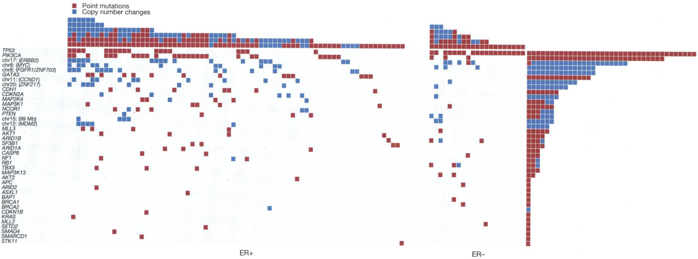

Figure 2 | The landscape of driver mutations in breast cancer. Each of the 40 cancer genes in which a driver mutation or copy number change has been identified is listed down the left-hand side. The number of mutations in each gene in the 100 tumours is shown (rows), as is the number of driver mutations in each breast cancer (columns). Point mutations and copy number changes are coloured red and blue, respectively.

neoplastic transformation of human cells[25]. Our systematic genome analysis now provides a direct survey of the landscape of driver mutations in breast cancer.

Somatic driver point mutations and/or copy number changes in at least 40 cancer genes were implicated in the development of the 100 breast cancers (Fig. 2, Supplementary Tables 3 and 4, and Supplementary Methods). The maximum number of mutated cancer genes in an individual cancer was 6, but 28 cases only showed a single driver. Thus, there seems to be substantial variation in the number of drivers. In some cases, the presence of multiple drivers was associated with subclonal evolution of the cancer (Supplementary Statistical Analyses). However, in others multiple drivers were in the root cancer clone. Seven of the 40 cancer genes (*TP53*, *PIK3CA*, *ERBB2*, *MYC*, *FGFR1/ZNF703*, *GATA3* and *CCND1*) were mutated in more than 10% of cases. Collectively these contributed 58% of driver mutations (144 of 250). Therefore, 33 mutated cancer genes, each contributing relatively infrequently, were responsible for the remaining 42% of driving genetic events. We observed 73 different combinations of mutated cancer genes. Thus, most breast cancers differed from all others (Fig. 2 and Supplementary Fig. 2). This assessment of the genetic diversity of breast cancer is probably conservative because, for several reasons, it underestimates the number of mutated cancer genes in each case.

At present, we know little about the mutational processes responsible for the generation of somatic mutations in breast and other cancers. In the 100 breast cancers analysed here, there was substantial variation in the total numbers of base substitutions and indels between individual cases (Fig. 3a). There was also considerable diversity of mutational pattern, ranging from cases in which C•G → T•A transitions predominated to cases in which all transitions and transversions made equal contributions (Fig. 3b and Supplementary Fig. 3). Taken together, the results suggest that multiple distinct mutational processes are operative. For most of these processes, the underlying mechanism is unknown.

To illustrate one mutational signature in detail, we selected the ER+ breast cancer with the largest number of base substitutions in the series, PD4120 (Fig. 3a, asterisk; Fig. 4). The mutation spectrum of this case was distinctive, featuring C•G → T•A, C•G → G•C and C•G → A•T mutations and very few mutations at A•T base pairs (Fig. 4a). To characterize this process further, we examined the sequence context in which the mutations occurred (in the following discussion, mutations at C•G base pairs are represented as the change at the C base) and found pronounced overrepresentation of thymine immediately 5′ to the mutated cytosines. Thus, in PD4120 the large majority of mutations were of cytosine at TpC dinucleotides (Fig. 4b).

To obtain further insight into the underlying mechanism in this case, we looked for differences in mutation prevalence between the transcribed and untranscribed strands of the 21,416 genes analysed ('strand bias') and found a higher prevalence of C → T, C → G and C → A mutations on transcribed strands ($P = 0.02$) (Fig. 4c and Supplementary Table 7). This strand bias raises the possibility that transcription-coupled nucleotide excision repair (NER) has been operative. NER removes bulky DNA adducts that distort the DNA

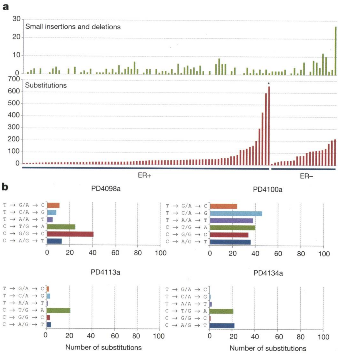

Figure 3 | The variation in numbers and types of mutation between individual breast cancers. a, Numbers of small indels and base substitutions in the protein-coding exons of each of the 100 breast cancers studied. The cases are ranked according to the number of base substitutions. *Breast cancer PD4120 (see main text). **b,** Mutation spectrum of four primary tumours with diverse mutational patterns.

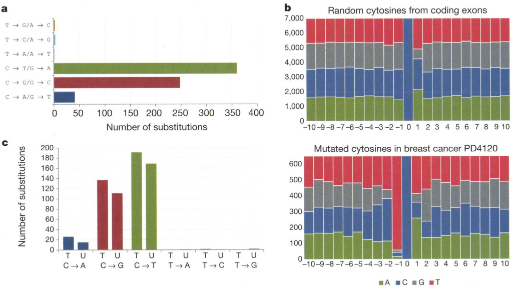

Figure 4 | The mutational signature of ER+ breast cancer PD4120. a, The mutational spectrum. **b,** The sequence context of C → T, C → G and C → A mutations. The central blue bar indicates the position of the mutated cytosine and the bases 5′ and 3′ are numbered on the horizontal axis. **c,** Strand bias of mutations showing substitutions at C bases and at T bases according to whether they are on the transcribed (T) or untranscribed (U) strands of the genes screened.

double helix, notably pyrimidine dimers due to ultraviolet light exposure or adducts due to mutagens in tobacco smoke[26]. There is a form of NER, recruited by RNA polymerase II, that is operative only on the transcribed strand of each gene and thus introduces a strand bias for mutations[27]. Therefore, one hypothesis to account for the strand bias in PD4120 is past involvement of NER, in turn implicating exposure to a bulky DNA-damaging agent, either of endogenous or exogenous origin. However, we cannot exclude the possibility that other DNA damage or repair processes generate a strand bias. At least eight additional cancers in this series had a very similar mutational spectrum, sequence context and strand bias (Supplementary Fig. 4 and Supplementary Statistical Analysis). None had been treated before excision of the cancer.

The somatic mutations in a cancer genome accumulate over a patient's lifetime, during the lineage of mitotic divisions from the fertilized egg to the cancer cell. Some are acquired while cells in the lineage are biologically normal, whereas others are acquired after acquisition of the neoplastic phenotype. However, the relative proportions accumulated in these two phases are unknown. To explore this question, we examined the relationship between the total numbers of somatic base substitutions and the age at diagnosis in the 100 tumours (Fig. 5). In both ER+ and ER− cancers, no correlation was observed ($P = 0.33$ and 0.14 respectively). If most somatic mutations in a cancer genome are acquired in normal tissues before neoplastic transformation, the later the onset of the cancer the longer this part of the lineage is likely to have been and, consequently, the higher the number of mutations. The absence of a correlation therefore suggests that most mutations in breast cancer genomes occur after the initiating driver event.

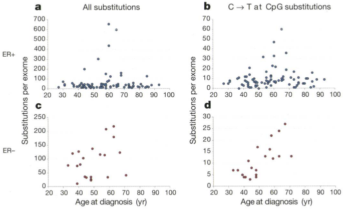

Figure 5 | The relationship between age at breast cancer diagnosis and all substitutions, and for C → T substitutions at CpG sites. a, b, Data from the 79 ER+ breast cancers. **c, d,** Data from the 21 ER− breast cancers.

We then considered separately the subset of somatic mutations constituted by C•G → T•A substitutions at CpG dinucleotides, because this mutational pattern is observed in non-diseased tissues, manifesting prominently in normal germline variation. This subset showed a strong positive correlation with the age at cancer diagnosis in ER− cancers ($P = 1.2 \times 10^{-7}$), supporting the proposition that it is enriched in mutations occurring in normal tissues and that, overall, other mutation classes occur later. By contrast, ER+ cancers showed no correlation between C•G → T•A substitutions at CpG dinucleotides and age at diagnosis ($P = 0.27$). The basis for this pronounced difference is unclear, but potentially highlights a profound divergence in the dynamics of mutation acquisition between these two major subclasses of breast cancer.

In clinical practice, breast cancers are graded microscopically on the basis of mitotic counts, pleomorphism of cancer cell nuclei and extent of tubule formation, which are then collected into an overall grade score. High scores indicate large numbers of mitoses, substantial tumour cell pleomorphism and little tubule formation, and are generally associated with more rapid progression. Significant correlations were not observed between numbers of driver mutations and grade scores (Supplementary Statistical Analysis). However, there were strong positive correlations between the total number of substitutions (that is, drivers and passengers) and mitosis and tubule scores ($P = 0.0002$ and 0.002 respectively), which remained significant after multiple testing corrections. The causal relationships between these features are unclear. However, because most substitutions are likely to be biologically inert passengers, it is possible that the biological state of high-grade breast cancers may be responsible for generating increased numbers of mutations, rather than the converse.

The panorama of mutated cancer genes and mutational processes in breast cancer is becoming clearer, and a sobering perspective on the complexity and diversity of the disease is emerging. Driver mutations are operative in many cancer genes. A few are commonly mutated, but many infrequently mutated genes collectively make a substantial contribution in myriad different combinations. Multiple somatic mutational processes have been operative. Ultimately, characterization of the genomes of breast cancer, and others, will provide a robust and biologically meaningful classification generating insights into the clinical heterogeneity of the disease and influencing strategies to find new modes of prevention and treatment.

METHODS SUMMARY

DNAs from breast cancers and normal tissues from the same individuals were subjected to in-solution enrichment for the coding exons of 21,416 genes and 1,664 micro RNAs (Agilent 50 Mb Exome) and subsequently sequenced on Illumina GAIIX machines. The average exome coverage (at a minimum depth of ×30) was 70%. Following alignment to the reference genome using BWA[28], somatic substitutions and small indels were identified using CaVEMan and Pindel calling algorithms, respectively[3,29]. DNAs from cancers were also hybridized to Affymetrix SNP6 arrays and analysed using the ASCAT algorithm[30] for copy number and zygosity changes. Confirmation by orthogonal sequencing technologies was attempted for all putative somatic mutations and follow-up of a subset of genes in additional case series was undertaken by targeted PCR and Illumina sequencing. Identification of genes showing evidence of selection was conducted as previously described[3].

Informed consent was obtained from all subjects and ethical approval obtained from Cambridgeshire 3 Research Ethics Committee (ref 09/H0306/36).

Full Methods and any associated references are available in the online version of the paper at www.nature.com/nature.

Received 21 June 2011; accepted 6 March 2012.

Published online 16 May; corrected 20 June 2012 (see full-text HTML version for details).

1. Stratton, M. R., Campbell, P. J. & Futreal, P. A. The cancer genome. *Nature* **458,** 719–724 (2009).
2. Greenman, C., Wooster, R., Futreal, P. A., Stratton, M. R. & Easton, D. F. Statistical analysis of pathogenicity of somatic mutations in cancer. *Genetics* **173,** 2187–2198 (2006).
3. Varela, I. *et al.* Exome sequencing identifies frequent mutation of the SWI/SNF complex gene PBRM1 in renal carcinoma. *Nature* **469,** 539–542 (2011).
4. Keshet, Y. & Seger, R. The MAP kinase signaling cascades: a system of hundreds of components regulates a diverse array of physiological functions. *Methods Mol. Biol.* **661,** 3–38 (2010).
5. Su, G. H. *et al.* Alterations in pancreatic, biliary, and breast carcinomas support MKK4 as a genetically targeted tumor suppressor gene. *Cancer Res.* **58,** 2339–2342 (1998).
6. Carpten, J. D. *et al.* A transforming mutation in the pleckstrin homology domain of AKT1 in cancer. *Nature* **448,** 439–444 (2007).
7. Park, H. S. *et al.* Akt (protein kinase B) negatively regulates SEK1 by means of protein phosphorylation. *J. Biol. Chem.* **277,** 2573–2578 (2002).
8. Carnero, A., Blanco-Aparicio, C., Renner, O., Link, W. & Leal, J. F. The PTEN/PI3K/AKT signalling pathway in cancer, therapeutic implications. *Curr. Cancer Drug Targets* **8,** 187–198 (2008).
9. Wu, G. S. The functional interactions between the MAPK and p53 signaling pathways. *Cancer Biol. Ther.* **3,** 146–151 (2004).
10. Horlein, A. J. *et al.* Ligand-independent repression by the thyroid hormone receptor mediated by a nuclear receptor co-repressor. *Nature* **377,** 397–404 (1995).
11. Merrell, K. W. *et al.* Differential recruitment of nuclear receptor coregulators in ligand-dependent transcriptional repression by estrogen receptor-alpha. *Oncogene* **30,** 1608–1614 (2010).
12. Jones, S. *et al.* Frequent mutations of chromatin remodeling gene ARID1A in ovarian clear cell carcinoma. *Science* **330,** 228–231 (2010).
13. Reisman, D., Glaros, S. & Thompson, E. A. The SWI/SNF complex and cancer. *Oncogene* **28,** 1653–1668 (2009).
14. Wiegand, K. C. *et al.* ARID1A mutations in endometriosis-associated ovarian carcinomas. *N. Engl. J. Med.* **363,** 1532–1543 (2010).
15. Spirin, K. S. *et al.* p27/Kip1 mutation found in breast cancer. *Cancer Res.* **56,** 2400–2404 (1996).
16. Tigli, H., Buyru, N. & Dalay, N. Molecular analysis of the p27/kip1 gene in breast cancer. *Mol. Diagn.* **9,** 17–21 (2005).
17. Chu, I. M., Hengst, L. & Slingerland, J. M. The Cdk inhibitor p27 in human cancer: prognostic potential and relevance to anticancer therapy. *Nature Rev. Cancer* **8,** 253–267 (2008).
18. Han, J. *et al.* Tbx3 improves the germ-line competency of induced pluripotent stem cells. *Nature* **463,** 1096–1100 (2010).
19. Howard, B. & Ashworth, A. Signalling pathways implicated in early mammary gland morphogenesis and breast cancer. *PLoS Genet.* **2,** e112 (2006).
20. Bamshad, M. *et al.* Mutations in human TBX3 alter limb, apocrine and genital development in ulnar-mammary syndrome. *Nature Genet.* **16,** 311–315 (1997).
21. Fillmore, C. M. *et al.* Estrogen expands breast cancer stem-like cells through paracrine FGF/Tbx3 signaling. *Proc. Natl Acad. Sci. USA* **107,** 21737–21742 (2010).
22. Ghoussaini, M. *et al.* Genome-wide association analysis identifies three new breast cancer susceptibility loci. *Nature Genet.* **44,** 312–318 (2012).
23. Varghese, J. S. & Easton, D. F. Genome-wide association studies in common cancers–what have we learnt? *Curr. Opin. Genet. Dev.* **20,** 201–209 (2010).
24. Miller, D. On the nature of susceptibility to cancer. *Cancer* **46,** 1307–1318 (1980).
25. Schinzel, A. C. & Hahn, W. C. Oncogenic transformation and experimental models of human cancer. *Front. Biosci.* **13,** 71–84 (2008).
26. Shuck, S. C., Short, E. A. & Turchi, J. J. Eukaryotic nucleotide excision repair: from understanding mechanisms to influencing biology. *Cell Res.* **18,** 64–72 (2008).
27. Fousteri, M. & Mullenders, L. H. Transcription-coupled nucleotide excision repair in mammalian cells: molecular mechanisms and biological effects. *Cell Res.* **18,** 73–84 (2008).
28. Li, H. & Durbin, R. Fast and accurate long-read alignment with Burrows-Wheeler transform. *Bioinformatics* **26,** 589–595 (2010).
29. Ye, K., Schulz, M. H., Long, Q., Apweiler, R. & Ning, Z. Pindel: a pattern growth approach to detect break points of large deletions and medium sized insertions from paired-end short reads. *Bioinformatics* **25,** 2865–2871 (2009).
30. Van Loo, P. *et al.* Allele-specific copy number analysis of tumors. *Proc. Natl Acad. Sci. USA* **107,** 16910–16915 (2010).

Supplementary Information is linked to the online version of the paper at www.nature.com/nature.

Acknowledgements This work was supported by the Wellcome Trust (grant reference 077012/Z/05/Z) and Breakthrough Breast Cancer. P.J.C. is personally funded through a Wellcome Trust Senior Clinical Research Fellowship (grant reference WT088340MA). P.V.L. is a postdoctoral researcher at the Research Foundation - Flanders (FWO) and is a visiting scientist at the Wellcome Trust Sanger Institute, supported by a travel grant from the FWO. I.V. is supported by a fellowship from The International Human Frontier Science Program Organization. A.-L.B.-D. and A.L. are funded by the Norwegian Research Council, The Norwegian Cancer Society, The Radium Hospital Foundation and Health Region SØ. A.V.S. was supported by an 'Interface INSERM' grant. J.S.R.-F. is funded in part by Breakthrough Breast Cancer and is a recipient of the 2010 CRUK Future Leaders Prize. D.E. is a Principal Research Fellow of Cancer Research UK. A.T. receives financial support from the Department of Health via the National Institute for Health Research comprehensive Biomedical Research Centre award to Guy's and St Thomas' NHS Foundation Trust in partnership with King's College London, and from King's College Hospital NHS Foundation Trust in conjunction with The Experimental Cancer Medicine Centre Initiative jointly funded by Cancer Research UK, the National Institute for Health Research, the Welsh Assembly Government, the HSC R&D Office for Northern Ireland and the Chief Scientist Office, Scotland. C.D. and C.S. received partial funding from the MEDIC foundation and the Fonds National de Recherche Scientifique. J.M. and J.F. are funded in part by a research grant from the Netherlands Genomics Initiative/Netherlands Organization for Scientific Research. The INCa-Synergie facility received support from the Institut National du Cancer, the Fondation Synergie-Lyon-Cancer, the Canceropole Lyon Auverge Rhone Alpes and the Centre Leon Berard. A.C.V. is funded by The Ludwig Institute for Cancer Research. L.v.'t.V. and A. Broeks receive funding from the Dutch Genomics Initiative-Cancer Genomics Center. We also acknowledge support for sample collection, banking and processing from the Biological Resource Center of Institut Curie; the Breakthrough Breast Cancer Unit; P. Watson and the BCCA Tumour Tissue Repository; the Centre for Translational Genomics; A. Lane and P. T. Simpson; the Australian Biospecimens Network; the Breast Unit at Royal Brisbane and Women's Hospital; the Dana-Farber/Harvard SPORE in breast cancer (reference CA089393); A. M. Sieuwerts; and the Singhealth Tissue Repository, Singapore. We are grateful also for the support of T. B. Tean, and acknowledge the input and guidance of P. Spellman and A. Ashworth.

Author Contributions P.J.S., P.S.T. and H.D. performed analysis of the sequence data, aided by S.N.Z., I.V., G.R.B., L.R.Y., E.P., D.J.M., M.S.-C. and R.R. P.V.L. performed analysis of the SNP6 data. C.G., D.C.W., K.W.L. and D.E. performed the statistical investigations. S. Martin coordinated sample acquisition and pathology review. S. McLaren coordinated sample processing. D.B., A. Butler, J.G., J.H., M.J., A.J., D.J., A.M., K.R. and J.T. performed informatics investigations. A.C., C.L. and L.M performed technical investigations. A.L., OSBREAC, M.T.M.L., C.-Y.S., B.T.K.T., B.W.H., A. Broeks, A.C.V., G. Turashvili, J.M., A.F., P.M., S.-F.C., G. Thomas, S.B., O.M., S.R.L., M.v.d.V., L.v.'t.V., J.F., C.D., C.S., A.T., C.C., J.S.R.-F., S.A.J.R.A., A.V.S., A.-L.B.-D. and A.R. contributed samples, clinical data and scientific advice. P.J.C. and P.A.F. directed the research and contributed to the manuscript. M.R.S. directed the research and wrote the manuscript.

Author Information Genome sequence data have been deposited at the European Genome-phenome Archive under accession number EGAD00001000133. Affymetrix SNP6 data have been deposited under accession number E-MTAB-1110. Reprints and permissions information is available at www.nature.com/reprints. The authors declare no competing financial interests. Readers are welcome to comment on the online version of this article at www.nature.com/nature. Correspondence and requests for materials should be addressed to M.R.S. (mrs@sanger.ac.uk).

The Oslo Breast Cancer Consortium (OSBREAC) Rolf Karesen[1,2], Ellen Schlichting[1], Bjorn Naume[2,3], Torill Sauer[2,4] & Lars Ottestad[3]

[1]Department of Breast and Endocrine Surgery, Oslo University Hospital, 0424 Oslo, Norway. [2]Medical Faculty, University of Oslo, 0424 Oslo, Norway. [3]Department of Oncology, Oslo University Hospital, 0424 Oslo, Norway. [4]Department of Pathology, Oslo University Hospital, 0424 Oslo, Norway.

LETTER

doi:10.1038/nature11154

Sequence analysis of mutations and translocations across breast cancer subtypes

Shantanu Banerji[1,2,3]†*, Kristian Cibulskis[1]*, Claudia Rangel-Escareno[4]*, Kristin K. Brown[5]*, Scott L. Carter[1], Abbie M. Frederick[1], Michael S. Lawrence[1], Andrey Y. Sivachenko[1], Carrie Sougnez[1], Lihua Zou[1], Maria L. Cortes[1], Juan C. Fernandez-Lopez[4], Shouyong Peng[2], Kristin G. Ardlie[1], Daniel Auclair[1], Veronica Bautista-Piña[6], Fujiko Duke[1], Joshua Francis[1], Joonil Jung[1], Antonio Maffuz-Aziz[6], Robert C. Onofrio[1], Melissa Parkin[1], Nam H. Pho[1], Valeria Quintanar-Jurado[4], Alex H. Ramos[1], Rosa Rebollar-Vega[4], Sergio Rodriguez-Cuevas[6], Sandra L. Romero-Cordoba[4], Steven E. Schumacher[1,2], Nicolas Stransky[1], Kristin M. Thompson[1], Laura Uribe-Figueroa[4], Jose Baselga[3,7], Rameen Beroukhim[1,2,3,8], Kornelia Polyak[2,3,9], Dennis C. Sgroi[3,10], Andrea L. Richardson[2,3,11], Gerardo Jimenez-Sanchez[4]†, Eric S. Lander[1,3,12], Stacey B. Gabriel[1], Levi A. Garraway[1,2,3], Todd R. Golub[1,3,13,14], Jorge Melendez-Zajgla[4], Alex Toker[3,5], Gad Getz[1], Alfredo Hidalgo-Miranda[4] & Matthew Meyerson[1,2,3,8]

Breast carcinoma is the leading cause of cancer-related mortality in women worldwide, with an estimated 1.38 million new cases and 458,000 deaths in 2008 alone[1]. This malignancy represents a heterogeneous group of tumours with characteristic molecular features, prognosis and responses to available therapy[2–4]. Recurrent somatic alterations in breast cancer have been described, including mutations and copy number alterations, notably *ERBB2* amplifications, the first successful therapy target defined by a genomic aberration[5]. Previous DNA sequencing studies of breast cancer genomes have revealed additional candidate mutations and gene rearrangements[6–10]. Here we report the whole-exome sequences of DNA from 103 human breast cancers of diverse subtypes from patients in Mexico and Vietnam compared to matched-normal DNA, together with whole-genome sequences of 22 breast cancer/normal pairs. Beyond confirming recurrent somatic mutations in *PIK3CA*[11], *TP53*[6], *AKT1*[12], *GATA3*[13] and *MAP3K1*[10], we discovered recurrent mutations in the *CBFB* transcription factor gene and deletions of its partner *RUNX1*. Furthermore, we have identified a recurrent *MAGI3–AKT3* fusion enriched in triple-negative breast cancer lacking oestrogen and progesterone receptors and *ERBB2* expression. The MAGI3–AKT3 fusion leads to constitutive activation of AKT kinase, which is abolished by treatment with an ATP-competitive AKT small-molecule inhibitor.

Breast cancers are classified according to gene-expression subtypes: luminal A, luminal B, Her2-enriched (Her2 is also known as ERBB2), and basal-like[14]. Luminal subtypes are associated with expression of oestrogen and progesterone receptors and differentiated luminal epithelial cell markers. The subtypes differ in genomic complexity, key genetic alterations and clinical prognosis[2–4,15]. To discover genomic alterations in breast cancers, we performed whole-genome and whole-exome sequencing of 108 primary, treatment-naive, breast carcinoma/normal DNA pairs from all major expression subtypes (Table 1 and Supplementary Tables 1–3), 17 cases by whole-exome and whole-genome sequencing, 5 cases by whole-genome sequencing alone, and 86 cases by whole-exome sequencing alone.

In total, whole-exome sequencing was performed on 103 tumour/normal pairs, 54 from Mexico and 49 from Vietnam, targeting 189,980 exons comprising 33 megabases (Mb) of the genome and with a median of 85.1% of targeted bases covered at least 30-fold across the sample set. This analysis revealed a total of 4,985 candidate somatic substitutions (see https://confluence.broadinstitute.org/display/CGATools/MuTect for methods and data sets) and insertions/deletions (indels, see https://confluence.broadinstitute.org/display/CGATools/Indelocator for methods) in the target protein-coding regions and the adjacent splice sites, ranging from 14 to 307 putative events in individual samples (Supplementary Table 4). These mutations represented 3,153 missense, 1,157 silent, 242 nonsense, 97 splice site, 194 deletions, 110 insertions and 32 other mutations (Supplementary Table 5). The total mutation rate was 1.66 per Mb (range 0.47–10.5) with a non-silent mutation rate of 1.27 per Mb (range 0.31–8.05), similar to previous reports in breast carcinoma[6–9]. The mutation rate in breast cancer exceeds that of haematologic malignancies and prostate cancer, but is significantly lower than in lung cancer and melanoma[10,16–19]. The most common

Table 1 | Sample collections successfully completed sequencing and analysis

Patients	Mexico $N = 56$	Vietnam $N = 52$
Median age (range)	54 (37–92)	48 (31–81)
Source of normal DNA	Blood	Adjacent tissue
Pathology subtype (percent)		
Ductal	46 (82%)	41 (79%)
Lobular	4 (7%)	0 (0%)
DCIS	0 (0%)	9 (17%)
Other	6 (11%)*	2 (4%)†
Stage		
0	0 (0%)	9 (17%)
I	8 (14%)	3 (6%)
II	36 (64%)	31 (60%)
III	12 (21%)	9 (17%)
Expression subtype (per cent)‡		
Luminal A	24 (43%)	14 (27%)
Luminal B	13 (23%)	9 (17%)
Her2	9 (16%)	12 (23%)
Basal	5 (9%)	8 (15%)
Unknown	2 (4%)	3 (6%)
Normal-like	3 (5%)	6 (11%)

* Includes tubular carcinoma, medullary carcinoma, mucinous carcinoma and mixed carcinoma (3).
† Includes mucinous carcinoma (2).
‡ Based on PAM-50 classification.
DCIS, ductal carcinoma *in situ*.

---

[1]The Broad Institute of MIT and Harvard, Cambridge, Massachusetts 02142, USA. [2]Department of Medical Oncology, Dana-Farber Cancer Institute, Boston, Massachusetts 02215, USA. [3]Harvard Medical School, Boston, Massachusetts 02115, USA. [4]Instituto Nacional de Medicina Genómica, Mexico City 01900, Mexico. [5]Department of Pathology, Beth Israel Deaconess Medical Center, 330 Brookline Avenue, Boston, Massachusetts 02215. [6]Instituto de Enfermedades de la Mama FUCAM, Mexico City 04980, Mexico. [7]Division of Hematology and Oncology, Massachusetts General Hospital, Boston, Massachusetts 02114, USA. [8]Department of Cancer Biology, Dana-Farber Cancer Institute, Boston, Massachusetts 02215, USA. [9]Department of Medicine, Brigham and Women's Hospital, Boston, Massachusetts 02115, USA. [10]Department of Pathology, Massachusetts General Hospital, Boston, Massachusetts 02114, USA. [11]Department of Pathology, Brigham and Women's Hospital, Boston, Massachusetts 02115, USA. [12]Massachusetts Institute of Technology, Cambridge, Massachusetts 02139, USA. [13]Department of Pediatric Oncology, Dana-Farber Cancer Institute, Boston, Massachusetts 02215, USA. [14]Howard Hughes Medical Institute, Chevy Chase, Maryland 20815, USA. †Present addresses: Department of Medical Oncology, CancerCare Manitoba, Winnipeg, Manitoba R3E 0V9, Canada (S.B.); Global Biotech Consulting Group, Mexico City 01900, Mexico (G.J.-S.).

*These authors contributed equally to this work.

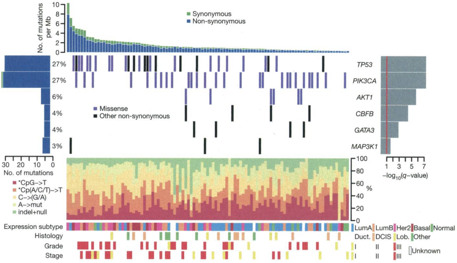

Figure 1 | Most significantly mutated genes in breast cancer as determined by whole-exome sequencing ($n = 103$). Upper histogram, rates of sample-specific mutations (substitutions and indels). Green, synonymous; blue, non-synonymous. Left histogram, number of mutations per gene and percentage of samples affected (colour coding as in upper histogram). Central heat map, distribution of significant mutations across sequenced samples ('Other non-synonymous' mutations: nonsense, indel and splice-site). Right histogram, $-\log_{10}$ score of MutSig q value. Red line at $q = 0.1$. Lower chart: top, rates of non-silent mutations within categories indicated by legend; bottom, key molecular features of samples in each column. DCIS, ductal carcinoma *in situ*; Duct., infiltrating ductal carcinoma; Lob., infiltrating lobular carcinoma; Lum, luminal.

mutation events observed are C to T transition events in CpG dinucleotides (Fig. 1 and Supplementary Fig. 4).

We performed validation experiments on 494 candidate mutations (representing all significantly mutated genes and genes in significantly mutated gene sets) using a combination of mass-spectrometric genotyping, 454 pyrosequencing, Pacific Biosciences sequencing and Illumina sequencing of matched formalin-fixed paraffin-embedded tissue, and confirmed the presence of 94% of protein-altering point mutations (Supplementary Table 4 and Supplementary Fig. 5); this validation rate is consistent with previous results that 95% of point mutations can be validated with orthogonal methods[16,17]. Only 18 out of 39 (46%) indels among significantly mutated genes were confirmed.

Six genes were found to be mutated with significant recurrence in the 103 whole-exome sequenced samples, by analysis with the MutSig algorithm[16,17] (https://confluence.broadinstitute.org/display/CGATools/MutSig) at a false discovery rate (FDR) < 0.1 after correction for multiple hypothesis testing (Supplementary Table 6a), manual review of reads, and subsequent orthogonal confirmation of somatic events (Fig. 1 and Supplementary Fig. 6). One gene, *CBFB*, is identified for the first time as a significantly mutated gene in breast cancer or any other epithelial cancer, to our knowledge, whereas the other five genes (*TP53*, *PIK3CA*, *AKT1*, *GATA3* and *MAP3K1*) have previously been reported as mutated in breast cancer[7,10,13]. This significantly mutated genes list, as any list produced by a statistical method, is probably incomplete and reflects the statistical power of our cohort size—larger sample sets will provide further statistical power.

Somatic mutations in *TP53* and *PIK3CA* were each present in 27% of samples, consistent with published frequencies[10,20] (Fig. 1). *TP53* mutations occur in samples with a higher mutation rate (t-test $P = 0.0079$ comparing samples with mutation rates greater than or less than the median 1.66 mutations per Mb) and were distributed across the gene in sites reported in COSMIC (http://www.sanger.ac.uk/genetics/CGP/cosmic/). Also, using the ABSOLUTE algorithm for determining allele-specific copy number[21], we observed that 21 out of 31 *TP53* mutations were homozygous (Supplementary Table 4). *PIK3CA* mutations were clustered in the helical (amino acids 542/545; 40%) and kinase domains (amino acid 1047; 47%)[20]. Six samples harboured the *AKT1* E17K mutation that alters the pleckstrin-homology (PH) domain and leads to activation of the kinase[12]. *AKT1* and *PIK3CA* mutations, which activate the phosphatidylinositol-3-kinase (PI3K) pathway, were mutually exclusive in our data set. *MAP3K1*, recently reported as mutated in oestrogen-receptor-positive breast cancers[10], harboured five mutations in three patients with oestrogen-receptor-positive disease, and followed a pattern consistent with positive selection for recessive inactivation of the gene. In total, two frameshift, two nonsense and one missense mutation, combined with a homozygous deletion spanning the coding region were observed. Although the point mutations seemed to be heterozygous by copy-number analysis, two patients harboured dual mutations, consistent with compound heterozygous inactivation, although confirmatory phasing data were not available. The *GATA3* transcription factor gene harboured mutations in four patients with luminal tumours, including three previously unknown frameshift mutations near the 3′-end of the coding sequence. We also identified one previously described splice-site mutation that disrupts zinc-finger domains in GATA3 required for DNA binding[13].

CBFB, encoding the core-binding-factor beta subunit, was mutated in four oestrogen-receptor-positive samples, with one nonsense mutation and three truncating frameshift mutations (Fig. 2a). *CBFB* somatic mutations have been noted in isolated cases of breast cancer[6,10]. This is the first report of these mutations recurring at a significant rate above background; the sample size is not sufficient to determine whether these mutations are specific for oestrogen-receptor-positive subtypes. *CBFB* encodes the non-DNA-binding component of a heterodimeric protein complex, together with the DNA-binding RUNX proteins encoded by *RUNX1*, *RUNX2* and *RUNX3*. Copy-number analysis, using the ABSOLUTE algorithm[21], provides further evidence for loss of function of the RUNX1/CBFB complex in breast cancer: the cases with *CBFB* mutations seem to have hemizygous deletions of one parental allele, whereas two additional cases harbour homozygous deletions of *RUNX1* (Fig. 2b, c and Supplementary Figs 7 and 8). Oncogenic rearrangements of *RUNX1* or *CBFB* are common in acute myeloid leukaemia[22,23] (including the *CBFB–MYH11* translocation believed to have dominant negative function[22]). This is to our knowledge the first report of inactivation of this transcription factor complex in epithelial cancers.

Significance analysis restricted to somatic mutations in genes reported in COSMIC revealed three significantly mutated genes,

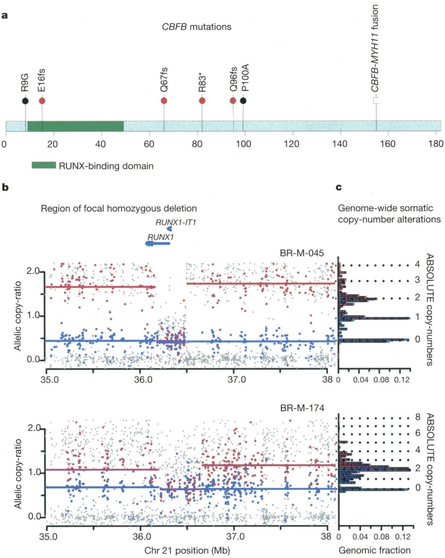

Figure 2 | *CBFB* mutations and *RUNX1* deletions. a, *CBFB* coding region diagram, RUNX-binding domain in green. Mutations identified in this study (red bullets), previously identified mutations[6,10] (black bullets), and known *CBFB–MYH11* fusion indicated. **b**, Allelic copy ratios for the 3-Mb region surrounding *RUNX1* in samples BR-M-045 and BR-M-174. Dots indicate copy-ratios for individual SNP alleles. Red, higher copy-ratio allele for informative SNPs that are heterozygous in matched normal DNA; blue, lower-copy ratio SNPs; grey, uninformative SNPs (homozygous in matched normal). Lines indicate inferred segmental copy-ratios. Red, higher-copy segment; blue, lower-copy segment; purple, equal-copy segment. **c**, Histogram depicting bins of segmented copy number (*y* axis), with inferred integral copies shown by dotted lines; the length of each horizontal block corresponds to the fraction of the haploid genome at the copy number level, or 'genomic fraction' (*x* axis).

PIK3CA, *TP53* and *ERBB2*, the latter below the significance threshold in the complete analysis (Supplementary Table 7). *ERBB2* contained somatic mutations in three samples, with two being identical S310F mutations (these two samples are distinct on the basis of their germline and somatic genotypes). The S310F mutation can activate ERBB2 and is transforming *in vitro* (personal communication from H. Greulich). Neither sample with the S310F activating mutation has *ERBB2* amplification (Supplementary Fig. 9). The two samples belong to the Her2-enriched and luminal B subtypes, which typically have *ERBB2* amplification; this supports the notion that the observed mutations have a driving role in these tumours[10,24].

To identify candidate genomic rearrangements, we applied the dRanger algorithm[16,17] to the 22 cases with paired tumour/normal whole-genome sequencing data (Supplementary Table 8). The rate of rearrangements ranged from a median of 30 rearrangements per sample in the luminal A subtype (range 0–218) to the basal-like and Her2-enriched subtypes with a median of 237 and 246 rearrangements, respectively (Supplementary Fig. 10); the rates are similar to a recent report[15]. We performed polymerase chain reaction (PCR) amplification on a subset of the candidate rearrangements (Supplementary Methods) and confirmed 89 out of 165 events (54%). No rearrangement was seen in more than one sample (Supplementary Table 8). In addition, we did not identify rearrangements previously observed by DNA sequencing[15] nor by complementary DNA (cDNA)-sequencing, including MAST and NOTCH family-gene fusions[25].

The discovery of recurrent driver rearrangements in other epithelial cancers[26,27] led to a closer examination of the list of confirmed rearrangements. In a triple-negative, basal-like subtype tumour, we observed a rearrangement between the genes *MAGI3* (membrane-associated guanylate kinase, WW and PDZ domain containing 3) on chromosome 1p and *AKT3* (v-akt murine thymoma viral oncogene homologue 3) on chromosome 1q, resulting in a balanced translocation from intron 9 in *MAGI3* to intron 1 of *AKT3* (Fig. 3a). The previously unknown fusion genes were confirmed in tumour DNA by sequencing the product of PCR amplification (Fig. 3b). The *MAGI3* disruption is complemented by a hemizygous deletion of the other allele (Supplementary Fig. 11a). The expression levels of individual exons of *MAGI3* and *AKT3* correspond to the predicted

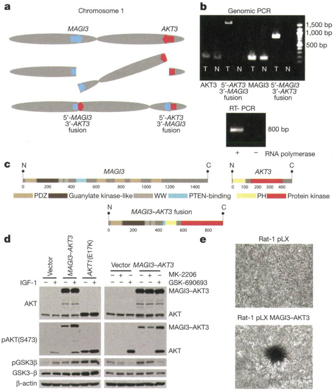

Figure 3 | *MAGI3–AKT3* fusion gene. a, Diagram of balanced translocation between *MAGI3* and *AKT3*. **b**, Top, genomic DNA PCR for *AKT3*, *MAGI3* and both fusion products in tumour (T) and normal (N). Bottom, cDNA PCR of fusion gene in tumour. **c**, Above, MAGI3 and AKT3 protein domains; below, putative fusion protein. **d**, Immunoblots of lysates from ZR-75 cells transfected with vector, *MAGI3–AKT3* fusion, or *AKT1* E17K mutant, grown in low-serum media, for the indicated antibodies. Left, infected cells with and without insulin growth factor 1 (IGF-1) stimulation; right, treatment of vector or *MAGI3–AKT3* overexpressing cells with AKT inhibitors MK-2206 and GSK-690693. **e**, Focus formation assays with Rat-1 cells expressing pLX control or *MAGI3–AKT3*, and stained with crystal violet.

5′-*MAGI3–AKT3*-3′ fusion (Supplementary Fig. 11b), with this sample having the highest *AKT3* expression in the data set. Expression of the fusion gene was confirmed in the tumour sample by PCR amplification of the cDNA (Fig. 3b).

The rearrangement produces an in-frame fusion gene with a predicted MAGI3–AKT3 fusion protein that combines MAGI3 lacking the second PDZ domain, reported to bind to PTEN and be required for the inhibitory effect of PTEN on the PI3K pathway[28], together with an AKT3 region that retains an intact kinase domain but has a disruption of the pleckstrin homology domain before the glutamate at position 17 (Fig. 3c). *AKT3* shares significant homology to *AKT1* and is reported to be the dominant AKT family member expressed in hormone-receptor-negative breast cancers[29]. Together, the *MAGI3–AKT3* translocation and deletion of *MAGI3* could result in the combined loss of function of a tumour suppressor gene (*PTEN*) and activation of an oncogene (*AKT3*).

To evaluate oncogenic activity of the *MAGI3–AKT3* fusion, we expressed the fusion gene ectopically in ZR-75 cells. The MAGI3–AKT3 fusion protein is constitutively phosphorylated at serine 473 in the AKT3 kinase domain (numbered according to the wild-type protein) in the absence of growth factors (Fig. 3d); ectopically expressed AKT1 with an engineered E17K mutation is likewise constitutively phosphorylated (Fig. 3d), as previously reported[12]. Constitutive activation of the MAGI3–AKT3 kinase in turn activates downstream pathways as demonstrated by phosphorylation of GSK3β, an AKT substrate (Fig. 3d). Phosphorylation of GSK3β by the MAGI3–AKT3 fusion can be inhibited with an ATP-competitive small molecule AKT inhibitor, GSK-690693, but not with an allosteric AKT inhibitor, MK-2206, that interacts with the PH domain of AKT (Fig. 3d). Overexpression of the *MAGI3–AKT3* fusion gene in Rat-1 fibroblast cell lines led to loss of contact inhibition and focus formation (Fig. 3e).

We screened 235 additional breast cancer samples for the presence of the 5′-*MAGI3–AKT3*-3′ fusion event by PCR with reverse transcription (RT–PCR) of cDNA followed by Sanger sequencing of breakpoints. The fusion was present in 8 of the 235 samples, including 5 out of 72 triple-negative (oestrogen-receptor-, progesterone-receptor- and Her2-negative) samples (Supplementary Fig. 12).

The power provided by whole-genome and whole-exome sequencing of a relatively large and diverse breast cancer sample set has enabled several significant discoveries, including the identification of recurrent inactivating mutations in *CBFB* and of a recurrent translocation of *MAGI3–AKT3*. The mutations in *CBFB*, *RUNX1* and *GATA3* suggest the importance of understanding epithelial cell differentiation and its regulatory transcription factors in breast cancer pathogenesis. The recurrent genomic fusion involving *AKT3* suggests that the use of ATP-competitive AKT inhibitors should be evaluated in clinical trials for the treatment of fusion-positive triple-negative breast cancers, a subtype where limited therapeutic options exist beyond systemic cytotoxic chemotherapy.

METHODS SUMMARY

All samples were obtained under institutional IRB approval and with documented informed consent. Breast cancer specimens from Mexico were paired with peripheral blood normal DNA whereas the Vietnamese samples were paired with DNA from normal adjacent breast tissue. Tumour RNA for each case was analysed on exon arrays to determine breast cancer expression subtype using the PAM50 classification method, whereas tumour/normal DNA pairs were analysed for copy number, allelic imbalance, and ancestry using single nucleotide polymorphism (SNP) arrays. A total of 108 samples, 17 both whole-genome sequencing and whole-exome sequencing, 86 whole-exome sequencing only, and 5 whole-genome sequencing only, passed initial qualification metrics, library construction, and successfully achieved desired sequencing depth (100× whole-exome sequencing; 30× whole-genome sequencing) on the Illumina sequencing platform (Supplementary Figs 1–3, Supplementary Tables 2 and 3). Tumour-specific point mutations, small insertions/deletions (indels), and rearrangements were detected by comparing tumour DNA to its paired normal DNA and using a series of algorithms to identify somatic events (Supplementary Fig. 2)[16,17]. Additional mutation calling was performed separately on tumour and normal DNA to identify germline mutation events that may confer susceptibility to breast carcinoma. Allele-specific copy number of each gene/mutation was determined using the HAPSEG and ABSOLUTE analysis methods. Confirmation of point mutations and indels was performed using mass-spectrometry-based genotyping and orthogonal next-generation sequencing methods, whereas putative in-frame genomic rearrangements were PCR-amplified from DNA to confirm the presence of the event.

A complete description of the materials and methods is provided in the Supplementary Information. Access to the data and computational algorithms used in this study can be found at https://confluence.broadinstitute.org/display/CGATools/Home.

Received 16 June 2011; accepted 20 April 2012.

1. Jemal, A. *et al.* Global cancer statistics. *CA Cancer J. Clin.* **61,** 69–90 (2011).
2. Sørlie, T. *et al.* Gene expression patterns of breast carcinomas distinguish tumor subclasses with clinical implications. *Proc. Natl Acad. Sci. USA* **98,** 10869–10874 (2001).
3. Chin, K. *et al.* Genomic and transcriptional aberrations linked to breast cancer pathophysiologies. *Cancer Cell* **10,** 529–541 (2006).
4. Gatza, M. L. *et al.* A pathway-based classification of human breast cancer. *Proc. Natl Acad. Sci. USA* **107,** 6994–6999 (2010).
5. King, C. R., Kraus, M. H. & Aaronson, S. A. Amplification of a novel v-*erb*B-related gene in a human mammary carcinoma. *Science* **229,** 974–976 (1985).
6. Sjöblom, T. *et al.* The consensus coding sequences of human breast and colorectal cancers. *Science* **314,** 268–274 (2006).
7. Wood, L. D. *et al.* The genomic landscapes of human breast and colorectal cancers. *Science* **318,** 1108–1113 (2007).
8. Shah, S. P. *et al.* Mutational evolution in a lobular breast tumour profiled at single nucleotide resolution. *Nature* **461,** 809–813 (2009).
9. Ding, L. *et al.* Genome remodelling in a basal-like breast cancer metastasis and xenograft. *Nature* **464,** 999–1005 (2010).

10. Kan, Z. *et al.* Diverse somatic mutation patterns and pathway alterations in human cancers. *Nature* **466,** 869–873 (2010).
11. Samuels, Y. *et al.* High frequency of mutations of the *PIK3CA* gene in human cancers. *Science* **304,** 554 (2004).
12. Carpten, J. D. *et al.* A transforming mutation in the pleckstrin homology domain of AKT1 in cancer. *Nature* **448,** 439–444 (2007).
13. Usary, J. *et al.* Mutation of *GATA3* in human breast tumors. *Oncogene* **23,** 7669–7678 (2004).
14. Sorlie, T. *et al.* Repeated observation of breast tumor subtypes in independent gene expression data sets. *Proc. Natl Acad. Sci. USA* **100,** 8418–8423 (2003).
15. Stephens, P. J. *et al.* Complex landscapes of somatic rearrangement in human breast cancer genomes. *Nature* **462,** 1005–1010 (2009).
16. Berger, M. F. *et al.* The genomic complexity of primary human prostate cancer. *Nature* **470,** 214–220 (2011).
17. Chapman, M. A. *et al.* Initial genome sequencing and analysis of multiple myeloma. *Nature* **471,** 467–472 (2011).
18. Pleasance, E. D. *et al.* A comprehensive catalogue of somatic mutations from a human cancer genome. *Nature* **463,** 191–196 (2010).
19. Pleasance, E. D. *et al.* A small-cell lung cancer genome with complex signatures of tobacco exposure. *Nature* **463,** 184–190 (2010).
20. Bachman, K. E. *et al.* The *PIK3CA* gene is mutated with high frequency in human breast cancers. *Cancer Biol. Ther.* **3,** 772–775 (2004).
21. Carter, S. L. *et al.* Absolute quantification of somatic DNA alterations in human cancer. *Nature Biotechnol.* doi:10.1038/nbt.2203 (29 April 2012).
22. Cameron, E. R. & Neil, J. C. The *Runx* genes: lineage-specific oncogenes and tumor suppressors. *Oncogene* **23,** 4308–4314 (2004).
23. Shigesada, K., van de Sluis, B. & Liu, P. P. Mechanism of leukemogenesis by the inv(16) chimeric gene *CBFB/PEBP2B-MHY11*. *Oncogene* **23,** 4297–4307 (2004).
24. Stephens, P. *et al.* Lung cancer: intragenic ERBB2 kinase mutations in tumours. *Nature* **431,** 525–526 (2004).
25. Robinson, D. R. *et al.* Functionally recurrent rearrangements of the MAST kinase and Notch gene families in breast cancer. *Nature Med.* **17,** 1646–1651 (2011).
26. Soda, M. *et al.* Identification of the transforming *EML4–ALK* fusion gene in non-small-cell lung cancer. *Nature* **448,** 561–566 (2007).
27. Tomlins, S. A. *et al.* Recurrent fusion of *TMPRSS2* and ETS transcription factor genes in prostate cancer. *Science* **310,** 644–648 (2005).
28. Wu, Y. Interaction of the tumor Suppressor PTEN/MMAC with a PDZ domain of MAGI3, a novel membrane-associated guanylate kinase. *J. Biol. Chem.* **275,** 21477–21485 (2000).
29. Nakatani, K. *et al.* Up-regulation of Akt3 in estrogen receptor-deficient breast cancers and androgen-independent prostate cancer lines. *J. Biol. Chem.* **274,** 21528–21532 (1999).

Supplementary Information is linked to the online version of the paper at www.nature.com/nature.

Acknowledgements We would like to thank all patients who contributed samples to this study. This study was a collaboration of the Broad Institute in Cambridge, Massachusetts, USA, and the National Institute of Genomic Medicine (INMEGEN) in Mexico City, Mexico. The work was conducted as part of the Slim Initiative for Genomic Medicine, a project funded by the Carlos Slim Health Institute in Mexico. This work is part of a global effort in collaboration with the International Cancer Genome Consortium (ICGC). The authors would also like to acknowledge J. Barretina and H. Greulich for their critical review of the manuscript. In addition, we would like to acknowledge the technical expertise and data generation efforts of The Broad Institute Biological Samples, Genome Sequencing, and Genetic Analysis Platforms. S.B. has received fellowship support co-sponsored by CancerCare Manitoba and the University of Manitoba. K.K.B. is a recipient of the John Gavin Post-doctoral Fellowship, Genesis Oncology Trust of New Zealand. R.R.-V. and S.L.R.-C. received a scholarship from the Mexican Council of Science and Technology (CONACyT). R.B. is a V Foundation Scholar. A.T. is funded by NIH grant CA122099. This work was partially supported by the Dana-Farber/Harvard SPORE in breast cancer under NCI grant reference CA089393.

Author Contributions S.B., K.C., C.R.E., L.Z., M.S.L., A.Y.S, A.H.R., N.S., G.G., A.H.M. and M.M. performed sequencing data analysis. S.B., A.M.F. and J.F. planned and performed fusion gene PCR and cloning. K.K.B. and A.T. planned and performed fusion gene biochemical and transformation experiments. F.D. and J.J. performed quantitative PCR experiments. C.R.-E. and J.C.F.-L. performed ancestry analysis. C.R.-E., J.C.F.-L., L.Z. and S.P. performed expression analysis. S.L.C. and G.G. performed ABSOLUTE analysis. R.R.-V., L.U.-F., S.E.S. and R.B. performed experimental work on SNP arrays and DNA copy number analysis. K.C., R.C.O. and M.P. performed mutation and rearrangement validation analysis. C.S., M.L.C., K.G.A., D.A., V.B.-P., V.Q.-J. and S.L.R.-C. collected data, processed and analysed genetic material, and provided data management. S.B., K.G.A. D.A., R.R.-V., S.L.R.-C., A.M.-A., S.R.-C., K.M.T., D.C.S., A.L.R. and A.H.-M. collected patient materials. S.B., K.C., C.R.-E., S.L.C., L.Z., A.M.F., J.C.F.-L., N.H.P., and M.M. contributed text and figures including Supplementary Information. All authors contributed to the final manuscript. K.P., D.C.S., A.L.R. and E.S.L. provided critical review of the manuscript. J.B., G.J.-S., E.S.L., S.B.G., L.A.G., T.R.G., J.M.-Z., G.G., A.H.-M. and M.M. provided leadership for the project.

Author Information Sequence data have been deposited in the dbGaP repository (http://www.ncbi.nlm.nih.gov/gap) under accession number phs000369.v1.p1. Reprints and permissions information is available at www.nature.com/reprints. This paper is distributed under the terms of the Creative Commons Attribution-Non-Commercial-Share Alike licence, and is freely available to all readers at www.nature.com/nature. Readers are welcome to comment on the online version of this article at www.nature.com/nature. The authors declare competing financial interests: details accompany the full-text HTML version of the paper at www.nature.com/nature. Correspondence and requests for materials should be addressed to M.M. (matthew_meyerson@dfci.harvard.edu), A.H.-M. (ahidalgo@inmegen.gob.mx), A.T. (atoker@bidmc.harvard.edu) or G.G. (gadgetz@broadinstitute.org).

doi:10.1038/nature11059

Astrocyte glypicans 4 and 6 promote formation of excitatory synapses via GluA1 AMPA receptors

Nicola J. Allen[1]†, Mariko L. Bennett[1], Lynette C. Foo[1], Gordon X. Wang[2], Chandrani Chakraborty[1], Stephen J. Smith[2] & Ben A. Barres[1]

In the developing central nervous system (CNS), the control of synapse number and function is critical to the formation of neural circuits. We previously demonstrated that astrocyte-secreted factors powerfully induce the formation of functional excitatory synapses between CNS neurons[1]. Astrocyte-secreted thrombospondins induce the formation of structural synapses, but these synapses are postsynaptically silent[2]. Here we use biochemical fractionation of astrocyte-conditioned medium to identify glypican 4 (Gpc4) and glypican 6 (Gpc6) as astrocyte-secreted signals sufficient to induce functional synapses between purified retinal ganglion cell neurons, and show that depletion of these molecules from astrocyte-conditioned medium significantly reduces its ability to induce postsynaptic activity. Application of Gpc4 to purified neurons is sufficient to increase the frequency and amplitude of glutamatergic synaptic events. This is achieved by increasing the surface level and clustering, but not overall cellular protein level, of the GluA1 subunit of the AMPA (α-amino-3-hydroxy-5-methyl-4-isoxazole propionic acid) glutamate receptor (AMPAR). Gpc4 and Gpc6 are expressed by astrocytes *in vivo* in the developing CNS, with Gpc4 expression enriched in the hippocampus and Gpc6 enriched in the cerebellum. Finally, we demonstrate that Gpc4-deficient mice have defective synapse formation, with decreased amplitude of excitatory synaptic currents in the developing hippocampus and reduced recruitment of AMPARs to synapses. These data identify glypicans as a family of novel astrocyte-derived molecules that are necessary and sufficient to promote glutamate receptor clustering and receptivity and to induce the formation of postsynaptically functioning CNS synapses.

To understand how astrocytes regulate functional synapse formation, we examined postsynaptic function, AMPAR levels and AMPAR localization at synapses between purified retinal ganglion cells (RGCs) cultured alone or with a feeder layer of astrocytes (Supplementary Fig. 1a–d). Astrocytes strengthen individual excitatory glutamatergic synapses in RGCs, as shown by increased frequency and amplitude of miniature excitatory postsynaptic currents[1] (mEPSCs) (Fig. 1a–c). In RGCs, mEPSCs are mediated purely by AMPARs, composed of combinations of four subunits, GluA1 to GluA4, forming tetramers[1,3]. Astrocytes do not greatly alter total AMPAR levels in RGCs (except for a small significant increase in GluA4), and thus do not induce the synthesis of new AMPARs or block the degradation of existing receptors (Fig. 1d, e). Astrocytes do, however, increase surface levels of all AMPAR subunits on RGCs by a factor of three, as shown by surface biotinylation and quantitative western blotting (Fig. 1f, g). Surface staining for GluA1-containing AMPARs demonstrated that the increased surface receptors are clustered together in puncta throughout the dendrites (Fig. 1h–j). These results demonstrate that astrocyte-derived signals lead to increased surface levels and clustering of pre-existing AMPARs.

We previously identified thrombospondins and hevin as astrocyte-secreted proteins sufficient to induce structural synapse formation, but the synapses so formed are postsynaptically silent because they lack AMPARs[2,4]. Therefore, we used biochemistry to identify the astrocyte-secreted factor that is sufficient to induce functional synapse formation. Astrocytes were maintained in minimal medium and the factors they secreted collected as astrocyte-conditioned medium (ACM), which was concentrated and fed to RGCs, and was sufficient to induce functional synapse formation as assessed by electrophysiological recording of total synaptic activity and mEPSCs (Supplementary Fig. 1c, e–g). Analysis of ACM by two-dimensional electrophoresis revealed that hundreds of proteins were present, and size-exclusion experiments demonstrated the activity factor to be relatively large, between 100 and 300 kDa (Supplementary Fig. 2). To narrow down candidate factors present in ACM, we conducted affinity column fractionation, initially using individual columns and then combining them in series (Supplementary Fig. 3). In the final fractionation scheme, the unbound proteins were taken from a heparin column, bound and eluted from an anion column, and then bound and eluted from a hydrophobic interaction column. This final eluted protein fraction was fed to RGCs, and as it was unclear whether the activity factor would be sufficient to induce synapses directly, thrombospondin was included to induce structural synapse formation. This final fraction was sufficient to induce a large increase in synaptic activity (Fig. 1k), contained 1% of the starting protein (Supplementary Table 1) and was sixfold enriched for functional activity. This fraction was analysed by mass spectrometry and contained approximately 25 candidate factors (Supplementary Table 2).

To identify which candidate protein was sufficient to enhance synaptic activity, we overexpressed them in COS-7 cells (which do not secrete endogenous synaptogenic factors (Supplementary Fig. 4)) and fed the conditioned medium to RGCs along with thrombospondin. Most of the candidates lacked activity, whereas medium conditioned by Gpc4-expressing COS-7 cells was sufficient to induce a large increase in synaptic activity (Supplementary Fig. 4 and Fig. 1l). Western blotting of conditioned media from RGCs, cultured astrocytes and immunopanned astrocytes (that closely resemble *in vivo* mature astrocytes[5]) demonstrated that astrocytes and not neurons secrete Gpc4 *in vitro* (Supplementary Fig. 5). Glypicans are a conserved family of heparan sulphate proteoglycans, with six members (Gpc1 to Gpc6) in mammals, and Gpc4 is homologous to *Drosophila* Dally-like[6]. The 63-kDa core protein is heavily glycosylated and can be in excess of 200 kDa in mass. Glypicans are tethered to the extracellular face of the plasma membrane of cells by GPI (glycosyl phosphoinositide) linkages[7,8], which can be cleaved by endogenous phospholipases, thus releasing the protein.

Having demonstrated that Gpc4 is sufficient to enhance total synaptic activity, we asked whether this was due to effects on postsynaptic strengthening of synapses. In subsequent experiments, RGCs were treated with purified Gpc4 (Supplementary Fig. 6a, b), in the absence of thrombospondin, to assess specific effects of Gpc4 on synapse formation and function. Gpc4 was sufficient to strengthen individual

---

[1]Stanford University School of Medicine, Department of Neurobiology, 299 Campus Drive, Fairchild Science Building D231, Stanford, California 94305-5125, USA. [2]Stanford University School of Medicine, Department of Molecular and Cellular Physiology, 279 Campus Drive, Beckman Center B100, Stanford, California 94305-5125, USA. †Present address: Molecular Neurobiology Laboratory, The Salk Institute for Biological Studies, 10010 North Torrey Pines Road, La Jolla, California 92037, USA.

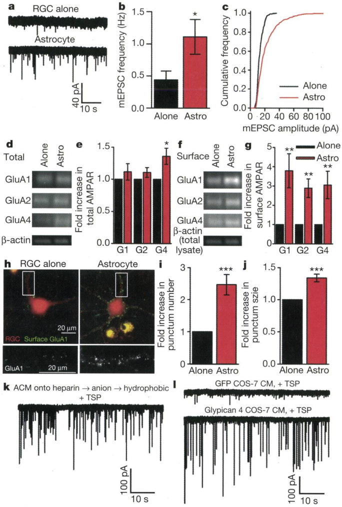

Figure 1 | Astrocyte signals strengthen synapses by recruitment of surface AMPARs. **a–c**, Example mEPSC recordings (**a**) show that frequency (**b**) and amplitude (**c**) are significantly increased in RGCs cultured with astrocytes. Average mEPSC amplitude: 12.2 ± 0.5 pA (RGCs alone, $N = 13$ cells), 20.4 ± 1.7 pA (astrocytes, $N = 14$, $P < 0.0002$). **d, e**, Astrocytes do not alter total AMPAR levels in RGCs. Western blots (**d**) of RGC lysates for AMPAR subunits GluA1 (G1), GluA2 (G2) and GluA4 (G4), and β-actin loading control, and quantification of band intensity relative to RGC alone (**e**). $N = 7$ experiments. **f, g**, Astrocytes increase surface AMPARs in RGCs. Western blots (**f**) of surface AMPAR subunits GluA1, GluA2 and GluA4, and β-actin loading control from total lysate (same experiment as **d**), and quantification of band intensity relative to RGC alone (**g**). $N = 16$ experiments. **h–j**, Astrocytes cluster GluA1-containing AMPARs on the RGC surface. Example images (**h**) of surface GluA1 (green) and RGC processes (red); bottom panel, enlargement of GluA1 (boxed white). Quantification of number (**i**) and size (**j**) of GluA1 clusters. $N = 10$ experiments. **k**, Total synaptic activity induced by final protein fraction from column fractionation of ACM. **l**, Total synaptic activity in RGCs cultured in COS-7-cell-conditioned medium (COS-7 CM) transfected with a control protein (green fluorescent protein (GFP)) or Gpc4, plus thrombospondin (TSP). $*P < 0.05$, $**P < 0.01$, $***P < 0.001$; error bars, s.e.m.

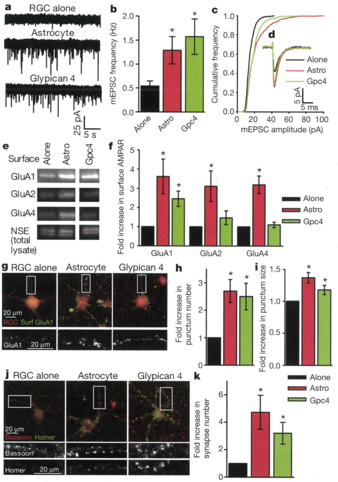

Figure 2 | Gpc4 is sufficient to strengthen glutamatergic synapses and increase surface GluA1-containing AMPARs. **a–d**, Example mEPSC recordings (**a**) show that frequency (**b**) and amplitude (**c**) are significantly increased in RGCs cultured with Gpc4. Average traces aligned by rise time (**d**). Average mEPSC amplitude: 13.8 ± 0.7 pA (RGC alone, $N = 16$ cells), 20.0 ± 1.2 pA (astrocyte, $N = 16$, $P < 0.05$), 17.8 ± 1.4 pA (Gpc4, $N = 13$, $P < 0.05$). **e, f**, Gpc4 increases surface GluA1 AMPARs in RGCs. Western blots (**e**) of surface AMPAR subunits GluA1, GluA2 and GluA4 and neuron-specific enolase (NSE) loading control from total lysate, and quantification of band intensity relative to RGC alone (**f**). For full blot results, see Supplementary Fig. 9. $N = 6$ experiments for GluA1 and GluA2; $N = 3$ for GluA4. **g–i**, Gpc4 clusters GluA1-containing AMPARs on the RGC surface. Example images (**g**) of surface GluA1 (green) and RGC processes (red); bottom panel, enlargement of GluA1 (boxed white). Quantification of number (**h**) and size (**i**) of GluA1 clusters. $N = 7$ experiments. **j, k**, Gpc4 induces structural synapses. Example images (**j**) of presynaptic (bassoon, red) and postsynaptic (homer, green) staining; bottom panels, enlargements of the respective markers (boxed white). Quantification of synapse number (**k**) (co-localization of pre- and postsynaptic puncta). $N = 6$ experiments. $*P < 0.05$; error bars, s.e.m.

synapses, as shown by increased mEPSC frequency and amplitude, although the very large-amplitude events induced by astrocytes were absent (Fig. 2a–d and Supplementary Fig. 7). To determine whether increased synaptic activity was due to increased numbers of AMPARs on the cell surface, we isolated surface receptors and analysed them by western blotting. Gpc4 induced a 2.5-fold increase in surface GluA1, comparable to that observed in the presence of astrocytes; however, there was less of an increase in surface levels of the other subunits (Fig. 2e, f and Supplementary Fig. 9). Thus, Gpc4 specifically recruits GluA1-containing AMPARs, and astrocytes release additional factors that bring GluA2, GluA3 and GluA4 AMPAR subunits to the synapse. Surface staining for GluA1 revealed a 2.5-fold increase in the number of receptor clusters on RGCs exposed to Gpc4, and a 20% increase in size, comparable to astrocytes (Fig. 2g–i). Gpc4-induced clustering of GluA1 on RGCs is dose dependent, being effective at 0.1–10 nM (comparable to levels in ACM) and ineffective at higher concentrations (Supplementary Fig. 6c, d). These experiments demonstrate that Gpc4 is sufficient to strengthen pre-existing synapses by increasing mEPSC amplitude; however, we also observed an increase in the number of mEPSCs and GluA1 clusters on RGCs, suggesting that Gpc4 can induce new structural synapses. We assessed synapse number by counting co-localization of pre- and postsynaptic markers, and observed a significant threefold increase in synapse number in RGCs treated with Gpc4 compared with RGCs grown alone (Fig. 2j, k). This demonstrates that Gpc4 is synaptogenic, although to a lesser degree than astrocytes.

The glypicans are a gene family with six members in mouse and human; *Gpc6* is the most homologous to *Gpc4* (ref. 9). We identified both Gpc4 and Gpc6 in the fractionation positive fraction (Supplementary Table 2), so we assessed whether Gpc6 is also synaptogenic. Gpc6 was sufficient to recruit GluA1 to the neuronal surface, and also induced structural synapse formation to the same extent as Gpc4 (Supplementary Fig. 8). To determine whether Gpc4 and Gpc6 are necessary for ACM to enhance postsynaptic activity, we used short interfering RNA (siRNA) to reduce expression of both in astrocytes, and confirmed protein reduction in ACM by western blotting (Supplementary Fig. 10a). ACM with reduced Gpc4 and Gpc6 was unable to significantly increase mEPSC amplitude in RGCs (Fig. 3a–c) and unable to cluster GluA1 on the neuronal surface (Fig. 3d and Supplementary Fig. 10c, d). Overexpression of the human form of Gpc4, which is resistant to the siRNA, rescued the ability of ACM to cluster GluA1 receptors on the neuronal surface (Fig. 3d). The use of siRNA against individual glypicans was not as effective in reducing the ability of ACM to enhance total synaptic activity (Supplementary Fig. 10b). ACM with reduced levels of Gpc4 and Gpc6 still induced a significant increase in structural synapse formation, presumably owing to the presence of other synaptogenic proteins such as thrombospondin and hevin[2,4] (Fig. 3e). These results show that Gpc4 and Gpc6 are necessary components of ACM for enhancing postsynaptic activity, and that there is functional redundancy between family members.

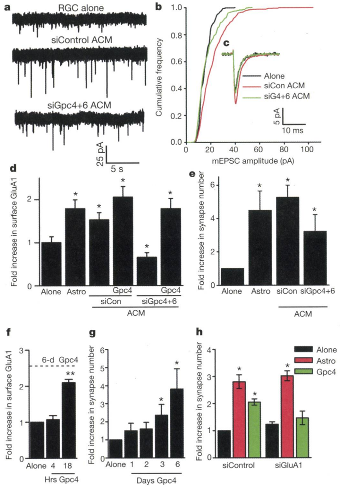

Figure 3 | Gpc4 and Gpc6 are necessary for ACM to cluster surface GluA1, and mechanism of action. a–c, Reduction of Gpc4 and Gpc6 levels in ACM reduces its ability to increase mEPSC amplitude in RGCs. Example mEPSC recordings (**a**), cumulative amplitude plot (**b**) and average traces aligned by rise time (**c**). Average mEPSC amplitude: 14.6 ± 0.6 pA (RGC alone, $N = 8$ cells), 20.6 ± 0.9 pA (siRNA control ACM, $N = 10$, $P < 0.05$), 16.0 ± 1.0 pA (siRNA Gpc4 and Gpc6 ACM, $N = 11$, $P = 0.3$). **d**, Reduction of Gpc4 and Gpc6 levels in ACM prevents GluA1 surface clustering, which is rescued by expression of siRNA-resistant Gpc4. $N = 30$ cells per condition. **e**, Reduction of Gpc4 and Gpc6 levels in ACM does not prevent ACM-induced structural synapse formation. $N = 3$ experiments. **f**, Time course of Gpc4-induced surface clustering of GluA1 shows 18 h of treatment is required to increase surface GluA1 levels. Dashed line, 6-d data from Fig. 2h. $N = 3$ experiments (4 h), 4 (18 h). **g**, Gpc4 does not rapidly induce structural synapse formation and requires 3 d of treatment. $N = 5$ experiments (1 d), 3 (2 d), 6 (3 d), 3 (6 d). **h**, Surface clustering of GluA1 is necessary for Gpc4-induced synapse formation, shown by the inability of Gpc4 to induce synapse formation in RGCs lacking GluA1. $N = 5$ experiments. $^{*}P < 0.05$, $^{**}P < 0.0001$; error bars, s.e.m.

To examine the time course of Gpc4 effects, we assayed surface clustering of GluA1 after 4 h and 18 h of treatment. There was no increase in receptor recruitment after 4 h, but after 18 h there was a significant increase in surface GluA1, to the same level as after 6 d (time point previously used; Fig. 3f and Supplementary Fig. 11a, b). Thus, Gpc4 does not immediately capture GluA1 AMPARs on the surface of the cell, which suggests that downstream signalling cascades are involved. We examined structural synapse formation at 4 h, 18 h, 1 d, 2 d, 3 d and 6 d after Gpc4 addition, and found that synapse number only significantly increased after 3 d (Fig. 3g and Supplementary Fig. 11c, d). Therefore, Gpc4 first clusters GluA1-containing AMPARs on the cell surface, and only then recruits postsynaptic scaffolding molecules. This suggests that clustering of GluA1 is a necessary step in Gpc4-induced synapse formation. To test this hypothesis, we used siRNA to decrease GluA1 in RGCs, and asked whether Gpc4 could still induce structural synapse formation (Supplementary Fig. 11e). Whereas astrocytes still increased synapse formation in RGCs lacking GluA1, Gpc4 did not (Fig. 3h). This mechanism of synaptogenesis is distinct from that of thrombospondin, which induces structural synapses that are postsynaptically silent[2]. Thus, astrocytes can induce excitatory synapse formation by at least two distinct mechanisms (Supplementary Fig. 19).

Because they are heparan sulphate proteoglycans, glypicans can interact with signalling receptors and morphogens (for example Wnt, fibroblast growth factor, Hedgehog and bone morphogenetic protein) via their sugar chains[10]. We generated a 'mutant' form of Gpc4 lacking glycosylation sites to investigate whether glycosylation is necessary for the synaptogenic effects of Gpc4 (Supplementary Fig. 12a). Glycosylation-deficient Gpc4 could not cluster GluA1 or induce structural synapse formation (Supplementary Fig. 12b, c and Supplementary Fig. 6d). Comparison by mass spectrometry of co-purified factors between full and mutant Gpc4 produced by HEK cells showed few differences between them, and these factors were not detected when Gpc4 was purified from astrocytes (data not shown), which can induce an increase in synaptic activity (Fig. 2a–d). We nevertheless tested a number of known glypican interactors for their ability to cluster surface GluA1 on RGCs and found none to be effective (Supplementary Fig. 12d). Thus, modification of Gpc4 by heparan sulphate is necessary for its synaptogenic activity, and this may be due to the necessity of heparan sulphate for structural interaction with a receptor rather than delivery of associated morphogens, as has been shown for Dally-like binding to its receptor LAR[11].

We next investigated the roles of Gpc4 and Gpc6 in developmental synapse formation and maturation *in vivo*. *In situ* hybridization revealed overlapping messenger RNA expression throughout the brain during postnatal development, particularly in the cortex, with Gpc4 enriched in the hippocampus and Gpc6 enriched in the cerebellum (Fig. 4a and Supplementary Fig. 13a). Prior gene profiling of purified forebrain CNS cells showed that messenger RNA for both Gpc4 and Gpc6 is highly enriched in astrocytes compared with neurons[12] (Supplementary Fig. 14a), which we confirmed using quantitative real-time PCR of purified astrocytes and neurons from the cortex and hippocampus (Supplementary Fig. 14b, c). Combining *in situ*

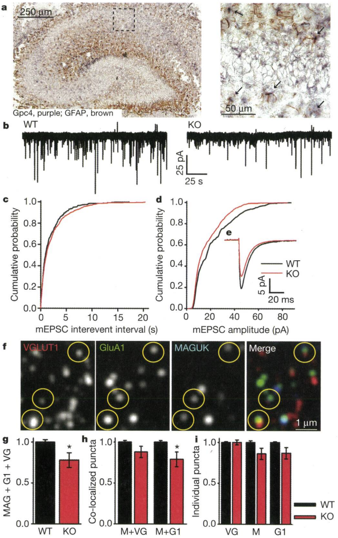

Figure 4 | Mice deficient in Gpc4 have weaker excitatory synapses *in vivo*. **a**, *In situ* hybridization of Gpc4 messenger RNA in P6 mouse hippocampus. Left: Gpc4 (purple) is expressed in synaptic regions and co-localizes with astrocytes (glial fibrillary acidic protein (GFAP), brown). Right: enlargement of boxed region; arrows mark Gpc4-positive astrocytes. **b–e**, Mice lacking Gpc4 (KO) have weaker excitatory synapses in CA1 pyramidal neurons at P12. Example mEPSC recordings (**b**), cumulative probability plot of mEPSC interevent interval (**c**) (no significant difference in frequency: wild type, 0.88 ± 0.25 Hz; *Gpc4*-knockout, 0.55 ± 0.08 Hz; $P = 0.16$), cumulative probability plot of mEPSC amplitude (**d**) (significant decrease in amplitude: wild type, 20.67 ± 2.16 pA; *Gpc4*-knockout, 16.07 ± 0.96 pA; $P < 0.05$), average traces aligned by rise time (**e**). $N = 9$ cells (*Gpc4*-knockout, five mice), 6 (wild type, five mice). **f–i**, Mice lacking Gpc4 recruit fewer GluA1 AMPARs to synaptic sites in hippocampal CA1 at P12. Example array tomography image (**f**) from wild type; VGLUT1 (red), GluA1 (green), MAGUK (blue), triple co-localization (yellow circles). There is a significant decrease in triple co-localization of VGLUT1 + MAGUK + GluA1 in *Gpc4*-knockout mice (**g**). There is no significant difference in structural synapse number (VGLUT1 + MAGUK), but there is a significant decrease in GluA1 association with MAGUK in *Gpc4*-knockout mice (**h**) and no difference in individual synaptic markers (**i**). $N = 10$ arrays per genotype from four wild-type and four *Gpc4*-knockout mice. $*P < 0.05$; error bars, s.e.m.

hybridization for Gpc4 with immunostaining for the astrocyte marker GFAP demonstrated that hippocampal astrocytes express Gpc4 at early postnatal periods (P6–P14) during the initiation of synaptogenesis[13], and that astrocytic expression decreases with maturation (P21) and switches to subsets of neurons (Fig. 4a and Supplementary Fig. 13b–d). Therefore, developing astrocytes express different glypicans with distinct but overlapping regional patterns.

To determine the *in vivo* function of Gpc4, we examined synapse formation and function in hippocampal area CA1 of *Gpc4*-knockout mice, and chose this region because Gpc4 is enriched here (Supplementary Fig. 13a) and Gpc4 and Gpc6 have redundant functions *in vitro*. We recorded mEPSCs from CA1 pyramidal neurons in acute hippocampal slices from *Gpc4*-knockout and wild-type littermate controls at P12, during functional synapse formation, and at P24, when more mature synapses are present. We observed a significant (22%) decrease in the amplitude of mEPSCs at P12, and at P24 a significant shift in amplitude distribution remained (Fig. 4b–e and Supplementary Figs 15 and 16). These effects were not due to gross differences in dendritic architecture or neuronal membrane properties (Supplementary Fig. 17), or to changes in total levels of synaptic proteins (Supplementary Fig. 18). We used array tomography to address whether the decreased mEPSC amplitude was due to a defect in structural synapse formation or to reduced recruitment of GluA1 receptors to synapses in hippocampal area CA1. Functional excitatory synapses were classified by triple co-localization of the presynaptic vesicular marker VGLUT1 with the postsynaptic density marker MAGUK, plus GluA1 at the postsynaptic side (Fig. 4f). There is a significant (22%) decrease in this class of synapse at P12 in *Gpc4*-knockout mice (Fig. 4g). This decrease is not due to a difference in the number of individual puncta (Fig. 4i) or to less structural synapse formation (VGLUT1 + MAGUK is not altered), but to a significant decrease in the co-localization of GluA1 with MAGUK (Fig. 4h). Therefore, the same number of synapses form in *Gpc4*-knockout mice as in wild type, but these synapses recruit fewer GluA1 AMPARs, probably leading to the observed physiological defect of smaller mEPSCs. The amplitude decrease observed is similar to that seen when the GluA1 subunit of the AMPAR is removed from CA1 pyramidal neurons[14,15], and this is the subunit we have shown to be recruited to the surfaces of RGCs by Gpc4 *in vitro* (Fig. 2e, f).

Here we have identified glypicans as a novel family of astrocyte-secreted proteins that regulate glutamate receptor clustering and excitatory synapse formation in neurons. Other secreted factors have been described that can induce structural synapses that are postsynaptically silent (thrombospondins and hevin[2,4]), increase surface AMPAR levels (neuronal pentraxins and tumour necrosis factor-α (refs 16, 17)) or alter AMPAR mobility and synaptic plasticity (extracellular matrix molecules[18]). Glypicans are the first non-neuronal secreted factors to be identified that are sufficient to induce functional synapses that cluster pre- and postsynaptic density proteins, are postsynaptically active and contain surface AMPARs. We have demonstrated that astrocytes increase GluA1 to GluA4 on the surfaces of neurons and that Gpc4 and Gpc6 specifically regulate GluA1 surface expression, indicating that astrocytes produce multiple factors that regulate the surface expression of different AMPAR subunits. Notably, specific AMPAR subunits may be used for the developmental initiation of synapse formation and also for the strengthening of synapses during long-term potentiation, with GluA1 used during synapse initiation and GluA2 and GluA3 used during synapse maturation[19–22]. This would be consistent with a role for glypicans in initiating nascent synapse formation by recruiting postsynaptic GluA1, followed by the action of additional factors that induce synapse maturation. Astrocytes may control these events by releasing distinct factors, including glypicans and thrombospondin, with spatiotemporal specificity, providing a new mechanism by which astrocytes control the formation and maturation of neural circuitry.

An attractive candidate receptor for inducing the actions of Gpc4 and Gpc6 is LAR, a protein tyrosine phosphatase receptor. *Drosophila* Dally-like can bind to and signal through LAR[11], and removal of LAR family members from mammalian hippocampal neurons reduces their ability to form synapses and to recruit AMPARs to synapses[23]. Mice lacking Gpc6 die shortly after birth[24] from apparent breathing difficulties (N.J.A. and B.A.B., unpublished observations), suggesting neural dysfunction, which is reminiscent of the phenotype observed in neuroligin-triple-knockout mice[25]. In addition, mutations in Gpc6 have been associated with attention deficit hyperactivity disorder[26] and neuroticism[27] in humans, disorders in which synaptic dysfunction has been implicated. Thus, the identification of glypicans as regulators of functional synapse formation has important implications for the formation of appropriate neuronal circuits in development and disease.

METHODS SUMMARY

For detailed methods, see Methods.

Purification and culture of RGCs and astrocytes. RGCs were purified by sequential immunopanning to greater than 99% purity from P5–P7 Sprague-Dawley rats (Charles Rivers) and cultured in serum-free medium containing BDNF, CNTF and forskolin on laminin-coated coverslips at 50,000 cells per well, as previously described[1,2]. Cortical astrocytes (MD astrocytes) were prepared as described in ref. 1. RGCs were cultured for 7–10 d to allow robust process outgrowth, and were then cultured with astrocyte inserts, ACM, COS-7-conditioned media, thrombospondin, Gpc4 or Gpc6 for an additional 6 d unless stated otherwise.

Column fractionation procedure. ACM (3.3 mg), collected from 10 × 15 cm plates of astrocytes, was diluted in ethanolamine buffer and passed over a heparin column to which the protein of interest did not bind. The unbound fraction was collected and passed over an anion column (Q column), to which the protein of interest did bind. The NaCl (salt) concentration was increased to 0.5 M to remove irrelevant proteins, and then to 2 M to elute proteins of interest. The 0.5–2 M anion column eluate was passed over a hydrophobic interaction column (phenyl (low sub)), to which the protein of interest did bind. The bound proteins were eluted by decreasing the NaCl concentration from 2 M to 0 M. This final eluate contained 32 µg protein (Supplementary Table 1) and was sixfold enriched for functional activity, and was analysed by mass spectrometry.

Mice. *Gpc4*-knockout mice were obtained from Genentech/Lexicon and were generated by homologous recombination targeting exon 3, confirmed by Southern blotting[24]. No Gpc4 was detected by western-blotting-conditioned media prepared from *Gpc4*-knockout astrocytes, demonstrating that no functional protein was being secreted (Supplementary Fig. 5c).

Full Methods and any associated references are available in the online version of the paper at www.nature.com/nature.

Received 15 December 2010; accepted 16 March 2012.
Published online 27 May 2012.

1. Ullian, E. M., Sapperstein, S. K., Christopherson, K. S. & Barres, B. A. Control of synapse number by glia. *Science* **291,** 657–661 (2001).
2. Christopherson, K. S. *et al.* Thrombospondins are astrocyte-secreted proteins that promote CNS synaptogenesis. *Cell* **120,** 421–433 (2005).
3. Traynelis, S. F. *et al.* Glutamate receptor ion channels: structure, regulation, and function. *Pharmacol. Rev.* **62,** 405–496 (2010).
4. Kucukdereli, H. *et al.* Control of excitatory CNS synaptogenesis by astrocyte-secreted proteins Hevin and SPARC. *Proc. Natl Acad. Sci. USA* **108,** E440–E449 (2011).
5. Foo, L. C. *et al.* Development of a method for the purification and culture of rodent astrocytes. *Neuron* **71,** 799–811 (2011).
6. Ybot-Gonzalez, P., Copp, A. J. & Greene, N. D. Expression pattern of glypican-4 suggests multiple roles during mouse development. *Dev. Dyn.* **233,** 1013–1017 (2005).
7. Song, H. H. & Filmus, J. The role of glypicans in mammalian development. *Biochim. Biophys. Acta* **1573,** 241–246 (2002).
8. Watanabe, K., Yamada, H. & Yamaguchi, Y. K-glypican: a novel GPI-anchored heparan sulfate proteoglycan that is highly expressed in developing brain and kidney. *J. Cell Biol.* **130,** 1207–1218 (1995).
9. De Cat, B. & David, G. Developmental roles of the glypicans. *Semin. Cell Dev. Biol.* **12,** 117–125 (2001).
10. Van Vactor, D., Wall, D. P. & Johnson, K. G. Heparan sulfate proteoglycans and the emergence of neuronal connectivity. *Curr. Opin. Neurobiol.* **16,** 40–51 (2006).
11. Johnson, K. G. *et al.* The HSPGs Syndecan and Dally-like bind the receptor phosphatase LAR and exert distinct effects on synaptic development. *Neuron* **49,** 517–531 (2006).
12. Cahoy, J. D. *et al.* A transcriptome database for astrocytes, neurons, and oligodendrocytes: a new resource for understanding brain development and function. *J. Neurosci.* **28,** 264–278 (2008).
13. Hsia, A. Y., Malenka, R. C. & Nicoll, R. A. Development of excitatory circuitry in the hippocampus. *J. Neurophysiol.* **79,** 2013–2024 (1998).
14. Lu, W. *et al.* Subunit composition of synaptic AMPA receptors revealed by a single-cell genetic approach. *Neuron* **62,** 254–268 (2009).
15. Andrasfalvy, B. K., Smith, M. A., Borchardt, T., Sprengel, R. & Magee, J. C. Impaired regulation of synaptic strength in hippocampal neurons from GluR1-deficient mice. *J. Physiol. (Lond.)* **552,** 35–45 (2003).
16. O'Brien, R. J. *et al.* Synaptic clustering of AMPA receptors by the extracellular immediate-early gene product Narp. *Neuron* **23,** 309–323 (1999).
17. Beattie, E. C. *et al.* Control of synaptic strength by glial TNF-α. *Science* **295,** 2282–2285 (2002).
18. Frischknecht, R. *et al.* Brain extracellular matrix affects AMPA receptor lateral mobility and short-term synaptic plasticity. *Nature Neurosci.* **12,** 897–904 (2009).
19. Kumar, S. S., Bacci, A., Kharazia, V. & Huguenard, J. R. A developmental switch of AMPA receptor subunits in neocortical pyramidal neurons. *J. Neurosci.* **22,** 3005–3015 (2002).
20. Friedman, H. V., Bresler, T., Garner, C. C. & Ziv, N. E. Assembly of new individual excitatory synapses: time course and temporal order of synaptic molecule recruitment. *Neuron* **27,** 57–69 (2000).
21. Groc, L., Gustafsson, B. & Hanse, E. AMPA signalling in nascent glutamatergic synapses: there and not there! *Trends Neurosci.* **29,** 132–139 (2006).
22. Malinow, R. & Malenka, R. C. AMPA receptor trafficking and synaptic plasticity. *Annu. Rev. Neurosci.* **25,** 103–126 (2002).
23. Dunah, A. W. *et al.* LAR receptor protein tyrosine phosphatases in the development and maintenance of excitatory synapses. *Nature Neurosci.* **8,** 458–467 (2005).
24. Tang, T. *et al.* A mouse knockout library for secreted and transmembrane proteins. *Nature Biotechnol.* **28,** 749–755 (2010).
25. Varoqueaux, F. *et al.* Neuroligins determine synapse maturation and function. *Neuron* **51,** 741–754 (2006).
26. Lesch, K.-P. *et al.* Molecular genetics of adult ADHD: converging evidence from genome-wide association and extended pedigree linkage studies. *J. Neural Transm.* **115,** 1573–1585 (2008).
27. Calboli, F. C. *et al.* A genome-wide association study of neuroticism in a population-based sample. *PLoS ONE* **5,** e11504 (2010).

Supplementary Information is linked to the online version of the paper at www.nature.com/nature.

Acknowledgements We thank R. Winant for mass spectrometry analysis, A. Olson for array tomography assistance, S. Pasca for assistance with quantitative real-time PCR and M. Fabian for technical assistance with cell cultures. This project was funded by a NIDA grant to B.A.B. (R01DA015043). N.J.A. was supported by a Human Frontiers Long Term Fellowship. S.J.S. is supported by grants R01NS0725252 and R01NS077601 from the NIH/NINDS.

Author Contributions N.J.A. and B.A.B. designed the experiments and wrote the manuscript; N.J.A., M.L.B., L.C.F. and C.C. performed and analysed the experiments; and G.X.W. and S.J.S. assisted with data analysis.

Author Information Reprints and permissions information is available at www.nature.com/reprints. The authors declare competing financial interests: details accompany the full-text HTML version of the paper at www.nature.com/nature. Readers are welcome to comment on the online version of this article at www.nature.com/nature. Correspondence and requests for materials should be addressed to N.J.A. (nallen@salk.edu).

LETTER

doi:10.1038/nature11093

PGC7 binds histone H3K9me2 to protect against conversion of 5mC to 5hmC in early embryos

Toshinobu Nakamura[1]†, Yu-Jung Liu[2], Hiroyuki Nakashima[2], Hiroki Umehara[2], Kimiko Inoue[3], Shogo Matoba[3], Makoto Tachibana[4], Atsuo Ogura[3], Yoichi Shinkai[4] & Toru Nakano[1,2]

The modification of DNA by 5-methylcytosine (5mC) has essential roles in cell differentiation and development through epigenetic gene regulation[1]. 5mC can be converted to another modified base, 5-hydroxymethylcytosine (5hmC), by the tet methylcytosine dioxygenase (Tet) family of enzymes[2,3]. Notably, the balance between 5hmC and 5mC in the genome is linked with cell-differentiation processes such as pluripotency and lineage commitment[4–7]. We have previously reported that the maternal factor PGC7 (also known as Dppa3, Stella) is required for the maintenance of DNA methylation in early embryogenesis, and protects 5mC from conversion to 5hmC in the maternal genome[8,9]. Here we show that PGC7 protects 5mC from Tet3-mediated conversion to 5hmC by binding to maternal chromatin containing dimethylated histone H3 lysine 9 (H3K9me2) in mice. In addition, imprinted loci that are marked with H3K9me2 in mature sperm are protected by PGC7 binding in early embryogenesis. This type of regulatory mechanism could be involved in DNA modifications in somatic cells as well as in early embryos.

Maternal-genome chromatin bears considerable DNA methylation and contains H3K9me2 (ref. 10). Conversely, little DNA methylation remains and no H3K9me2 is present in the chromatin of the paternal genome. We found that DNA methylation of naked DNA and chromatin DNA did not lead to substantial differences in the binding of PGC7 to DNA (Supplementary Figs 1, 2a and 3 and Supplementary Discussion). By contrast, compared with the nucleosomes purified from wild-type embryonic stem (ES) cells, PGC7 showed significantly weaker binding to the nucleosomes purified from ES cells lacking G9a (also known as Ehmt2)—an H3K9me2-specific lysine methyltransferase—in which H3K9me2 was absent, without affecting DNA methylation status (Fig. 1a, b and Supplementary Figs 2b and 4a, b)[11]. However, PGC7 bound to nucleosomes purified from rescued *G9a* knockout (*G9a*$^{-/-}$) ES cells, which expressed the short or long form of G9a (*G9a*$^{-/-}$-G9a(S) and *G9a*$^{-/-}$-G9a(L), respectively), with comparable affinity to the nucleosomes of wild-type ES cells (Fig. 1a, b). Next, we conducted a chromatin-immunoprecipitation (ChIP) assay in PGC7-null and PGC7-expressing ES cells using an anti-PGC7 antibody. As shown in Fig. 1c, nucleosomes that were bound by PGC7 specifically contained H3K9me2. H3 with other methylation modifications, however, did not show binding to PGC7. We confirmed the H3K9me2-dependent PGC7 association with chromatin in wild-type, DNA methyltransferase triple-knockout (*Dnmt1*$^{-/-}$ *Dnmt3a*$^{-/-}$ *Dnmt3b*$^{-/-}$) mutants[12] and G9a-null ES cells using a stepwise salt-extraction method[13]. PGC7 and H3 were similarly extracted from the nuclear pellets of wild-type, *Dnmt1*$^{-/-}$ *Dnmt3a*$^{-/-}$ *Dnmt3b*$^{-/-}$ and G9a (*G9a*$^{-/-}$-G9a(S) ES cells (Fig. 1d and Supplementary Fig. 5a, b). By contrast, PGC7 was extracted from nuclear pellets of *G9a*$^{-/-}$ ES cells under a lower NaCl concentration compared with that in wild-type and *Dnmt1*$^{-/-}$ *Dnmt3a*$^{-/-}$ *Dnmt3b*$^{-/-}$ cells (Fig. 1d and Supplementary Fig. 5a, b), showing that PGC7 binding to chromatin without H3K9me2 was weaker. These two experiments indicate that the association between PGC7 and chromatin is dependent on the presence of H3K9me2.

We studied the *in vitro* binding of PGC7 to various histone peptides to see whether PGC7 directly binds to H3K9me2. Although all histone peptides containing residues 1–21 bound to PGC7 to some extent, H3K9me2 bound to PGC7 most strongly (Fig. 1e). The same binding assay using truncated versions of PGC7, namely PGC7ΔC (containing amino acids 1–75) and PGC7ΔN (containing amino acids 76–150), showed that PGC7 bound to H3K9me2 by its amino terminus (Supplementary Fig. 6). Next, we carried out a competitive-binding assay to determine the binding strength of PGC7 and H3K9me2. As shown in Fig. 1f, only the excess amount of H3K9me2, but not that of the other peptides, outcompeted the binding of PGC7 to H3K9me2, indicating that the binding of PGC7 to H3K9me2 was stronger than that of other histone modifications.

PGC7 binding was higher at two representative H3K9me2-enriched loci, *Magea2* and *Wfdc15a*, but not at the control *Pou5f1* locus (Fig. 1g). By contrast, such enrichment was not observed under the G9a-null condition (Fig. 1g). These data clearly demonstrate that PGC7 specifically binds to the loci marked with H3K9me2 *in vivo*. Meanwhile, micrococcal nuclease (MNase) activity was inhibited significantly by the enforced expression of PGC7 and PGC7ΔNES, a nuclear export signal deleted mutant of PGC7 (ref. 8), in wild-type and *Dnmt1*$^{-/-}$ *Dnmt3a*$^{-/-}$ *Dnmt3b*$^{-/-}$ ES cells (Supplementary Fig. 5c–f and Supplementary Discussion). However, neither PGC7 nor PGC7ΔNES reduced MNase sensitivity in G9a$^{-/-}$ ES cells, indicating that the protective function of PGC7 required H3K9me2 (Supplementary Fig. 5a, b, g and h). These results indicate that the protective function of PGC7 is dependent on H3K9me2, but not DNA methylation.

We next asked whether the H3K9me2-dependent binding of PGC7 occurs under physiological conditions during early embryogenesis. Both the paternal and maternal pronuclei stained positively with anti-PGC7 antibody after conventional paraformaldehyde (PFA) fixation (PFA–Triton (PT) condition in Fig. 2a, b and Supplementary Fig. 7). However, the staining pattern was completely different when zygotes were treated with Triton X-100 before PFA fixation[14] (Triton–PFA (TP) condition in Fig. 2a, b and Supplementary Fig. 7). Under TP conditions, only the maternal pronucleus was labelled with the anti-PGC7 antibody, indicating that PGC7 in the paternal pronucleus was eluted by Triton X-100. In other words, PGC7 was tightly attached to a type of 'architecture' that was present in the maternal, but not the paternal, pronuclei.

Considering the maternal pronucleus-specific localization of H3K9me2 (Fig. 2b) and the results of our experiments using ES cells (Fig. 1), we hypothesized that chromatin containing H3K9me2 is the crucial structure to which PGC7 strongly binds in the maternal pronucleus. To test this hypothesis we expressed Jhdm2a (also known as

---

[1]Department of Pathology, Graduate School of Medicine, Osaka University, Osaka 565-0871, Japan. [2]Graduate School of Frontier Biosciences, Osaka University, Osaka 565-0871, Japan. [3]RIKEN BioResouce Center, Tsukuba, Ibaraki 305-0074, Japan. [4]Experimental Research Center for Infectious Diseases, Institute for Virus Research, Kyoto University, Kyoto 606-8507, Japan. †Present address: Nagahama Institute of Bio-Science and Technology, Shiga 526-0829, Japan.

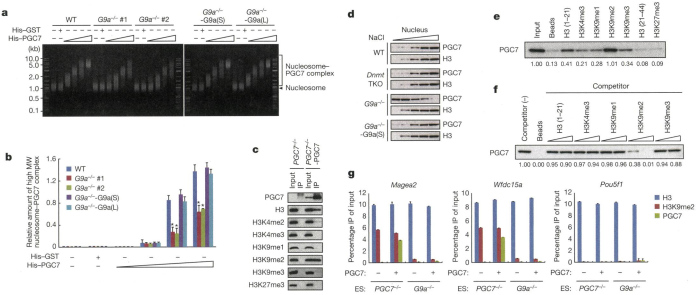

Figure 1 | Preferential binding of PGC7 to H3K9me2-marked chromatin. **a**, **b**, Electrophoretic gel-mobility shift assay of His–PGC7. Nucleosomes (approximately 10 μg) purified from wild-type (WT) and $G9a^{-/-}$ ES cells, and $G9a^{-/-}$ ES cells in which $G9a^{-/-}$-G9a(S) and $G9a^{-/-}$-G9a(L) forms of G9a were expressed were incubated with increasing concentrations of His–PGC7 (2.5, 5, 10 and 20 μg). The binding mixtures were analysed on agarose gels (**a**). Ratios of high-molecular-weight (MW) PGC7–nucleosome complex (>5 kb) were determined using NIH Image J (**b**). Error bars indicate s.d. ($n = 3$). Binding affinities were significantly different between wild-type and $G9a^{-/-}$ ES cells ($*P < 0.005$, t-test). His–glutathione S-transferase (GST; 20 μg) was used as a negative control in both experiments. Similar results were obtained in at least three independent experiments and representative results are shown. **c**, Histone-methylation status of PGC7-containing chromatin. Anti-PGC7 antibody was used to immunoprecipitate chromatin from $PGC7^{-/-}$ ES cells stably expressing PGC7. Immunoprecipitates (IP) and aliquots of the input protein were analysed by immunoblotting with antibodies against various histone modifications. Essentially the same results were obtained in two independent experiments. **d**, Chromatin-binding status of PGC7 in ES cells. Nuclei were isolated from stable-PGC7-expressing wild-type, $Dnmt1^{-/-}$ $Dnmt3a^{-/-}$ $Dnmt3b^{-/-}$ triple knockout (*Dnmt* TKO), $G9a^{-/-}$ or $G9a^{-/-}$-G9a(S) ES cells and were treated with DNase I under various concentrations of NaCl (100, 200, 300, 400 and 500 mM) to separate nuclear extract from nuclear debris. Equivalent amount of aliquots were analysed by immunoblotting with anti-PGC7 or anti-H3 antibodies. **e**, *In vitro* assay of the binding of recombinant PGC7 to various H3 tail peptides. Recombinant His–PGC7 and histone H3 tail peptides with various methylation modifications were used in an *in vitro* peptide-binding assay. Binding characteristics were analysed by immunoblotting with anti-PGC7 antibody. Similar results were obtained in three independent experiments. **f**, PGC7 competitive peptide-binding assay. N-terminal biotinylated H3K9me2 peptide was immobilized on streptavidin–sepharose beads and incubated with recombinant His–PGC7 in the presence of increasing amounts of unmodified H3 or the indicated methylated H3 peptides. Binding characteristics were analysed by immunoblotting with anti-PGC7 antibody. Similar results were obtained in two independent experiments. **g**, Concomitant binding of PGC7 to the chromatin loci marked with H3K9me2 in ES cells. A ChIP analysis using the indicated antibodies was conducted in the $PGC7^{-/-}$ and $G9a^{-/-}$ ES cells with or without enforced PGC7 expression. The percentages of each PCR product in the immunoprecipitated sample per those of the input samples are shown (mean and s.d., $n = 3$). Anti-mouse or -rabbit IgG was used for the negative controls and the signals per total input of the negative controls were <0.12% in all genes examined (data not shown).

Kdm3a), an H3K9 methylation/dimethylation-specific demethylase[15], in zygotes to erase H3K9 dimethylation. This involved injection of *Jhdm2a* polyadenylated messenger RNA and its inactive mutant, which contains a histidine to alanine point mutation (*Jhdm2a(H1122A)*) in the JmjC domain and does not possess histone-demethylase function (Supplementary Figs 8, 9 and Supplementary Discussion).

As expected, Jhdm2a expression abolished H3K9 methylation and dimethylation (Fig. 2c, d and Supplementary Fig. 10) but did not affect H3K9 trimethylation (Supplementary Fig. 11). Microinjection of *Jhdm2a* mRNA abolished PGC7 staining of the maternal pronuclei (Fig. 2e and Supplementary Fig. 12), resulting in the well-correlated PGC7 and H3K9me2 staining patterns under the TP condition (Supplementary Fig. 13). These data clearly indicate that the structure to which PGC7 strongly binds in the maternal pronucleus is H3K9me2-containing chromatin. Next, we examined whether DNA methylation was maintained after Jhdm2a expression. As shown in Fig. 3f, g, DNA methylation was not retained after H3K9me2 demethylation by Jhdm2a. In addition, the H3K9me2 and methylated-cytosine staining intensities were well correlated (Supplementary Fig. 14), and DNA methylation in the maternal pronucleus was not maintained at the pronuclear (PN) 5 stage without PGC7, as reported previously[8]. Embryonic development was impaired by reducing methylated H3K9, and the accessibility of the antibodies to chromatin is shown in Supplementary Figs 15 and 16 and Supplementary Discussion. Taken together, these observations indicate that PGC7 protects methylated DNA by binding to chromatin regions containing H3K9me2.

Next, we confirmed the importance of PGC7 binding to H3K9me2-containing chromatin in a different context. DNA methylation of paternally imprinted genes such as the differentially methylated regions (DMRs) of the *Dlk1–Gtl2* domain (where *Gtl2* is also known as Meg3), *H19* and *Rasgrf1* is protected during the active demethylation in normal mouse development[16]. However, DNA methylation of *H19* and *Rasgrf1* DMRs was not maintained, whereas that of the *Dlk1–Gtl2* DMR was maintained in PN5-stage embryos derived from PGC7-null oocytes. It is reasonable to assume that epigenetic modifications of *H19* and *Rasgrf1* differ from those of *Dlk1–Gtl2*, and that epigenetic modifications residing only in the former genes are responsible for the protective function of PGC7. Although the histones in nucleosomes are replaced by protamine during spermiogenesis, a recent epigenomic analysis of human and mouse sperm revealed that histone-containing nucleosomes are preferentially retained at loci of developmental importance, including imprinted gene clusters, homeobox-containing (*Hox*) gene clusters and Nanog homeobox (*Nanog*), but not in the intergenic regions of protein kinases, cyclic-AMP-dependent catalytic β (*Prkacb*), or zona pellucida glycoprotein 4 pseudogene (*Zp4-ps*)[17,18]. Thus, we carried out a ChIP analysis of the above-mentioned paternally imprinted genes (*Dlk1–Gtl2*, *H19* and *Rasgrf1*) and three maternally imprinted genes (paternally expressed genes 1, 3 and 5 (*Peg1* (*Mest*), *Peg3*, *Peg5* (*Nnat*)),

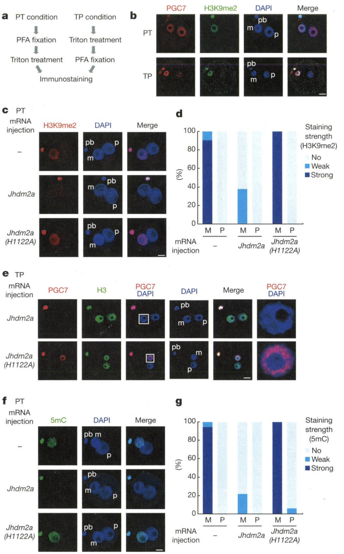

Figure 2 | Protection of the maternal genome from DNA demethylation by PGC7 through H3K9me2-containing chromatin in early embryos. **a**, Schematic diagram of the two pre-treatment procedures: PT and TP conditions. **b**, After PT or TP treatment, immunostaining was performed with the indicated antibodies (m, maternal pronuclei; p, paternal pronuclei; pb, polar body). PGC7 and H3K9me2 are shown in red and green, respectively; nuclei were stained with DAPI (blue). A total of 38 and 42 zygotes were stained, under PT and TP conditions, respectively. **c**, **d**, H3K9 dimethylation after microinjecting *Jhdm2a* or *Jhdm2a* mRNA coding for the H1122A mutation (*Jhdm2a (H1122A)*). Zygotes were injected with *Jhdm2a* or *Jhdm2a(H1122A)* mRNA and cultured for 4.5 h in potassium-enriched simplex optimized medium (KSOM). H3K9 dimethylation was analysed using anti-H3K9me2 antibody (H3K9me2, red; DAPI, blue) (**c**). A total of 32 and 34 zygotes were injected with *Jhdm2a* and *Jhdm2a(H1122A)*, respectively. A total of 55 non-injected zygotes were analysed as controls. The strength of the H3K9me2 staining in maternal (M) and paternal (P) pronuclei was analysed (**d**). **e**, Analysis of PGC7 localization after microinjecting *Jhdm2a* or *Jhdm2a(H1122A)* mRNA. Zygotes were stained after TP fixation. PGC7 and histone H3 are shown in red and green, respectively; nuclei are stained with DAPI (blue). **f**, **g**, The methylation status of the parental genome after microinjecting *Jhdm2a* or *Jhdm2a(H1122A)* mRNA. Zygotes were injected with *Jhdm2a* mRNA and cultured for 4.5 h in KSOM. Demethylation of the parental genome was analysed using anti-5mC antibody (5mC, green; DAPI, blue) (**f**). A total of 33 and 34 zygotes were injected with *Jhdm2a* and *Jhdm2a(H1122A)* mRNA, respectively, and 41 non-injected zygotes were analysed as controls. The strength of 5mC staining in the maternal and paternal pronuclei was analysed (**g**). Scale bar, 20 μm.

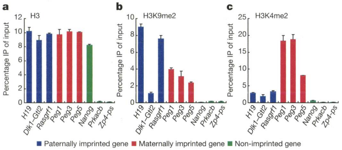

Figure 3 | Remaining H3K9me2 at the DMRs of two paternally imprinted genes, *H19* and *Rasgrf1*, in mature sperm. **a–c**, A ChIP–quantitative (q)PCR analysis of mature sperm was conducted using anti-H3 (**a**), -H3K9me2 (**b**) and -H3K4me2 (**c**) antibodies. *H19*, *Dlk1–Gtl2*, *Rasgrf1*, *Peg1*, *Peg3*, *Peg5*, *Nanog*, *Prkacb* and *Zp4-ps* were analysed by qPCR. The mean and s.d. ($n = 3$) of the percentage of each PCR product in the immunoprecipitated sample compared with that in the input sample is shown. Anti-mouse or -rabbit IgG was used as a negative control. The signals per total input of the negative controls were $<0.16\%$ for all genes examined (data not shown).

as well as the promoter and intergenic regions of three non-imprinted genes (*Nanog*, *Prkacb* and *Zp4-ps*) in mature mouse sperm.

Histone enrichment was detected at all DMRs of the analysed imprinted genes and at the *Nanog* promoter region, but not at the *Prkacb* and *Zp4-ps* intergenic regions (Fig. 3a) as reported for human sperm. Notably, H3K9me2 was enriched at the *H19* and *Rasgrf1* DMRs (Fig. 3b), but enrichment was not observed at the DMR of the paternally imprinted domain *Dlk1–Gtl2*. Considering that the *Nanog*-promoter region from the paternal genome was demethylated in wild-type zygotes, even in the presence of PGC7 (ref. 19), H3K9me2 should be crucial for the PGC7 protective function. These observations strongly suggest that the remaining H3K9me2 is important for protecting the *H19* and *Rasgrf1* DMRs against active DNA demethylation after fertilization. It is reasonable to conclude that this protection is mediated by PGC7 binding at the loci containing H3K9me2. H3K4me2 was enriched at all maternally imprinted genes examined but not at the paternally imprinted genes (Fig. 3c and Supplementary Discussion. Taking the dynamics of H3K9me2 into account (see Supplementary Discussion), in the maternal genome and two paternally imprinted loci, the binding of PGC7 to H3K9me2-containing chromatin is critical for the protection of DNA methylation.

We and another group found that the Tet3-mediated conversion of 5mC to 5hmC takes place in the paternal genome but not in the maternal genome[9,20,21]. We also showed that this conversion occurred in the maternal genome of zygotes derived from PGC7-null oocytes. These observations prompted us to analyse the effects of H3K9me2 on 5hmC status as an analogy to the PGC7-dependent regulation of zygotic 5mC. As shown in Fig. 4a, eradicating H3K9me2 by expressing Jhdm2a induced hydroxymethylation of the maternal genome, and the levels of H3K9me2 exhibited an inverse correlation with those of 5hmC (Supplementary Fig. 17). In addition, RanBP5–mER (RanBP5 fused to a mutated oestrogen receptor) expression, which inhibits PGC7 function by driving the subcellular protein out of the nucleus[8] (Supplementary Fig. 18), also induced maternal-genome hydroxymethylation (Fig. 4a). Although it has been reported that acetylation of H3K9 decreases in *Jhdm2a*$^{-/-}$ testes[22], this effect was negligible in our experimental system (Supplementary Fig. 19). Taken together, these results indicate that PGC7 protected 5mC from the Tet3-mediated conversion to 5hmC through binding to H3K9me2-containing chromatin, which is essentially identical to the model in which 5mC is protected from active demethylation.

Tet3 was detectable in both paternal and maternal pronuclei under PT conditions (Fig. 4b, c). However, Tet3 was detected only in paternal pronuclei under TP conditions (Fig. 4b, c), indicating that Tet3 was tightly bound to a structure that existed in the paternal but not the maternal chromatin. Furthermore, Tet3 was detectable in the maternal pronucleus after microinjecting *Jhdm2a* or *RnaBP5–mER* mRNA and

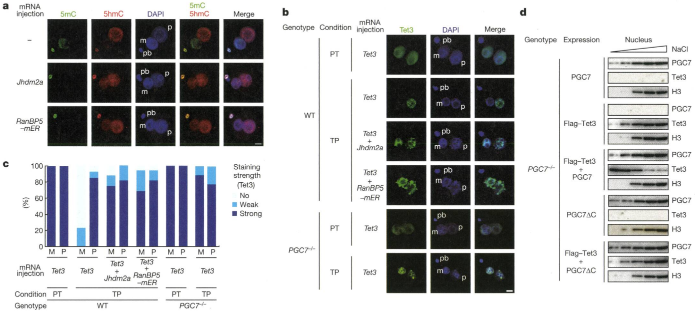

Figure 4 | Protection of the conversion of 5mC to 5hmC by PGC7 through H3K9me2-containing chromatin in early embryos. **a**, 5mC and 5hmC status after the microinjection of *Jhdm2a* or *RanBP5-mER* mRNA. Zygotes were injected with *Jhdm2a* or *RanBP5-mER* mRNA and cultured for 4.5 h in KSOM. The 5mC and 5hmC states were analysed using anti-5mC and anti-5hmC antibodies (5mC, green; 5hmC, red; DAPI, blue). Scale bar, 20 μm. **b**, **c**, Flag-tagged *Tet3* mRNA was injected into zygotes obtained from wild-type or $PGC7^{-/-}$ female mice with or without *Jhdm2a* or *RanBP5-mER* mRNA and cultured for 4.5 h in KSOM. After PT or TP treatment as described in the Fig. 2 legend, immunostaining was performed using an anti-Flag antibody. Tet3 is shown in green; nuclei were stained with DAPI (blue). Ten zygotes obtained from wild-type female mice injected with Flag-tagged *Tet3* (Flag–*Tet3*) mRNA were stained with the anti-Flag antibody under PT conditions; 13 zygotes were injected with Flag–*Tet3* mRNA alone and 16 zygotes were injected with *Tet3* and *Jhdm2a* mRNA or with *Tet3* and *RanBP5-mER* mRNA. These embryos were stained with anti-Flag antibody under TP conditions. Zygotes obtained from $PGC7^{-/-}$ female mice were injected with Flag–*Tet3* mRNA. A total of 6 and 9 zygotes were stained with the anti-Flag antibody under PT and TP conditions, respectively (**b**) and the percentage of Flag staining in maternal (M) and paternal (P) pronuclei is shown (**c**). Scale bar, 20 μm. **d**, Effect of PGC7 on the chromatin binding of Tet3 in ES cells. Nuclei were isolated from $PGC7^{-/-}$ ES cells transfected with full-length PGC7, Flag–*Tet3*, PGC7 and Flag–*Tet3*, PGC7ΔC, and both PGC7ΔC and Flag–*Tet3*. These nuclei were treated with DNase I under various concentrations of NaCl (100, 200, 300, 400 and 500 mM) to separate nuclear extract from nuclear debris. Equivalent amount of aliquots were analysed by immunoblotting with anti-PGC7, anti-Flag and anti-H3 antibodies as described.

was also detectable both in maternal and paternal pronuclei of PGC7-null fertilized eggs under TP conditions (Fig. 4b, c and Supplementary Fig. 20). These data clearly indicate that the tight binding of Tet3 to chromatin was inhibited by intranuclear PGC7 through its binding to H3K9me2-containing chromatin. Although we examined direct binding of PGC7 to Tet3, no obvious binding was observed (data not shown).

To examine the effect of PGC7 on Tet3 in more detail, we carried out a stepwise salt-extraction analysis using the $PGC7^{-/-}$ ES cells. As shown in Fig. 4d, PGC7 considerably reduced the binding of Tet3 to chromatin, which was as tight as that of H3 without PGC7. By contrast, PGC7ΔC did not show this effect despite having a chromatin-binding affinity similar to that of full-length PGC7. Moreover, the expression of PGC7ΔC did not inhibit the endonuclease activity in the MNase assay, like Tet3 binding (Supplementary Fig. 21), indicating that the inhibitory effect of PGC7 on Tet3 was not caused by competitive binding. PGC7 inhibited MNase digestion of the linker part of chromatin by binding to H3K9me2, a modified histone tail, as described in the discussion of the MNase assay of $G9a^{-/-}$ ES cells (Supplementary Fig. 5). PGC7 (~17 kDa) is a relatively small protein compared to the histone octamer (~100 kDa) and the deleted carboxy-terminal part of PGC7 (~8 kDa), which is essential for the inhibitory effect on both Tet3 binding and MNase activity. Therefore, it is probably too small to have a marked steric effect. Meanwhile, it is conceivable that the distribution of H3K9me2, through which PGC7 binds to chromatin, is not sufficiently dense. Considering these points, although we cannot exclude it completely, the possibility of a steric effect seems improbable. Therefore, we prefer the hypothesis that PGC7 inhibits the activity of the enzyme(s) acting on DNA, such as Tet3 and MNase, by means of a change in chromatin configuration.

Although 5mC has been the only recognized DNA modification for many years in mammals, several reports have described a novel 5hmC DNA modification[2,3]. The discovery of 5hmC raises numerous questions, including its function, tissue localization and regulatory mechanisms of modification. The tight differential regulatory patterns of 5mC and 5hmC in paternal and maternal pronuclei imply that 5hmC is important[9,20,21]. Here, we showed the molecular function of PGC7 during the modification as a first step towards understanding the regulatory mechanisms of 5-hydroxymethylation in DNA. It is noteworthy that regulation of reciprocal DNA methylation and hydroxymethylation was controlled by the same protein, PGC7, through binding to H3K9me2-containing chromatin. Two recent studies have raised the possibility that 5hmC is an intermediate during DNA demethylation and that the Tet family are the critical enzymes for this process[23,24]. Our conclusion is consistent with this notion, and the inhibition of Tet3 activity through the binding of PGC7 to H3K9me2 would explain the regulatory function of PGC7 in global DNA demethylation during early embryonic development (Supplementary Fig. 22).

METHODS SUMMARY

Details of cell culture, gel-shift assay, ChIP–western blotting, sperm collection, chromatin preparation, Plasmids, global DNA methylation analysis, MNase assay, histone peptide-binding assay, stepwise salt extraction, zygote collection and culture, triton treatment of zygotes, immunohistochemistry, ChIP–quantitative PCR and sperm chromatin preparation can be found in Methods.

Full Methods and any associated references are available in the online version of the paper at www.nature.com/nature.

Received 2 July 2011; accepted 28 March 2012.

Published online 3 June 2012.

1. Feng, S., Jacobsen, S. E. & Reik, W. Epigenetic reprogramming in plant and animal development. *Science* **330**, 622–627 (2010).
2. Tahiliani, M. *et al.* Conversion of 5-methylcytosine to 5-hydroxymethylcytosine in mammalian DNA by MLL partner TET1. *Science* **324**, 930–935 (2009).

3. Kriaucionis, S. & Heintz, N. The nuclear DNA base 5-hydroxymethylcytosine is present in Purkinje neurons and the brain. *Science* **324,** 929–930 (2009).
4. Koh, K. *et al.* Tet1 and Tet2 regulate 5-hydroxymethylcytosine production and cell lineage specification in mouse embryonic stem cells. *Cell Stem Cell* **8,** 200–213 (2011).
5. Ficz, G. *et al.* Dynamic regulation of 5-hydroxymethylcytosine in mouse ES cells and during differentiation. *Nature* **473,** 398–402 (2011).
6. Williams, K. *et al.* TET1 and hydroxymethylcytosine in transcription and DNA methylation fidelity. *Nature* **473,** 343–348 (2011).
7. Wu, H. *et al.* Dual functions of Tet1 in transcriptional regulation in mouse embryonic stem cells. *Nature* **473,** 389–393 (2011).
8. Nakamura, T. *et al.* PGC7/Stella protects against DNA demethylation in early embryogenesis. *Nature Cell Biol.* **9,** 64–71 (2007).
9. Wossidlo, M. *et al.* 5-Hydroxymethylcytosine in the mammalian zygote is linked with epigenetic reprogramming. *Nature Commun.* **2,** 241 (2011).
10. Santos, F., Peters, A. H., Otte, A. P., Reik, W. & Dean, W. Dynamic chromatin modifications characterise the first cell cycle in mouse embryos. *Dev. Biol.* **280,** 225–236 (2005).
11. Tachibana, M. *et al.* G9a histone methyltransferase plays a dominant role in euchromatic histone H3 lysine 9 methylation and is essential for early embryogenesis. *Genes Dev.* **16,** 1779–1791 (2002).
12. Tsumura, A. *et al.* Maintenance of self-renewal ability of mouse embryonic stem cells in the absence of DNA methyltransferases Dnmt1, Dnmt3a and Dnmt3b. *Genes Cells* **11,** 805–814 (2006).
13. Ge, Y. Z. *et al.* Chromatin targeting of *de novo* DNA methyltransferases by the PWWP domain. *J. Biol. Chem.* **279,** 25447–25454 (2004).
14. Hajkova, P. *et al.* Genome-wide reprogramming in the mouse germ line entails the base excision repair pathway. *Science* **329,** 78–82 (2010).
15. Yamane, K. *et al.* JHDM2A, a JmjC-containing H3K9 demethylase, facilitates transcription activation by androgen receptor. *Cell* **125,** 483–495 (2006).
16. Olek, A. & Walter, J. The pre-implantation ontogeny of the H19 methylation imprint. *Nature Genet.* **17,** 275–276 (1997).
17. Hammoud, S. S. *et al.* Distinctive chromatin in human sperm packages genes for embryo development. *Nature* **460,** 473–478 (2009).
18. Brykczynska, U. *et al.* Repressive and active histone methylation mark distinct promoters in human and mouse spermatozoa. *Nature Struct. Mol. Biol.* **17,** 679–687 (2010).
19. Farthing, C. R. *et al.* Global mapping of DNA methylation in mouse promoters reveals epigenetic reprogramming of pluripotency genes. *PLoS Genet.* **4,** e1000116 (2008).
20. Iqbal, K., Jin, S. G., Pfeifer, G. P. & Szabo, P. E. Reprogramming of the paternal genome upon fertilization involves genome-wide oxidation of 5-methylcytosine. *Proc. Natl Acad. Sci. USA* **108,** 3642–3647 (2011).
21. Gu, T. *et al.* The role of Tet3 DNA dioxygenase in epigenetic reprogramming by oocytes. *Nature* **477,** 606–610 (2011).
22. Liu, Z. *et al.* Jmjd1a demethylase-regulated histone modification is essential for cAMP-response element modulator-refulated gene expression and spermatogenesis. *J. Biol. Chem.* **285,** 2758–2770 (2010).
23. Ito, S. *et al.* Tet proteins can convert 5-methylcytosine to 5-formylcytosine and 5-carboxylcytosine. *Science* **333,** 1300–1303 (2011).
24. He, Y. F. *et al.* Tet-mediated formation of 5-carboxylcytosine and its excision by TDG in mammalian DNA. *Science* **333,** 1303–1307 (2011).

Supplementary Information is linked to the online version of the paper at www.nature.com/nature.

Acknowledgements We thank M. Okano, H. Niwa and H. Kimura for providing *Dnmt1*$^{-/-}$ *Dnmt3a*$^{-/-}$ *Dnmt3b*$^{-/-}$ ES cells, plasmids and antibody. We also thank N. Asada for assistance, and A. Mizokami and M. Imaizumi for secretarial assistance. This work was supported in part by grants from the Ministry of Education, Science, Sports, Culture and Technology of Japan.

Author Contributions T. Nakamura and T. Nakano conceived the project and wrote the manuscript. T. Nakamura designed and performed the all experiments and evaluated the results. Y.-J.L., H.N. and H.U. propagated *PGC7*$^{-/-}$ mice. K.I., S.M. and A.O. performed some of the experiments. M.T. and Y.S. provided *G9a*$^{-/-}$ ES cells and related materials.

Author Information Reprints and permissions information is available at www.nature.com/reprints. The authors declare no competing financial interests. Readers are welcome to comment on the online version of this article at www.nature.com/nature. Correspondence and requests for materials should be addressed to T.Nakamura (tnakamura@nagahama-i-bio.ac.jp) or T.Nakano (tnakano@patho.med.osaka-u.ac.jp).

doi:10.1038/nature10831

Experimental adaptation of an influenza H5 HA confers respiratory droplet transmission to a reassortant H5 HA/H1N1 virus in ferrets

Masaki Imai[1], Tokiko Watanabe[1,2], Masato Hatta[1], Subash C. Das[1], Makoto Ozawa[1,3], Kyoko Shinya[4], Gongxun Zhong[1], Anthony Hanson[1], Hiroaki Katsura[5], Shinji Watanabe[1,2], Chengjun Li[1], Eiryo Kawakami[2], Shinya Yamada[5], Maki Kiso[5], Yasuo Suzuki[6], Eileen A. Maher[1], Gabriele Neumann[1] & Yoshihiro Kawaoka[1,2,3,5]

Highly pathogenic avian H5N1 influenza A viruses occasionally infect humans, but currently do not transmit efficiently among humans. The viral haemagglutinin (HA) protein is a known host-range determinant as it mediates virus binding to host-specific cellular receptors[1–3]. Here we assess the molecular changes in HA that would allow a virus possessing subtype H5 HA to be transmissible among mammals. We identified a reassortant H5 HA/H1N1 virus—comprising H5 HA (from an H5N1 virus) with four mutations and the remaining seven gene segments from a 2009 pandemic H1N1 virus—that was capable of droplet transmission in a ferret model. The transmissible H5 reassortant virus preferentially recognized human-type receptors, replicated efficiently in ferrets, caused lung lesions and weight loss, but was not highly pathogenic and did not cause mortality. These results indicate that H5 HA can convert to an HA that supports efficient viral transmission in mammals; however, we do not know whether the four mutations in the H5 HA identified here would render a wholly avian H5N1 virus transmissible. The genetic origin of the remaining seven viral gene segments may also critically contribute to transmissibility in mammals. Nevertheless, as H5N1 viruses continue to evolve and infect humans, receptor-binding variants of H5N1 viruses with pandemic potential, including avian–human reassortant viruses as tested here, may emerge. Our findings emphasize the need to prepare for potential pandemics caused by influenza viruses possessing H5 HA, and will help individuals conducting surveillance in regions with circulating H5N1 viruses to recognize key residues that predict the pandemic potential of isolates, which will inform the development, production and distribution of effective countermeasures.

Although H5N1 viruses continue to cause outbreaks in poultry and there are cases of human infection in Indonesia, Vietnam, Egypt and elsewhere (http://www.who.int/influenza/human_animal_interface/H5N1_cumulative_table_archives/en/index.html), they have not acquired the ability to cause human-to-human transmission. Investment in H5N1 vaccines has therefore been questioned. However, because humans lack immunity to influenza viruses possessing an H5 HA, the emergence of a transmissible H5-HA-possessing virus would probably cause a pandemic. To prepare better for such a scenario, it is critical that we understand the molecular changes that may render H5-HA-possessing viruses transmissible in mammals. Such knowledge would allow us to monitor circulating or newly emerging variants for their pandemic potential, focus eradication efforts on viruses that already have acquired subsets of molecular changes critical for transmission in mammals, stockpile antiviral compounds in regions where such viruses circulate, and initiate vaccine generation and large-scale production before a pandemic. Therefore, we studied the molecular features that would render H5-HA-possessing viruses transmissible in mammals.

Previous studies suggested that HA has a major role in host-range restriction of influenza A viruses[1–3]. The HA of human isolates preferentially recognizes sialic acid linked to galactose by α2,6-linkages (Siaα2,6Gal), whereas the HA of avian isolates preferentially recognizes sialic acid linked to galactose by α2,3-linkages (Siaα2,3Gal)[3]. A small number of avian H5N1 viruses isolated from humans show limited binding to human-type receptors, a property conferred by several amino acid changes in HA[4–9]. None of the H5N1 viruses tested transmitted efficiently in a ferret model[10–13], although, while our paper was under review, one study[14] reported that a virus with a mutant H5 HA and a neuraminidase (NA) of a human virus in the H5N1 virus background caused respiratory droplet transmission in one of two contact ferrets.

To identify novel mutations in avian H5 HAs that confer human-type receptor-binding preference, we introduced random mutations into the globular head (amino acids 120–259 (H3 numbering), which includes the receptor-binding pocket) of A/Vietnam/1203/2004 (H5N1; VN1203) HA (Supplementary Fig. 1). Although this virus was isolated from a human, its HA retains avian-type receptor-binding properties[6,15]. We also replaced the multibasic HA cleavage sequence with a non-virulent-type cleavage sequence, allowing us to perform studies in biosafety level 2 containment (http://www.who.int/csr/resources/publications/influenza/influenzaRMD2003_5.pdf). The mutated polymerase chain reaction (PCR) products were cloned into RNA polymerase I plasmids[16] containing the VN1203 HA complementary DNA, which resulted in *Escherichia coli* libraries representing the randomly generated HA variants. Sequence analysis of 48 randomly selected clones indicated an average of 1.0 amino acid changes per HA globular head (data not shown). To generate an H5N1 virus library, plasmids for the synthesis of the mutated HA gene and the unmodified NA gene of VN1203 were transfected into human embryonic kidney (293T) cells together with plasmids for the synthesis of the six remaining viral genes of A/Puerto Rico/8/34 (H1N1; PR8), a laboratory-adapted human influenza A virus.

Turkey red blood cells (TRBCs; which possess both Siaα2,6Gal and Siaα2,3Gal on their surface (data not shown)) were treated with *Salmonella enterica* serovar Typhimurium LT2 sialidase, which preferentially removes α2,3-linked sialic acid (that is, avian-type receptors), creating TRBCs that predominantly possess Siaα2,6Gal on the cell surface (Siaα2,6-TRBCs; Supplementary Fig. 2). The virus library was then adsorbed to Siaα2,6-TRBCs at 4 °C and extensively washed to remove nonspecifically or weakly bound viruses. Bound viruses were eluted by incubation at 37 °C for 30 min, and then diluted to approximately ~0.5 viruses per well (on the basis of a pilot experiment that

---

[1]Department of Pathobiological Sciences, University of Wisconsin-Madison, Madison, Wisconsin 53711, USA. [2]ERATO Infection-Induced Host Responses Project, Saitama 332-0012, Japan. [3]Department of Special Pathogens, International Research Center for Infectious Diseases, Institute of Medical Science, University of Tokyo, Tokyo 108-8639, Japan. [4]Department of Microbiology and Infectious Diseases, Kobe University, Hyogo 650-0017, Japan. [5]Division of Virology, Department of Microbiology and Immunology, Institute of Medical Science, University of Tokyo, Tokyo 108-8639, Japan. [6]Health Science Hills, College of Life and Health Sciences, Chubu University, Kasugai, Aichi 487-8501, Japan.

assessed the approximate number of eluted viruses). We screened one-third of the library (that is, 2.1×10^6 viruses) in three separate selection experiments (that is, 0.7×10^6 viruses per experiment) and isolated 370 viruses that bound to Siaα2,6-TRBCs (Supplementary Fig. 2). Individual viruses were then grown in Madin-Darby canine kidney (MDCK) cells modified to overexpress Siaα2,6Gal (AX4 cells[17]), and screened again for their ability to agglutinate Siaα2,6-TRBCs (Supplementary Fig. 2). The parental control virus (designated VN1203/PR8) with avian-type receptor-binding specificity agglutinated untreated TRBCs (which possess both human- and avian-type receptors on their surface), but not TRBCs possessing predominantly human-type receptors (Siaα2,6-TRBCs; Supplementary Table 1). By contrast, of the 370 viruses originally isolated, nine agglutinated Siaα2,6-TRBCs, albeit with different efficiencies (Supplementary Table 1). All nine viruses possessed mutations in the region targeted for random mutagenesis; one mutant also possessed an additional mutation (E119G) in an area that was not targeted for mutation. Most of the mutations clustered around the receptor-binding pocket (Fig. 1a). Several of the selected viruses possessed mutations known to increase binding to human-type receptors, including N186K (ref. 9), S227N (ref. 5) and Q226L (which confers human-type receptor binding together with G228S)[15] (all shown in blue in Fig. 1a). The identification of known determinants of human-type receptor-binding specificity from a library of random mutants validates our approach. Notably, our screen also identified mutations not previously associated with receptor-binding specificity.

Although viruses were diluted to ~0.5 viruses per well for amplification in AX4 cells, we cannot exclude the possibility that some wells were infected with more than one virus, resulting in mixed populations. To confirm the significance of the identified mutations in HA for human-type receptor binding, the mutations were engineered into a VN1203/PR8 virus (possessing an avirulent HA cleavage site sequence, as described earlier). All nine mutants were generated; however, after two passages in MDCK cells, the S136N mutation reverted to the wild-type sequence. This mutant was excluded from further evaluation.

First, we confirmed the binding of the remaining eight variants to Siaα2,6-TRBCs (Supplementary Table 1). For comparison, we included a VN1203/PR8 virus with two changes in its HA (Q226L and G228S) previously shown to have increased binding to Siaα2,6Gal[6,15]. Indeed, compared to the wild-type VN1203/PR8 virus, the Q226L/G228S mutant displayed an increased ability to bind to human-type receptors. For the recreated variants, haemagglutination titres were higher and slightly different from the initial characterization, which we attribute to biological differences (the initial characterization was carried out with non-concentrated cell culture supernatant and potentially mixed virus populations, whereas the recreated viruses were concentrated and purified) and to experimental differences (that is, differences between the TRBC batches or the efficiency of α2,3-sialidase treatment, or both). Collectively, however, these experiments demonstrate that this random mutagenesis approach allows the identification of hitherto unrecognized amino acid substitutions that permit avian virus HAs to bind to human-type receptors.

To characterize further the receptor-binding properties of the selected variants, we used solid-phase binding assays in which sialylglycopolymers were absorbed to plates, which were then incubated with virus (Fig. 2a). A virus possessing the HA and NA genes of the seasonal human A/Kawasaki/173/2001 (H1N1; K173) virus and the remaining genes from PR8 (K173/PR8) served as a control virus with typical human-type receptor specificity. Indeed, K173/PR8 preferentially bound to Siaα2,6Gal. In contrast, VN1203/PR8 bound to only Siaα2,3Gal. As reported elsewhere[6,15], the Q226L/G228S mutations led to increased binding to Siaα2,6Gal. Variants I202T/R220S, W153R/T160I, N169I/H184L/I217M and H130Q/K157E resembled VN1203/PR8 in their binding to glycans, despite the fact that these mutants weakly agglutinated Siaα2,6-TRBCs (see Supplementary Table 1). These viruses may have bound to glycans on TRBCs that were different from Siaα2,6Galβ1,4GlcNAc used in this study. However, variants N186K/M230I, S227N/G228A and Q226L/E231G showed an appreciable increase in binding to Siaα2,6Gal but also retained binding capacity for Siaα2,3Gal. Of all of the variants tested, only E119G/V152I/N224K/Q226L exhibited specificity for only Siaα2,6Gal. Thus, only one H5 HA variant with receptor-binding capability akin to that of seasonal influenza viruses was isolated from the library screen of 2.1×10^6 viruses. To identify the amino acid change(s) responsible for the conversion from Siaα2,3Gal to Siaα2,6Gal recognition in the E119G/V152I/N224K/Q226L virus HA, we tested the amino acid changes at positions 119, 152, 224 and 226 individually and in various combinations. Solid-phase binding assays demonstrated that the N224K/Q226L combination is critical for the shift from Siaα2,3Gal to Siaα2,6Gal recognition (Fig. 2b); Q226L in combination with V152I also conferred weak binding to α2,6-glycans.

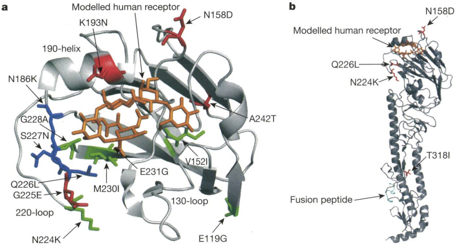

Figure 1 | Localization of amino acid changes identified in this study on the three-dimensional structure of the monomer of VN1203 HA (Protein Data Bank accession 2FK0)[15]. **a**, Close-up view of the globular head of VN1203 HA. Mutations known to increase affinity to human-type receptors are shown in blue. Amino acid changes not previously known to affect receptor binding are shown in green. Additional mutations that occurred in the HA of H5 avian–human reassortant viruses during replication and/or transmission in ferrets are shown in red. **b**, The positions of four mutations in the HA of H5 transmissible reassortant mutant virus, HA(N158D/N224K/Q226L/T318I)/CA04, are highlighted in red. The fusion peptide of HA is shown in cyan. All mutations are shown with H3 numbering. Images were created with MacPymol (http://www.pymol.org/).

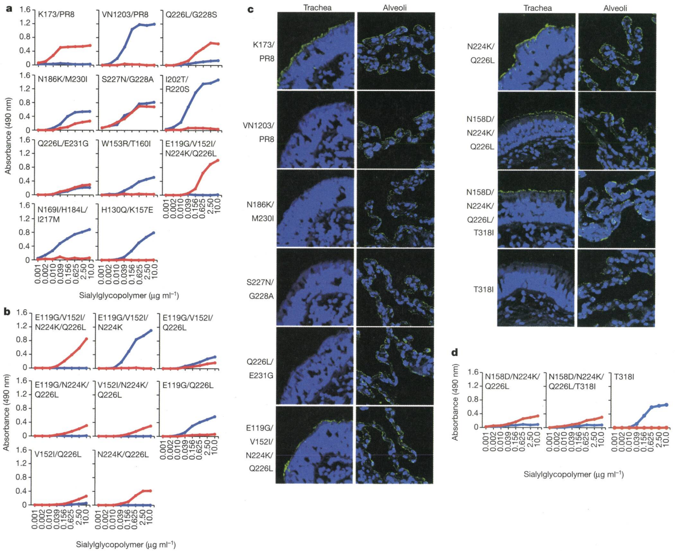

Figure 2 | Characterization of the receptor-binding properties of isolated viruses. **a**, Binding of VN1203 mutants to sialylglycopolymers in solid-phase binding assays. A human virus (K173/PR8), an avian virus (VN1203/PR8) and mutant VN1203/PR8 viruses were compared for their ability to bind to sialylglycopolymers containing either α2,3-linked (blue) or α2,6-linked (red) sialic acids. **b**, Identification of mutations that confer binding to human-type receptors. **c**, Binding of VN1203 mutant viruses to human respiratory tissues. K173/PR8, VN1203/PR8 and mutant VN1203/PR8 viruses were incubated with human tissue sections and then stained with either anti-K173 antiserum (green) or anti-VN1203 HA antibodies (green). All sections were subsequently incubated with labelled secondary antibodies and Hoechst dye (blue). **d**, Characterization of the receptor-binding properties of N158D/N224K/Q226L, N158D/N224K/Q226L/T318I and T318I viruses. The direct binding of virus to sialylglycopolymers containing either α2,3-linked (blue) or α2,6-linked (red) sialic acids was determined as described in panel **a**.

To assess the effect of enhanced α2,6-glycan recognition on the attachment of viruses to human respiratory tracts, sections of tracheal and lung tissues were exposed to K173/PR8 (human-type receptor binder), VN1203/PR8 (avian-type receptor binder) and mutant VN1203/PR8 viruses (Fig. 2c). Because the N186K/M230I, S227N/G228A, Q226L/E231G, E119G/V152I/N224K/Q226L and N224K/Q226L mutants exhibited appreciable binding to Siaα2,6Gal (Fig. 2a, b), the attachment of these mutants was also tested. On tracheal sections, the K173/PR8 virus bound extensively to ciliated epithelial cells (Fig. 2c and Supplementary Fig. 3), whereas the VN1203/PR8 virus bound poorly. By contrast, on lung sections, both viruses bound extensively to the alveolar epithelial surface (both type I and II pneumocytes; Fig. 2c and Supplementary Fig. 4). The binding patterns of these viruses correlate with the distribution of Siaα2,3Gal (that is, avian-type receptors; present in lung epithelia) and Siaα2,6Gal (that is, human-type receptors; present in both trachea and lung epithelia) on the tissues, as observed with lectin staining[18] (Supplementary Fig. 5). Like the human K173/PR8 virus, the E119G/V152I/N224K/Q226L and N224K/Q226L mutants exhibited strong binding to the ciliated epithelial cells of the trachea (Fig. 2c and Supplementary Fig. 3). By contrast, the N186K/M230I, S227N/G228A and Q226L/E231G mutants displayed little-to-no binding to tracheal epithelia (Fig. 2c), despite their binding to Siaα2,6Gal (Fig. 2a). A number of sialylated oligosaccharides with differing branching patterns and chain lengths are thought to be present on the cell surface[19]. We therefore speculate that the mutants can recognize a short glycan structure such as Siaα2,6Galβ1,4GlcNAc, but may not recognize longer, more complex glycan structures, which are possibly required for binding to human tracheal epithelium. On the other hand, all mutants bound to alveolar epithelial cells (both type I and II pneumocytes; Fig. 2c and Supplementary Fig. 4). When the tissue sections were pre-treated with *Arthrobacter ureafaciens* sialidase (which cleaves all non-reducing terminally branched and unbranched sialic acids), virus binding to the tissues was substantially reduced (Supplementary Fig. 6a–c), confirming the sialic acid binding specificity of the virus. These data indicate that alterations in the receptor specificity of the E119G/V152I/N224K/Q226L and N224K/Q226L mutants have profound effects on virus attachment to human respiratory epithelium.

In an avian H3 HA, the Q226L mutation changed the binding preference from avian- to human-type[20]. A previous study found that the Q226L mutation on an H5 HA does not confer efficient binding to α2,6-glycans in a glycan array[15]; however, when tested in combination with G228S, increased binding to human-type receptors, but not a complete switch from avian- to human-type receptor-binding specificity, was observed[15]. By contrast, here we found that Q226L in combination with N224K resulted in a switch from Siaα2,3Gal to Siaα2,6Gal binding in an H5 HA and allowed virus binding to human tracheal epithelia (Fig. 2c). The receptor-binding domain of HA is formed by the 190-helix at the top of HA, the 220-loop at the edge of the globular head, and the 130-loop at the other edge of the globular head (Fig. 1a). Crystal structure analysis revealed that the 220-loop of avian H5 HA is closer to the opposing 130-loop than in human H3 HA, indicating that a wider binding site for human H3 HA, compared to that of avian H5 HA, may be required to optimize contacts with the larger Siaα2,6-glycans[21]. N224 lies on the turn leading into the 220-loop, adjacent to position 226 (Fig. 1a). Replacement of N224 may alter the orientation of the 220-loop and thus optimize contacts between L226 and Siaα2,6Gal-containing receptors, thereby increasing the preference for α2,6 linkages.

Recent studies reported that 2009 pandemic H1N1 and H5N1 viruses show high genetic compatibility[22,23]. These two viruses have been isolated from pigs[24–28], which have been considered as 'mixing vessels' for the reassortment of avian, swine and human strains. Thus, the coexistence of H5N1 and 2009 pandemic H1N1 viruses could provide an opportunity for the generation of transmissible H5 avian–human reassortants in mammals. Therefore, we generated reassortant viruses possessing the mutant VN1203 HAs generated above, and the seven remaining gene segments from a prototype 2009 pandemic H1N1 virus (A/California/04/2009, CA04). Experiments with viruses possessing the wild-type HA cleavage site were performed in enhanced biosafety level 3 (BSL3+) containment laboratories approved for such use by the Centers for Disease Control and Prevention (CDC) and the United States Department of Agriculture (USDA). Because efficient human-to-human transmission is a critical feature of pandemic influenza viruses, we examined the growth and transmissibility of reassortant viruses in ferrets, which are widely accepted as an animal model for influenza virus transmissibility and pathogenesis studies. Because the E119G/V152I/N224K/Q226L and N224K/Q226L variants bound extensively to human tracheal epithelia (Fig. 2c), we generated by reverse genetics (rg) three H5 reassortant viruses possessing the VN1203 HA or mutant HAs (all with the wild-type multibasic cleavage site) and the remaining genes from the CA04 virus. The VN1203 HA mutants tested included the one containing four mutations, E119G, V152I, N224K and Q226L (designated rg(E119G/V152I/N224K/Q226L)/CA04), and another containing two mutations, N224K and Q226L (designated rg(N224K/Q226L)/CA04).

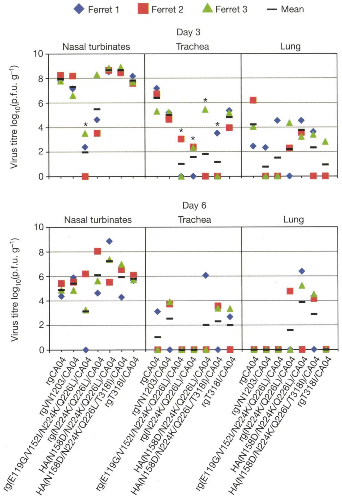

Figure 3 | Virus replication in respiratory organs. Ferrets were infected intranasally with 10^6 p.f.u. of virus. Three ferrets per group were killed on days 3 and 6 after infection for virus titration. Virus titres in nasal turbinates, trachea and lung were determined by use of a plaque assay on MDCK cells. Horizontal bars show the mean. Asterisks indicate virus titres significantly different from that of rgCA04 (Dunnett's test; $P < 0.05$).

To determine whether the introduced HA mutations affected the replication of the H5 reassortant viruses, six ferrets were inoculated intranasally with 10^6 plaque-forming units (p.f.u.) of virus. On day 3 after infection, a recombinant virus whose genes all came from CA04, rgCA04, replicated efficiently in the respiratory organs of infected animals, and was isolated from the colon, but not from any other organs tested (Fig. 3 and Supplementary Table 2). A virus possessing H5 VN1203 HA and the remaining genes from CA04 (designated rgVN1203/CA04) replicated to titres comparable to those of rgCA04 in nasal turbinates, but substantially less in the lungs. By contrast, the two H5 reassortant viruses with HA mutations (rg(E119G/V152I/N224K/Q226L)/CA04 and rg(N224K/Q226L)/CA04) were severely limited in their replicative ability in trachea. Although virus titres in nasal turbinates and lung were not statistically different between rg(N224K/Q226L)/CA04 and rgCA04, the virus titre in nasal turbinates was significantly lower in animals inoculated with rg(E119G/V152I/N224K/Q226L)/CA04 than in animals inoculated with rgCA04 (Dunnett's test; $P = 0.0002$; Fig. 3). Notably, rgVN1203/CA04 (avian-type receptor binder) replicated efficiently in nasal turbinates of ferrets, which have a similar sialic acid receptor distribution pattern to that of the human respiratory tract[29,30]. The reason for this discrepancy is unclear; however, replication of avian H5N1 viruses in ferret nasal turbinates has been reported[12,13].

Although virus titres in respiratory organs were generally lower on day 6 after infection than on day 3 after infection, rg(N224K/Q226L)/CA04 still showed high levels of replication at day 6 after infection; titres in nasal turbinates ranged from $10^{4.6}$ to $10^{8.1}$ p.f.u. g^{-1} (Fig. 3). Sequence analysis of viruses in nasal turbinates on day 6 after infection revealed that viruses in ferret 2 and ferret 3 possessed N158D and N158K mutations in their HA (in addition to the original two mutations), respectively, leading to the loss of the glycosylation site at position 158 (that is, 158N-S-T to 158D-S-T or 158K-S-T; Fig. 1a and Supplementary Table 3). In nasal turbinates on day 6 after infection, the titre of the virus with the N158D/N224K/Q226L mutations ($10^{8.1}$ p.f.u. g^{-1}; see Fig. 3, ferret 2 of rg(N224K/Q226L)/CA04) was approximately four orders of magnitude higher than that of the original rg(N224K/Q226L)/CA04 ($10^{4.6}$ p.f.u. g^{-1}; Fig. 3, ferret 1 of rg(N224K/Q226L)/CA04), whereas the virus with the N158K/N224K/Q226L mutations ($10^{5.6}$ p.f.u. g^{-1}; Fig. 3, ferret 3 of rg(N224K/Q226L)/CA04) grew to one order of magnitude higher than the original mutant. These data indicate that the additional mutation N158D improved the replication of rg(N224K/Q226L)/CA04 in ferrets. To test the effect of this mutation on the replication of H5 reassortant viruses in ferrets, we examined the replicative ability of a virus with the triple N158D/N224K/Q226L HA substitutions in ferrets. This HA(N158D/N224K/Q226L)/CA04 virus replicated efficiently in infected animals, except in the trachea (Fig. 3 and Supplementary Table 2). On day 3 after infection, this virus was isolated from the brain of two of the three animals tested, although we did not observe neurological signs in these animals. These results indicate that the N158D mutation contributed to the efficient growth in the nasal turbinates of ferrets of an H5 reassortant virus with the N224K/Q226L mutations. Removal of the glycosylation site at position 158 has been reported to result in enhanced binding of H5N1 viruses to human-type receptors in combination with the Q226L/G228S mutations[7]. A previous study showed that H5N1 viruses lacking this glycosylation site transmit efficiently by direct contact among guinea-pigs[31]. By contrast, H5N1 viruses that acquire this glycosylation site lose the ability to transmit among guinea-pigs. Therefore, we speculated that the loss of the glycosylation site in HA(N158D/N224K/Q226L)/CA04 virus may affect its transmissibility in ferrets.

To assess the ability of H5 reassortant viruses with human-type receptor specificity to transmit between ferrets, we placed naive ferrets in wireframe cages next to ferrets inoculated with 10^6 p.f.u. of rgCA04, rgVN1203/CA04, rg(N224K/Q226L)/CA04, or HA(N158D/N224K/Q226L)/CA04 (Supplementary Fig. 7). Similar to previous experiments[32], rgCA04 was efficiently transmitted via respiratory droplets to all three contact ferrets, as evidenced by the detection of virus in nasal washes and haemagglutination inhibition (HI) antibody in these animals (Table 1 and Fig. 4). By contrast, rgVN1203/CA04 and rg(N224K/Q226L)/CA04 were not transmitted; neither virus shedding nor seroconversion was detected in any contact animals, despite the binding of the latter to Siaα2,6Gal. This result was consistent with that of previous studies in which human-type receptor recognition was shown to be necessary but not sufficient for respiratory droplet transmission of an H5N1 virus in a ferret model[12,14]. In the HA(N158D/N224K/Q226L)/CA04-inoculated group, virus was recovered from two of the six contact ferrets (pairs 1 and 2) between days 5 and 7 after contact. Moreover, seroconversion was detected in five animals including those from which virus was recovered. No animals died in the course of these transmission experiments. This finding demonstrates the generation of an H5 HA that supports virus transmission by respiratory droplets among ferrets.

To determine whether additional mutations occurred in the HA of HA(N158D/N224K/Q226L)/CA04 during transmission, viral RNA was analysed from nasal washes of inoculated and contact ferrets (Fig. 4 and Supplementary Table 4). On day 5 after infection, the A242S and T318I mutations in HA were present in five (pairs 1, 3, 4, 5 and 6) and one (pair 2) of the six inoculated animals, respectively. Viruses derived from the contact animals of pair 1 on day 7 after contact had two changes in HA (K193N and A242S) (Fig. 1a), whereas those derived from the contact animals of pair 2 contained a single change in HA (T318I) (Fig. 1b), indicating that additional changes in HA occurred during the infection of ferrets with HA(N158D/N224K/Q226L)/CA04. No mutations in the remaining genes were detected in any of these viruses from nasal washes compared with the CA04 virus sequences.

Because HA(N158D/N224K/Q226L)/CA04 was isolated from only one-third of the contact animals, we isolated a virus from the nasal wash of the contact ferret that shed a high titre ($10^{7.5}$ p.f.u. ml^{-1}) of virus on day 7 after contact (pair 2) (Fig. 4d) to evaluate the replication and transmissibility of that virus in ferrets. This mutant virus, designated HA(N158D/N224K/Q226L/T318I)/CA04, replicated efficiently in the nasal turbinates and was isolated from brain tissue (Fig. 3 and Supplementary Table 2). In the transmission study, four of the six contact ferrets were positive for virus between days 3 and 7 after contact, and all contact animals were seropositive; no animals died in the course of the transmission experiments (Table 1; Fig. 4e and Supplementary Fig. 8). Notably, this transmission pattern is comparable to that of the 1918 pandemic H1N1 virus when tested under the same experimental conditions; the 1918 pandemic virus was recovered from the nasal wash of two of three contact animals (our own unpublished data). Sequence comparison of viruses from inoculated and contact animals identified mutations at positions 225 and 242 as well as a reversion at position 224 (Fig. 1a and Supplementary Table 5) (in addition to the original four mutations) although the 224 reversion was found only in viruses from inoculated ferrets. Collectively, these findings demonstrate that four amino acid substitutions (N158D/N224K/Q226L/T318I) in H5 HA confer efficient respiratory droplet transmission in ferrets to a virus possessing an H5 HA in a 2009 pandemic H1N1 backbone. We also confirmed that recombinant viruses possessing the three HA mutations N158D, N224K and Q226L, or the four HA mutations N158D, N224K, Q226L and T318I, and the NA of VN1203 in a PR8 backgrand (designated N158D/N224K/Q226L or N158D/N224K/Q226L/T318I, respectively) preferentially bind to Siaα2,6Gal and attach to human tracheal epithelia (Fig. 2c, d).

HA(N158D/N224K/Q226L/T318I)/CA04 transmitted by respiratory droplet more efficiently than HA(N158D/N224K/Q226L)/CA04, raising the possibility that the T318I mutation is involved in the efficient transmission of avian H5N1/pandemic H1N1 reassortants. To explore the functional role of this mutation in respiratory droplet transmission, we generated an H5 reassortant expressing the H5 HA with the T318I mutation and examined its receptor-binding specificity and transmissibility. This reassortant (designated rgT318I/CA04) bound to only Siaα2,3Gal and showed little binding to human tracheal epithelia (Fig. 2c, d). rgT318I/CA04 did not transmit via respiratory droplet among ferrets (Table 1 and Fig. 4f), although it replicated in nasal turbinates and trachea as efficiently as rgCA04 (Fig. 3 and Supplementary Table 2). These results indicate that the T318I mutation alone is not sufficient for H5 reassortant viruses to transmit efficiently among ferrets.

Table 1 | Transmission in ferrets inoculated with H5 avian–human reassortant viruses

Virus	Inoculated ferrets			Contact ferrets	
	Weight loss (%)*	Peak virus titre in nasal wash (mean $\log_{10}$(p.f.u. ml^{-1})) (days after inoculation)	Seroconversion (positive and total numbers) (HI titre)†	Virus detection in nasal wash (positive and total numbers)	Seroconversion (positive and total numbers) (HI titre)
rgCA04	3 of 3 (15.1)	7.5 (1)	3 of 3 (≥1,280, ≥1,280, ≥1,280)	3 of 3	3 of 3 (≥1,280, ≥1,280, ≥1,280)
rgVN1203/CA04	3 of 3 (5.9)	5.3 (5)	3 of 3 (80, 40, 80)	0 of 3	0 of 3 (<10, <10, <10)
rg(N224K/Q226L)/CA04	2 of 3 (7.8)‡	3.9 (5)	3 of 3 (≥1,280, ≥1,280, ≥1,280)	0 of 3	0 of 3 (<10, <10, <10)
HA(N158D/N224K/Q226L)/CA04	6 of 6 (5.7)	6.7 (3)	6 of 6 (640, ≥1,280, ≥1,280, 640, ≥1,280, ≥1,280)	2 of 6	5 of 6 (160, 320, 20, 160, 40, <10)
HA(N158D/N224K/Q226L/T318I)/CA04	6 of 6 (9.8)	6.1 (5)	6 of 6 (≥1,280, ≥1,280, 640, ≥1,280, ≥1,280, ≥1,280)	4 of 6	6 of 6 (640, 640, ≥1280, 80, ≥1,280, 320)
rgT318I/CA04	3 of 5 (1.5)§	5.6 (3)	5 of 5 (40, 20, 20, 40, 40)	0 of 5	0 of 5 (<10, <10, <10, <10, <10)

* Maximum percentage weight loss is shown.

† Haemagglutination inhibition (HI) assays were carried out with homologous virus and turkey red blood cells.

‡ One animal did not lose any body weight.

§ Two animals did not lose any body weight.

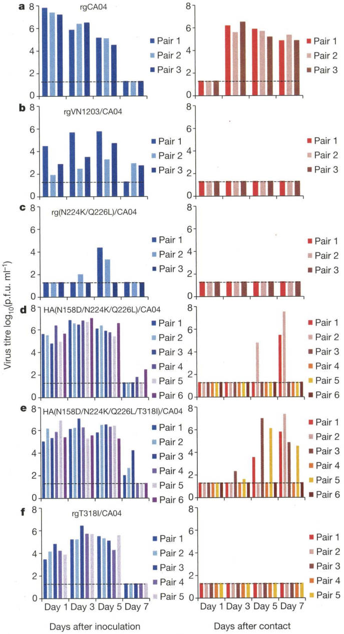

Figure 4 | Respiratory droplet transmission of H5 avian–human reassortant viruses in ferrets. a–f, Groups of three, five, or six ferrets were inoculated intranasally with 10^6 p.f.u. of rgCA04 (**a**), rgVN1203/CA04 (**b**), rg(N224K/Q226L)/CA04 (**c**), HA(N158D/N224K/Q226L)/CA04 (**d**), HA(N158D/N224K/Q226L/T318I)/CA04 (**e**), or rgT318I/CA04 (**f**). One day after infection, three, five, or six naive ferrets were placed in adjacent cages. Nasal washes were collected every other day from both inoculated (left panel) and contact (right panel) animals for virus titration. Virus titres in organs were determined by using a plaque assay on MDCK cells. The lower limit of detection is indicated by the horizontal dashed line.

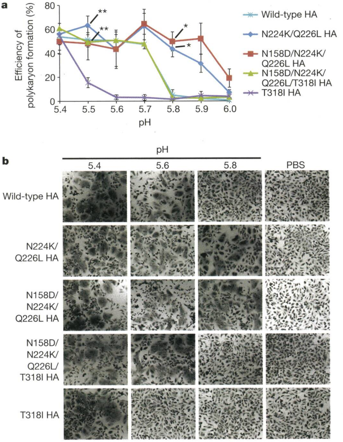

Figure 5 | Polykaryon formation by HeLa cells expressing wild-type or mutant HAs after acidification at low pH. a, The efficiency of polykaryon formation over a pH range of 5.4–6.0 was estimated from the number of nuclei in polykaryons divided by the total number of nuclei in the same field. The mean and standard deviations determined from five randomly chosen fields of cell culture are shown. Single asterisks indicate values significantly different between the wild-type HA and the N224K/Q226L or N158D/N224K/Q226L HA (Tukey test; $P < 0.05$). The double asterisk indicates values significantly different between the T318I HA and the N224K/Q226L or N158D/N224K/Q226L HA (Tukey test; $P < 0.05$). **b**, Representative fields of cells expressing the indicated HAs and exposed to pH 5.4, 5.6, or 5.8 are shown. Images were taken at ×10 magnification.

Influenza virus HA protein has membrane-fusion as well as receptor-binding activity. Notably, in the three-dimensional model of influenza A virus HA, residue 318 is located proximally to the fusion peptide (Fig. 1b), which has key roles in the membrane fusion process. To assess the effect of HA mutations on low-pH-induced membrane fusion activity, we examined the pH at which the fusion activity of wild-type and mutant HA was activated (Fig. 5). The wild-type HA had a threshold for membrane fusion of pH 5.7; the N224K/Q226L and N158D/N224K/Q226L mutations raised the threshold for fusion to >pH 5.9, whereas the T318I mutation reduced the threshold for fusion to pH 5.5. The N158D/N224K/Q226L/T318I mutations showed wild-type fusogenic properties (that is, a threshold at pH 5.7). The HA of influenza virus undergoes a low-pH-dependent conformational change, which is required for fusion of the viral envelope with the target membrane[33]. Such a conformational change to a fusion-active form can also lead to viral inactivation. Therefore, sustained and efficient human-to-human transmission of virus may require a certain level of stability of the HA protein in an acidic environment, as the pH of human nasal mucosa, where human influenza viruses replicate primarily, is approximately pH 5.5–6.5 (ref. 34). Our findings suggest that an increase in the pH threshold for fusion as a result of the N224K/Q226L mutations that shift the HA receptor recognition from avian-type to human-type may reduce HA protein stability; however, the T318I mutation decreases the pH threshold for fusion activity, resulting in a stable mutant HA.

Because heat treatment at neutral pH is also known to promote a fusogenic form of HA protein[35,36] and serve as a surrogate assay for HA stability[37], we next tested whether the HA mutations described above affect the heat stability of the HA protein. Wild-type and mutant HA viruses were incubated at 50 °C for various times, after which the loss of infectivity and haemagglutination activity were determined. The wild-type and N224K/Q226L viruses lost most of their infectivity by heating for 60 min (>5.5-log$_{10}$ decrease in titre; Fig. 6a), whereas the

N158D/N224K/Q226L and N158D/N224K/Q226L/T318I mutants exhibited considerable tolerance to high temperature (3.9- and 3.4-$\log_{10}$ decrease after a 60-min incubation, respectively) and the T318I mutant was most resistant (only a 1.4-$\log_{10}$ decrease under the same conditions). In haemagglutination assays, the N224K/Q226L mutant HA lost activity more rapidly than did the wild-type HA, and N158D/N224K/Q226L lost activity more rapidly than did the N158D/N224K/Q226L/T318I mutant (Fig. 6b). Thus, addition of the N158D mutation to the N224K/Q226L HA increased HA stability and subsequent addition of the fourth mutation, T318I, rendered the HA protein even more stable. Taken together, these results suggest that the addition of the T318I mutation to H5 HAs that preferentially recognize human-type receptors restores HA protein stability, thereby allowing a virus carrying the N158D/N224K/Q226L/T318I mutations in HA to transmit efficiently via respiratory droplet among ferrets. In conclusion, a fine balance of mutations affecting different functions in HA (such as receptor-binding specificity and HA stability) may be critical to confer transmissibility in ferrets.

We next compared the pathogenicity in ferrets of H5 avian–human reassortants with that of the pandemic H1N1 virus CA04 (Fig. 7, Supplementary Information and Supplementary Figs 9–11). The control virus, rgCA04, caused substantial body weight loss (15.1%) (Table 1 and Supplementary Fig. 9). By contrast, the four reassortant viruses caused only modest weight loss (<10%) in most of the animals. However, no statistically significant differences in body weight loss were found between the reassortant viruses and rgCA04. Pathological examination revealed similar histological changes and levels of viral antigens in the nasal mucosa of rgCA04-, HA(N158D/N224K/Q226L)/CA04- and HA(N158D/N224K/Q226L/T318I)/CA04-infected ferrets (Fig. 7a, b). In the rgVN1203/CA04 and rg(N224K/Q226L)/CA04 groups, however, less tissue damage was found in the nasal mucosa compared with the rgCA04 group on day 3 after infection (Dunnett's test; $P = 0.0057$ and 0.0175, respectively; Fig. 7b). In addition, all three

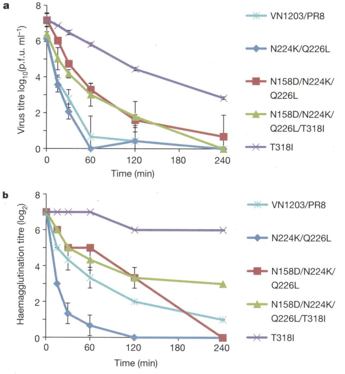

Figure 6 | Effect of heat treatment on the infectivity and haemagglutination activity of viruses. Aliquots of a virus stock containing 128 HA units were incubated for the times indicated at 50 °C. **a**, Virus titres in heat-treated samples were determined by plaque assays on MDCK cells. **b**, Haemagglutination titres in heat-treated samples were determined by using haemagglutination assays with 0.5% TRBCs. Each point represents the mean ± standard deviation from triplicate experiments.

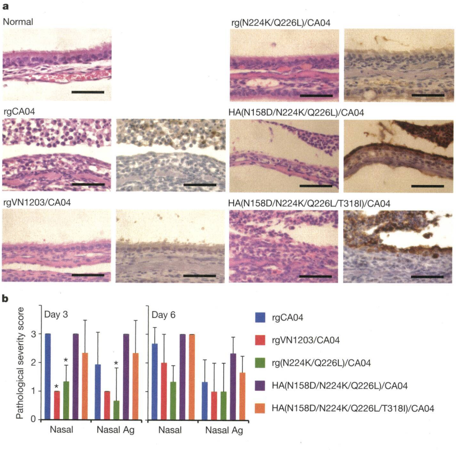
a
Normal
rg(N224K/Q226L)/CA04
rgCA04
HA(N158D/N224K/Q226L)/CA04
rgVN1203/CA04
HA(N158D/N224K/Q226L/T318I)/CA04
b
Pathological severity score
3
2
1
0
Day 3
Day 6
Nasal
Nasal Ag
Nasal
Nasal Ag
rgCA04
rgVN1203/CA04
rg(N224K/Q226L)/CA04
HA(N158D/N224K/Q226L)/CA04
HA(N158D/N224K/Q226L/T318I)/CA04

Figure 7 | Pathological analyses of H5 avian–human reassortant viruses. **a**, Representative histological changes in nasal turbinates from influenza-virus-infected ferrets. Three ferrets per group were infected intranasally with 10^6 p.f.u. of virus, and tissues were collected on day 3 after infection for pathological examination. Uninfected ferret tissues served as negative controls (normal). Left panel, haematoxylin-and-eosin staining. Right panel, immunohistochemical staining for viral antigen detection (brown staining). Scale bars, 50 μm. **b**, Pathological severity scores in infected ferrets. To represent comprehensive histological changes, respiratory tissue slides were evaluated by scoring the pathological changes and viral antigen expression levels. The pathological scores were determined for each animal in each group ($n = 3$ per group on days 3 and 6 after infection) using the following scoring system: 0, no pathological change/antigen negative; 1, affected area (<30%) or only interstitial lesion/rare viral antigens; 2, affected area (<80%, ≥30%)/moderate viral antigens; 3, severe lesion (≥80%)/many viral antigens. Nasal, pathological changes in the nasal mucosa; nasal Ag, viral antigens in the nasal mucosa. Asterisks indicate virus pathological scores significantly different from that of rgCA04 (Dunnett's test; $P < 0.05$). Error bars denote standard deviation.

viruses caused lung lesions (Supplementary Information and Supplementary Figs 10 and 11).

To assess whether current control measures may be effective against the H5 transmissible reassortant mutant virus, we examined the reactivity of sera from individuals vaccinated with an H5N1 prototype vaccine[38] against a virus possessing the N158D/N224K/Q226L/T318I mutations in HA. We found that pooled human sera from individuals immunized with this vaccine reacted with the virus possessing the mutant H5 HA (N158D/N224K/Q226L/T318I) at a higher titre than with a wild-type H5 HA virus (VN1203/PR8; Supplementary Table 6), indicating that current H5N1 vaccines would be efficacious against the H5 transmissible reassortant mutant virus. In addition, the H5 transmissible reassortant mutant virus (HA(N158D/N224K/Q226L/T318I)/CA04) was highly susceptible to a licensed NA inhibitor, oseltamivir (Supplementary Table 7). These experiments show that appropriate control measures would be available to combat the transmissible virus described in this study.

Currently, we do not know whether the mutations that we identified in this study that allowed the HA(N158D/N224K/Q226L/T318I)/CA04 virus to be transmissible in ferrets would also support sustained human-to-human transmission. In particular, we wish to emphasize that the transmissible HA(N158D/N224K/Q226L/T318I)/CA04 virus possesses seven segments (all but the HA segment) from a human pandemic 2009 H1N1 virus. Human-virus-characteristic amino acids in these seven segments may have critically contributed to the respiratory droplet transmission of the HA(N158D/N224K/Q226L/T318I)/CA04 virus in ferrets. Examples include amino acids in the PB2 polymerase protein that confer efficient replication in mammalian, but not avian, cells[39–43]. As the PB2 gene of the HA(N158D/N224K/Q226L/T318I)/CA04 virus is of human virus origin, the virus possesses high replicative ability in mammalian cells. In contrast, most avian virus PB2 proteins lack these human-type amino acids, although one of these changes (a glutamic-acid-to-lysine mutation at position 627) is found in highly pathogenic avian H5N1 viruses circulating in the Middle East[44]. As a second example, the viral NA gene may contribute to viral transmissibility. The NA protein cleaves α-ketosidic linkages between a terminal sialic acid and an adjacent sugar residue, an activity that balances the sialic-acid-binding activity of HA. A recent study found that a human virus NA gene was critical to confer limited transmissibility to a mutant H5 avian-human reassortant virus[14]. In general, a human-type receptor recognizing H5 HA alone may not be sufficient to confer transmissibility in mammals, but may have to act together with other human-virus-characteristic traits (in PB2, NA, and/or other viral proteins). Therefore, at this point we cannot predict whether the four mutations in the H5 HA identified here would render a wholly avian H5N1 virus transmissible.

Three of the residues identified here (N224, Q226 and T318) have been strictly conserved among H5 HA proteins isolated since 2003. However, as H5N1 viruses continue to evolve and infect people, receptor-binding variants of H5N1 viruses, including avian–human reassortant viruses as tested here, may emerge. One of the four mutations we identified in our transmissible virus, the N158D mutation, results in loss of a glycosylation site. Many H5N1 viruses isolated in the Middle East, Africa, Asia and Europe do not have this glycosylation site. Therefore, only three nucleotide changes are needed for the HA of these viruses to support efficient transmission in ferrets. In addition, the H5N1 viruses circulating in these geographic areas also possess a glutamic-acid-to-lysine mutation at position 627 in the PB2 protein, which promotes viral replication in certain mammals, including humans[40,45]. Therefore, these viruses may be several steps closer to those capable of efficient transmission in humans and are of concern.

Our study highlights the pandemic potential of viruses possessing an H5 HA. Although current vaccines may protect against a virus similar to that tested here, the continued evolution of H5N1 viruses reinforces the need to prepare and update candidate vaccines to H5 viruses. The amino acid changes identified here will help individuals conducting surveillance in regions with circulating H5N1 viruses (for example, Egypt, Indonesia, Vietnam) to recognize key residues that predict the pandemic potential of isolates. Rapid responses in a potential pandemic situation are essential in order to generate appropriate vaccines and initiate other public health measures to control infection. Furthermore, our findings are of critical importance to those making public health and policy decisions.

Our research answers a fundamental question in influenza research: can H5-HA-possessing viruses support transmission in mammals? Moreover, our findings have suggested that different mechanisms (that is, receptor-binding specificity and HA stability) may act in concert for efficient transmissibility in mammals. This knowledge will facilitate the identification of additional mutations that affect viral transmissibility; the monitoring of this expanded set of changes in natural isolates may improve our ability to assess the pandemic potential of H5N1 viruses. Thus, although a pandemic H5N1 virus may not possess the amino acid changes identified in our study, the findings described here will advance our understanding of the mechanisms and evolutionary pathways that contribute to avian influenza virus transmission in mammals.

METHODS SUMMARY

Viruses. All recombinant viruses were generated by using reverse genetics essentially as described previously[16]. All experiments with the viruses possessing the wild-type HA cleavage site were performed in an enhanced biosafety level 3 (BSL3+) containment laboratory approved for such use by the CDC and the USDA.

Infection and transmission in ferrets. Six–ten-month-old female ferrets (Triple F Farms) were intramuscularly anaesthetized and intranasally inoculated with 10^6 p.f.u. (500 μl) of virus. On days 3 and 6 after infection, ferrets were killed for virological and pathological examinations. The virus titres in various organs were determined by use of plaque assays in MDCK cells.

For transmission studies in ferrets, animals were housed in adjacent transmission cages that prevented direct and indirect contact between animals but allowed spread of influenza virus through the air (Showa Science; Supplementary Fig. 7). Ferrets were intranasally inoculated with 10^6 p.f.u. (500 μl) of virus (inoculated ferrets). Twenty-four hours after infection, naive ferrets were each placed in a cage adjacent to an inoculated ferret (contact ferrets). To assess viral replication in the nasal turbinates, we determined viral titres in nasal washes collected from virus-inoculated and contact ferrets on day 1 after inoculation or co-housing, respectively, and then every other day. Animal studies were performed in accordance with Animal Care and Use Committee guidelines of the University of Wisconsin-Madison.

Biosafety and biosecurity. All recombinant DNA protocols were approved by the University of Wisconsin-Madison's Institutional Biosafety Committee after risk assessments were conducted by the Office of Biological Safety, and by the University of Tokyo's Subcommittee on Living Modified Organisms, and, when required, by the competent minister of Japan. In addition, the University of Wisconsin-Madison Biosecurity Task Force regularly reviews the research program and ongoing activities of the laboratory. The task force has a diverse skill set and provides support in the areas of biosafety, facilities, compliance, security and health. Members of the Biosecurity Task Force are in frequent contact with the principal investigator and laboratory personnel to provide oversight and assure biosecurity. Experiments with viruses possessing the wild-type HA cleavage site were performed in enhanced BSL3 containment laboratories approved for such use by the CDC and the USDA. Ferret transmission studies were conducted by three scientists with both DVM and PhD degrees who each had more than a minimum of 6 years of experience with highly pathogenic influenza viruses and animal studies with highly pathogenic viruses. Our staff wear powered air-purifying respirators that filter the air, and disposable coveralls; they shower out on exit from the facility. The containment facilities at University of Wisconsin-Madison were designed to exceed standards outlined in Biosafety in Microbiological and Biomedical Laboratories (5th edition; http://www.cdc.gov/biosafety/publications/bmbl5/BMBL.pdf). Features of the BSL3-enhanced suites include entry/exit through a shower change room, effluent decontamination, negative air-pressure laboratories, double-door autoclaves, double HEPA-filtered exhaust air, and gas decontamination ports. The BSL3-Agriculture suite features include all those listed for BSL3-enhanced plus HEPA-filtered supply and double-HEPA-filtered exhaust air, double-gasketed watertight and airtight seals, airtight dampers on all ductwork, and the structure was pressure-decay tested during commissioning. The University of Wisconsin-Madison facility has a dedicated alarm system that monitors all building controls and sends alarms (~500 possible alerts). Redundancies and emergency resources are built-in to the facility including two air handlers, two compressors, two filters each place filters are needed, two effluent sterilization tanks, two power feeds to the building, an emergency generator in case of a power failure and other physical containment measures in the facility that operate without power. Biosecurity monitoring of the facility is ongoing. All personnel undergo Select Agent security risk assessment by the United States Criminal Justice Information Services Division and complete rigorous biosafety, BSL3 and Select Agent training before participating in BSL3-level experiments. Refresher training is scheduled on a regular basis. The principal investigator participates in training sessions and emphasizes compliance to maintain safe operations and a responsible research environment. The laboratory occupational health plan is in compliance with the University of Wisconsin-Madison Occupational Health Program. Select agent virus inventory is checked monthly and submitted to the University of Wisconsin-Madison Research Compliance Specialist. Virus inventory is submitted 1–2 times per year to the file holder in the Select Agent branch of the CDC. The research program, procedures, occupational health plan, documentation, security and facilities are reviewed annually by the University of Wisconsin-Madison Responsible Official and at regular intervals by the CDC and the Animal and Plant Health Inspection Service (APHIS) as part of the University of Wisconsin-Madison Select Agent Program.

Full Methods and any associated references are available in the online version of the paper at www.nature.com/nature.

Received 18 August 2011; accepted 9 March 2012.
Published online 2 May 2012.

1. Glaser, L. *et al.* A single amino acid substitution in 1918 influenza virus hemagglutinin changes receptor binding specificity. *J. Virol.* **79,** 11533–11536 (2005).
2. Matrosovich, M. *et al.* Early alterations of the receptor-binding properties of H1, H2, and H3 avian influenza virus hemagglutinins after their introduction into mammals. *J. Virol.* **74,** 8502–8512 (2000).
3. Rogers, G. N. & Paulson, J. C. Receptor determinants of human and animal influenza virus isolates: differences in receptor specificity of the H3 hemagglutinin based on species of origin. *Virology* **127,** 361–373 (1983).
4. Auewarakul, P. *et al.* An avian influenza H5N1 virus that binds to a human-type receptor. *J. Virol.* **81,** 9950–9955 (2007).
5. Gambaryan, A. *et al.* Evolution of the receptor binding phenotype of influenza A (H5) viruses. *Virology* **344,** 432–438 (2006).
6. Stevens, J. *et al.* Recent avian H5N1 viruses exhibit increased propensity for acquiring human receptor specificity. *J. Mol. Biol.* **381,** 1382–1394 (2008).
7. Wang, W. *et al.* Glycosylation at 158N of the hemagglutinin protein and receptor binding specificity synergistically affect the antigenicity and immunogenicity of a live attenuated H5N1 A/Vietnam/1203/2004 vaccine virus in ferrets. *J. Virol.* **84,** 6570–6577 (2010).
8. Watanabe, Y. *et al.* Acquisition of human-type receptor binding specificity by new H5N1 influenza virus sublineages during their emergence in birds in Egypt. *PLoS Pathog.* **7,** e1002068 (2011).
9. Yamada, S. *et al.* Haemagglutinin mutations responsible for the binding of H5N1 influenza A viruses to human-type receptors. *Nature* **444,** 378–382 (2006).
10. Jackson, S. *et al.* Reassortment between avian H5N1 and human H3N2 influenza viruses in ferrets: a public health risk assessment. *J. Virol.* **83,** 8131–8140 (2009).
11. Maines, T. R. *et al.* Lack of transmission of H5N1 avian-human reassortant influenza viruses in a ferret model. *Proc. Natl Acad. Sci. USA* **103,** 12121–12126 (2006).
12. Maines, T. R. *et al.* Effect of receptor binding domain mutations on receptor binding and transmissibility of avian influenza H5N1 viruses. *Virology* **413,** 139–147 (2011).
13. Yen, H. L. *et al.* Inefficient transmission of H5N1 influenza viruses in a ferret contact model. *J. Virol.* **81,** 6890–6898 (2007).
14. Chen, L. M. *et al.* *In vitro* evolution of H5N1 avian influenza virus toward human-type receptor specificity. *Virology* **422,** 105–113 (2012).
15. Stevens, J. *et al.* Structure and receptor specificity of the hemagglutinin from an H5N1 influenza virus. *Science* **312,** 404–410 (2006).
16. Neumann, G. *et al.* Generation of influenza A viruses entirely from cloned cDNAs. *Proc. Natl Acad. Sci. USA* **96,** 9345–9350 (1999).
17. Hatakeyama, S. *et al.* Enhanced expression of an α2,6-linked sialic acid on MDCK cells improves isolation of human influenza viruses and evaluation of their sensitivity to a neuraminidase inhibitor. *J. Clin. Microbiol.* **43,** 4139–4146 (2005).
18. Shinya, K. *et al.* Avian flu: influenza virus receptors in the human airway. *Nature* **440,** 435–436 (2006).
19. Varki, A. Glycan-based interactions involving vertebrate sialic-acid-recognizing proteins. *Nature* **446,** 1023–1029 (2007).
20. Rogers, G. N. *et al.* Host-mediated selection of influenza virus receptor variants. Sialic acid-α2,6Gal-specific clones of A/duck/Ukraine/1/63 revert to sialic acid-α2,3Gal-specific wild type *in ovo*. *J. Biol. Chem.* **260,** 7362–7367 (1985).
21. Ha, Y., Stevens, D. J., Skehel, J. J. & Wiley, D. C. X-ray structures of H5 avian and H9 swine influenza virus hemagglutinins bound to avian and human receptor analogs. *Proc. Natl Acad. Sci. USA* **98,** 11181–11186 (2001).
22. Cline, T. D. *et al.* Increased pathogenicity of a reassortant 2009 pandemic H1N1 influenza virus containing an H5N1 hemagglutinin. *J. Virol.* **85,** 12262–12270 (2011).
23. Octaviani, C. P., Ozawa, M., Yamada, S., Goto, H. & Kawaoka, Y. High level of genetic compatibility between swine-origin H1N1 and highly pathogenic avian H5N1 influenza viruses. *J. Virol.* **84,** 10918–10922 (2010).
24. Li, H. *et al.* Isolation and characterization of H5N1 and H9N2 influenza viruses from pigs in China [in Chinese]. *Chin. J. Prev. Vet. Med.* **26,** 1–6 (2004).
25. Nidom, C. A. *et al.* Influenza A (H5N1) viruses from pigs, Indonesia. *Emerg. Infect. Dis.* **16,** 1515–1523 (2010).
26. Pasma, T. & Joseph, T. Pandemic (H1N1) 2009 infection in swine herds, Manitoba, Canada. *Emerg. Infect. Dis.* **16,** 706–708 (2010).
27. Pereda, A. *et al.* Pandemic (H1N1) 2009 outbreak on pig farm, Argentina. *Emerg. Infect. Dis.* **16,** 304–307 (2010).
28. Welsh, M. D. *et al.* Initial incursion of pandemic (H1N1) 2009 influenza A virus into European pigs. *Vet. Rec.* **166,** 642–645 (2010).
29. Xu, Q., Wang, W., Cheng, X., Zengel, J. & Jin, H. Influenza H1N1 A/Solomon Island/3/06 virus receptor binding specificity correlates with virus pathogenicity, antigenicity, and immunogenicity in ferrets. *J. Virol.* **84,** 4936–4945 (2010).
30. van Riel, D. *et al.* Human and avian influenza viruses target different cells in the lower respiratory tract of humans and other mammals. *Am. J. Pathol.* **171,** 1215–1223 (2007).
31. Gao, Y. *et al.* Identification of amino acids in HA and PB2 critical for the transmission of H5N1 avian influenza viruses in a mammalian host. *PLoS Pathog.* **5,** e1000709 (2009).
32. Itoh, Y. *et al.* *In vitro* and *in vivo* characterization of new swine-origin H1N1 influenza viruses. *Nature* **460,** 1021–1025 (2009).
33. Skehel, J. J. & Wiley, D. C. Receptor binding and membrane fusion in virus entry: the influenza hemagglutinin. *Annu. Rev. Biochem.* **69,** 531–569 (2000).
34. England, R. J., Homer, J. J., Knight, L. C. & Ell, S. R. Nasal pH measurement: a reliable and repeatable parameter. *Clin. Otolaryngol. Allied Sci.* **24,** 67–68 (1999).
35. Carr, C. M., Chaudhry, C. & Kim, P. S. Influenza hemagglutinin is spring-loaded by a metastable native conformation. *Proc. Natl Acad. Sci. USA* **94,** 14306–14313 (1997).
36. Haywood, A. M. & Boyer, B. P. Time and temperature dependence of influenza virus membrane fusion at neutral pH. *J. Gen. Virol.* **67,** 2813–2817 (1986).
37. Krenn, B. M. *et al.* Single HA2 mutation increases the infectivity and immunogenicity of a live attenuated H5N1 intranasal influenza vaccine candidate lacking NS1. *PLoS ONE* **6,** e18577 (2011).
38. Treanor, J. J., Campbell, J. D., Zangwill, K. M., Rowe, T. & Wolff, M. Safety and immunogenicity of an inactivated subvirion influenza A (H5N1) vaccine. *N. Engl. J. Med.* **354,** 1343–1351 (2006).
39. Bussey, K. A., Bousse, T. L., Desmet, E. A., Kim, B. & Takimoto, T. PB2 residue 271 plays a key role in enhanced polymerase activity of influenza A viruses in mammalian host cells. *J. Virol.* **84,** 4395–4406 (2010).
40. Hatta, M., Gao, P., Halfmann, P. & Kawaoka, Y. Molecular basis for high virulence of Hong Kong H5N1 influenza A viruses. *Science* **293,** 1840–1842 (2001).
41. Li, Z. *et al.* Molecular basis of replication of duck H5N1 influenza viruses in a mammalian mouse model. *J. Virol.* **79,** 12058–12064 (2005).
42. Mehle, A. & Doudna, J. A. Adaptive strategies of the influenza virus polymerase for replication in humans. *Proc. Natl Acad. Sci. USA* **106,** 21312–21316 (2009).
43. Yamada, S. *et al.* Biological and structural characterization of a host-adapting amino acid in influenza virus. *PLoS Pathog.* **6,** e1001034 (2010).
44. Salzberg, S. L. *et al.* Genome analysis linking recent European and African influenza (H5N1) viruses. *Emerg. Infect. Dis.* **13,** 713–718 (2007).
45. Subbarao, E. K., London, W. & Murphy, B. R. A single amino acid in the PB2 gene of influenza A virus is a determinant of host range. *J. Virol.* **67,** 1761–1764 (1993).

Supplementary Information is linked to the online version of the paper at www.nature.com/nature.

Acknowledgements The authors would like to acknowledge D. Holtzman for his contributions to the initial concept for this project and thoughtful scientific discussions. We thank M. McGregor, R. Moritz, L. Burley, K. Moore, A. Luka, J. Bettridge, N. Fujimoto and M. Ito for technical support, S. Watson for editing the manuscript, and the National Institute of Hygiene and Epidemiology, Hanoi, Vietnam for the A/Vietnam/1203/2004 (H5N1) virus, which was obtained from the CDC. This work was supported by the Bill & Melinda Gates Foundation (Grants 48339 and OPPGH5383), by a Grant-in-Aid for Specially Promoted Research from the Ministry of Education, Culture, Sports, Science, and Technology of Japan, by ERATO (Japan Science and Technology Agency), and by the National Institute of Allergy and Infectious Diseases Public Health Service Research grants. The following reagents were obtained from the NIH Biodefense and Emerging Infections Research Resources Repository, NIAID, NIH: polyclonal anti-monovalent influenza subvirion vaccine rgA/Vietnam/1203/2004 (H5N1), (antiserum, Human), high tire pool, NR-4109 and low titre pool, NR-4110.

Author Contributions M.I., T.W., M.H., S.C.D., M.O., K.S., G.Z., A.H., H.K., S.W., C.L., S.Y., M.K., Y.S., E.A.M., G.N. and Y.K. designed the experiments; M.I., T.W., M.H., S.C.D., M.O., K.S., G.Z., A.H., H.K., S.W., C.L., S.Y. and M.K. performed the experiments; M.I., T.W., M.H., S.C.D., M.O., K.S., G.Z., A.H., H.K., S.W., C.L., E.K., S.Y., M.K., Y.S., E.A.M., G.N. and Y.K. analysed the data; M.I., T.W., M.H., S.C.D., K.S., E.A.M., G.N. and Y.K. wrote the manuscript; M.I., T.W. and M.H. contributed equally to this work.

Author Information Reprints and permissions information is available at www.nature.com/reprints. This paper is distributed under the terms of the Creative Commons Attribution-Non-Commercial-Share Alike licence, and is freely available to all readers at www.nature.com/nature. The authors declare competing financial interests: details accompany the full-text HTML version of the paper at www.nature.com/nature. Readers are welcome to comment on the online version of this article at www.nature.com/nature. Correspondence and requests for materials should be addressed to Y.K. (kawaokay@svm.vetmed.wisc.edu).

COLUMN A passion for science can have some undesirable consequences **p.431**

CAREERS BLOG News and discussion on research jobs **go.nature.com/z8g4a7**

NATUREJOBS For the latest career listings and advice **www.naturejobs.com**

S. YAKOV/SHUTTERSTOCK

LIFE SCIENCES

All jazzed up

Bioscience is thriving in New Orleans as the city bounces back from multiple disasters.

BY AMANDA MASCARELLI

In New Orleans, Louisiana, in 2009, three men hatched a plan to start a business. One man, Mark Heiman, was then a chief scientific officer at pharmaceutical company Eli Lilly, based in Indianapolis, Indiana; another, Dale Pfost, was a serial biotechnology entrepreneur; and the third, John Elstrott, was a professor of entrepreneurship at Tulane University in New Orleans and chair of Whole Foods Market, a natural-foods supermarket chain based in Austin, Texas. Their meeting led to the creation in 2010 of New Orleans biotechnology start-up NuMe Health, which develops food compounds that promote the growth of healthy microbes in the gut. The founders attribute the partnership's creation not only to the pooling of their respective strengths, but also, says Heiman, to "the magic" of New Orleans: the city's innovative spirit, already known to inspire greatness in food and music. Increasingly, bioscience researchers are trying to capture the same inspiration.

This bioscience renaissance is powered by a programme of investment by the state and federal governments and by the private sector, much of which was spurred by the effort to help the region to recover from the ravages of Hurricane Katrina in 2005. The area is also benefiting from research funds resulting from the Deepwater Horizon oil spill in 2010 (see 'Investment after the spill')."This part of the country has become very attractive to people who are very idealistic and want to make a difference," says Vijay John, a chemical engineer at Tulane. "A lot of risk-taking young people have moved in. There's a sense of commitment, of community."

BIOSCIENCE ON THE BAYOU

Not long ago, New Orleans and the surrounding area had virtually no start-up companies. But in the past few years, nearly 60 have sprung up, many in the biosciences sector, attracting the attention of big-time investors, out-of-state venture-capital funds and pharmaceutical companies. Although the city is certainly not yet an established biotechnology hub, onlookers see the potential for significant growth.

"I'm beginning to see a critical mass of these elements of an entrepreneurial environment come together," says Tom Dickerson, adviser to Louisiana Fund I, a US$26-million health-care venture-capital fund based in Baton Rouge. The region offers a cost of living that is below the US average, as well as robust tax incentives for investors and start-ups and a strong pool of talent from research and educational institutions.

Although start-ups often rely on just a handful of employees, the smattering of new businesses is already creating opportunities for research jobs and internships at all levels, from undergraduates to junior and senior researchers. The biotechnology boom is also offering scientists a chance to see their ▶

▶ work commercialized, says Dickerson, noting that technology-transfer opportunities have become a tool for attracting top-quality researchers to universities.

The heart of the local biotechnology movement is BioDistrict New Orleans, a 6-square-kilometre state-supported economic-development area established in the business district in 2005. It draws together intellectual resources from the city's research institutions, including Tulane University, Xavier University of Louisiana, Louisiana State University (LSU) Health Sciences Center and Delgado Community College. One big project in the district is the Louisiana Cancer Research Center, a $102-million facility that has created 235 jobs — mostly in research — and drawn nearly $155 million in research grants. In 2011, officials also broke ground on the state's new teaching hospital, the University Medical Center, and construction has begun on the New Orleans Veterans Affairs Medical Center.

INCUBATING INNOVATION

Another key component of the BioDistrict is the 6,000-square-metre New Orleans BioInnovation Center, a non-profit life-sciences business incubator focused on university research and located on Canal Street near the French Quarter — close to the hub of New Orleans' economic activity, and to Tulane and the LSU Health Sciences Center.

The idea for the innovation centre took root in 2002, when Louisiana's governor was seeking ways to spur economic development, forge a 'knowledge economy' rather than relying on tourism, and revive an area full of empty hotels and office buildings. "Everyone was looking for ways to rejuvenate the area while at the same time providing this kind of resource to the universities," says Aaron Miscenich, who became president of the centre in 2004.

At the time, there was little local precedent for translating research into products. Miscenich didn't see much of a culture of entrepreneurship. "There was brilliant research being done in the city, but none was being brought to market," he says. "Historically, the technologies were either leaving the state or just sitting in filing cabinets." And before Katrina, there was little economic investment to support such ventures, he adds.

> *"As some of these ventures succeed, hopefully they can spool up into larger-scale operations serving a national and global market."*

When the hurricane hit, plans for the facility ground to a halt. "The level of uncertainty in our community was just staggering," says Miscenich. In late 2005 and early 2006, centre principals re-evaluated the business model, says Miscenich, and cut the projected size of the centre by half, but the state of Louisiana stepped in to provide $47 million in construction costs, and building went ahead. The BioInnovation Center opened in 2011 and the state currently supports most of the facility's annual operational costs.

The centre houses around 20 tenants, from biotechnology start-ups and a clinical-research organization (CRO) to intellectual-property attorneys and venture capitalists. Ultimately, it will provide space for up to 50 companies, which Miscenich hopes will draw well-established businesses and CROs to the city to create a wealth of research positions. "As some of these ventures succeed, hopefully they can spool up into larger-scale operations serving a national and global market," says Michael Bernstein, provost at Tulane. He is optimistic that companies will remain and generate more jobs.

THE SEEDS OF A HUB

Collaborations are already developing. NuMe Health is a tenant of the BioInnovation Center, and Heiman, who says the centre helps spur alliances, has built promising relationships with two companies in the building. "That led to a volley of brainstorming and an outline of potential new areas for our companies," he says. Heiman notes that Louisiana offers several incentives for start-ups, including an angel-investor tax credit and a 'phase zero' grant that funds companies to draw up proposals for higher-level funding; such schemes helped his company get off the ground, he says, and should draw other businesses.

Sudhir Sinha, a scientist turned entrepreneur, sold one biotechnology company in 2008 and was planning to retire when he learned about the opportunities at the BioInnovation Center. He rented space in the incubator to launch a new business, InnoGenomics, which specializes in techniques for extracting forensic information from trace amounts of degraded DNA samples found at crime scenes. He got the company under way with start-up capital, including a $150,000

ENVIRONMENTAL SCIENCE

Investment after the spill

Environmental researchers in New Orleans and the surrounding area are benefiting from the silver lining of a rather large cloud: an influx of research dollars after the Deepwater Horizon oil spill in the Gulf of Mexico in 2010.

BP, the operator of the well that spewed almost 5 million barrels of oil into the Gulf, pledged to provide US$500 million over ten years to support research related to the spill and its impacts on ecosystems. The company established the Gulf of Mexico Research Initiative (GoMRI), which so far has awarded eight grants to consortia made up of research institutions from around the region.

"With the federal and state budgets declining so drastically, it's one of the few sources of external research money right now," says Nancy Rabalais, director of the Louisiana Universities Marine Consortium based in Chauvin, which has received one of the grants. The disaster brought national attention to some of the Gulf region's pressing long-term problems, such as land loss and hypoxia in coastal waters. Ultimately, she says, this has produced a shift in conservation: from small-scale mitigation projects to whole-ecosystem restoration.

The Louisiana Universities Marine Consortium's GoMRI project focuses on assessing the effects of the spill on coastal ecosystems and will create 25–30 positions, says Rabalais. Graduate students, postdoctoral researchers and research assistants will study marsh degradation and the effects of the oil on organisms living in shallow waters near the continental shelf. The 12 institutions comprising the consortium will collectively receive $12 million, divided among all of them, over three years.

The demand for researchers is also growing in the private sector, says Ralph Portier, an environmental scientist at Louisiana State University (LSU) in Baton Rouge. LSU has just approved a PhD programme in environmental sciences, set to begin in autumn 2012, which will focus on research related to the oil spill. The university also offers a master's degree in environmental sciences, the "scientific equivalent of an MBA", says Portier: companies send policy specialists and other employees without research backgrounds to develop expertise in areas such as soils and coastal restoration. "Employees go back to their companies with the environmental training needed to function as environmental-scientist planners and managers," says Portier.

The region is a hotspot of pressing environmental issues, adds Portier, noting its constellation of ecological attributes — including the Mississippi River, wetlands and agricultural land — and development challenges resulting from industrialization of oil and gas resources in the Gulf. "There are lots of issues, lots of problems and lots of opportunities," he says. **A.M.**

grant from the US National Science Foundation, and received help in developing his commercialization plan from graduating MBA students and interns at the centre. In the past year, InnoGenomics has created five full-time lab-research positions; Sinha anticipates adding several more in the next 12–18 months, including jobs for undergraduates and postdocs in biochemistry and molecular biology.

Another tenant, energy-technology company ReactWell, has taken advantage of the centre's non-profit status, core laboratory facility and access to Tulane's office of technology transfer, says founder Brandon Iglesias. In April, Iglesias won $20,000 in start-up capital from the Tulane Business Plan Competition and the Domain Companies New Orleans Entrepreneur Challenge, to develop ways to use underground geothermal reactors to create synthetic crude oil from algal biomass. "It's quite scary to be in a start-up because the risk is pretty high," he says. "But I can't think of a more important issue to be working on than energy security." Iglesias says that New Orleans' location on the major waterway of the Mississippi River, close to the oil and gas industry and aquaculture in the Gulf of Mexico, gave him ready access to experts in his field.

The city still faces formidable challenges. More start-up capital is needed for new companies, and researchers at local universities aren't necessarily trained to meet businesses' needs.

"We have these institutions in place to help with training, but we just need to make sure that the programming they're providing matches the needs of the companies that we're putting together," says Miscenich. He adds that, for the city to succeed as a biohub, it must be able to retain talent. Louisiana must maintain its tax incentives and business infrastructure, and encourage an influx of established pharmaceutical firms and CROs to buoy the young companies and bring new jobs to the area.

"We need to come up with a business rationale to keep these companies in New Orleans," says Miscenich. "It's not just going to be the good food or the music; it's going to be because it makes economic sense to the company." ■

Amanda Mascarelli *is a freelance science writer based in Denver, Colorado.*

CLARIFICATION

In the Turning Point on Mayim Bialik (*Nature* **485**, 669; 2012) the quote about Stephen Hawking attributed to Kaley Cuoco was said by her character Penny during the show.

COLUMN

Piled too high

A passion for science is admirable, but can have unwanted outcomes, argues **Mariano A. Loza-Coll**.

An independent film about the pursuit of a science PhD became a hit last year — at least among the fledgling scientists that it represents. Thousands flocked to see *The PhD Movie*, based on the hugely popular comic strip *Piled Higher and Deeper* by Jorge Cham, a former mechanical engineer, at hundreds of on-campus screenings in several countries. Not bad for a film produced, directed and acted in by graduate students and researchers at the California Institute of Technology in Pasadena, and funded on a shoe-string budget.

Why the popularity? The film puts the plight of the PhD student on the big screen, giving student audiences a chance to laugh at themselves in recognition of the years of schooling, hard work and frustration that they are undertaking.

But I would argue that there is another reason: the film tackles some of the negative aspects of pursuing a PhD and a science career. At its climax, *The PhD Movie* raises a question that crosses many students' minds: why bother? The answer it provides resonates with the audience: "Everybody is here because they want to be here … You have to embrace the things you're passionate about."

Yet the passion that drives many scientists to investigate the natural and physical world can also get them into trouble. It compels them to push the boundaries of science, but not always with healthful long-term consequences.

Hard work and a stubborn can-do attitude are admirable and rewarding. We put hours, days and months into experiments that don't work, because we're passionate about the exhilarating moments when they do. But the trade-offs and downsides are many. The romantic ideal of the scientist as an independent academic investigator uncovering knowledge can convince some very smart people to accept mediocre pay and delays in starting a family, settling down, buying a house and planning for retirement — with no guarantees that these sacrifices are worthwhile. That is the drama so nicely portrayed in *The PhD Movie*.

The film could be seen as a warning, showing budding researchers that they need to be realistic about their career expectations. But I see it as much more. It is a wake-up call for scientists and non-scientists alike. After all, it is not scientists, but the rest of society that may suffer most if scientists end up burning out. To ensure that scientists can cure diseases, feed the hungry and prevent environmental catastrophes, we should select them on the basis of their intelligence, effectiveness and focus, not their personal sacrifices, obsession and stamina.

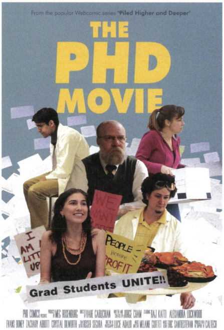
From the popular Webcomic series "Piled Higher and Deeper"
THE PHD MOVIE
I AM LITT UP
WE WANT
PEOPLE Before PROFIT
Grad Students UNITE!!
PHD COMICS MEG ROSENBURG VAHE GABUCHAN JORGE CHAM RAJ KATTI ALEXANDRA LOCKWOOD
EVANS BONEY ZACHARY ABBOTT CRYSTAL DILWORTH ROSER SEGURA LUCIE ABALO MELANIE CUTTET ERIC SANTIESTEVAN CALTECH

WWW.PHDCOMICS.COM

Why, then, isn't society at large demanding changes? I suspect that most people just don't know or understand what it takes to advance as a scientist. In the interests of science outreach, *The PhD Movie* and similar films should be distributed more widely to society at large (it can be viewed for a small fee at www.phdmovie.com).

We can use such films to start a conversation about how to nurture the practitioners and purveyors of science. With a good dose of sarcasm, *The PhD Movie* shows how graduate students spend much of their day second-guessing why they would spend another minute doing science. Another film, the 2009 documentary *Naturally Obsessed* (www.naturallyobsessed.com), shows how capable, aspiring science graduate students become 'drop-outs' and 'sell-outs' for reasons that have nothing to do with intelligence and drive.

Scientists complain about how we are portrayed in popular culture. Maybe it is time to start sharing who we are, and what we do. ■

Mariano A. Loza-Coll *is a postdoc in genetics at the Salk Institute for Biological Studies in La Jolla, California.*

naturejobs

European Head Office, London naturejobs@nature.com
The Macmillan Building, 4 Crinan Street, London NI 9XW, UK
Tel: +44 (0) 20 7843 4961 Fax: +44 (0) 20 7843 4996

European Manager: Nils Moeller,+44 (0) 20 7843 4953	n.moeller@nature.com
Southwest UK/RoW: Emma Hare, +44 (0) 20 7843 4944	e.hare@nature.com
Northeast UK/Ireland: Matthew Ward, +44 (0) 20 7014 4059	m.ward@nature.com
France/Switzerland/Belgium: Julie Aramburu, +44 (0) 20 7843 4994	j.aramburu@nature.com
Scandinavia/Spain/Portugal/Italy: Megan Ball, +44 (0) 20 7843 4973	m.ball@nature.com
North Germany/The Netherlands/Eastern Europe: Kristin Doelling, +44 (0) 20 7843 4970	k.doelling@nature.com
South Germany/Austria: Maria Kubalova, +44 (0) 20 7014 4084	m.kubalova@nature.com
Natureevents: Matthew Clare, +44 (0) 20 7014 4015	m.clare@nature.com
Business Development Manager, Middle East: Jon Giuliani, +44 (0) 20 7843 4922	j.giuliani@nature.com

USA Head Office, New York naturejobs@us.nature.com
75 Varick Street, 9th Floor, New York, NY 10013-1917
Tel: +1 800 989 7718 Fax: +1 800 989 7103

US Sales Manager: Ken Finnegan, +1 212 726 9248	k.finnegan@us.nature.com

Japan Head Office, Tokyo
Chiyoda Building, 2-37 Ichigayatamachi, Shinjuku-ku, Tokyo 162-0843
Tel: +81 3 3267 8751, Fax: +81 3 3267 8746

Asia-Pacific Sales & Business Development Manager: Yuki Fujiwara, +81-3-3267-8765	y.fujiwara@natureasia.com
Business Development Manager, Greater China/Singapore: Gloria To, +852 2811 7191	g.to@natureasia.com

India
3a, 4th Floor, DLF Corporate Park, Gurgaon, 122 002, India

Advertisement Sales: Vikas Chawla, +91 1242881057	v.chawla@nature.com

---

Lund University invites applications for following position

Professor

in Physiology in particular Cardiovascular Physiology

Ref. no. PA 2012/137

Information see:
www.med.lu.se/medarbetare/
lediga_anstaellningar
Closing date 4 September 2012

LUND UNIVERSITY
Faculty of Medicine

W225701R

LSUHealthNewOrleans

HEALTH SCIENCES CENTER
School of Medicine
Department of Microbiology, Immunology & Parasitology

WILLIAM & SARAH JANE PELON ENDOWED CHAIR

LSU Health-New Orleans School of Medicine is initiating a search for an Endowed Faculty Chair in the Department of Microbiology, Immunology and Parasitology. Candidates will be considered for appointment as Professor on the tenure track, and should have a strong record of research accomplishment, lead an active, nationally funded research program, and have a commitment to developing collaborative translational research programs involving multiple investigators. The ideal candidate will have a Ph.D. and/or M.D degree, demonstrated team-building ability, and a strong track record of developing translational research from basic scientific observations. Expertise in all areas of host/pathogen interaction will be considered, but special consideration will be given to those complementing existing core departmental strengths in HIV, HIV-related infections, and sexually transmitted diseases. LSU Health-NO School of Medicine offers a highly interactive and collegial environment, with a strong history of collaborative research programs and state-of-the-art infrastructure, including core laboratories in genomics, proteomics, imaging, and flow cytometry. Excellent opportunities exist for interaction with clinical departments, and with research Centers of Excellence in Vaccine Development, Cancer, Alcohol and Drug Abuse, Cardiovascular Biology, and Neuroscience. Anticipated duties and responsibilities will include sustaining an exceptional research program, mentoring of graduate students and postdoctoral fellows, and participation in departmental and school graduate and undergraduate teaching programs. The institution offers competitive start-up packages and salaries. Qualified investigators interested in learning more about the position should email Dr. Alistair Ramsay in the MIP Department (aramsa@lsuhsc.edu). Applicants should send their curriculum vitae that includes a full list of publications, previous and current research funding, teaching experience, a statement of research plans, and the names of three references to: keigen@lsuhsc.edu

LSU Health-NO is an EEO/AA Employer. Reference # 82 41017 033

NW225726R

The University of Edinburgh

The University of Edinburgh is an exciting, vibrant, research led academic community offering opportunities to work with leading international academics whose visions are shaping tomorrow's world.

Lectureship in Terrestrial Vegetation Ecology

£37,012- £44,166

Applications are invited for a Lectureship in the area of Terrestrial Vegetation Ecology. You will be expected to develop an outstanding programme of research relevant to ecological and environmental science questions, founded on the observation and analysis of processes and the interpretation of data related to terrestrial vegetation ecology, likely making use of advanced statistical tools. Example areas of application might include the analysis of trophic networks, material and energy flows, plant-herbivore and plant-soil interactions, or impacts of climate change on plant community distribution. This research programme will be of international standing and should lead to significant impacts within the particular field of speciality. You will also be expected to lead delivery of undergraduate courses in Ecological and Environmental Sciences and in related ecological undergraduate courses in Geography, and may contribute to the delivery of postgraduate Masters Programmes (e.g., Ecosystem Services).

This is an open-ended post from 01 October 2012.

Apply online, view further details or browse more jobs at our website. Alternatively, telephone the recruitment line on 0131 650 2511. Ref: 3015845N. Closing date 25 July 2012.

Committed to Equality and Diversity

The University of Edinburgh is a charitable body, registered in Scotland, with registration number SC005336.

www.jobs.ed.ac.uk

U225758RL

WATCH THIS AD COME TO LIFE IN YOUR HANDS

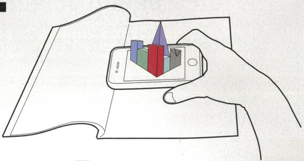

Download the Kaust AR App and experience this interactive ad in 3D!

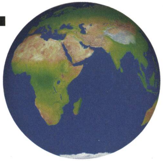

What you will discover:

The King Abdullah University of Science and Technology (KAUST) is an international, graduate level, Research University located on the Red Sea. We have used augmented reality technology to create a 3D interactive experience of the KAUST campus (newly opened in September 2009). Come and discover the research departments at KAUST and our current job vacancies available through **naturejobs.com**.

How to interact with this ad:

Download your '**Kaust AR App**' from your App Store, Google Play or visit **bit.ly/kaust-app**. After launching the application, simply point your camera at this ad (hold your camera 12-24 inches away from this page) and the globe will spin to life, opening up to reveal the KAUST campus. The KAUST Augmented Reality Application was developed in association with *Naturejobs* and Inition.

naturejobs.com

جامعة الملك عبدالله للعلوم والتقنية
King Abdullah University of Science and Technology

INITION
Everything in 3D

nature publishing group npg

Download the Kaust AR App from bit.ly/kaust-app

Available on the App Store

ANDROID APP ON Google play

Android is a trademark of Google Inc.

RW225621R

Professor and Senior Lecturer/Associate Professor

in Infectious Medicine

Linköping University is one of Sweden's six large universities, currently enrolling 27,300 students. The Faculty of Health Sciences runs the most highly rated MD program in Sweden, as well as a number of other strong educational programs in Health Care and Life Sciences; it trains a large number of health care professionals and researchers, typically graduating 140 MDs and 50 PhDs annually, and has strong research within several areas of the medical sciences. The Department of Clinical and Experimental Medicine has 400 employees, and hosts several strategic research centers, i.e., infectious disease, neuromedicine and regenerative medicine. The department is seeking two new faculty members; one Professor and one Senior Lecturer/Associate Professor in Infectious Medicine (encompassing medical microbiology, clinical microbiology and virology, and infectious diseases). The positions focus on research and teaching, and the successful applicant is expected to establish an independent research group conducting research within infectious medicine. The positions can be combined with clinical positions in clinical microbiology or infectious diseases.

For more details regarding the position and to submit an application please go to: http://www.liu.se/en/job/. For more details regarding the University, the Faculty of Health Sciences and the region, please visit: http://www.hu.liu.se, http://www.liu.se

LINKÖPINGS UNIVERSITET

Linköping University
expanding reality

Dnr LiU-2012-00732, LiU-2012-00733

W225722R

---

nature

Ecology and Evolution Editor

Nature the international weekly journal of science, seeks to appoint a Locum Ecology and Evolution Editor to join a team dedicated to publishing the world's best original research in the biological sciences.

This position is a locum position covering a Paternity leave for a 6-7 month period starting in December 2012.

The successful candidate will play a key role in determining how biological sciences are represented - through the selection and preparation of manuscripts for publication and by acting as *Nature*'s interface with the relevant research communities. These are demanding and intellectually stimulating positions, and call for a keen interest in the practice and communication of science.

The ideal candidate will have a strong track record of research in ecology and evolution and ideally theoretical biology, but highly qualified candidates from other areas of the biological sciences are also encouraged to apply. Applicants should hold or expect shortly to receive a PhD or equivalent degree.

This position is preferably based in *Nature*'s London office but positions in US offices may also be considered.

Please apply by sending your CV, covering letter (including your class of degree, a brief account of your research and other relevant experience, and details of your current salary) and a concise discussion of recent scientific developments which you have found particularly exciting (stating why).

Please upload your application to job http://jobs.macmillan.com/ - ref. **NPG/062/12**.

nature publishing group npg

IN225428R

IIF cnic

International Incoming Fellowships for Young Group Leaders

Opportunities for YOUNG GROUP LEADERS in Biomedical Research at the Spanish National Centre for Cardiovascular Research CNIC, Madrid - Spain

The CNIC is dedicated to excellence in cardiovascular research and to translating new knowledge into real improvements in clinical practice.

The scientific project of the centre has been structured in three areas:

- Cardiovascular Development and Repair Department (CDR)
- Vascular Biology and Inflammation Department (VBI)
- Epidemiology, Atherothrombosis and Imaging Department (EAI)

To be eligible, candidates must:

- Hold a PhD/ MD degree
- Demonstrate a minimum of three years' postdoctoral/post MD experience in centres of international reference
- Candidates must not have resided or carried out their main activity in Spain for more than twelve months in the last three years

The CNIC can offer you:

- A 3-year contract
- An internationally competitive salary
- Contribution to research and training
- State of the art infrastructure and latest generation of technological equipment
- Scientific-technical support and complementary training

Deadline for submission of proposals: 20 July 2012.

CNIC is an inclusive, equal opportunity employer, irrespective of nationality, ethnic origin, gender, marital or parental status, sexual orientation, creed, disability, age or political belief. Confidentiality is guaranteed throughout the selection process and all current regulations relating to the protection of personal data will be strictly adhered to.

For further information and applications, please visit www.cnic.es

MINISTERIO DE ECONOMÍA Y COMPETITIVIDAD Fundaciónprocnic cnic MARIE CURIE ACTIONS

W225650R

Cluster of Excellence

EXZELLENZCLUSTER
CellNetworks

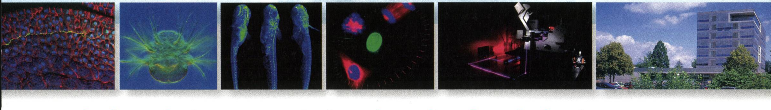

From molecular mechanisms to a quantitative understanding of complex functions

Within the **German excellence initiative**, the cluster *CellNetworks* has the central aim to define behavior and dynamic alterations of complex intra- and intercellular networks and to develop a systemic understanding of their regulation and interplay. This will depend on a closely interactive collaboration between scientists from different disciplines and requires methodological and technological advances. Ultimately, an integrated view should be generated which is detailed enough to allow mathematical modeling and simulation of biological processes. Please visit www.cellnetworks.uni-hd.de

Within *CellNetworks*, we offer **5 junior groups** as outlined below. Junior group leaders will receive an attractive package, support for 5 years and a prolongation option for a start-up professorship of up to six years. *CellNetworks* places particular emphasis on recruiting female scientists for group leader positions and applications from female scientists will be preferentially considered. Under German Law disabled applicants with full qualifications are to be preferred. All junior groups are invited to become *CellNetworks* members. Membership entails participation in our intramural funding programs and access to our numerous core facilities.

Junior Group in Regulated Protein Turnover

This group will be based at the Center for Molecular Biology of the University of Heidelberg (ZMBH) and is expected to work on mechanisms and cellular roles of regulated protein degradation. Among the main fields of interest are the ubiquitin-proteasome system and autophagy. The successful candidate should have an internationally visible track record of research and submit a cutting edge research proposal. The group will be integrated into the departmental structure of the ZMBH with full access to all facilities and is expected to interact with other groups on campus working on protein biochemistry. The ZMBH maintains a strategic Alliance with the cell and tumor biology program of the German Cancer Research Center (DKFZ). For more information about the ZMBH, please visit *www.zmbh.uni-heidelberg.de*

Junior Group in Chemical Biology

The group will be based at the Heidelberg University Biochemistry Center (BZH; www.uni-heidelberg.de/zentral/bzh). Applicants are expected to have a strong background in chemical biology and a research interest in gene regulation, RNA metabolism or membrane biology. The group will be integrated into the departmental structure of BZH and have access to all facilities. It will be associated with the Collaborative Research Center (SFB) 638: Dynamics of macromolecular complexes in biosynthetic transport or the Collaborative Research Center (TR) 83: Molecular Architecture and Cellular Functions of Lipid/Protein-Assemblies.

Junior Group in Quantitative Cell-Matrix-Interaction

This group will be established in close cooperation with the Institute for Physical Chemistry at the University of Heidelberg and the Max Planck Institute for Intelligent Systems, Department New Materials and Biosystems. Applicants should work on important biological and medical research questions investigated by quantitative methods and have an excellent track record on quantitative analysis of spatially and temporally resolved cell-matrix interactions. Special interest should be on technologies such as microfluidics, microscopy, spatial patterning of ligands, and its application towards single cells and collective phenomena within cell networks. The group will be fully integrated into the Physical Chemistry Institute and the MPI for Intelligent Systems. Please visit *www.is.mpg.de/de/spatz* and *www.uni-heidelberg.de/fakultaeten/chemgeo/pci/*

Junior Group on Stem Cells, Development, Metabolism and Organismal Environment

This group will be established at the Centre for Organismal Studies Heidelberg (COS; www.cos.uni-heidelberg.de) and work on a research topic linking the control of metabolism to stem cells, development and organismal environment. With this research topic they will ideally integrate with the COS departments as well as foster close interactions with research groups working on related topics on Heidelberg Campus, EMBL and KIT. The applicant should have a strong background in developmental biology and/or metabolism and a research interest in the mechanistic level of the interplay of organism function and the environment. The group will be fully integrated into the infrastructure and have access to all core facilities and equipment of COS Heidelberg including metabolomics, microscopy, new generation sequencing, and high throughput technologies. In addition, there is the possibility to join collaborative research activities on stem cell research (SFB 873) and planned activities on organism-environment interactions.

Junior Group on Cellular Networks in Viral Infection

This group will be established in the Department of Infectious Diseases and closely collaborate with other groups in the Virology and Molecular Virology units at the University. Applicants should work on an important human pathogen and have an excellent track record. Among the main fields of interest are quantitative real-time analysis of pathogen replication, pathogen-induced alterations of cellular networks and host immune responses, and analyses of assemblies using high resolution light and cryo-electron microscopy as well as systems biology approaches. The group will be fully integrated into the Department of Infectious Diseases and the newly developing Centre for Integrative Infectious Disease Research. It will have access to the entire infrastructure including P3-containment facilities as well as core facilities for microscopy and high throughput technologies. Translational research aspects can be pursued through the recently established German Centre for Infection Research (DZIF), where Heidelberg is a partner site. *Please visit us at www.klinikum.uni-heidelberg.de/Kraeusslich.6551.0.html*

Applications for junior group leader positions (referring to the specific position) including the usual documents and a proposal for a cutting edge research program should be sent no later than **23 July 2012 to**

Prof. Hans-Georg Kräusslich
CellNetworks Coordinator
Im Neuenheimer Feld 267
69120 Heidelberg, Germany
or to: cellnetworks@bioquant.uni-heidelberg.de

UNIVERSITÄT
HEIDELBERG
ZUKUNFT
SEIT 1386

W225776R

Imperial College London

Faculty of Natural Sciences
Department of Life Sciences
Division of Ecology and Evolution

3 Academic Positions in Ecology and Evolution

Lecturer salary: £43,350 - £48,400 p.a.
Reader minimum starting salary: £53,450 p.a.
Chair minimum starting salary: £68,170 p.a.

The Division of Ecology and Evolution is looking to make 3 academic appointments in the broad areas of Ecology & Evolution. The posts will be based at the Silwood Park Campus. We anticipate that most appointments will be at Lecturer level. However, there is potential for appointments to be made at more senior academic levels, and welcome applications from more senior researchers. The goal is to improve fundamental scientific understanding of biological and ecological processes and systems. The research will focus on solving ecological, evolutionary and environmental challenges and could fit into a range of disciplines, from ecology, evolution, genomics, conservation science or environmental biology, and focus on microbes, plants, animals or whole ecosystems.

For an informal discussion about the posts please contact Professor Austin Burt, Head of Division, (a.burt@imperial.ac.uk).

Our preferred method of application is online via our website http://www3.imperial.ac.uk/employment (please select "Job Search" then enter the job title or vacancy reference number including spaces – **NS 2012 126 JT** into "Keywords"). Please complete and upload an application form as directed.

Alternatively, if you are unable to apply online, please contact Mrs Diana Anderson by e-mail: d.anderson@imperial.ac.uk to request an application form.

POSITIVE ABOUT DISABLED PEOPLE

Closing date: 18 July 2012.

Stonewall
DIVERSITY CHAMPION

Committed to equality and valuing diversity. We are also an Athena Bronze SWAN Award winner, a Stonewall Diversity Champion and a Two Ticks Employer.

U225755R

---

www.cardiff.ac.uk/jobs

CARDIFF UNIVERSITY
PRIFYSGOL CAERDYDD

Two Faculty Positions in Astrophysics

School of Physics and Astronomy

The School of Physics and Astronomy at Cardiff University has immediate vacancies for two permanent faculty appointments in Astrophysics. We are seeking experts in observational and theoretical studies of star-formation and/or extra-solar planetary systems to conduct world-class research and research-led teaching at undergraduate and postgraduate level. The appointments will be at any level from Lecturer to Professor depending on the experience of the candidate; we expect at least one of the appointments to be at a junior level.

Physics and Astronomy at Cardiff University has undergone substantial expansion in the past few years and has very strong research groups in gravitational-wave physics, astronomical instrumentation, extragalactic astronomy and cosmology, star-formation and condensed matter physics. There are presently 18 academic staff involved in astrophysics and relativity, with 15 post-doctoral researchers and 22 PhD students.

The appointment will be made at a level commensurate with experience.

Salary:
Lecturer: £30122 - £35938 per annum
Senior Lecturer: £38140 - £44166 per annum
Reader: £45486 - £52706 per annum
Chair: A point on the professorial salary scale

Informal enquiries can be made to the Head of School, Professor Walter Gear, via email Walter.gear@astro.cardiff.ac.uk or alternatively contact Cardiff University, School of Physics and Astronomy,The Parade, Cardiff CF24 3AA. Tel: +44 (0)29 2087 5526 or visit htttp://www.astro.cardiff.ac.uk/research/starformation.

To work for an employer that values and promotes equality of opportunity, please visit www.cardiff.ac.uk/jobs and search for vacancy number 135BR.

Closing date: 14 July 2012.

U225759R

---

naturejobs

Need help with your career?
Ask the Expert on **naturejobs.com**

- **Browse past Q&A**
- **Get professional advice**
- **Email your questions**

Ask the Expert is located in the **Career Toolkit** section of **naturejobs.com**

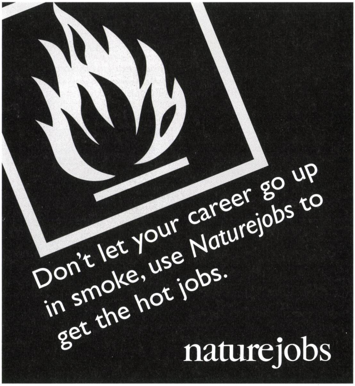
Don't let your career go up in smoke, use Naturejobs to get the hot jobs.
naturejobs

Universität
Konstanz

The University of Konstanz belongs to the universities in Germany whose “Future concepts for top-class research at universities” is promoted within the framework of the Excellence Initiative of the German federal and state governments.

Konstanz Research School Chemical Biology:

Research and Graduate Training at the Interface of Chemistry and Biology

The Konstanz Research School Chemical Biology *(KoRS-CB)* is an interdisciplinary initiative of the Departments of Biology, Chemistry, and Computer & Information Science at the University of Konstanz and is supported by the German Excellence Initiative.

KoRS-CB guides talented graduate students to scientific excellence. The research projects are dedicated to the following research areas: Synthetic Chemistry, Cellular Biochemistry, Biophysics, Biomedicine, and Computational Life Science.

The individually tailored training programme – fully in English language – and the intensive supervision by an interdisciplinary thesis committee are the basic elements for the excellent educational standards of the graduate school.

KoRS-CB will accept new fellows in **October 2012**. Thus, *KoRS-CB* is offering

Fellowships for Ph.D. Students

to highly motivated and enthusiastic students with a keen interest in interdisciplinary research and with an excellent degree (Master or Diploma) in Biology, Chemistry, Computational Life Science, or related areas.

The research projects and the application procedure are specified on our website: http://www.chembiol.uni-konstanz.de/application-procedure.html .

Please send your application under the reference number 2012/099 to the *KoRS-CB* office in one single pdf file via e-mail: chembiol@uni-konstanz.de **by 1 August 2012**.

ChemicalBiology
University of Konstanz

Contact: Dr. Heike Brandstädter, GM
e-mail: chembiol@uni-konstanz.de
phone: +49(0)7531/88-2237

Detailed information on the research and training programme is provided on our homepage: http://www.chembiol.uni-konstanz.de

W225769R

Universität
Konstanz

The University of Konstanz belongs to the universities in Germany whose “Future concepts for top-class research at universities” is promoted within the framework of the Excellence Initiative of the German federal and state governments.

The *Zukunftskolleg* of the University of Konstanz is offering:

A. up to fifteen ZIF Marie Curie 2-year Postdoctoral Fellowships in any discipline represented at the University of Konstanz (Salary Scale 13 TV-L)

for researchers in the early stage of their career, so as to enable them to develop and implement individual and independent research projects. Fellowships will begin on March 1, 2013, and end on February 28, 2015. **Reference number 2012/110**

B. up to eight ZIF Marie Curie 5-year Research Fellowships in any discipline represented at the University of Konstanz (Salary Scale 14 TV-L)

for the development and implementation of individual research projects. Fellowships will begin on March 1, 2013, and end on February 28, 2018. **Reference number 2012/111**

C. up to five 5-year Research Fellowships in any discipline represented at the University of Konstanz (Salary Scale 14 TV-L)

for the development and implementation of individual research projects. Fellowships will begin on March 1, 2013, and end on February 28, 2018. **Reference number 2012/109**

Applications should be submitted in English **before August 26, 2012, to zukunftskolleg@uni-konstanz.de with the respective reference number in the subject line of the e-mail.**

Zukunftskolleg
frei • kreativ • verbindend

Contact: Anda Lohan LLM
e-mail: **Anda.Lohan@uni-konstanz.de**
phone: +49 (0) 75 31/88-48 21

Detailed information is available on our website: http://www.zukunftskolleg.uni-konstanz.de

W225768R

UNIVERSITY OF PITTSBURGH
CENTER FOR ENERGY

R.K. Mellon Endowed Faculty Positions in Energy

As part of the University of Pittsburgh’s strategic expansion of its Center for Energy (*www.energy.pitt.edu*), the Swanson School of Engineering invites exceptional applicants for endowed faculty positions at all ranks in the following key research areas:

- **Energy delivery and reliability,** with an emphasis on electric power transmission and distribution systems, advanced power electronics technologies (FACTS and DC systems), power system modeling and analysis, power system operation and control, and renewable energy integration.
- **Materials for energy-related applications,** with an emphasis on experimental and/or computational efforts on structural and functional materials used in harsh service environments, and therefore including corrosion engineering, catalysts, energy storage, thermo-electrics and sensors.

These key areas also complement our existing and emerging research and education activities in *carbon management and utilization, unconventional gas resources,* and *direct energy conversion and recovery.*

Established as part of a recent $22 million gift from the Richard King Mellon Foundation, a total of four endowed faculty positions are available: two Professor-level appointments as *R.K. Mellon Chairs in Energy* and two Assistant/Associate Professor appointments as *R.K. Mellon Faculty Fellows in Energy.*

The successful candidates will greatly benefit from the resources fostered by the University of Pittsburgh’s extensive facilities, research partnerships, and close proximity to numerous energy-related companies and research laboratories. For instance, the Department of Energy’s National Energy Technology Laboratory (NETL) recently formed a Regional University Alliance (RUA) for energy technology innovation that is in partnership with the University of Pittsburgh and four other nationally recognized universities.

Interested candidates or candidate teams should apply with a **single pdf file** of the following: a cover letter; a full curriculum vita; statements describing teaching and research interests and plans; copies of three representative publications; and the names and contact information for at least three references. Questions and nominations should be addressed to **Prof. Brian Gleeson, Director of the Center for Energy at cfenergy@pitt.edu.**

For the R.K. Mellon Chair in Energy position, please apply at: RKMChairSearch@engr.pitt.edu

For the R.K. Mellon Faculty Fellow in Energy positions, please apply at: RKMFellowSearch@engr.pitt.edu

Screening begins immediately and will continue until the search is closed. The University of Pittsburgh is an Affirmative Action, Equal Opportunity Employer

NW225771R

United Nations
Educational, Scientific and
Cultural Organization

REGIONAL CENTRE FOR BIOTECHNOLOGY

an institution of education, training & research

(Established by the Dept of Biotechnology, Govt. of India under the auspices of UNESCO)

Adv. No. 5/2012

Leadership Position in Technology Platforms in Interdisciplinary Biomedical Research

Regional Centre for Biotechnology (RCB), an institution of education, training and research established by the Govt. of India under the auspices of UNESCO, is looking for dynamic, result-oriented and dedicated aspirants at leadership position at the Advanced Technology Platforms Centre, a major research resource of NCR Biotech Science Cluster of which RCB is a partner institution. Applications/nominations from/ for suitable candidates are invited for a position at the level of Scientist 'H'. The candidate should have Ph. D. in any area of Natural Sciences, Medicine or Engineering and an experience of at least 15 years as Principal Investigator in interdisciplinary biomedical research using diverse technology platforms including experience of guiding research at doctoral level in Universities/Institutions/Industrial Research Laboratories. Experience of establishing and managing any of the technology platforms for innovative research in interdisciplinary biomedical areas at the leading levels will be an added advantage. Curriculum vitae containing relevant details, list of publications and the names of three potential referees along with their electronic mail addresses may be sent to the Executive Director, Regional Centre for Biotechnology, 180, Udyog Vihar, Phase-I, Gurgaon- 122016, India with an advance copy to the e-mail address: **office@rcb.res.in** latest by August 15, 2012. Only the short-listed candidates will be contacted for further discussions. A detailed version of the advertisement can be found on the RCB website: **http://www.rcb.res.in** and **www.rcb.ac.in** .

RW225803R

8
Chemokines and
AACR-IASLC Joint
Noncoding RNAs
2 more...
9
Full Moon
10
11
12
Human Amyloid
13
14
15
16
The 1st IFReC-SIgN
Animal Minds: From
17
Fundamentals of
18
21
Seminar
Exhibition
Networking event
Space launches
International Observance
Training course
Public talk
Award Announcements
Publication date
Astronomical event
Workshop
Historical Date
Conference

DISCOVER SCIENCE EVENTS — SYNC YOUR CALENDAR TODAY.

CALENDAR VIEW NOW AVAILABLE AT NATUREEVENTS.COM

- It's easy to sync our events database with your online or mobile calendar
- Find important dates in the science calendar, not just conferences
- See events specially selected by Nature editors
- Match calendar events to your subject and location preferences

nature publishing group npg

NYU·poly

POLYTECHNIC INSTITUTE OF NYU

Director, Bioengineering Institute, New York University

New York University is creating an innovative Institute for Bioengineering that will cross multiple disciplines and schools of the university. It is intended to foster close collaboration particularly among the Polytechnic Institute (NYU-Poly), Courant Institute, Faculty of Arts and Science, Center for Neural Science, Colleges of Dentistry and Nursing, as well as the School of Medicine. The combined expertise and talent available in these units is already considerable. Part of the Institute's new activities will occur on the Campus of NYU-Poly in Brooklyn while the part particularly devoted to applied biomedical research and development will be housed in a new building under construction in Manhattan near the Medical School, cohabiting with the College of Dentistry and Nursing.

We are seeking applications and nominations for the Institute Director. The primary responsibilities of the Director are to provide leadership and vision for collaborative bioengineering research among these units, recruit qualified faculty, generate resources, establish interdisciplinary Masters and Ph.D. Programs, and interface with peer departments and institutes elsewhere. The faculty of the new Institute will have tenure and teaching responsibilities in one of the units of NYU but conduct research that is not constrained by disciplinary or geographic boundaries within NYU. We are particularly interested in an individual who embraces academic entrepreneurship and whose research supports NYU-Poly's core values of invention, innovation and entrepreneurship in an academic setting. World-class visibility in one or several of the bioengineering areas will be required. Some examples are implant and instrument design, therapeutic devices, biomedical imaging and diagnostics, biomaterials, biomedical simulation, modeling and data analysis, genomic engineering, and neuro-engineering, but this list is not exclusionary.

Applications for the position should consist of a CV, a list of publications, a history of grant support, a summary of entrepreneurial activities, and a statement of research and teaching interests. They should be sent electronically to Dir_Bioeng_Inst@poly.edu at the Provost's Office at NYU-Poly, with "Bioengineering Institute Director" in the subject line. Applications will be accepted until the position is filled, but those received prior to June 30, 2012 will be assured of consideration.

NYU and NYU-Poly are Equal Opportunity/Affirmative Action Employers. All candidates are encouraged to apply.

NW225613R

---

naturejobs

Scientists stay informed of the latest:

- Hot jobs
- Career news
- Announcements

Sign-up to our **FREE** jobseeker newsletter:
naturejobs.com/newsletter

UNIVERSITY *of* CALIFORNIA, SAN DIEGO
SCHOOL OF MEDICINE

Faculty Position in Nephrology-Hypertension and Pharmacology/Physiology

The Division of Nephrology-Hypertension in the Department of Medicine (http//med.ucsd.edu) at the University of California, San Diego is committed to academic excellence and diversity within the faculty, staff, and student body.

The Division is seeking an established investigator in kidney physiology/pharmacology who can lead a research and teaching program involving multiple faculty in the division and collaborative research across divisions at UCSD and the VA. The successful candidate should have strong basic research recognition with a track record of top-tier research publications; the research orientation should include studies of nephron function possibly by micropuncture techniques and a strong background in genetic approaches to examining kidney function using knockout animals and molecular biologic techniques.

The candidate should possess an M.D., Ph.D. or combined degrees and a record of experience and excellence in teaching at the level of preclinical curriculum and training of postdoctoral research fellows. A record of extramural funding is required and evidence of capacity to acquire funding from private pharmaceutical sources as well. Recognition amongst peers should be in evidence on an international level by a record of invited editorials, reviews and chapters in major texts and teaching vehicles. A record of successful collaborative research and leadership in research organization should also be obvious. Successful candidates will demonstrate strong or potential accomplishments in areas contributing to diversity, equity and inclusion, and a desire to play a leadership role in advancing UC San Diego's commitment to achieving excellence and diversity.

Salary is commensurate with qualifications and based on University of California pay scales.

Review of applications will begin August 15, 2012, and continue until the position is filled.

Interested individuals should send their CV, reference list and a statement summarizing their experience and professional contributions in the area of equity and diversity to:

Roland C. Blantz, M.D.
Chair, Search Committee (9111-H)
9500 Gilman Drive # 0505
La Jolla, CA 92093-0505
rblantz@ucsd.edu

UCSD is an Affirmative Action/Equal Opportunity Employer with a strong institutional commitment to excellence through diversity.

NW225690R

DANA-FARBER
CANCER INSTITUTE

Assistant Professor

The Dana-Farber Cancer Institute, Brigham and Women's Hospital and the Department of Medicine, Harvard Medical School, invite applications for a full-time appointment at the Assistant Professor level. This individual will develop an independent, disease-based laboratory research program focused on solid tumors housed in the Division of Molecular and Cellular Oncology and will interface with the relevant clinical research program within the Division of Solid Tumor Oncology. Candidates with an interest in squamous cell carcinomas are especially encouraged to apply. The candidate must have an MD and/or PhD and a proven track record of outstanding laboratory research.

The candidate will work principally at the Dana-Farber Cancer Institute, an NCI-designated Comprehensive Cancer Center, and at the Brigham and Women's Hospital. The academic appointment will be at the Assistant Professor level. Salary and benefits will be competitive.

Interested candidates must submit a curriculum vitae, a research plan and three letters of reference to: William Hahn, MD, PhD, Chief, Division of Molecular and Cellular Oncology, Dana-Farber Cancer Institute, 450 Brookline Avenue, Boston, MA 02215. Please send submissions via email to: MCO_SEARCH@DFCI.HARVARD.EDU.

HARVARD
MEDICAL SCHOOL

BRIGHAM AND
WOMEN'S HOSPITAL

Dana-Farber Cancer Institute/Brigham and Women's Hospital/Harvard Medical School are Equal Opportunity/Affirmative Action Employers actively committed to increasing the diversity of our faculty: people with disabilities, veterans, women and members of underrepresented minority groups are therefore strongly encouraged to apply.

NW225656R

Institut Pasteur

Director of the Institut Pasteur

The Search Committee invites expression of interest from potential candidates for the position of Director of the Institute.

Since its creation in 1887, the Institut Pasteur has been a world leader in basic biological and biomedical research as well as a renowned teaching center. The Institute is an independent, non-profit, private foundation with a commitment both to fundamental research in the life sciences and to the understanding and prevention of infectious diseases. In the context of biomedicine and public health, in addition to major discoveries in microbiology, virology, immunology and vaccines, it also has a major commitment to cross-disciplinary approaches, and has extended its focus to other biomedical fields. The Director will join an exciting and innovative academic environment on the campus, where more than 2500 people work, in central Paris.

The Director will provide the executive leadership and will develop an ambitious and strategic vision for the scientific activities of the Institut Pasteur. He/She will be responsible for the successful translation of basic science into improvement of human health, and will forge industrial partnerships and oversee the fundraising efforts of the Institute. The Director's responsibilities include catalysis of cooperative research between the 30 Institutes making up its outstanding international network.

The Search Committee encourages expression of interest from scientists of the highest international standing, with experience of scientific management and French language skills, irrespective of their nationality or their experience of working in France. Letters of interest should be sent to Professor Daniel Louvard, Chair of the Search Committee, c/o Lisa Riffaud, Institut Pasteur, 28 rue du Dr Roux, 75015 Paris or by e-mail to ipsc@pasteur.fr, before October 1st, 2012. The new director will be appointed in spring, 2013 to take up the position on the 1st October, 2013.

W225796R

UNIVERSITY OF
LIVERPOOL

Faculty of Health and Life Sciences
Institute of Integrative Biology

Postdoctoral Research Associate (Genomics/Bioinformatics)

£31,020 - £33,884 pa

You will join a BBSRC funded project to undertake the generation, analysis, interpretation and presentation of next-generation sequence data derived from transcriptome analysis in Arabidopsis and wheat. The project involves the Centre for Genomic Research, a leading laboratory for the application of genomic technologies and bioinformatic analyses. You should have a PhD in a biology related subject. The post is available for 3 years. **Job Ref: R-579868/N**

Institute of Ageing and Chronic Disease
Department of Eye and Vision Science

Postdoctoral Research Associate

£31,020 pa

This project, funded by the Leverhulme Trust, is to investigate saccadic eye movement control in large groups of participants drawn from different cultural groups in order to establish whether recently reported differences in saccades are due to cultural/environmental factors, or are culturally independent. It involves recording and analysing saccades using various eyetrackers, and analysis of large datasets. You should have a degree in Neuroscience, Psychology, Optometry, Orthoptics or a related discipline, with a relevant PhD. Previous experience of human visuomotor research, the use of visual stimulation, and particularly the use of eye tracking equipment, would be an advantage. The post is available until 31 August 2014. **Job Ref: R-579798/N**

Closing date for both posts: 20 July 2012

For full details, or to request an application pack, visit www.liv.ac.uk/working/job_vacancies/ or e-mail jobs@liv.ac.uk
Please quote job ref in all enquiries.

COMMITTED TO DIVERSITY AND EQUALITY OF OPPORTUNITY

Stonewall DIVERSITY CHAMPION

POSITIVE ABOUT DISABLED PEOPLE

U225754R

> "When trying to recruit good scientists for such a remote institutions like ours, in the Canary Is., the high visibility and wide-range exposure that Naturejobs provides has been crucial. I'm very happy to have international candidates who applied to our position from places ranging between St. Petersburg and Cincinnati. Thanks a lot!"

Eduardo Salido, MD, PhD,
Hospital Universitario de Canarias

naturejobs

a**nature**conference

Nature Immunology and HudsonAlpha Institute for Biotechnology present:

HudsonAlpha - Nature Conference on Immunogenomics

The first HudsonAlpha - Nature Conference on Immunogenomics will bring together four areas to shape this emerging field: scientists in genomics and genetics, immunology, bioinformatics and methodology, and clinical research. We expect our invited talks to cover a range of topics: large-scale immune sequencing projects of the repertoire of T- and B-cell diversity, and clinical implications; epigenetics and the immune system; developmental lineage of immune cells; genetic and environmental contributions to autoimmunity; drug development for autoimmune conditions; pharmacogenomics and the immune response; gene regulation and cell-type identity and high-resolution transcriptome analyses.

October 1-3, 2012
The Jackson Center, Huntsville, AL, USA

KEYNOTE SPEAKERS

Daniel Kastner (National Institute of Arthritis and Musculoskeletal and Skin Diseases, National Institutes of Health, USA)
Stephen Quake (Stanford University, USA)
Ugur Sahin (Translational Oncology at the University Medical Center of the Johannes Gutenberg University Mainz, Germany)

SPEAKERS

Christophe Benoist
S. Louis Bridges, Jr.
Christopher Glass
Jian Han
Robert Holt
John O'Shea
Robert Plenge
Harlan Robins
Ellen Rothenberg
Harinder Singh
Casey Weaver
Wenzhong Xiao

ORGANIZERS:

S. Louis Bridges, Jr (University of Alabama Birmingham, USA)
Laurie Dempsey (*Nature Immunology*, USA)
Chris Gunter (HudsonAlpha Institute for Biotechnology, USA)
Jian Han (HudsonAlpha Institute for Biotechnology / iCubate / iRepertoire, USA)
Robert Holt (Michael Smith Genome Sciences Centre, BC Cancer Agency, Canada)
Robert Plenge (Harvard Medical School / Brigham & Women's Hospital, USA)
Ellen Rothenberg (California Institute of Technology, USA)

Abstract submission deadline: July 13, 2012
Early registration deadline: August 3, 2012
For more information and to register visit:
www.nature.com/natureconferences/haig2012

nature immunology

HUDSONALPHA
INSTITUTE FOR BIOTECHNOLOGY

IN225038E

SPOTLIGHT ON GENETICS

The changing role of model organisms in genetics

Advances in sequencing technology are giving researchers access to a wide range of genomes, from microbes to mammals. What does the future hold for traditional models?

> *"The only people we'll go after are those who think at a systems-wide scale, rather than classically trained reductionists."*
>
> **Eric Schadt, Mount Sinai School of Medicine**

EVOLUTIONARY BIOLOGIST Thomas Hunt Morgan may have immortalized the role of *Drosophila melanogaster* in genetics research, but the fruitfly was not his first choice of experimental model. Seeking a short-lived organism that could be easily bred in the laboratory under changing conditions, he tried the mouse, rat, pigeon and even a plant louse before settling on *Drosophila*. A century after Morgan's seminal work on sex-linked inheritance, scientists still use the fruitfly to investigate and demonstrate basic genetic principles. But it is far from the only tool available to modern geneticists.

Techniques for sequencing genes and genomes have developed at ever-increasing rates, and the turn of the 21st century was dotted with announcements of successful genome-sequencing projects, from yeast in 1997 to the tomato in May this year (go.nature.com/Zpz7sB). "What you're seeing is a dramatic expansion in the number of organisms and strains you can study," says Eric Schadt, chair of the department of genetics and genomics sciences at Mount Sinai School of Medicine in New York. The ease with which sequencing technologies can be applied to all manner of species presents a potential conundrum for researchers: should they continue to work on the established models or start afresh with some of the myriad organisms now available?

Advances in sequencing technology could lead to a revolution in research on the fruitfly *Drosophila melanogaster*.

EYE OF SCIENCE/SCIENCE PHOTO LIBRARY

The Big Five

The well-established 'big five' model organisms for genetics research, as described by Michael Snyder, director of Stanford University Center for Genomics and Personalized Medicine, are yeast, mouse, the nematode *Caenorhabditis elegans*, thale cress (*Arabidopsis thaliana*) and *Drosophila*. Snyder says the number one reason for working with these standard models these days is the wealth of biological information available about them and innumerable proven experimental techniques. His lab tests virtually every technical process on yeast before applying it to other model organisms or humans. "You have this vast database that lets you make connections you wouldn't otherwise make, and discover things you wouldn't normally look for," he says. "That's hard to beat."

Stéphane Noselli, director of the Institute of Biology Valrose (iBV) in Nice, France, who works primarily on *Drosophila*, agrees: "You can answer so many difficult questions with this small organism, from gene function to cell biology and physiology. It's a complete system."

Researchers at contract research organization KeyGene, based in the Netherlands, use *Arabidopsis* to validate new techniques and technologies for crop breeding. "*Arabidopsis* provides us with an ideal test system because it has a small genome that has been sequenced to a high level of accuracy and isn't expensive to use," explains chief scientific officer Michiel van Eijk.

The quantity of genetic information available for these standard model systems is just one of their advantages. They are all relatively sturdy organisms, and — with the exception of the mouse, whose maintenance is more complicated — they are inexpensive and easy to grow in the lab.

Emerging models

While basic cellular or biological problems are more easily solved with standard organisms, established models have been less useful in other, more complex areas. A lack of suitable systems for modeling ageing, for example, has encouraged researchers to branch out. Anne Brunet, Snyder's colleague at Stanford University, works on the killifish *Nothobranchius furzeri*. These fish live in African ponds that regularly dry out, so they complete their life cycle in a couple of months – perfect for studying the ageing process. Eugene Berezikov, one of the first recruits to the European Research Institute for the Biology of Ageing, which opened at University Medical Center Groningen in the Netherlands in January this year, is developing genomic tools to analyse the flatworm *Macrostomum lignano*. The worm's regeneration capabilities make it an ideal ageing model, while its small size, physical transparency and simple culturing techniques mean it can

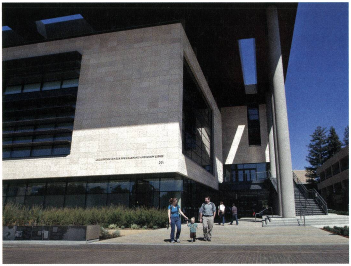

Stanford University, where all biology students take programming courses.

NORBERT VON DER GROEBEN/STANFORD SCHOOL OF MEDICINE

be easily handled in the lab.

The challenge of new models is that researchers start with little established biological knowledge. According to the NCBI's PubMed database there have only been 10 research papers published on *M. lignano*, and just eight on *N. furzeri*; a stark contrast to the figure of 15,477 for *D. melanogaster*. However, Brunet says the hard work that goes into developing a new model organism is worthwhile — as well as providing a valuable new experimental model to a range of scientific communities, it can also be an excellent career move. “Dario Valenzano, who was a graduate student when he jumpstarted the *N. furzeri* project, has set up the model entirely from scratch, developing the first linkage map and creating the first transgenic lines,” she says. “He's now likely to focus on this in his own lab.”

Advances in sequencing technologies could soon resolve the dearth of data for new models. The availability of cheaper, faster sequencers — Life Technologies now offer a bench-top model that can sequence a genome in a day at a cost of US$1,000 — has led to a plethora of ambitious projects that aim to reveal the genomes of everything from microbes to mammals over the coming years. In October 2011 a group of international researchers published the first findings from the 29 Mammals Project (go.nature.com/omuX3z), an initiative launched in 2005 to identify functional elements of the human genome by comparing it with those of other mammals. The project, led by the Broad Institute in the United States, has sequenced the genomes of 24 mammals, including the rhesus macaque, rat and cow, adding to the five pre-existing sequenced mammalian genomes (human, chimpanzee, mouse, dog and opposum). The Chinese genomics institute BGI, which operates a network of the world's biggest genome-sequencing centres, is involved in over 20 sequencing projects. It aims to sequence 10,000 microbial genomes, 1,000 plant and animal genomes and 10,000 vertebrate genomes, in collaboration with numerous institutions worldwide.

Researchers considering a move to a new model organism need to have a thorough understanding of its biology, says iBV's Noselli. “It involves a lot of investment,” he says. The developmental biology department at the Pasteur Institute in Paris, France, now uses *Drosophila*, chick, zebrafish and the emerging vertebrate model organism amphioxus, a fish-like marine animal also known as the lancelet, but this only came about after years of investment in a solid research base of mouse genetics.

In with the old

Although sequencing is opening up a vast array of research avenues, Schadt at Mount Sinai cautions that adapting existing technologies for novel organisms is going to be “a much longer road than we appreciate”. He argues that the best short-term use of new tools is to give geneticists a more sophisticated view of existing model organisms; in fact, he believes the field is heading for a revolution in *Drosophila* studies. He and his colleagues have just recruited additional staff to expand on promising work in a *Drosophila* lab at Mount Sinai. “It would be really difficult to develop it all from scratch in a new system,” he says. “It's hard to justify.”

Both Schadt and Guilio Superti-Furga, scientific director of the Center for Molecular Medicine (CeMM) in Vienna, Austria, predict that technological advances will encourage researchers to further study wild-type strains of existing mutant models, rather than moving straight into new systems. New mutations in established model organisms are also attracting interest. “Some groups are using genome-wide association studies to identify every potential disease risk gene, and making mouse models for each of them,” says Christine Van Broeckhoven, professor of molecular biology and genetics at Antwerp University and a director at life sciences research institute VIB in Belgium.

KeyGene's van Eijk adds that researchers will continue to revert to model organisms when faced with the unknown. “Once each technological barrier is broken, there are more questions,” he says. “It will always be the case that a limited number of model species stay ahead.”

Technically minded

As well as influencing which model genetic organisms will be used in the future, the vast quantities of data generated by collaborative genome-sequencing efforts is changing the field of genetics as a whole. Many leading departments are looking towards informatics-driven investigations and scientists are no longer being hired purely for their laboratory experience. Institutions list bioinformatic and statistical skills as key criteria when taking on new staff. “Investigators must be able to use all the new literature and databases,” says CeMM's Superti-Furga. “The next generation of researchers require much more computational skill.” Schadt agrees that geneticists need experience of a quantitative subject to be competitive in the field: “Ten years from now you'll be a dinosaur — extinct — if you don't”. Knowledge of systems biology is also an asset, he adds. “The only people we'll go after are those who think at a systems-wide scale, rather than classically trained reductionists.”

Many institutions have already embedded bioinformatics in their degree programmes. At Stanford University all biological sciences students now have to take programming classes, and the University of Washington set up an interdisciplinary computational molecular biology PhD more than a decade ago.

Robert Desnick, dean for genetics and genomic medicine at Mount Sinai, says computational genomics will be particularly important in research into human disease. Being trained in both computational genomics and biology is “going to pay off at every level of science,” he says.

Practical experience of sequencing is also advantageous. For example, the New York Genome Center (NYGC), an independent biomedical research start-up scheduled to begin operations in 2012, is currently “aggressively recruiting lab technicians with experience with Illumina HiSeq technology,” according to founding executive director Nancy Keller. The majority of the centre's initial 500 staff will be sequencing and bioinformatics professionals. NYGC's initial research focus will be human genomics, but it will also support the mouse genetics carried out at its founding institutions. “We expect that our focus and mission will evolve over time, and we are open to expanding in the future into other model organisms,” says Keller.

Stanford's Snyder says it is important to recognise the intrinsic value of traditional models in translational research as they can help accelerate the discovery of clinically relevant findings. “What we know about the cell cycle was pioneered in yeast; neurobiology, from flies and worms,” he says. “That background information can't be understated in terms of its value.”

So while there is certainly a place within the genetics field for research and development involving new model organisms, the traditional ones are by no means redundant. ■

Nature editorial staff have no responsibility for content

iit @SEMM
ISTITUTO ITALIANO
DI TECNOLOGIA

Center for Genomic Science of IIT@SEMM

The Center for Genomic Science of IIT@SEMM (http://genomics.iit.it) located in Milan, Italy, is an outstation of the Istituto Italiano di Tecnologia. The Center benefits from state-of-the art technological platforms including a high-throughput cell-based screening unit, next-generation DNA sequencing and others.

The following post-doctoral positions are available:

Pos. 1, 2 **Cancer Biology:** Genome, epigenome and transcriptome dynamics in mouse tumor models; forward and reverse genetic screens for modifiers of tumor progression. The projects will involve work with animal models and advanced molecular/cellular biology. PI: Stefano Campaner (Pos. 1), Bruno Amati (Pos. 2).

Pos. 3 **microRNA biology:** miRNA-mediated regulatory loops and gene expression mechanisms controlling stem cell self-renewal and fate specification in the mouse mammary gland. The project will involve isolation of mouse primary cells, FACS-based cell purification, organoid culture and transplantation. PI: Francesco Nicassio.

Pos. 4 **Drug Development:** Quantitative chemical proteomics applied to the identification of cellular proteins targeted by selected drugs. Collaborative project with the group of Dr. Tiziana Bonaldi at the European Institute of Oncology (IEO).

Pos. 5 **Computational Biology:** Development of pipelines for the automatic analysis and integration of different genome-wide datasets (RNA-seq, ChIP-seq, DNA methylation, long-range DNA interactions, mutational analysis); development of statistical and visualization tools. Familiarity with the Linux environment, programming skills (especially in R) will be advantageous; previous experience in genomics is not mandatory. PI: Bruno Amati, with computational supervision by Mattia Pelizzola and Marco Morelli.

Pos. 6 **Computational Biology:** Meta-analysis of somatic mutations in cancer with the goal of identifying driver mutations and specific mutation patterns. Proficiency in using JavaEE technology, mySQL databases, the Hibernate object relations management framework, statistics or grid computing will be advantageous. PI: Heiko Muller.

Pos. 7 **Computational Biology:** Analysis of imaging data from genome-wide siRNA screens; bioinformatic analysis of an ubiquitin-dependent signaling pathway. Proficiency with statistics, programming (R, C++ or Python), automated image analysis or analysis of large datasets will be advantageous. PI: Mark Wade

The positions will be subject to Post-doctoral contracts and require a PhD degree with or without post-doctoral experience. Candidates should be proficient with the relevant methods and technologies. Applications should be e-mailed to positions_semm@iit.it and should include a CV, the e-mail addresses of 3 referees and a short statement on professional skills and interests (1 page max). Candidates should indicate in the title to which of the above position(s) they are applying, and should ask three referees to send their reference letters directly to the same e-mail address. Selected candidates will be initially interviewed by Skype.

Application deadline: July 9, 2012

In order to comply with the Italian law (art. 23 of Privacy Law of the Italian Legislative Decree n. 196/03), we kindly ask every candidate to provide his/her consent to allow IIT to process his/her personal data. We inform you that the information you provided will be used solely for the purpose of assessing your professional profile to meet the requirements of Istituto Italiano di Tecnologia. Your data will be processed by Istituto Italiano di Tecnologia, with headquarters in Genoa, Via Morego, 30, acting as the Data Holder, using computer and paper based means, observing the rules on protection of personal data, including those relating to the security of data. Please also note that, pursuant to art. 7 of Legislative Decree 196/2003, you may exercise your rights at any time as a party concerned by contacting the Data Manager. The Italian Institute of Technology is an Equal Opportunity Employer that actively seeks diversity in the workforce.

W225598R

MSSM

MOUNT SINAI
SCHOOL OF
MEDICINE

A post-doctoral scientist position is available for translational research of genitourinary (GU) cancers in the Tisch Cancer Institute at Mount Sinai Medical Center. The qualified candidate will work with other members of the GU Cancer Research Program (http://www.mssm.edu/research/programs/genitourinary-cancer-research/about-us) to better understand the biology of the GU cancers in order to benefit the clinical management of the disease. Key projects will involve development and validation of immune gene signatures and biomarkers related to the prognosis and treatment of GU cancer.

The qualified candidate should have a Ph.D. in a related field, highly experienced with immunology, cell and molecular biology and biochemistry.

Experience with gene expression profiling, multiplex PCR is a plus. Effective written and verbal communication skills are required.

Strong work ethic, creativity, and enthusiasm required.

Candidate should send a CV, three letters of reference, and a summary of their research to Yixuan Gong, PhD to Yixuan.Gong@mssm.edu.

NW225653R

EGL
Charitable Foundation

The EGL Charitable Foundation
invites you to apply to the

Gruss Lipper Post-Doctoral Fellowship Program

Eligibility

- Israeli citizenship
- Candidates must have completed PhD and/or MD/PhD degrees in the Biomedical Sciences at an accredited Israeli University/Medical School or be in their final year of study
- Candidates must have been awarded a postdoctoral position in the U.S. host research institution.

Details regarding the fellowship are available at www.eglcf.org

NW224959R

ONE
PIECE OF DNA

Everyday, the people at Life Technologies work together to create breakthrough products that dramatically improve the lives of others.

Convicted in 1988 of a crime he did not commit, Herman Atkins spent more than 11 years in prison before the analysis of DNA evidence proved his innocence. The DNA analysis that set Herman free was made possible by the people at Life Technologies. We are more than 10,000 people dedicated to solving some of the most difficult biological challenges of the 21st century.

Join in to stand out.
Visit lifetechnologies.com/careers

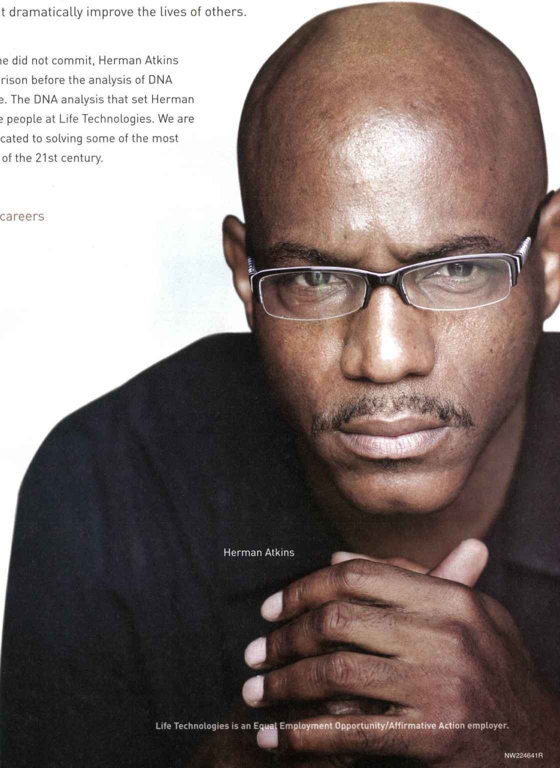

Herman Atkins

life technologies™

Life Technologies is an Equal Employment Opportunity/Affirmative Action employer.

NW224641R

Max Planck Institute for Plant Breeding Research

A new department of Comparative Development and Genetics at the Max Planck Institute for Plant Breeding Research (MPIPZ) is seeking a group leader in the area of:

Computational Modelling of Morphogenesis

The Department will operate under the direction of Honorary Professor Miltos Tsiantis and will investigate problems of plant development and evolution. The successful applicant will contribute to existing research projects and build independent research activity aimed at understanding plant morphogenesis and its diversity. The successful applicant will work with other research groups in the Department and will also participate in national and international Graduate Partner Programs and bids for external funding. Core funding is available to support activity of the group.

We are seeking a scientist with a PhD and an outstanding record of internationally competitive research accomplishments in computer science and its application in understanding morphogenesis, particularly through the use of geometric models. Experience with the effective and creative use of biological imaging data to support quantitative studies of development would be a strong advantage. A demonstrable ability to collaborate smoothly and synergistically in the context of interdisciplinary projects involving external collaborations is essential. Payment and benefits are according to the German TVöD. The position will initially be for five years. Exceptional candidates may be considered for a tenure track appointment pending review.

The Max Planck Institute aims to increase the proportion of women in so far underrepresented areas. Disabled applicants with equal qualifications will be given preferential treatment.

The Max Planck Institute for Plant Breeding Research (MPIZ) in Cologne (http://www.mpipz.mpg.de/2169/en) is one of the world's premier sites committed to basic research and training in plant science. The institute has four science departments, three independent research groups and specialist support, totaling 400 staff including externally funded positions.

Interested candidates are invited to send applications consisting of:

- a brief cover letter explaining their background and motivation for applying for this post,
- a statement of research plans (up to a page long),
- a full CV including the contact details three referees indicating the reference number by post to:

Max Planck Institute for Plant Breeding Research
Dept. of Developmental Genetics
Carl-von-Linné-Weg 10
D-50829 Cologne, Germany
e-mail: Christiane Wojtera, wojtera@mpipz.mpg.de

MAX-PLANCK-GESELLSCHAFT

Applications will be evaluated until a suitable candidate is identified.
For informal enquiries please contact miltos.tsiantis@plants.ox.ac.uk.

W225668R

Max Planck Institute for Plant Breeding Research

A new Department of Comparative Development and Genetics at the Max Planck Institute for Plant Breeding Research (MPIPZ) is seeking a group leader in the area of:

Bioinformatics

The Department will operate under the direction of Honorary Professor Dr. Miltos Tsiantis and will investigate problems of plant development and evolution. The successful applicant will contribute to existing research projects and build independent research activity in comparative plant biology using high throughput sequencing (HTS) datasets. S/he will be instrumental in building bioinformatics capability within the new department and will develop strong synergies with colleagues pursuing genetic and computational modeling approaches to study morphogenesis. S/he will participate in national and international Graduate Partner Programs and external funding bids.

We seek a candidate with a PhD and an outstanding record of internationally competitive research accomplishments in bioinformatics and the creative use of HTS datasets to shed new light on biological problems in genetics, development and evolution. Candidates must be highly interactive and willing and able to collaborate smoothly with both biologists and computational scientists. High-level expertise in gene expression analysis and regulatory genome annotation is of particular interest. Payment and benefits are according to the German TVöD. The position will be for five years in the first instance.

The Max Planck Institute aims to increase the proportion of women in so far underrepresented areas. Disabled applicants with equal qualifications will be given preferential treatment.

The Max Planck Institute for Plant Breeding Research (MPIPZ) in Cologne (http://www.mpipz.mpg.de/2169/en) is one of the world's premier sites committed to basic research and training in plant science. The institute has four science departments, three independent research groups and specialist support, totaling 400 staff including externally funded positions.

Interested candidates are invited to send applications consisting of:

- a brief cover letter explaining their background and motivation for applying for this post,
- a statement of research plans (up to a page long),
- a full CV including the contact details three referees indicating the reference number by mail by post or email to:

Max Planck Institute for Plant Breeding Research
Dept. of Developmental Genetics
Carl-von-Linné-Weg 10
D-50829 Cologne, Germany
e-mail: Christiane Wojtera, wojtera@mpipz.mpg.de

MAX-PLANCK-GESELLSCHAFT

Applications will be evaluated until a suitable candidate is identified.
For informal enquiries please contact miltos.tsiantis@plants.ox.ac.uk.

W225667R

naturejobs

Follow market trends in the News & Comment section of naturejobs.com

- Special reports
- New research opportunities
- Regional features and sector updates

Max Planck Institute for Plant Breeding Research

A new department of Comparative Development and Genetics at the Max Planck Institute for Plant Breeding Research (MPIPZ) is offering

Max Planck postdoctoral research fellowships

in the area of plant development and diversity. The Department will operate under the direction of Honorary Professor Dr. Miltos Tsiantis and will investigate problems of plant development and evolution.

We are seeking to recruit individuals with high level expertise and productivity in the following areas: molecular genetics, computational modelling of morphogenesis, bioinformatics, evolutionary genetics and cell biology. Applicants must be highly motivated and have demonstrable ability, evidenced by their publication record, to produce work of excellent quality and international impact. Applicants must be willing and able to work in a highly collaborative environment and to interact smoothly and productively with group members and external collaborators. The ability to write clearly and succinctly is highly desirable and it is expected that successful applicants will have high-level publications commensurate with their career stage.

The Max Planck Institute aims to increase the proportion of women in so far underrepresented areas. Disabled applicants with equal qualifications will be given preferential treatment.

The Max Planck Institute for Plant Breeding Research (MPIPZ) (http://www.mpipz.mpg.de/) is one of the world's premier sites committed to research into fundamental processes and training in plant biology. There are four science departments, three independent research groups and specialist support, totaling ~ 400 staff including externally funded positions.

Please send your application including • a cover letter summarizing your qualifications and your motivation for joining the department, • a CV with a full publication list and • names and contacts of two referees.

The application should be submitted electronically as one file to Christiane Wojtera
wojtera@mpipz.mpg.de

MAX-PLANCK-GESELLSCHAFT

W225670R

---

imb Institute of Molecular Biology

2012 IMB Conference
DNA Demethylation, Repair and Beyond

Mainz, Germany 18th - 21st October 2012

Speakers

Geneviève Almouzni
CNRS Institut Curie, Paris

Rafael Ariza
IMIBIC, University of Córdoba

Thomas Carell
Ludwig Maximilians University Munich

Jean-Marc Egly
IGBMC, Illkirch-Graffenstaden

Bernd Epe
Mainz University

Óscar Fernández-Capetillo
CNIO, Madrid

Nicole Francis
Harvard University, Cambridge

Jan Hoeijmakers
Erasmus Medical Center, Rotterdam

Penny Jeggo
University of Sussex, Brighton

Bernd Kaina
University Medical Center, Mainz

Markus Löbrich
Technical University Darmstadt

Wolf Reik
Babraham Institute, Cambridge

Primo Schär
University of Basel

Wim Vermeulen
Erasmus Medical Center, Rotterdam

Jörn Walter
Saarland University, Saarbrücken

Guoliang Xu
CAS, Shanghai

Yi Zhang
University of North Carolina, Chapel Hill

Keynote Speakers

Azim Surani
Gurdon Institute, University of Cambridge

Anjana Rao
La Jolla Institute for Allergy & Immunology

Scientific Organisers

Helle Ulrich CRUK London Research Institute
Christof Niehrs IMB, Mainz
George Reid IMB, Mainz
Holger Richly IMB, Mainz

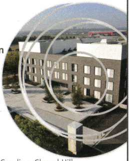

Institute of Molecular Biology
www.imb-mainz.de/2012Conference | events@imb-mainz.de

W222572EL

Bringing jobseekers and recruiters together.

Academic • Industry • Government

events · announcements · prospects · regions · careers & recruitment
spotlight · special reports · job channels · focus · movers

Search now at **naturejobs.com**

naturejobs
making science work

REPROGRAPHICS: CTT, London E17 6BU UK and **The Charlesworth Group,** Wakefield, UK.
PRINTED BY: William Gibbons & Sons Ltd, UK; **Publishers Press**, Lebanon Junction, Ky, USA and **Obun Printing Co. Inc,** Tokyo, Japan

21ST-CENTURY GIRL

A child out of time.

BY ADRIAN TCHAIKOVSKY

"Do you dream of mammoths?" a talk-show host once asked me. I knew not to give him my first choice of answer; that would have enlightened his audience over the course of three and a half hours — so long as they had the basic grounding in biosciences required to understand it. I also knew enough to avoid my second answer, which was that his question was unintelligent, and that the entire interview had taken time I could have spent better in the laboratory.

What I actually said was: "No more than you do," and the sound that the audience made told me that they liked that. I had gained their sympathy somehow. I couldn't see precisely the mechanism by which this had happened, but I filed the memory away with all the others, my empirical evidence of the human condition by which I attempt to govern my social interaction with my fellow hominids.

Another one I get is: "You must have had a difficult childhood." That throws me because it isn't a question, and so you can't really answer it. It's a statement, to which the only response, if response is even required, is: "Yes." Of course I must. Why say the obvious, except that interviews are all about them saying the obvious, and me replying with lies and simplifications because that is, I have learned, what they want to hear.

When I was 15, my foster-parents took me aside for The Talk. The bulk of my difficult childhood was behind me, although I had yet to learn most of the coping strategies I now rely on. I was essentially friendless, more comfortable interacting online than off, an academic overachiever and unable to understand why that didn't come with the positive social pay-off that I had been led to expect. I didn't like crowds or strangers much. My world was comfortable with only a few other people in it.

No different, really, from hundreds of other children across the world.

I had thought that I knew what The Talk was going to be. They had never said, but I knew I wasn't their natural offspring, by deduction from first principles. I didn't look like them. I was built differently, and I'd spent ages looking at my face in the mirror, tracing the contours of nose and chin and forehead. I was a striking girl. People who know about me now say I'm ugly, but that's a judgement influenced by their foreknowledge — they think I *should* be ugly, and so they recast my features in that unflattering light. Striking, is the word I prefer. Not even unique, if you take each feature on its own. Not resembling my foster-parents, though.

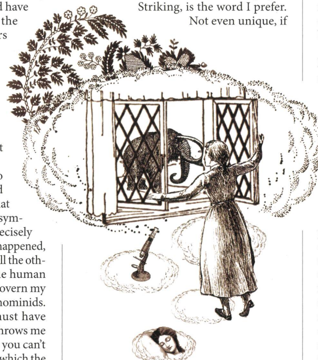

JACEY

I know, I told them. *I'm adopted*. They were unsure how to proceed. I could see that this was not, in fact, what The Talk was to be about. Perhaps I shouldn't have said anything, but that is something I still have difficulties with: knowing when to withhold knowledge. It seems so counter-intuitive to do so.

We had The Talk, at last. I wonder how many other disaffected, unsociable children wait for just that revelation: *you are something special; there is a reason why you are not like them*. The Talk was about adoption, in a way, about telling me who my parents were. My mother was stem-cell research and my father was gene sequencing.

When I was 20, and had been accepted for my doctorate, I made the decision to go public. You will recall the media storm. Nobody knew quite what to do with me. The geneticists behind my genesis had done something unethical, and yet at the same time their detractors wanted to study me. There were legal battles, in which I was a determined participant. If I was to be a test subject, stripped of human rights, then at the same time my reviled creators were guilty of nothing more than making a *thing*. Alternatively, if they had broken the boundaries of professional ethics, then it could only be because I was a human being.

➲ NATURE.COM
Follow Futures on Facebook at:
go.nature.com/mtoodm

In having me raised among their own kind, in showing that I was intellectually, and at least borderline socially, functional, they sealed their own professional fate and secured mine. They must have known. They have been forgiven, since, because genius is too valuable a quality to waste. As for me …

I did not go into my current discipline purely because of my unique past. I became a geneticist because it is an area in which my cognitive strengths shine. My ability to find patterns in complex data, and to focus without distraction on the small details of my work, is as apposite for the minutiae of modelling gene-sequencing outcomes as it would have been for the painstaking production of exacting stone tools. In fact, the further I progress in my profession, the more I meet people who are just like me, despite our different heritages — and the less our different heritages matter in any meaningful way.

I will have sisters, soon, and brothers, as close to me as blood-kin. That project is proceeding specifically because I have been more than a success: I and my people have valuable intellectual traits that the world can use. I am not working on that team, though. I have other genomes to sequence, other verdicts of history to reverse.

And still people want to know, "What's it like, being you? What is it like to be brought back, to be taken from your proper time?" And I answer that this is my time, that I am a child of the twenty-first century. And if I, *Homo sapiens neoneanderthalensis*, did not evolve to live in cities and use the Internet and make advances in the field of genetics, then neither did *Homo sapiens sapiens*, and we will both have to make do.

And why would I need to dream of mammoths when these days I can step out of my office and just watch them? ■

Adrian Tchaikovsky *was born in Lincolnshire, studied psychology and zoology at Reading and now practises law in Leeds. More of his work can be found at www.shadowsoftheapt.com.*

7,000 Recombinant Human Proteins

More Assays!
Better Assays!

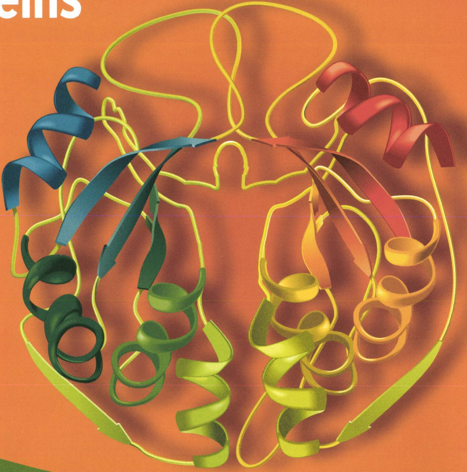

The Largest Collection of Mammalian Cell-Derived Proteins

Protein functional studies

Compound screening

Immunogens for antibody production

Assay standards: ELISA, Mass Spec, and more

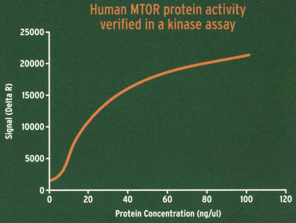

Human MTOR protein activity verified in a kinase assay

ORIGENE
Your Gene Company

origene.com/protein

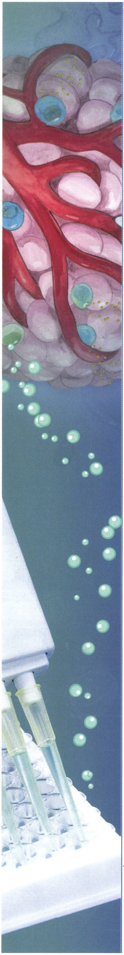

R&D Systems Tools for Cell Biology Research™

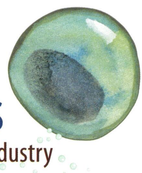

Quantikine® ELISA Kits

Setting the Standard for the Life Science Industry

R&D Systems has over 25 years of experience developing and manufacturing products for cytokine research and today we offer **the most referenced selection of ELISA kits in the industry**. Our Quantikine ELISA Kits are designed to provide the highest levels of specificity, accuracy, and sensitivity in analyte quantification. For each kit we develop, we take every step possible to ensure that it will provide customers with reliable, consistent results without the need for further assay optimization. These standards have made Quantikine Kits the top choice of life science researchers.

- More than 300 complete, ready-to-run Quantikine ELISA Kits are currently available
- Each Quantikine ELISA measures a specific protein in a designated set of complex sample types utilizing two highly specific antibodies
- During development, each kit undergoes rigorous testing to ensure optimal assay performance

Measurement of IL-17A/F in Mouse Spleen Cell Culture Supernates using the Mouse IL-17A/F Heterodimer Quantikine ELISA Kit

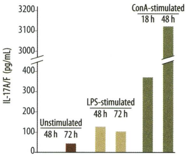

Measurement of IL-1β and IL-1α in Supernates from Human PBMCs using the Human IL-1α Quantikine or the IL-1β QuantiGlo ELISA Kit

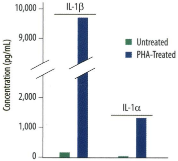

For more information, please visit our website at

www.RnDSystems.com/ELISAQuality

For research use only. Not for use in diagnostic procedures.

R&D Systems, Inc. www.RnDSystems.com

R&D Systems Europe, Ltd. www.RnDSystems.com

R&D Systems China Co., Ltd. www.RnDSystemsChina.com.cn

R&D SYSTEMS®